AFRL-ML-WP-TR-2001-4104

LOW-TEMPERATURE PLASMA COATING FOR ALUMINUM

DR. HIROTSUGU YASUDA
CENTER FOR SURFACE SCIENCE & PLASMA TECHNOLOGY
UNIVERSITY OF MISSOURI-COLUMBIA
COLUMBIA, MO 65211

DR. GORDON P. BIERWAGEN
NORTH DAKOTA STATE UNIVERSITY
FARGO, ND 51802

DR. JOAN E. DEFFEYES
BOEING
ST. LOUIS, MO 63105

DR. DAVID WIELICZKA
PHYSICS DEPARTMENT
UNIVERSITY OF MISSOURI-KANSAS CITY
KANSAS CITY, MO 64110

MARCH 2001

FINAL REPORT FOR PERIOD 29 JUNE 1996 – 31 MARCH 2001

**MATERIALS AND MANUFACTURING DIRECTORATE
AIR FORCE RESEARCH LABORATORY
AIR FORCE MATERIEL COMMAND
WRIGHT-PATTERSON AIR FORCE BASE, OH 45433-7750**

Report Documentation Page

Report Date	Report Type	Dates Covered (from... to)
00032001	N/A	-

Title and Subtitle		Contract Number
Low-Temperature Plasma Coating for Aluminum		
		Grant Number
		Program Element Number

Author(s)		Project Number
Yasuda, Hirotsugu; Bierwagen, Gordon P.; Deffeyes, Joan E.; Wieliczka, David		
		Task Number
		Work Unit Number

Performing Organization Name(s) and Address(es)	Performing Organization Report Number
Center for Surface Science & Plasma Technology University of Missouri-Columbia Columbia, MO 65211	

Sponsoring/Monitoring Agency Name(s) and Address(es)	Sponsor/Monitor's Acronym(s)
Materials and Manufacturing Directorate Air Force Research Laboratory Air Force Materiel Command Wright-Patterson AFB, OH 45433-7750	
	Sponsor/Monitor's Report Number(s)

Distribution/Availability Statement
Approved for public release, distribution unlimited

Supplementary Notes
The original document contains color images.

Abstract

Subject Terms

Report Classification	Classification of this page
unclassified	unclassified

Classification of Abstract	Limitation of Abstract
unclassified	UU

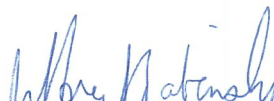**Number of Pages**
426

NOTICE

Using government drawings, specifications, or other data included in this document for any purpose other than government procurement does not in any way obligate the US Government. The fact that the government formulated or supplied the drawings, specifications, or other data does not license the holder or any other person or corporation or convey any rights or permission to manufacture, use, or sell any patented invention that may relate to them.

This report is releasable to the National Technical Information Service (NTIS). At NTIS, it will be available to the general public, including foreign nations.

This technical report has been reviewed and is approved for publication.

ELIZABETH S. BERMAN, Materials Engineer
Coatings Team
Nonstructural Materials Branch

JEFFREY S. ZABINSKI, Chief
Nonstructural Materials Branch
Materials and Manufacturing Directorate

ROBERT M. SUSNIK, Deputy Chief
Nonmetallic Materials Division
Materials and Manufacturing Directorate

Do not return copies of this report unless contractual obligations or notice on a specific document requires its return.

1. AGENCY USE ONLY (Leave blank)	2. REPORT DATE MARCH 2001	3. REPORT TYPE AND DATES COVERED Final, 6/29/1996 - 3/31/2001	

4. TITLE AND SUBTITLE
LOW-TEMPERATURE PLASMA COATING FOR ALUMINUM

5. FUNDING NUMBERS
C: F33615-96-C-5055
PE: 62102F
PR: 4347
TA: 65
WU: 03

6. AUTHOR(S)
DR. HIROTSUGU YASUDA
DR. GORDON P. BIERWAGEN
DR. JOAN E. DEFFEYES
DR. DAVID WIELICZKA

7. PERFORMING ORGANIZATION NAME(S) AND ADDRESS(ES)

CENTER FOR SURFACE SCIENCE & PLASMA TECHNOLOGY UNIVERSITY OF MISSOURI-COLUMBIA COLUMBIA, MO 65211

NORTH DAKOTA STATE UNIVERSITY FARGO, ND 51802

BOEING ST. LOUIS, MO 63105

PHYSICS DEPARTMENT UNIVERSITY OF MISSOURI-KANSAS CITY KANSAS CITY, MO 64110

8. PERFORMING ORGANIZATION REPORT NUMBER

9. SPONSORING / MONITORING AGENCY NAME(S) AND ADDRESS(ES)

MATERIALS AND MANUFACTURING DIRECTORATE
AIR FORCE RESEARCH LABORATORY
AIR FORCE MATERIEL COMMAND
WRIGHT-PATTERSON AIR FORCE BASE, OH 45433-7750
POC: Dr. Elizabeth S. Berman, AFRL/MLBT, (937) 255-2465

10. SPONSORING / MONITORING AGENCY REPORT NUMBER

AFRL-ML-WP-TR-2001-4104

11. SUPPLEMENTARY NOTES

12a. DISTRIBUTION / AVAILABILITY STATEMENT
Approved for public release; distribution unlimited.

12b. DISTRIBUTION CODE

13. ABSTRACT *(Maximum 200 Words)*

The primary objective of this research project was to provide an alternative corrosion protection through means of processes more environmentally benign than conventional methodologies. Hexavalent chromium (Cr+6) has historically been acknowledged to exhibit the technological forefront in corrosion protection of aluminum alloys. The Systems Approach Interface Engineering (SAIE) concept, adopted in this project, emphasizes the fact that the corrosion protection of a metal depends on the overall corrosion protective behavior of an entire systems, including the bulk characteristics of the coatings(s) and interfacial factors. The primary methodologies used were plasma processing. The technology showed superior corrosion resistant results to traditional aircraft coating systems. This technology is applicable to aircraft piece parts.

14. SUBJECT TERMS
plasma processing, corrosion resistant, corrosion protection aluminum parts, environmental benign, chromate replacement

15. NUMBER OF PAGES
428

16. PRICE CODE

17. SECURITY CLASSIFICATION OF REPORT Unclassified	18. SECURITY CLASSIFICATION OF THIS PAGE Unclassified	19. SECURITY CLASSIFICATION OF ABSTRACT Unclassified	20. LIMITATION OF ABSTRACT SAR

Table of Contents

Table of Contents (Cont.)

Low Temperature Plasma Coating for Aluminum

**U. of Missouri - Columbia, U. of Missouri - K.C.,
Boeing-St. Louis, North Dakota State University**

- **Objectives**
  - Non-chromated finish system for aluminum detail parts including Ion Vapor Deposited (IVD) aluminum coated parts
  - Low/no VOC/HAP organic coatings
  - Permanent systemis an ultimate goal

- **Milestones/Accomplishments**
  - "Barrier-Adhesion" principle for damaged surface- and pitting- corrosion protections was established.
  - Equally good corrosion protection was obtained with E-coat and water-born spray primers without corrosion inhibitor, which out performed control with CC coating and a solvent borne chromated primer.
  - A hybrid process of IVD and cathodic plasma polymerization showed practical feasibility.

- **Approach**
  - ➤ System Approach Interface Engineering for corrosion protection system without chromate conversion coating and chroomate in primers.
  - ➤ Combination of Ion Vapor Deposited Aluminum Coating (IVD) and Cathodic Plasma Polymerization in situ
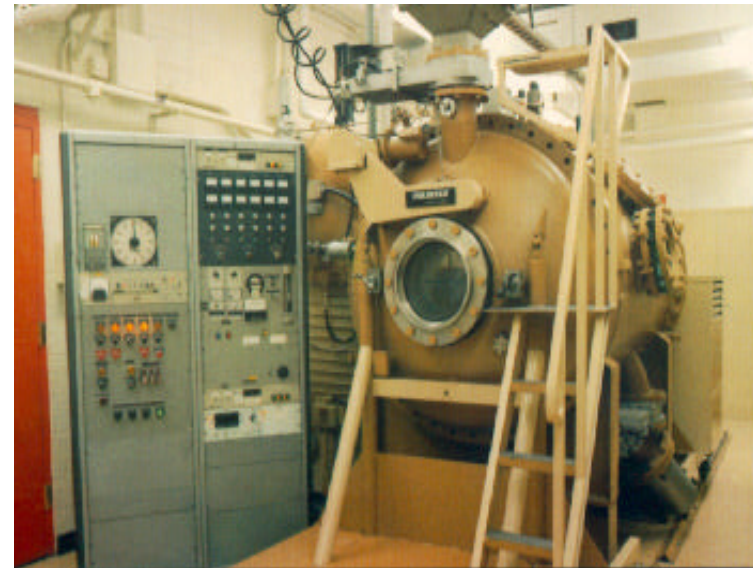
Executive Summary

Corrosion on a coated aluminum alloy can be viewed as occurring based on the following two important modes of corrosion. 1). Corrosion that occurs at and in the vicinity of the damaged, or scribed, coating, which could be termed "damaged surface corrosion". 2). Corrosion that occurs under the undamaged coating, which often appears as many small pits. This corrosion can be referenced under the general category of "pitting corrosion".

Examining over several thousands of corrosion test specimens, which were subjected to SO_2 salt spray and Prohesion salt spray tests through the course of this project, it became quite clear that the corrosion damage, which can be expressed by the width of corrosion along the scribed line or by the percent of corroded area, is primarily the consequence of "corrosion-induced de-lamination of the coating". In other words, the salt spray tests tell how severe, or how slight, the corrosion-induced de-lamination occurred during the period of salt spray exposure. De-lamination of the coating precedes the corrosion under the coating.

Pitting corrosion, on the other hand, occurs without gross de-lamination of the coating during the normal duration of salt spray tests (e.g., one to three months). Only the removal of the coating after the salt spray tests can reveal this effect. Pitting corrosion occurs when the barrier characteristics of a coating are poor, and also when the adhesion is poor under the influence of water permeation.

The combination of chromate conversion coating and chromated primer prohibits, or minimizes the occurrence of corrosion at damaged sites. Thus it diminishes or minimizes the driving force for the corrosion-induced de-lamination of the coating. On the other hand, the inclusion of corrosion inhibitors (e.g., chromates) in the coating damages the barrier characteristics of the bulk phase of the coating and also makes the adhesion water sensitive. Thus, the chromated corrosion protection coating minimizes the damaged surface corrosion, but does not prevent pitting corrosion.

Electrochemical corrosion protection requires the presence of water at the site of corrosion in order to facilitate the electrochemical reactions. Therefore, a superb barrier could not be used in such an approach. Tenacious adhesion of an excellent barrier, insensitive to water and salts, is the basis for the System Approach Interface Engineering (SAIE), principle in the foundation of this study. The two types of approaches are fundamentally incompatible. The choice between the two must be made on the merits of the desired results.

In contrast to conventional corrosion protection, which can be categorized under the general term "electrochemical corrosion protection", the approach taken for this project could be viewed as corrosion protection fundamentally based on the "barrier-adhesion" principle. The adhesion in this approach must be "water insensitive adhesion", which is primarily based on covalent bonding of a primer to the nano-film to the substrate alloy.

The coatings produced utilizing the "barrier-adhesion" principle protect aluminum alloys in a completely different manner than conventional electrochemical inhibiting methods. There is no corrosion inhibitor involved in the system, and no inhibition of corrosion occurs at the damaged

site. However, because of tenacious, water-insensitive, adhesion of the coating to the metal surface, de-lamination of the coating from the damaged sites cannot occur. Without opening a new surface, the corrosion at the damaged sites cannot propagate, or proceeds very slowly. In many cases, the exposed surface passivates itself, for all practical purposes, and the corrosion width does not increase much beyond the original width of the scribed line.

Because of the water-insensitive adhesion, and the good barrier characteristics of the coating, no pitting corrosion was found with coatings formed based on the "barrier-adhesion" principle. Pitting corrosion was only found on the controls, which were chromate conversion coated and then coated with a chromated primer. Thus, this approach was found to be very effective in minimizing both "damaged surface corrosion" and "pitting corrosion".

Cathodic plasma polymerization, or plasma chemical vapor deposition (PCVD), of trimethylsilane (TMS) applied to an appropriately prepared aluminum alloy surface yields a roughly 50 nm thick layer of an amorphous $Si_kC_yH_z$ network (nano-film), which is covalently bonded to the aluminum oxide at the interface. A primer coating applied to the surface of the nano-film is covalently bonded via the reaction of peroxides, which are formed by the reaction of oxygen with Si dangling bonds (free radicals) when the coated surface is exposed to ambient oxygen. Thus the TMS nano-film works as an interlayer to allow the formation of coating system that is bonded primer to the metal surface via an interactive covalent network. The plasma polymerization process is a one-minute deposition process, during which the temperature of the substrate alloy only rises approximately 2-3 °C. Minimization of this temperature increase was found to be an important factor for yielding a good corrosion protection system for aluminum alloys.

It was decided that the most practical way to utilize the plasma polymerization technique in the corrosion protection of aluminum alloys for aerospace applications is to combine it with current Ion Vapor Deposition (IVD) of pure aluminum, which is currently a standard technique that is available at both the OEM manufacturers and also at the depot maintenance facilities. Since E-coat (electrochemical paint application) has never been used for IVD coated parts or components, our efforts have shifted to the establishment of an IVD/plasma polymerization hybrid process for spray primer application. It was found that IVD/plasma coating/non-chromated water borne primer out performed the current system of IVD/chromate conversion coating/chromated solvent borne primer.

Within the scope of the IVD/plasma coating hybrid process, **the main goal of this study; i.e., to develop a chromate-free coating system and to eliminate or minimize VOC and HAP, has been successfully accomplished. It is estimated that the hybrid process would reduce the total operational cost of the current IVD application, even without counting the huge environmental remediation costs that can be avoided via this approach.** Furthermore, this study has clearly established that a new alternative approach to the corrosion protection of aluminum alloys exists, which does not rely on electrochemical corrosion protection. The "barrier-adhesion" principle is the foundation of this new approach, and should be the root of future advanced corrosion protection schemes for aluminum alloys.

1. Introduction

The primary objective of this research project was to provide an alternative corrosion protection through means of processes more environmentally benign than conventional methodologies. Cr^6 has historically been acknowledged to exhibit the technological forefront in corrosion protection of aluminum alloys. Technologies to take advantages of the electrochemical corrosion protection provided by Cr^6, such as chromate conversion coatings and chromated primers, have been developed and are widely used today. The mainstays of corrosion protection, and probably the only currently reliable and practical corrosion protection approaches, for aluminum alloys today are based on the electrochemical corrosion protection provided by Cr^6.

While chromates provide sufficient corrosion protection of aircraft aluminum alloys, the environmental concerns and health hazards caused by chromium have become quite serious in recent years. In order to protect workers and the environment , the use of chromium and chromates is in the process of being phased out. It is imperative to find alternative methods that can provide equivalent, or better, corrosion protection than that provided by the Cr based corrosion protection methods, before the phase-out can be completed.

In the search for alternative methods, two major approaches can be conceived. One is the search for environmentally benign corrosion inhibitors other than chromium. Another approach is to find a way to protect aluminum alloys without using any corrosion inhibitors. Alternative corrosion inhibitors, which are aimed at replacing chromium with the same functional effect, are generally other heavy metals. The principle of this approach is the selection of lesser evils. The other approach, which was adopted in this research project, is to eliminate all potentially hazardous materials altogether and establish completely different corrosion protection mechanisms.

The System Approach Interface Engineering (SAIE) concept, adopted in this project, emphasizes the fact that the corrosion protection of a metal depends on the overall corrosion protective behavior of an entire system, including the bulk characteristics of the coating(s) and interfacial factors. In other words, without tailoring interfaces, the mere combination of effective protection layers does not lead to an excellent corrosion protection system.

In contrast to conventional corrosion protection, which can be generally termed "electrochemical corrosion protection", the approach taken in this project could be viewed as corrosion protection based on the "barrier-adhesion" principle. The adhesion in this approach must be "water insensitive adhesion" that is one which is primarily based on covalent bonding of a nano-film of plasma polymer of amorphous $Si_kC_yH_z$ to the substrate, and also the covalent bonding of the primer to the nano-film.

In this final report, important topics were selected and are presented in the format of publication in scientific or technical journals. Accordingly, some figures and tables appear more than once in different chapters for different topics, for ease of reading. Numbers for figures, tables, and references are given within a particular chapter.

2. "Barrier-Adhesion" Principle for Corrosion Protection

H. K. Yasuda, Q. S.Yu, C. M. Reddy, C. E. Moffitt, D. M. Wieliczka, and J. E. Deffeyes

Abstract

The "barrier-adhesion" principle for corrosion protection of aluminum alloys is presented. The corrosion that occurs in a coated aluminum alloy can be viewed as pertaining to one of the two following corrosion modes of. 1). Corrosion that occurs at and in the vicinity of a damaged coating (damaged surface corrosion, such as that associated with scribed corrosion testing). 2). Corrosion that occurs under the undamaged coating, which often appears as many small pits (pitting corrosion). The damaged surface corrosion was found to be a consequence of corrosion-induced de-lamination of the coating, which enhances the propagation of corrosion from the damaged site. With a coating system that contains corrosion inhibitors, the corrosion at the damaged site is suppressed to prevent de-lamination. It was found that if a good barrier was adhered to the metal surface by the tenacious water-insensitive adhesion, the corrosion-induced de-lamination could be prevented without corrosion inhibitors in the primer. Pitting corrosion is then seen to be a consequence of the formation of localized micro de-lamination, which is caused by a poor barrier and poor (water-sensitive) adhesion. The effective incorporation of corrosion inhibitors makes the barrier characteristics of coating poor, and also makes the adhesion to the metal surface more water-sensitive. Accordingly, it was found that a coating with corrosion inhibitors reduces the damaged surface corrosion, but tends to enhance pitting corrosion. The coating based on the "barrier-adhesion" principle was found to prevent both the damaged surface corrosion and pitting corrosion.

Introduction

The corrosion protection of a metal depends on the overall performance of the entire corrosion protecting system as a whole. The basic factors involved in the corrosion protecting system under consideration include: the stability of the alloy components and metal oxides covering the top surface of a metallic substrate; the modification of oxides by a conversion coating; the adhesion of a primer; the corrosion inhibitor or passivation agent incorporated in the primer; the barrier characteristics of the primer, etc. An attempt to improve a factor does not necessarily result in better performance of the system. The concept of system approach interface engineering (SAIE) is based on the tailoring of various interfaces to accomplish the optimum overall corrosion protection by the system as a whole.

Corrosion of a metal is an electrochemical process, and the corrosion protection of a metal generally relies on electrochemical passivation of the corrosion process. The latter process, however, must be incorporated into a coating, for practical application. Electrochemical corrosion as well as electrochemical passivation requires the presence of water, because both processes need electrolytic solutions to proceed. The water necessary for electrochemical passivation is generally provided from the environment where the corrosion occurs, when a coating is damaged. In the case of an un-damaged coating, water and corrosive components such as salt and oxygen are provided by transport through the coating. The combination of poor adhesion of paint and inferior barrier characteristics of a coating, with regard to water and salts, could introduce clustered water (liquid water as opposed to molecular water) with salts at the

coating/metal interface. Hence providing the electrolytic environment for corrosion to proceed, without conspicuous damage to the coating.

While the majority of corrosion tests focus on the corrosion of damaged surfaces, a substantial amount of damage to most coated objects might occur in the second process described above. The major tool to combat the corrosion that occurs via this route is the combination of good barrier characteristics and water insensitive adhesion of the coating. Systems without any corrosion inhibitor, which have excellent water insensitive adhesion and good barrier characteristics, have shown remarkably good results in salt spray corrosion tests with scribed surfaces [1-4]. It is important to note that the scribed line did not advance in such systems and the exposed surface in the scribed line did not show any conspicuously different corrosion compared to the controls with corrosion inhibitors. In light of these very promising results, which were obtained without the use of corrosion inhibitors, factors involved in both approaches, i.e., electrochemical protection versus barrier/adhesion protection, are critically examined in this chapter.

EXPERIMENTAL

Materials

7.62 cm by 15.2 cm by 0.08 cm aluminum alloys panels, including AA2024-T3 ([2B]), AA7075-T6 ([7B]), Alclad 2024-T3 ([2A]), Alclad 7075-T6 ([7A]), were procured from Q-Panel Lab Products (Cleveland, OH). Ion vapor deposition (IVD) aluminum-coated 2024-T3 ([2I]) panels (7.62 cm by 15.24 cm by 0.081 cm) were prepared at The Boeing Company, St. Louis, MO. Two types of controls, chromate conversion coated (Iridite 14-2) and then non-chromated cathodic E-coated (CC/E1) or chromated spray primer (Deft 44-GN-36) coated (CC/A) alloy panels, were used in this study. These later panels were also prepared at The Boeing Company in St. Louis.

The chemicals used in the chemical cleaning of the aluminum alloy panels were: Turco 4215-S, a commercial alkaline cleaner purchased from Turco Products, Inc., Wilmington, CA; Amchem 7, a commercial deoxidizer purchased from Amchem Products, Inc., Ambler, PA; Nitric acid (65%) purchased from Fisher Scientific.

The following chemicals were used in plasma pretreatment and plasma polymerization process. The diatomic gases, oxygen (99.9%) and hydrogen (99%), were procured from Airgas. Trimethlysilane (TMS) gas of 97% minimum purity was procured from PCR, Inc. (Gainesville, FL) and Lancaster Synthesis, Inc. (Windham, NH). All the gases and monomers were used as received without any further purification.

Two kinds of proprietary experimental cathodic E-coat, designated as E1 and E2 were used in this study. The spray primers employed in this study were Deft 44-GN-36 (Deft Corporation, Irvine, CA), Spraylat EWDY048 (Spraylat Corporation, Chicago, IL), and Dexter 10-PW-22-2 (Dexter Corporation, Waukegan, IL) spray primers.

Surface preparation

Acetone wiping with Kimwipes® was first used to clean the ink marks and loose organic matter from the surfaces of the Al panels. The chemical cleaning of the aluminum alloy panels was performed by Alkaline cleaning and Deoxidization. The Turco 4215-S alkaline solution was prepared and used per McDonnell Douglas Process Specification P.S. 12030 (The Boeing Company, St. Louis). The Amchem 7 deoxidizer solution was combined with nitric acid, prepared and used per McDonnell Douglas Process Specification P.S. 12050.1 (The Boeing Company, St. Louis).

Alkaline cleaning of Al panels was performed by immersion in an alkaline bath at 65 ^{0}C (150 ^{0}F) for about 25 minutes, or until each panel became water break free when rinsed with DI water; they were then thoroughly rinsed with DI water. In the case of deoxidization, the panels first went through the alkaline cleaning process and were then immersed in a deoxidization bath at room temperature for 10 minutes, rinsed with DI water, immersed in DI water for 5 minutes and finally air-dried.

Before plasma polymer deposition, plasma pretreatment by simple gas plasmas was applied to aluminum panel surfaces to remove possible contaminants and thus to promote plasma polymer adhesion. TMS was mainly used as the monomer of direct current (d.c.) cathodic plasma polymerization. Plasma conditions for sample preparation and the sample identification codes are summarized in Table 1.

Plasma reactor system and operation

The DC plasma reactor system used in this study was a bell jar type reactor. The d.c. plasma generator was an MDX-1K Magnetron Drive power supply (Advanced Energy Industries, Inc.). Two anodes consisting of stainless steel plates ($25.4 \times 25.4 \times 0.16$ cm), with magnetron enhancement, were placed 15.5 cm apart in parallel. An iron ring (17.5 cm outside diameter, 13.8 cm inside diameter, 0.16 cm thick) and an iron center plate (5 cm in diameter, 0.16 cm thick) were attached coaxially on the backside of each anode plate as magnetic field distributor. Eight pieces of permanent magnet bars were equidistantly attached on the iron ring and iron plate with the south-pole pointing to the center of the iron plate. The magnetic field strength of each magnet ranged from 700 to 800 Gauss. Two Al panels (forming a 15.2 cm by 15.2 cm square) were placed in the middle of the two parallel anodes and used as the cathode of the plasma system. The detailed operation procedures of such a reactor system have been described elsewhere [1].

To conduct plasma deposition in a closed reactor system, the anode assembly was removed and the grounded reactor wall was used as the anode during operation. The reactor chamber was first pumped down to < 1 mTorr. The reactor chamber was then isolated from the pump system by closing the main valve located in between. TMS gas controlled by an MKS mass flow meter (model 247C) was then fed into the reactor. After the system pressure reached the preset point, TMS gas feeding was stopped and DC power was then applied to initiate the glow discharge to start cathodic polymerization.

Table 1
Sample identification codes

Identification Code	Meaning and Conditions
[2B]	2024-T3 aluminum alloy
[7B]	7075-T6 aluminum alloy
[2A]	Alclad 2024-T3 aluminum alloy
[7A]	Alclad 7075-T6 aluminum alloy
[2I]	IVD Al-coated 2024-T3 aluminum alloy
(Ace)*	Acetone wiping with Kimwipes® tissue
(Alk)	Alkaline cleaning (65 ^{0}C, 25 min)
(Dox)	Deoxidization (room temperature, 10 min, always preceeded by alkaline cleaning)
(O)	O_2 plasma treatment (on Al panel surface: 2 sccm O_2, 100 mTorr, 40 W, 2 min; on TMS polymer surface: 2 sccm O_2, 50 mTorr, 10 W, 1 min)
(AH)	Ar + H_2 plasma treatment (1 sccm Ar + 2 sccm H_2, 50 mTorr, 80 W, 10 min)
(Ar)	Ar plasma treatment (2 sccm Ar, 10 W, 1 min)
T	TMS DC cathodic polymerization with anode magnetron enhancement in a flow reactor system (1 sccm TMS, 50 mTorr, 5 W, 1 min)
TO	TMS + O_2 DC cathodic polymerization with anode magnetron enhancement in a flow reactor system (1 sccm TMS + 1 sccm O_2, 50 mTorr, 5 W, 1 min)
Tfs	TMS DC cathodic polymerization without using anode assembly in a flow reactor system (TMS 25 mTorr, DC 1000 V, 2 min)
Tcs	TMS DC cathodic polymerization without using anode assembly in a close reactor system (1 sccm TMS, 50 mTorr, 5 W, 1 min)
CC	Chromate conversion coating (Iridite 14-2)
A	Deft spray primer 44-GN-36 (chromated)
E1	Cathodic E-coat 1 (non-chromated)
E2	Cathodic E-coat 2 (with proprietary inhibitors)
D	Spraylat spray primer EWDY048 (non-chromated)
X	Dexter spray primer 10-PW22-2 (non-chromated)
/	Process separation mark

* Code used in parenthesis indicates the surface cleaning process, code used without parenthesis indicates coating process.

Application of primers

Electrodeposition of cathodic e-coats was carried out in a one gallon electrocoat bath using an Al panel as the cathode and a stainless steel strip (1.5"×10") as the anode. A Darrah Digital® DC power source with variable voltage capability was used for the electrodeposition.

Spray primers were sprayed onto the Al substrates with an airbrush. After painting, primer-coated samples were cured according to the stipulations provided by the primer suppliers. After curing, the thickness of the primer coatings was controlled to be around 1.0 mil (25.4 µm).

Tests and Measurements

Adhesion tests

Adhesion performance was first evaluated via the tape test according to the guidelines of the American Society for Testing and Materials (ASTM 3359-93B) [5]. This testing method provides semi-quantitative results given in grades of 0 to 5. Poor adhesion can be easily detected by this simple test. When the test result reaches the grade of 5, this simple test cannot distinguish between results. However, if samples are exposed to some adhesion-damaging environment before the tape test, it is possible to further distinguish the level or nature of adhesion.

The boiling water test is such a modification of the tape test. In this process, the test specimens are prepared according to the standard procedure described above. Instead of applying the tape test directly, the specimens are placed in boiling water for a predetermined period of time. In this study, 1, 4, and 8 hours were used. Samples initially immersed in boiling water (with pre-scribed marks) were subjected to the tape test. Because the interface between the coating and the substrate metal is exposed to boiling water, the water sensitivity of the adhesion can easily be detected by this test.

NMP (N-methyl pyrrolidone) paint removal time test (NMP time) as described elsewhere [6,7] was also used to evaluate the adhesion level of the electocoatings (E-coats) to the alloy substrates. The NMP time is the time needed for an E-coat layer to separate from its substrate when an E-coated sample (1.0 cm diameter) is immersed in 60 ^{0}C NMP.

SO$_2$ and Prohesion salt spray tests

The alloy panels with various low-temperature plasma interface-engineered, primer-coated surfaces were evaluated for corrosion performance at Boeing, St. Louis, MO. Two kinds of accelerated corrosion tests were conducted on all the samples, including the two types of control panels: SO$_2$ salt spray test performed per the American Standards for Testing Methods (ASTM) G85-94-A4, and Prohesion salt spray test performed per the American Standards for Testing Methods (ASTM) G85-94-A5, respectively [8].

After completing corrosion testing exposure, the panels were rinsed with distilled water and visual observations were made. The panels were then subjected to Turco-5469 paint stripper solution to strip off the E-coat or spray primers (including the samples and the controls) from the

scribed surface, so that the effect of corrosion beneath the coatings and away from the scribes could be viewed. These panels were then used to estimate the average corrosion creep widths [9], in order to compare the corrosion performance of the different sample systems.

Filiform corrosion test

Filiform Corrosion is a special type of corrosion that occurs under coatings on metal substrates that is characterized by a definite threadlike structure and directional growth (ASTM D2803 para. 3.1.1) [10]. Before the test, diagonal lines were scribed in each panel forming an "X" in the coating surface film exposing the metal substrate. Each specimen edge and back surface were then covered with a protective tape. The panels were placed vertically, with the long dimension horizontal, in a desiccator containing 1000 ml of 12 N hydrochloric acid (HCl). The panels were exposed for one hour at 77 ^{0}C while being supported approximately two inches above the liquid level. Upon completion of the one hour HCl exposure, the specimens were immediately placed, without rinsing, in a 104±3 ^{0}F (40±2 ^{0}C), 80±5% RH environmental chamber for 2000 hours. Panels were held with the long dimension at a 6^0 inclination from vertical and with the coated side facing upward. Visual observations were not made during the exposure.

XPS surface analysis

X-ray photoelectron spectroscopy (XPS), also referred to as ESCA (electron spectroscopy for chemical analysis), data was acquired with a Kratos AXIS HS instrument, using the Mg-Kα flood source operated at ~217 watts (15 mA, 14.5 kV). XPS data were acquired in the hybrid mode of the instrument, which combines electrostatic and magnetic lensing. The 2 mm aperture, used in the hybrid mode, limits collection to a spot size on the order of 200-300 μm. All spectra were collected with the analyzer set at a pass energy of 80 eV, including the individual core spectra. This gives a FWHM of just over 1.4 eV for the Ag 3d line. This lower resolution setting was used to minimize collection time and thus the exposure of the films to extended x-ray and secondary electron fluxes, since these could tend to modify organic components. This also allowed for much more practical sputter depth profiling of the films, not included in this discussion, as well as for the collection of the Si KLL Auger spectra, which have a substantially smaller signal strength, at the same resolution as the photoelectron spectra. The preferred use of the flood Mg source was based on the desire to collect Si KLL Auger spectra, which can not be excited with an Al monochromatic source. Charge compensation was made with the manufacturer's proprietary system, at settings of: -1.5 V charge balance voltage, 1.85 A filament current, and –0.5 V bias voltage.

RESULTS AND DISCUSSION

The corrosion that occurs in a coated aluminum alloy can be viewed in one of the following two corrosion models. 1). Corrosion that occurs at and in the vicinity of the damaged, or scribed, coating. This corrosion is termed "damaged surface corrosion". 2). Corrosion that occurs under the undamaged coating, which often appears as many small pits. This corrosion is termed "pitting corrosion".

Examining some few hundreds of corrosion test specimens [1-4], which were subjected to SO_2 salt spray (4 weeks) and Prohesion salt spray (12 weeks) tests, it became quite clear that the

corrosion damage, which can be expressed by the widths of corrosion along the scribed line or by the percent of corroded area, is the consequence of "corrosion-induced de-lamination of the coating". In other words, the salt spray tests show how badly or how little the corrosion induced de-lamination occurred during the period of salt spray exposure. The de-lamination of the coating seems to precede the occurrence of corrosion under the coating.

Pitting corrosion, on the other hand, occurs without gross de-lamination of the coating during the normal duration of salt spray tests (e.g., one to three months), and only removing the coating after the salt spray tests can reveal the pits themselves. Pitting corrosion occurs when the barrier characteristics of the coatings system are poor, and also when the adhesion of the coatings is poor under the influence of water permeation. In this case, localized micro de-lamination of the coating occurs at the site of pitting corrosion. The basic principle for this phenomenon has been recently presented [11,12,13]

The combination of chromate conversion coating and chromated primer prohibits or minimizes the occurance of corrosion at the damaged sites. Thus it diminishes, or minimizes, the driving force for the corrosion-induced de-lamination of the coating. On the other hand, the inclusion of corrosion inhibitors (chromates) in the coating damages the barrier characteristics of the bulk phase of the coating and also makes the adhesion water sensitive. Consequently, the chromated coating could effectively prevent damaged surface corrosion, but does not prevent the occurance of pitting corrosion, and may even promote pitting corrosion.

There are obvious fundamental requirements that must be fulfilled in order to have an effective coating system with electrochemical inhibitors, or passivation agents, incorporated in a coating layer. First, the inhibitor must be able to migrate within a coating layer. Second, a sufficient amount should be incorporated in the coating to assure continued passivation. The third, not so obvious, requirement is that the coating should have relatively high water permeability in order to provide enough water necessary to allow the function of aqueous electrochemical corrosion inhibition at the site of corrosion, particularly for undamaged surface corrosion. In other words, a super barrier to water cannot and should not be used with corrosion inhibitors. These requirements make the barrier characteristics of the coating poorer and also the adhesion more water-sensitive.

An evaluation procedure designed to allow for the results of salt spray corrosion tests to be numerically ranked was developed [9]. These methods enable corrosion test results to be dealt with in a statistical manner. In order to compare the relative extent of the damaged surface corrosion and of the pitting corrosion, the percent of the corroded area in the tested surface is used, and summarized in Table 2. It is important to note that pitting corrosion was found only on chromate conversion coated controls (one with chromated spray primer and another with E-coat). It is also important to note that E-coat directly applied on alloy surfaces, without chromate conversion coating, performed as good as, or even better than, chromate conversion coated controls in salt spray tests, and no pitting corrosion was found with those systems.

Table 2. Average percent corrosion area of SO_2 (3 weekw) and Prohesion salt spray (12 weeks) tested aluminum panels.

Substrates	Coating Systems	Pitting Corrosion (%)		Along the Scribe (%)	
		SO_2	Prohesion	SO_2	Prohesion
[2A]	CC/A	0.33 ± 0.06	-0-	20.4	10.1
	CC/E1	-0-	-0-	8.95	44.1
	(Ace)/E1	-0-	-0-	5.16	4.03
	(Ace/O)/TO/E1	-0-	-0-	4.39	3.79
[2B]	CC/A	1.05 ± 0.17	1.8 ± 0.7	4.56	8.89
	CC/E1	0.68 ± 0.04	1.5 ± 0.3	4.44	14.2
	(Dox)/E1	-0-	-0-	7.41	4.74
	(Alk)/TO/E1	-0-	-0-	2.07	2.79
[7B]	CC/A	0.41 ± 0.16	1.7 ± 0.7	3.08	4.74
	CC/E1	1.9 ± 0.4	1.5 ± 0.3	2.96	11.5
	(Dox)/E1	-0-	-0-	4.21	6.52
	(Alk/AH)/T/E1	-0-	-0-	19.5	5.16

The first control is a panel with chromate conversion coating and a chromated primer designated as A (see Table 1 for sample designation). The second control has chromate conversion coating and E-coat (E1). After the salt spray test, the primer was removed, and the now-exposed surface of each panel was placed on a scanner and the corresponding digital image was created. The control, CC/A is a typical sample representing the corrosion protection afforded by means of electro-chemical corrosion protection. The second control, CC/E1 is the sample representing the hybrid of electro-chemical corrosion protection and barrier protection. The third sample, (Ace)/E1, is the sample representing the corrosion protection by barrier/water-insensitive adhesion principle without plasma coating. The fourth sample is the sample representing the corrosion protection by "barrier-adhesion" principle by means of plasma interface engineering. With a good corrosion resistant surface, such as Alclad, the corrosion protection by barrier/water-insensitive adhesion seems to work much better than the electrochemical corrosion protection. These results also indicate that these two basic approaches are incompatible. Placing chromate conversion coating on the substrate ruins the good interactive coating aspect of E-coat.

A good barrier cannot be used in the electrochemical corrosion protection scheme as mentioned earlier. When corrosion inhibitors are incorporated in a primer, it is necessary to reduce the barrier characteristics of a coating. When the barrier characteristic is lowered, it also reduces the water-insensitive adhesion. Comparing two E-coats, of which one was intended to achieve what was just described, one can see the effect of these two inter-related factors on adhesion and corrosion protection. Two prototype E-coats, E1 and E2, are compared. E2 is designed to incorporate a proprietary (non-chromate) corrosion inhibitor by sacrificing barrier characteristic of the primer. Table 3 summarizes the adhesion characteristics of these two E-coats. While the dry tape test cannot distinguish the level of adhesion, NMP immersion time and the wet tape test clearly indicate that the adhesion of E2 is more water-sensitive.

Table 3. Comparison of adhesive characteristics of two E-coat systems (scale 0-5 indicates poor (0) to excellent (5) performance).

Substrate	Pretreatment	Tape test rating				NMP Time (min)	
		E1		E2		E1	E2
		Dry	Water Boiled for 1, 4, 8 hrs	Dry	Water Boiled for 1, 4, 8 hrs		
[2A]	(Ace/O)/TO	5	3, 3, 2	5	0, --	>120	5
[2B]	(Alk)/TO	5	3, 3, 2	5	4, 0, --	>120	75
[7B]	(Dox)/T	5	3, 3, 2	5	0, --	15	2

The coatings formed using the "barrier-adhesion" principle protect aluminum alloys in a completely different manner. There is no corrosion inhibitor involved in the system, and no inhibition of corrosion occurs at the damaged site. However, because of the tenacious water-insensitive adhesion between the coating and the metal surface, de-lamination of the coating from the damaged sites cannot occur. Without opening a new surface, the corrosion at the damaged sites cannot propagate, or proceeds very slowly. In many cases, the exposed surface passivates itself, in all practical senses, and the corrosion width does not increase much beyond the original width of the scribed line. Because of water-insensitive adhesion and the good barrier characteristics of the coating, no pitting corrosion was found with coatings formed with the "barrier-adhesion" principle. Pitting corrosion examples were only found on controls, which are chromate conversion coated and coated with a chromated primer. Thus, this approach was found to be very effective in minimizing both "damaged surface corrosion" and "pitting corrosion".

Fig. 1 shows the scanned images of panels after the Prohesion salt spray test. On both samples, E-coat was applied directly on alkaline cleaned 2024-T3 aluminum alloys. Sample E2 showed numerous pitting corrosion sites, reflecting the lower barrier characteristic of this coating. When these E-coats were applied on chromate conversion coated substrate, however, CC/E2 performs better than CC/E1 in Prohesion salt spray test, which indicates that E2 achieved what it was designed to accomplish with the inhibiting agents. Without chromate conversion coating, the performance of E2 was found to be inferior to that of E1. These comparisons confirm the basic principle that the corrosion protection afforded by a particular scheme depends on the system as a whole. The modification of one component; e.g., primer composition, without consideration of matching with other factors, usually does not yield improved corrosion protection by the system.

To this point, the results shown have been for E-coat, which confirm that E-coat (E1) is a good primer for the creation of water-insensitive adhesion to an excellent barrier by means of an interactive coating application. Good corrosion protection by barrier/water-insensitive adhesion can be also obtained with the application of spray primers. Waterborne spray primers, including both chromated and non-chromated primers, were applied on aluminum alloys with the appropriate surface preparation and plasma deposition of an ultra-thin plasma polymer. Similar trends to the E-coated Al panels were observed on spray primer coated Al alloys. As shown in Fig. 2, after the Prohesion salt spray test, numerous pits due to pitting corrosion were observed on chromated primer coated [7B] surfaces ([7B](Dox)/T/F/A) but not on non-chromated primer coated [7B] surfaces ([7B](Dox)/Tfs/(Ar)/X).

A non-chromated, waterborne primer applied to [2B] alloy samples, with the appropriate surface preparation and plasma deposition of an ultra-thin plasma polymer, was also compare to controls, which were prepared by depositing a chromated primer on chromate conversion coated Al substrate. The same comparison was also performed for IVD Al-coated 2024-T6 substrates. In the latter case, the primer could not be removed from the IVD Al coated panels that were treated with the plasma polymer prior to spray primer application. It is interpreted that the water born spray paint penetrates into the column structure of the top surface of the IVD Al coated substrates when the surface energy was modified by the application of a plasma polymer. This effect could be viewed as interactive coating with a porous surface.

[2B](Alk)/E1   [2B](Alk)/E2
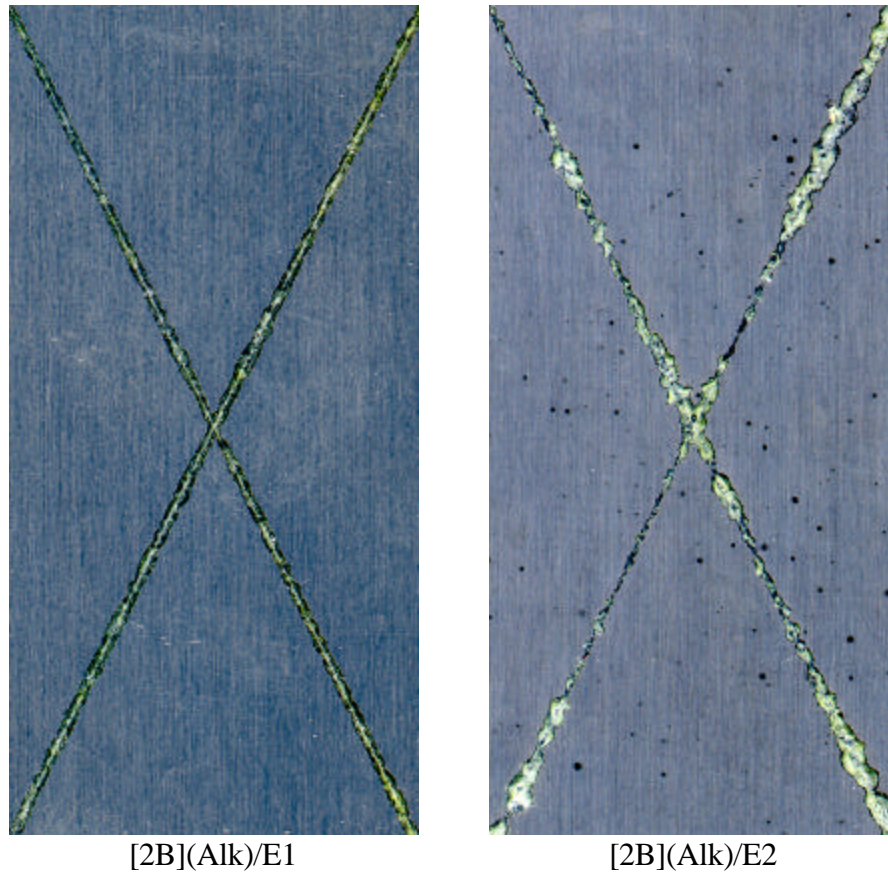
Figure 1. Comparison of the two E-coat coated aluminum panels after Prohesion salt spray tests. E-coats were removed after the test.

When a test panel is subjected to an environment that is less corrosive such as the Filiform Test, the water-sensitivity of the adhesion of a primer shows more clearly. In the Filiform Test, coated panels are exposed to HCl vapor for a fixed period of time, and then kept in a high humidity-high temperature chamber. The evaluation is made without removing the primer. The changes observable along the scribed lines are compared in this test. Fig. 3 shows the scanned surface of Filiform tested panels, which depicts the lateral advance of the de-lamination of non-chromated, water-born spray primer applied to 7075-T6 with plasma interface engineering, and also that for a chromated spray primer (organic solvent) applied on a chromate conversion coated panel.   The

plasma interface engineered samples coated with non-chromated, water-born primer show no sign of damage to the scribed lines.

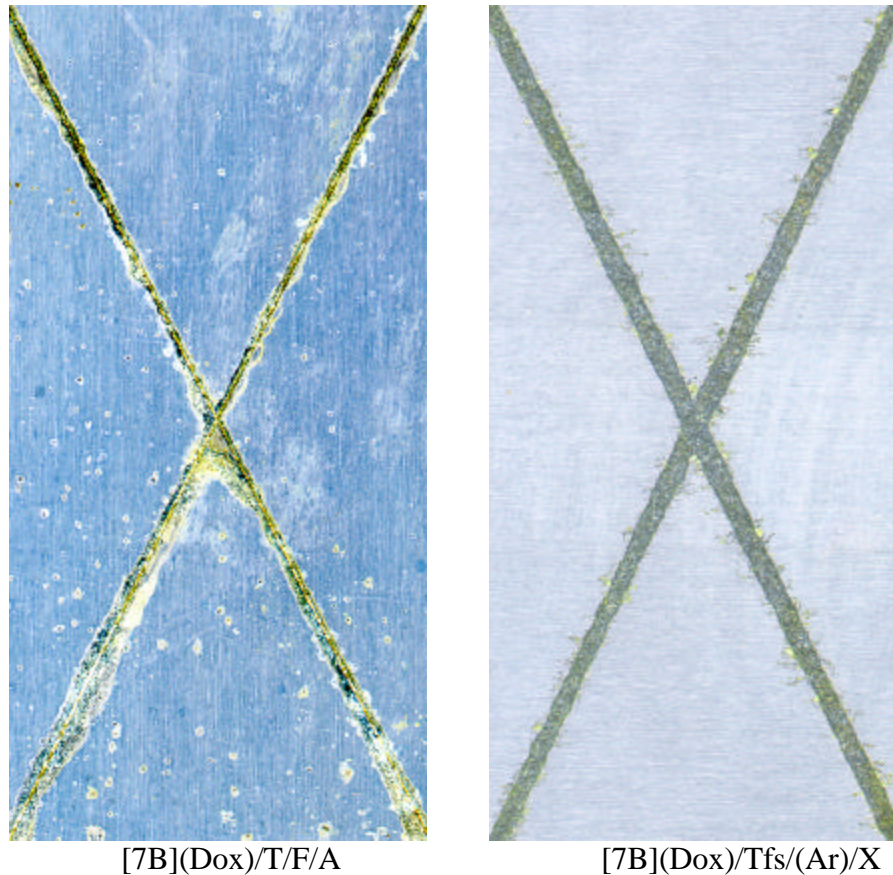|	
[7B](Dox)/T/F/A	[7B](Dox)/Tfs/(Ar)/X

Figure 2. Comparison of chromated primer coated Al panel ([7B](Dox)/T/F/A) with non-chromated primer coated Al panel ([7B](Dox)/Tfs/(Ar)/X) after Prohesion salt spray test. Primers were removed after the test.

Cathodic plasma polymerization or plasma chemical vapor deposition (PCVD) of trimethylsilane (TMS) applied to an appropriately prepared aluminum alloy surface, employed in this study, yields a roughly 50 nm thick layer of amorphous $Si_xC_yH_z$ network, which is covalently bonded to aluminum oxide at the intersurface. The XPS cross-sectional profiles given in Fig. 4 show the conspicuous shifts in O1s and Si2p at the interface that indicate the changes of chemical bonds. A primer coating applied on the surface of the nano-film is covalently bonded via the reaction of peroxides, which are formed by the reaction of oxygen with Si dangling bonds (free radicals) when the coated surface is exposed to ambient oxygen [15]. Thus the TMS nano-film works as an interlayer to form a covalently bonded network between primer and the metal surface. An unparalleled level of water-insensitive adhesion between the two interfaces, and the cohesive integrity and strength of the nano-film distinguish it from other interfacial modifications such as the use of silane coupling agents.

The water-insensitive adhesion between the water-born primers and the surface of the nano-film depends on the interfacial tension and also on the cohesive integrity of the nano-film. A general approach to this avenue is that polar groups are introduced to the surface in order to improve adhesion of water-born paints. While the polar groups increase the adhesion characteristics, they also increase the surface energy, which makes the adhesion water-sensitive and often increases the water permeability.
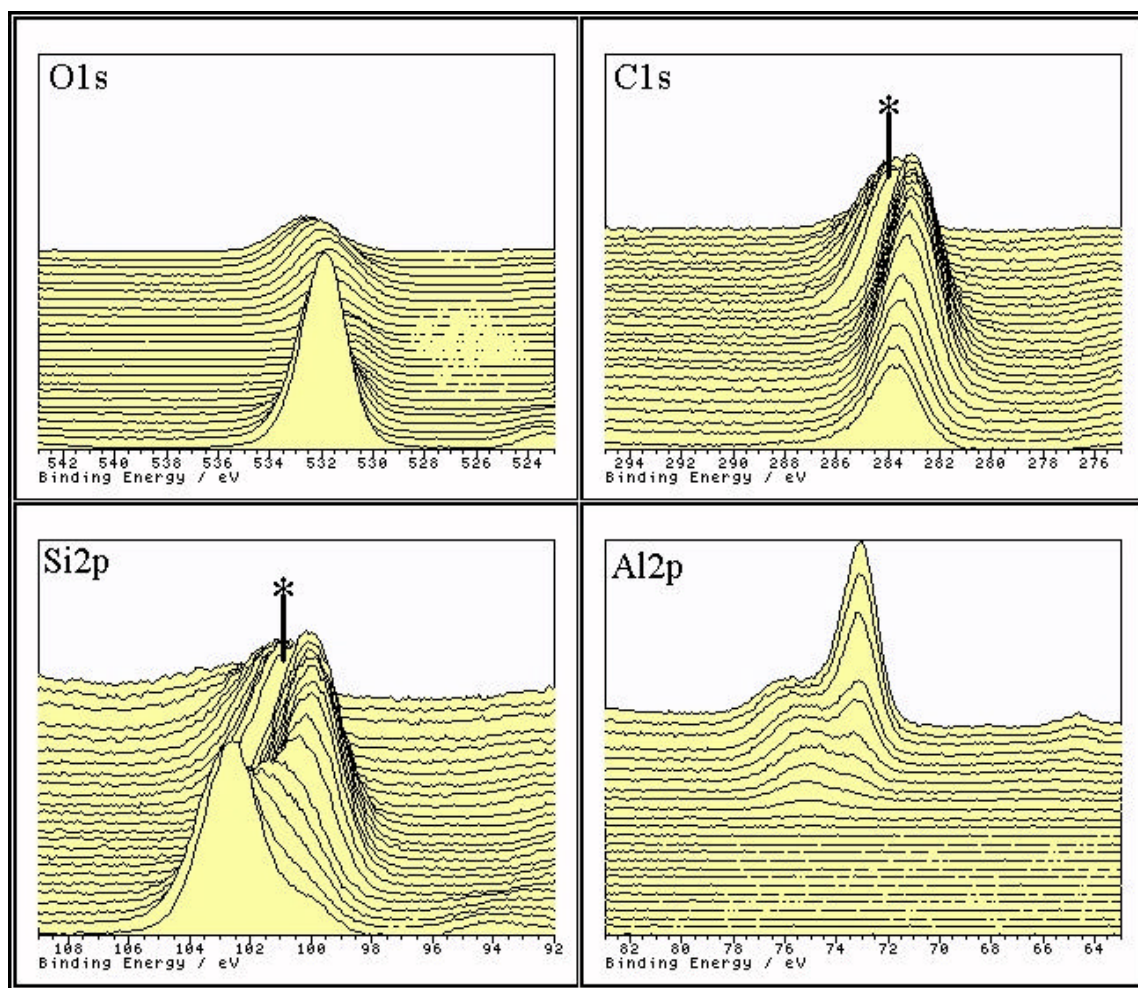
Figure 4. Combined spectra from depth profile of closed system TMS film treated with an O_2 plasma after deposition. The asterisk marked line indicates the interface region. Shifts in C1s, O1s, and Si2p observed at the interface indicate the change of chemical bonds at the interface.

The same principle applies to plasma surface modification. It is generally observed that O_2 plasma treatment of a polymer surface dramatically increases the adhesion of paint applied on the treated surface. The adhesion thus created, however, is sensitive to water, and the wet adhesion is poor [15]. This aspect can be seen in the difference of the wet adhesion and the dry adhesion depicted in Table 4. A plasma polymer of TMS deposited on an aluminum sheet in a flow system reactor is very hydrophobic and the adhesion of a water-born primer to this surface

is poor (tape test result is 0). Oxygen plasma treatment of the plasma polymer increases the dry adhesion test dramatically (tape test result increases to 5), however, it does not survive boiling water for one hour.

[7B]CC/A　　　　　　　　　　　　[7B](Dox/O)/Tcs/(Ar)/X
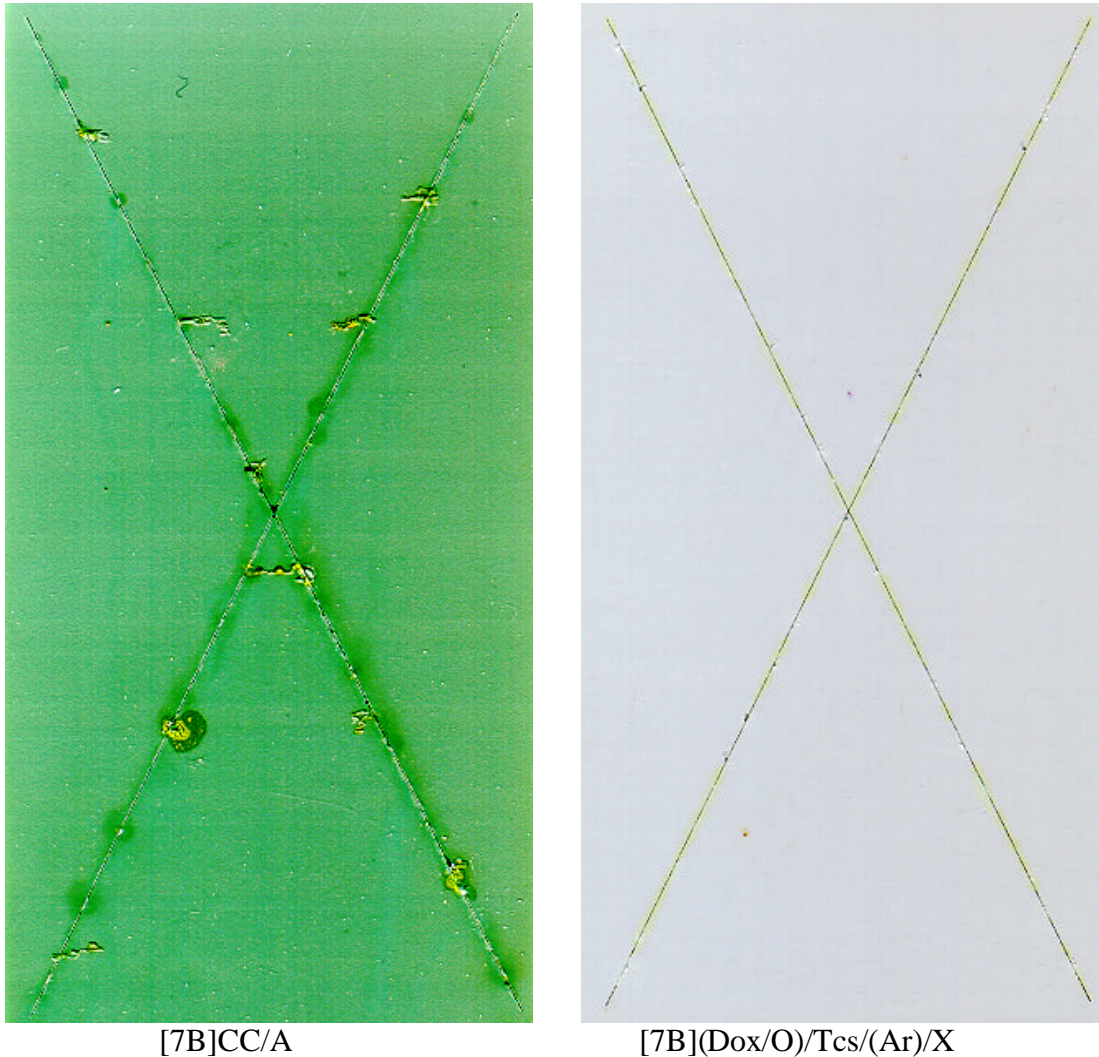
Figure 3. Scanned images of Filiform tested 7075-T6 aluminum panels. Paints were not removed.

The same plasma polymer deposited in a closed system reactor has a graded elemental composition with a carbon-rich top surface, and the oligomers content is much lower [16,17], both of which increase the level of adhesion. The adhesion of the same water-borne primer is excellent and survives 8 hour immersion in boiling water. When this surface is treated with O_2 plasma, the adhesion does not survive one hour of boiling, while the dry tape test still remains at the level of 5. The water-sensitivity of adhesion depends on the chemical nature of the top surface as depicted by XPS data shown in Figure 5. Water-insensitive tenacious adhesion, coupled with good transport barrier characteristics, provides excellent corrosion protection, as

14

supported by experimental data [1-4], and constitutes the basic principle for the "barrier-adhesion" approach.

Table 4. Surface treatment effect of TMS by succeeding plasmas on adhesion of spray paint primer (Spraylat EWDY048 (primer D)) to TMS plasma coated [7A](Ace/O) aluminum panels (scale 0-5 indicates poor (0) to excellent (5) performance).

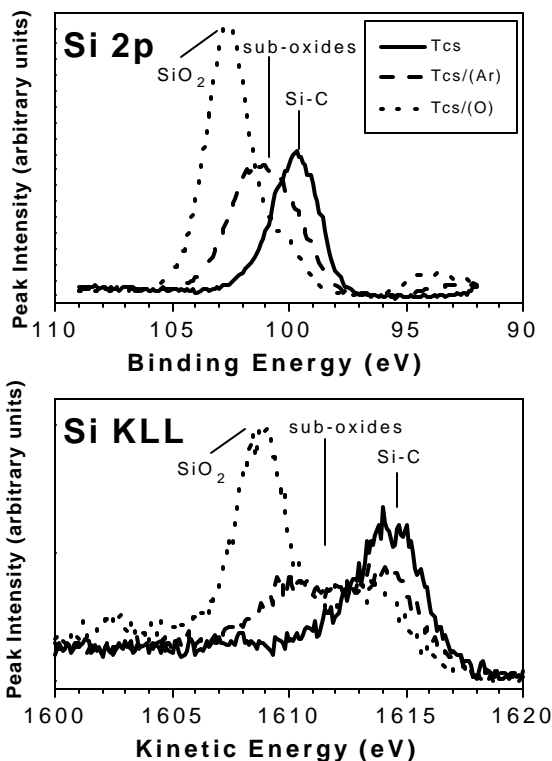| Plasma systems	Coating systems	Tape test rating	
		Dry	Water boiled for 1, 4, 8 hrs
Flow system	T_{fs}/D	0	---
	$T_{fs}/(O)/D$	5	0, ---
	$T_{fs}/(Ar)/D$	5	3, 3, 2
Closed system	T_{cs}/D	5	5, 5, 5
	$T_{cs}/(O)/D$	5	0, ---
	$T_{cs}/(Ar)/D$	5	5, 5, 5

Figure 4. Si 2p photoelectron and Si KLL x-ray induced Auger spectra from the top surface of TMS plasma coatings (produced in a close reactor system) with and without second surface treatment by O_2 or Ar plasma corresponding to the adhesion data shown in the bottom half of Table 4.

The incorporation of electrochemical corrosion inhibitors is the current mainstream approach for corrosion protection, and these methods have been advanced nearly to the limit of this type of approach, and often incorporate chemicals with undesirable environmental implications. In long-term corrosion protection, the loss of the inhibitors due to them leaching out of the system is a serious drawback. The difficulty of creating water insensitive adhesion, while still maintaining the inhibitor mobility and water molecules in the coating layer, is another limitation. The "barrier-adhesion principle" coatings are free of these problems and limitations. Furthermore, they are environmentally benign and free from the health hazards associated with conventional schemes.

Corrosion protecting coatings based on the barrier-adhesion principle has shown to provide excellent corrosion protection of aluminum alloys, which are environmentally benign and without health hazards associated with corrosion inhibitors. The coating based on this principle could prevent both damaged surface corrosion and pitting corrosion, which are difficult to simultaneously achieve with coatings based solely on the electrochemical corrosion protection such as chromate conversion coating and/or chromated primers.

References
1. C. M. Reddy, Q.S. Yu, C. E. Moffitt, D. M. Wieliczka, , R. Johnson, J. E. Deffeyes, and H. K. Yasuda, "Improved Corrosion Protection of Al Alloys by Low Temperature Plasma Interface Engineering: Part I-Alclad 2024-T3 ", *Corrosion*, 56 (2000): p. 819.
2. Q.S. Yu, C. M. Reddy, C. E. Moffitt, D. M. Wieliczka, R. Johnson, J. E. Deffeyes, and H. K. Yasuda, "Improved Corrosion Protection of Al Alloys by Low Temperature Plasma Interface Engineering: Part II-AA 2024-T3 ", *Corrosion*, 56 (2000): p. 887.
3. C. E. Moffitt, C. M. Reddy, Q.S. Yu, D. M. Wieliczka, R. Johnson, J. E. Deffeyes, and H. K. Yasuda, "Improved Corrosion Protection of Al Alloys by Low Temperature Plasma Interface Engineering: Part III-AA 7075-T6", *Corrosion*, 56 (2000): p. 1032
4. Q.S. Yu, C. M. Reddy, C. E. Moffitt, D. M. Wieliczka, R. Johnson, J. E. Deffeyes, and H. K. Yasuda, "Improved Corrosion Protection of Al Alloys by Low Temperature Plasma Interface Engineering: Part IV-Spray Paint Primer Coated Al Alloys ", *Corrosion*, submitted.
5. ASTM standards D3369-93B, Annual book of ASTM standards, Vol. 06.01.
6. W. J. van Ooij and A. Sabata, "Effects of Paint Adhesion on the Underfilm Corrosion of Painted Precoated Steels", *CORROSION/91*, Paper No. 417 (Houston, TX, NACE international, 1991).
7. T.F. Wang, T.J. Lin, D.J. Yang, J.A. Antonelli, H.K. Yasuda, *Prog. Org. Coat*., 28 (1996): p. 291-297.
8. ASTM standards G85-94-Annex A4 and A5, Annual book of ASTM standards, Vol. 03.02.
9. C. M. Reddy, H. K. Yasuda, C. E. Moffitt, D. M. Wieliczka, J. E. Deffeyes, *Plat. Surf. Fin.*, 86 (1999): p.77.
10. Filiform standards ASTM D2803-93 para. 3.1.1, Annual book of ASTM standards, Vol. 03.02.
11. Sungyung Lee, "Effects of Plasma Polymer on the Multi-Stress Aging of Organic Insulation and Proposed Degradation Mechanisms", Ph.D. Dissertation, University of Missouri-Columbia, 1995.
12. M. Chen, Q.S. Yu, C.M. Reddy, H.K. Yasuda, *Corrosion*, 56 (2000): p. 709.

13. H.K. Yasuda, C.M. Reddy, Q.S. Yu, J.E. Deffeyes, G.P. Bierwagen, and L. He, *Corrosion*, in press.

14. Q.S. Yu, Y-S. Lin, H.K. Yasuda, "Durable Bonding Characteristics of Plasma Treated Thermoplastic Olefins by Low-Temperature Cascade Arc Torches", *Prog. Org. Coat*., in press.

15. Qingsong Yu, C.E. Moffitt, D.M. Wieliczka, Hirotsugu Yasuda, "Deposition of Trimethylsilane (TMS) in Glow Discharges: Part III; DC Cathodic Polymerization In a Closed Reactor System", J. Vac. Sci., and Tech., submitted.

16. H. K. Yasuda, Q. S.Yu, C. M. Reddy, C. E. Moffitt, and D. M. Wieliczka, "Effects of Wall Contamination on Consecutive Plasma Processes", J. Vac. Sci., and Tech., in press.

3. Quantifying Corrosion Test Results

Chandra M. Reddy, H. K. Yasuda, J. Deffeyes, and D. M. Wieliczka

Abstract

The performance ranking of panels subjected to corrosion testing is difficult to perform when the panels have similar response to the corrosive environment. A method of imaging the panels, quantifying the corrosion, and normalizing the resulting values provides a process for accurately ranking the corrosion performance. This method also minimizes operator bias.

Introduction

The quantification of corrosion test results is often performed by counting visible corrosion pits, or measuring a "typical" distance the corrosion is observed away from a scribe line. Often these methods result in a lack of precision in quantifying the corrosion test results because the assessment of the corrosion is somewhat subjective. In this section we present a better way to quantify the results on standard corrosion tests such as ASTM 117B neutral salt spray, SO_2 salt spray, Prohesion testing, outdoor exposure, or any other method which involves exposure of a flat test surface to a corrosive environment. Corrosion testing on coated test panels may be performed for either quality control, coating development, or process development purposes. In many instances there is a substantial benefit from quantifying these test results.

The standard approach to recording corrosion test results is to have a researcher visually assess the extent of corrosion on test panels, sometimes attempting to assign a number rating to each panel in the test. It is difficult for that one researcher to be consistent in ranting panels from month to month, year to year. It is nearly impossible for a second researcher to score the panels the same as the first researcher. Thus personnel changes or absences can result in skewed test results, and even without these problems the subjective results are less than ideal.

Quality control records will give more statistically significant information about the process if the test results can be objectively measured and the trends quantified. Trend analysis and statistical process control methods can then be used to identify processing problems and reduce process variability. Ultimately this approach reduces cost because out-of-tolerance conditions, and associated rework, are reduced.

Process development work or coatings development work in which the corrosion resistance of an applied coating is being optimized benefits from quantifying the corrosion test results. Trends in corrosion resistance as a function of process parameters or coating deposition parameters can be more easily spotted if meaningful quantification of the corrosion test results can be accomplished. Perhaps most importantly, test panels run months or years apart can be compared in a meaningful way because the results have been objectively quantified.
The results presented in this section were obtained with relatively expensive imaging equipment and automated image-processing software. However, even the average shop will likely have

access to personal computer equipment and software that would be suitable for applying this technique. What is required is an input device, such as a flatbed scanner, and some type of image analysis software that can analyze an image and give the user quantitative counts of pixels of various colors.

Corrosion Width Measurement

The corrosion performance of panels with different low temperature plasma interface engineered surfaces of Al alloys was determined at Boeing St. Louis (Annual Progress Report #1, AF F33615-96-C-5055, July 1997,) using two types of accelerated corrosion tests. SO_2 and Prohesion salt spray tests per ASTM G85 A4 and A5 [1], respectively, were performed on panels of Al alloys 2024-T3 bare, Alclad 2024-T3 and 7075-T6 bare. The panels with the low temperature plasma interface engineered surfaces were compared to two types of control panels. The controls were: 1) chromate conversion coated preparation followed by an E-coat (CC E-coat) and chromate conversion coated followed by Deft primer (CC Deft). The controls were selected to compare the protection of the new systems with those currently in use. The panels were scribed with an X shape across the surface from corner to corner prior to placing them in the salt spray test chambers.

After completing test cycles in SO_2 or Prohesion salt spray, the panels were rinsed with distilled water and visual observations were made. The panels were then subjected to Turco stripper solution to remove the E-coat for observation of the corrosion away from the scribe. Average corrosion widths of these stripped panels were determined following the procedures described in the next paragraph.

The corrosion was quantified using image analysis software [2] and a flatbed scanner [3]. A portion of each panel with the intersection of the scribe at the center, approximately 4 cm of scribe length on each side of center, was imaged. The scanned area of the panels was fixed at ~27 cm^2 using the imaging software to fix the scanned area and the images were scanned at 450x900-pixel resolution for accurate image analysis. Two methods were used depending on the extent of corrosion, percent area by color contrast or area morphometry. The percent area by color contrast method was used for calculation of the corroded area for panels that exhibited smaller corrosion areas. The area morphometry method was used to calculate the areas of the panels with large corrosion areas to speed up the process. The corrosion width was determined by dividing the area as measured with either method by the total length of the scribe within the scanned area. The corrosion widths, as presented here, include the original scribe width.

Percent Area by Color Contrast

This data set allows for the calculation of percent area for different regions distinguished by the apparent color contrast. The images typically have corroded and non-corroded areas that could be distinguished by color contrast. The percent area of corroded and non-corroded regions are then calculated by setting the threshold for each color. By modifying the threshold intensity of the three colors, red, green, and blue, the corresponding region of the image could be isolated. Once satisfactory thresholds are achieved, percent areas is determined by computing the isolated region based on pixel values. The pixel area is converted into cm^2 through the calibration

procedure of the software.   For panels that showed little color contrast, food dye was used to enhance the contrast between corroded and non-corroded areas.

The corrosion widths of a set of panels, for a given pretreatment, were averaged to obtain the average corrosion width and standard deviation. Actual corrosion creep could be calculated by scanning the panel prior to the corrosion test. This value could then be subtracted from the corrosion width determined after the exposure.

Area Morphometry Method

This method provides for a quick calculation of corroded and non-corroded regions of the test panel and was used to calculate the respective areas of panels with larger corroded areas. Once the panel image is imported into the Optimas software window, the area morphometry tool is selected. The areas to be measured are then drawn from the area morphometry window and the area, perimeter, position etc of the highlighted region is determined.

Fig. 1 shows the typical images of three Alclad panels tested with SO_2 salt spray. The panels are a) chromate conversion coated followed by priming with e-coat; b) chromate conversion coated followed by priming with Deft; and c) plasma coated followed by priming with e-coat. The corroded area and corrosion width is given in Table 1.   Although the panel with the plasma deposited film followed by priming with e-coat is visually better, the use of the corrosion width provides a method for quantifying the improvement in the corrosion performance. Also the factor of ~2 difference in corrosion width between the two chromate conversion coated panels is difficult to obtain from the qualitative difference observed from the scanned images.   It can be seen from this comparison of three panels that the use of the measured corrosion width makes the differentiation of corrosion performance much easier.

From this simple example comparing three panels, it is obvious that the quantification of the corrosion width using the flatbed scanner and image analysis software provides a more accurate determination of the performance of the protection system. This technique has allowed for the easy ranking of 1200 panels which have been subjected to both SO_2 salt spray and prohesion testing. The use of the qualitative comparison would not have allowed for such an accurate ranking of the results.

Table 1

Corrosion area and width as determined using the Optimus image analysis software and an HP flatbed scanner.

Sample	Corrosion Area (cm^2)	Corrosion Width (mm)
Chromate Conversion coated / Ecoat primer	2.45	1.53
Chromate Conversion coated / Deft primer	5.89	3.68
Plasma Polymer coated / Ecoat primer	0.77	0.48

| A | B | C |

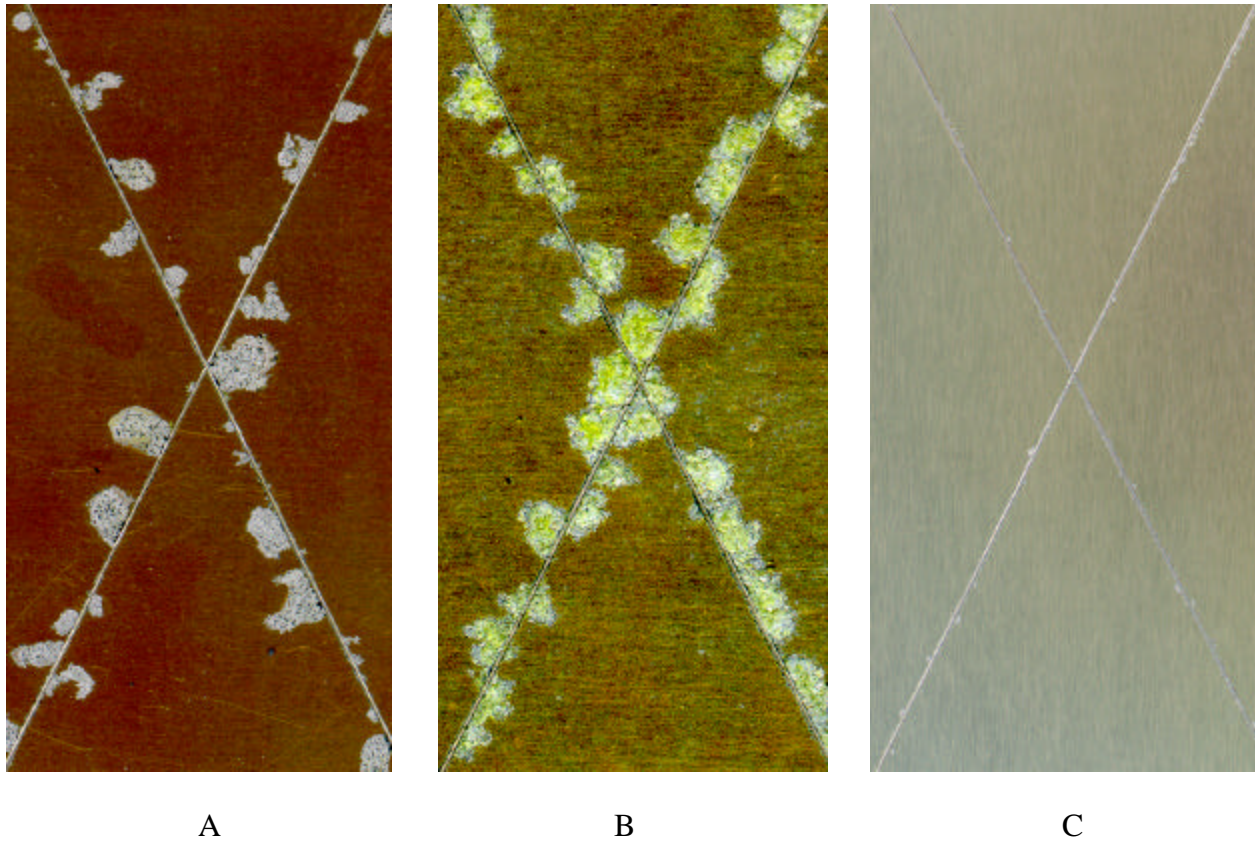Figure 1. Alclad 2024 SO$_2$ Salt Spray Tested Panels (4 Weeks). A – Chromate Conversion coat with E-coat primer. B – Chromate Conversion coat with Deft primer. C – Plasma Polymer coat with E-coat primer. Total Scanned Area is 27 cm^2.

Reference

1 (ASTM G85 -94, Standard Practice for Modified Salt Spray (Fog) Testing, Annex A4 and Annex A5)
2 OPTIMAS 6.1, Optimas™ Corporation
3 Hewlett Packard DeskScan II

4. Improved Corrosion Protection of Al Alloys by System Approach Interface Engineering: Part I - Alclad 2024-T3

C. M. Reddy, Q. S.Yu, C. E. Moffitt, D. M. Wieliczka, R. Johnson, J. E. Deffeyes, and H. K. Yasuda

Abstract

This study investigates the development of chromate-free corrosion protection systems for Alclad 2024-T3 aluminum alloy ([2A]) based on the concept of System Approach Interface Engineering (SAIE) by chemical and plasma techniques. Anode magnetron enhanced d.c. cathodic plasmas were used to treat [2A] surface and to create interface engineered systems of cathodic E-coat/plasma polymer/plasma treated [2A]. Plasma polymer coatings provided not only a corrosion resistant layer on [2A] surface but also an excellent adhesion base for subsequent cathodic E-coat. When tested by SO_2 and Prohesion salt spray tests, these plasma modified systems showed excellent corrosion protection characteristics. The corrosion test results of both SO_2 and Prohesion salt spray tests showed that most of these plasma polymer coated systems outperformed or performed comparably to the two types of controls used in this study, i.e., chromate conversion coated and then E-coated or chromated primer (Deft 44-GN-36) painted [2A] panels. The sample surface preparation effect on corrosion performance of these plasma interface engineered systems was also studied and X-ray photoelectron spectroscopy (XPS) has been used to monitor the surface composition changes on [2A] surfaces.

Introduction

The System Approach Interface Engineering (SAIE) concept adopted in this study emphasizes the fact that the corrosion protection of a metal depends on the overall corrosion protective behavior of an entire system.[1] The factors to be considered in a corrosion protection system include the bulk characteristics of the coating(s),[2-4] interfacial factors,[3] and the surface-state of the substrate [5,6] on which a protective coating system is applied. The surface state onto which a plasma polymer or a primer coating will be applied directly depends on the preceding process step, which must be tailored for a particular desired outcome.

The term "surface state" is used to describe the properties of materials in the top surface region that are significantly different from those in the bulk phase of the same material.[7-10] The concept of "surface state" is important to recognize the nature of treatment that is applied to a surface. The term "state" is used in a similar context in solid-state, liquid-state, gas-state, etc. The importance of "surface state" in this context can be visualized by the following examples. The contact electrification of surfaces occurs as a consequence of the exchange of electrons in the process of equilibrating the surface states. The surface state of water is recognized as "vicinal water". It is now generally accepted that water and aqueous solutions on close proximity to a solid surface exhibit physical properties that are uniquely different from those of the bulk. Specifically, viscosity,[11, 12] dielectric constant,[11-13] surface tension,[11, 14] hydrogen ion concentration,[14] and consequently, pH of this vicinal water (surface state of water) have been found to be significantly different from the corresponding bulk liquid properties. The surface

state of the interfacing solid dictates the properties of this vicinal water and the extent of wetting. Conversely, the surface state of a polymer is influenced by the surface state of water in contact with the polymer. It was found that the transition temperature of surface configuration change reflects nothing but the transition temperature of vicinal water recognized as the Drost-Hansen temperature [7].

The essence of interface engineering lies in the tailoring of surfaces to facilitate the equilibration of surface states of different materials. Low temperature plasma processes, such as gas plasma treatment and plasma polymerization, have unique advantages in that active or depositing species strongly interact with the surface of the substrate, and modify the surface state. An ultra-thin layer of plasma polymer, e.g., thickness less than 50 nm, can be viewed as a new surface state because such a thin layer does not develop a characteristic bulk phase. Contact electrification measurements indicate that surface electrons are still influenced by those from the substrate, up to a film thickness of roughly 20 nm. Thus, plasma polymer modification and polymerization could be considered as a means to create an entirely new grafted surface state on a substrate.

Although low temperature plasma treatment and plasma polymerization are heavily used in this study, SAIE does not necessarily require low temperature plasma processes. Some excellent corrosion protecting systems that do not include plasma processes have been found as a fringe benefit of this study, as will be seen in this series of studies of various aluminum alloys. It is important to note, however, that the deposition process in such systems (electrolytic coating) also strongly interacts with the substrate, and is not a passive coating process. These results are a consequence of (non-plasma) interface engineering.

Various chemical treatments, such as alkaline cleaning and deoxidization, were used (chemical interface engineering) to prepare the surface state on which plasma treatments and/or plasma polymerization were applied. The optimal surface treatment was found to be dependent on the type of alloy used as the substrate. A primer coating is applied on the plasma interface engineered surface to complete the corrosion protective coating system used in this study.

The interfacial system under examination is schematically depicted in Fig. 1. The top layer of an aluminum alloy is generally covered with hydrated mixed oxides. Either alkaline cleaning or a combination of alkaline cleaning and deoxidization removes major organic contaminants and this potentially unstable oxide layer. A thin layer of plasma polymer is deposited on the stabilized oxide layer thus created.

The plasma polymerization employed in this study is a one-minute deposition process, during which the temperature of the substrate alloy rises approximately 2-3 °C. Minimization of this rise in temperature was found to be an important factor in yielding a good corrosion protection system. The effectiveness of plasma polymerization depends on the preparation (interface engineering) of the surface onto which a plasma polymer deposits. In the interface engineering, gas plasma such as plasmas of oxygen, argon, etc. are also used in the pretreatment (cleaning) of the chemically prepared surface prior to the deposition of a plasma polymer. The optimum combination of these low temperature plasma processes constitutes low temperature plasma interface engineering, which compliments chemical interface engineering.

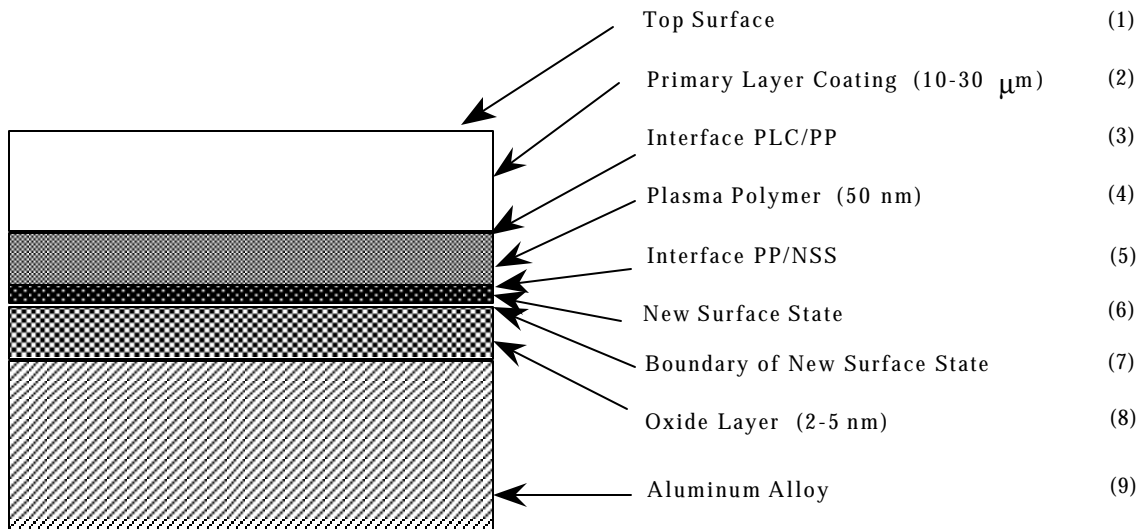| Top Surface | (1) |
Primary Layer Coating (10-30 μm)	(2)
Interface PLC/PP	(3)
Plasma Polymer (50 nm)	(4)
Interface PP/NSS	(5)
New Surface State	(6)
Boundary of New Surface State	(7)
Oxide Layer (2-5 nm)	(8)
Aluminum Alloy	(9)

Figure 1. Schematic diagram of SAIE system.

Using the aluminum sheet substrate as the cathode of a D.C. glow discharge, cathodic plasma polymerization is carried out.[5] Cathodic plasma polymerization is not commonly used, but has unique advantages for corrosion protection of aluminum alloys, which will be seen in this series of studies.

A primer is applied on the surface of the plasma polymer. The thickness of the plasma polymer layers employed in this study is roughly 50 nm on average, and that of the primer layer is about 30,000 nm. Primers used in this study included E-coat and spray primers, but no topcoat was applied.

The method described in this series of papers deals with corrosion protection of aluminum alloys without utilizing chromate conversion or inhibitors based on heavy metals. The method is not meant as a replacement of chromate conversion coating or chromated inhibitors in all applications, but provides an alternative principle and approach to corrosion protection.

Aircraft skins are readily accessible for inspection and conventional repair, but various internal structural components are neither easily accessible nor easily remedied after the onset of corrosion. Because of the tenacious adhesion of plasma coatings, plasma processes may be more useful in difficult to inspect/repair areas, i.e., internal structures of an aircraft. Thus this method is aimed at the corrosion protection of detailed parts rather than easily accessible aircraft skin. The potential long service-life protection offered by these plasma-based systems appears to fit well with the needs of particular detailed parts and internal structural components that cannot be addressed in standard maintenance cycles.

According to the SAIE concept, the mere combination of effective protection layers without tailoring interfaces does not lead to an excellent corrosion protection system. The main objective of the study is to find alternative corrosion protection methods by means of environmentally

benign processes, eliminating health concerns and environmentally hazardous materials from corrosion protection systems. The optimization of processes is done considering the whole corrosion protecting system.

The contents of this introduction are applicable to all three parts of this series of studies, but are omitted in Part II and Part III. This section is the first of three parts dealing with corrosion protection of aluminum alloys used in the production of aircraft. Part I deals with clad aluminum alloy (AA) 2024-T3.

Experimental

Materials

Alclad 2024-T3 Al alloy ([2A]) panels (3"×6"×0.032") used for the present study were procured from Q-Panel Lab Products (Cleveland, OH). The cladding has a specified composition of, in wt%, Cu 0.1, Si+Fe 0.7, Mg 0.05, Mn 0.05, Zn 0.1 Ti 0.03, others 0.3 and Al balance. Two types of controls, chromate conversion coated (Iridite 14-2) and then BASF E-coated or Deft primer (44-GN-36) coated (CC Deft) Alclad 2024-T3 panels, were used in this study. These later panels were prepared at The Boeing Company in St. Louis.

The chemicals used in chemical cleaning of aluminum alloy panels were: Turco 4215S, a commercial alkaline cleaner purchased from Turco Products, Inc., Wilmington, CA; Amchem 7, a commercial deoxidizer purchased from Anchem Products, Inc., Ambler, PA; Nitric acid (65%) purchased from Fisher Scientific.

The following chemicals were used in plasma pretreatment and plasma polymerization process. The diatomic gases, hydrogen (99%), oxygen (99.9%) and nitrogen (99.99%), were procured from Airgas. Trimethlysilane (TMS) gas of 97% minimum purity was procured from PCR, Inc. (Gainesville, FL) and Lancaster Synthesis, Inc. (Windham, NH). Methane (CH_4) was purchased from Scot Specialty Gases, Inc. (Plumsteadville, PA), and Hexafluoroethane (HFE) from Specialty Gases (Maumee, OH). All the gases and monomers were used as received without any further purification.

Surface preparation

As obtained, Alclad 2024-T3 panels had shiny surfaces with panel identification ink marks. Acetone wiping with Kimwipes® was first used to clean the ink marks and loose organic matter from the surfaces of the panels. The chemical cleaning of the aluminum alloy panels was performed by Alkaline cleaning and Deoxidization provided by The Boeing Company at St. Louis. Alkaline solution of Turco 4215S was prepared and used per McDonnell Douglas Process Specification P.S. 12030 (The Boeing Company, St. Louis). Deoxidizer solution of Amchem 7 combined with nitric acid was prepared and used per McDonnell Douglas Process Specification P.S. 12050.1 (The Boeing Company, St. Louis).

Alkaline cleaning of [2A] panels was performed by immersion in an alkaline bath at 65 ^{0}C (150 ^{0}F) for about 25 minutes, or until each panel became water break free when rinsed with DI water;

they were then thoroughly rinsed with DI water. In the case of deoxidization, the panels first went through the alkaline cleaning process and were then immersed in a deoxidization bath at room temperature for 10 minutes, rinsed with DI water, immersed in DI water for 5 minutes and finally air-dried.

Before plasma polymer deposition, plasma pretreatment by simple gas plasmas was applied to aluminum panel surfaces to remove possible contaminants and thus to promote plasma polymer adhesion. TMS was mainly used as the monomer of d.c. cathodic plasma polymerization. Plasma conditions for sample preparation and the sample identification codes are summarized in Table 1.

Table 1. Sample identification codes

Identification Code	Meaning and Conditions
[2A]	Alclad 2024-T3 aluminum alloy
(Ace)*	Acetone wiping with Kimwipes$^®$ tissue
(Alk)	Alkaline cleaning (65 ^{0}C, 25 min)
(Dox)	Deoxidization (room temperature, 10 min, always preceeded by alkaline cleaning)
(O)	O_2 plasma treatment (2 sccm O_2, 100 mTorr, 40 W, 10 min)**
(N)	N_2 plasma treatment (2 sccm N_2, 50 mTorr, 80 W, 10 min)
(AH)	Ar + H_2 plasma treatment (1 sccm Ar + 2 sccm H_2, 50 mTorr, 80 W, 10 min)
T	TMS plasma polymerization (1 sccm TMS, 50 mTorr, 5 W, 1 min)
TH	TMS + H_2 plasma polymerization (1 sccm TMS + 2 sccm H_2, 50 mTorr, 5 W, 1 min)
TO	TMS + O_2 plasma polymerization (1 sccm TMS + 1 sccm O_2, 50 mTorr, 5 W, 1 min)
TN	TMS + N_2 plasma polymerization (1 sccm TMS + 1 sccm N_2, 50 mTorr, 5 W, 1 min)
F	HFE plasma polymerization (1 sccm HFE, 50 mTorr, 5 W, 1 min)
CC	Chromate conversion coating (Iridite 14-2)
E	Cathodic E-coat (nonchromated)
A	Deft primer 44-GN-36 (chromated)
/	Process separation mark

*   Code used in parenthesis indicates the surface cleaning process, code used without
     parenthesis indicates coating process,
** Plasma duration in minute was used as noted in table unless otherwise specified with a
     superscript on the code.

Plasma reactor system and operation

The d.c. plasma reactor system used in this study was a bell jar type reactor as depicted in Fig. 2. The d.c. plasma generator was an MDX-1K Magnetron Drive power supply (Advanced Energy

Industries, Inc.). Two anodes consisting of stainless steel plates (25.4 × 25.4 × 0.16 cm) with magnetron enhancement were placed 15.5 cm apart in parallel. An iron ring (17.5 cm outside diameter, 13.8 cm inside diameter, 0.16 cm thick) and an iron center plate (5 cm in diameter, 0.16 cm thick) were attached coaxially on the backside of each anode plate as magnetic field distributor. Eight pieces of permanent magnet bars were equidistantly attached on the iron ring and iron plate with the south pole pointing to the center of the iron plate. The magnetic field strength of each magnet ranged from 700 to 800 Gauss. Two [2A] panels (forming a 6"×6" square) were placed in the middle of the two parallel anodes and used as the cathode of the plasma system.

The cleaned [2A] panels were placed inside the plasma reactor as the cathode. The reactor chamber was first pumped down to less than 1 mTorr with the vacuum system (Edward Booster with mechanical pump, capacity 240 m^3/h at 0.3 mbar). A monomer or a gas mixture depending on the type of process was then fed into the reactor chamber. An MKS mass flow meter (Model 247 C) was used for monitoring the monomer/gas flow rates and an MKS pressure controller (Model 252 A) was used to control the gas pressure in the reactor chamber. After the system pressure stablized, d.c. power was applied to create the plasma for a preset operation time. After the plasma operation, the residual gases were pumped out and the system pressure allowed to return to the background pressure. The vacuum of the reactor system was then released and the samples were then removed for further sample preparation steps.

Application of Primer

E-coat was applied as the primary layer on top of the plasma polymer coated and pretreated panels. The cathodic E-coat used was a mixture of 44 wt% resin emulsion (BASF U32CD033A), 8 wt% paste (BASF U32AD290), 48 wt% deionized (DI) water and 4 vol% additive (BASF 20CD0043).

Electrodeposition was carried out in a one gallon electrocoat bath using an Alclad 2024-T3 panel as the cathode and stainless steel strip (1.5"×10") as the anode. A Darrah Digital® DC power source with variable voltage capability was used for the electrodeposition. The d.c. power source was operated in galvano-potentiostatic mode at 250V and less than 1.0 ampere for 2 minutes. This mode keeps a constant current of 1.0 ampere in the initial stage of coating as the voltage is increased to the final voltage. The final voltage is then maintained as the current decreases. The electrocoated panels were then thoroughly rinsed with DI water to wash off any loose E-coat material. Panels were allowed to dry in air for 30 minutes and then baked in an oven for 30 minutes at 149 ^{0}C (300°F). The thickness of the cured electrocoat films after baking was about 25 μm as measured using an Elcometer® 355 with a non-ferrous probe.

XPS analysis

X-ray photoelectron spectroscopy (XPS) data was acquired with a Kratos AXIS HS instrument, using the Mg-Kα flood source operated at ~217 watts (15 mA, 14.5 kV). It is probably better to use the term electron spectroscopy for chemical analysis (ESCA) in this instance since relevant Auger electrons were collected to enhance the chemical information obtained from the samples, but the convention is more often to use the term XPS. All of the XPS data were acquired in the

hybrid mode of the instrument, which combines electrostatic and magnetic lensing. The 2 mm aperture, used in the hybrid mode, limits collection to a spot size on the order of 200-300 μm. All spectra were collected with the analyzer set at a pass energy of 80 eV, including the individual core spectra. This gives a FWHM of just over 1.4 eV for the Ag 3d line. All depth profiling was done at 90 degree take-off angle. Charge compensation was made with the manufacturer's proprietary system, at settings of: -1.5 V charge balance voltage, 1.85 A filament current, and –0.5 V bias voltage.
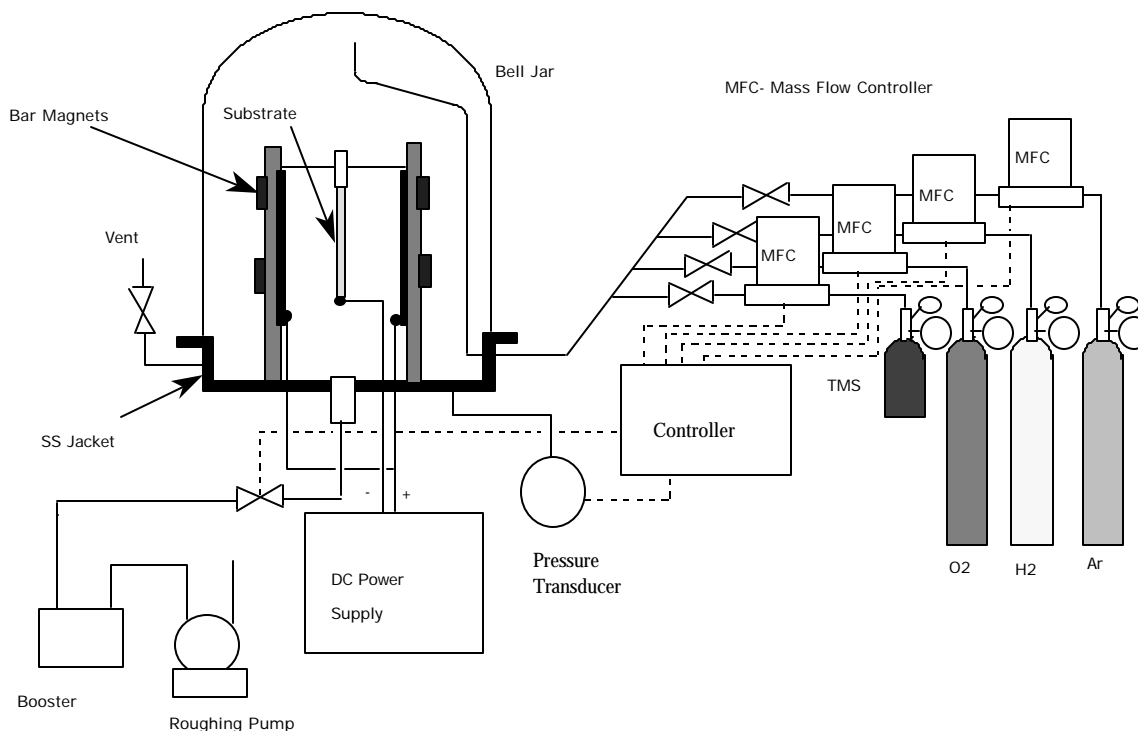

Figure 2. Schematic diagram of DC bell jar reactor system.

XPS depth profiles were done with a rastered Ar^+ beam. The beam energy was 4 kV at a filament emission of 10 mA. This gives a current of about 1μA at the sample in a spot size of ~1.1 mm, which was rastered over an area of approximately 3x3 mm^2. Data were collected from near the center of this area.

Polarization Resistance (R_p) Measurements

A linear polarization technique was used to evaluate the R_p values of [2A]. All the measurements were carried out in an aqueous salt solution (0.5% NaCl + 0.35% $(NH_4)_2SO_4$) performed with an EG&G Potentiostat/Galvanostat Model 273A that was controlled by 352 SoftCorr^{TM} III Corrosion Measurement Software. A [2A] panel was used as the working

electrode, a graphite rod (0.6 cm diameter) as counter electrode, and Ag/AgCl (0.197 V vs. NHE) as reference electrode. The exposed surface area of the panel was 3×3 cm^2 and the rest of the panel surface was covered with insulating tape. The experiments were conducted after immersion for about 50 minutes when the open circuit potential became stable. During the Linear Polarization measurement, a controlled-potential scan over a small range (±17 mV with scan rate 2 mV/min) with respect to the corrosion potential (Ecorr) was applied to the electrochemical electrodes.

Corrosion tests and evaluation

Panels with various low temperature plasma modified interfaces were evaluated for corrosion performance at Boeing, St. Louis. Two types of accelerated corrosion tests, i.e. SO$_2$ salt spray and Prohesion cyclic salt spray, were used in this study. SO$_2$ (4 weeks) salt spray test was performed per ASTM G85-94, annex A4.[15] Prohesion (12 weeks) cyclic salt spray tests was performed per ASTM G85-94, annex A5.[15] The tests were performed on all the samples along with two types of control panels.

After completing corrosion testing exposure, the panels were rinsed with distilled water and visual observations were made. The panels were then subjected to Turco-5469 paint stripper solution (Turco Products, Inc., Cornwells Heights, PA) to strip off the E-coat (all samples and the first control) or Deft primer (second control) from the scribed surface, so that the effect of corrosion beneath the coatings and away from the scribes could be viewed. These stripped panels were used to estimate the average corrosion creep widths, in order to compare the corrosion performance of the different sample systems.

The average corrosion widths of the Prohesion and SO$_2$ salt spray tested panels were estimated using OPTIMAS 6.1 software.[16] For each panel, about 4 cm of scribe length on either side of the center of the X shaped scribe were scanned using an HP DeskScan II. The scanned area was fixed at approximately 27 cm^2, and the scanned images were utilized for corrosion area measurements. For the most accurate estimation obtainable by OPTIMAS 6.1, the percent area method was used to calculate the corroded area of panels with small corrosion widths. To calculate the corroded areas of panels with large corrosion widths, the less time consuming morphometry method was used. The corrosion widths of each set of panels were averaged to determine average corrosion width and standard deviation.

Results and Discussion

The corrosion resistance of aluminum and Al alloys is largely due to the protective oxide film which can attain a thickness of about 10 Å within seconds on a freshly exposed aluminum surface.[17] A good corrosion protection system should include protection of the oxide layer, and, in addition, should provide a good adhesive base for subsequent paint. The conventional corrosion protection system of aluminum alloys consists of the application of a chromate conversion coating following alkaline cleaning and deoxidization of the surface. The purpose of pretreatments is to remove the contaminants and any defective oxide left after part forming, and thus create a clean surface on which chromium oxide can be grown, which then acts as the

corrosion protective layer and also the adhesive base. The effect of these chemical pretreatments on [2A] surface composition is determined by the XPS analysis.

Effect of Initial Cleaning Processes: XPS Study

XPS studies of [2A] samples after different initial cleaning processes have shown some interesting results. Alkaline cleaning is observed to leave a Cu-enriched surface, and alkaline cleaning followed by deoxidization greatly increases the level of enrichment. The extent of this copper enrichment can be seen in the spectra displayed in Fig. 3. A summary of these is shown in copper and oxygen depth-profile summary graphs (Fig. 4). Although the sputter step resolution is somewhat low, it is apparent on observation that the enriched copper layer lies beneath the oxide. The maximum copper signal is at the second data point for both the alkaline cleaned and the deoxidized samples. By this time the oxygen signal had dropped by more than half on the alkaline cleaned sample, and was less than 10% of the initial value on the deoxidized sample. This elevated copper level persists after the oxygen signal has dropped further in both samples shown.

The reason copper is seen in the spectra from the non-sputtered surface is due to the finite sampling depth of XPS. Distinct metallic aluminum signals were also observed in the Al 2p and Al KLL Auger spectra from the thinner oxides on the treated samples. The origin of the copper must be from dissolution of the alloy matrix, but whether just from the cladding or added to by dissolution of the core is not clear. Cu is thought to plate out of solution at cathodic sites on alloy surfaces.[18] Although the cladding material (AA1050 for these samples or those that are comparable to the specified AA1230 cladding) has a listed maximum Cu concentration of only 0.1wt%, this appears to be large enough to leave enrichments.[19] Precipitates may be exposed in the oxide etching processes, and any Cu freed in the etching of the solid solution portion of the alloy matrix may contribute to the enrichment. Upon removal from solution, the expansive aluminum oxide grows, covering the alloy. This may only partially or thinly cover the enriched deposits, weakening the oxide coating when compared to that formed on pure aluminum surfaces.

It is possible that the edges of the Alclad samples, where the core alloy is exposed to the solution, may contribute additional copper to the process. These measurements were repeated on samples treated in fresh solutions, void of any Cu contamination from any previous treatments, with the same result. Attempts at masking the edges to keep the core material from being exposed continued to show similar levels of enrichment. Since there was no way to verify that the mask had not been breached, this was considered inconclusive. Samples prepared for XPS analysis were cut from full panels prior to chemical cleaning and some large variations in enrichment were observed with different sized samples. A sample cut from full sized alclad panels that were chemically cleaned prior to cutting was cut and analyzed which showed little to no enrichment, for the detection limits of the technique. Differences in baths used and the ages of the solutions might contribute to these observed differences.

The second potential source of the copper is the preferential dissolution of aluminum as compared to Cu intermetallic phases in the matrix. This is considered the source of enrichments beneath anodic oxides on alloys,[20-24] and the case in enrichments beneath the oxide formed after

caustic dissolution of relatively pure aluminum,[19] as well as the source of enrichments beneath oxides formed after the etching of high copper alloys.[25]
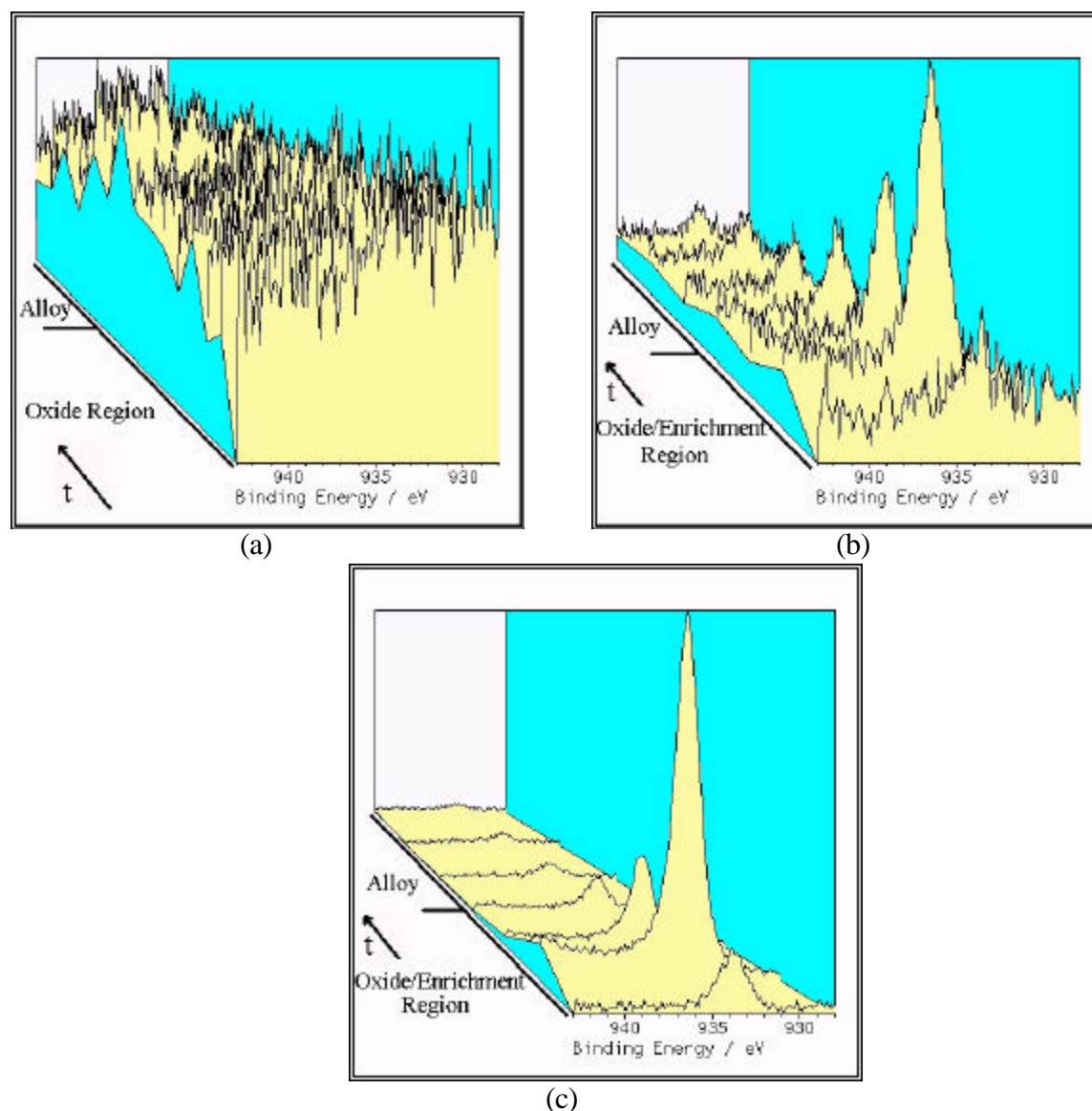

(a)

(b)

(c)

Figure 3. Cu 2p 3/2 photoelectron spectra from XPS depth profile runs on [2A] surfaces, a) native surface, b) alkaline cleaned surfaces, and c) alkaline cleaned and deoxidized surface. The arrow shows the direction of sputtering time into the alloy. The levels of the peak intensity changes are seen in Figure 4.

The summary depth-profiles were compiled from total photoelectron peak areas, independent of changes in chemical state. The copper 2p spectra from these samples show very little binding energy variation from bulk AA2024 copper 2p spectra or similar enrichments observed on AA2024 (part II of this series). The copper 2p 3/2 binding energy of the deposits and the bulk AA2024 is quite similar to that of $CuAl_2$, having a value of 933.8eV in the highest enrichment

and shifting to slightly lower binding energy as the level decreases. Although CuO has a similar binding energy, the absence of the satellite structure associated with CuO seems to indicate that this is not a copper oxide.[26] As pointed out earlier, Fig. 4 shows that the maximum Cu content on the chemically-cleaned samples occurs after the oxide is removed, as is particularly noticeable in the profile from the deoxidized sample. This fact, accompanied by the lack of the oxide satellite, seems to indicate that the Cu enrichment is associated with a Cu-Al intermetallic state on the surface of the bulk alloy, beneath the oxide. It should also be noted that no black deposits associated with smutting were observed, and that the deposits focused on here are on the order of a few nanometers in thickness at most.
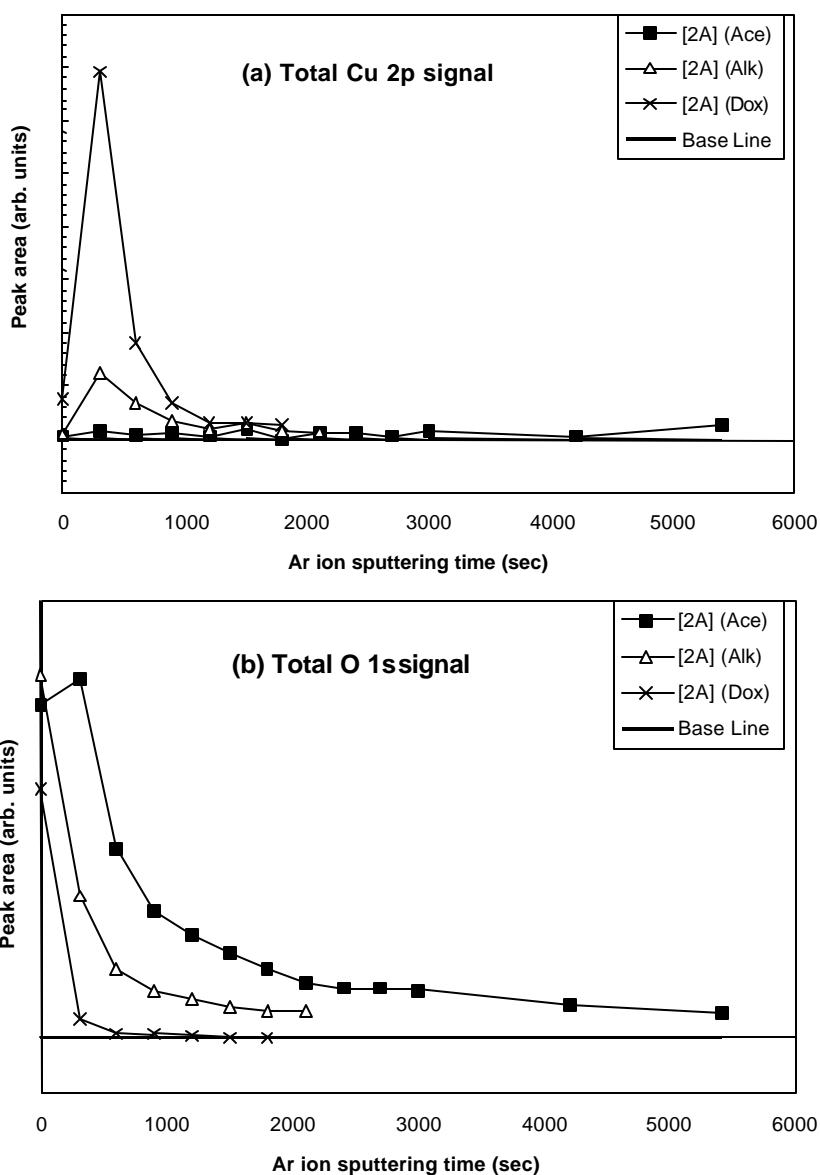

Figure 4. XPS depth-profile summary graphs of (a) Cu 2p and (b) O 1s peak area as a function of sputtering time.

Effect of Initial Cleaning Processes and Plasma Polymer Deposition: Polarization Resistance
Measurements

Polarization resistance (R_p) was used to evaluate the effect of chemical cleaning and plasma
polymer coating on corrosion resistance of [2A]. Fig. 5 shows the R_p values of [2A] with three
different chemical pretreatments and with a TMS plasma polymer on each of the three pretreated
surfaces, as well as on the control [2A]CC surfaces. It can be seen that the R_p value of [2A] were
decreased to some extent by pretreatment of alkaline cleaning, and were drastically reduced by
alkaline cleaning plus deoxidization. As observed in the XPS results shown in Fig. 4, the
accumulation of Cu elements and removal of oxide layer on [2A] surfaces were presumed
responsible for the reduction in corrosion resistance of these chemically pretreated [2A] panels.

In contrast, a significant increase of the R_p values was observed in Fig. 5 with the application of
a thin layer of TMS plasma polymers (~ 50 nm) on these chemically treated [2A] surfaces. It
was also noted that these TMS plasma polymer coated [2A] samples have the same level of R_p
values as the [2A]CC controls. These results clearly indicate that these plasma polymer coatings
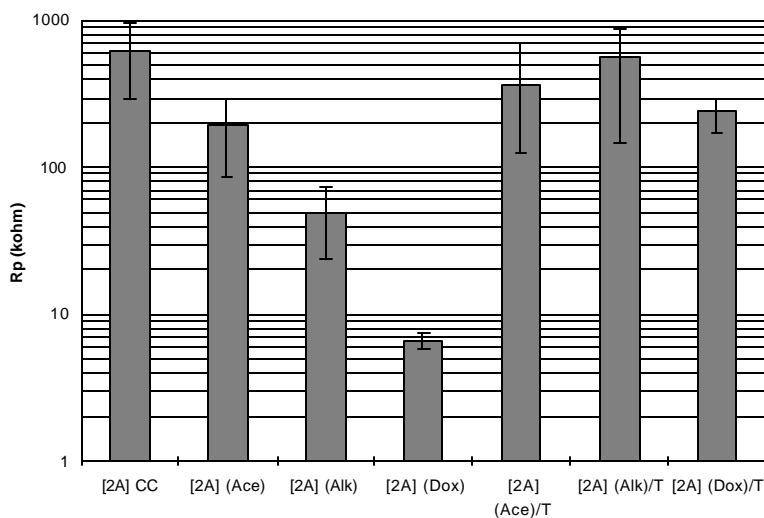have a good corrosion resistance property.

Figure 5. Polarization resistance of [2A] panels with different chemical pretreatments and TMS
plasma polymer coated surfaces.

From Fig. 5, it was also noticed that a simple solvent acetone cleaning of [2A] surfaces gave
higher R_p values as compared to alkaline cleaning and deoxidization processes. As confirmed by
XPS data in Fig. 4, it is clearly evident that the [2A] surface, which has a stable aluminum oxide
layer with a minimum of alloying elements beneath the oxide layer or penetrating through it,
should not be damaged. The acetone cleaning, which removed only surface contamination but
did not induce any surface composition change, seems to be a suitable surface pretreatment
method of [2A]. With the aid of low-temperature plasma interface engineering, therefore, an

excellent corrosion protection performance was anticipated for these acetone cleaned [2A] samples. A short plasma sputter cleaning was employed on the acetone-wiped surface to remove tougher organic contaminants and to promote plasma polymer adhesion.

Corrosion Protection Properties: Evaluated by SO_2 and Prohesion Salt Spry Tests

Two types of corrosion evaluation tests, SO_2 and Prohesion salt spray tests were employed for the evaluation of corrosion protection characteristics of painted plasma systems. The SO_2 salt spray test was chosen to speed up differentiation of the corrosion protection properties of the different systems investigated. The Prohesion cyclic salt spray test, which is chemically milder than the SO_2 salt spray test, was conducted for a longer period, 2000 hours. It is considered a more realistic test, as it better simulates actual service conditions of an aircraft in which both wet and dry periods occur.

Fig. 6 shows typical scanned images of SO_2 salt spray tested panels, two controls and two plasma polymer treated panels. By visual observation, one can easily see that the corrosion performance of the plasma polymer treated panels, [2A](Ace/O/N)/TN/E and [2A](Dox/AH)/TH/E, is far better than that of the control panels, [2A]CC/E and [2A]CC/A. Fig. 7 shows typical scanned images of the surfaces of controls and plasma interface engineered systems of [2A](Ace/O)/TH/E and [2A](Ace/O)/TN)/E after Prohesion salt spray corrosion testing and subsequent e-coat stripping. Both plasma-treated panels show excellent corrosion protection performance as compared to the control panels. All [2A] panels with different plasma treatments and plasma polymer coatings, which were corrosion tested in both SO_2 and Prohesion salt spray tests, were similarly scanned and the corrosion width was evaluated as described in the experimental procedures.

Fig. 8 shows the comparison of average corrosion widths of Prohesion and SO_2 salt spray tested panels of different plasma-modified samples and the controls. For each system tested, the corrosion widths obtained after Prohesion salt spray testing are plotted below those obtained after SO_2 salt spray testing. This figure shows that all SAIE series-I (plasma system with acetone wiping) and series-II (plasma systems with Deoxidization pretreatment) plasmas on [2A] out-performed both controls in SO_2 salt spray testing. In Prohesion salt spray testing, all E-coated SAIE series-I and series-II plasma treatments out-performed [2A]CC/E controls; however, some did not perform as well as [2A]CC/A controls.

It can be seen from Fig. 8, that the Prohesion salt spray results show larger corrosion widths from systems with series-II plasmas, which were prepared on the deoxidized surfaces. As discussed before, the deoxidation pretreatment thinned the surface oxide and also caused copper enrichment on sample surfaces. This directly correlates to the increased corrosion widths in Prohesion testing. When exposed to solutions of electrolytes, copper rich deposits such as second phase precipitates and $CuAl_2$ from overaging act as cathodic sites in the formation of local galvanic/corrosion cells. The less noble aluminum matrix is then preferentially attacked and corrosion is enhanced. Similar behavior with the enriched copper layer is thought to contribute to the lowered Prohesion performance of the series II samples.

To take advantage of the protective nature of the surface oxide formed during and after the rolling process, it appears best not to perform these chemical modifications to this oxide when applying low temperature plasma interface engineering to aluminum alloys. In order to achieve better adhesion of E-coat to the surfaces, plasma treatment with O_2 for a short time (e.g., 2 minutes), to clean the organic residue and promote adhesion to the following plasma polymer deposition, seems to be a sufficient modification to the as-rolled surface.

[2A] CC/E

[2A] CC/A

[2A] (Ace/O/N)/TN/E

[2A] (Dox/AH)/TH/E

Figure 6. Scanned images of SO_2 salt spray tested (4 Weeks) [2A] panels. Total scanned area is 27 cm^2 and total scribe length within the scanned area is 16 cm.
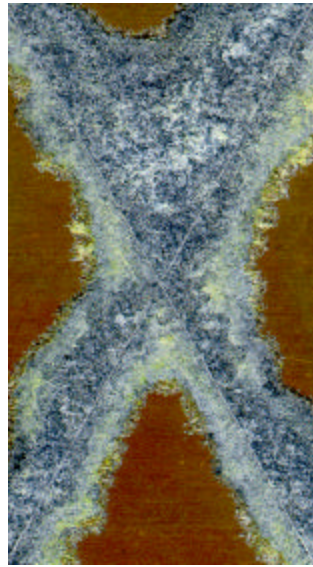
[2A] CC/E   [2A] CC/A

[2A] (Ace/O)/TH/E   [2A] (Ace/O)/TN/E

Figure 7. Scanned images of Prohesion salt spray tested (12 Weeks) [2A] panels. Total scanned area is 27 cm^2 and total scribe length within the scanned area is 16 cm. The white spots on [2A] (Ace/O)/TN/E are paint which could not be stripped with Turco paint stripper.

Examination of the corrosion of damaged surfaces using optical microscopic images

Observation of damaged (scribed) surface corrosion indicates that the corrosion takes place as a result of the delamination of paint and that it creeps underneath poorly adhered organic paint films. Whenever the adhesion is strong, the corrosion does not creep underneath the paint films. To examine this phenomenon, optical microscopic imaging of several corrosion-tested panels was carried out.
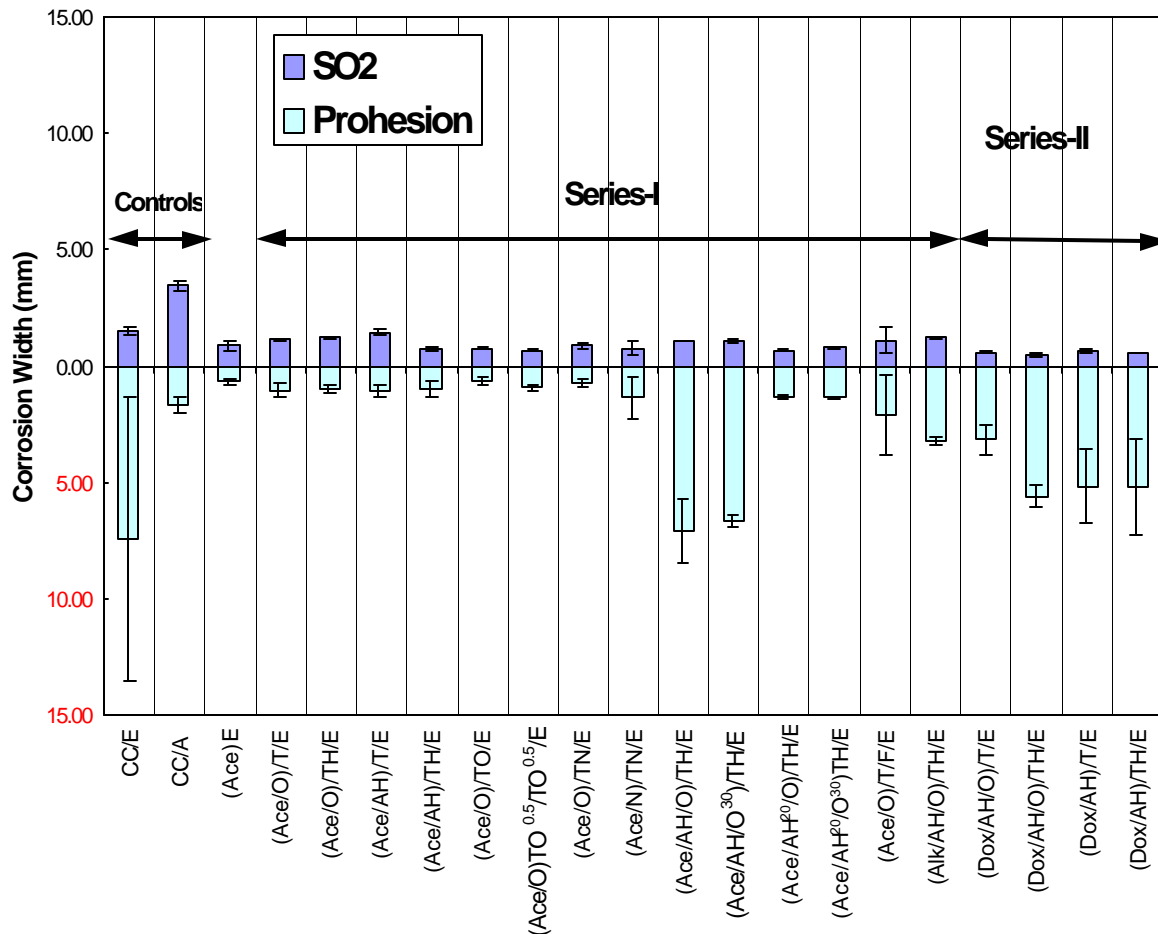

Figure 8. Average corrosion widths of Prohesion (12 weeks) and SO_2 salt spray (4 weeks) tested surfaces of control, acetone-cleaned and plasma-modified [2A] panels. All samples were E-coated except the CC/A control. Series-I indicates plasma systems with acetone wiping and series-II indicates plasma systems with Deoxidization pretreatment of [2A] surfaces.
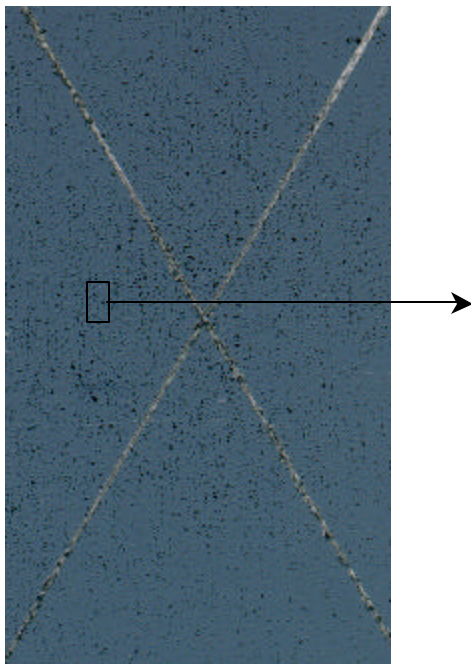
Optical microscopic pictures of Prohesion and SO_2 salt spray tested panels of Alclad 2024-T3 were taken to examine the profiles of corrosion on the scribed surfaces. The optical microscope is equipped with a camera, which was used to take the pictures of the scribes at the intersection of the X shape for all the corrosion-tested surfaces at 50X magnification. About 2 mm $\times$ 3 mm area of the panels was used in taking the pictures. Pictures of all plasma treated, E-coated substrate surfaces were compared with those of the controls, [2A]CC/E and [2A]CC/A.
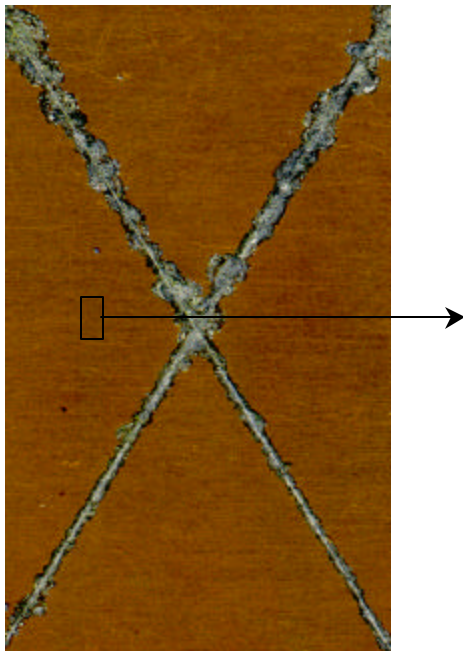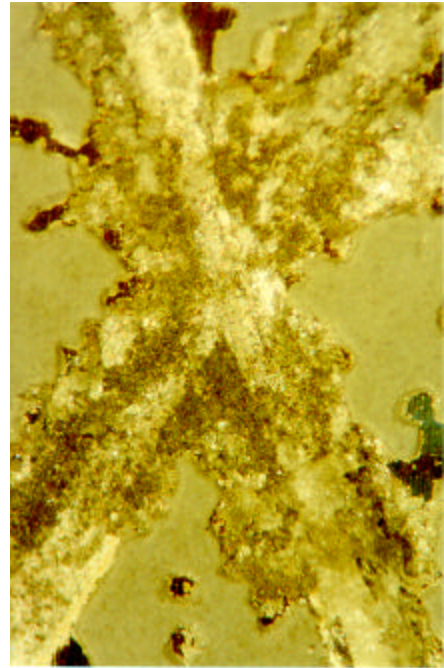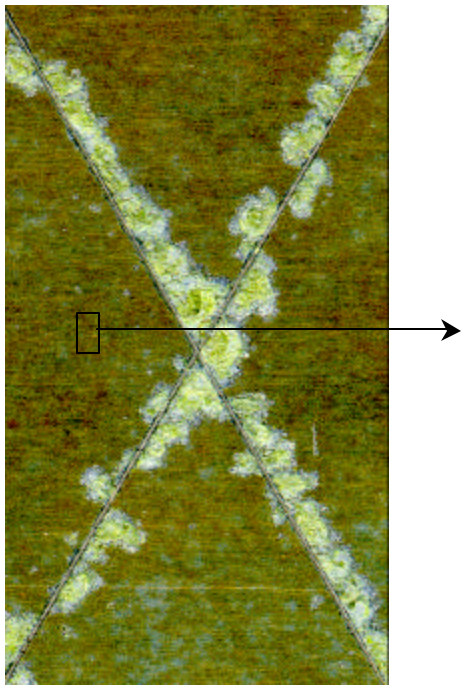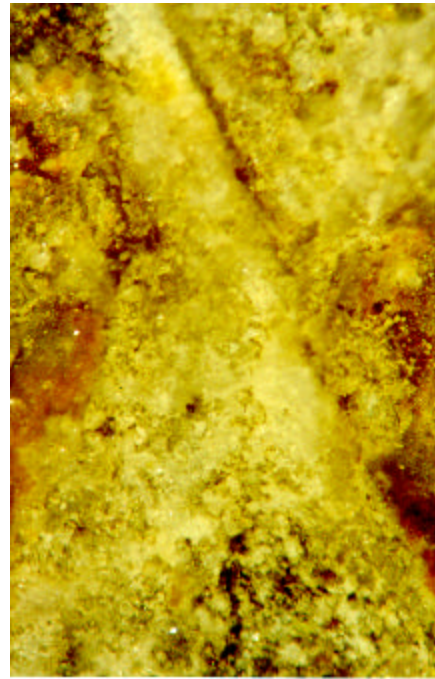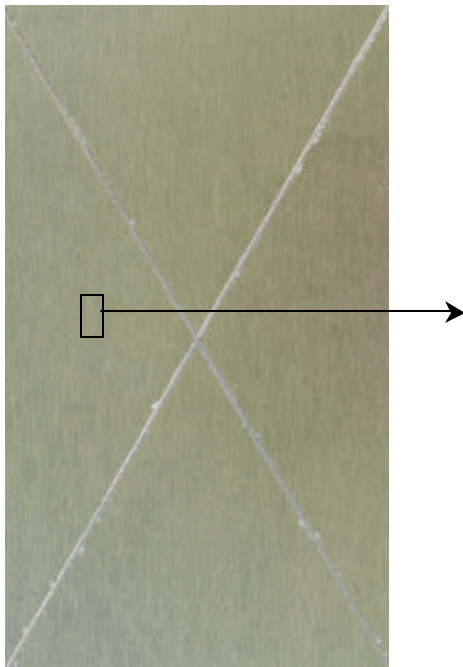
[2A] CC/A

[2A] CC/A

[2A] (Ace/O)/T/F/E

[2A] (Ace/O)/T/F/E

Figure 9. Scanned pictures (left column, actual sample size is 27 cm^2) and optical microscope pictures (right column, actual sample size is 2 mm $\times$ 3 mm) of Prohesion salt spray tested (12 weeks) [2A] panels. [2A] (Ace/O)/T/F/E shows the E-coat still adhering after attempted removal with Turco paint stripper.
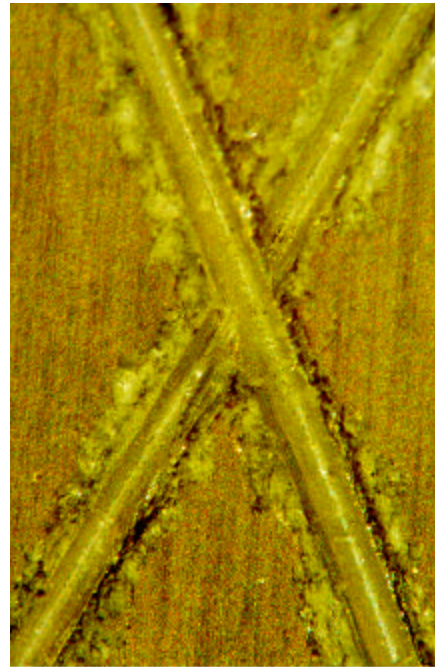
[2A] CC/A

[2A] CC/A

[2A] (Ace/O)/TH/E

[2A] (Ace/O)/TH/E

Figure 10. Scanned pictures (left column, actual sample size is 27 cm^2) and optical microscope pictures (right column, actual sample size is 2 mm $\times$ 3 mm) of SO$_2$ salt spray tested (4 weeks) [2A] panels.

Optical microscopic pictures provided details on how corrosion takes place in and around the scribed surface during Prohesion and SO_2 salt spray tests. The typical optical microscopic pictures are shown in Figs. 9 and 10. From these figures, it can be seen that there are many corrosion products on the surface. Even though corrosion products are apparent on the scribes, the pictures show that the corrosion creeps into the interface more than into the scribe itself. To demonstrate the corrosion width difference between the controls and the plasma-treated surfaces, the scanned surfaces of these panels are also shown in Figs. 9 and 10. As seen from the corrosion widths (Fig. 8), both control panels showed larger corrosion widths than many of the plasma systems, also indicating that plasma interface engineered systems provide stronger adhesion to paint films and thus better corrosion protection performance than chromate conversion coatings. This phenomenon is also evident from the optical microscope pictures, which show corrosion moving more into the paint metal interface on the control panel surfaces.

Conclusion

The significance of the SAIE approach is clearly evident in the test results presented. Chromate conversion coating, which was prepared with alkaline cleaning and deoxidization, showed the highest Rp value, and the E-coat used in this study was shown to be an excellent barrier. However, when these two layers are combined, it resulted in the worst corrosion test result in Prohesion salt spray tests. This is a good example attesting to the statement made in the introduction that a mere combination of excellent layers does not yield excellent corrosion protection. The surface state of aluminum on as-rolled Alclad 2024-T3 consists of stable aluminum oxide that can be considered a very good corrosion resistant layer. Any chemical or severe plasma treatment disturbs this stable oxide layer and yields inferior corrosion resistance when E-coat is applied.

Another important fact revealed by this study is that chromate conversion coating applied onto Alclad, according to the conventional procedure, is not a good combination in the context of SAIE. A chromated spray primer on CC coating was found not to be as effective either, and the combination gave the worst result in SO_2 salt spray test. This might imply that the presence of corrosion inhibitors is not essential in corrosion protection of Alclad.

It is also important to point out that E-coat applied onto acetone cleaned Alclad yielded excellent corrosion performances, better than chromate conversion coated controls. This indicates that the tenacious adhesion of E-coat to the stable oxide is sufficient to provide excellent corrosion protection. The application of chromate conversion coating evidently ruins the situation, because the adhesion of E-coat to CC coating is not as strong. Optical microscopic investigation on the corrosion tested [2A] surfaces clearly indicates that corrosion on the damaged surfaces proceeds mainly via paint delamination. Plasma polymers provide tenacious water-insensitive adhesion and consequently prevent corrosion from creeping into the paint-metal interface, whereas the chromate conversion coated control surfaces show corrosion that has spread out from the scribes.

Reference

1. H. Yasuda, Q. Yu, M. Chen and C. M. Reddy. Effect of Interfacial Factors on Corrosion Protection, Presented at Workshop on Advanced Metal Finishing Techniques for Aerospace Applications (Keystone Resort, Keystone, Colorado, August 23-28, 1998).
2. Sungyung Lee, Effects of Plasma Polymer on the Multi-Stress Aging of Organic Insulation and Proposed Degradation Mechanisms (Ph.D. Dissertation, University of Missouri-Columbia, 1995).
3. G.W. Walter, Corrosion Science, **26** (1986): p. 27.
4. H. Leidheiser, Jr., Corrosion, **38** (1982): p. 376.
5. T.F. Wang, T.J. Lin, D.J. Yang, J.A. Antonelli, H.K. Yasuda, Prog. Org. Coat., **28** (1996): p. 291.
6. H.K. Yasuda, T.F. Wang, D.L. Cho, T.J. Lin, J.A. Antonelli, Prog. Org. Coat., **30** (1996): p. 31.
7. H. Yasuda, E.J. Charlson, E.M. Charlson, T. Yasuda, M. Miyama, and T. Okuno, Langmuir, **7** (1991): p. 2394.
8. T. Yasuda, T. Okuno, M. Miyama, and H. Yasuda, Langmuir, **8** (1992): p. 1425.
9. E.M. Charlson, E.J. Charlson, S. Burkett, and H. Yasuda, IEEE Trans. on Electrical Insulation, **27** (1992): p. 1136.
10. H. Yasuda, Mackromol. Chem.: Macromol. Symp. **70/71** (1993): p.29.
11. W. Drost-Hansen, Ind. Eng. Chem. **61** (1969): p. 10.
12. J.T. Davies and E.K. Rideal, Interfacial Phenomena, 2nd Ed. (Academic Press, London, 1963): p. 369
13. C.F. Hazelwood, Cell-Associated Water (Academic Press, New York, 1979): p. 165.
14. R.A. Peters, "interfacial Tension and Hydrogen-Ion Concentration", Proc. Royal Soc. London, series A1, 33 (1931): p.140.
15. ASTM G85-94, Standard Practice for Modified Salt Spray (Fog) Testing, Annex A4 and Annex A5.
16. C.M. Reddy, H.K. Yasuda, C.E. Moffitt, D.M. Wieliczka and J. Deffeyes, Plating and Surface Finishing, **86** (1999): p. 77.
17. L. L. Shreir, R. A. Jarman, and G. T. Burstein (eds.). Corrosion, 3rd ed, Vol. 2, Chap. 10 (Buttersworth-Heinemann, Jordan Hill, 1994).
18. K. Kowal, J. DeLuccia, J. Y. Josefowicz, C.Laird, and G.C. Farrington. J. Electrochem. Soc. **143** (1996): p. 2471-2481.
19. X. Wu and K. Hebert, J. Electrochem. Soc., **143** (1996): p. 83-91.
20. H. Habazaki, K. Shimizu, P. Skeldon, G. E. Thompson, G. C. Wood and X. Zhou, Trans IMF, **75** (1997): p.18-23.
21. X. Zhou, G. E. Thompson, H. Habazaki, K. Shimizu, P. Skeldon, and G. C. Wood, Thin Solid Films, **293** (1997): p. 327-332.
22. K. Shimizu, K. Kobayashi, G. E. Thompson, P. Skeldon, and G. C. Wood, Corrosion Sci., **39** (1997): p. 281-284.
23. H. Habazaki, M. A. Paez, K. Shimizu, P. Skeldon, G. E. Thompson, G. C. Wood and X. Zhou, Corrosion Sci., **38** (1996): p. 1033-1042.
24. M. A. Paez, T. M. Foong, C. T. Ni, G. E. Thompson, K. Shimizu, H. Habazaki, P. Skeldon, and G. C. Wood, Corrosion Sci., **38** (1996): p. 59-72.
25. T. S. Sun, J. M. Chen, J. D. Venables, and R. Hopping, Appl. Surf. Sci., **1** (1978): p. 202-214.
26. S. Hüfner, in Photoemission in Solids II: Case Studies, L. Ley and M. Cardona eds. (Spriger-Verlag, Berlin, 1979): p. 173-216.

5. Improved Corrosion Protection of Al Alloys by System Approach Interface Engineering: Part II - AA 2024-T3

Q. S. Yu, C. M. Reddy, C. E. Moffitt, D. M. Wieliczka, R. Johnson, J. E. Deffeyes, and H. K. Yasuda

Abstract

This study investigates the development of a chromate-free corrosion protection systems for AA 2024-T3 [2B] based on the concept of System Approach Interface Engineering (SAIE) by chemical and plasma techniques. An anode magnetron enhanced D.C. cathodic plasma process was used to enhance the bonding to and the protection offered by a cathodically electrodeposited, epoxy-based primer (E-coat) on [2B]. Corrosion test results of both SO_2 and prohesion salt spray tests indicated that superior corrosion protection properties of [2B] were achieved with the aid of plasma interface engineering, tailoring specific properties of the interfaces. Many of these plasma polymer enhanced systems on [2B] outperformed the controls used in this study: chromate conversion coated and then Deft primer (Deft 44-GN-36) coated [2B], as well as chromate conversion coated and then cathodic E-coated [2B]. The corrosion protection properties of [2B] were found to be strongly dependent on the surface preparation of the alloy, which was investigated by X-ray photoelectron spectroscopy (XPS). Plasma polymer coated systems prepared on alkaline cleaned [2B] surfaces displayed enhanced corrosion protection properties.

Introduction

This section is the second of three parts dealing with System Approach Interface Engineering (SAIE) by means of chemical and (low temperature) plasma interface engineering. It is aimed at achieving improved corrosion protection of aluminum alloys used for the production of aircraft without employing heavy metal containing chemicals such as chromate conversion coatings and chromated primers. The main objective of the study is to find alternative corrosion protection methods by means of environmentally benign processes, eliminating health concerns and environmentally hazardous materials from corrosion protection systems. This paper, part II, deals with AA 2024-T3 ([2B]) as the substrate.

Experimental

Materials

The 3"×6"×0.032" Al alloy panels used for the present study were AA 2024-T3 (2024 specifications are by composition in wt%: Si 0.5, Fe 0.5, Cu 3.8-4.9, Mn 0.3-0.9, Mg 1.2-1.8, Cr 0.1, Zn 0.25, Ti 0.15, total of others 0.15, and Al remainder)[2] procured from Q-Panel Lab Products (Cleveland, OH). All the other materials used in this study are identical to what was described in Part I of this series. [1]

Sample preparation

In the present study, the [2B] systems modified in the plasma interface engineering process are grouped into four different SAIE series. Series-I samples were prepared on acetone-wiped surfaces to investigate the corrosion protective property of plasma processes, eliminating any effects of wet chemical processes. Series-II and Series-III samples were prepared on chemically cleaned surfaces with plasma pretreatment. Effect of cathodic E-coating voltage was investigated by E-coating SAIE Series-II plasmas at 250V and SAIE Series-III plasmas at 170V keeping other parameters the same. Series IV samples were prepared by omitting the extended plasma pretreatment and depositing the plasma polymers on alkaline-cleaned panels only. The objective of this series was to investigate the effect of alkaline cleaning on the corrosion performance of plasmas on [2B] without plasma pretreatment. For ease of identification of process parameters, identification codes were used. Codes and process details are summarized in Chapter 4, Table 1 (page 26). [2B] is used to denote AA 2024-T3.

Corrosion tests and surface analysis

Two types of accelerated corrosion tests, SO_2 (4 weeks) salt spray test performed per ASTM G85-94-annex A4 and Prohesion (12 weeks) cyclic salt spray tests performed per ASTM G85-94-annex A5, were used to examine the corrosion protection performance of the coating systems on [2B]. Polarization resistance (R_p) measurements were used to evaluate the effect of surface cleaning and plasma polymer coating on corrosion resistance of [2B]. X-ray photoelectron spectroscopy (XPS) was employed to monitor the surface composition change of [2B] after the surface preparation.

The detailed description of the test methods and experimental procedures used in this study was given in Part I of this series. [1]

Results and Discussion

The corrosion resistance of aluminum and Al alloys is largely due to the protective oxide film which can attain a thickness of about 10 Å within seconds on a freshly exposed aluminum surface.[3] A good corrosion protection system should include protection of the oxide layer, and, in addition, should provide a good adhesive base for a subsequent coating layer (paint). The conventional corrosion protection system for aluminum alloys consists of the application of a chromate conversion coating following alkaline cleaning and deoxidization of the surface. The purpose of pretreatments is to remove the contaminants, and thus create a clean surface on which chromium oxide can be grown, which then acts as the corrosion protective layer and also the adhesive base. The experimental results obtained in Part I of this series study indicated that these chemical cleaning processes significantly changed the surface composition of Alclad 2024-T3 aluminum alloy ([2A]) and consequently affected its corrosion protection characteristics.[1] In the present study, therefore, the effect of these chemical pretreatments on [2B] surface composition is first investigated by XPS analysis.

Effect of Chemical Pretreatments: XPS Study

The effects of three chemical pretreatments on AA2024-T3 were analyzed using XPS sputter depth profiling. The three treatments analyzed were the acetone wash (Ace), alkaline cleaning (Alk), and alkaline cleaning followed by deoxidization (Dox). Both the Alk sample and the Dox sample were inserted into the XPS chamber load lock and were under vacuum within five minutes of the final deionized water rinse stage of the cleaning. The results of this analysis, Figs. 1-3, imply some specific changes in surface chemical composition.

Fig. 1 shows the effects of each cleaning method on the thickness of the oxide layer. The oxide layer remaining after alkaline cleaning is thinner than the native oxide, and the oxide layer left on the Dox surface is thinner still. Using a Ta_2O_5 sputter rate of 0.58nm/min, which was obtained just prior to the depth profile and calculated at the 50% level of the O 1s peak, the oxide on the acetone wiped panel is calculated to be roughly 30nm thick. A metallic component first appeared in the Al 2p and Al KLL spectra after 900 seconds of sputtering, indicating that the thickness calculation with the tantalum oxide sputter rate is an overestimation. This overestimation is likely due to surface roughness limiting the removal of the oxygen signal from the aluminum alloy and possibly the tantalum oxide reference. The Alk sample did have a slight shoulder on the Al 2p spectrum due to metallic aluminum on the unsputtered surface, which steadily increased with sputtering time. It also had a small metallic peak in the KLL Auger spectrum, where the metallic and oxide components are much more separated. The Dox sample had a distinct metallic 2p peak evident and a stronger metallic KLL Auger peak on the unsputtered surface, indicating that this oxide layer is indeed quite thin, on the order of just a few nanometers at most.
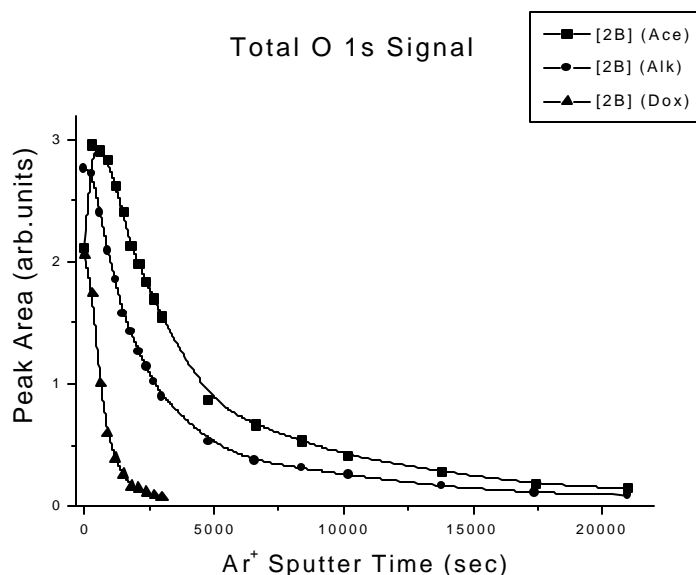

Figure 1. Total O 1s signal measured by XPS analysis of chemically pretreated and native (Ace) surfaces of AA 2024-T3 ([2B]).

In an attempt to better assess oxide thickness after the chemical treatments, Strohmeier's method for determining oxide thickness[4] was employed on the spectra from the surface prior to sputtering. The asymmetric Al 2p peak from a sputtered aluminum sample having no copper content was used as the model lineshape for the metallic component of the spectrum, in the software. Likewise, a sputter-cleaned oxygen-free, high conductivity (OFHC) Cu sample was used to determine ratio of Cu 3p to Cu 2p 3/2 peak area so that the contribution to the Al 2p spectrum from the Cu 3p could be accounted for by the measurement of the Cu 2p intensity on the un-sputtered alloy surfaces. The Cu 3p peak from the OFHC copper was also used as a model peak in the curve fitting of the Al 2p spectral region, and its intensity was restricted to be the same fraction (.206) of the Cu 2p 3/2 peak as measured on the pure Cu. Besides metallic Al, oxidized Al and Cu 3p peaks, an additional peak at higher binding energy (~77.8eV) was necessary to obtain a reasonable fit to the data and was included as part of the oxide component.

This additional peak could be a modeling problem indicative of differences in the attenuation of Cu 3p and Cu 2p electrons in the oxide, which is not unreasonable due to their differences in kinetic energy when emitted. This might also be indicative of the formation of some oxy-fluoride[5] on the surface of the oxide formed after deoxidation, due to remnants from the sodium bifluoride in the deoxidizer solution, since some fluorine was observed in the long range survey spectra from deoxidized samples. Values of 2.4nm and 2.2nm were used as the effective attenuation lengths of the 2p electrons in the oxide and metal respectively. These were the values used in the original reference[4], which still seem to fit within the range identified in a recent review[5]. Likewise, an aluminum atomic density ratio of 1.5 was used. The result of this procedure yields an oxide thickness of ~5.4nm on the alkaline cleaned sample and ~3.9nm on the deoxidized sample.

The thickness determined by this method, on these particular samples, is somewhat tenuous, since there is no accounting for how the enriched Cu layer beneath the oxide affects the attenuation of the metallic aluminum electrons, nor does it account for electron emission from possible aluminum in this layer in the form of an intermetallic. If the layer is pure copper and additional attenuation is the only effect, then the oxide calculated here is an overestimate of the thickness, since electrons from the oxide would not be attenuated. As noted by Strohmeier, this technique also fails to take the adventitious carbon layer and hydration effects into account, but can be used to get a feel for relative thickness differences.

Applying this same procedure in an iterative fashion after each of the first few sputter cycles on the deoxidized sample, and plotting the results, allowed for a linear fit of the thickness with sputter time. This generated a sputter rate of 0.24nm/min for aluminum oxide, indicating that the use of the Ta_2O_5 reference may overestimate the thickness by almost double in a case such as this.

The native oxide was seen to agree with the assessment that it is composed of an outer hydrated region above a non-hydrated region[4,5,7], both of which had some magnesium incorporated throughout.[8] Atomic ratios for the acetone cleaned native surface, calculated after the first sputter cycle to reduce the carbon contribution, are: (in atomic %), O-50.7%, C-1.7%, Al-16.4%, Mg-31.2%, and Cu-not detectable. All of the Mg spectra were consistent with oxidized species, hydrated to perhaps $Mg(OH)_2$ or a hydrated spinel in the outer layer, and a non-hydrated species

beneath.[9] The outer layer had Mg 2p spectra with a binding energy of 49.3 eV, which quickly decreased with sputtering, while a peak at 51.6 eV increased and maintained the same binding energy as it was eventually eroded with sputtering. These changes corresponded to similar changes in the oxidized aluminum 2p signal, indicating similar hydration effects on the surface of the mixed oxide. The precise identification of these states was difficult to determine.

Although charge neutralization was used during the entire depth profile, the acetone wiped native surface had a fairly complex carbon spectrum, which greatly complicated the analysis. Two distinctly visible peaks required a third component for a reasonable fit of the data. A high binding energy peak at 288.0 eV is likely a carbonate or C=O bond, while two peaks were present at lower binding energy (283.6 eV and 284.8 eV). All were nearly nonexistent after the first sputter cycle, indicating that they were remnant contaminants from the rolling and marking processes not fully removed by acetone cleaning, or could be residue from the acetone. This same structure was observed on panels of other alloys from the same manufacturer. The neutralizing scheme actually overcompensates for sample charging on thick insulators, pushing the binding energy of the C 1s line lower than the accepted adventitious level. As will be discussed shortly for the aluminum spectrum, the changes in depth maintained consistency with the earlier asserted hydrated mixed Al-Mg oxide above a non-hydrated mixed oxide, but the absolute binding energies from the top surface are somewhat suspect.
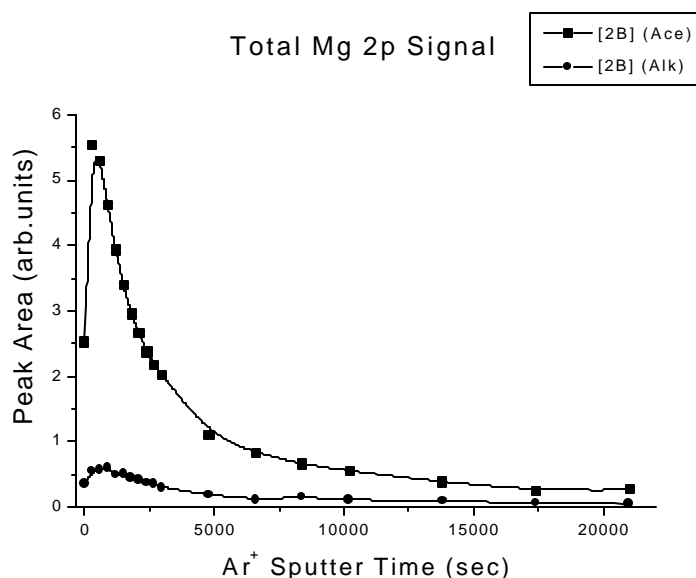

Figure 2. Total Mg 2p signal measured by XPS analysis of chemically pretreated and native (Ace) surfaces of AA 2024-T3 ([2B]). The Mg 2p signal from the (Dox) surface is not shown in this figure, because the intensities were below detection limits.

From Fig. 2 it is evident that after alkaline cleaning the Mg levels in the oxide have been dramatically reduced. After deoxidization, the Mg level in the oxide diminished to the point that

the Mg2p signal was undetectable, hence no trace for the deoxidized sample is shown in the figure. Unfortunately, the Mg 2p signal is not the strongest magnesium photoelectron line. The 1s is, but it cannot be excited with an Mg anode, as used in the depth profiles. The Mg 2p signal was undetectable in the bulk alloy with this source, although some concentration of Mg in the bulk alloy was confirmed with an Al Kα monochromatic source. Hence, the detection of magnesium in the samples using the Mg anode as the depth profiling x-ray source was limited to some value above 2% by weight.

The oxide left after alkaline cleaning is thicker than the oxide left after the deoxidization process, as shown in the depth profile (Fig. 1). The thickness of the inner barrier oxide on aluminum is temperature dependent[10]. Since alkaline cleaning takes place at approximately 65°C and the deoxidization process takes place at room temperature, it is possible that the inner barrier layer left after alkaline cleaning is thicker than that left after the deoxidization process. The solution chemistries also play a critical role in these values of thickness. In either case, the barrier layer is covered with the accepted thin, hydrated oxide layer after rinsing and the passing of time necessary to load the sample into the vacuum chamber.
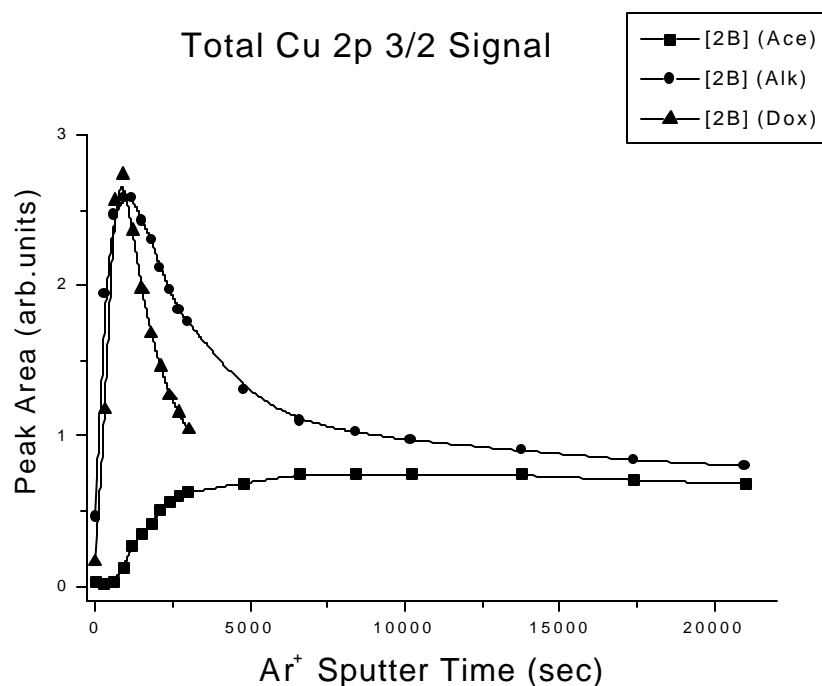

Figure 3. Total Cu 2p$^{3/2}$ signal measured by XPS analysis of chemically pretreated and native (Ace) surfaces of AA 2024-T3 ([2B]).

Fig. 3 displays the depth summary generated by the Cu2p 3/2 spectral area. It is quite apparent that the copper levels in the near surface region beneath the oxide are enriched by alkaline cleaning and by alkaline cleaning followed by deoxidization. A copper-enriched surface generally causes accelerated electrochemical corrosion due to galvanic interactions with the bulk alloy. The replacement of the hydrated, mixed oxide layer with a thin oxide layer containing little Mg seems to negate some of the electrochemical activity. It is thought that the incorporation of Mg in the native film acts to destabilize the oxide from a corrosion perspective, allowing easier transport of solute ions to the metal interface.[11-13]

Chemical States in the Interface

All of the summary depth profiles presented in Fig. 1-3 were compiled from total photoelectron peak areas, independent of changes in chemical state. The unique identification of specific chemical states in a complex system, such as the plasma-film/alloy interface region and the oxide on the treated alloy, is not straightforward. Due to the nature of certain chemical state changes, some information about the compounds involved in the interface has been gleaned.

It was mentioned earlier that the state of the Mg in the oxide region on the native, untreated alloy was consistent with a hydrated phase on the surface above a non-hydrated layer. The same scenario holds for the Al-O structure into which the Mg incorporates on the native surface. The top hydrated layer of the Alk and Dox treated samples appears similar to various mineral phases such as $AlO(OH)$ (boehmite), $Al(OH)_3$, and hydrated Al_2O_3, having a modified Auger parameter of 1460.5. The underlying barrier layer is consistent with the accepted amorphous Al_2O_3 designation,[8-10] with a modified Auger parameter of 1461.6.

The Cu2p spectra from the interface region show little variation in binding energy from those in the bulk alloy, having a position corresponding to a designation of $CuAl_2$ (BE of 933.9). This tends to indicate similar local bonding in the copper atoms, although the copper in the bulk alloy is considered to be at sites in the aluminum matrix and not in a $CuAl_2$ structure. The alkaline cleaned surface, however, does show some indication of oxidized Cu species above the main enrichment. A unique identification of this oxidized region is difficult due to effects such as possible reduction during ion and electron bombardment.

Effect of Initial Cleaning Processes and Plasma Polymer Deposition: Polarization Resistance Measurements

Polarization resistance (R_p) is defined as the charge transfer resistance of the solution-metal interface. In the present study, polarization resistance (R_p) was used to evaluate the effect of chemical cleaning and plasma polymer coating on corrosion resistance of [2B].

Fig. 4 shows the polarization resistance of the [2B] panels with different chemical pretreatment and with a TMS plasma polymer deposited on them. The alkaline-cleaned (Alk) and alkaline-cleaned, deoxidized (Dox) surfaces had higher polarization resistance than acetone-wiped (Ace) surfaces, which implies that these surfaces showed higher corrosion resistance. This supports the XPS finding that chemical cleaning of [2B] eliminated the channels of magnesium-rich, mixed oxides which penetrate the aluminum oxide on the native surface,[14] replacing this native

structure with a more stable barrier oxide layer. The native oxide on [2B] had a higher Mg concentration than the bulk composition, this Mg incorporated in the native oxide most likely diffused during solution heat treatment in manufacturing of the alloy panels. Though the Cu concentration on [2B] surfaces increased after alkaline cleaning and after alkaline cleaning followed by deoxidization, the Mg concentration decreased to the level of base alloy elemental concentrations. These more stable oxide layers improve the adhesion of plasma polymers.[15]

Plasma polymer coated [2B] surfaces showed higher polarization resistance than native and chemically cleaned surfaces. Thus, the corrosion resistance of plasma polymer coated [2B] was much higher than that of the barrier type oxides formed after chemical cleaning. Also, as is evident from the higher polarization resistance of the plasma polymers, they are good barriers to water, oxygen and corrosive species, even under an externally applied potential.[16] The R_p values of the plasma polymer coated surfaces of [2B] were nearly equal to or higher than those of the chromate conversion coated [2B]CC surfaces, suggesting that the plasma polymer coating process should offer higher corrosion resistance.
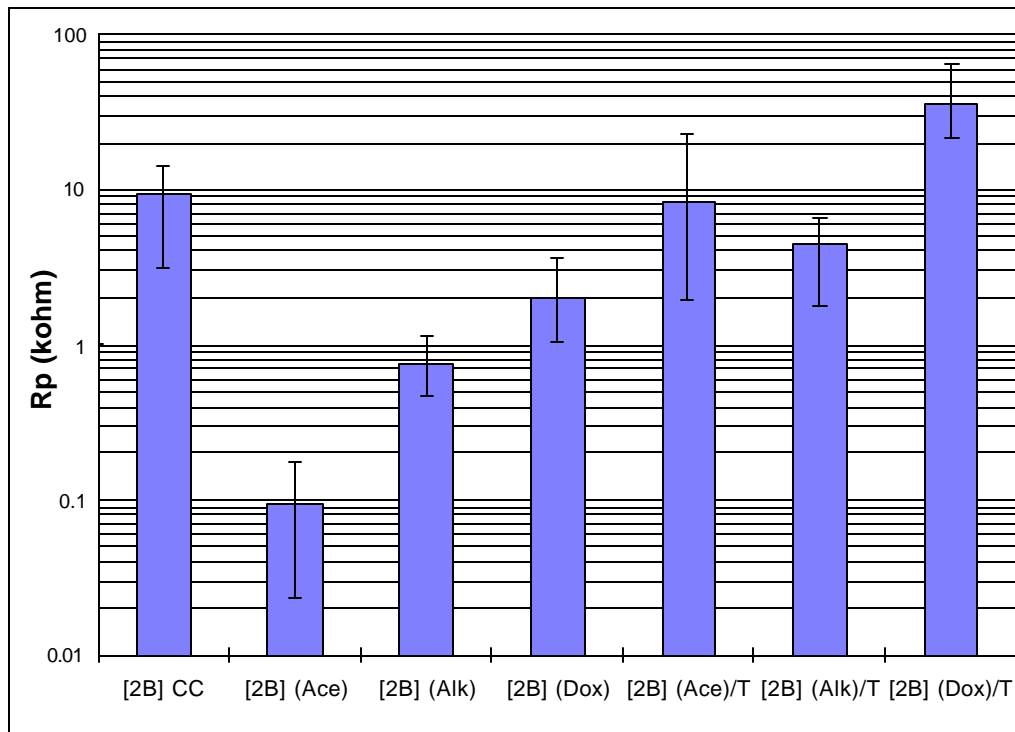

Figure 4. Polarization resistance of AA 2024-T3 ([2B]) panels with different chemical pretreatments and plasma polymer coated surfaces.

Corrosion Protection Characteristics: Evaluated by SO_2 and prohesion Salt Spray Tests

Two types of corrosion evaluation tests, SO_2 and prohesion salt spray, were employed for the evaluation of corrosion protection characteristics of the plasma systems on [2B] surfaces. The SO_2 salt spray test was chosen to speed up differentiation of the corrosion resistance of the

different systems investigated. The prohesion test, which is a chemically milder test than the SO_2 salt spray test, was conducted for a longer period, 2000 hours; it is considered a more realistic test, as it better simulates the actual corrosive environment found in service.
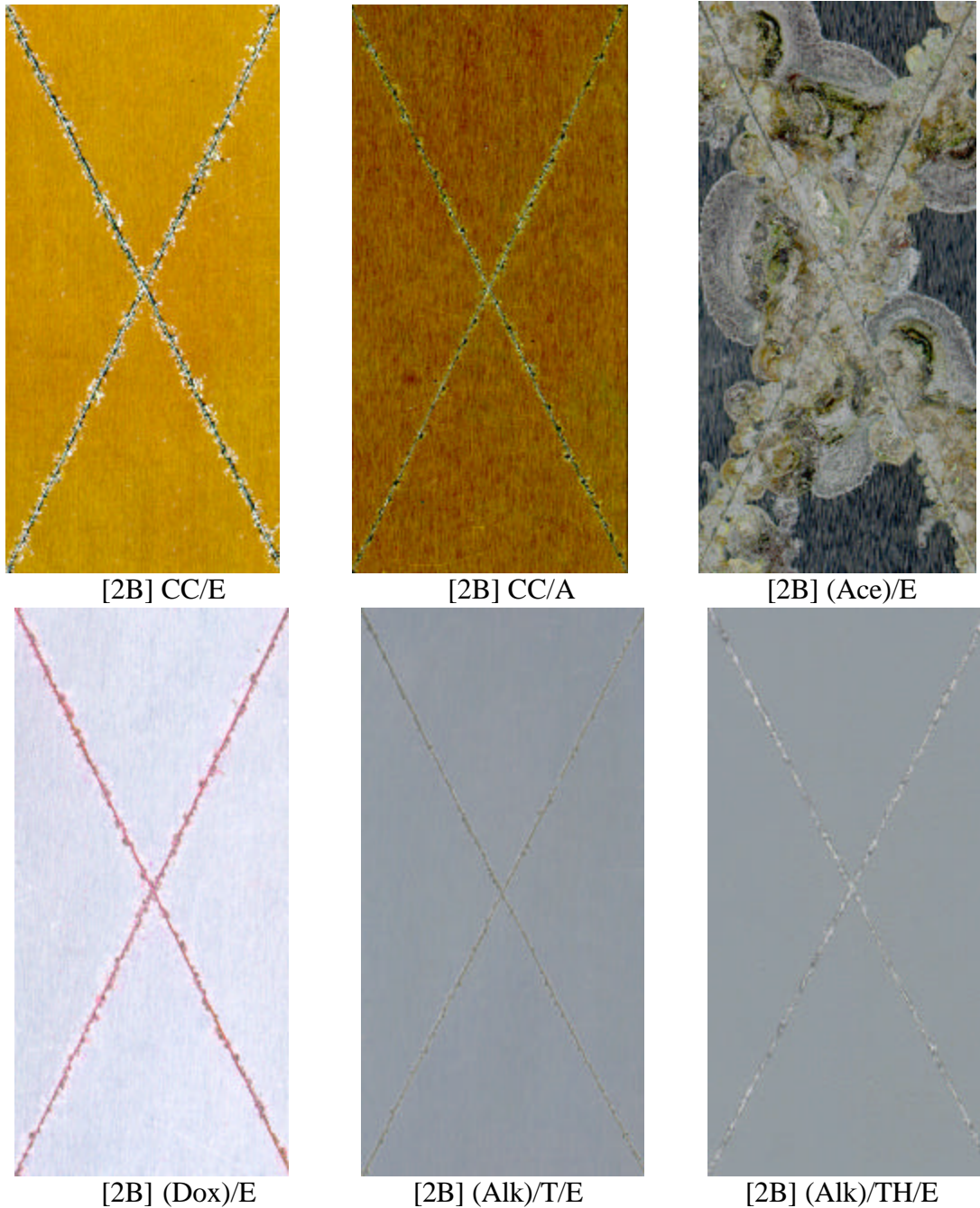

[2B] CC/E   [2B] CC/A   [2B] (Ace)/E

[2B] (Dox)/E   [2B] (Alk)/T/E   [2B] (Alk)/TH/E

Figure 5. Scanned images of SO_2 salt spray tested (4 weeks) panels of AA 2024-T3 ([2B]). Total scanned area is 27 cm^2 and total scribe length within the scanned area is 16 cm.

Figs. 5 & 6 show the scanned images of SO_2 and prohesion salt spray tested panels of [2B], respectively. Visual observation of these images reveals that panels that were only acetone-wiped and E-coated ([2B](Ace)/E) provided poor corrosion resistance. In contrast the plasma modified [2B] panels showed excellent corrosion resistance even after 12 weeks of exposure to prohesion salt spray, outperforming both controls of [2B]CC/E and [2B]CC/A.
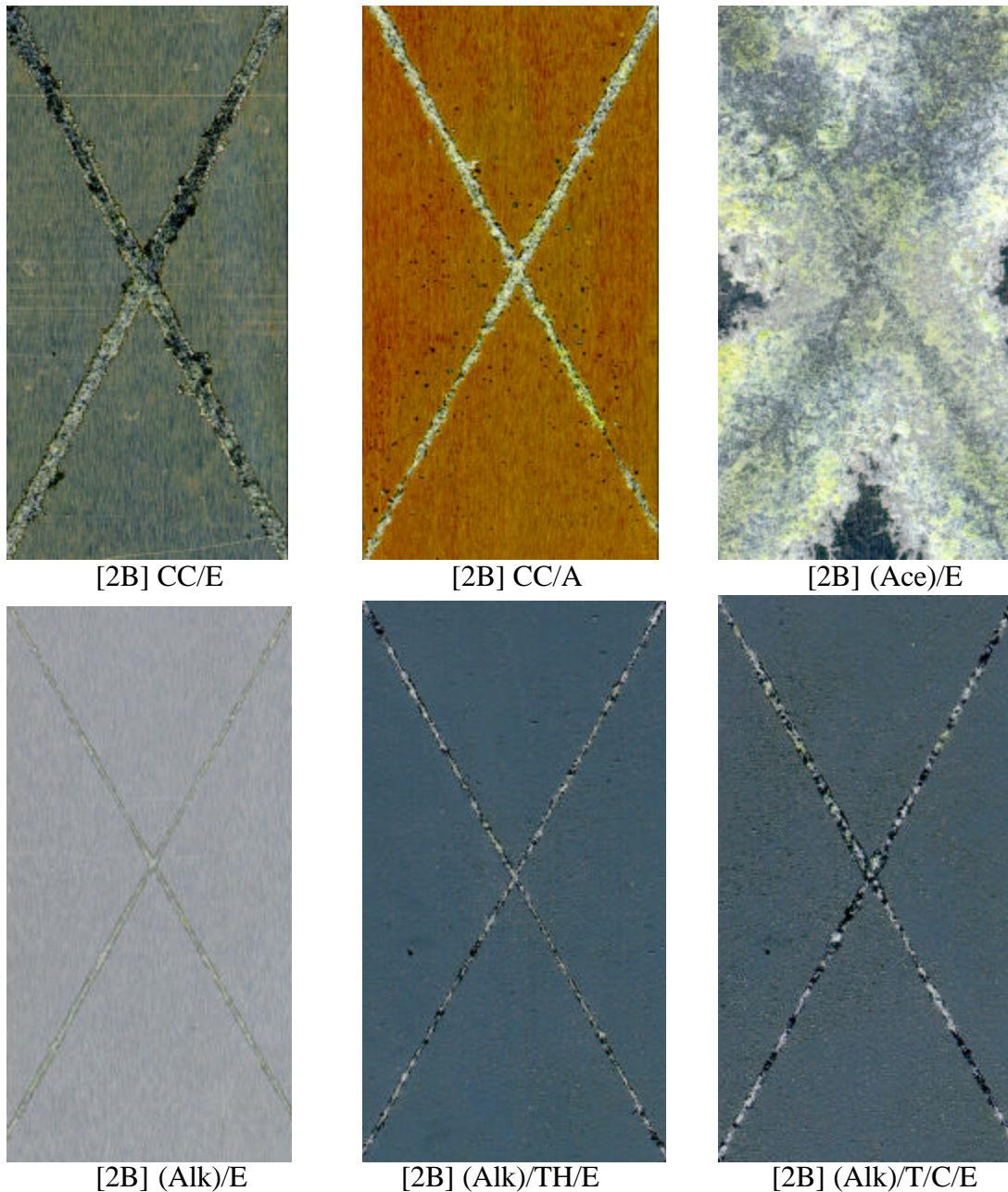

[2B] CC/E	[2B] CC/A	[2B] (Ace)/E
[2B] (Alk)/E	[2B] (Alk)/TH/E	[2B] (Alk)/T/C/E

Figure 6. Scanned images of prohesion salt spray tested (12 weeks) panels of AA 2024-T3 ([2B]). Total scanned area is 27 cm^2 and total scribe length within the scanned area is 16 cm.
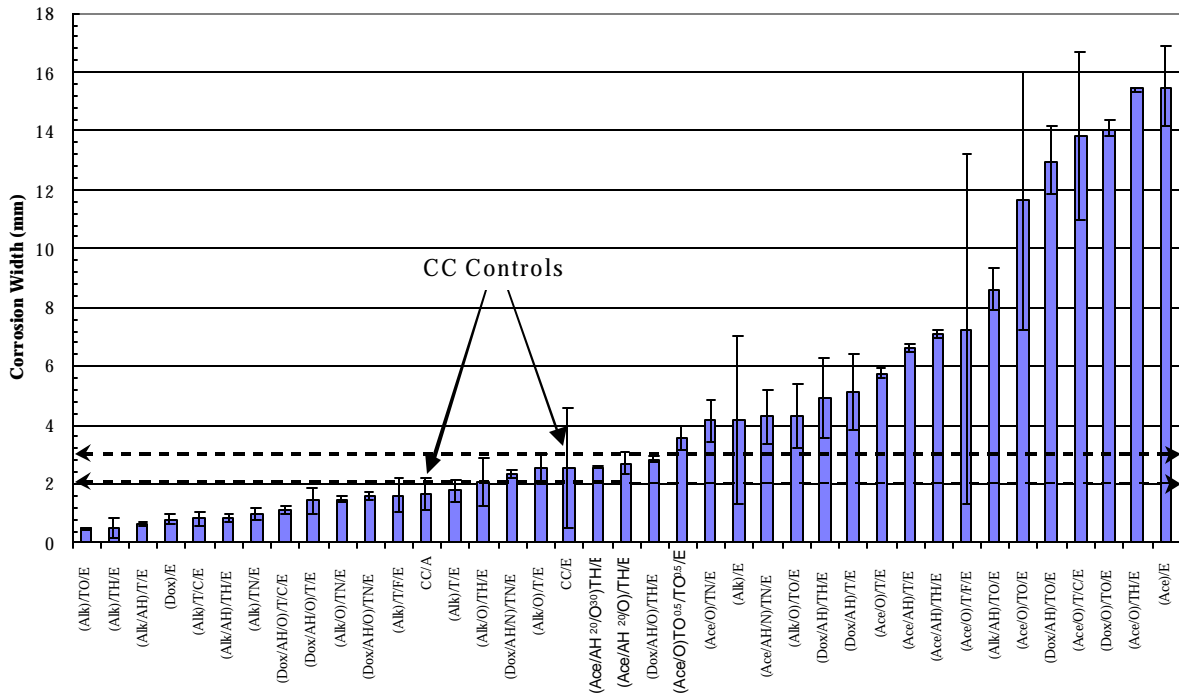
Figure 7. Average corrosion widths of prohesion salt spray tested (12 weeks) control, acetone-cleaned, alkaline-cleaned and various plasma treated AA 2024-T3 ([2B]) systems.
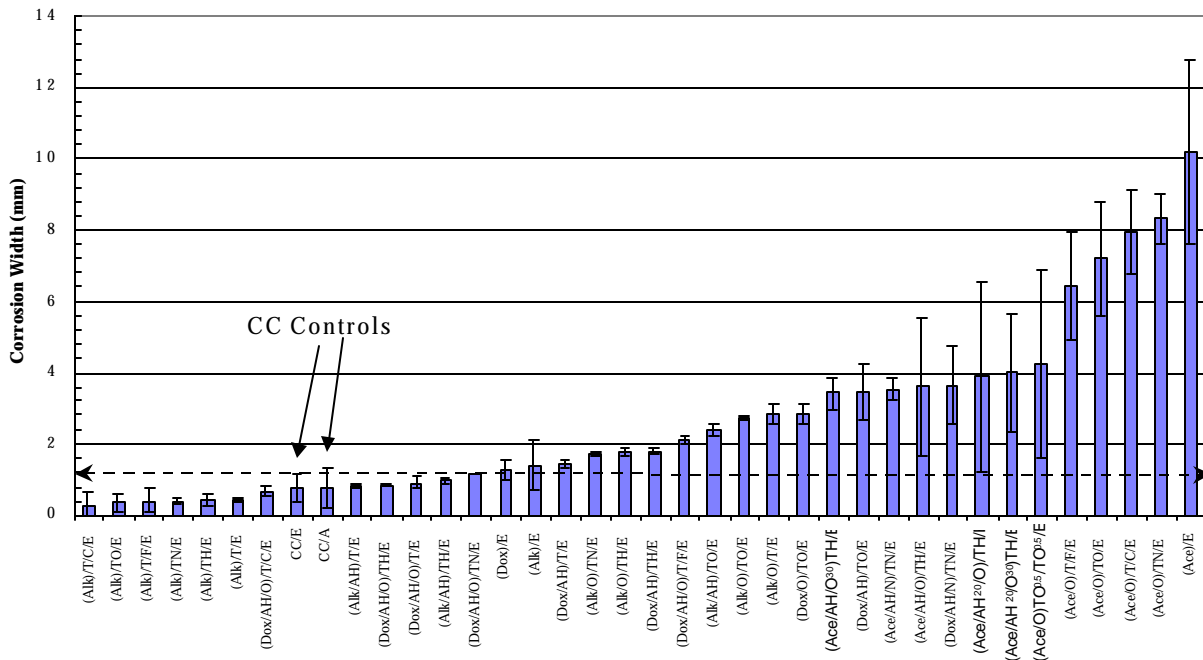

Figure 8. Average corrosion widths of SO_2 salt spray tested (4 weeks) control, acetone-cleaned, alkaline-cleaned and various plasma treated AA 2024-T3 ([2B]) systems.

The control panels had much improved performance over the acetone-wiped surface ([2B](Ace)/E) in both tests, but the [2B]CC/A panels displayed numerous pitting corrosion areas away from the scribe in prohesion salt spray testing, indicating that the Deft primer may have poor barrier properties. This pitting corrosion away from the scribe was clearly observed on both controls when examined under a microscope. The deoxidized (Dox) surface, Fig. 5, and the alkaline-cleaned (Alk) surface, Fig. 6, also showed improved corrosion performance when only coated with cathodic E-coat after the chemical treatment, without any plasma polymer deposition. These E-coated Dox and Alk panels showed corrosion resistance performance comparable to that of the control panels.

Figs. 7 & 8 show the ascending order of average corrosion widths for [2B] panels after prohesion and SO_2 salt spray testing, respectively. The corrosion widths of several of the plasma based systems evinced better performance than both controls in SO_2 as well as prohesion salt spray tests. Figs. 7 & 8 indicate that corrosion performance improves with all of the plasma film systems when compared to [2B] (Ace)/E. The corrosion performance of the alkaline-cleaned surfaces with plasma pretreatment and an applied plasma film is clearly better than that of acetone-wiped and deoxidized surfaces with plasma pretreatment and plasma films. XPS analysis showed that alkaline-cleaned and deoxidized surfaces have a significant concentration of Cu, while the acetone-cleaned surfaces are composed of Mg-Al oxides with no copper. The (Alk) treated surfaces had very little Mg and the (Dox) surfaces had no measurable Mg, which was in higher concentrations on (Ace) cleaned surfaces. The high Mg concentration in the oxide on the (Ace) cleaned surfaces is thought to be composed of Mg oxide channels[14] that allow the electrolyte to penetrate the oxide more easily, which could be the reason why acetone-wiped surfaces coated with E-coat displayed larger corrosion areas.

Correlation of SO_2 and Prohesion Salt Spray Tests

Figs. 9 & 10 show a comparison of the corrosion performance of different series of plasma modified [2B] specimens in both SO_2 and prohesion testing. The corrosion performance results for both tests roughly correlate linearly. Thus, if the corrosion performance of a plasma treatment is good in SO_2 testing, then its performance is also good in prohesion testing.

Series-I samples on (Ace) cleaned surfaces with plasma pretreatment, either O_2 or $Ar+H_2$, and plasma polymer deposited on top of these plasma-treated surfaces, showed large corrosion widths as compared to the control panels (Figs. 9). Extended plasma pretreatment by either O_2 or $Ar+H_2$ resulted in migration of Mg to the substrate surface (Fig. 11) due to an inadvertent large rise in substrate temperature. The sample shown in Fig. 11-c was alkaline cleaned and deoxidized and was pretreated with plasmas of $Ar+H_2$ and then N_2 prior to film deposition in a slightly different D.C. reactor. A temperature rise up to 250°C was observed on panels in the D.C. reactor used in this corrosion study and additional heat driven Mg migration into the oxide was observed in related XPS experiments. This was observed on panels where the Mg-rich, native oxide was stripped with chemical cleaning prior to plasma polymer deposition. These highly defective Mg-rich oxides are thought to be similar to pure Mg oxides and thus more soluble than aluminum oxides that do not contain magnesium[11,12,17], corroding more readily and providing paths for the formation of local galvanic cells. The poor performance of the series-I samples is likely due to the extended plasma cleaning of acetone cleaned panels.
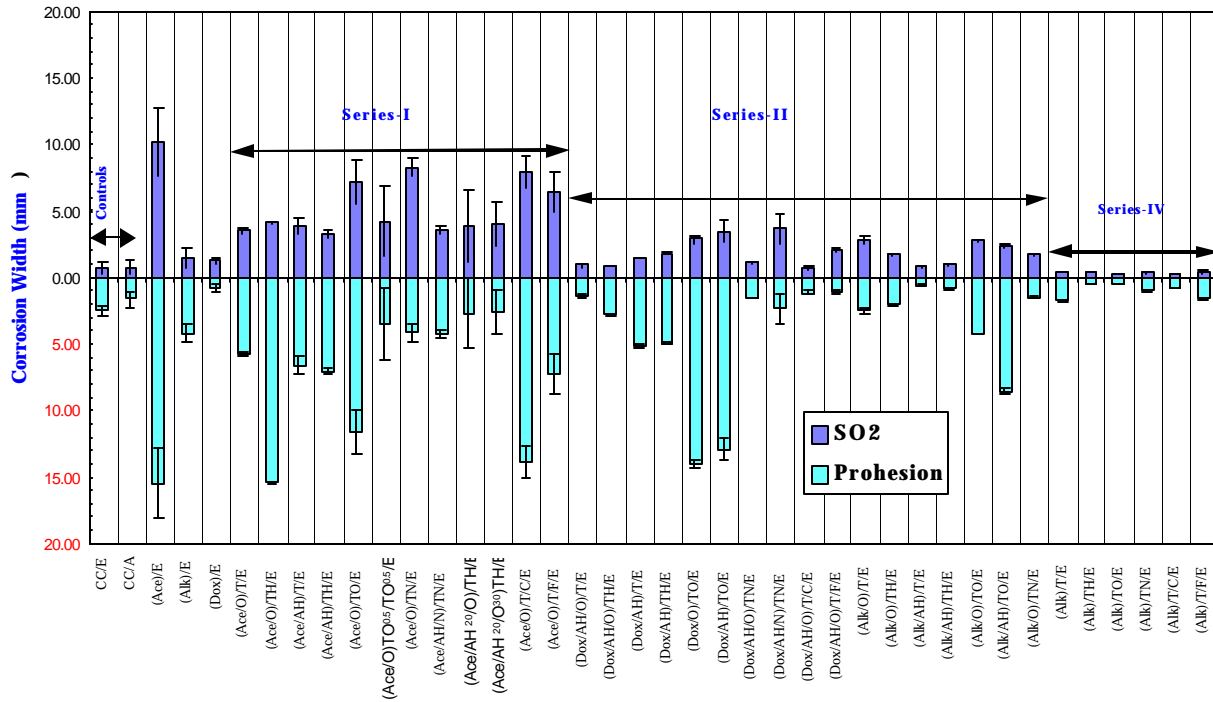
Figure 9. Comparison of average corrosion widths from panels of different series used in the plasma interface engineering of AA 2024-T3 ([2B]) panels and the control panels after prohesion salt spray testing (12 weeks) and SO_2 salt spray testing (4 weeks).
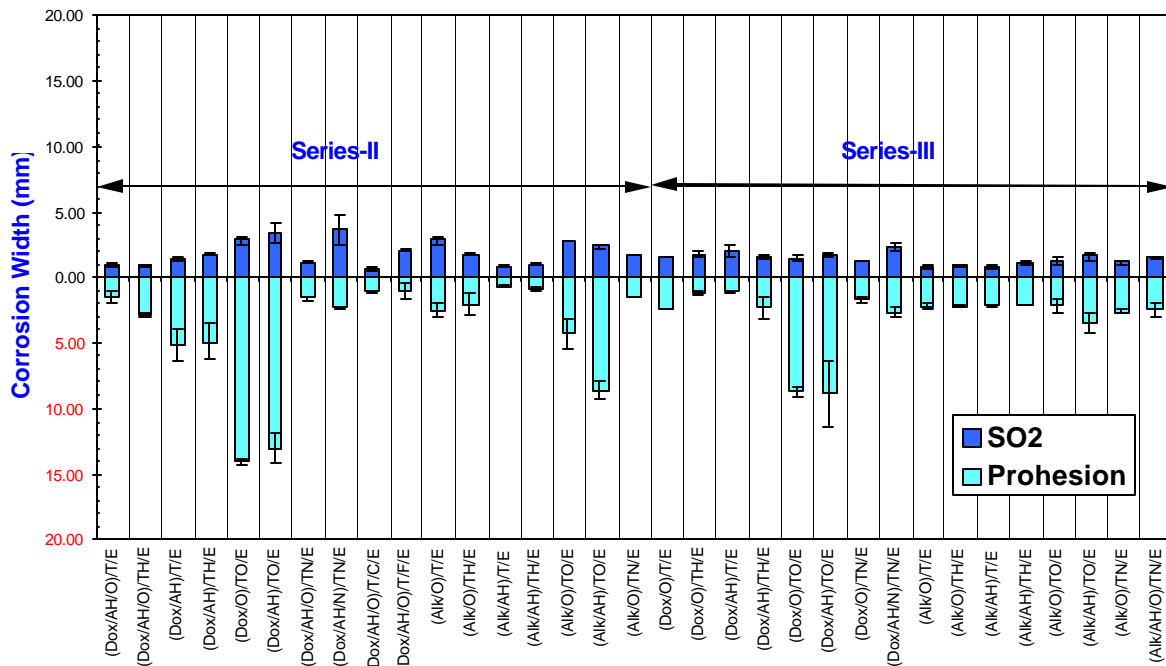

Figure 10. Comparison of average corrosion widths of Series-II (E-coating voltage 250 V) and Series-III (E-coating voltage 170 V) plasma modified AA 2024-T3 ([2B]) samples after SO_2 salt spray (4 weeks) and prohesion salt spray (12 weeks) tests.

Series-I: no wet chemical process and with plasma pretreatment, E-coating voltage 250 V;
Series-II: with wet chemical cleaning and plasma pretreatment, E-coating voltage 250 V;
Series-IV: with (Alk) cleaning but no plasma pretreatment, E-coating voltage 200 V.
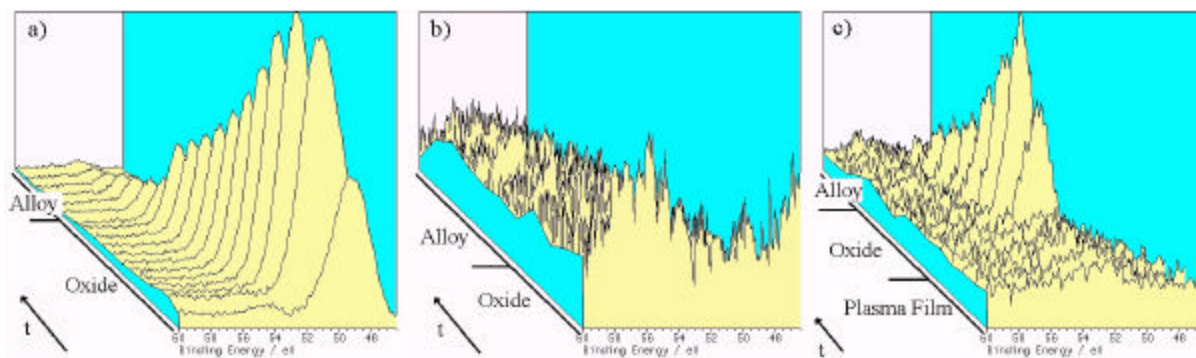

Figure 11. Mg 2p spectra from depth profiles showing Mg migration into the oxide layer due to heating during extended plasma pretreatments. The three samples are: a) the native acetone cleaned surface, b) alkaline cleaned and deoxidized, and c) alkaline cleaned and deoxidized followed by 10 minutes of Ar+H_2 plasma treatment and 10 minutes of N_2 plasma treatment prior to deposition of a plasma polymer from TMS + N_2. The arrow indicates the evolution as a function of sputtering time, but spacing between spectra is not linear but rather a spectral index. The lines mark the different regions on the samples, as obtained from spectra of the other constituent elements.

The likely enhanced the Mg concentration in the already Mg rich native oxide, produced additional defects created by the sputtering, and possibly caused the precipitation of copper phases related to increased aging of the alloy from the temperature increase. The process has since been optimized, and temperature increases of only 2-3 $^{\circ}$C are now more typical. Although the corrosion widths on the Series -I modified surfaces are larger than those on the controls, there was no pitting corrosion away from the scribed surfaces observed on the Series-I specimens (Figs. 5 & 6).

Series-II samples employed chemical pretreatment along with extended plasma pretreatment, which again resulted in poor performance on [2B](Fig. 9). The corrosion performance of (Alk) cleaning with plasma pretreatment of [2B] showed improvement over that of Series-I, but still not comparable with that of the controls. As just discussed, the reason appears related to the significant migration of Mg to the surface from the heating experienced during extended plasma pretreatment, Series-III samples were prepared to see the effect of cathodic E-coating voltage on corrosion performance of [2B] with similar plasma pretreatments and plasma polymer coatings that were employed in Series-II samples. Fig. 10 shows the comparison of the average corrosion widths of Series-II samples (E-coating voltage 250 V) and Series-III (E-coating voltage 170 V) samples after SO_2 and Prohesion salt spray tests. Regardless of the difference in E-coating voltage, the samples with the same plasma treatments and plasma coatings have very similar

corrosion performance in both Series-II and Series-III, having no significant difference observed on the corrosion widths, as seen inFig. 10.

(Alk) cleaning of [2B] surfaces improved the corrosion performance of the Series-II samples, but (Dox) had a negative effect on the corrosion resistance of the same plasma systems. This might result from the larger copper enrichment as observed by XPS analysis shown inFig. 3, coupled with the increase of magnesium in the oxide from the extended plasma cleaning. Series-IV specimens, which were made by depositing plasma polymers directly on (Alk)-cleaned surfaces of [2B], omitting the extended plasma pretreatment with O_2 or Ar+H_2, outperformed both controls. As evidenced by the XPS study, Series-IV samples had reduced magnesium concentrations in the oxide, as compared to the acetone wiped surface, via the alkaline cleaning process and eliminated magnesium migration into the remaining oxide by omitting prolonged plasma pretreatment.

Pitting Corrosion away from the Scribe on [2B]CC/E and [2B]CC/A control panels

Pitting corrosion away from the scribe was observed on almost all panels of both controls after the corrosion tests. Pitting corrosion away from the scribe occurs when the polymer paint films (in this case E-coat and Deft primer) have a high permeability to corrosive species like H_2O, O_2 and Cl^-. The pitting corrosion area was determined through image analysis and penetrant dye testing, as discussed below.

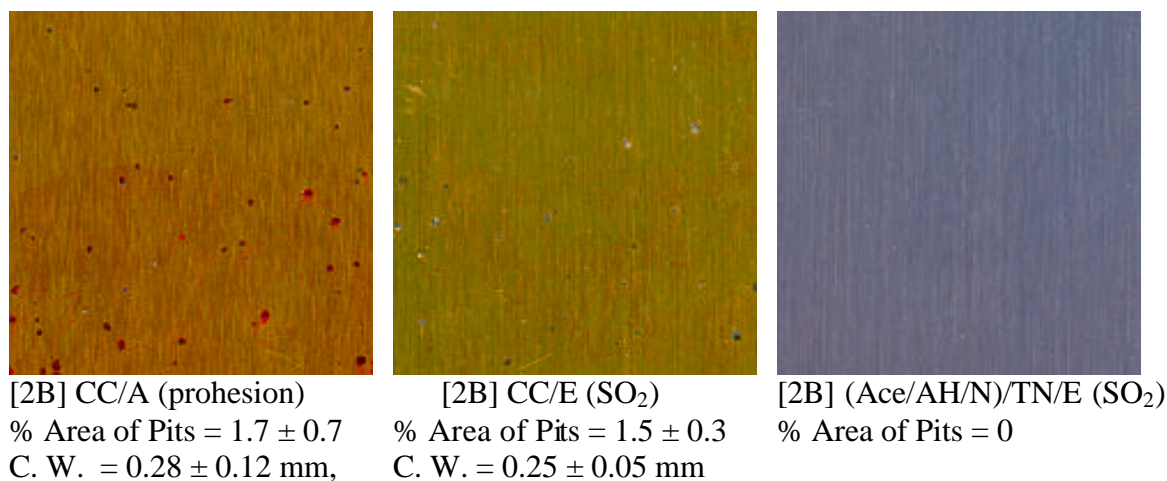| [2B] CC/A (prohesion)	[2B] CC/E (SO$_2$)	[2B] (Ace/AH/N)/TN/E (SO$_2$)
% Area of Pits = 1.7 ± 0.7	% Area of Pits = 1.5 ± 0.3	% Area of Pits = 0
C. W. = 0.28 ± 0.12 mm,	C. W. = 0.25 ± 0.05 mm	

Figure 12. Scanned pictures of corrosion-tested panels showing pitting corrosion away from the scribed surface of chromate conversion coated controls and plasma polymer coated AA 2024-T3 ([2B]). C. W. is the average corrosion width.

[2B]CC/E and [2B]CC/A control panels exposed to SO_2 and prohesion testing displayed numerous pitting corrosion areas away from scribed surface which were visible to the unaided eye. The panels with pitting corrosion were scanned over a small portion (2 cm $\times$ 2 cm) of the surface away from the scribe. These scanned pictures were used for calculating the percent area

of pits using OPTIMAS 6.1 software. Representative pictures of these surfaces are shown in Fig. 12, which clearly elucidates the pitting corrosion on the control panels. This pitting corrosion was not observed on the plasma polymer coated panels.

Further study of pitting corrosion was made using a penetrant dye inspection/photography technique at Boeing, St. Louis. Penetrant inspection is routinely performed on structural aircraft parts to check for material defects such as cracks or porosity. Fig. 13 shows the typical results of such a surface inspection of control panels and plasma polymer enhanced [2B] panels. These images were made by exposing the panel to fluorescent dye, washing off the dye, applying a developer to the panel that pulls trapped dye to the surface, and finally photographing the panel under black light. The pitting corrosion on the control panels is quite obvious in the pictures shown inFig. 13. Corrosive species along with water permeated through the paint film on the controls forming pools of solution at metal/primer interface that caused corrosion. The absence of pitting on the plasma-modified surface confirms that the plasma polymer coating overcomes this problem by offering a good water-insensitive barrier on [2B] surfaces.

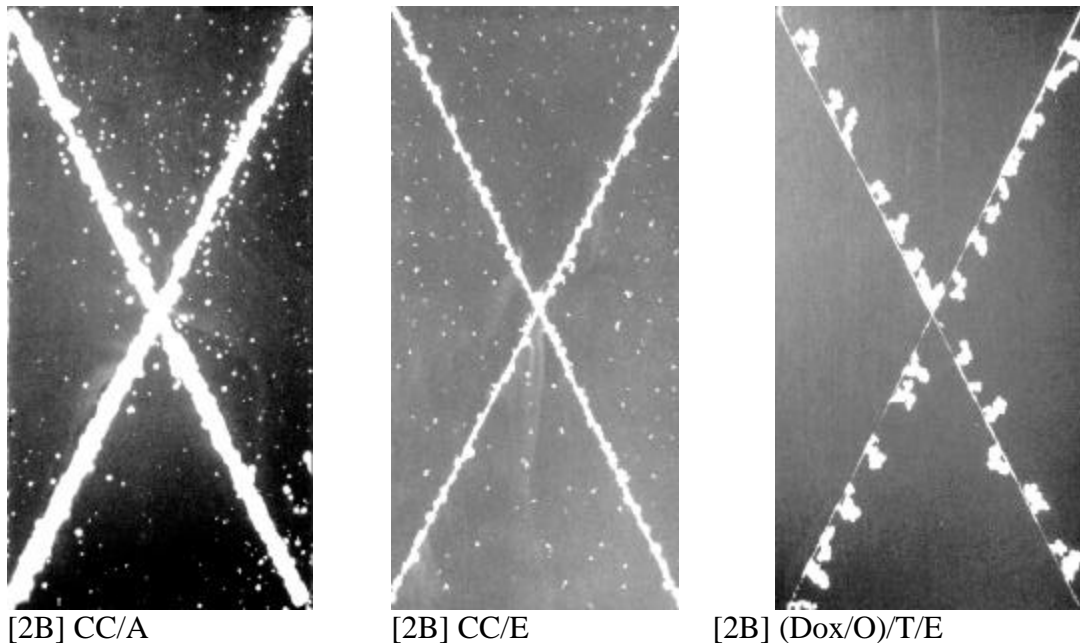| [2B] CC/A | [2B] CC/E | [2B] (Dox/O)/T/E |

Figure 13. Penetrant inspection/photographs of chromate conversion coated controls and plasma polymer coated AA 2024-T3 ([2B]).

Mechanism of Corrosion Protection of Al Alloy AA 2024-T3 by Low Temperature Plasma Interface Engineering

Adhesion of the cathodic E-coat to the plasma polymer surfaces is an important parameter in the corrosion protection of Al alloys. In general, the adhesion performance of E-coat applied onto plasma polymers was found to be far superior to that of the control panels. NMP (N-methylpyrrolidinone) paint delamination was not observed after 120 minutes for E-coat on

plasma polymer surfaces[18,19] as compared to a maximum time for complete delamination of 5 minutes for E-coat on chromate conversion coating;[2B] CC/E panels. The adhesion performance of cathodic E-coat on the plasma polymer surfaces could not be differentiated by the conventional tape test (ASTM D3359-93B), since E-coat on all of the combinations of plasma polymers achieved the maximum rating of the tape test method.

Good corrosion protection characteristics were obtained with strong water-insensitive adhesion of cathodic E-coat to plasma-modified surfaces of [2B] prepared on (Alk) cleaned surfaces. Plasma polymer coated surfaces provided extremely good adhesion for E-coat films, and showed excellent corrosion resistance, and there was no pitting corrosion away from the scribe. The following corrosion protection mechanism of these plasma interface engineered [2B] systems is proposed. The major factors influencing the corrosion of a damaged (scribed) surface protection system and those for an undamaged system are depicted in Fig. 14.
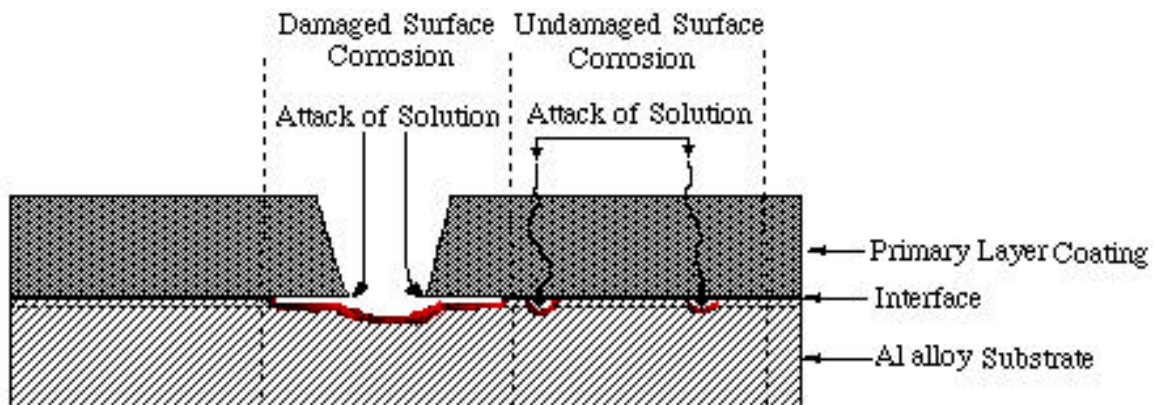

Figure 14. Schematic representation of damaged and undamaged surface corrosion of coated Al alloys.

There are at least five important factors to be considered in the corrosion protection of an Al alloy panel with a good barrier coating system as a whole: (i) salt intrusion resistance of the top surface; (ii) barrier properties of the bulk phase of the coating; (iii) type and nature of passivating agents, if any; (iv) adhesion characteristics of the coating-metal interface; and (v) the surface character (oxides) of the metal substrate.

All of the systems with plasma polymer modified interfaces on [2B] showed no pitting corrosion away from the damaged surface (scribe), suggesting that such systems have good barrier characteristics. In an undamaged corrosion protection system (the surface away from the scribe), all chemical species that are involved in the corrosion process of the substrate metal, such as H_2O, O_2 and CI, must penetrate the barrier. Therefore, the permeability of the coating is a dominant factor. In a damaged corrosion protection system (the surface along the scribe), the metal surface is directly exposed to the corrosive environment where the coating is breached and the supply of the corrosive species does not rely on transport through the coating. Consequently, the barrier characteristics of a coating are much less important in a damaged area.

When water molecules permeate the coating and reach the interface, the adhesion of a coating becomes a crucial important factor in an undamaged corrosion protection system. Water permeates a flawless polymer layer by the diffusion of dissolved individual molecules but not as bulk (liquid) water. In general, water molecules that reach the interface have a stronger association with conventional polymers and also with the metal surface than the adhesive interaction between the conventional polymer coating and the metal. This leads to localized delamination of the coating. Once a void is formed at the interface, water tends to cluster together to form liquid phase water. Water-insensitive adhesion is important to prevent this phenomenon. It is important to recognize that it is impossible to prevent transport of water with an organic polymer layer. It is simply a time-dependent event, determined by the water transport resistance of the coating.

In a damaged corrosion protection system, the adhesion of a coating becomes the most important factor, because both liquid water and corrosive species attack the interface. A water-delaminated coating layer does not provide any corrosion protection. Thus, water-insensitive adhesion of a coating to a substrate is a mandatory requirement for the prevention of corrosion-induced delamination.

The corrosion characteristics of the surface of the substrate (i.e., pure aluminum oxide, mixed oxides, chromium oxide or plasma polymer) in an undamaged corrosion protection system become important as enough water and corrosive species reach the interface. Corrosion becomes the driving force in the delamination of a coating and in the propagation of surface corrosion only after the transport of corrosive species to the interface and creation of micro-voids. Hence, the degradation of the main barrier layer can be considered the dominant factor.

Corrosion begins immediately in a damaged corrosion protection system, regardless of the conditions of the undamaged area. The result of this factor is two-fold: the immediate corrosion of the exposed surface and the initiation of surface corrosion that does not depend on barrier characteristics of the coating. Corrosion of exposed surface area proceeds until a significant barrier-type layer of corrosion products builds up, slowing down further corrosion. The propagation of surface corrosion beneath the coating near the damage depends on the adhesion of the coating. Good adhesion between the surface and the coating layer will ultimately limit surface corrosion, particularly once the build-up of corrosion products inhibits further corrosion into the damaged region.

Conclusions

In contrast to Alclad 2024-T3, studied in Part I of this series, bare AA 2024-T3 has a significantly lower Rp value than pure aluminum. Alkaline cleaning and alkaline cleaning plus deoxidization increase the Rp value, indicating chemical treatment of the surface is necessary for this alloy. Plasma surface treatment, with or without chemical treatment, employed in this study (10 minutes treatment) raised the temperature of the substrate above 200 ^{o}C, which caused the migration of Mg to the surface, yielding poor corrosion protection.

XPS surface analysis results indicated that the native surface of [2B] has a high Mg concentration, which was then associated with a decrease in its corrosion resistance. Chemical cleaning of these alloy surfaces by alkaline cleaning and deoxidization procedures leaves an

enriched Cu concentration on the surface, but reduces the Mg concentration to the bulk level or below it. Similar behavior has been observed in etching processes, with similar conclusions drawn regarding the effects.[7]

An anode magnetron enhanced D.C. cathodic plasma technique was successfully applied to AA 2024-T3 aluminum alloys ([2B]) to develop environmentally benign corrosion protection systems, i.e. plasma interface engineered systems of cathodic E-coat/plasma polymer/[2B] in this study. The corrosion test results from SO_2 and prohesion salt spray tests clearly showed that plasma interface engineered systems provided excellent corrosion protection of [2B].

It is also important to point out that E-coat directly applied onto alkaline cleaned and deoxidized 2B surface showed excellent corrosion protection, indicating that good adhesion of an excellent barrier could match the corrosion protection of chromate conversion coated controls. This is also an example of SAIE, i.e., a chemically interface engineered corrosion protection system.

The plasma polymers provided good water-insensitive adhesion, which prevents corrosion from creeping into the paint-metal interface. The corrosion process on the damaged surfaces (scribe) of these plasma polymer coated [2B] systems did not show any worse damage of the metal in the scribe than the chromate controls. The good water-insensitive adhesion of the plasma polymers prevented corrosion of the undamaged surfaces, whereas the control panels showed pitting corrosion away from the scribe.

The results obtained in this study indicate that the corrosion protection of [2B] depends on three major factors: the stability of the surface of the metal substrate (i.e., pure aluminum oxide, mixed oxides, chromium oxide or plasma polymer), the barrier characteristics of the primer film system and the adhesion properties of the coating-metal interface. Good corrosion protection characteristics were obtained with strong water-insensitive adhesion of cathodic E-coat to selectively chosen plasma polymers deposited on alkaline cleaned [2B] surfaces, i.e., plasma interface engineered surfaces.

Reference

1. C. M. Reddy, Q. Yu, H. K. Yasuda, C. E. Moffitt, D. M. Wieliczka, R. Johnson and J. E. Deffeyes, "Improved Corrosion Protection of Al Alloys by Low Temperature Plasma Interface Engineering: Part I-Alclad 2024-T3 ", submitted to *Corrosion*.
2. ASM Specialty Handbook: Aluminum and Aluminum Alloys, American Society for Metals, 1993.
3. L. L. Shreir, R. A. Jarman, and G. T. Burstein (eds.). Corrosion, 3rd ed. (Buttersworth-Heinemann, Jordan Hill, 1994; Vol. 1,) Chap. 4.
4. B.R. Strohmeier, Surf. and Interface Anal., 15 (1990) p. 51-56.
5. B.R. Strohmeier, Appl. Surf. Sci. 40 (1989) p. 249-263.
6. C. J. Powell and A. Jablonski, J. Phys. Chem. Ref. Data, 28 (1999) p. 19-62.
7. E. McCafferty and J. P Wightman, Surf. and Interface Anal., 26 (1998) p. 549-564.
8. S. Wernick, and R. Pinner. Surface treatment and finishing of Aluminum and its Alloys, 3rd ed. (Robert Draper, Teddington, 1976).

9.   C.D. Wagner, in Practical Surface Analysis:Volume1-Auger and X-ray Photoelectron Spectroscopy, 2nd Ed., D. Briggs and M. P. Seah ed. (Wiley, 1995), pp. 601-2.

10. Metals Handbook, 9th Edition, Volume 13: Corrosion (American Society for Metals, 1987) p.583.

11. T. S. Sun, J. M. Chen, J. D. Venables, and R. Hopping, Appl. Surf. Sci., **1** (1978) p.202-214.

12. M. Textor and R. Grauer, Corrosion Sci., **23** (1983) p. 41-53.

13. A. J. Kinloch in Polymer Surfaces and Interfaces, eds. W. J. Feast and H. S. Munro (Wiley, New York, 1987) p. 75-97.

14. K. Wefers, Aluminum, **57** (1981) p. 722-726.

15. DARPA Annual Progress Report #2, Contract AF F33615-96-C-5055 (July 24, 1998).

16. N. Pommier, L. Thiery, M. P. Gigandet, and M. Tachez, Annales de Chimie-Science des Materiaud, **23**(1-2) (1998) p. 397-400.

17. Handbook of Chemistry and Physics, 66th ed., R. C. Weast ed. (CRC press, 1985) B-69, B-111.

18. W. J. van Ooij and A. Sabata, *CORROSION/91* (Houston, TX, NACE, 1991) Paper No. 417.

19. C. M. Reddy, C. M. Weikart and H. Yasuda, "Effect of Interfacial Tension Minimizing on Adhesion of Cathodic E-coat", to be published in J. Adhesion.

6. Improved Corrosion Protection of Al Alloys by System Approach Interface Engineering: Part III - AA 7075-T6

C. E. Moffitt, C. M. Reddy, Q. S. Yu, D. M. Wieliczka, R. Johnson, J. E. Deffeyes, and H. K. Yasuda

Abstract

This study investigates the development of chromate-free corrosion protection systems for AA 7075-T6 [7B] based on the concept of System Approach Interface Engineering (SAIE) by means of chemical and plasma techniques. An anode magnetron enhanced d.c. cathodic plasma process was used to enhance the interfacial bonding and the protection offered by a cathodically electrodeposited, epoxy-based primer (E-coat) on [7B]. Corrosion test results indicated that superior corrosion properties were achieved on [7B] with the aid of plasma interface engineering, tailoring specific properties of the interfaces. When tested in SO_2 salt spray, several of these plasma modified systems outperformed and many of them performed comparably to the controls used in this study: chromate conversion coated and then Deft primer coated (Deft 44-GN-36) [7B] panels, as well as chromate conversion coated and then cathodic E-coated [7B] panels. When tested by the prohesion salt spray method, the corrosion protection performance of the best systems was close to or equal to the controls. The corrosion protection properties of [7B] were found to be strongly dependent on the surface preparation of the alloy, which was investigated by X-ray photoelectron spectroscopy (XPS). Plasma polymer coated systems prepared on [7B] surfaces, with a deoxidization process in combination with the E-coat, displayed the most enhanced corrosion resistance.

Introduction

This section is the third of three parts dealing with System Approach Interface Engineering (SAIE) by means of chemical and (low temperature) plasma interface engineering. Part III, deals with AA 7075-T6 ([7B]) as the substrate. A full introduction to the subject with background information can be found in part I of this series, which focuses on Alclad 2024-T3 ([2A]).[1]

Experimental

Materials

The 3"×6"×0.032" Al alloy panels used for the present study were AA 7075-T6 ([7B]) procured from Q-Panel Lab Products (Cleveland, OH). Hexamethyldisiloxane (HMDSO, 99.5+%) was purchased from Aldrich Chemical Campany, Inc. (Milwaukee, WI), hexamethyldisilazane (HMDSZ, 99.0% min.) were purchased from PCR Incorporated (Gainesville, FL). Liquid monomers were degassed by a freezing-thawing process three times and their vapors then used. All the other materials used in this study are identical to what was described in Part I of this series. [1]

Sample preparation

In the present study, the individual systems investigated in the plasma interface engineering of [7B] are grouped into five different series. Series-I samples were prepared on acetone-wiped surfaces to investigate the corrosion protective property of plasma processes eliminating any effects of wet chemical processes. Series-II and Series-III samples were prepared on chemically cleaned surfaces with plasma pretreatment. Effect of cathodic E-coating voltage was investigated by E-coating SAIE Series-II plasmas at 250V and SAIE Series-III plasmas at 170V keeping other parameters the same. Series IV samples were prepared by omitting the extended plasma pretreatment and depositing the plasma polymers on alkaline-cleaned panels only. The objective of this series was to investigate the effect of alkaline cleaning on the corrosion performance of plasmas on [7B] without plasma pretreatment. During the course of this study, it was discovered that Series-IV samples did not perform as well as the controls on this alloy; therefore, process conditions were modified and Series-V samples were prepared on deoxidized surfaces with no plasma pretreatment. Series-V plasma films included additional monomers like Hexamethyldisiloxane (HMDSO) and Hexamethyldisilazane (HMDSZ), which were not used in the other series. The same codes and process details summarized in Chapter 4 are used also in this chapter. [7B] is used to denote AA 7075-T6.

Corrosion tests and surface analysis

Two types of accelerated corrosion tests, SO_2 (4 weeks) salt spray test performed per ASTM G85-94-annex A4 and Prohesion (12 weeks) cyclic salt spray tests performed per ASTM G85-94-annex A5, were used to examine the corrosion protection performance of the coating systems on [7B]. Polarization resistance (R_p) measurements were used to evaluate the effect of surface cleaning and plasma polymer coating on corrosion resistance of [7B]. X-ray photoelectron spectroscopy (XPS) was employed to monitor the surface composition change of [7B] after the surface preparation.

All the test methods and experimental procedures used in this study were described in detail in Part I[1] except for the following.

Scanning Electron Microscopy (SEM) analysis

To investigate the micro-pitting areas, Scanning Electron Microscopy (SEM) analysis was carried up on the corrosion tested [7B] panels after primer coating was stripped off by Turco5469 paint stripper solution. The SEM samples of 10 mm × 10 mm was prepared from the tested [7B] panels by cutting from where no pits visible to the unaided eyes. SEM measurement was performed with an Amray model 1600T SEM apparatus. A tungsten filament was used as the electron source. A 10 KeV accelerator voltage was used for scanning the sample surfaces.

Results and Discussion

The surface oxide on Al alloys offers relatively good corrosion protection in mildly corrosive environments. Aluminum corrodes in high (greater than 11.5) and low (less than 2.0) pH solutions with specific exceptions like strong acid solutions of high redox potential, e.g., concentrated nitric acid in which aluminum passivates.[3] A corrosion protection system should

include protection of the oxide and, in addition, should provide a good adhesive base for subsequent coating. The conventional corrosion protection system consists of alkaline cleaning and deoxidization of the surface followed by the application of a chromate conversion coating. The purpose of pretreatments is to remove the surface contaminants, and thus create a clean surface on which chromium oxide can be grown, which then acts as the corrosion protective layer and also the adhesive base. The experimental results presented in Parts I and II of this series indicated that these chemical cleaning processes significantly changed the surface composition of Alclad 2024-T3 ([2A]) and AA 2024-T3 ([2B]) aluminum alloys, and consequently affected the corrosion protection characteristics of the alloys.[1,2] In the present study, therefore, the effect of these chemical pretreatments on [7B] surface composition was first investigated by XPS analysis.

Effect of Chemical Cleaning Pretreatments: XPS Study

XPS analysis of [7B] surfaces was performed to examine changes resulting from the application of different cleaning methods. The results reveal that the chemical cleaners change the elemental composition of the surface and could play an important role in the corrosion performance of the alloy. XPS depth profiles of the alloy after each of the three cleaning techniques (acetone wiping (Ace), alkaline cleaning (Alk), and alkaline cleaning followed by deoxidization (Dox)) are shown in Fig. 1. They show the comparison of total photoelectron peak areas as a function of sputtering time, and therefore imply elemental concentration changes as a function of depth.
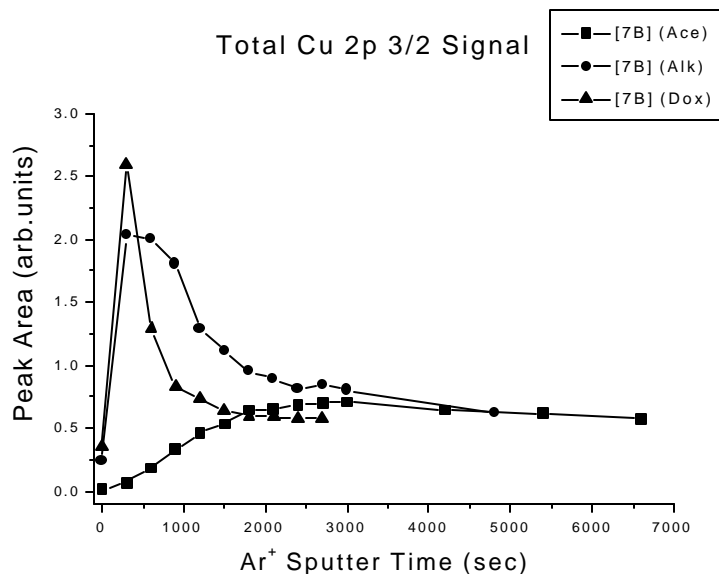

Figure 1. Cu 2p3/2 photoelectron peak area as a function of sputtering time for AA7075-T6 ([7B]) after each of three chemical pretreatments.

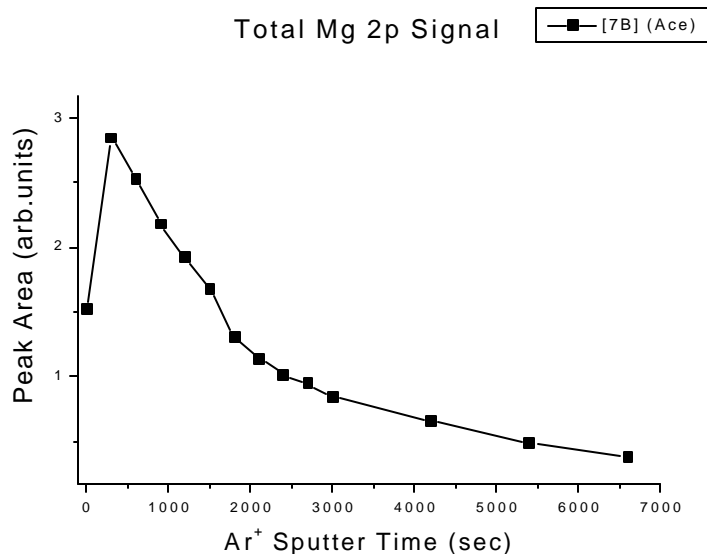Total Mg 2p Signal   ■— [7B] (Ace)

Figure 2. Mg 2p photoelectron peak area as a function of sputtering time for AA7075-T6 ([7B]) after each of three chemical pretreatments. No signal was received from (Alk) or (Dox) surfaces.

Total O 1s Signal
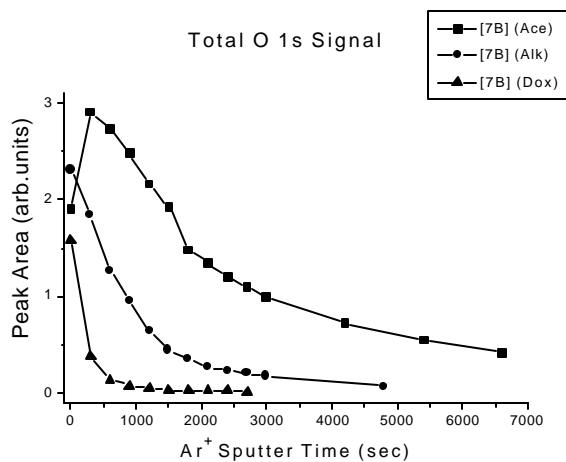
■— [7B] (Ace)
●— [7B] (Alk)
▲— [7B] (Dox)

Figure 3. O 1s photoelectron peak area as a function of sputtering time for AA7075-T6 ([7B]) after each of three chemical pretreatments.

It becomes quite apparent, upon observation of the data in Fig. 1, that the copper levels in the near surface region beneath the oxide are dramatically enhanced, and thus could play a significant role in local galvanic activity. While the Cu levels increase after each of the chemical cleaning techniques, the enriched magnesium-containing oxide structure seen on the native, as-received surface is removed and replaced with an oxide having no significant Mg content (Fig. 2). Fig. 3 indicates that the chemical cleaners do indeed leave thinner oxides on the surface, with the deoxidizer leaving the thinnest structure. Finally, Fig. 4 indicates that the

alkaline cleaner alone leaves a highly zinc-enriched structure on the surface. This zinc enrichment appears to be in the form of an oxide, which is probably hydrated on its topmost surface.
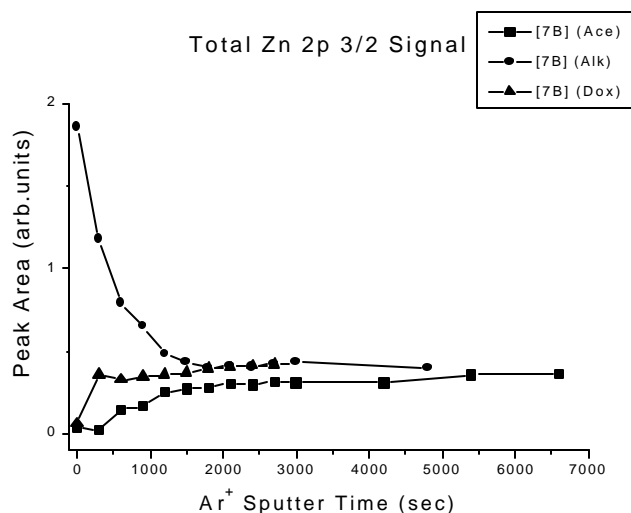

Figure 4. Zn 2p 3/2 photoelectron peak area as a function of sputtering time for AA7075-T6 ([7B]) after each of three chemical pretreatments.

While a copper-enriched surface has the implication of always causing accelerated electrochemical corrosion, replacing the native, hydrated (possibly better phrased as hydroxylated),[4] mixed Al-Mg oxide[5] layer with a thin stable oxide layer seems to allow the plasma films to tightly adhere to the alloy surface. This adhesion, coupled with the barrier properties of the films, appears to provide additional protection of the oxide layer from contact with corrosive agents. Such agents, if they were to penetrate the oxide and reach the metallic alloy, act as electrolytes in local galvanic cell formation.

The thickness of the oxide layer remaining after alkaline cleaning is reduced from that of the native oxide (Fig. 3). The relative thicknesses of the barrier and hydroxylated layers after using this cleaning method may be slightly altered, since the thickness of the barrier layer is temperature dependent.[6] Alkaline cleaning is performed at an elevated temperature (65 °C), and may therefore leave a thicker barrier-type oxide, covered by a hydrated oxide layer. Both of these layers have little or no magnesium incorporation after the treatment. Deoxidization after alkaline cleaning substantially reduces the total oxide thickness even further, but uses an entirely different chemistry, so the inferred temperature dependence of the thicker oxide after alkaline cleaning may be oversimplified. Using the sputter rate calculated from a Ta_2O_5 sample, the native oxide is calculated to be just over 20nm thick. The oxides left after either chemical cleaning method were thin enough to see metallic contributions in both the Al 2p and KLL spectra, with the Dox sample having the largest metallic contribution, indicating that the oxides were in the range of just a few nanometers after chemical cleaning.

Using the method of Strohmeier[7], treating the Cu 3p contribution and Al metallic lineshape in the manner discussed in Part II of this series, the oxide on the deoxidized sample is calculated to be roughly 3.3nm thick. The same cautions apply as discussed regarding 2024 in Part II, due to effects of the enriched copper layer, beneath the oxide, on metal Al 2p electrons originating in the alloy. It was considered even less appropriate to attempt to use this technique on the alkaline cleaned sample, due to the enriched Zn in the oxide, which would effect the attenuation length in an additional unknown manner. Observing that the oxygen signal in the depth profile of the as-received, native surface persists for approximately 10x that of the deoxidized sample, this seems to correlate to the thickness calculated by the Ta_2O_5 sputter rate. The actual thickness of this oxide is not assumed so straightforward, however. A metallic Al signal was observed even after the first sputter cycle of 300 seconds, although an additional 1500 seconds of sputtering remained before the oxygen signal decreased to even 50% of its maximum value. This discrepancy also arose on as-received 2024 in part II of this series and is quite possibly due to non-uniform coverage by a duplex, Mg containing oxide film, as pointed out by Wefers[5].

Deoxidization fully strips the native, magnesium-containing oxide, whereas less aggressive alkaline cleaning was seen to occasionally leave some magnesium-containing oxide complex on sample surfaces. Fig. 4 only shows the magnesium intensity from a native, acetone-wiped surface, because no appreciable Mg 2p signal was measured on either the Alk or the Dox surfaces that were depth profiled in this set.

All of the summary depth profiles presented here were compiled from total elemental photoelectron peak areas, independent of changes in chemical state. The unique identification of specific chemical states in a complex system, such as that of the alloy oxide after these pretreatments, is not trivial. Due to the nature of certain chemical state changes, some information about the compounds involved in the interface has been gleaned.

The copper 2p spectra from the interface show little variation in binding energy to those from the bulk alloy. Angular depth profiling of a polished [7B] sample, which was then alkaline cleaned, did show some variation in photoelectron binding energy and principal Auger electron kinetic energy for the copper spectra[8]. Unfortunately the designation as a particular chemical state is not straightforward,[9] and no absolute conclusions could be drawn. It does appear that the copper enrichments are in a metallic state, as the spectra are quite similar to those of the copper in the bulk alloy, as well as $CuAl_2$, with a binding energy of 933.9 eV. No satellite structure, as is characteristic of CuO, was observed either. The observation that the maximum copper concentration is evident only after some oxide is sputtered correlates well to a metallic state deposited at cathodic sites on the alloy surface and covered with the expansive aluminum oxide structure. This also correlates with preferential dissolution of aluminum from the matrix, as is the case shown in anodic oxidation studies[10-12], and is the suggested mechanism for enrichment in etching environements[13].

In a similar fashion, the zinc 2p photoelectron and Auger KMM lines showed certain changes with different take-off angle, but failed to give any unique identification. The sputtering depth profile does show two specific states, with the higher binding energy state at 1023.4eV binding energy being removed first. The remaining enrichment has a binding energy of 1021.9eV. This seems to indicate a hydrated (or hydroxylated) oxide on the topmost surface above a non-

hydrated oxide. The take-off angle variations confirmed the two layer observation. The oxide designation seems to be born out in the nature and position of the maximum zinc concentration, with the maximum at the topmost surface and an ever-decreasing amount beneath it. The determination of this chemical state is even more convoluted, due to the fact that mixed zinc-aluminate structures have binding energies very similar to those of metallic zinc.[14]

The chemical state of aluminum on the surface also has a multitude of possible configuration designations. The state in the hydroxylated outer layer corresponds to various mineral phases such as AlO(OH) (boehmite), Al(OH)$_3$, having a modified Auger parameter of 1460.6 on the acetone cleaned surface and 1461.4 on both the Alk and Dox surfaces. The exact chemistry is difficult to distinguish because many of the mineral phases have values in this same range.[14] Spectra from the non-hydrated barrier region of the oxide indicate possible combinations of Al$_2$O$_3$ and MgAl$_2$O$_4$ (spinel) on the native surface, with a modified Auger parameter of 1461.7. The non-hydrated region appears mostly comprised of Al$_2$O$_3$ on the chemically cleaned surfaces, possibly a zinc aluminate in the case of alkaline cleaning alone. When capped with a plasma polymer, depth profiles show that the state of the aluminum is seen to be consistent with the many oxides, as well as mixed states with plasma film components.

Effect of Initial Cleaning and Plasma Polymer Deposition: Polarization Resistance (R$_p$) Measurements

Linear polarization resistance (R$_p$) is defined as the charge transfer resistance of the solution-metal interface. The linear polarization technique was employed to measure the R$_p$ values of the Al alloy surfaces after different pretreatments. In the present study, polarization resistance (R$_p$) was used to evaluate the effect of chemical cleaning and plasma polymer coating on corrosion resistance of [7B]. Each panel was masked with insulating tape so as to only expose a square region of dimension 3cm by 3cm to the electrolyte aqueous salt solution (aqueous salt solution of 0.5% NaCl + 0.35% (NH$_4$)$_2$SO$_4$).

Fig. 5 shows the polarization resistance of [7B] with pretreatments of acetone wiping, alkaline cleaning, deoxidization, and plasma polymer deposition. Whereas deoxidized (Dox) surfaces show a level of polarization resistance similar to that of acetone-wiped (Ace) surfaces of this alloy, the polarization resistance of alkaline-cleaned (Alk) surfaces is dramatically lower. This decreased R$_p$ value on Alk surfaces correlates to the observation of higher Zn concentrations remaining on the surfaces after the Alk pretreatment. Although the Cu concentration is slightly higher after Dox than Alk, the Zn enrichment is eliminated after the deoxidization step. Something associated with this higher Zn concentration on the Alk surfaces seems to decrease the polarization resistance of these surfaces.

Deoxidized surfaces of [7B] with a plasma polymer coating ([7B] (Dox)/T) showed higher polarization resistance than the chemically deoxidized surfaces without a plasma polymer. This indicates the added corrosion resistance offered by plasma polymer films is much higher than that of the barrier type oxides, formed after chemical cleaning, alone. As compared to the chromate conversion coated surfaces ([7B] CC), the deoxidized and plasma polymer coated ([7B] (Dox)/T) surfaces showed higher R$_p$ values, suggesting that these surfaces have higher corrosion resistance.
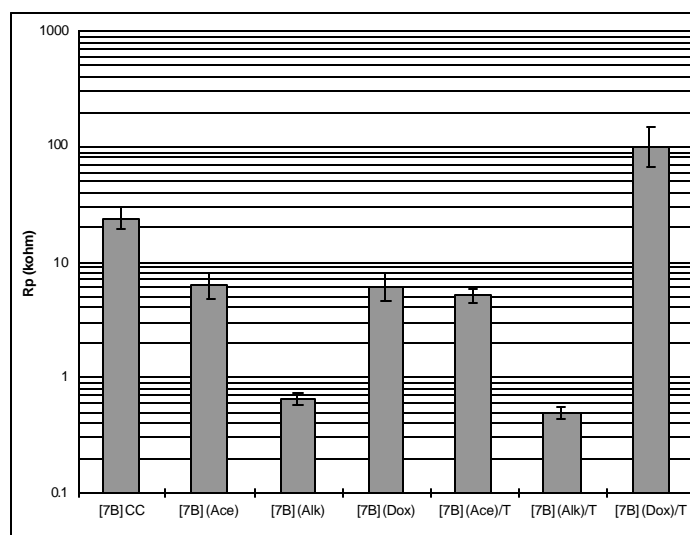
Figure 5. Polarization resistance of 3cm x 3cm exposed regions of AA 7075-T6 ([7B]) panels with different chemical pretreatments and plasma polymer coated surfaces.

Corrosion Protection Characteristics: Evaluated by SO_2 and Prohesion Salt Spray Tests

Two types of corrosion evaluation tests, SO_2 and prohesion salt spray, were employed for the evaluation of corrosion protection characteristics of the plasma systems on [7B]. The SO_2 salt spray test was chosen to speed up differentiation of the corrosion resistance of the various systems investigated. The prohesion test, which is a chemically milder test than the SO_2 salt spray test, was conducted for a longer period, 2000 hours; it is considered a more realistic test, as it better simulates actual service conditions.

Fig. 6 & 7 show typical scanned images of SO_2 and prohesion salt spray tested [7B] panels, respectively. Visual observation of these images reveals that the plasma modified panels of [7B] have outperformed both control panels in the SO_2 salt spray test. These plasma film combinations were prepared on deoxidized [7B] surfaces without any plasma cleaning pretreatment. Fig. 6 also shows an image of a panel that had simply been deoxidized prior to the application of E-coat, which performed excellently in the SO_2 salt spray test.

Prohesion salt spray tested panels in Fig. 7 show that [7B] (Alk/AH)/T/E and [7B] (Alk/O)/TH/E systems performed comparably to the controls. Deft primer coated control panels ([7B] CC/A) displayed extensive pitting corrosion away from the scribe in both tests, indicating that Deft primer may have poor barrier properties. This pitting corrosion away from the scribe was observed on both controls when examined by scanning electron microscopy (SEM).

Observations concerning the pitting corrosion away from the scribe are presented in the latter part of this section. The deoxidized surface in Fig. 6 & 7 shows good corrosion performance when only coated with cathodic E-coat after the chemical treatment, without any plasma polymer deposition. This corrosion resistance was comparable to that of primer coated control panels. Fig. 8 & 9 show the ascending order of average corrosion widths of the various panels after prohesion and SO_2 salt spray testing, respectively.
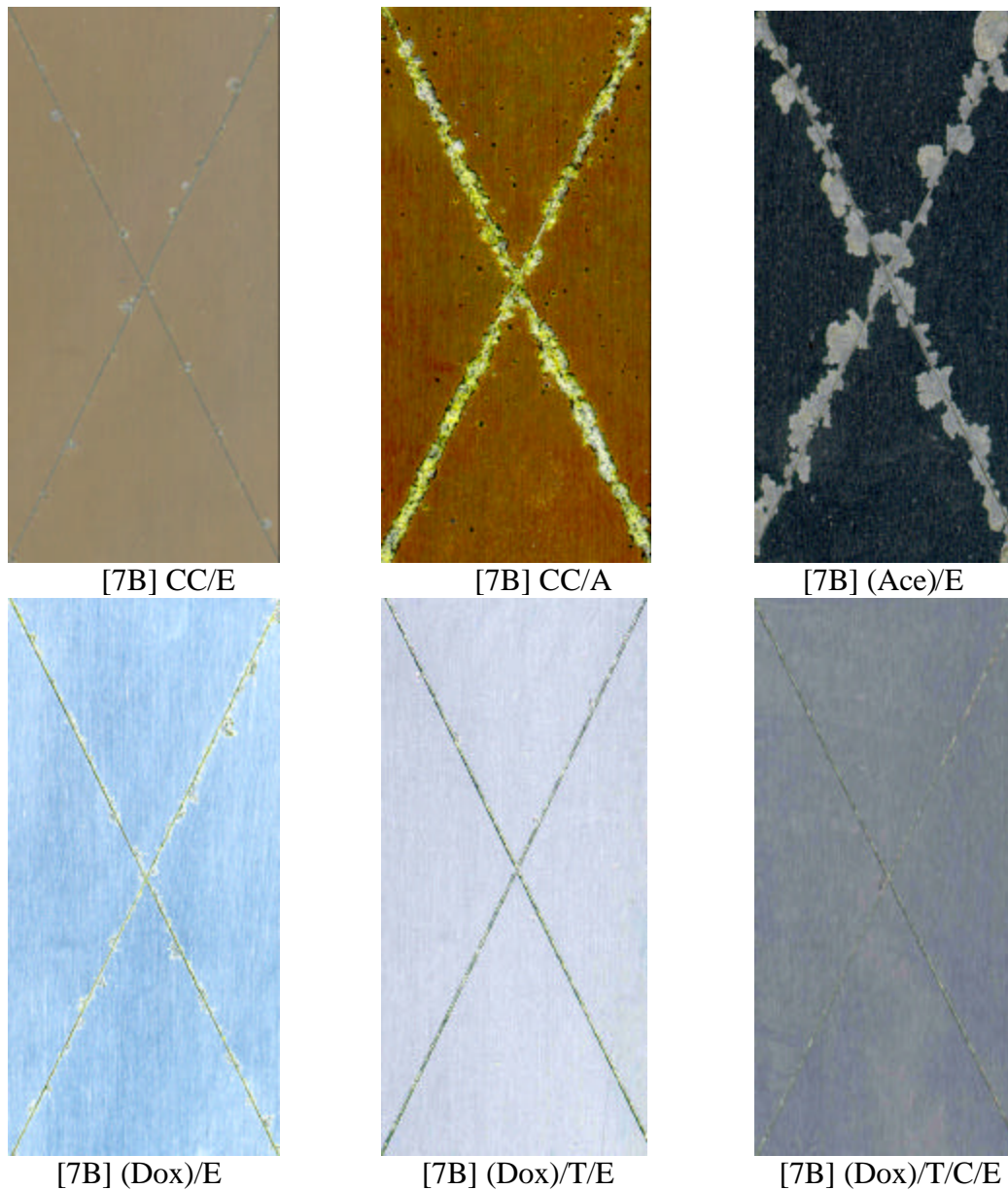
[7B] CC/E	[7B] CC/A	[7B] (Ace)/E
[7B] (Dox)/E	[7B] (Dox)/T/E	[7B] (Dox)/T/C/E

Figure 6. Scanned images of SO_2 salt spray tested (4 Weeks) panels of AA 7075-T6 ([7B]). Total scanned area is 27 cm^2 and total scribe length within the scanned area is 16 cm.

The corrosion widths of samples with a direct application of plasma polymer to deoxidized [7B] panels with no extended plasma cleaning (Series-V samples) displayed corrosion performance superior to that of both controls in SO_2 salt spray testing. Prohesion salt spray tested panels of several modified systems showed corrosion widths comparable to those of the controls.

Fig. 8 & 9 indicate that corrosion performance improves with most of the panels employing plasma films as compared to acetone-wiped, E-coated panels, but some of the plasma modified samples have inferior corrosion performance to just acetone-wiped surfaces. The corrosion performance of deoxidized surfaces with an applied plasma polymer film in the SO_2 salt spray

test is clearly better than that of the alkaline-cleaned surfaces with the same plasma polymer coating. This could be due to the reduction of Zn concentrations on the deoxidized surfaces (XPS results in Fig. 4).
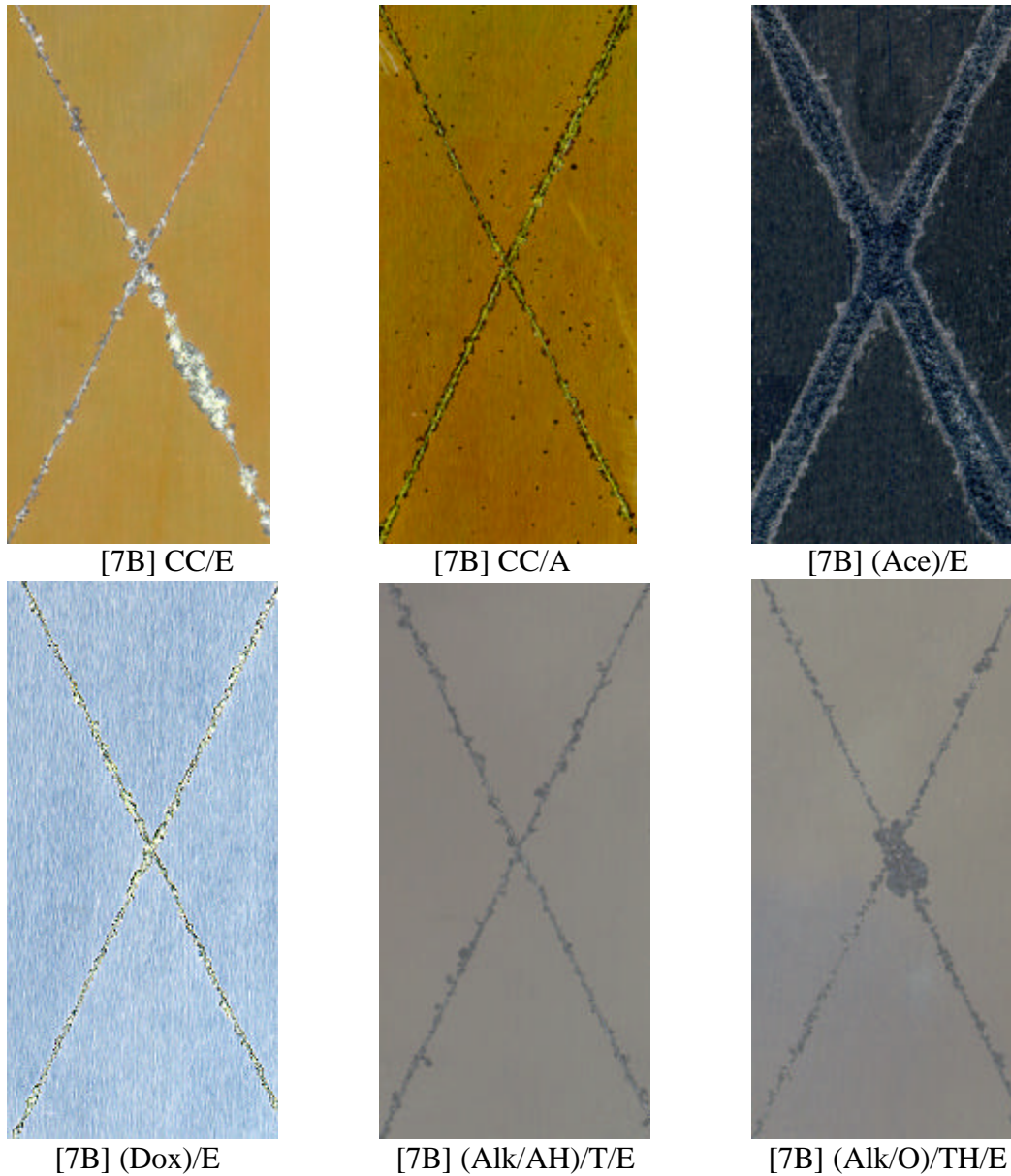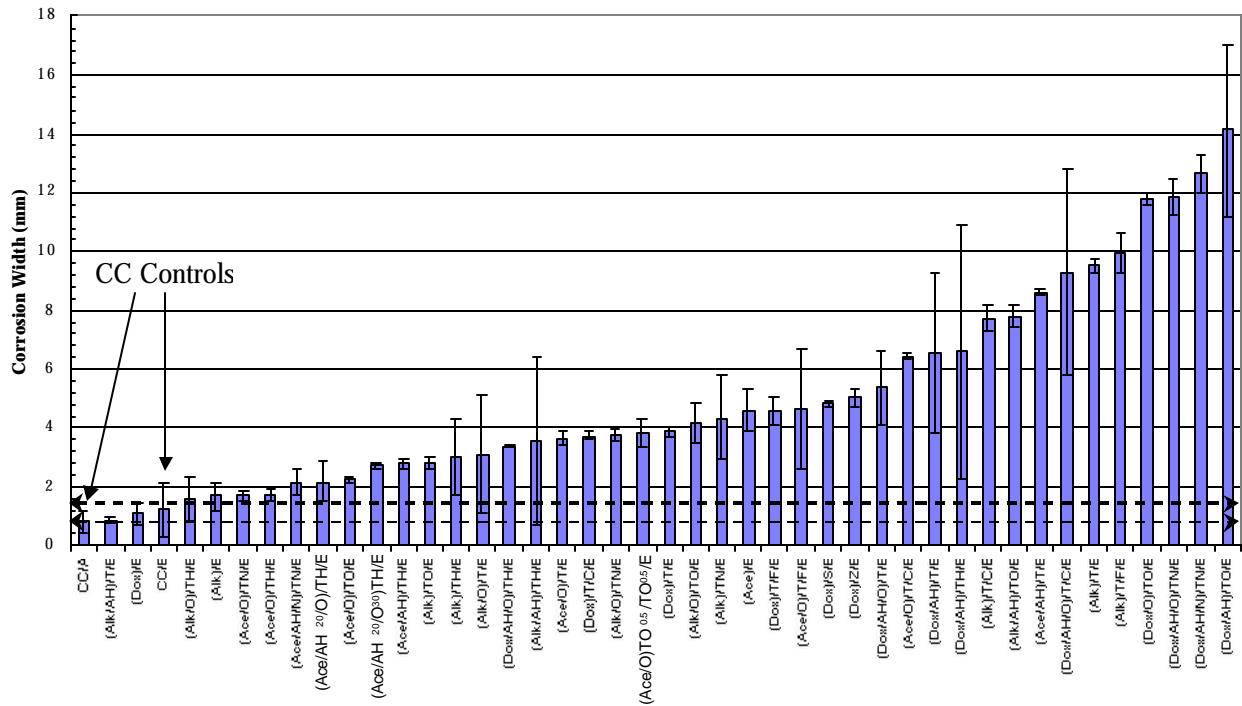

[7B] CC/E	[7B] CC/A	[7B] (Ace)/E
[7B] (Dox)/E	[7B] (Alk/AH)/T/E	[7B] (Alk/O)/TH/E

Figure 7. Scanned images of prohesion salt spray tested (12 Weeks) panels of AA 7075-T6 ([7B]). Total scanned area is 27 cm^2 and total scribe length within the scanned area is 16 cm.

Figure 8. Average corrosion widths of prohesion salt spray tested (12 weeks) control, acetone-cleaned, alkaline-cleaned, and various plasma modified AA 7075-T6 ([7B]) systems.
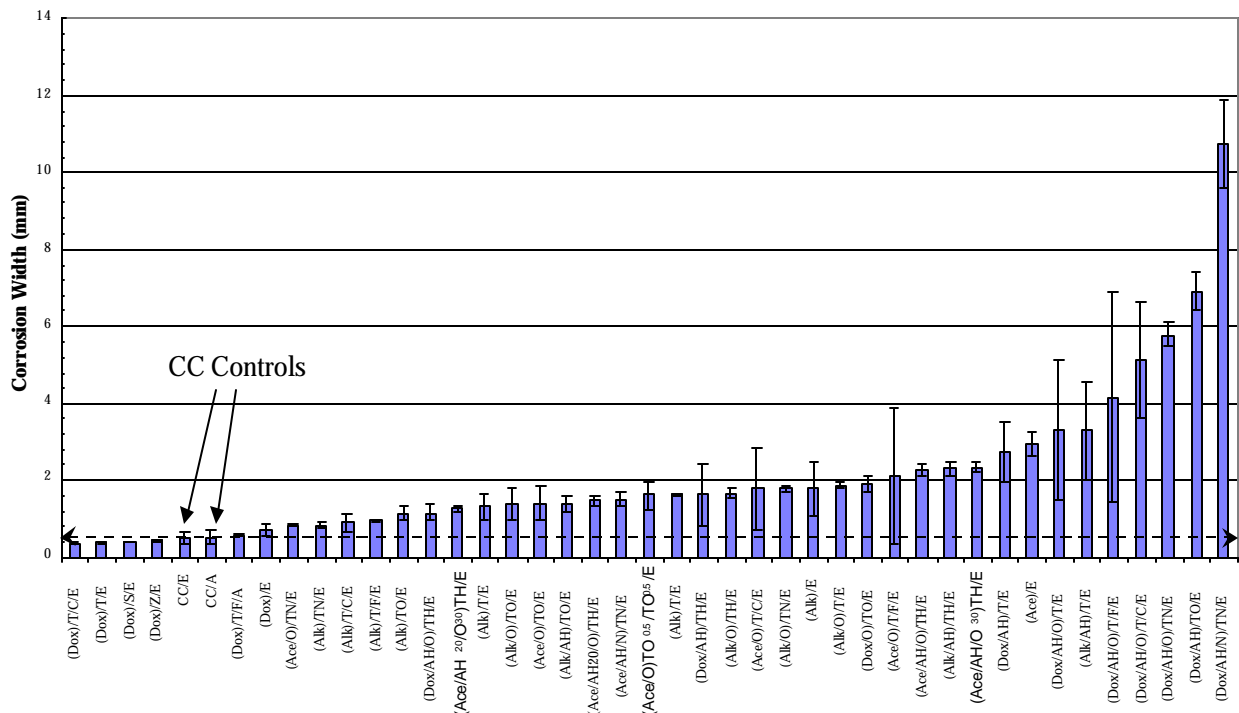
Figure 9. Average corrosion widths of SO_2 salt spray tested (4 weeks) control, acetone-cleaned, alkaline-cleaned, and various plasma modified AA 7075-T6 ([7B]) systems.

Though the Cu concentration is higher than that on acetone-wiped surfaces, the Mg concentration on both alkaline-cleaned and deoxidized surfaces is much lower. These results indicate that reduction of Zn as well as Mg concentrations from the surface oxide greatly improves the corrosion performance of [7B].

It is clear from the figures that most of the plasma polymer coated, deoxidized [7B] panels (Series-V samples) have outperformed both controls in the SO_2 salt spray test. There are several of the modified systems with corrosion performance in the prohesion salt spray test comparable to that of the controls.

Correlation of SO_2 and Prohesion Salt Spray Tests

Fig. 10 shows a comparison of the corrosion performance of samples in both SO_2 and prohesion salt spray testing. The corrosion performance results for both tests roughly correlate linearly with few exceptions. Thus, if the corrosion performance of a plasma system is good in SO_2 testing, its performance is also good in prohesion testing.

Series-I samples, with acetone-wiped surfaces and an extended plasma pretreatment, either O_2 or $Ar+H_2$, and having a plasma polymer deposited on top of these plasma-pretreated surfaces, showed large corrosion widths as compared to the control panels (CC/A and CC/E in Fig. 10). Extended plasma pretreatment was found to heat substrate panels to more than 250°C in the D.C. reactor used in this study. This heating has been associated with the migration of Mg into the interface oxide, as discussed in part II of this series. Heating from extended plasma pretreatment is also seen to drive similar Mg enrichment of the interface oxide on [7B] as seen in Fig. 11, where progressively longer $Ar+H_2$ plasma pretreatment times were used in a slightly different D.C. reactor. The modifications to this reactor were such that the flux was different than in the specific reactor used in the corrosion study.

The temperature changes were a different function of plasma time, but temperature effects on the Mg migration were consistently observed in several experiments. This was observed on panels where the Mg-rich, native oxide had been stripped with chemical cleaning prior to the plasma film deposition. Similar thermal migration has been related to the formation of magnesium containing oxide channels in the aluminum oxide.[5] Oxides of magnesium are more soluble in caustic environments than pure oxides of aluminum,[15] thus allowing corrosive solutions to more readily penetrate the protective oxide and reach the underlying alloy, destabilizing the interface.[13,16,17] The extended plasma cleaning of panels that were only acetone cleaned in advance likely contributes significantly to the poor performance of the series-I samples, due to enhancement of the Mg concentration in the already Mg rich native oxide, additional defects created by the sputtering, and any precipitation of copper phases related to increased aging of the alloy from the temperature increase. Although the corrosion widths are larger than those of the controls, there was no pitting corrosion away from the scribed plasma polymer modified surfaces of Series-I samples.

Series-II employed chemical treatment along with plasma pretreatment, which again resulted in poor performance of these systems on this alloy (Fig. 10). Series-II plasma films on [7B] demonstrated diminished performance on both (Dox) and (Alk) chemically pretreated surfaces as compared to Series-I samples. As just mentioned, the heat-induced magnesium migration into the

surface oxide during extended plasma pretreatment on both Dox and Alk surfaces correlates to their hindered corrosion resistance.

Series-III samples were prepared to see the effect of cathodic E-coating voltage on corrosion protection performance of [7B] with plasma pretreatments and plasma polymer coatings employed in Series-II samples. Quite similar to the results shown in Part II,[2] the samples with the same plasma treatments and plasma coatings have very similar corrosion performance in both Series-II and Series-III regardless of the E-coating voltage difference, so the corrosion test results of Series-III samples were not shown in Fig. 10.

Alkaline cleaning of [7B] showed a somewhat negative effect on the performance of the plasma modified specimens in prohesion salt spray testing, whereas deoxidization showed a definite increase in the corrosion protection offered in SO_2 salt spray testing. The poor performance of Series-IV coatings is attributed to the higher Zn concentration on alkaline-cleaned [7B] surfaces, as exemplified by the XPS surface analysis results discussed earlier. Series-V samples, which were prepared by omitting the plasma pretreatment with O_2 or $Ar+H_2$ and depositing plasma polymers directly on deoxidized [7B] surfaces, outperformed both controls in SO_2 salt spray testing. Prohesion salt spray tested panels with Series-V coatings have corrosion widths comparable to those of the E-coated controls (CC/E), but they did not perform as well as the Deft primer coated controls (CC/A).

Pitting Corrosion Away from the Scribe on [7B] CC/E and [7B] CC/A Panels

Pitting corrosion away from the scribe was observed on almost all panels of both controls tested alongside plasma interface engineered [7B] systems. The pitting corrosion area was determined through image analysis and SEM analysis.

The CC/A and CC/E panels exposed to SO_2 and prohesion salt spray testing displayed numerous pitting corrosion areas away from the scribed surface which were visible to the unaided eye. The panels with pitting corrosion were scanned over a small portion (2×2 cm^2) of the surface. These scanned pictures were used in calculating the percent area of pits using OPTIMAS 6.1 software. Representative pictures of these surfaces are shown in Fig. 12. As seen from Fig. 12, the absence of pitting corrosion on the plasma-modified surface confirms that the plasma polymer coated surfaces overcome pitting corrosion away from the scribe by offering a good water-insensitive adhesion of the E-coat.

The scanned images of the tested panels did not reveal smaller features such as micro pits (those on the order of microns in size). Therefore, to investigate the micro-pitted areas on control as well as on plasma polymer coated panels, further study of pitting corrosion was made by SEM. The sample surfaces used for SEM analysis evinced no pits visible to the unaided eye. Fig. 13 & 14 show comparative SEM pictures of these areas. Evident in these pictures are several pits up to a few microns in size on the [7B] CC/E and [7B] CC/A control surfaces. In contrast, [7B] (Dox)/T/E panels did not show any pitting corrosion after both SO_2 and Prohesion salt spray tests.
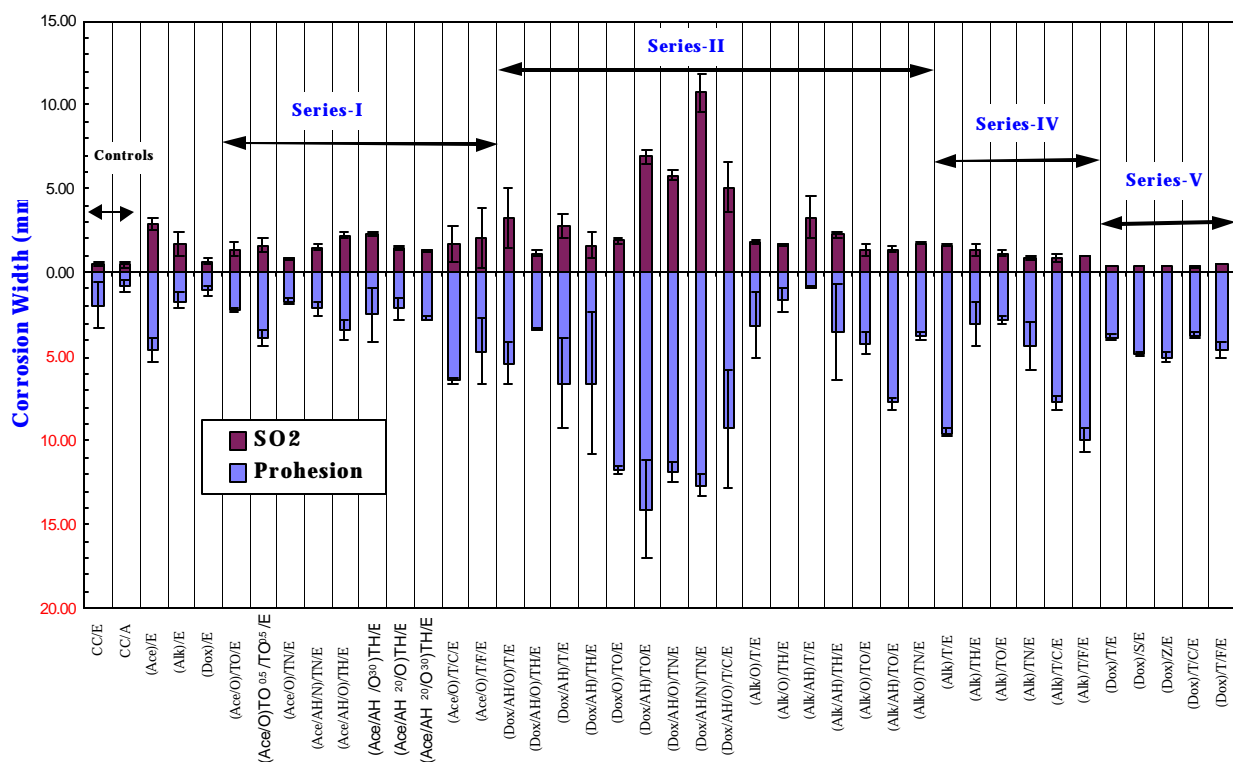
Figure 10. Comparison of average corrosion widths of different sample series used in the plasma interface engineering of AA 7075-T6 ([7B]) and the controls after prohesion salt spray testing (12 weeks) and SO$_2$ salt spray testing (4 weeks). Series-I: no wet chemical process and with plasma pretreatment, E-coating voltage 250 V; Series-II: with wet chemical cleaning and plasma pretreatment, E-coating voltage 250 V; Series-IV: with (Alk) cleaning but no plasma pretreatment, E-coating voltage 200 V; Series-V: with (Dox) but no plasma pretreatment, E-coating voltage 200 V.

 Mechanism of Corrosion Protection of Al Alloys by Low Temperature Plasma Interface Engineering Systems

As was the case for AA2024-T3 ([2B]) in part II of this series,[2] the adhesion performance of cathodic E-coat on plasma polymer coated [7B] could not be differentiated by the conventional tape test (ASTM D3359-93B), since E-coat on all of the combinations of plasma polymers achieved the maximum tape test rating. So, the adhesion characteristics of the cathodic E-coat were again evaluated by the N-methylpyrrolidinone (NMP) paint delamination method.[18] Similar to combined systems on [2B], NMP paint delamination was not observed after 120 minutes for E-coat on plasma polymer coated [7B] as compared to a maximum time for complete delamination of 5 minutes for E-coat on the chromate conversion coated [7B] controls.[19] This extremely strong adhesion evidently plays a crucial role in the excellent corrosion protection performance of plasma interface engineered [7B] systems.
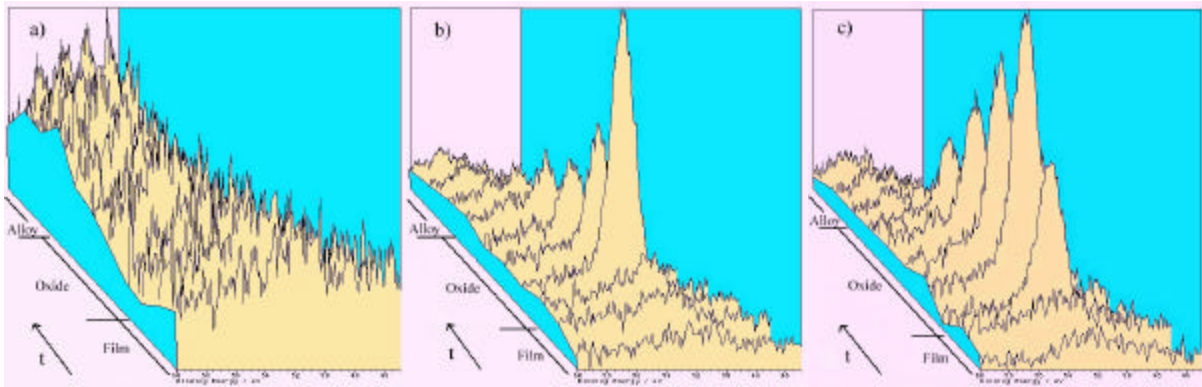
Figure 11. Mg 2p spectra from depth profiles through plasma film, oxide, and into the alloy substrate for alkaline-cleaned, deoxidized substrates with a) 5 minutes, b) 10 minutes and c) 20 minutes of argon/hydrogen plasma pretreatment prior to film deposition. These show Mg migration into the oxide layer due to heating during extended plasma pretreatment. The arrow indicates the evolution as a function of sputtering time. The spacing between spectra is not linear but rather a spectral index that is consistent between samples.
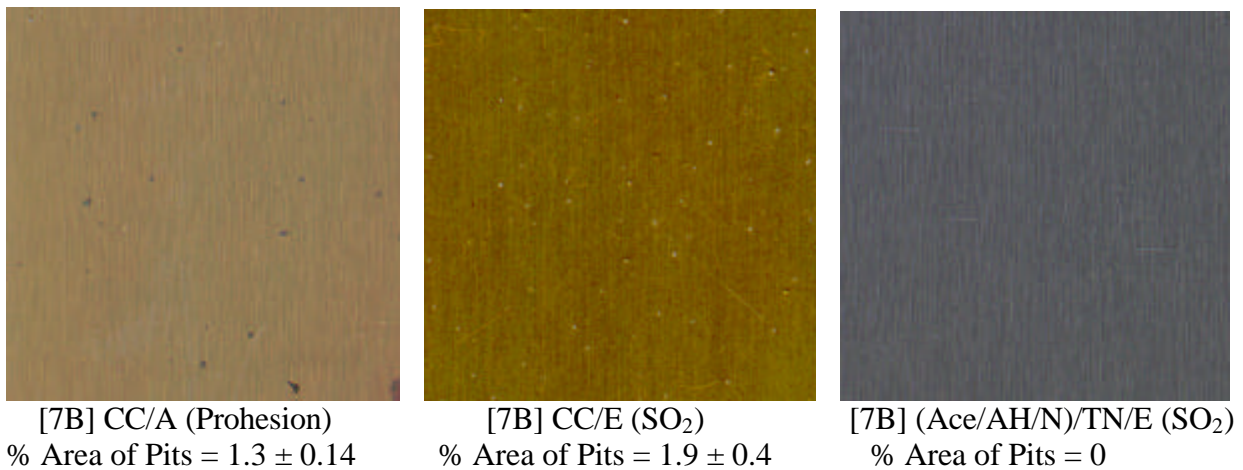
[7B] CC/A (Prohesion)	[7B] CC/E (SO$_2$)	[7B] (Ace/AH/N)/TN/E (SO$_2$)
% Area of Pits = 1.3 ± 0.14	% Area of Pits = 1.9 ± 0.4	% Area of Pits = 0

Figure 12. Scanned pictures of corrosion-tested panels showing pitting corrosion areas away from the scribed surface of chromate conversion coated controls and plasma coated AA 7075-T6 ([7B]).

As discussed in Part II of this series,[2] there are at least five important factors to be considered in the corrosion protection of an Al alloy panel with a good barrier coating system as a whole: (i) salt intrusion resistance of the top surface; (ii) barrier properties of the bulk phase of the coating; (iii) type and nature of passivating agents, if any; (iv) adhesion characteristics of the coating-metal interface; and (v) the surface state (i.e. pure aluminum oxide, mixed oxides, chromium oxide or plasma polymers) of the metal substrate.
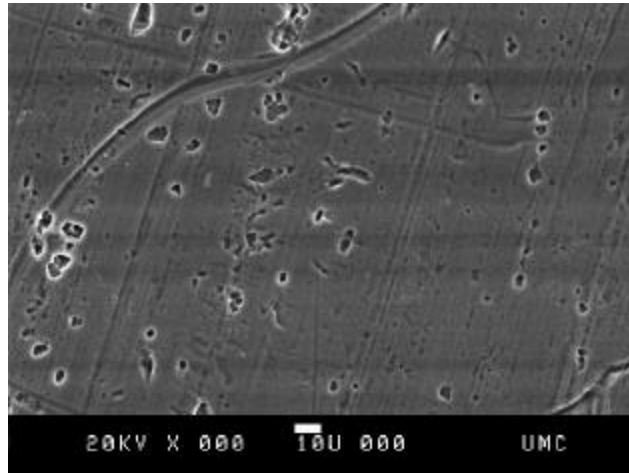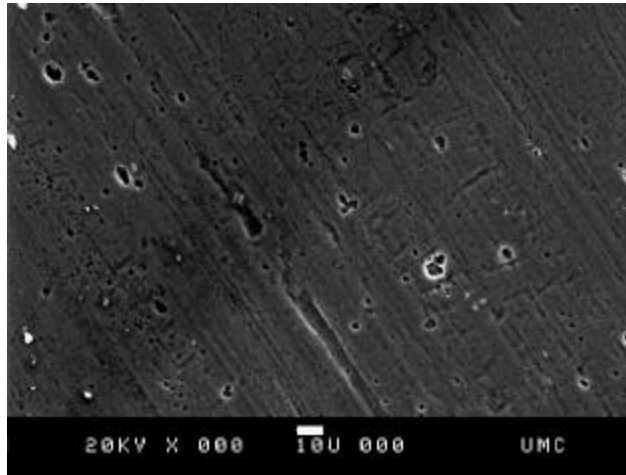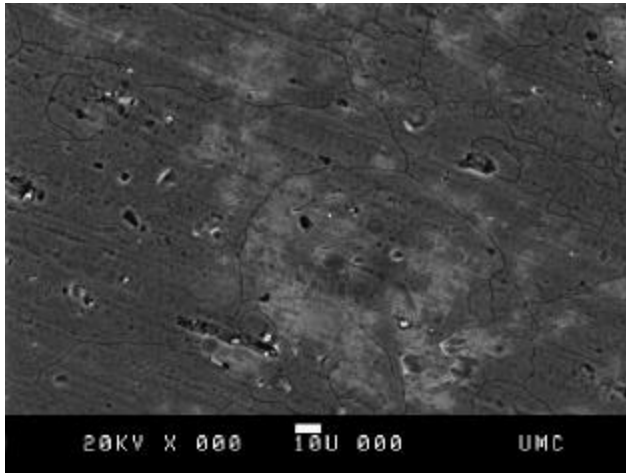
[7B] CC/E
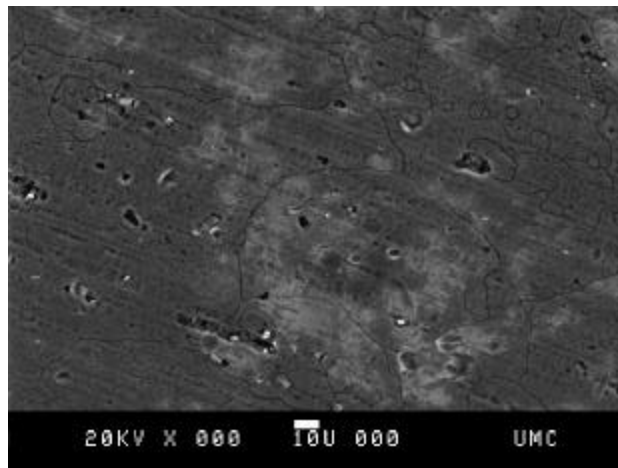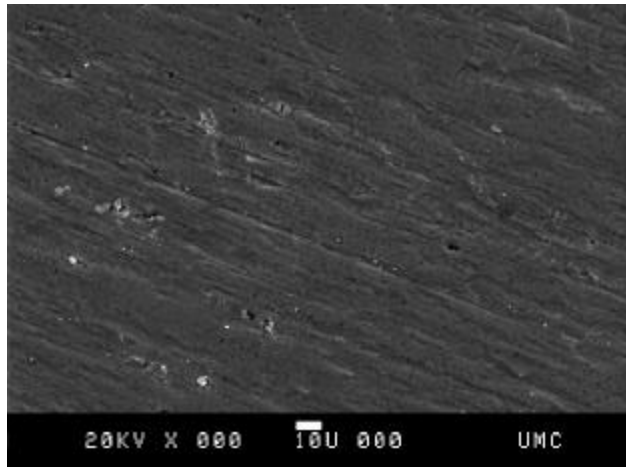

[7B] CC/A
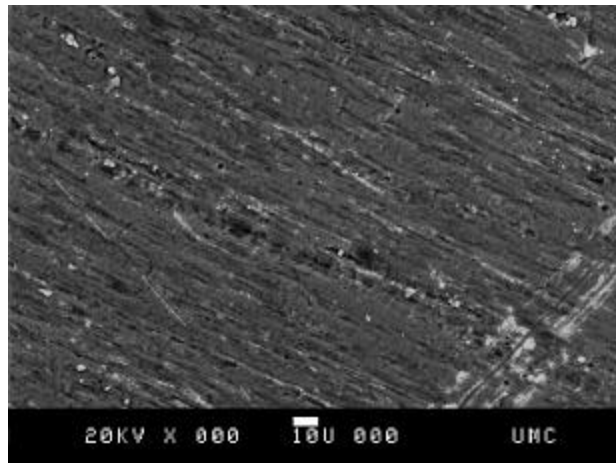
[7B] (Dox)/T/E

Figure 13. SEM pictures of SO_2 salt spray tested panels of AA 7075-T6 ([7B]) after primer coatings were stripped off.

[7B] CC/E

[7B] CC/A

[7B] (Dox)/T/E

Figure 14. SEM pictures of Prohesion salt spray tested panels of AA 7075-T6 ([7B]) after primer coatings were stripped off.

 The salt intrusion resistance of the top surface (Factor i) of E-coat deposited on plasma modified [7B] systems is not different from that of the top surface of E-coat deposited on a chromate conversion coated system. Therefore, the salt intrusion characteristics are likely to be similar in both systems. This means, in either case, the same contribution will be made from this factor to the corrosion protection system. Additionally, in the plasma polymer modified systems there is no passivating or sacrificial agent employed in any of the processes in the development of a corrosion protection system using E-coat as the top layer. Thus, a passivating agent (Factor iii) is not a factor contributing to the good corrosion protection properties of these systems.

Consequently, the main reasons for the good corrosion protection properties of the plasma interface engineered [7B] systems must lie in the remaining three factors. As seen from corrosion test results, plasma polymer coated systems provided excellent corrosion resistance after scribing and did not allow pitting corrosion away from damaged surface area (scribe). Among the remaining three factors, therefore, the strong adhesion and durability of the entire interface system evidently played a crucial role in the corrosion protection of [7B].

In a damaged (scribed) corrosion protection system, the wet adhesion of a coating becomes the most important factor, because both liquid water and corrosive species attack the interface. A water-delaminated coating layer does not provide any corrosion protection. Thus, water-insensitive adhesion of a coating to a substrate is a mandatory requirement for the prevention of corrosion-induced delamination.

The plasma polymer coated systems showed no pitting corrosion away from damaged surface area (scribe), suggesting that such systems have good undamaged surface corrosion resistance characteristics. In an undamaged corrosion protection system, all chemical species involved in the corrosion of the substrate metal, such as H_2O, O_2, and Cl^-, must permeate through the barrier. Therefore, the permeability of the coating seems to be a dominant factor for pitting corrosion.

When water molecules permeate through the coating and reach the interface, the adhesion of a coating becomes a crucial factor in an undamaged corrosion protection system. Water permeates through a flawless polymer layer by the diffusion of dissolved individual molecules but not as bulk (liquid) water. In general, water molecules that reach the interface have a stronger association with conventional polymers and also with the metal surface than the adhesive interaction between the conventional polymer coating and the metal, leading to localized de-laminations of the coating. Once a void is formed at the interface, water tends to cluster together to form liquid phase water. Water-insensitive adhesion is crucial in the prevention of this phenomenon. It is important to recognize that it is impossible to prevent transport of water within an organic polymer layer. It is simply a time dependent-event, determined by the water transport resistance of the coating.

In an undamaged corrosion protection system, the corrosion characteristics of the surface of the substrate (i.e., pure aluminum oxide, mixed oxides, chromium oxide, or plasma polymer) become important as enough water and corrosive species reach the interface. Corrosion becomes the driving force for the de-lamination of a coating and the propagation of surface corrosion only after the transport of corrosive species to the coating-metal interface and the creation of micro-voids. The extremely strong adhesion at coating-metal interface achieved by plasma interface

engineering evidently could prohibit the creation of micro-voids at the interface and hence protect the metal from corrosion.

It is interesting to point out that pit-corrosion away from the scribe lines were observed with both controls; i.e., E-coat on CC and Deft chromated primer on CC, probably reflecting the weaker adhesion compared to plasma interface engineered samples. The more pit-corrosions were found with the spray primer, which turned out to be the best performer (the smallest corrosion width) in Prohesion salt spray test. In this case the corrosion inhibitor is indeed working, but cannot stop pit-corrosions under the un-damaged coating. For effective corrosion inhibition, the coating should be loose enough to allow efficient movement of inhibitor, which is a contradicting requirement for being a good barrier. When the corrosion under an undamaged coating becomes an important issue, a corrosion protection system based on the tenacious water-insensitive adhesion by SAIE has advantages over conventional approaches with corrosion inhibitors.

Conclusions

The results obtained in this study indicate that the corrosion protection of [7B] depends on three major factors, the stability of the metal surface, the barrier characteristics of the primer film, and the adhesion of the polymer primer film to the substrate. Good corrosion protection was obtained with strong adhesion of cathodic E-coat to plasma polymer coated surfaces prepared on deoxidized alloy panels. The native, as-received surface of this alloy is largely composed of magnesium-containing oxides, which appear to decrease the corrosion resistance of the surface. Chemical cleaning of [7B] by alkaline cleaning is seen to leave enriched Cu and Zn concentrations on the surface and a deoxidization procedure enhances the Cu enrichment while removing the Zn enrichment. Similar results regarding removal of enriched Mg and the enrichment of Cu in etching solutions have been observed, with similar conclusions drawn regarding the effect of the Mg containing oxide on corrosion in adhesive bonding[13]. Although the Mg concentration on alkaline-cleaned surfaces is comparable to that on deoxidized surfaces, the deoxidizing process removes the enriched zinc levels left in the oxide on the alkaline-cleaned surfaces. It is not clear whether the superior corrosion resistance of the deoxidized surface results from a thinner passive film, with less defects due to removal of the zinc enrichment, or from reduced chemical activity promoted by the removal of the zinc enrichment.

Plasma polymers provide good water-insensitive adhesion, which prevents corrosion from creeping into the interface. Good water-insensitive adhesion of the plasma polymers prevents corrosion of the undamaged surfaces, whereas the control panels display pitting corrosion in undamaged areas away from the scribe. It is also important to recognize that E-coat applied to deoxidized [7B] showed excellent corrosion protection with no pit-corrosion away from the scribe lines. This is another example of SAIE prepared corrosion protection system, again emphasizing the importance of water-insensitive adhesion in corrosion protection.

Reference

1. C. M. Reddy, Q. Yu, H. K. Yasuda, C. E. Moffitt, D. M. Wieliczka, R. Johnson and J. E. Deffeyes, "Improved Corrosion Protection of Al Alloys by Low Temperature Plasma Interface Engineering: Part I-Alclad 2024-T3 ", submitted to *Corrosion*.
2. C. M. Reddy, Q. Yu, H. K. Yasuda, C. E. Moffitt, D. M. Wieliczka, R. Johnson and J. E. Deffeyes, "Improved Corrosion Protection of Al Alloys by Low Temperature Plasma Interface Engineering: Part II-AA 2024-T3 ", submitted to *Corrosion*.
3. L. L. Shreir, R. A. Jarman, and G. T. Burstein eds. Corrosion, 3rd ed. (Buttersworth-Heinemann, Jordan Hill, 1994) Vol. 1, Chap. 4.
4. E. McCafferty and J.P. Wightman, Surface and Interface Analysis, **26** (1998) p. 549.
5. K. Wefers, *Aluminum*, **57** (1981) p. 722.
6. J. R. Davis ed., ASM Metals Handbook, 9th Edition, Volume 13: Corrosion (American Society of Metals, 1987) p. 583.
7. B.R. Strohmeier, Surf. and Interface Anal., 15 (1990) p. 51-56
8. C. E. Moffitt, D. M. Wieliczka, and H. K. Yasuda, Proceedings of the Air Force Research Laboratory's Workshop on Advanced Metal Finishing Techniques for Aerospace Applications, (Keystone, Colorado, 1998) submitted to Surf. Coat. Technol.
9. B. R. Strohmeier, D. E. Leyden, R. S. Field, and D. M. Hercules, J. Catalysis, **94** (1985) p. 514.
10. H. Habazaki, K. Shimizu, P. Skeldon, G. E. Thompson, G. C. Wood and X. Zhou, Trans IMF, **75** (1997) p.18-23.
11. X. Zhou, G. E. Thompson, H. Habazaki, K. Shimizu, P. Skeldon, and G. C. Wood, Thin Solid Films, **293** (1997) p. 327-332.
12. H. Habazaki, M. A. Paez, K. Shimizu, P. Skeldon, G. E. Thompson, G. C. Wood and X. Zhou, Corrosion Sci., **38** (1996) p. 1033-1042.
13. T. S. Sun, J. M. Chen, J. D. Venables, and R. Hopping, Appl. Surf. Sci., **1** (1978) p. 202-214.
14. C.D. Wagner. in Practical Surface Analysis, 2nd Ed., Vol. 1, D. Briggs and M. P. Seah eds. (Wiley 1990) p. 595.
15. Handbook of Chemistry and Physics, 66th ed., R. C. Weast ed. (CRC press, 1985) B-69, B-111.
16. M. Textor and R. Grauer, Corrosion Sci., **23** (1983) p. 41-53.
17. A. J. Kinloch in Polymer Surfaces and Interfaces, eds. W. J. Feast and H. S. Munro (Wiley, New York, 1987) p. 75-97.
18. W. J. van Ooij and A. Sabata, "Effect of paint adhesion on the underfilm corrosion of painted precoated steels," CORROSION/91 (Houston, TX, NACE, 1991) Paper No. 417.
19. R. G. Buchheit, M. D. Bode, and G. E. Stoner, Corrosion, **50(3)** (1994) p. 205-214.

7. Improved Corrosion Protection of Al Alloys by System Approach Interface Engineering: Part IV; Spray Paint Primer Coated Al Alloys

Q. S. Yu, C. M. Reddy, C. E. Moffitt, D. M. Wieliczka, J. E. Deffeyes, and H. K. Yasuda

Abstract

This study investigates the development of a chromate-free coating system for the corrosion protection of aluminum alloys based on the concept of system approach interface engineering (SAIE) by chemical and plasma techniques. The aluminum alloys investigated include AA2024-T3 ([2B]), AA7075-T6 ([7B]), Alclad 2024-T3 ([2A]), Alclad 7075-T6 ([7A]), Plate stock AA2124-T851 ([2P]), and Plate stock AA7050-T7451 ([7P]). Direct current (DC) cathodic plasma processes were used to enhance the bonding to and the protection offered by spray paint primers on aluminum alloys. Besides anode magnetron enhancement, the DC cathodic plasma processes were also operated with the anode assembly removed of, a more practical approach for industrial applications. With appropriate application, DC cathodic plasma coatings provided not only a corrosion resistant layer on aluminum alloy surfaces but also excellent adhesion bases for spray paint primers, including both chromated and non-chromated water borne primers. When tested by sulfur dioxide (SO_2) salt spray and Prohesion salt spray tests, most of these plasma modified coating systems showed excellent corrosion protection characteristics. All the **chromate-free (water born)** coating systems based on the SAIE concept outperformed or performed comparably to the chromated controls used in this study (i.e. chromate conversion coated and then chromated primer coated aluminum alloys). In contrast, many of the plasma coating systems based on **chromated** primers showed more corrosion on AA2024-T3 ([2B]) and AA7075-T6 ([7B]) as compared to their controls. The chromated primer coated AA2024-T3 ([2B]) and AA7075-T6 ([7B]) showed severe pitting corrosion away from the scribed lines in both SO_2 and Prohesion salt spray tests, which were scarcely observed, and in most of the cases did not occur, on **non-chromated** primer coated aluminum alloys with the plasma surface modification.

Introduction

This section is a follow-up to three series sections [1-3] dealing with system approach interface engineering (SAIE) by means of chemical and (low temperature) plasma techniques. The project is aimed at achieving improved corrosion protection of aluminum alloys, used for the production of aircraft, without using heavy metal-containing chemistries such as chromate conversion coatings and chromated primers. The main objective of the study was to find alternative corrosion protection methods by means of a more environmentally benign process, eliminating health concerns and environmentally hazardous materials from corrosion protection systems.

The aluminum alloys that have been investigated in our previous studies, including [2B], [7B], and [2A], are materials used for aircraft skins. Aircraft skins are readily accessible for inspection and conventional repair, but various internal structural components are neither easily accessible nor easily remedied after the onset of corrosion. Because of the tenacious adhesion of plasma

coatings, plasma processes may be more useful in difficult to inspect/repair areas, i.e., internal structures of an aircraft. Thus this method is aimed at the corrosion protection of detailed parts rather than easily accessible aircraft skin. The potential long service-life protection offered by these plasma-based systems appears to fit well with the needs of particular detailed parts and internal structural components that cannot be addressed in standard maintenance cycles. Therefore, another two aluminum alloys, i.e., Plate stock AA2124-T851 ([2P]) and Plate stock AA7050-T7451 ([7P]), which are usually used for internal structural parts of aircraft, were introduced and investigated in the present study.

The previous three series papers[1-3] have investigated the SAIE coating systems that were based on a cathodic electrodeposited, chromate-free epoxy-based primer (E-coat) on Alclad 2024-T3 ([2A]), AA2024-T3 ([2B]), and AA7075-T6 ([7B]). This paper deals with spray paint primer coated aluminum alloys by employing the SAIE concept. The use of non-chromated, water borne primers are of special interest in the present study because of the complete elimination of hazardous chromates and significant reduction of "Volatile Organic Compounds" (VOC) in the coating systems.

Experimental

<u>Materials and sample preparation</u>

Al alloy panels of AA 2024-T3 sheet (denoted as [2B]), AA 7075-T6 ([7B]), Alclad 2024-T3 ([2A]), and Alclad 7075-T6 ([7A]) with dimensions of 7.62 cm by 15.2 cm by 0.081 cm were procured from Q-Panel Lab Products (Cleveland, OH). AA 2124-T851 cut from plate ([2P]) with dimension of 7.62 cm by 15.2 cm by 0.33 cm, and AA 7050-T7451 cut from plate ([7P]) with dimension of 7.62 cm by 12.7 cm by 0.33 cm were prepared at Boeing, St. Louis, MO. Two types of controls that are typical to current aerospace industry usage were utilized in this study: (1) chromate conversion-coated (Iridite 14-2), chromated primer-coated (Deft 44-GN-36 or 44-GN-72) panels (denoted as CC/A or CC/A1), and (2) chromate conversion-coated (Iridite 14-2), E-coated panels (henceforth denoted as CC/E1). These controls were also prepared at Boeing, St. Louis, MO.

Due to the unavailability of the BASF cathodic E-coat that was used as the second control in parts 1 through 3 of this series, a new PPG Cathodic E-coat, designated as E2 was used in this study. The chromated spray primers employed in this study were water borne Deft 44-GN-36 (A) or 44-GN-72 (A1) (Deft Corporation, Irvine, CA) and solvent borne Courtauld 519X303 (G) (Courtauld Aerospace, Glendale, CA). The non-chromated spray primers were water borne Dexter 10-PW-22-2 (X) (Dexter Corporation, Waukegan, IL) and water borne Spraylat EWAE118 (D) (Spraylat Corporation, Chicago, IL).

All the other materials used in the present study are identical to what was described in part 1 of this series[1]. Except for the plasma deposition step when the anode assembly was removed, the sample preparation procedures were the same as Part 2 (Chapter 5) of this series. The sample identification codes and associated plasma conditions for sample preparation are summarized in Table 1.

Table 1. Sample identification codes and associated plasma conditions for sample preparation.

Identification Code	Meaning and Conditions
[2A]	Alclad 2024-T3
[7A]	Alclad 7075-T6
[2B]	AA 2024-T3
[7B]	AA 7075-T6
[2P]	Plate stock AA 2124-T851
[7P]	Plate stock AA 7050-T7451
(Ace)*	CH_3COCH_3 wiping with Kimwipes® tissue
(Alk)	Alkaline cleaning (65 ^{o}C, 25 min)
(Dox)	Deoxidization (room temperature, 10 min, always preceded by alkaline cleaning)
(O)	O_2 plasma pretreatment (on Al surface: 1 sccm O_2, 100 mtorr, 40 W, 2 min; on TMS polymer surface: 1 sccm oxygen, 50 mtorr, 10 W, 1 min)
(Ar)	Ar plasma treatment (1 sccm argon, 50 mtorr, 10 W, 1 min)
T	TMS plasma polymerization with anode magnetron enhancement (1 sccm TMS, 50 mtorr, 5 W, 1 min)
F	HFE plasma polymerization (1 sccm HFE, 50 mtorr, 5 W, 1 min)
Tfs	TMS plasma polymerization without anode assembly in a flow reactor (1 sccm TMS, 50 mtorr, 5 W, 1 min)
Tcs	TMS plasma polymerization without anode assembly in a closed reactor (25 mtorr TMS, 1000 V, 2 min)
CC	Chromate conversion coating (Iridite 14-2)
A	Deft spray primer 44-GN-36 (chromated, water borne)
A1	Deft spray primer 44-GN-72 (chromated, water borne)
G	Courtauld spray primer 519X303 (chromated, solvent borne)
E2	Proprietary cathodic E-coat (non-chromated)
X	Dexter spray primer 10-PW-22-2 (non-chromated, water borne)
D	Spraylat spray primer EWAE118 (non-chromated, water borne)
/	Process separation mark

*: Code used in parentheses indicated the surface treatment process; code used without parentheses indicates coating process.

Plasma reactor system and operation

DC cathodic polymerization and plasma treatment was carried out in a bell jar reactor, which was described in detail in part 1 of this series[1]. The system was exactly the same as described in part 1, except when the anode assembly was removed and the grounded reactor wall was used as anode during the operation in certain situations explored. A pair of Al panels was placed inside the plasma reactor as the cathode (i.e. substrate for deposition). Plasma treatment by simple gases, such as oxygen or argon, was conducted in a flow system similar to that described in part 1.

To conduct plasma deposition in a closed reactor system, a new approach in this study, the reactor chamber was first pumped down to < 1 mtorr. The reactor chamber was then isolated from the pumping system by closing the main valve located in between. Trimethylsilane (TMS) gas, controlled by an MKS mass flow meter (model 247C), was then fed into the reactor. After the system pressure reached a preset point, TMS gas feeding was stopped and DC power was then applied to initiate the glow discharge to start cathodic polymerization.

Application of primers

Primers were sprayed onto the substrates with an airbrush. After painting, primer-coated samples were cured according to the stipulations provided by the primer suppliers. After curing, the thickness of primer coatings was measured with an Elcometer 355 (Elcometer Inc., Rochester Hill, Michigan). The thickness of the primer coatings was controlled to be around 1.0 mil (25.4 μm).

Tests and measurements

X-ray photoelectron spectroscopy (XPS) data was acquired with a Kratos AXIS HS instrument, using the Mg-Kα flood source operated at ~217 watts (15 mA, 14.5 kV) or an Al monochromatic source at the same power. Spectra displayed in this paper were recorded with 20eV pass energy when the monochromator was used, or 80eV when the flood source was used in conjunction with sputter depth profiling and the collection of Bremsstrahlung excited Si Auger electrons. The resolution of the Ag 3d 5/2 peak (FWHM) at these pass energies is <0.7e V for the monochromatic source and <1.5eV for the flood source. Electron flood charge neutralization was used in both cases.

A linear polarization technique was used to evaluate the R_p values of plasma coated aluminum panels.[4] All the measurements were carried out in an aqueous salt solution (0.5% NaCl + 0.35% $(NH_4)_2SO_4$) performed with an EG&G Potentiostat/Galvanostat Model 273A that was controlled by 352 SoftCorr[TM] III Corrosion Measurement Software.

A standard tape test (ASTM D3359-93B) was first used to evaluate the adhesion performance of the coating systems.[5] For stronger adhesion, an accelerated adhesion test developed by Sharma and Yasuda[6,7] was utilized to further examine adhesive characteristics of the samples. In such test, cross-shaped cuts were first made on the coated specimen in accordance with the tape test procedure. Specimens are then immersed in boiling water and periodically examined via the tape test. In the aerospace industry, Turco paint stripper solution (Turco 5469, Turco Products, Inc., Cornwells Heights, PA) is commonly used to strip the primer coatings off of painted aircraft parts during maintenance and repair procedures. For most painted systems, Turco solution can delaminate the paint within several minutes of application. In this study, the time required to delaminate the paint is taken as a third measure of the adhesive strength of the coating/Al alloy interface of the investigated systems.

Two types of accelerated corrosion tests, SO_2 (4 weeks) salt spray test performed per ASTM G85-94-annex A4[8] and Prohesion (12 weeks) cyclic salt spray tests performed per ASTM G85-

94-annex A5,[8] were used to examine the corrosion protection performance of the coating systems on aluminum alloys.

Results and Discussion

Because the aim of this project is the complete elimination of heavy metals from the coating systems, an approach that primarily relies on tenacious water-insensitive adhesion and good barrier characteristics of a primer has been taken in this study. It should be pointed out that this approach is theoretically incompatible with the primers that have corrosion inhibitors, e.g., chromated primers. This is because a primer with super barrier characteristics would not allow the migration of inhibitors and would not provide enough water for their electrochemical reaction to form corrosion protection products.

Chromated primers applied to chromate conversion coated Al alloys are the most common method used for corrosion protection of Al alloys in the aerospace industry. According to the concept of system approach interface engineering (SAIE), the corrosion protection of a metal depends on the overall protective behavior of an entire system.[1] Optimization of the process steps has to be done considering the whole corrosion protecting system. In other words, the mere combination of effective protection layers without tailoring interfaces and considering their role in the whole system does not lead to an excellent corrosion protection system. In order to elucidate the SAIE concept further, both **chromated** and **non-chromated** spray primers were employed to generate two types of plasma coating modified systems, and their corrosion protection behaviors were investigated in this study.

Chromated Primer Coating Systems

Interface Engineering — Adhesion of the primers to the plasma polymer surfaces is an important parameter in the corrosion protection of aluminum alloys[9]. Regardless of the hazardous nature, excellent primer adhesion is one of the main reasons for the continuing use of chromate conversion coating in industry. To some extent, plasma polymer coatings that are produced by a vacuum process, which is more environmentally clean, play a similar role to chromate conversion coatings. Plasma polymer coatings are highly chemically inert and will function as corrosion resistant layers on metal surfaces. Moreover, an appropriate application of plasma coating can produce extremely strong adhesion to a metal surface and also provide an excellent adhesion base for succeeding spray primers.[10-12]

Table 2 summarizes the adhesion test results of chromated primers on plasma polymer coated aluminum alloys. It can be seen that direct application of trimethylsilane (TMS) plasma coatings to Al alloys did not give good primer adhesion. However, an appropriate combination of plasma coatings of TMS followed by Hexafluoroethane (C_2F_6, abbreviated as HFE), designated as T/F in Table 2, remarkably increased the primer adhesion of Al alloys. As seen in Table 2, the paints applied to T/F plasma treated Al alloys could not be stripped by the conventional, commercial Turco 5469 paint stripping solution . The strong adhesion achieved with primers applied to T/F plasma treated Al alloys was also water-insensitive. As listed in Table 2, a wet adhesion test, which is the standard tape test performed after boiling the painted specimen, with prior cross-cuts, in water for up to 8 hours, gave the highest tape test ratings of 5. In other words, tenacious

and water-insensitive adhesion has been achieved between these primers and the plasma treated Al alloys.

Table 2. The adhesion test results of chromated spray primers (Deft 44-GN-36 (A) and Courtauld 519X303 (G)) to Al alloys prepared with chemical cleanings and plasma surface treatments. Scale 0 - 5 indicates poor (0) to excellent (5) performance.

Substrate	Surface Preparation	Primer A			Primer G		
		Tape Test	Boiling 1,4,8 hrs	Turco Time	Tape Test	Boiling 1,4,8 hrs	Turco Time
[2B]	(Alk)	5	3, 3, 3	~ 5 min	5	5, 5, 5	~30 min
	(Alk)/T	0	---	---	0	---	---
	(Alk)/T/F	**5**	**5, 5, 5**	**> 24 hrs**	**5**	**5, 5, 5**	**> 24 hrs**
[7B]	(Dox)	4	4, 4, 4	~ 30 min	5	4, 4, 4	~ 30 min
	(Dox)/T	0	---	---	0	---	---
	(Dox)/T/F	**5**	**5, 5, 5**	**> 24 hrs**	**5**	**5, 5, 5**	**> 24 hrs**
[2A]	(Ace)	3	---	~ 5 min	5	4, 4, 4	~ 5 min
	(Ace/O)/T	0	---	---	0	---	---
	(Ace/O)/T/F	**5**	**5, 5, 5**	**> 24 hrs**	**5**	**5, 5, 5**	**> 24 hrs**
[7A]	(Ace)	3	---	~ 5 min	5	4, 4, 4,	~ 5 min
	(Ace/O)/T	0	---	---	0	---	---
	(Ace/O)/T/F	**5**	**5, 5, 5**	**> 24 hrs**	**5**	**5, 5, 5**	**> 24 hrs**

The poor primer adhesion of the as-deposited TMS plasma coating can be ascribed to its low surface energy (with a water surface contact angle of 120 degree) and also the possible existence of oligomers on the surface. However, the T/F plasma coating also has low surface energy, with a water surface contact angle of about 110 degrees. Therefore, the existence of a certain amount of oligomers on the as-deposited TMS plasma-coating surface, which acts as a weak boundary layer for primer adhesion, seems to be the main reason for its poor primer adhesion performance. It has been reported that plasma polymerization of organosilicons contains small amounts of oligomeric product.[13,14]

Due to its excellent primer adhesion performance, a more detailed surface analysis of the T/F plasma coating was performed with x-ray photoelectron spectroscopy (XPS). Fig. 1 shows the typical XPS spectrum from the surface of plasma T/F coatings. The C 1s spectral region for the T/F surface has distinct contributions from carbon bound to fluorine in various combinations. The high electronegativity of fluorine causes a very large change in carbon's local electronic environment in C-F bonding. This has the effect of spreading out the individual spectral lines and allowing for better identification of the individual contributions, which also aids in the identification of the polymer bonds present in the film. This spectrum of polymer component lines is similar to those of many other fluorocarbon plasma polymers.[15]

The XPS information indicated that the HFE plasma polymerization process deposited a film of roughly 20 Å on the TMS coating, which is about 500 Å thick itself. HFE does not normally polymerize without a source of hydrogen in this process environment, but has been shown to be

polymerizable under certain conditions with the addition of a reducing agent.[16] In most cases it is mixed with H_2. The HFE plasma polymers whose spectra are presented in Fig. 1 were made without an additional hydrogen source. It thus appears that the hydrogenated nature of the TMS films acts as the hydrogen source for the plasma polymerization of HFE. In a sense, the plasma polymerization process using HFE to form the thin surface plasma coating helps to remove and/or fix the oligomeric products that existed on the as-deposited TMS coating surface, and thus significantly improves the primer adhesion performance.
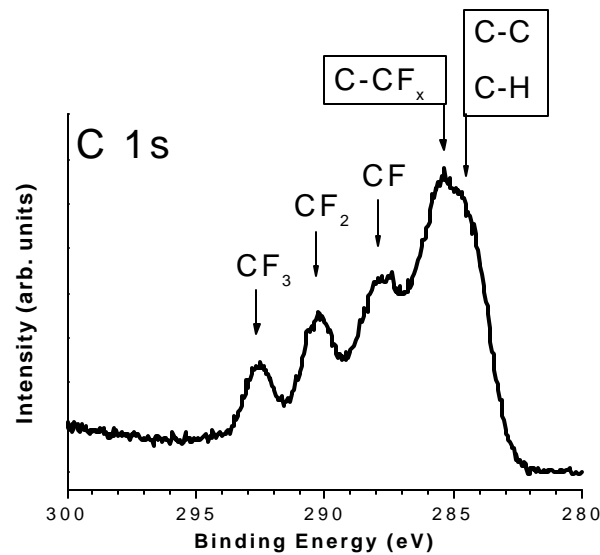
Figure 1. C1s monochromatic XPS spectrum from HFE plasma polymers deposited on top of TMS plasma coatings.

Polarization Resistance (Rp)
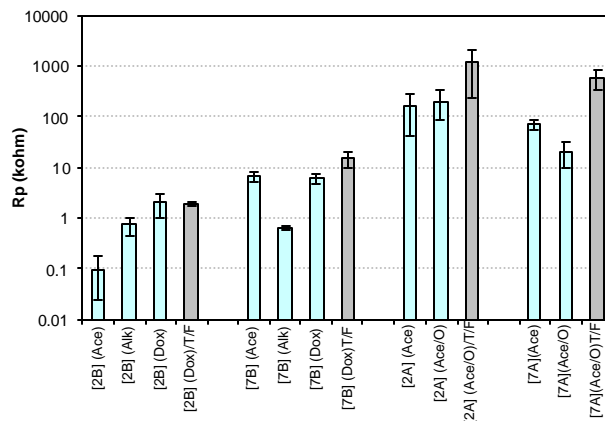
Figure 2. Rp values of AA2024-T3 ([2B]), AA7075-T6 ([7B]), Alclad 2024-T3 ([2A]), and Alclad 7075-T6 ([7A]) panels with different chemical pretreatments and plasma polymer-coated surfaces.

The surface state of a metal is another important factor that will greatly influence the corrosion protection performance of a coating system. As presented in parts I to III of this series, a proper surface preparation of the Al alloys not only affects the adhesion performance of the coating system but also changes the corrosion protection characteristics of the Al alloy.[1-3]

Fig. 2 shows the Rp values of several kinds of Al alloys with different chemical pretreatments and plasma T/F coated surfaces. As seen in Fig. 2, Deoxidization (Dox) is a very suitable surface preparation for [2B] and [7B] because it increased the corrosion resistance of these Al alloys. As reported in part I of this series,[1] either Alkaline (Alk) or Deoxidization (Dox) degraded the corrosion resistance of Alclad Al alloy of [2A] and gave worse corrosion results in the salt spray tests. In the present study, therefore, Alclad Al alloys of [2A] and [7A] were not treated with these chemical cleaning processes prior to plasma surface treatment. In most cases, as noted from Fig. 2, the application of a thin layer of T/F plasma polymers evidently increased the corrosion resistance of the Al alloys. Because of its excellent primer adhesion characteristics, it was anticipated that plasma T/F coating should contribute significantly to the corrosion protection characteristics of the coating systems thus formed.

Corrosion Test Results

Two types of corrosion evaluation tests, SO_2 and Prohesion salt spray tests, were employed for the evaluation of corrosion protection characteristics of the primer coating systems achieved with the aid of DC cathodic polymerization and treatment. The 4-week SO_2 salt spray test was chosen to speed up differentiation of the corrosion protection properties of the different systems investigated. The Prohesion cyclic salt spray test, which is chemically milder than the SO_2 salt spray test, was conducted for a longer period, 12 weeks. The Prohesion cyclic salt spray test is considered a more realistic test, as it better simulates actual service conditions of an aircraft in which both wet and dry periods occur.

The corrosion test results were evaluated and the corrosion widths along the scribe lines were calculated according the procedures described in part I of this series[1]. Fig. 3 shows the comparison of average corrosion widths of (a) SO_2 salt spray tested and (b) Prohesion salt spray tested Al alloy panels and their corresponding control panels. After 4 weeks of SO_2 salt spray test, as shown in Fig. 3(a), most of the **chromated** primer coated [2B] and [7B] panels, including those with excellent adhesion achieved by plasma T/F, showed much larger corrosion widths than their controls ([2B]CC/A and [7B]CC/A). This result evidently elucidated that the application of chromated primers with tenacious adhesion to plasma T/F treated [2B] and [7B] could not provide corrosion protection as good as the control systems. In contrast, with the same SO_2 salt spray test as shown in Fig. 3(a), chromated primer coated [2A] and [7A] gave better or comparable corrosion results to their controls. The inherent noble aluminum oxide (Al_2O_3) on the Alclad surface, and the lack of any cathodic alloying component enrichments,[17] obviously played a positive role in the corrosion protection of these Al alloys. The prolonged Prohesion salt spray test results are shown in Fig. 3(b).
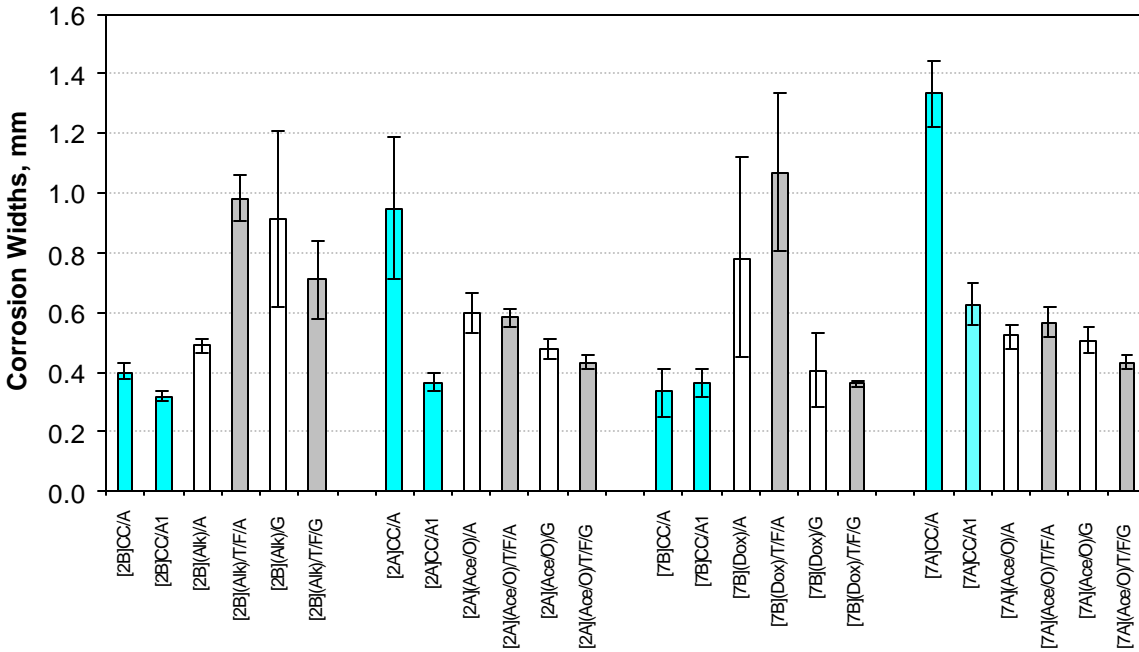
(a) SO$_2$ salt spray test results
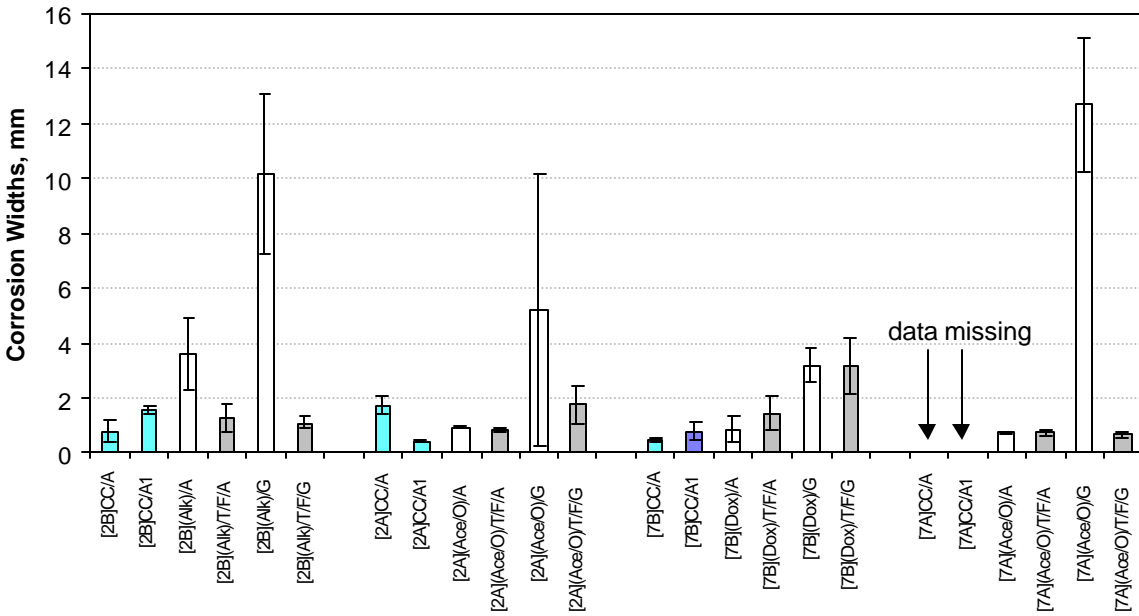
(b) Prohesion salt spray test results

Figure 3. Corrosion widths of (a) SO$_2$ salt spray and (b) Prohesion salt spray tested Al panels with chromated plasma coating systems prepared by anode magnetron plasmas and their corresponding chromated controls.
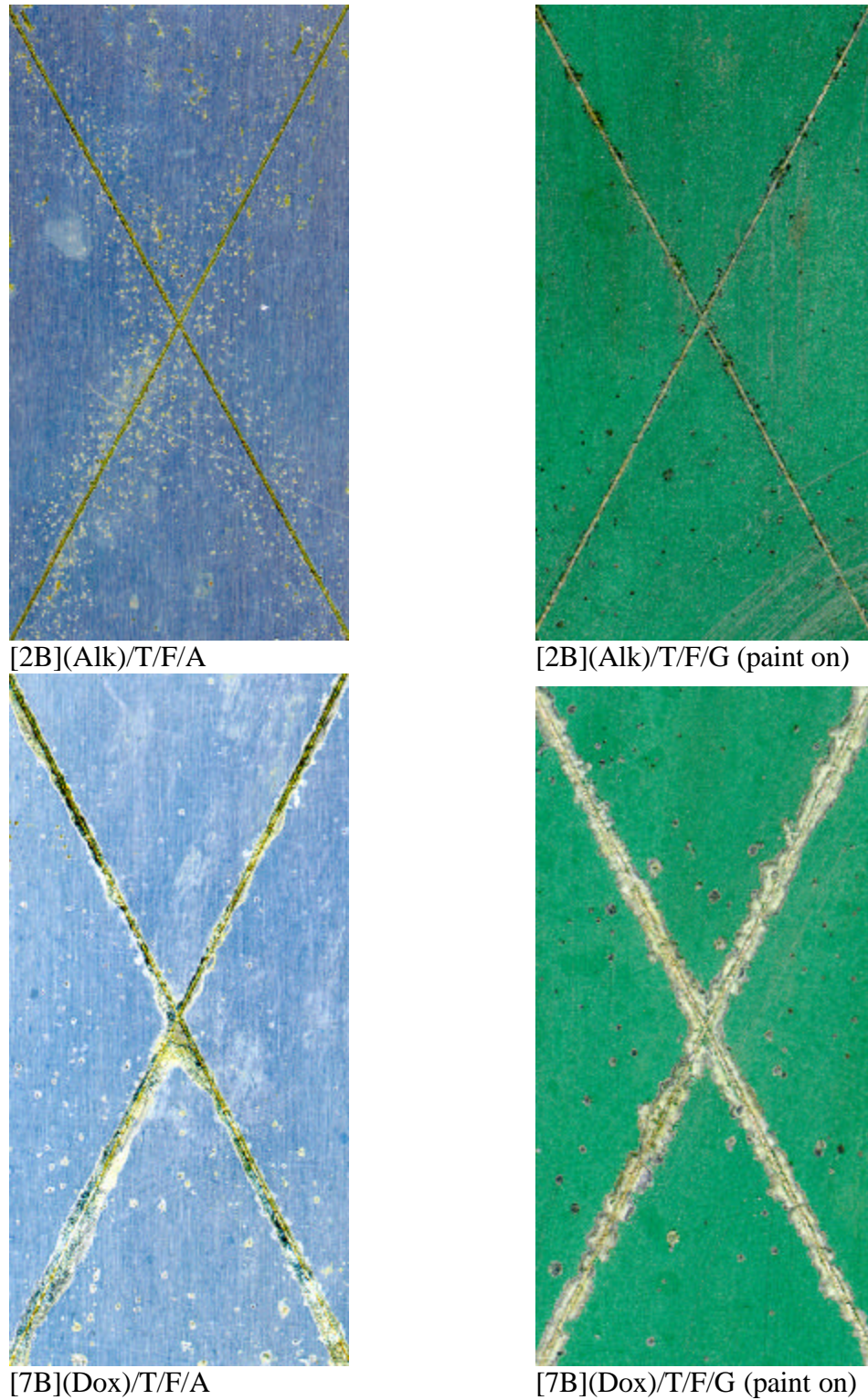
[2B](Alk)/T/F/A

[2B](Alk)/T/F/G (paint on)

[7B](Dox)/T/F/A

[7B](Dox)/T/F/G (paint on)

Figure 4. Scanned images of Prohesion salt spray tested Al panels with chromated plasma coating systems prepared by anode magnetron plasmas. Primer G could not be removed from the whole Al panel due to the strong adhesion, and only the portion with pitting corrosion occurred underneath could be stripped off with paint stripper solution.

It can be clearly seen that the tenacious and water-insensitive adhesion achieved by plasma T/F are differentiated in the results of the 12-week Prohesion salt spray test. These chromated primer coating systems with good adhesion, including these either achieved by chromate conversion coating designated as (CC)/A or plasma T/F coating designated as T/F/A in Fig. 3(b), showed very similar corrosion widths after the test. In contrast, the chromated primer coating systems without good adhesion, which were obtained with direct application of primers to the Al alloy surfaces, showed very large corrosion widths after the test.

After SO_2 and Prohesion salt spray tests, severe pitting corrosion was found on almost all the chromated primer coated [2B] and [7B] panels but not on [2A] and [7A] panels. Fig. 4 shows the typical scanned images of prohesion salt spray tested [2B] and [7B] Al alloy panels. Although a strong and water-insensitive adhesion exists on these, as noted in the adhesion testing results in table 2, the plasma coating systems based on chromated primers could not prevent the occurrence of pitting corrosion on [2B] and [7B] surfaces.

In summary of the corrosion test results elucidated in Fig. 3 & 4, the combination of a chromated primer with tenacious and water-insensitive adhesion could not provide satisfactory corrosion protection on these Al alloys. In a sense, chromated primer is good for corrosion protection when combined with chromate conversion coatings, but not the case in the absence of chromate conversion coatings, which probably due to its high water permeability that allows corrosion inhibitors to migrate and function. In other words, the chromated primers did not provide good enough barrier characteristics to yield good corrosion protection without chromate conversion coating. Pitting corrosions are due to the poor barrier characteristics of the chromated primers.
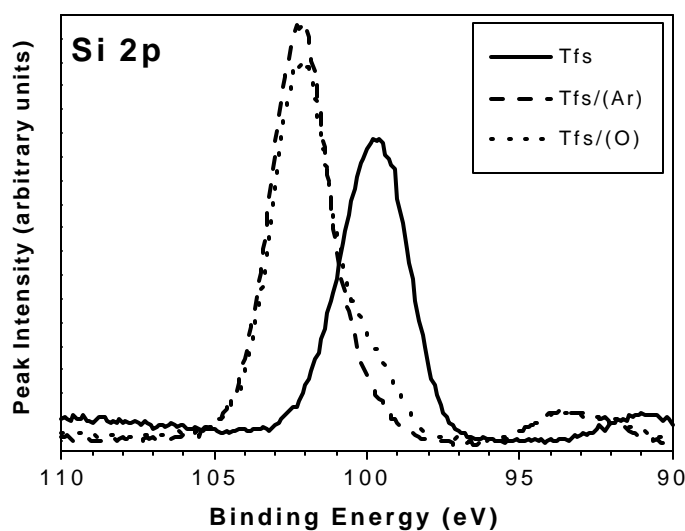
Non-Chromated Primer Coating Systems

The complete elimination of heavy metals and other hazardous compounds from the coating systems was the main objective of this study. Chromated spray primers with hazardous chromate components do not fit such an objective. Therefore, two kinds of **non-chromated and water borne** spray primers, i.e., Spraylat EWAE118 (D) and Dexter 10-PW-22-2 (X), were selected to produce chromate-free plasma coating systems for corrosion protection of Al alloys.

DC cathodic polymerization employed in the previous section was carried out with the substrate (the cathode) negatively charged and the anode assembly grounded. Because of limitation of its size and shape, the use of the anode assembly is impractical for large-scale operation as noted earlier. In contrast, DC cathodic polymerization without using the anode assembly is a more practical approach for industrial application, with an evident advantage that the size and number of the substrates (used as cathode) are no longer restricted by the anode assembly. In a separate study,[11] it was found that the removal of the anode assembly neither changed the plasma deposition process nor degraded the plasma coating properties as compared to anode magnetron plasmas. In this study, therefore, the DC cathodic polymer polymerization was modified and carried out without using an anode assembly, i.e., with the reactor wall acting as a grounded anode.
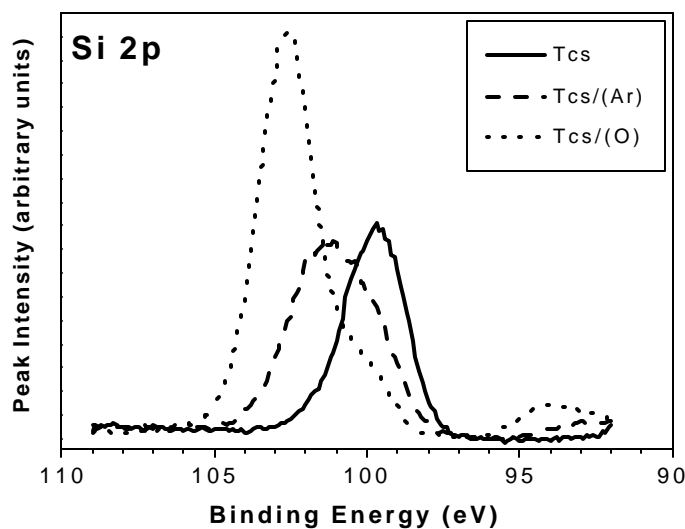
(a) Closed system TMS

(b) Flow system TMS

Figure 5. Si 2p photoelectron spectra from the top surface of TMS plasma coatings produced in (a) closed reactor system and (b) flow reactor system with and without second surface treatment by O_2 or Ar plasmas.

DC cathodic polymerization in flow and closed reactor systems

In an industrial scale vacuum reactor that has a large volume, the DC cathodic polymerization process in a closed reactor system, as opposed to a pumped flowing monomer system, can more efficiently utilize the monomers and thus significantly reduce the cost associated with usage of

monomer gases[12]. In order to investigate the consequences of this type of plasma deposition process, DC cathodic polymerization of TMS on Al alloy surfaces was carried out in both flow and closed reactor deposition systems, and the results were compared.

Table 3 summarizes the adhesion test results of the chromated spray primers to no anode assembly plasma treated [7A] panels. As compared to Table 2, it can be seen that the T/F plasma coatings produced with no anode assembly plasmas gave similar primer adhesion to those T/F plasma polymers obtained with anode magnetron plasmas. As noticed in Table 2, some other plasma coating systems, such as plasma Tfs/(Ar) and Tcs/(Ar), also provided excellent primer adhesion.

Since the it was observed that fluorine contamination was a possibility and had potentially detrimental effects,[18, 19] the excellent primer adhesion achieved with Tfs/(Ar) and Tcs/(Ar), shown in Table 3, has significant importance in the practical application of the plasma technique without any of the potentially deleterious effects of fluorine based systems. Ar plasma treatment on both flow system TMS (Tfs) and closed system TMS (Tcs) polymers were then investigated as an additional system modification which could provide strong adhesion without the incorporation of fluorine containing monomers, in the quest to produce chromate-free coatings systems. If fruitful, this has the additional benefit of using monomers with none of the environmental implications of fluorocarbons or chemistries containing any chromates.

Table 3. Adhesion test results of chromated primers (Deft 44-GN36 (A) and 44-GN-72 (A1)) to no anode assembly plasma treated 7A(Ace/O). Scale 0 - 5 indicates poor (0) to excellent (5) performance.

Plasma Systems	Plasma Coatings	Primer A			Primer A1		
		Tape Test	Boiling 1,4,8 hrs	Turco Time	Tape Test	Boiling 1,4,8 hrs	Turco Time
Flow	**Tfs**	0	---	< 5 min	0	---	~ 6 min
	Tfs/F	5	5, 5, 5	> 24 hrs	5	5, 5, 5	> 24 hrs
	Tfs/ (Ar)	5	5, 4, 3	~ 20 min	5	5, 5, 3	~ 1.5 hrs
Close	**Tcs**	5	4, 3, 3	~ 5 min	5	3, 3, 3	~ 10 min
	Tcs/(Ar)	5	4, 3, 2	~ 20 min	5	5, 4, 4	> 24 hrs

Table 4. The adhesion test results of non-chromated primers (Spraylat EWAE118 (D) and Dexter 10-PW-22-2 (X)) to no anode assembly plasma treated 7A(Ace/O). Scale 0 - 5 indicates poor (0) to excellent (5) performance.

Plasma Systems	Plasma Coatings	Primer D			Primer X		
		Tape Test	Boiled 1,4,8 hrs	Turco	Tape Test	Boiling 1,4,8 hrs	Turco
Flow	**Tfs**	2	---	---	3	0, ---	~ 10 min
	Tfs/(Ar)	5	5, 3, 3	~ 15 min	5	5, 5, 5	~13 hrs
Close	**Tcs**	5	4, 4, 4	~ 12 hrs	5	5, 5, 5	~30 min
	Tcs/(Ar)	5	5, 5, 5	>24 hrs	5	5, 5, 5	> 24 hrs

Table 4 summarizes the adhesion test results of non-chromated primers (Spraylat EWAE118 (D) and Dexter 10-PW-22-2(X)) to plasma coatings deposited without an anode assembly, which were produced in both flow and closed system deposition processes. As noted in Table 4, closed system TMS plasma polymers (Tcs) showed superior primer adhesion performance to similar ones obtained from a flow system (Tfs). Similar to chromated primers, summarized in Table 2, tenacious and water-insensitive primer adhesion was always achieved with closed system TMS plasma polymers treated with subsequent Ar plasma applications (Tcs/(Ar)).

XPS surface analysis was employed to investigate the chemical structures of TMS plasma coatings produced in both flow reactor system and closed reactor system. Fig. 5 & 6 summarize the XPS results from the TMS plasma films produced in the closed reactor system (Fig. 5a & 6a) and the flow reactor system (Fig. 5b & 6b), with and without second plasma surface treatments.

As observed from Fig. 5, TMS plasma films produced from closed and flow systems both have a surface chemical structure with carbon-silicon bonds similar to silicon carbide bonding, with the Si 2p binding energy close to 99.5 eV. The second O_2 plasma treatment on these TMS films changes the silicon surface structure to one primarily composed of silicon-oxygen bonds, with the Si 2p binding energy shifted to 103 eV, similar to that of SiO_2. As seen from Fig. 5 b, the Ar plasma treatment on flow system TMS polymers resulted in effects similar to O_2 plasma treatment, although this cannot be a direct modification in the case of the Ar treatment. The oxidation of the Si sites must happen after the plasma treatment, when the sample is exposed to atmosphere prior to XPS analysis. In contrast, as noted in Fig. 8a, the Ar plasma treatment on closed system TMS polymers has a surface composed of intermediary bonding and is thought to be some silicon-oxycarbide bonding or Si_2O bonding with various possible silicon sub-oxides[20-22].

Fig. 6 shows C/Si ratios formed from XPS sputter depth profiles of the TMS plasma polymers with and without additional plasma treatment. As deposited, without a second plasma treatment, the closed system TMS plasma film (Tcs) has a surface that is carbon rich (with C/Si ratio of ~ 4.7) and low oxygen content (with O/Si ratio of ~ 0.7). From Fig. 6(a), it is observed that the as-deposited TMS plasma film shows a gradual compositional change from the surface with more carbon (C/Si ratio of ~ 4.7) to lower carbon (C/Si ratio of ~ 1.7) in the bulk film. This also manifests itself as a much higher C/Si ratio at the surface than the bulk value, which is unique to this film, since in the flow system film the bulk level is immediately reached after the first sputter, with no gradual change. The argon plasma treatment of flow system TMS polymers had a similar ratio in the depth profile as oxygen plasma treatment, shown in Fig. 6b. In contrast, as noted in Fig. 6a, the argon plasma modified the surface of the closed system TMS film to an intermediary position with a smaller amount of carbon loss near the surface.

In order to study the surface property change of TMS plasma polymers with succeeding plasma treatment, the water contact angle change was studied as a function of the plasma power input for the second plasma treatment and the results are shown in Fig. 7. Reflecting the C-rich top surface, the as deposited TMS plasma polymer prepared by the closed system reactor (Tcs) has significantly lower contact angle (~ 80 degree) than that prepared by a flow system reactor (~ 120 degree), the values at zero power in Fig. 7. It can be seen that the Ar plasma treatment lowered the water contact angles to similar levels for both closed system TMS polymers (Tcs/(Ar)) and flow system samples (Tfs/(Ar)). On the other hand, it has been well documented

that argon plasma treatment on an organic surface could produce a more cohesive skin to enhance primer adhesion through crosslinking effects on the top surface.[23]
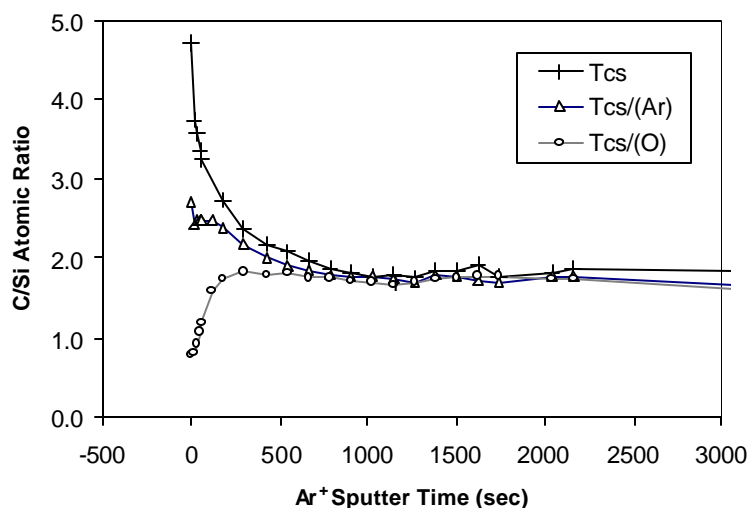
(a) Closed system TMS
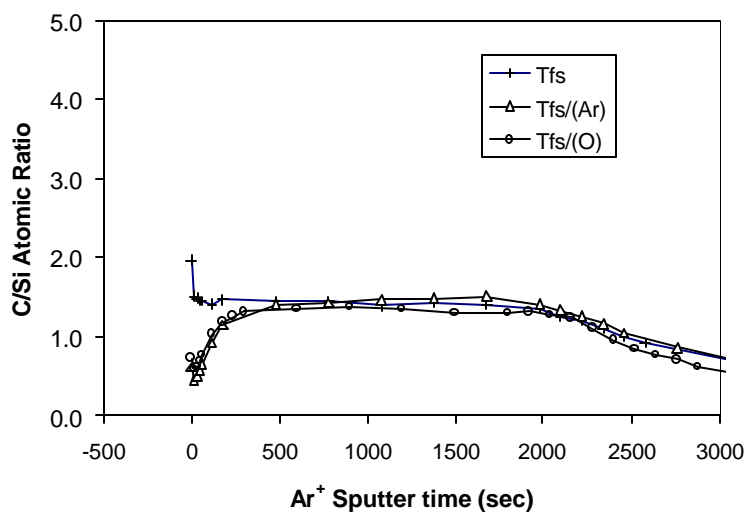
(b) Flow system TMS

Figure 6. Cross-sectional profile of C/Si ratios in plasma polymers of TMS prepared in a (a) closed reactor system and (b) flow reactor system with and without second surface treatment by O_2 or Ar plasmas.

Fig. 8 shows the comparison of Rp values of TMS plasma coated [7A] prepared in flow (Tfs) and closed (Tcs) reactor systems, both with and without succeeding O_2 or Ar plasma treatment. It can be seen that the succeeding O_2 plasma treatment reduced the corrosion resistance of Tcs but not Tfs. In contrast, the Ar plasma treatment did not degrade the corrosion resistance of both Tfs and Tcs. Since good adhesion was achieved with chromate-free spray primers on both

Tfs/(Ar) and Tcs/(Ar) plasma treated Al alloys, which was shown in Table 4, excellent corrosion protection of Al alloys was anticipated with these chromate-free plasma coating systems.
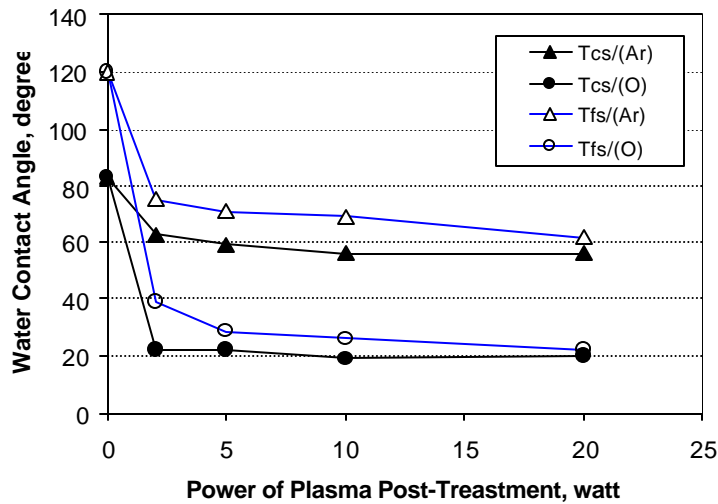
Figure 7. Water contact-angle change of closed system and flow system TMS polymer surfaces with the power input of argon and oxygen plasma post-treatment.
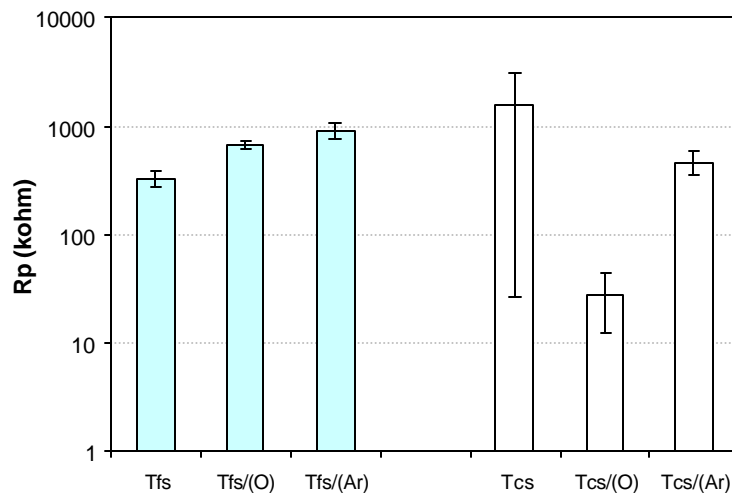
Figure 8. Rp values of TMS plasma coated Alclad 7075-T6 aluminum panels prepared in a flow reactor system and closed reactor system without using anode assembly.

Corrosion test results

SO$_2$ salt spray and Prohesion salt spray tests were again used to evaluate the corrosion protection characteristics of these chromate-free plasma coating systems on several kinds of aluminum alloys, including both skin type Al alloys ([2A], [2B], and [7B]) and internal structural Al alloys ([2P] and [7P]). Fig. 9 summarizes the corrosion widths along the scribed lines that were calculated from (a) SO$_2$ salt spray tested and (b) Prohesion salt spray tested Al alloy panels and

their corresponding control panels. As seen from Fig. 9, the corrosion test results evidently showed that the plasma coating systems based on the chromate-free spray primers provided excellent corrosion protection for the Al alloys studied.
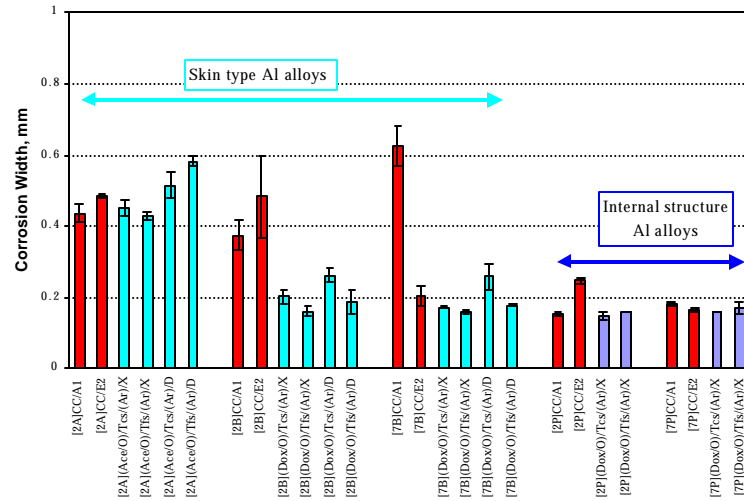
(a) SO2 salt spray test results
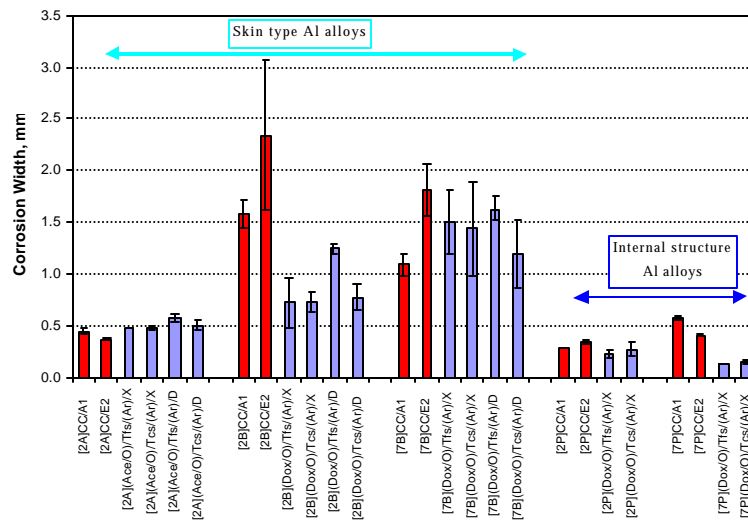
(b) Prohesion salt spray test results

Figure 9. Corrosion widths of (a) SO_2 salt spray and (b) Prohesion salt spray tested Al panels with chromate-free plasma coating systems prepared without using anode assembly and their corresponding chromated controls.

All the plasma coated Al panels, including those prepared in flow and closed reactor systems, showed comparable corrosion widths to, and in many cases much lower corrosion widths than, their corresponding controls. It is also seen in Fig. 9 that the plasma coating systems prepared in both flow (Tfs) and closed (Tcs) reactor systems showed very similar corrosion test results after the salt spray tests. The application of these chromate-free plasma coating systems to internal

structural Al alloys ([2P] and [7P]) gave very small corrosion widths, which were less than 0.2 mm after 4 weeks of SO_2 salt spray test and less than 0.3 mm after 12 weeks of Prohesion salt spray test. These results indicated that the plasma coating system combinations explored in this study are very suitable for the corrosion protection of aircraft internal structural Al alloys.

It should be pointed out that the pitting corrosion, which had severe occurrence on chromated primer coated [2B] and [7B] panels shown in Fig. 4, was significantly diminished and, in most of the cases, eliminated with the application of non-chromated primers for the chromate-free plasma coating systems. Fig. 10 shows the typical scanned images of Prohesion tested [2B], [7B], [2P], and [7P] Al panels, which were protected with chromate-free plasma coating systems during the tests. As observed in Fig. 10, a very slight amount of small pits was observed on the [2B] surface. There was no pit on [7B], [2P], and [7P] Al surfaces after both SO_2 salt spray and Prohesion salt spray tests. In Fig. 10, the primers are still in place on the [2P] and [7P] panels, because they had such strong adhesion to the plasma treated Al surfaces that the Turco paint stripping solution could not strip them, even with prolonged application for several days. The results shown in Fig. 9 & 10 demonstrate that the chromate-free plasma coating systems not only provide excellent corrosion protection on a damaged (scribed) Al alloy surface, but also prevent the occurrence of pitting corrosion of an undamaged Al alloy surface (away from the scribe lines). Since water borne primers (primer X and D in Fig. 9 & 10) was used, the VOC problem, which is often encountered in industrial coating process, can be also avoided with application of the plasma coating systems developed in the present study.

Conclusions

1. With the aid of DC cathodic polymerization and treatment, tenacious and water-insensitive adhesion can be achieved with spray primers on different types of Al alloys. The spray primers include both chromated and non-chromated primers.

2. The significance of the SAIE concept adopted in this series study is clearly demonstrated with the corrosion test results presented. The mere combination of a chromated primer (with excellent corrosion inhibitors) and tenacious adhesion, which was provided by plasma interface modification, did not provide good corrosion protection of Al alloys. In spite of strong primer adhesion to the Al surface, severe pitting corrosion occurred on these chromated primer coated [2B] and [7B] panels in both 4 weeks of SO_2 and 12 weeks of Prohesion salt spray tests. In contrast, the chromate-free plasma coating systems, which were produced based on the SAIE approach by combining the superior barrier performance of a primer with tenacious and water-insensitive adhesion, not only provide excellent corrosion protection on damaged (scribed) Al alloy surfaces, but also prevent the occurrence of pitting corrosion of undamaged Al alloy surfaces (away from the scribe lines).

3. Based on the SAIE approach, excellent corrosion protection of Al alloys has been achieved with chromate-free plasma coating systems. This accomplishment indicates that hazardous chromates can be completely eliminated from coating systems for corrosion protection of Al alloys. Since the spray primers used were water borne, the VOC problem, which is often encountered in industrial coating process, can be also avoided with application of the plasma coating systems developed in the present study.

[2B](Dox)/Tfs/(Ar)/X　　　　　　　　　[7B](Dox)/Tfs/(Ar)/X

[2P](Dox)/Tfs/(Ar)/X　　　　　　　　　[7P](Dox)/Tfs/(Ar)/X
　　(paint on)　　　　　　　　　　　　　　(paint on)

Figure 10. Scanned images of Prohesion salt spray tested Al panels coated with non-chromated primers prepared in a flow reactor system and closed reactor system without using anode assembly. Primer X could not be removed from plasma treated [2P] and [7P] surface due to the strong adhesion.

4. Superior corrosion protection results have also been achieved on [2P] and [7P] panels with the chromate-free plasma coating systems. These results indicate that the chromate-free plasma coating systems, which have tenacious adhesion to the Al alloys, may be a good fit in the long-term corrosion protection of internal structural components of aircraft that cannot be addressed in standard maintenance cycles.

Reference

[1] C. M. Reddy, Q.S. Yu, C. E. Moffitt, D. M. Wieliczka, , R. Johnson, J. E. Deffeyes, and H. K. Yasuda, "Improved Corrosion Protection of Al Alloys by Low Temperature Plasma Interface Engineering: Part I-Alclad 2024-T3 ", Corrosion, 56 (2000): p. 819.

[2] Q.S. Yu, C. M. Reddy, C. E. Moffitt, D. M. Wieliczka, R. Johnson, J. E. Deffeyes, and H. K. Yasuda, "Improved Corrosion Protection of Al Alloys by Low Temperature Plasma Interface Engineering: Part II-AA 2024-T3 ", Corrosion, 56 (2000): p. 887.

[3] C. E. Moffitt, C. M. Reddy, Q.S. Yu, D. M. Wieliczka, R. Johnson, J. E. Deffeyes, and H. K. Yasuda, "Improved Corrosion Protection of Al Alloys by Low Temperature Plasma Interface Engineering: Part III-AA 7075-T6", Corrosion, 56 (2000): p. 1032

[4] "SoftCorr^{TM} III Corrosion Measurement Software Instruction Manual", EG&G Instruments Corp., 1997.

[5] ASTM standards D3359-93B, Annual book of ASTM standards, Vol. 06.01.

[6] A. Sharma and H. Yasuda, J. Vac. Sci. Tech., 21(4) (1982): p. 994.

[7] A. Sharma and H. Yasuda, J. Adhesion, 13 (1982): p. 201.

[8] ASTM standards G85-94-Annex A4 and A5, Annual book of ASTM standards, Vol. 03.02.

[9] M. Chen, Q.S. Yu, C.M. Reddy, H.K. Yasuda, Corrosion, 56 (2000): p. 709.

[10] Q.S. Yu, J.E. Deffeyes, H.K. Yasuda, " Corrosion Protection of Ion Vapor Deposition (IVD) Al-Coated Al Alloys by Low-temperature Plasma Interface Engineering: part I: DC Cathodic Polymerization with Anode Magnetron Enhancement", Prog. Org. Coat., accepted.

[11] Q.S. Yu, J.E. Deffeyes, H.K. Yasuda, " Corrosion Protection of Ion Vapor Deposition (IVD) Al-Coated Al Alloys by Low-temperature Plasma Interface Engineering: part II: DC Cathodic Polymerization under Conditions of IVD", Prog. Org. Coat., Submitted.

[12] Q.S. Yu, C.E. Moffitt, D.M. Wieliczka, J.E. Deffeyes, H.K. Yasuda, " Corrosion Protection of Ion Vapor Deposition (IVD) Al-Coated Al Alloys by Low-temperature Plasma Interface Engineering: part III: DC Cathodic Polymerization in a Closed Reactor System", Prog. Org. Coat., Submitted.

[13] A.M. Wrobel, M. Kryszewski, M. Gazicki, J. Macromol. Sci.-Chem., A20 (1983): p.583.

[14] M. Gazicki, A.M. Wrobel, M. Kryszewski, J. Appl. Polym. Sci., 21 (1977): p. 2013.

[15] R. d'Agostino, F. Cramarossa, F. Fracassi, F. Illuzzi, "Plasma Polymerization of Fluorocarbons", in Plasma Deposition, Treatment, and Etching of Polymers, R. Agostino, Ed., Academic Press, Inc., Boston, 1990: p. 95.

[16] T. Msuoka, and H. K. Yasuda, J. Polym. Sci., Polym. Chem. Ed., 20 (1982): p. 2633.

[17] C.E. Moffitt, D.M Wieliczka, and H.K. Yasuda, "An XPS Study of the Elemental Enrichment on Aluminum Alloy Surfaces from Chemical Cleaning", Surface and Coatings Technology, in press.

[18] C.E. Moffitt, C.M. Reddy, Q.S. Yu, D.M Wieliczka, and H.K. Yasuda, Appl. Surf. Sci., 161 (2000): p. 481-496.

[18] C.E. Moffitt, C.M. Reddy, Q.S. Yu, D.M Wieliczka, and H.K. Yasuda, Appl. Surf. Sci., 161 (2000): p. 481-496.

[19] H. K. Yasuda, Q. S.Yu, C. M. Reddy, C. E. Moffitt, and D. M. Wieliczka, "Effects of Wall Contamination on Consecutive Plasma Processes", J. Vac. Sci. Technol., submitted, 2000.

[20] F.J. Himpsel, F.R. McFeely, A. Taleb-Ibrahimi, J.A. Yarmoff, and G. Hollinger, Phys. Rev. B 38 (1988): p. 6084-6096.

[21] F.R. McFeely, K.Z. Zhang, M.M. Banaszak Holl, S. Lee, and J.E. Bender IV, J.Vac. Sci. Technol. B 14 (1996): p. 2824-2831.

[22] M.R. Alexander, R.D. Short, F.R. Jones, W. Michaeli, C.J. Blomfield, *Appl. Surf. Sci.* **137** (1999): p. 179-183.

[23] E.M. Liston, L. Martinu, M.R. Wertheimer, "Plasma surface modification of polymers for improved adhesion: a critical review" in Plasma Surface Modification of Polymers, Utrecht, The Netherlands, VSP 1994: p.3.

8. Corrosion Protection of Ion Vapor Deposited (IVD) Aluminum Alloys by Low-Temperature Plasma Interface Engineering:
Part I - DC Cathodic Plasma Polymerization with Anode Magnetron Enhancement

Qingsong Yu, Joan Deffeyes, Hirotsugu Yasuda

Abstract

Anode magnetron enhanced DC cathodic plasmas were used to treat IVD aluminum coated 2024-T3 and 7075-T6 Al alloys for the creation of plasma interface-engineered systems of IVD/plasma polymer/primer. Cathodic E-coat and three kinds of spray paints were employed as primers. Plasma treatment and polymerization on IVD-coated Al alloys provided an excellent adhesion base for succeeding primer coatings; extremely strong, water-insensitive adhesion was obtained between the plasma-treated IVD-coated Al alloys and primers. When evaluated by SO_2 and Prohesion salt spray testing, these plasma interface-engineered IVD/plasma polymer/primer systems showed excellent corrosion resistance. After 4 weeks of SO_2 salt spray testing, the systems outperformed the two conventional conversion-coated IVD Al alloy controls: chromate conversion-coated/BASF cathodic electrocoated and chromate conversion-coated/Deft primer(44-GN-36)-coated IVD Al alloys. After 12 weeks of Prohesion salt spray testing, the plasma interface-engineered IVD/plasma polymer/primer systems showed corrosion test results comparable to the Deft primer-coated controls and outperformed the BASF cathodic electrocoated controls.

Introduction

Ion vapor deposition (IVD) is a vacuum process that utilizes an ion plating technique to apply a uniform and highly adherent aluminum coating on different metallic materials. IVD-coated aluminum alloy aircraft parts have been in service in the aerospace industry for corrosion protection [1,2]. IVD aluminum coatings are used in the aerospace industry as an environmentally friendly replacement for cadmium plating per MIL-C-83488. IVD vacuum equipment is in-place at OEM's, military maintenance depots, and a number of coating/plating vendors. Fig. 1 shows a picture of a typical IVD deposition chamber and associated electronics, located at Boeing in St. Louis.

Historically, IVD was developed in the 1970's for use on fatigue critical aircraft parts. The aluminum coating provides good fatigue resistance because it is soft and thus is less prone to serve as a crack initiation layer. However, its benefits as an environmentally friendly coating have become increasingly appreciated as the use of heavy metals, such as cadmium, have become more highly regulated. Plating processes, such as cadmium plating, generate hazardous waste when disposal of spent plating solutions is necessary. The IVD process uses a high purity aluminum, and the waste generated is aluminum overspray, and is therefore not hazardous. However, for improved corrosion protection, a chromate conversion coating is applied to the aluminum. The hexavalent chromium in the conversion coat provides additional corrosion protection, but disposal of the spent conversion coat solution generates hazardous waste.

Additionally, chromated paint is typically required on top of the conversion coating to get acceptable corrosion protection in service. From an environmental standpoint, the ideal process would be one which uses IVD aluminum but which does not require the chromate conversion coating and which provides good corrosion protection when used with a nonchromated primer paint. This would minimize hazardous waste generated by the process and minimize the potential for worker exposure to harmful heavy metals.

The IVD process is similar to the familiar physical vapor deposition (PVD), with one major difference: during plating, the substrate is held at a high negative potential (~ 1 kV) with respect to the vacuum chamber and evaporation source [1,2]. This potential produces a DC glow discharge of inert argon gas in the deposition chamber. A number of the evaporated aluminum atoms are ionized by this argon glow discharge and accelerated toward the cathode (substrate). This produces stronger adhesion and increases the uniformity of the aluminum coating.

As applied, IVD aluminum has an open and columnar surface and therefore low density, as illustrated in Fig. 2. Because of this open structure, IVD aluminum is extremely susceptible to corrosion as applied. Thus, it is standard practice to use glass bead peening to densify the coating. Following the glass bead peening, chromate conversion coating is required to obtain the desired corrosion resistance and create a good adhesion base for subsequent primer coatings.
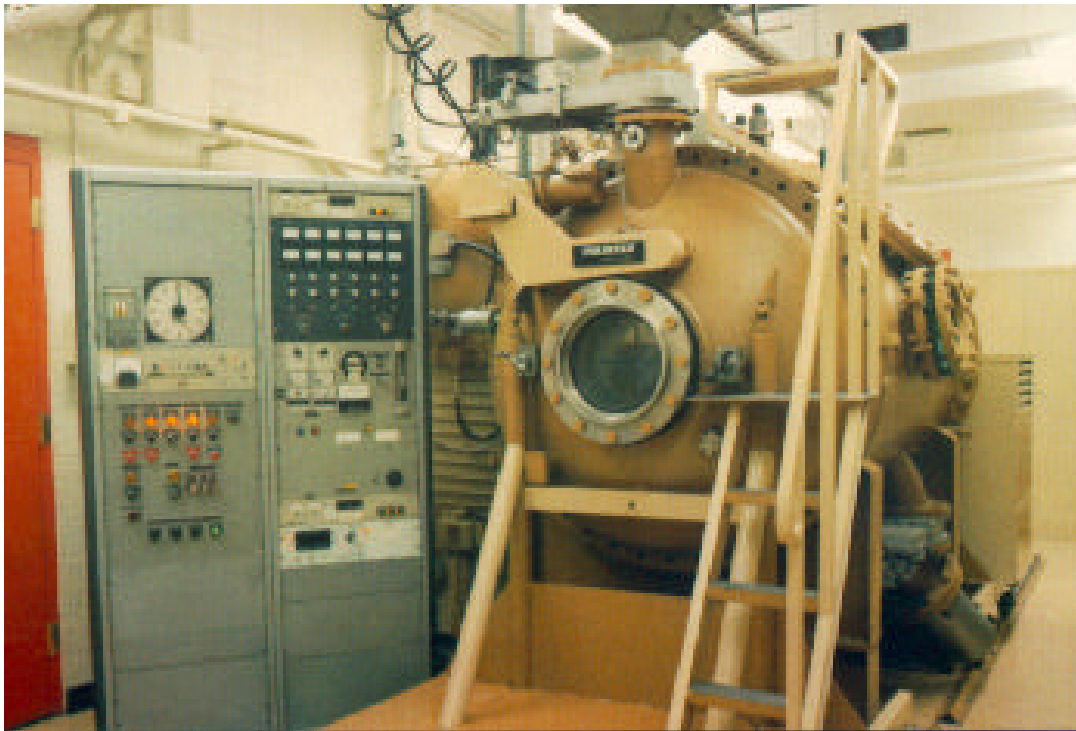
Figure 1. IVD deposition equipment in the production line at Boeing, St. Louis, MO.
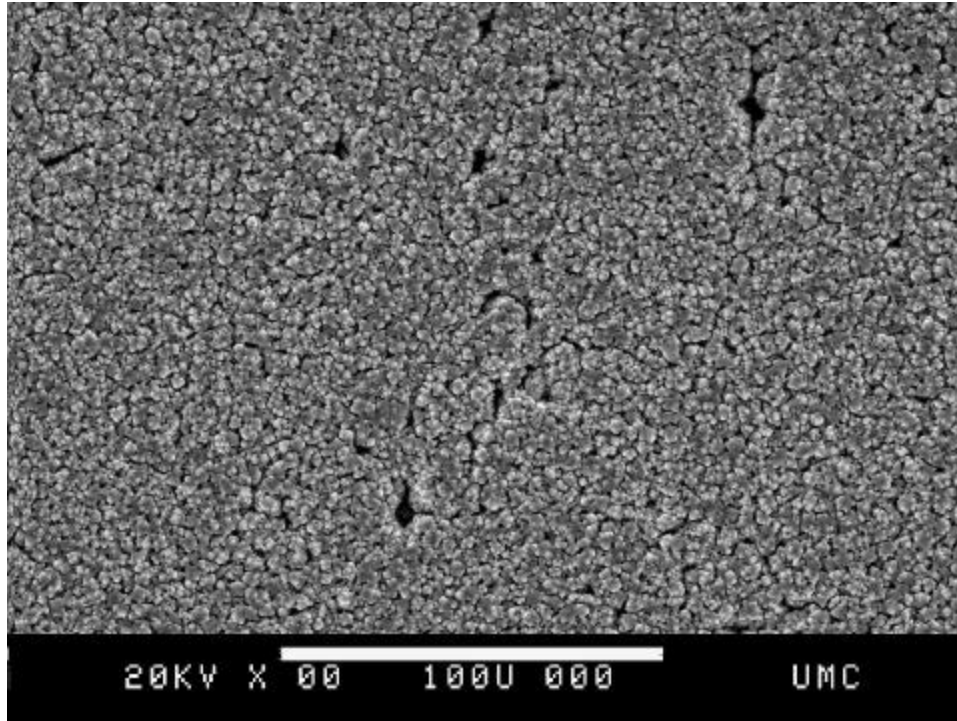
Figure 2. SEM picture of IVD aluminum coating on 7075-T6 substrate.

The plasma interface engineering employed in this study is a dry vacuum process based on low-temperature plasmas that are partially ionized gases. Depending on the types of gases employed, low-temperature plasmas can be utilized to clean and modify the surface of various materials, or to deposit a thin layer of plasma polymer coating with specific desired properties [4,5]. Plasma polymer coatings have many advantageous features, such as a pinhole-free structure, chemical inertness, and strong adhesion to almost all substrates. Applications of plasma polymer coatings for various purposes such as protective coating, surface modification, and adhesion promotion can be found in the literature [4,5,6,7]. Recently, low-temperature plasma interface engineering has been successfully applied for the corrosion protection of cold-rolled steel (CRS), and excellent corrosion protection was obtained with plasma interface-engineered CRS/plasma polymer/cathodic electrocoat (E-coat) systems [8,9].

Since low-temperature plasma processes are carried out under vacuum, low-temperature plasma interface engineering can take advantage of the existing IVD vacuum equipment and technology. In principle, plasma interface engineering can be performed in a continuous mode with IVD. Additionally, the typically disadvantageous porous IVD surface becomes an advantage in low-temperature plasma interface engineering. Gas phase species can penetrate into the micropores of IVD coatings to form an ideal transitional interface layer. The porous IVD surface also allows physical interlocking adhesion and provides high microscopic surface area for chemical bonding in plasma interface-engineered systems of IVD/plasma polymer/primer. One final benefit of the application of low-temperature plasma to IVD surfaces is the elimination of post-deposition peening and environmentally hazardous chromate conversion coating.

This chapter is the first in a series which will deal with corrosion protection of IVD-coated aluminum alloys via the application of plasma interface engineering.

Experimental

Materials

IVD aluminum-coated 7075-T6 panels (3×6 inches) were prepared at Boeing, St. Louis, MO. Two kinds of IVD aluminum coatings, Class I IVD (25 μm in thickness) and Class II IVD (12.5 μm in thickness) were employed in this study. Two peened IVD control panels of materials typical to current aerospace industry usage were utilized in this study: (1) chromate conversion-coated (Iridite 14-2), E-coated panels (henceforth denoted as CC/E) and (2) chromate conversion-coated (Iridite 14-2), Deft primer-coated (44-GN-36) panels (denoted as CC/A). These were also prepared at Boeing, St. Louis, MO.

Plasma reactor system and sample preparation procedure

Table 1. Sample identification codes and associated plasma conditions for sample preparation.

Identification Code	Meaning and Conditions
[2I]	IVD aluminum-coated 2024-T3 aluminum alloy
[7I]	IVD aluminum-coated 7075-T6 aluminum alloy
[7pI]	IVD aluminum-coated 7075-T6 aluminum alloy which has undergone glass bead peening
[2pI]	IVD aluminum-coated 2024-T3 aluminum alloy which has undergone glass bead peening
(O)	O_2 plasma pretreatment under the following conditions: 1 sccm O_2, 100 mTorr, 40 W, 2 min
T	TMS plasma polymerization under the following conditions: 1 sccm TMS, 50 mTorr, 5 W, 1 min
TO	Plasma polymerization of TMS and O_2 mixture under the following conditions: 1 sccm TMS + 1 sccm O_2, 50 mTorr, 5 W, 1 min
TN	Plasma polymerization of TMS and N_2 mixture under the following conditions: 1 sccm TMS + 1 sccm N_2, 50 mTorr, 5 W, 1 min
T/F	TMS plasma polymerization succeeded by HFE plasma treatment under the following conditions: 1 sccm HFE, 50 mTorr, 5 W, 1 min
CC	Chromate conversion coating (Iridite 14-2)
E	Cathodic E-coat, nonchromated
A	Deft primer 44-GN-36, chromated
D	Spraylat primer EDWY048, nonchromated
G	Courtaulds primer 519X303, chromated

The cathodic E-coat used was a mixture of 44 wt% resin emulsion (BASF U32CD033A), 8 wt% paste (BASF U32AD290), 48 wt% deionized (DI) water and 4 vol% additive (BASF 20CD0043). Deft 44-GN-36 (Deft Corporation, Irvine, CA), Courtaulds 519X303 (Courtaulds Aerospace, Glendale, CA), and Spraylat EDWY048 (Spraylat Corportion, Chicago, IL) spray primers were employed in this study.

Plasma treatment was carried out in a bell-jar type glass reactor. The system consists of six major components: the reactor chamber (approximately 75-liter capacity), anode magnetron electrode setup (two $25.4 \times 25.4 \times 0.16$ cm stainless steel plates with 8 bar magnets placed equidistantly on the back of each), monomer/gas feeding system, pressure and flow rate control systems, vacuum pump system (Edward Booster with mechanical pump, 240-m^3/h capacity at 0.3 mbar), and DC power source. DC power is supplied by an MDX-1K Magnetron Drive (Advanced Energy Industries, Inc.) and is controlled in power mode. Flow controller and pressure controllers (made by MKS) are used for monitoring flow rates of the monomer/gas and reactor chamber pressure. The detailed operation procedures of such a reactor system have been described elsewhere [8].

Oxygen plasma was used to pretreat the received IVD-coated panels to provide in-situ cleaning of organic contaminants before plasma polymer deposition. TMS monomer was employed in DC cathodic plasma polymerization. Sample identification codes and associated plasma conditions for sample preparation are summarized in Table 1.

Application of primers

Electrodeposition was carried out in a one gallon E-coat bath using the substrate as the cathode and a stainless steel strip (1.5"×10") as the anode. A Darrah Digital® DC power source with variable voltage facility was utilized. Electrodeposition was carried out in galvano-potentiostatic mode at 250 V and less than 1.0 ampere current for 2 minutes. This mode keeps a constant current of 1.0 ampere in the initial stage of coating as the voltage is increased to the final voltage. The final voltage is then maintained as the current decreases. Each E-coated panel was rinsed with deionized water to wash any loose E-coat from the surface. Panels were dried in air for 30 minutes and cured in an oven for 30 minutes at 300°F. After baking, the thickness of cured E-coat was 25 μm.

Primers were sprayed onto the substrates with an airbrush. After painting, primer-coated samples were cured according to the stipulations provided by the primer suppliers. After curing, the thickness of primer coatings was measured with an Elcometer 355 (Elcometer Inc., Rochester Hill, Michigan). The thickness of the primer coatings was controlled to be around 1.0 mil (25.4 μm).

Testing

Adhesion tests

Adhesion performance was first evaluated via the tape test according to the guidelines of the American Society for Testing and Materials (ASTM 3359-93B). This testing method provides

semi-quantitative results given in grades of 0 to 5. Poor adhesion can be easily detected by this simple test.

The upper limit of adhesive strength measurable by the tape test is relatively low, because the adhesive strength of the tape is limited. Therefore, the accelerated adhesion test developed by Sharma and Yasuda [10, 11] was utilized to further examine adhesive characteristics of the samples. The water sensitivity of adhesion is an important characteristic to consider when endeavoring to provide corrosion protection. Water-sensitive adhesion increases the chances of salt solution attacking the metal surface and thus resulting in corrosion. The accelerated adhesion test provides a means by which to evaluate this important factor. The method involves boiling specimens in water to accelerate water diffusion through the primer coating to the interface between primer and substrate. Before boiling, cross-shaped cuts 1 mm apart are made with a razor blade on the plasma polymer layer of each specimen in accordance with the tape test procedure. Specimens are then immersed in boiling water and periodically examined via the tape test.

In the aerospace industry, Turco paint stripper solution (Turco 5469, Turco Products, Inc., Cornwells Heights, PA) is usually used to strip the primer coatings off of painted aircraft parts during maintenance and repair procedures. For most painted systems, Turco solution can delaminate the paint within several minutes of application. In this study, the time required to delaminate the paint is taken as a third measure of the adhesive strength of the coating/metal interface of the investigated systems. Although there is no quantitative evidence suggesting that this time measurement is linearly proportional to adhesion strength, the method provides a means by which to qualitatively distinguish the levels of adhesion of primers to IVD-coated specimens.

Corrosion tests and evaluation

Panels with various low-temperature plasma interface-engineered, painted surfaces were evaluated for corrosion performance at Boeing, St. Louis, MO. Two kinds of accelerated corrosion tests were conducted on all the samples including the two types of control panels: SO_2 salt spray test performed per the American Standards for Testing Methods (ASTM) G85-94-A4, and Prohesion salt spray test performed per the American Standards for Testing Methods (ASTM) G85-94-A5, respectively [12]. 4 weeks of SO_2 salt spray testing was chosen to speed up differentiation of the corrosion protection performance of the various systems investigated. The Prohesion test, which is chemically milder than the SO_2 salt spray test, was conducted for a longer period, 12 weeks. It is considered a more realistic test, as it better simulates actual in-service conditions.

The average corrosion widths of the Prohesion and SO_2 salt spray tested panels were estimated using OPTIMAS 6.1 software [13]. For each panel, about 4 cm of scribe length on either side of the center of an X-shaped scribe were scanned using an HP DeskScan II. The scanned area was fixed at approximately 27 cm^2, and the scanned images were utilized for corrosion area measurements. Previously reported observation of damaged (scribed) surface corrosion indicates that corrosion creeps much more into the coating/substrate interface than into the scribe itself [14]. Corrosion width calculations provide a simple and meaningful method by which to quantitatively evaluate corrosion test results.

Results and Discussion

Adhesion enhancement by DC plasma treatment

Besides excellent barrier properties of the primer coating, good adhesion between a primer and metal base is essential to achieve effective corrosion protection of metallic materials. The use of conventional chromate conversion coatings continues, despite the inherent environmental and heath hazards, because the coatings provide excellent corrosion protection as well as good adhesion bases for subsequent primer coatings.

Low-temperature plasma interface engineering like that employed in this study has been well recognized as an environmentally clean technique which can produce a thin layer of corrosion resistant plasma polymer with strong adhesion to both the substrate and succeeding primer coatings. It should be noted that plasma deposited onto a metal substrate (usually the cathode) from DC discharge is a quite different than that from other sources. Because of the high negative potential applied to the cathode which results in strong ion bombardment of the surface, tenacious adhesion of plasma coatings to a metal surface can be easily achieved. In order to obtain effective corrosion protection of IVD-coated Al alloys, the adhesion behavior of primers to plasma interface-engineered IVD panels was first examined this study.

IVD/plasma polymer/E-coat systems

Cathodic E-coat is a coating system that has the following advantages: superior corrosion protection, high throw power, high coating utilization (>95%), a low level of pollution (aqueous system), and ease of automation. Recently, cathodic E-coat has been used as a primary layer coating or top coat in corrosion protection systems in the automotive, industrial, and appliance areas [15]. Cathodic E-coating is a fairly simple process that can be used on small and large scales. High throw power makes the process more attractive in practical applications involving IVD, as the E-coat penetrates into the pores of the IVD-coating, eliminating this IVD weakness.

Our preliminary results showed that, when E-coat was applied to Class I IVD (~ 25 μm in thickness), some blisters developed on the surface during the curing process. It was discovered that the use of Class II IVD (~ 12.5 μm in thickness) was helpful in eliminating this E-coat blistering during the curing process. Therefore, Class II IVD was selected for the studies performed on IVD/plasma polymer/E-coat systems.

As explained earlier, three kinds of adhesion tests were used to evaluate the interfacial adhesion behaviors of these systems; the results are summarized in Table 2. As is evident from the data, excellent water-insensitive adhesion was obtained for all of the plasma interface-engineered IVD/plasma polymer/E-coat systems examined.

In the case of direct application of E-coat to IVD specimens (one of the systems which showed excellent adhesion performance in both the tape test and the accelerated adhesion test), due to the high throw power of the E-coating process, the strong penetration of E-coat into the porous IVD structure creates mechanical interlocking and thus strong adhesion. Because of this development

of mechanical interlocking, neither the tape test nor the accelerated adhesion test could distinguish the effect of plasma treatment on adhesion performance.

To determine the significance of plasma treatment, the severe method involving commercial Turco paint stripper was used to evaluate the adhesion properties of these plasma interface-engineered IVD/plasma polymer/E-coat systems. As seen in Table 2, the typical Turco delamination time for E-coat on an IVD surface is only about 5 minutes. In contrast, the application of plasma polymers on IVD surfaces significantly increased the delamination resistance of E-coat in Turco solution. As noted in Table 2, the plasma interface-engineered IVD system [7I](O)T/F/E survived in Turco solution without delaminating for over 24 hours. Based on the Turco solution delamination times presented in Table 2, it is evident the application of plasma polymers played an important role in improving adhesion, which in turn had significant effects on the corrosion performance of the systems.

Table 2. Adhesion test results for E-coat on Class II IVD-coated 7075-T6 panels.

Initial Plasma(s) Prior to E-coating	Tape Test Rating		Delamination Time in Turco Solution
	Dry	After Boiling in H_2O for 1, 2, 4, 6, 8 hrs	
[7I]	5	5, 5, 5, 5, 5	~ 5 min
[7I](O)	5	5, 5, 5, 5, 5	~ 5 min
[7I](O)T	5	5, 5, 5, 5, 5	~ 5 min
[7I](O)TO	5	5, 5, 5, 5, 5	~ 20 min
[7I](O)TN	5	5, 5, 5, 5, 5	~ 20 min
[7I](O)T/F	5	5, 5, 5, 5, 5	> 24 hrs

IVD/plasma polymer/spray paint systems

In this study, T/F plasma polymer was also selected to improve the adhesion of different spray paints to IVD-coated panels. As presented in Table 2, T/F plasma polymer (DC plasma-polymerized TMS followed by HFE) gives rise to such strong adhesion of E-coat that Turco solution could not strip it over a 24-hour period. Since the formation of mechanical interlocking between primers and porous IVD surfaces could conceal the role of plasma treatment in enhancing adhesion, bare 7075-T6 aluminum alloy panels with smooth surfaces were first used as substrate to examine the effect of plasma treatment on the adhesion of spray paints.

Table 3 displays the adhesion test results for different spray primers applied to T/F plasma-treated bare 7075-T6 alloys. The results evince this special plasma polymer coating gave rise to excellent water-insensitive adhesion of all three primers: Turco solution could not delaminate any of the primers over a period of 24 hours. Additionally, up to 6 days aging of T/F plasma polymer in air prior to primer application did not degrade the excellent adhesion performance of the systems.

Table 4 contains the adhesion test results for IVD/T/F plasma polymer/spray paint systems. The coating of IVD aluminum panels with DC T/F plasma polymers gave rise to strong adhesion of subsequent spray paints. The spray paints could not be removed with the Turco solution.

Corrosion protection performance

SO$_2$ salt spray testing

Fig. 3 shows the scanned images of SO$_2$ salt spray tested IVD-coated 7075-T6 panels: one control, and two E-coated panels. The direct application of E-coat to IVD-coated panels (with no plasma treatment) did not provide corrosion protection as good as that of the conversion-coated control panel: more corrosion creepage was observed along the scribed lines on [7I]/E panels than on the [7pI]CC/E control panels. However, with the aid of plasma interface engineering, IVD/plasma polymer/E-coat systems outperformed the chromate conversion-coated [7pI]CC/E controls.

Table 3. Adhesion test results for primers applied to T/F plasma-treated bare 7075-T6 panels that had been pre-cleaned with alkaline and deoxidizer solutions prior to plasma treatment.

Primer	Exposure Time of T/F to Air Before Primer Application	Tape Test Rating		Delamination Time in Turco Solution
		Dry	After Boiling in H$_2$O for 1, 2, 4, 6, 8 hrs	
A	~ 10 min	5	5, 5, 5, 5, 5	> 24 hrs
	24 hrs	5	5, 5, 5, 5, 5	> 24 hrs
	48 hrs	5	5, 5, 5, 5, 5	> 24 hrs
	76 hrs	5	5, 5, 5, 5, 5	> 24 hrs
	6 days	5	5, 5, 5, 5, 5	> 24 hrs[*]
G	~ 10 min	5	5, 5, 5, 5, 5	> 24 hrs
	24 hrs	5	5, 5, 5, 5, 5	> 24 hrs
	48 hrs	5	5, 5, 5, 5, 5	> 24 hrs
	76 hrs	5	5, 5, 5, 5, 5	> 24 hrs
	6 days	5	5, 5, 5, 5, 5	> 24 hrs[*]
D	~ 10 min	4	4, 4, 4, 4, 4	> 24 hrs
	24 hrs	4	4, 4, 4, 4, 3	> 24 hrs
	48 hrs	4	4, 4, 4, 4, 4	> 24 hrs
	76 hrs	4	4, 4, 4, 4, 4	> 24 hrs
	6 days	4	4, 4, 4, 4, 4	> 24 hrs[*]

[*] A few blisters begin to develop after 24 hours in Turco solution.

Underneath the E-coat, corrosion creepage spread out from the scribed lines on both [7pI]CC/A and [7I]/E (Fig. 3). In contrast, on the IVD/plasma polymer/E-coat panel, because of the strong adhesion achieved by plasma interface engineering, no corrosion creepage occurred along the exposed scribed cross lines even after SO$_2$ salt spray testing.

Table 4. Adhesion test results for primers applied to Class I IVD-coated 7075-T6 panels.

Primers	Exposure Time of T/F to Air Before Primer Application	Tape Test Rating		Delamination Time in Turco Solution
		Dry	After Boiling in H_2O for 1, 2, 4, 6, 8 hrs	
A	N/A (no T/F)	5	5, 5, 5, 5, 5	> 24 hrs
	2 hrs	5	5, 5, 5, 5, 5	> 24 hrs
	4 days	5	5, 5, 5, 5, 5	> 24 hrs
G	N/A (no T/F)	5	5, 5, 5, 5, 5	> 24 hrs
	2 hrs	5	5, 5, 5, 5, 5	> 24 hrs
	4 days	5	5, 5, 5, 5, 5	> 24 hrs
D	N/A (no T/F)	5	5, 5, 5, 5, 5	~ 5 min
	2 hrs	5	5, 5, 5, 5, 5	> 24 hrs
	4 days	5	5, 5, 5, 5, 5	> 24 hrs

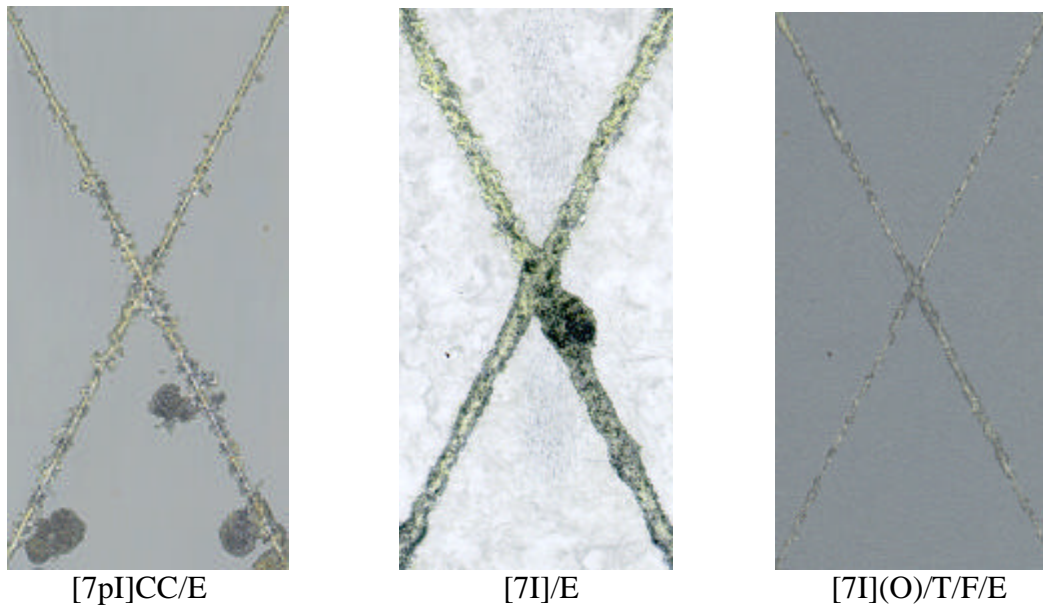[7pI]CC/E   [7I]/E   [7I](O)/T/F/E
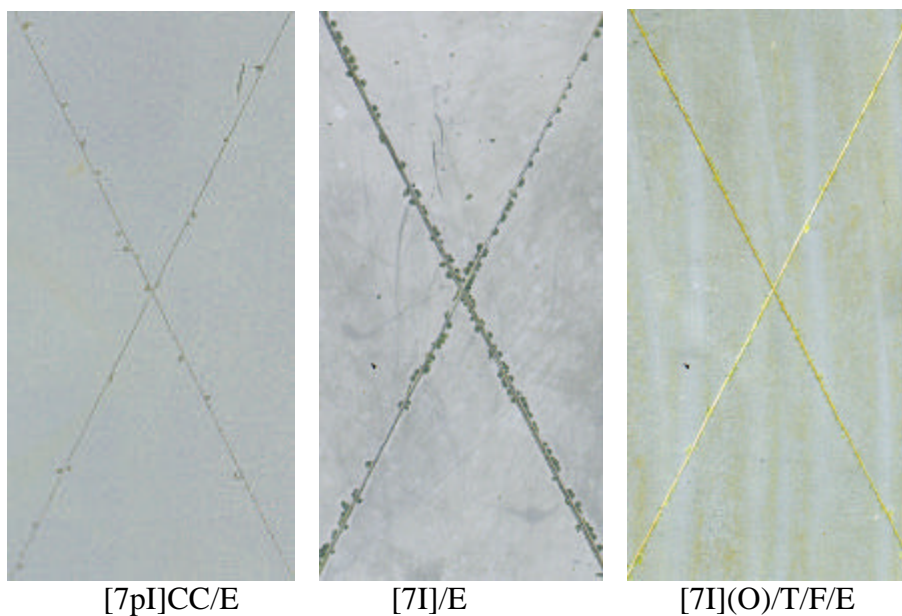
Figure 3. Scanned images of SO_2 salt spray tested (4 weeks) IVD-coated 7075-T6 panels. On each, the total scanned area is 27 cm^2, and the total scribe length within the scanned area is 16 cm.

All corrosion-tested panels were scanned and the corrosion widths along the scribed lines were calculated as described in the experimental procedures. Fig. 4 presents a comparison of the average corrosion widths of SO_2 salt spray tested panels of different plasma interface-engineered samples and the controls.
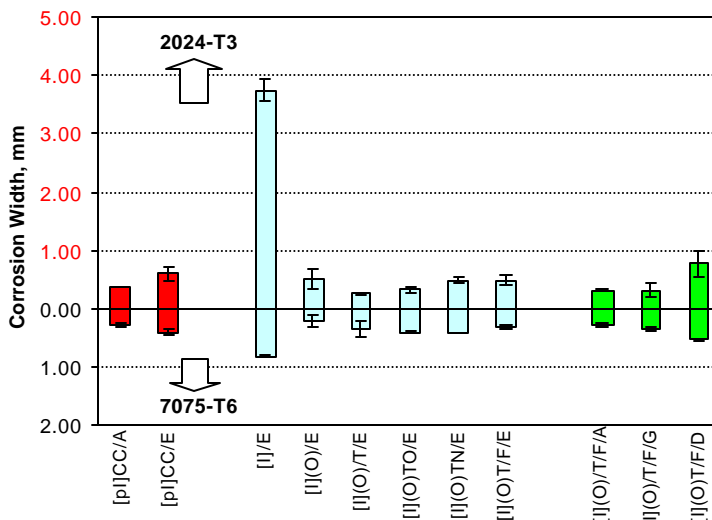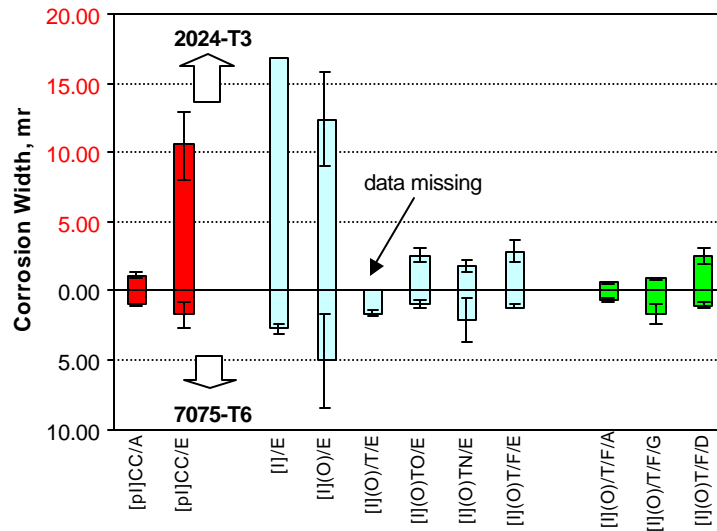
Figure 4. Average corrosion widths of SO_2 salt spray tested IVD aluminum-coated 2024-T3 and 7075-T6 panels: control, IVD/plasma polymer/E-coat, and IVD/plasma polymer/spray primer systems.

It is evident from Fig. 4 that the direct application of E-coat to IVD-coated panels without plasma treatment gave large corrosion width values after SO_2 salt spray testing. However, the plasma-tailored IVD systems on both 7075-T6 and 2024-T3 substrates displayed excellent corrosion protection. Most of the plasma-treated IVD samples outperformed or nearly outperformed both conventional conversion-coated IVD Al alloy controls.

Prohesion salt spray testing

Fig. 5 presents the scanned images of Prohesion salt spray tested IVD-coated 7075-T6 panels. After Prohesion salt spray testing, it was readily evident that plasma interface-engineered samples, like the [7I](O)T/F/E specimen pictured, showed much less corrosion creepage along the scribed cross lines than did the [7pI]CC/E control panels. As compared to the SO_2 salt spray tested samples displayed in Fig. 3, 12 weeks of Prohesion salt spray testing led to more corrosion on all samples.

An extensive spread of corrosion creepage from the scribed lines into the paint/metal interface was observed on both [7pI]CC/E and [7I]/E. This spread of corrosion apparently resulted from partial adhesion failure at the IVD/E-coat interface. In contrast, since strong adhesion prohibits corrosion propagation into the plasma modified paint/metal interface, the corrosion creepage was much narrower and more uniform on the plasma interface-engineered [7I]/T/F/E panel. This result is consistent with the finding that Turco stripper could not remove E-coat from the [7I]/T/F/E system (Table 2).

The corrosion widths of Prohesion salt spray tested aluminum panels were calculated and are summarized in Fig.6. As is evident from the data, after 12 weeks of Prohesion salt spray testing,

IVD/plasma polymer/spray paint systems showed better corrosion protection overall than IVD/plasma polymer/E-coat systems.

[7pI]CC/E   [7I]/E   [7I](O)/T/F/E

Figure 5. Scanned images of Prohesion salt spray tested IVD-coated 7075-T6 panels. On each, the total scanned area is 27 cm^2, and the total scribe length within the scanned area is 16 cm.

Figure 6. Average corrosion widths of Prohesion salt spray tested IVD aluminum-coated 2024-T3 and 7075-T6 panels: control, IVD/plasma polymer/E-coat, and IVD/plasma polymer/spray primer systems.

All the IVD/plasma polymer/spray paint systems outperformed BASF cathodic E-coated controls and showed corrosion test results comparable to those of the Deft primer-coated controls. In the IVD/plasma polymer/E-coat systems evaluated, only oxygen plasma treatment (without applying any plasma polymer coating prior to E-coating) did not provide good corrosion protection of IVD-coated panels; as a result, very large corrosion width values were obtained for both 7075-T6 and 2024-T3 oxygen plasma-treated substrates. Since strong adhesion was able to be achieved, the application of plasma polymers such as T, TO, TN, and T/F created IVD/plasma polymer/E-coat systems which also outperformed BASF cathodic E-coated controls and showed corrosion test results comparable to those of the Deft primer-coated controls.

From Figs. 4 & 6, it should be noted that, after both SO_2 and Prohesion salt spray testing, chromate-free systems including [I](O)T/F/E, [I](O)T/E, [I](O)TO/E, [I](O)TN/E, and [I](O)T/F/D gave rise to excellent corrosion protection of IVD-coated aluminum alloys; they outperformed BASF cathodic E-coated controls and showed corrosion test results comparable to those of the Deft primer-coated controls. Thus, without using the conventional chromate conversion coating method, excellent corrosion protection of IVD aluminum alloys can be achieved with chromate-free, plasma interface-engineered systems.

Conclusions

Low-temperature plasma interface engineering was successfully applied in the development of an environmentally benign corrosion protection process for IVD aluminum coated 7057-T6 and 2024-T3 Al alloys. Corrosion test results showed that many chromate-free, plasma interface-engineered systems outperformed or nearly outperformed the conventional conversion-coated IVD Al alloy controls, chromate conversion-coated/BASF cathodic electrocoated, and chromate conversion-coated/Deft primer-coated IVD aluminum alloys.

The adhesion of E-coat and spray primers to plasma polymer-coated IVD aluminum alloys was excellent. Tenacious adhesion of both E-coat and spray primers to IVD-coated aluminum alloys was achieved by the application of a special plasma polymer to IVD-coated aluminum substrates.

Observation of damaged (scribed) surface corrosion indicated that, due to adhesion failure, corrosion proceeds mainly into the IVD/primer interface. Enhanced adhesion can hinder this spread of corrosion. Corrosion test results showed corrosion spread outward from the scribed lines on the control panel surfaces. In contrast, the tenacious adhesion of primers achieved with plasma treatment significantly impeded corrosion propagation on the damaged surfaces of the plasma interface-engineered systems. The results of this study demonstrate that, without using conventional chromate conversion coatings, the enhanced adhesion and durability of plasma interface-engineered systems can produce excellent corrosion protection of IVD-coated aluminum alloys.

References

[1] B.T. Nevill, 36th Annual Technical Conference Proceedings-Society of Vacuum Coaters, Albuquerque, NM, USA, 1993, p. 379.

[2] K.E. Steube and L.E. McCrary, J. Vac. Sci. Technol., 11(1) (1974) 362.

[3] D.P. Monaghan, D.G. Teer, P.A. Logan, K.C. Laing, R.I. Bates, R.D. Arnell, Surf. Sci. Coat. Technol., 60 (1993) 592.

[4] H. Yasuda, *Plasma Polymerization*, Academic Press, Orlando, FL, 1985.

[5] H.V. Boenig, *Plasma Science and Technology*, Cornell University Press, Ithaca, NY, 1982.

[6] H. Yasuda, B.H. Chun, D.L. Cho, T.J. Lin, D.J. Yang, J.A. Antonelli, Corrosion, 52(3) (1996) 169.

[7] N. Morosoff, "An Introduction to Plasma Polymerization," in *Plasma Deposition, Treatment, and Etching of Polymers*, R. d'Agostino, ed., Academic Press, Inc., San Diego, USA, 1990, Chap. 1.

[8] T.F. Wang, T.J. Lin, D.J. Yang, J.A. Antonelli, H.K. Yasuda, Prog. Org. Coat., 28 (1996) 291.

[9] H.K. Yasuda, T.F. Wang, D.L. Cho, T.J. Lin, J.A. Antonelli, Prog. Org. Coat., 30 (1997) 31.

[10] A. Sharma and H. Yasuda, J. Vac. Sci. Tech., 21(4) (1982) 994.

[11] A. Sharma and H. Yasuda, J. Adhesion, 13 (1982) 201.

[12] ASTM G85-94, Standard Practice for Modified Salt Spray (Fog) Testing.

[13] C. Reddy, H. Yasuda, D. Weiliczka, J. Deffeyes, Plating and Surface Finishing, 86(10) (1999) 77.

[14] C.M. Reddy, Q.S. Yu, C.E. Moffitt, D.M. Wieliczka, J.E. Deffeyes, H.K. Yasuda, Corrosion, accepted.

[15] H.-J. Streitberger and R.P. Osterloh, "Interface Coatings-2," Wilson & Prosser, eds., Elsevier, London, 1987.

9. Corrosion Protection of Ion Vapor Deposition (IVD) Al-Coated Al Alloys by Low-temperature Plasma Interface Engineering: Part II - DC Cathodic Polymerization under conditions of IVD (Without Using Anode Assembly)

Qingsong Yu, Joan Deffeyes, Hirotsugu Yasuda

Abstract

DC cathodic polymerization of trimethylsilane (TMS) were carried out in a bell-jar reactor without using anode assembly, i.e., under the conditions similar to Ion Vapor Deposition (IVD) operation. In order to initiate the DC glow discharge, a negative potential was applied to IVD Al-coated aluminum panels that worked as the cathode and grounded reactor wall functioned as the anode. TMS plasma coatings obtained under such operation were studied in term of refractive indices, polarization resistance, and adhesion performance to subsequent spray paint primers. Experimental results indicated that the TMS plasma coatings obtained without anode assembly have the similar coating characteristics to those obtained by anode magnetron plasmas as used in part I of these series, which showed excellent corrosion protection of IVD Al-coated aluminum alloys. As a result, the plasma interface engineered coating systems of IVD/Plasma polymer/non-chromated primer obtained under such operation showed excellent corrosion protection of IVD Al-coated aluminum alloys, which outperformed the chromate conversion coated IVD controls after 4 weeks of SO_2 and 12 weeks Prohesion salt spray tests.

Introduction

This paper is the second of three parts dealing with corrosion protection of ion vapor deposition (IVD) Al-coated Al alloys via the application of low-temperature plasma interface engineering. It is aimed at achieving improved corrosion protection of aluminum alloys used for aircraft without using heavy metal-containing chemicals such as chromate conversion coatings and chromated primers.

Ion Vapor Deposition (IVD) of pure aluminum has been in service for about two decades in aerospace industry where substrate materials have typically been high strength steels, aluminum and titanium alloys [1]. In IVD process, a negative voltage is applied to the substrates with the evaporation source and the chamber becoming the anode (grounded) of the system [2]. This potential produces a DC glow discharge of inert argon gas in the deposition chamber. A portion of the evaporated aluminum atoms are ionized by this argon glow discharge and accelerated toward the cathode (substrate). This produces stronger adhesion and increases the uniformity of the aluminum coating.

As applied, IVD aluminum coating has an open and columnar surface and therefore low density. Because of this open structure, IVD aluminum is extremely susceptible to corrosion as applied. Thus, it is standard practice to use glass bead peening to densify the aluminum coating.

Following the glass bead peening, chromate conversion coating is required to obtain the desired corrosion resistance and create a good adhesion base for subsequent primer coatings.

Our recent results have demonstrated that DC cathodic polymerization with anode magnetron enhancement provides excellent corrosion protection of aluminum alloys and IVD Al-coated aluminum alloys [3-6]. Similar to IVD process, DC cathodic polymerization is usually carried out with the substrate (the cathode) negatively charged and anode assembly grounded. Since the anode has the same potential as the reactor chamber which are both grounded, there exists the possibility to conduct DC plasma polymerization without using an anode assembly but the chamber itself as the anode of the system.

Table 1 shows the comparison of typical operating parameters of IVD and DC cathodic polymerization process. It can be seen that striking similarities exist between DC cathodic polymerization and the industrial IVD process. Since it can utilize the existing IVD vacuum equipment in aerospace industry with no further investment cost, DC cathodic polymerization without anode assembly is a very promising way to apply this technique in practical applications. In this study, the possibility of DC cathodic polymerization has been investigated without using anode assembly, i.e., similar to IVD operations. The deposition behaviors and the plasma polymer film characteristics were also studied. An effort was especially made to compare the coating properties to those obtained with anode magnetron plasmas, which have demonstrated to provide excellent corrosion protection of aluminum alloys [3-6]. The corrosion protection properties of these plasma coating systems provided by DC cathodic polymerization under IVD conditions were also investigated on different IVD Al-coated aluminum alloys.

Table 1. Comparison of Ion Vapor Deposition (IVD) and DC cathodic polymerization processes.

Operating Parameters	IVD	DC Cathodic Polymerization
Power Supply	DC	DC
Cathode (- charged)	Substrate	Substrate
Anode (grounded)	Chamber & Evaporation Source	Chamber & Anode Assembly (usually)
Applied Voltage	Cleaning:-400 to –1000 V Deposition: -400 to –1000 V	Cleaning: -500 to –1000 V Polymerization: -500 to –1000 V
Base Pressure	≤ 0.08 mTorr	≤ 1.0 mTorr
System Pressure	~ 10 mTorr	10 to 100 mTorr
Deposition Controlling Factor	Evaporation Rate	Current Density

Experimental

Materials

118

IVD aluminum-coated Al alloy panels of 2024-T3 sheet (denoted as [2I]), 2124-T851 cut from plate (denoted as [2PI]), and 7050-T7451 cut from plate (denoted as [7PI]) were prepared at Boeing, St. Louis, MO. Class I IVD (25 μm in thickness) was employed in this study. The [2I] and [2PI] panels have the dimension of 7.62 cm by 15.2 cm by 0.33 cm and [7PI] panels have the dimension of 7.62 cm by 12.7 cm by 0.33 cm. Two types of peened IVD controls that are typical to current aerospace industry usage were utilized in this study: (1) chromate conversion-coated (Iridite 14-2), Deft primer-coated (44-GN-36) panels (denoted as CC/A) and (2) chromate conversion-coated (Iridite 14-2), E-coated panels (henceforth denoted as CC/E). These were also prepared at Boeing, St. Louis, MO.

The cathodic E-coat used was PPG ED6650 purchased PPG Industries, Cleveland, OH. Deft 44-GN-72 (Deft Corporation, Irvine, CA), Spraylat EWAE118 (Spraylat Corporation, Chicago, IL), and Dexter 10-PW-22-2 (Dexter Corporation, Waukegan, IL) spray primers were employed in this study.

All the other materials used in this study are identical to what was described in part 1 of this series.

Plasma reactor system and sample preparation procedures

DC cathodic polymerization and plasma treatment was carried out in a bell-jar type reactor. The system was exactly the same as described in part 1 of these series, except that the anode assembly was removed and the grounded reactor wall was used as anode during the operation. The detailed operation procedures of such a reactor system have been described elsewhere [3].

Oxygen plasma was used to pretreat the received IVD-coated panels to provide in-situ cleaning of organic contaminants before plasma polymer deposition. TMS monomer was employed in DC cathodic polymerization. Sample identification codes and associated plasma conditions for sample preparation are summarized in Table 2.

Application of primers

Primers were sprayed onto the substrates with an airbrush. After painting, primer-coated samples were cured according to the stipulations provided by the primer suppliers. After curing, the thickness of primer coatings was measured with an Elcometer 355 (Elcometer Inc., Rochester Hill, Michigan). The thickness of the primer coatings was controlled to be around 1.0 mil (25.4 μm).

Testing and measurements

Measurement of thickness and refractive index of plasma coatings

An AutoEL-II automatic ellipsometer (Rudolph Research Corporation), which is a null-seeking type with a 632.8 nm helium-neon laser light source, was used for measurement of the thickness and refractive index of deposited films in different glow discharges. For such a measurement, deposited films were all prepared on silicon wafers, which was sticking to IVD substrate (the

cathode) with a drop of Silver print during the deposition in order to achieve a good electrical contact in between.

Polarization Resistance (R_p) Measurements

A linear polarization technique was used to evaluate the R_p values of plasma coated aluminum panels. All the measurements were carried out in an aqueous salt solution (0.5% NaCl + 0.35% $(NH_4)_2SO_4$) performed with an EG&G Potentiostat/Galvanostat Model 273A that was controlled by 352 SoftCorr^{TM} III Corrosion Measurement Software. An aluminum panel was used as the working electrode, a graphite rod (0.6 cm diameter) as counter electrode, and Ag/AgCl (0.197 V vs. NHE) as reference electrode. The exposed surface area of the panel was 3×3 cm^2 and the rest of the panel surface was covered with insulating tape. The experiments were conducted after immersion for about 50 minutes when the open circuit potential became stable. During the Linear Polarization measurement, a controlled-potential scan over a small range (± 17 mV with scan rate 2 mV/min) with respect to the corrosion potential (Ecorr) was applied to the electrochemical electrodes.

Adhesion tests

Adhesion tests used in this study were exactly the same as described in part 1 of these series. Standard tape test (ASTM 3359-93B) was first used to evaluate the adhesion performance of the coating systems. For stronger adhesion, an accelerated adhesion test developed by Sharma and Yasuda [7, 8] was utilized to further examine adhesive characteristics of the samples. In such test, cross-shaped cuts were first made on the coated specimen in accordance with the tape test procedure. Specimens are then immersed in boiling water and periodically examined via the tape test.

In the aerospace industry, Turco paint stripper solution (Turco 5469, Turco Products, Inc., Cornwells Heights, PA) is usually used to strip the primer coatings off of painted aircraft parts during maintenance and repair procedures. For most painted systems, Turco solution can delaminate the paint within several minutes of application. In this study, the time required to delaminate the paint is taken as a third measure of the adhesive strength of the coating/IVD interface of the investigated systems.

Corrosion tests and evaluation

Two types of accelerated corrosion tests, SO_2 (4 weeks) salt spray test performed per ASTM G85-94-annex A4 [9] and Prohesion (12 weeks) cyclic salt spray tests performed per ASTM G85-94-annex A5 [10], were used to examine the corrosion protection performance of the coating systems on IVD coated aluminum alloys. The detailed description of the test methods and evaluation procedures [11] used in this study was given in Part I of this series [6].

Results and Discussion

Nature of Anode

DC cathodic polymerization employed in the previous study was carried out with the substrate (the cathode) negatively charged and anode assembly grounded [3]. Because of limitation of its size and shape, the use of anode assembly is impractical for large-scale operation. In contrast, DC cathodic polymerization without using anode assembly will be more compatible to industrial IVD processes. In this study, it was expected that the removal of anode assembly does not change the plasma deposition process and degrade the plasma coating properties as compared to anode magnetron plasmas.

Fig. 1 shows a comparison of operation parameters of DC plasmas (TMS and oxygen) conducted without anode assembly and with anode magnetron. In comparison with anode magnetron plasmas, for both TMS and oxygen gases, a higher voltage of about 100 V is necessary to sustain the plasmas at a certain power input with no anode assembly operation.

Similar to IVD Al coating process, plasma polymerization of TMS can be also conducted with voltage control mode instead of power control mode. The according deposition profiles are shown in Fig. 2. It can be seen that a very uniform deposition of TMS coatings can produced by no anode assembly operation. It is known that, in cathodic polymerization, the deposition rate was mainly controlled by the current density of the plasmas [12]. From Fig. 2, it can be noted that, regardless of the difference of operation mode, the similar current density produced the similar TMS coating thickness. These results also indicated that the current density is the controlling factor in DC cathodic polymerization process under conditions similar to IVD operation.
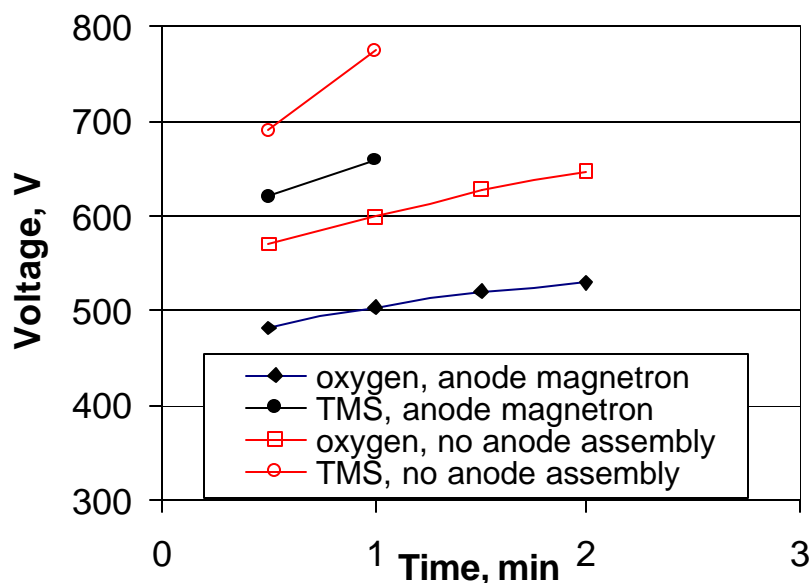
Figure 1. Voltage change with discharge time in DC anode magnetron plasmas and no anode assembly operation. Conditions are 1 sccm TMS, 50 mTorr, 5 watt, and 2 sccm oxygen, 100 mTorr, 40 watt.
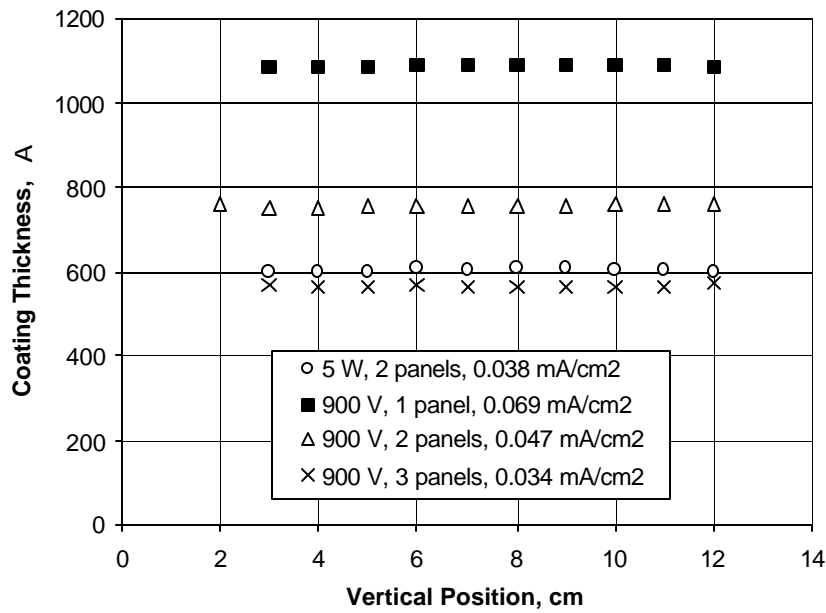
Figure 2. TMS deposition profile in no anode assembly plasmas with different operation modes. Conditions are 1 sccm TMS, 50 mTorr, 1 min.
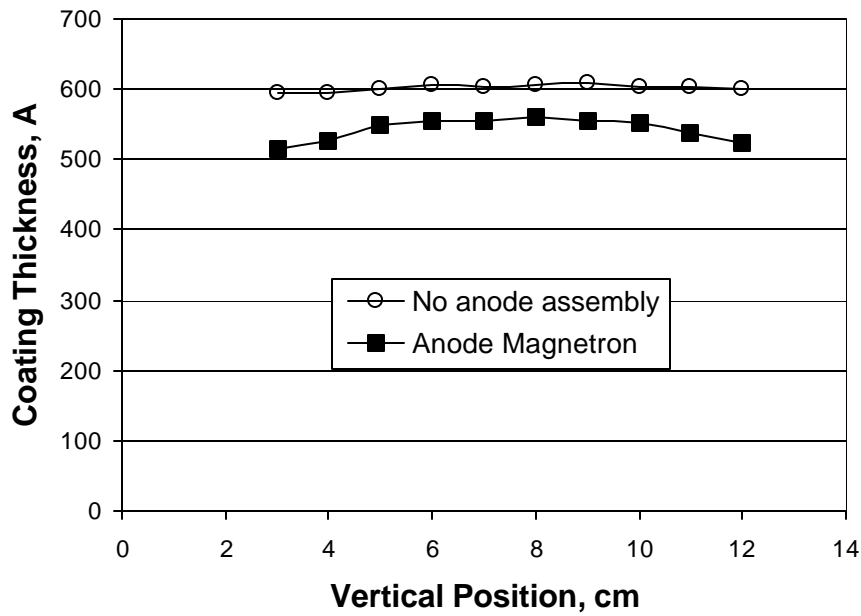
Figure 3. TMS deposition profile in no anode assembly and anode magnetron plasmas. Conditions are 1 sccm TMS, 50 mTorr, 5 watt, 1min.
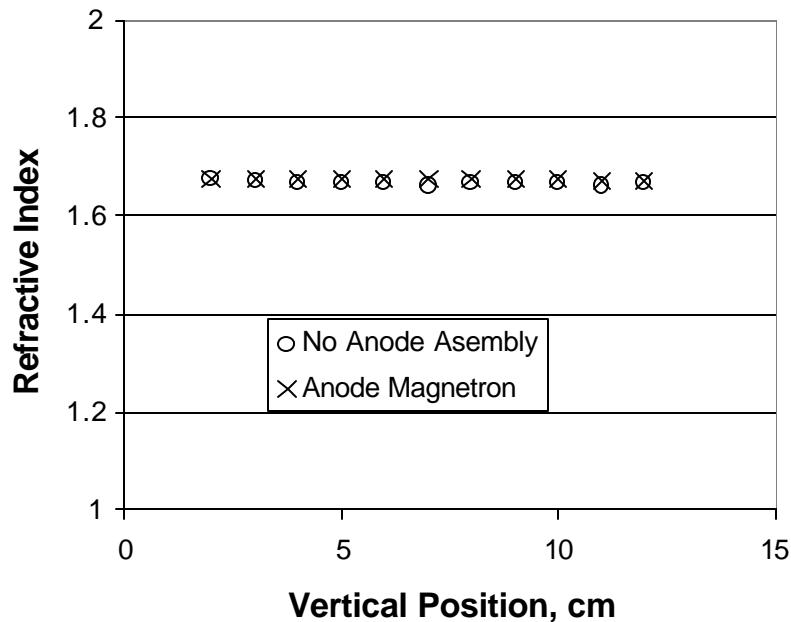
Figure 4. Refractive indices of TMS plasma coatings prepared by no anode assembly and anode magnetron plasmas. Conditions are 1 sccm TMS, 50 mTorr, 5 watt, 1 min.

The original purpose of using anode magnetron was to eliminate the edge effect of plasma etching and to lower the break down voltage. It was found, however, that the edge effect is not a serious problem in plasma deposition and the anode magnetron tends to yield a peak in the middle of a substrate [13].   Fig. 3 shows the deposition profile of TMS coatings produced by no anode assembly plasmas and anode magnetron plasmas. With similar plasma conditions, a similar TMS plasma coating thickness was obtained by no anode assembly operation to anode magnetron plasma. It was also noted that no anode assembly operation produced a more uniform TMS coating than anode magnetron plasmas, which showed a mild peak at the center of the substrate.

Coating properties

Our previous results have demonstrated that anode magnetron plasma coatings provided excellent corrosion protection of aluminum alloys. Therefore, the plasma coatings produced by no anode assembly plasmas have to be compared with those prepared by anode magnetron plasmas.

Refractive index is one of the simplest methods to describe the quality of plasma polymer coatings. Fig. 4 shows the refractive indices of TMS plasma polymer coatings produced by no anode assembly plasmas and anode magnetron plasmas. It can be seen that, at similar plasma conditions, no anode assembly plasma could produced TMS plasma coating with refractive indices identical to those prepared by anode magnetron plasmas.
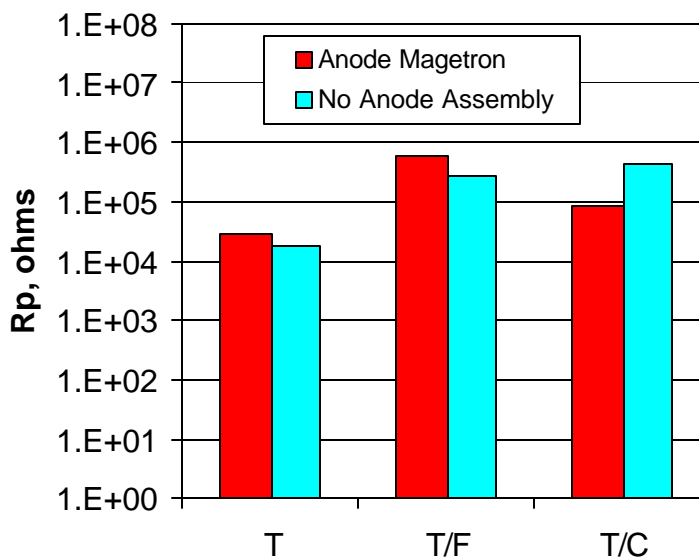
Figure 5. Polarization resistance of plasma polymer coated Alclad 7075-T6 alloys in 0.5% NaCl and 0.35% $(NH_4)_2SO_4$ aqueous solution.

DC polarization technique is very useful in predicting the corrosion protection properties of coatings on metal substrates. Our previous results indicated that the application of a thin layer of TMS plasma coatings (~ 50 nm) produced by anode magnetron plasmas significantly increased the R_p values on aluminum alloys [3-5]. To have a better control of the surface area exposed to electrolyte, Alclad 7075-T6 panels that have similar Al surface coatings to IVD aluminum but dense and smooth surface were used to examine the effects of DC plasma coatings on the polarization resistance of aluminum alloys. Fig. 5 compares the polarization resistance (R_p) of several plasma coated Alclad 7075-T6 panels. It can be seen that no anode-assembly plasmas and anode magnetron plasmas produced plasma coatings on Alclad 7075-T6 with very similar polarization resistance. This data indicated that no-anode assembly plasmas and anode magnetron plasmas produced plasma coatings with very similar corrosion protection properties.

Adhesion enhancement to subsequent spray primers

The corrosion protection of plasma interface engineered coating systems relies on the tenacious water-insensitive adhesion and good barrier characteristics of the coatings [3]. DC cathodic polymerization and plasma treatment have demonstrated to be an efficient method in improving the primer adhesion to metallic substrates [6, 14].

We have previously reported that a tenacious adhesion of several kinds of primers was achieved with application of plasma coatings by anode-magnetron plasmas [6]. Table 3 compares the adhesion test results of Deft primers (44-GN-36 and 44-GN-72) to plasma coatings prepared by no anode assembly and anode magnetron plasmas. As deposited IVD aluminum coating usually has a porous surface structure that can enhance the primer adhesion through mechanical interlocking mechanism. In order to exclusively examine the plasma treatment effect on primer

adhesion, Alclad 7075-T6 panels that have similar Al coating to IVD Al coatings but smooth surface were utilized as the substrates for DC plasma treatment in Table 3. It can be seen that no anode assembly and anode magnetron plasma polymers gave equivalent adhesion behaviors to Deft primers. It is worth to noted that, other than plasma T/F, plasma T/C, T/O, and T/Ar also gave good adhesion to Deft 44-GN-72 primer, which could not be stripped off by Turco stripper for over 24 hours.

Table 3. Adhesion test results of chromated primers (Deft 44-GN-36 and 44-GN-72) to plasma coated Alclad 7075-T6 alloy.

7A (Ace/O)	Plasma Mode	Deft 44-GN-36			Deft 44-GN-72		
		Dry Tape Test	Boiling Test (8 hrs)	Turco	Dry Tape Test	Boiling Test (8 hrs)	Turco
T	AM*	0	--	< 5 min	0	--	~ 6 min
	NA**	0	--	< 5 min	0	--	~ 6 min
T/F	AM	5	4	> 24 hrs	5	4	> 24 hrs
	NA	5	4	> 24 hrs	5	4	> 24 hrs
T/C	AM	5	4	~ 15 min	5	4	> 24 hrs
	NA	5	4	~ 15 min	5	4	> 24 hrs

As stated earlier, the main objective of this study is to improve the corrosion protection of IVD coated aluminum alloys without using hazardous heavy metals in the coating systems. Deft primers of both 44-GN-36 and 44-GN-72 contain a large amount of chromates, which are highly toxic chemical materials. In order to eliminate hazardous heavy metals in the plasma engineered coating systems, two other spray paint primers of Spraylat EWAE118 and Dexter 10-PW-22-2 that are chromate free were selected to produce the plasma interface engineered coating systems.

Table 4. Adhesion test results of non-chromated primers (Spraylat EWDY048 and Dexter 10-PW-22-2) to plasma coated Alclad 7075-T6 alloy under IVD conditions.

7A (Ace/O)	Spraylat EWAE118			Dexter 10-PW-22-2		
	Dry Tape Test	Boiling 1,4,8 hrs	Turco	Dry Tape Test	Boiling 1,4,8 hrs	Turco
T	2	---	---	3	0, ---	~10 min
T/(O)	5	0, ---	~ 5 min	5	5, 5, 5	~30 min
T/(Ar)	5	5, 3, 3	~ 15 min	5	5, 5, 5	~13 hrs

The adhesion performance of Spraylat EWAE118 and Dexter 10-PW-22-2 primers to DC plasma treated Alclad 7075-T6 aluminum alloys was evaluated and the adhesion test results were summarized in Table 4. It can be seen that an excellent adhesion was achieved on T/(Ar) treated aluminum surfaces for these two primers. They survived the tape test even after water boiling

for 8 hours. After the application of Turco paint stripper, Spraylat primer on T/(Ar) treated panels did not show any blisters in the beginning 15 min and Dexter primer stuck firmly to the T/(Ar) treated substrate for about 13 hours.

The poor primer adhesion of as deposited TMS plasma coating, which is shown in Table 3 & 4, can be ascribed to its low surface energy and also the possible existence of oligomers on the surface. It has been reported that plasma polymerization of organosilicons contains small amounts of oligomeric product [15, 16]. Therefore, there exist two very possible reasons for the primer adhesion improvement of TMS plasma coatings by second plasma treatment of argon or oxygen. The first is that, as shown in Fig. 6, argon or oxygen plasma treatment can significantly lower the TMS surface water contact angle, and thus produce a wetting surface for spray paint primers. Another reason is that argon or oxygen plasma treatment could eliminate the possible TMS oligomers and thus prevent the weak boundary layer formation on TMS coating surface.

Since the strong primer adhesion is the most crucial factor in inhibitor-free coating systems, the chromate-free primer coated IVD systems with application of plasma T/(Ar) treatment were selected for the further corrosion performance investigation through different corrosion tests.
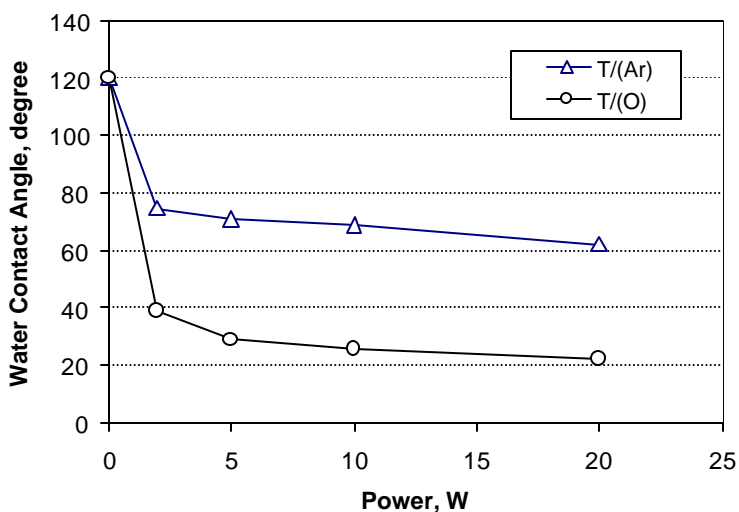
Figure 6. Water contact angle changes of TMS plasma polymer surface with input power of the second plasma treatment. Plasma conditions for plasma treatment are: 1 sccm Ar or oxygen, 50 mTorr, 1 min.

Corrosion test results

Two types of corrosion evaluation tests, SO_2 and Prohesion salt spray tests were employed for the evaluation of corrosion protection characteristics of plasma tailored coating systems achieved by DC cathodic polymerization and plasma treatment under the conditions of IVD. The 4 week SO_2 salt spray test was chosen to speed up differentiation of the corrosion protection properties of the different systems investigated. The Prohesion cyclic salt spray test, which is chemically milder than the SO_2 salt spray test, was conducted for a longer period, 12 weeks. It is considered

a more realistic test, as it better simulates actual service conditions of an aircraft in which both wet and dry periods occur.
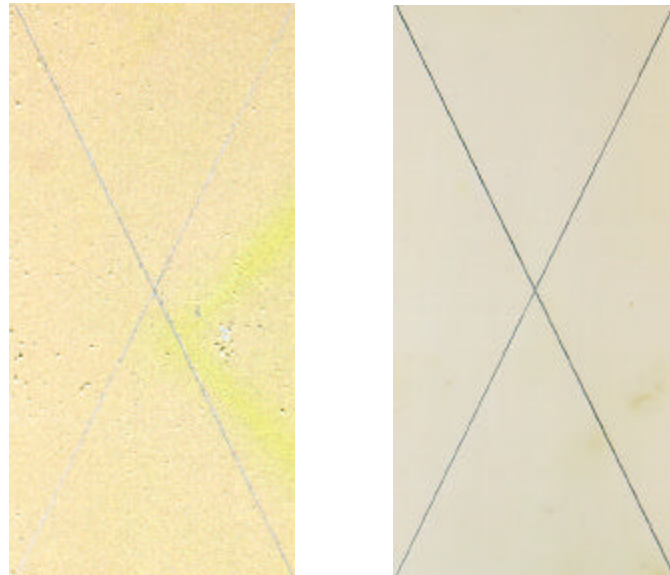
(a) SO_2 tested
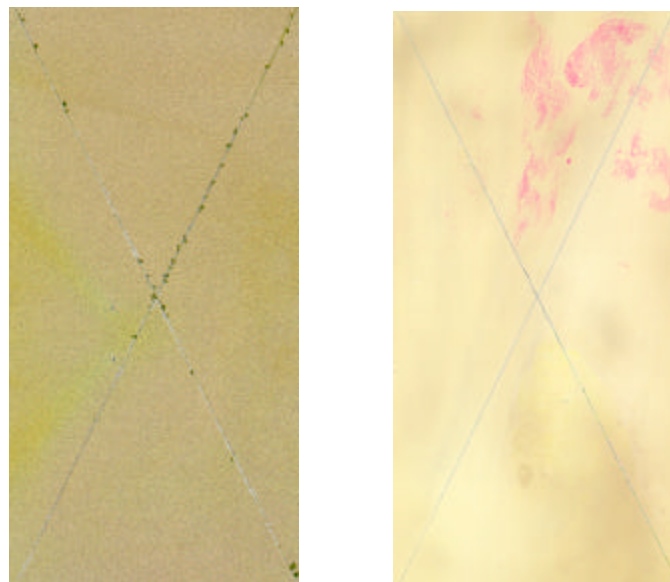
(b) Prohesion tested

Figure 7. Scanned images of (a) SO_2 salt spray tested and (b) Prohesion salt spray tested Chromate-free plasma coating systems of IVD 2024-T3 ([2I]) and their Chromated control panels, left column. Some blisters were observed on chromate conversion coatings after the paints were removed. Paints were still on the plasma prepared samples (right column) because they could not be removed by commercial Turco paint stripper solution.
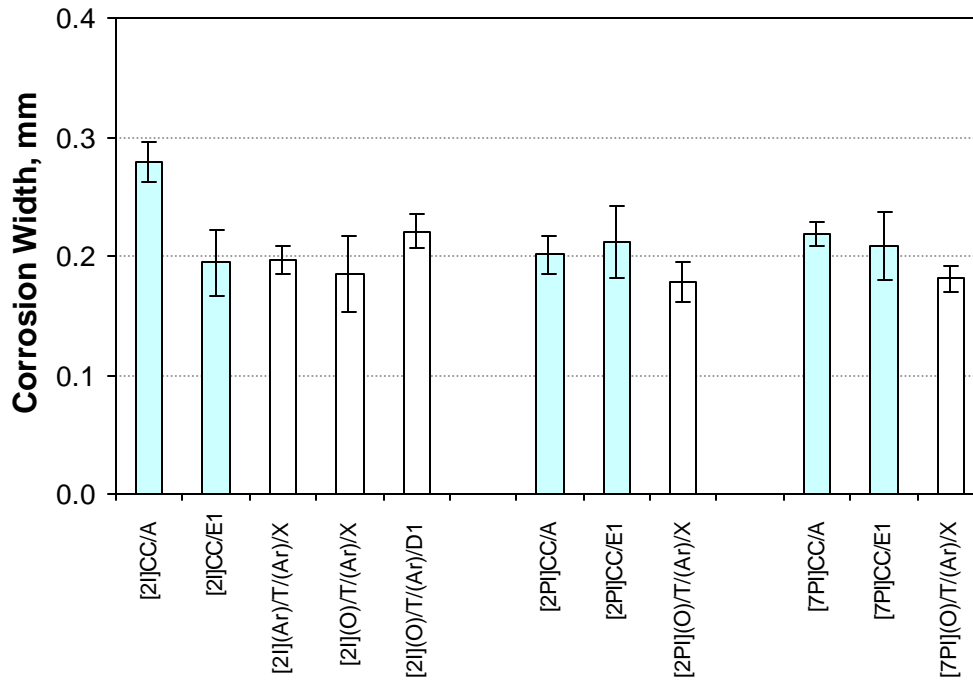
Figure 8. Corrosion widths of SO_2 salt spray tested Chromate-free plasma coating systems of IVD panels prepared under IVD conditions and their Chromated controls.

After 12 week Prohesion salt spray test, Deft primer coated IVD controls performed much better than the E-coated controls, although it was hard to distinguish the difference among the two controls with 4 week SO_2 salt spray test. Fig. 7(b) presents the typical scanned images of Prohesion salt spray tested IVD coated aluminum alloys. By visual observation, one easily can see that clear corrosion creepage appeared along the scribed lines for Deft primer coated controls ([2I]CC/A). In contrast, the chromate-free plasma coating systems of [2I](O)/T/(Ar)/X showed nearly no sign of corrosion on the whole panels.

All the Chromate-free plasma coating systems of IVD Al-coated Al alloys performed extremely well in SO_2 salt spray test. Fig. 7(a) shows the typical scanned images of SO_2 salt spray tested plasma coating systems of IVD panels and their Chromated controls.

After the SO_2 salt spray test, the Chromate-free plasma coating systems of both IVD Al-coated 2024-T3, plate stock 2124-T851 and 7050-T7451 (not shown in Fig. 7) showed no corrosion either along the scribe lines or away from the scribe. It should especially noted that these plasma tailored IVD coating systems are non-strippable with conventional paint strippers (Turco 5469).

The pattern seen on Prohesion salt spray tested sample (Fig. 7(b), right side) is the stain on the remaining paint caused by the Turco stripping test. In contrast, the control panels clearly showed some blisters on the Chromate conversion coating, which will very possibly influence the long-term corrosion performance of these coating systems.

The corrosion test results were evaluated and the corrosion widths along the scribe lines were calculated according the procedures described previously. Fig. 8 shows the comparison of average corrosion widths of SO$_2$ salt spray tested IVD panels of Chromate-free plasma coating systems and the Chromated controls. From Fig. 8, it can be noted that almost all the plasma coating systems outperformed their Chromated controls. One most important fact that should be pointed out here is the non-strippable nature of plasma coating systems on IVD panels, which will play a significant role in the long-term corrosion protection of Al alloys.

The corrosion widths of Prohesion salt spray tested were calculated and summarized in Fig. 9. As seen from Fig. 9, between the two types of IVD controls, E-coated IVD controls (CC/E) that is the combination coating systems of chromate conversion coating with non-chromated E-coat showed very large corrosion widths for all the IVD Al-coated aluminum alloys.
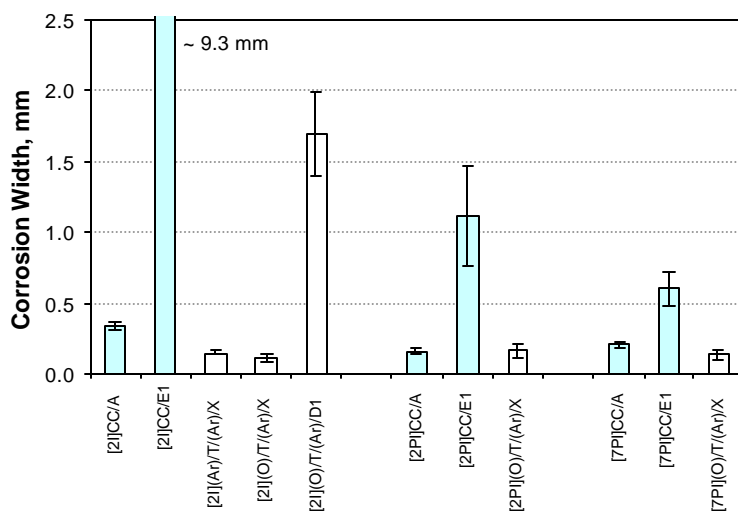
Figure 9. Corrosion widths of Prohesion salt spray tested Chromate-free plasma coating systems of IVD panels prepared under IVD conditions and their Chromated controls.

Among the three types of aluminum alloys employed in this study, all the chromate-free coating systems except [2I](O)/T/(Ar)/D1 achieved by DC plasma treatment performed extremely well after the Prohesion salt spray test. It can be seen that these plasma tailored coating systems showed very little corrosion widths and outperformed their corresponding chromated controls. The only one exception is [2I](O)/T/(Ar)/D1 specimen that performed well in the SO$_2$ salt spray test exhibited severe corrosion in Prohesion test with large corrosion widths. Since there is no any corrosion inhibitor existing in the plasma tailored coating systems, their excellent corrosion performance must resulted from the tenacious adhesion at the primer/IVD interface that was achieved by DC cathodic polymerization and plasma treatment under the condition of IVD operation.

It was noted that, from Fig. 9, the [2I](O)/T/(Ar)/D1 specimen that performed well in the SO$_2$ salt spray test exhibited much larger corrosion widths along the scribed lines and many pit

corrosion away from the scribed lines were visually observed after Prohesion test. The worse performance of Spraylat primer coated samples might resulted from its weaker adhesion to plasma treated IVD surface than Dexter primer, which have been shown earlier from the adhesion test results. Another possible reason might be due to its inferior barrier properties to Dexter primer because there was no pit corrosion observed for Dexter primer coated samples but many pits on Spraylat primer coated panels after the Prohesion test.

Conclusions

The experimental results presented in this study clearly indicated that the removal of anode assembly did not affect the DC cathodic polymerization process or degrade the resulted plasma coating properties. In comparison with anode magnetron plasmas that showed excellent corrosion protection of aluminum alloys, DC cathodic polymerization under such conditions similar to IVD operation provided plasma coatings with similar deposition rate, deposition uniformity, refractive index, polarization resistance, and excellent adhesion performance to subsequent spray paint primers. These results suggested that DC cathodic polymerization could be performed in an existing IVD equipment.

With the application of DC cathodic polymerization and plasma treatment under conditions similar to IVD process, the resulted chromate-free plasma coating systems provided excellent corrosion protection of IVD Al-coated aluminum alloys, which out performed chromated IVD controls in both the SO_2 and Prohesion salt spray tests. By eliminating the standard peening and conversion coating steps on IVD coated parts, chromate-free plasma coating systems will not only get rid of the environmentally hazardous chromates but also add potential cost savings for corrosion protection of IVD Al-coated aluminum alloys.

References

[1]   B.T. Nevill, 36th Annual Technical Conference Proceedings-Society of Vacuum Coaters, Albuquerque, NM, USA, 1993, p. 379.

[2]   K.E. Steube and L.E. McCrary, J. Vac. Sci. Technol., 1(1974): p.362.

[3]   C. M. Reddy, Q.S. Yu, C. E. Moffitt, D. M. Wieliczka, R. Johnson, J. E. Deffeyes, and H. K.Yasuda, "Improved Corrosion Protection of Al Alloys by System Approach Interface Engineering: Part I - Alclad 2024-T3", Corrosion, 56 (2000): p.819.

[4]   Q.S. Yu, C. M. Reddy, C. E. Moffitt, D. M. Wieliczka, R. Johnson, J. E. Deffeyes, and H. K. Yasuda, "Improved Corrosion Protection of Al Alloys by System Approach Interface Engineering: Part II - AA 2024-T3", Corrosion, 56 (2000): p.887.

[5]   C. E. Moffitt, C. M. Reddy, Q.S. Yu, D. M. Wieliczka, R. Johnson, J. E. Deffeyes, and H. K. Yasuda, "Improved Corrosion Protection of Al Alloys by System Approach Interface Engineering: Part III - AA 7075-T6", Corrosion, **56**, No. 10, 1032-1045, (2000).

[6]   Q.S. Yu, J. E. Deffeyes, and H. K. Yasuda, "Corrosion Protection of Ion Vapor Deposition (IVD) Al-coated Al Alloys by Low-Temperature Plasma Interface Engineering: Part I: DC Cathodic Polymerization with Anode Magnetron Enhancement", Prog. Org. Coat, submitted.

[7]   A. Sharma and H. Yasuda, J. Vac. Sci. Tech., 21(4) (1982): p.994.

[8]   A. Sharma and H. Yasuda, J. Adhesion, 13 (1982): p.201.

[9]   ASTM standards G85-94, Standard Practice for Modified Salt Spray (Fog) Testing, Annex 4.

[10]   ASTM standards G85-94, Standard Practice for Modified Salt Spray (Fog) Testing, Annex 5.

[11]   Chandra M. Reddy and H. K. Yasuda, D. M. Wieliczka, and J. Deffeyes, Plating and Surface Finishing, **86** (10), 77-79,(1999).

[12]   M. Miyama and H.K. Yasuda, J. Appl. Polym. Sci., 70 (1998): p. 237.

[13]   J. G. Zhao and H. K. Yasuda, "The Effect of Magnetic Field Configuration in the Cathodic Polymerization Systems with Two Anode Magnetrons", J. Vacuum Sci. & Tech., **in press**, (2000).

[14]   T.F. Wang, T.J. Lin, D.J. Yang, J.A. Antonelli, H.K. Yasuda, Prog. Org. Coat., 28 (1996): p.291.

[15]   A.M. Wrobel, M. Kryszewski, M. Gazicki, J. Macromol. Sci..-Chem., A20 (1983): p. 583.

[16]   M. Gazicki, A.M. Wrobel, M. Kryszewski, J. Appl. Polym. Sci., 21 (1977): p. 2013.

10. Corrosion Protection of Ion Vapor Deposition (IVD) Al-Coated Al Alloys by Low-Temperature Plasma Interface Engineering: Part III - DC Cathodic Polymerization in a Closed Reactor System

Qingsong Yu, C.E. Moffitt, D.M. Wieliczka, Joan Deffeyes, Hirotsugu Yasuda

Abstract

DC cathodic polymerization of trimethylsilane (TMS) and its mixtures with argon was conducted in a closed reactor system. The TMS deposition behavior and plasma parameters were examined with discharge time during the deposition process. The chemical composition of TMS plasma polymers was investigated by X-ray photoelectron spectroscopy (XPS) analysis. It was found that the TMS plasma coatings obtained under such operations have a distinct chemical structure that gradually changes from carbon rich at the top surface to silicon rich at the interface with the substrate. The coating characteristics of TMS plasma polymers were evaluated in term of refractive index, polarization resistance (Rp value), and adhesion performance to subsequent spray paint primers. Experimental data indicated that DC cathodic polymerization of TMS in a closed reactor system produced plasma coatings with superior coating properties, such as higher refractive index and stronger primer adhesion, to those obtained in a flow reactor system as employed in parts 1 and 2 of this series. As a result, the plasma interface engineered coating systems of IVD/Plasma polymer/Non-Chromated primer obtained under such a operation showed excellent corrosion protection of IVD Al-coated Al alloys, which outperformed the chromate conversion coated IVD controls after 4 weeks of SO_2 salt spray and 12 weeks of Prohesion salt spray tests.

Introduction

In our previous studies [1,2], efforts were made to utilize cathodic plasma polymerization of trimethylsilane (TMS) in conjunction with Ion Vapor Deposition (IVD) of pure Aluminum on aluminum alloys. The laboratory scale cathodic polymerization with anode magnetron applied on IVD Al coated substrate showed excellent corrosion protection characteristics of the corrosion protection systems without chromate conversion coating nor chromates in primers [1]. Cathodic plasma polymerization carried out under the operational conditions that are compatible with IVD operation also produced the same excellent corrosion protection [2].

In a separate study, it was found that the characteristics plasma deposition rate of Si-containing organic compounds is nearly six times greater than that of hydrocarbons [3]. In plasma polymerization, a significant extent of fragmentation of the original monomer molecules occurs, and direct deposition of the original molecules is an unlikely event. It is, therefore, anticipated that Si-containing moieties would deposit faster than C-based moieties leading to a Si-rich depositions from TMS, which contains one Si and three C in the original molecule. This difference in the characteristic deposition rates would be amplified if the plasma polymerization is carried out in a closed system, because the gas phase composition with respect to Si and C

changes continuously, and the composition of the deposition changes accordingly. Therefore, it is anticipated that the closed system deposition of TMS would lead to a graded composition film.

In the IVD coating process, the reactor is filled with argon gas to a certain pressure and the aluminum evaporation is arranged to face the parts [4,5]. Before initiating the ensuring plasma for the additional film deposition, the monomer gas has to be filled into the whole reactor to maintain a certain system pressure. If the reactor has a large volume, such as an industrial IVD reactor, large amounts of monomer gases will be necessary to fill the reactor to a certain pressure. In this case, if the plasma deposition is operated in a flowing mode in the aim of achieving a very thin plasma coating, very little amount of the monomers will be effectively utilized and most of them will be wasted and lost through the exhaust.

In contrast, DC cathodic polymerization in a closed system seems to be the most efficient way to operate plasma deposition in a large-scale reactor. In such a closed system, certain amounts of monomers can be introduced into the reactor to the minimum pressure required to start the plasma. Then, the feeding of monomer can be stopped and plasma deposition can be started. After the necessary coating thickness is achieved, the plasma can be stopped by an operator or possibly by the plasma system itself due to the conversion of gaseous monomers to solid coatings. In this operation mode, there is a minimum loss of gases and the most efficient utilization of the initial monomers. It is also possible to keep the argon that is used in IVD operation as an additional process gas in the plasma film deposition, if a closed system operation of TMS polymerization is utilized.

In order to explore the possibility of efficiently operating plasma deposition in an industrial IVD reactor, DC cathodic polymerization of trimethylsilane (TMS) in a closed system mode under conditions similar to the IVD operation was investigated. The corrosion protection properties of the plasma coatings obtained under such operation were also studied on IVD Al-coated Al alloys.

Experimental

Materials and sample preparation

All the materials used in the present study are identical to what was described in part 2 of this series [2]. Except the plasma deposition step, the sample preparation procedures were the same as part 2 of this series.

Plasma reactor system and operation

DC cathodic polymerization and plasma treatment was carried out in a bell jar reactor without using an anode assembly, which was described in detail in parts 1 and 2 of this series [1,2]. A pair of IVD panels was placed inside the plasma reactor as the cathode (i.e. substrate for deposition). Plasma treatment by simple gases, such as oxygen or argon, was conducted in a similar flow system to parts 1 and 2.

To conduct plasma deposition in a close reactor system, the reactor chamber was first pumped down to < 1 mTorr. The reactor chamber was then isolated from the pump system by closing the main valve located in between. TMS gas, controlled by an MKS mass flow meter (model 247C), was then fed into the reactor. After the system pressure reached the preset point, TMS gas feeding was stopped and DC power was then applied to initiate the glow discharge to start cathodic polymerization. In the case of TMS mixed with argon, Argon gas was fed into the reactor after TMS gas feeding was stopped. The TMS/Ar ratio was controlled and calculated by their partial pressures in the reactor system.

A residual gas analyzer (RGA) is connected to the plasma reactor (Leybold-Inficon Transpector 2 with a range of 200 amu controlled by Transpectorware[TM], version 3). The faraday cup sensor employed by this unit is attached to a Leybold-Inficon IPC-2 pressure converter system. The major components are the sampling valve, turbomolecular pump (Leybold-Inficon TMP-150), and rotary van pump. Quantitative RGA data were obtained by recording a mass spectrum for gases present in the isolated IPC-2 to correct background gases, then recording spectra of gases in the plasma reactor.

XPS analysis

X-ray photoelectron spectroscopy (XPS) data was acquired with a Kratos AXIS HS instrument, using the Mg-Kα flood source operated at ~217 watts (15 mA, 14.5 kV). It is probably better to use the term electron spectroscopy for chemical analysis (ESCA) in this instance since relevant Auger electrons were collected to enhance the chemical information obtained from the samples, but the convention is more often to use the term XPS. All of the XPS data were acquired in the hybrid mode of the instrument, which combines electrostatic and magnetic lensing. The 2 mm aperture, used in the hybrid mode, limits collection to a spot size on the order of 200-300 μm. All spectra were collected with the analyzer set at a pass energy of 80 eV, including the individual core spectra. This gives a FWHM of just over 1.4 eV for the Ag 3d line. All depth profiling was done at 90 degree take-off angle (surface normal). Charge compensation was made with the manufacturer's proprietary system, at settings of: -1.5 V charge balance voltage, 1.85 A filament current, and –0.5 V bias voltage.

XPS depth profiles were done with a rastered Ar^+ beam. The beam energy was 4 kV at a filament emission of 10 mA. This gives a current of about 1μA at the sample in a spot size of ~1.1 mm, which was rastered over an area of approximately 3x3 mm^2. Data were collected from near the center of this area.

2.4. Tests and measurements

An AutoEL-II automatic ellipsometer (Rudolph Research Corporation), which is a null-seeking type with a 632.8 nm helium-neon laser light source, was used for measurement of the thickness and refractive index of deposited films in different glow discharges.

A linear polarization technique was used to evaluate the R_p values of plasma coated aluminum panels [6]. All the measurements were carried out in an aqueous salt solution (0.5% NaCl + 0.35% $(NH_4)_2SO_4$) performed with an EG&G Potentiostat/Galvanostat Model 273A that was controlled by 352 SoftCorr[TM] III Corrosion Measurement Software.

Adhesion tests used in this study were exactly the same as described in part 1 of these series. Standard tape test (ASTM D3359-93B) was first used to evaluate the adhesion performance of the coating systems [7]. For stronger adhesion, an accelerated adhesion test developed by Sharma and Yasuda [8, 9] was utilized to further examine adhesive characteristics of the samples. In such test, cross-shaped cuts were first made on the coated specimen in accordance with the tape test procedure. Specimens are then immersed in boiling water and periodically examined via the tape test. In the aerospace industry, Turco paint stripper solution (Turco 5469, Turco Products, Inc., Cornwells Heights, PA) is commonly used to strip the primer coatings off of painted aircraft parts during maintenance and repair procedures. For most painted systems, Turco solution can delaminate the paint within several minutes of application. In this study, the time required to delaminate the paint is taken as a third measure of the adhesive strength of the coating/IVD interface of the investigated systems.

Two types of accelerated corrosion tests, SO_2 (4 weeks) salt spray test performed per ASTM G85-94-annex A4 [10] and Prohesion (12 weeks) cyclic salt spray tests performed per ASTM G85-94-annex A5 [10], were used to examine the corrosion protection performance of the coating systems on IVD coated aluminum alloys.

The detailed description of the test methods and evaluation procedures used in this study was given in Part I of this series [1].

Results and Discussion

Closed versus Flow System Plasma Polymerization

In a flow system plasma polymerization, the system pressure is continuously adjusted by controlling the opening of a throttle valve connected to the pumping system. Because of fragmentation of original monomer in a plasma state, the composition of gas phase changes on the inception of the plasma state. The increase in the total number of gas molecules is compensated by the increased pumping rate in a flow system (the flow system employed in this study), and a steady state flow of a consistent composition of gas phase is established at a pre-determined system pressure.

In a closed system plasma polymerization, a fixed amount of monomer molecules are contained in a reactor, and glow discharge is initiated. The system pressure in such a system (in a given volume) is proportional to the total number of gas phase molecules. The fragmentation of monomer molecules as well as the ablation of gaseous species from the deposited material will increase the pressure, while deposition will decrease the system pressure. Thus, the system pressure change with plasma polymerization time will indicate the change in the overall balance between the plasma fragmentation/ablation and the plasma film deposition.

Fig. 1 depicts the system pressure change in a closed system reactor when plasma polymerization of TMS is carried out. The system pressure continuously increases while the glow discharge is on, but remains at a constant value as soon as the glow discharge is turned off. This indicates that the total number of gas phase species increases with time in spite of the deposition of plasma

polymer of TMS. Fig. 2 depicts the change of gas phase species detected by a mass spectrometer during the plasma polymerization of TMS. The results indicate that the deposition of Si containing species takes place in the early stage of plasma polymerization, and the deposition of C containing species lags behind the deposition of Si-species. In the later stage, the main species that constitute the plasma phase is hydrogen.
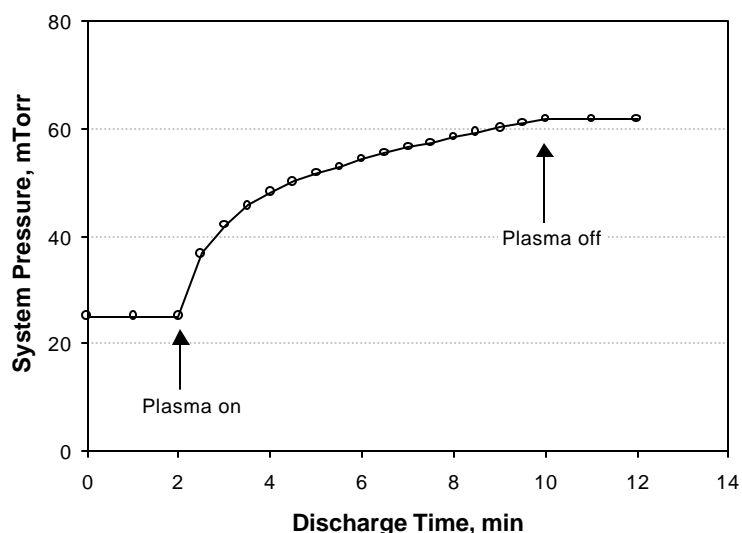
Figure 1. Increase of system pressure in closed system plasma polymerization of TMS. Plasma conditions are: 25 mTorr TMS, 2 panels of Alclad 7075-T6, DC 1000 V.
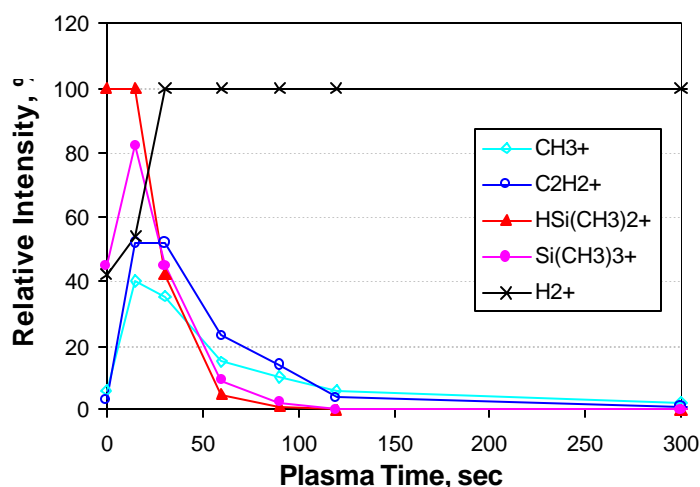
Figure 2. Change of gas phase species in plasma of TMS with plasma time. Plasma conditions are: 25 mTorr TMS, 2 panels of Alclad 7075-T6, DC 1000 V.
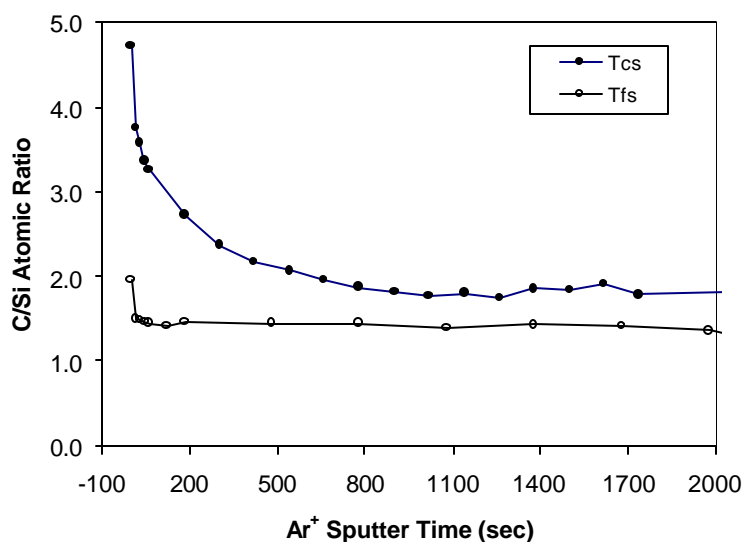
Figure 3. Cross-sectional depth profile of XPS measured C/Si ratios of plasma polymer films of TMS prepared in a flow system reactor (Tfs) and in a closed system reactor (Tcs).
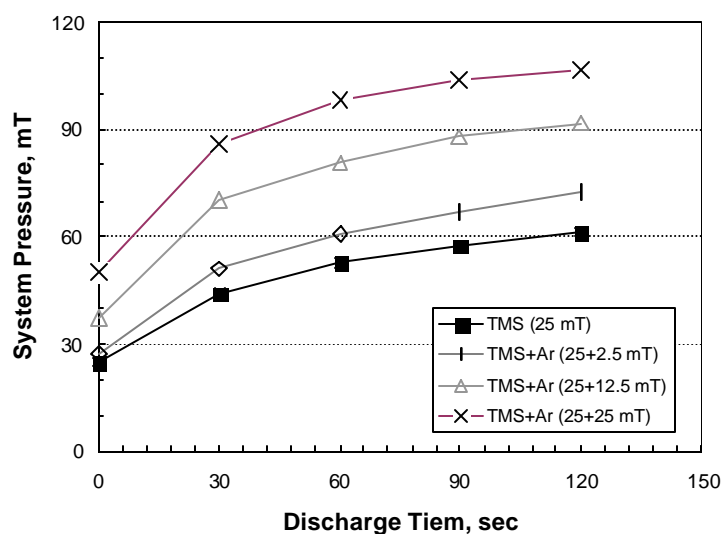
Figure 4. System pressure change with discharge time during plasma polymerization of TMS and its mixtures with argon at different ratios. Plasma conditions are Alclad 7075-T6 substrate, 25 mTorr TMS + Ar (based on TMS/Ar ratios), 2 panels of Alclad 7075-T6, DC **1000V.**

According to this scheme of plasma polymerization of TMS in a closed system, it is anticipated that the atomic composition of the plasma polymer should continuously change with the plasma polymerization time. Fig. 3 depicts comparison of XPS cross-section profile of C/Si ratios for plasma polymers deposited in a flow system reactor and that in a closed system reactor. The results clearly show that a closed system plasma polymerization of TMS indeed produces a film

with graded composition; i.e., with decreasing carbon content from the surface of the film into the interface with the substrate.

Considering the fact that the system pressure continues to increase after most of the polymerizable species are exhausted in the gas phase, plasma polymerization of TMS in a closed system can be visualized as a time-delayed, consecutive application of three fundamental processes. The sequence takes the order of 1) deposition of Si-species, 2) deposition of C-species, and 3) plasma treatment of the deposited plasma polymer by the non-polymer forming gas plasma.

Plasma parameter changes

Because of the objective of the present study, the initial system pressure of TMS was intentionally set to a lower value of 25 mTorr, rather than 50 mTorr that was used in parts 1 and 2 of this series [1,2]. Fig. 4 shows the system pressure change with discharge time during plasma polymerization of TMS only and its mixtures with argon gas at different ratios. DC cathodic polymerization of a TMS/Ar mixture has its advantages over that of pure TMS monomers, because the argon addition can help to achieve a more stable glow discharge. Also since inert argon gas is always present in the IVD process [4,5], DC cathodic polymerization of a TMS/Ar mixture can provide a more compatible process with the industrial IVD system. The result shown in Fig. 4 indicated that the pressure increase is more than the partial pressure of Ar added to the system.
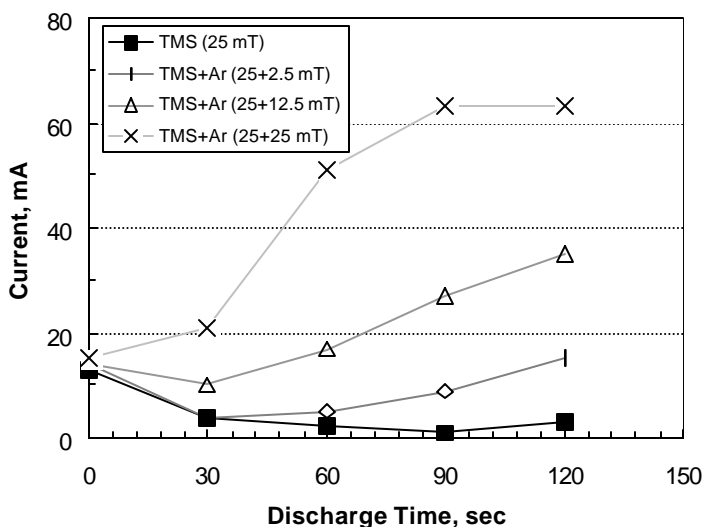
Figure 5. DC current change with discharge time during plasma polymerization of TMS and its mixtures with argon at different ratios. Plasma conditions are Alclad 7075-T6 substrate, 25 mTorr TMS + Ar (based on TMS/Ar ratios), 2 panels of Alclad 7075-T6, DC 1000V.

Fig. 5 shows the current change with discharge time during plasma polymerization of TMS and its mixtures with argon gas. It was noted that, for TMS monomer only, or its mixture with less argon addition (2.5 mTorr and 12.5 mTorr), the DC current to maintain the plasma dropped

down first after the plasma was ignited at a constant DC potential of 1000 V applied to the substrate. This phenomenon obviously resulted from disappearance of TMS monomers due to polymer deposition and the ionization difficulty of the gases produced from fragmentation of the TMS monomer. Therefore, the current decrease was not observed when a large amount of argon gases existed in the plasma system, such as 25 mTorr of argon mixed with TMS.
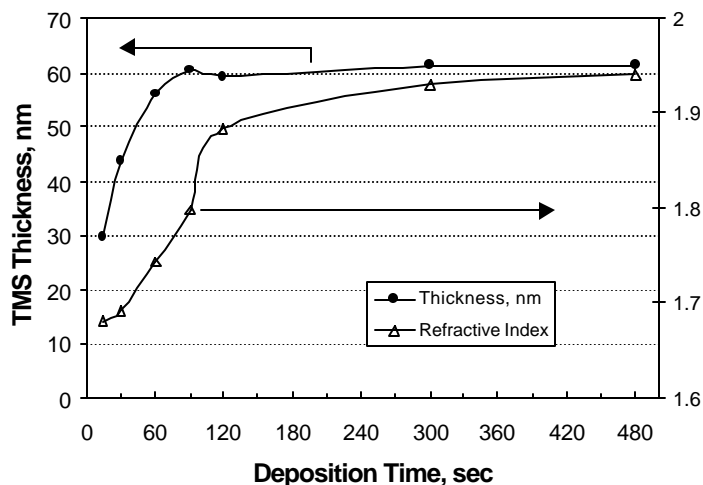
Figure 6. Thickness and refractive index changes of TMS plasma coatings with discharge time in a closed reactor system. Plasma conditions are: TMS 25 mT, 2 panels of Alclad 7075-T6, DC 1000 V.
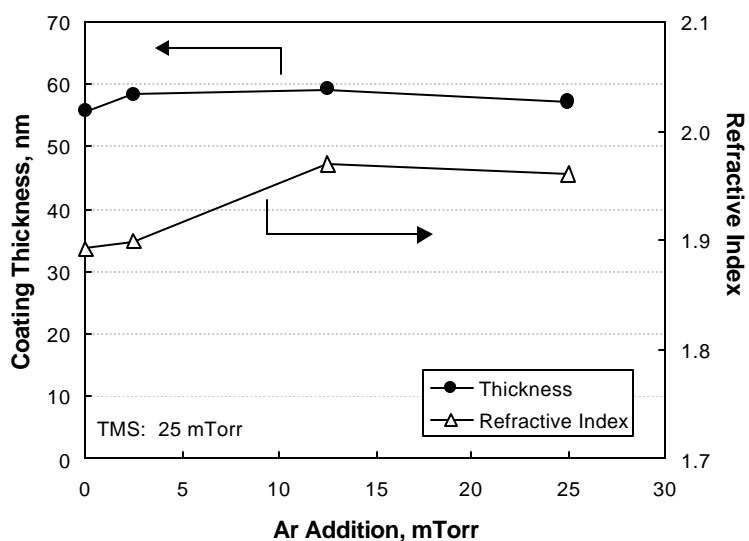
Figure 7. Thickness and refractive index changes of closed system TMS plasma coatings with argon pressure in the reactor system. Plasma conditions are: TMS 25 mT, 2 panels of Alclad 7075-T6, DC 1000 V, 2 min.

Coating properties

Fig. 6 shows the dependence of the thickness and refractive index of TMS plasma coating on the plasma polymerization time in a closed reactor system using TMS monomers. It can be seen that the coating thickness increased very fast in the first 90 seconds. After 90 seconds, the TMS coating thickness stopped growing with the deposition time. But the refractive index of TMS coating keep increasing with the deposition time. This increase obviously resulted from the continuing bombardment by the reactive species in the plasma.

Fig. 7 shows the changes of TMS plasma polymer thickness and refractive index with the addition of argon into the closed reactor system using TMS. It can be seen that the coating thickness of plasma polymers was solely determined by the amount of TMS monomer being filled into the reactor system. On the other hand, the addition of argon did not affect the coating thickness but increased the coating quality of TMS plasma polymers that was reflected from the increase of film refractive index.

XPS analysis of TMS films

Figs. 8 and 9 summarize the XPS results from three TMS plasma films produced in closed reactor system (Figs 8a and 9a) and flow reactor system (Figs 8b and 9b), with and without second plasma surface treatment. These films were deposited on Alclad 7075-T6 panels that were acetone cleaned and then oxygen plasma treated prior to film deposition. Alclad 7075-T6 panels with smooth surfaces were chosen for such a purpose because they provide similar Al coating surface to IVD Al-coated Al alloys. One film was removed from the reactor right after TMS plasma deposition, the second was treated with an argon plasma and the third with an oxygen plasma treatment after the TMS deposition.

As observed from Fig.8, TMS plasma films produced from close and flow systems both have a surface chemical structure similar to silicon carbide bonding with Si 2p bonding energy close to 99.5 eV. The second O_2 plasma treatment on these TMS films changed the surface structure to silicon oxide with Si 2p bonding energy shifted to 103 eV. As seen from Fig. 8b, the Ar plasma treatment on flow system TMS polymers resulted in the similar effects as O_2 plasma treatment. In contrast, as noted in Fig. 8a, the Ar plasma treatment on closed system TMS polymers has a surface composed of the intermediary bonding and is thought to be some silicon-oxycarbide bonding or Si_2O bonding with various possible silicon sub-oxides [11-13].

Fig. 9 shows C/Si ratios formed from the XPS sputter depth profiles of the TMS plasma polymers with and without additional plasma treatment. As deposited, without a second plasma treatment, the closed system TMS plasma film has a surface that is carbon rich (with C/Si ratio of ~ 4.7) and low oxygen content (with O/Si ratio of ~ 0.7). From Fig. 9a, it is observed that the as-deposited TMS plasma film shows a gradual structure change from the surface with more carbon (C/Si ratio of ~ 4.7) to lower carbon (C/Si ratio of ~ 1.7) in the bulk film. This also manifests itself as a higher C/Si ratio at the surface than the bulk value, which is unique to this film.
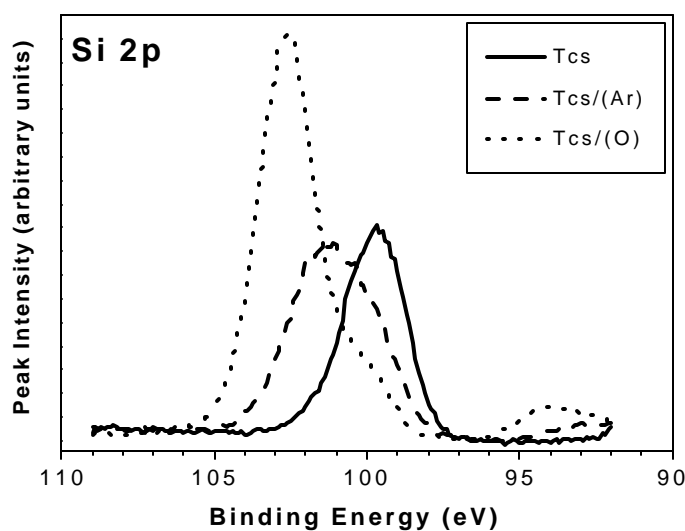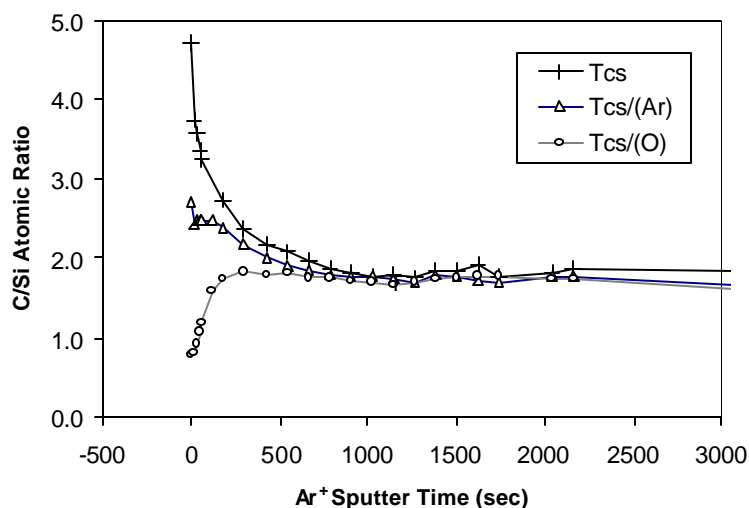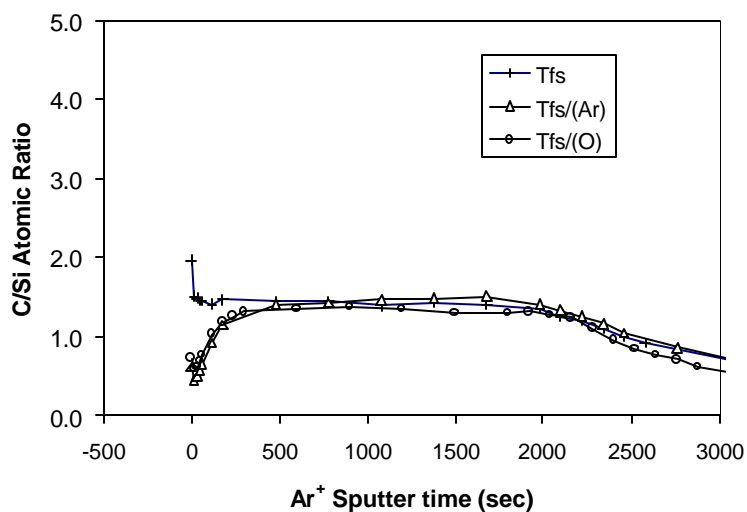
(a) Closed system TMS

(b) Flow system TMS

Figure 8. Si 2p photoelectron spectra from the top surface of TMS plasma coatings produced in (a) closed reactor system and (b) flow reactor system with and without second surface treatment by O_2 or Ar plasmas.

The O_2 plasma treatment on the TMS film, shown in Fig. 9, is seen to significantly reduce the incorporation of carbon in outer region of the TMS plasma films (including both closed system and flow system TMS polymers) and change the surface from a carbon rich state to one being rich in SiO_2 bonding. This result indicates that the O_2 plasma has the effect of removing carbon

from the film surface as a volatile compound and restructuring the surface into a silicon oxide rich layer.

(a) Closed system TMS

(b) Flow system TMS

Figure 9. Cross-sectional depth profile of XPS measured C/Si ratios of TMS plasma polymer films prepared in a (a) closed reactor system and (b) flow reactor system with and without second surface treatment by O_2 or Ar plasmas.

The argon plasma treatment of flow system TMS polymers had a similar ratio in the depth profile as oxygen plasma treatment, shown in Fig. 9b. In contrast, as noted in Fig. 9a, the argon plasma modified the surface of closed system TMS film to an intermediary position with a certain amount of carbon loss and silicon enrichment near the surface. The argon plasma treated closed system TMS film surface has a distinctly different silicon structure, somewhat

intermediary between the bulk and true silicon oxide as shown in Fig. 8. It is not asserted that the Ar treatment actually induces oxygen bonding simply by its own interaction. Rather, these samples were exposed to atmosphere prior to XPS analysis, hence any active sites formed during the Ar treatment then had ample time to react, forming oxygen bonds upon exposure to atmospheric gases.

Primer adhesion

From the XPS analysis results, it was found that TMS plasma coatings prepared in closed system have a carbon rich surface, which is similar to TMS polymers followed by methane plasma deposition, i.e. T/C as described in part 2 of this series, in a flow system. The adhesion study also showed that the T/C plasma treatment on aluminum alloy provided excellent adhesion to spray paint primers. In the present study, the primer adhesion performance of close system TMS plasma polymers was also examined and the results were summarized in Tables 2 and 3. Since the porous surface structure of IVD Al coating may conceal the plasma treatment effect on primer adhesion, Alclad 7075-T6 Al alloy panels were selected as the substrates for adhesion investigation based on the fact that they can provide smooth surfaces while still providing a similar Al coatings to that of IVD Al coatings.

Table 2 lists the adhesion test results of two chromated spray paint primers applied to these closed-system TMS plasma coatings with and without subsequent surface treatment by oxygen or argon plasmas. Due to their similar chemical structure to the flow system T/C plasma polymer, TMS plasma polymers prepared in a closed reactor have a much better primer adhesion than those produced in a flow reactor. Therefore, the more organic (carbon rich) top surface of closed system TMS coatings was considered as the main factor contributing to their superior primer adhesion performance to those prepared in flow system. Excellent primer adhesion performance was obtained on closed system TMS polymer surface with appropriate second argon plasma treatment, indicating that the intermediate bonding structures observed by the XPS analysis may play some strong role in primer adhesion.

Table 2. Adhesion performance in various adhesion tests, indicating the influence of second plasma treatment effects of TMS plasma films (under IVD conditions) on their adhesion performance to chromated primers (Deft 44-GN-36 and 44-GN-72). Substrates areAlclad 7075-T6 (7A(Ace/O)).

TMS Coating	2nd plasma (1 min)	Deft 44-GN-36			Deft 44-GN-72		
		Tape Test	Boiling 1,4,8 hrs	Turco	Dry Tape Test	Boiling 1,4,8 hrs	Turco time
Flow T$_{fs}$	---	0	---	< 5 min	0	---	~ 6 min
	C	5	4	~ 15 min	5	4	> 24 hrs
Closed T$_{cs}$	---	5	4, 3, 3	~ 5 min	5	3, 3, 3	~ 10 min
	(Ar)	5	4, 3, 2	~ 20 min	5	5, 4, 4	> 24 hrs

In order to produce chromate-free plasma coating systems, the adhesion of closed system TMS coatings to non-chromated primers (Spraylat EWAE118 and Dexter 10-PW-22-2) was also investigated, and the adhesion test results are summarized in Table 3. As noted in Table 3, closed system TMS plasma polymers showed superior primer adhesion performance to those obtained from a flow system. Similar to chromated primers, summarized in Table 2, excellent primer adhesion was always achieved with closed system TMS plasma polymers treated with subsequent Ar plasma applications.

Table 3. Adhesion performance in various adhesion testes, indicating the influence of second plasma treatment effects of TMS plasma films (under IVD conditions) on their adhesion performance to non-chromated primers (Spraylat EWAE118 and Dexter 10-PW-22-2). Substrates are Alclad 7075-T6 (7A(Ace/O)).

TMS Coating	2nd Plasma (1 min)	Spraylat EWAE118			Dexter 10-PW-22-2		
		Tape Test	Boiled 1,4,8 hrs	Turco	Tape Test	Boiling 1,4,8 hrs	Turco
Flow **T**fs	---	2	---	---	3	0, ---	~ 10 min
	(Ar)	5	5, 3, 3	~ 15 min	5	5, 5, 5	~13 hrs
Closed **T**cs	---	5	4, 4, 4	~ 12 hrs	5	5, 5, 5	~30 min
	(Ar)	5	5, 5, 5	>24 hrs	5	5, 5, 5	> 24 hrs
Closed **TAr (2:1)**	---	5	5, 5, 5	> 24 hrs	5	5, 5, 5	~ 14 hrs
Closed **TAr (1:1)**	---	5	5, 5, 5	>24 hrs	5	5, 5, 5	> 24 hrs
Closed **TAr (1:2)**	---	5	3, 3, 3	~ 10 min	5	5, 5, 5	~ 14 hrs

It should be pointed out that excellent primer adhesion was also obtained with TMS plasma polymers from a TMS+Ar mixture in a closed reactor system. This result indicated that, to achieve equally good primer adhesion, TMS polymerization with subsequent Ar plasma treatment could be replaced by one process of cathodic polymerization of a TMS+Ar mixture. Since the addition of argon to TMS can help stablize the gas discharge, the plasma polymerization of a TMS+Ar mixture is very important in the practical operation of plasma deposition process in conjunction with the industrial IVD process. Plasma polymerization of a mixture of TMS and argon in a closed system also has the advantage of being more compatible with the IVD process due to argon coexistence, excellent adhesion performance, and the benefit of one process of combining TMS plasma polymerization and second plasma treatment of the TMS polymers.

In order to study the surface property change of closed system TMS plasma polymers, the water contact angle change was studied as a function of the plasma power input for the second plasma treatment and the results are shown in Fig. 10. Reflecting the C-rich top surface, the plasma polymer of TMS prepared by the closed system reactor has significantly lower contact angle (~ 80 degree) than that for the sample prepared by a flow system reactor (~ 120 degree), without

post-deposition treatment (value from zero power in the graph). It can be seen that the second Ar or O$_2$ plasma treatment lowered the water contact angles on closed system TMS polymer surfaces, but not as much as the change introduced on the flow system sample. On the other hand, it has been well documented that argon plasma treatment on an organic surface could produce a more cohesive skin to enhance primer adhesion through crosslinking effects on the top surface [14].
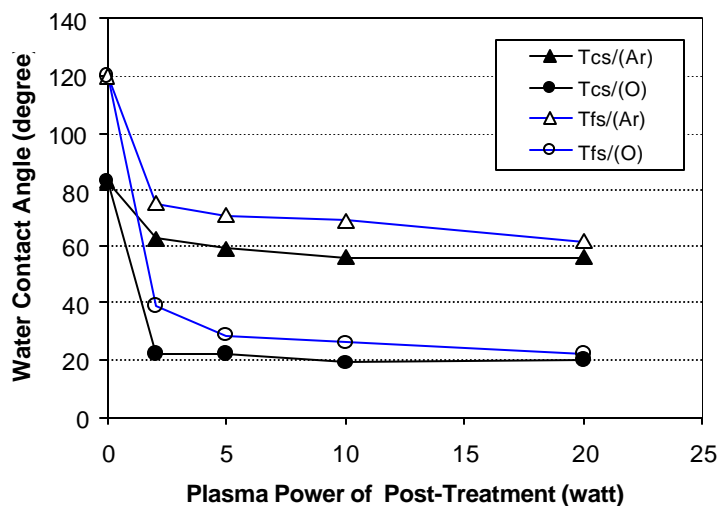
Figure 10. Water contact angle change of closed system and flow system TMS polymer surfaces with the power input of argon and oxygen plasma post-treatment.

Polarization resistance

Polarization resistance (Rp value), which is defined as the charge-transfer resistance of the solution-metal interface, has been considered as a very useful measure in predicting the corrosion protection properties of coatings on metal surfaces. It has been demonstrated that the application of a very thin layer of plasma coatings (~ 50 nm) could significantly increase the Rp values of aluminum alloys [15-17]. In the present study, the polarization resistance of TMS plasma-film coated Alclad 7075-T6 aluminum alloy was measured in an aqueous salt solution. Alclad 7075-T6 aluminum alloy was chosen for this purpose because it has a somewhat similar surface Al coating to IVD Al-coated substrate and it provides a smooth surface for a better control of surface area exposed to electrolyte.

Fig. 11 summarizes the DC measurement results of TMS plasma coated Alclad 7075-T6 panels under IVD conditions in both closed and flow reactor systems, with and without subsequent Ar plasma treatments. As seen from Fig. 11, TMS plasma coatings produced in a closed reactor system showed higher Rp values than those obtained in a flow reactor system. The second plasma treatment by Ar reduced the Rp values of TMS coatings, which are still comparable to the corresponding flow system TMS plasma coatings.

Besides the advantageous features described earlier, DC cathodic plasma polymerization of TMS mixed with argon also provides an opportunity to combine the two processes of TMS deposition

and second plasma treatment into only one step. From Fig. 11, it can be seen that TMS plasma coatings thus produced also maintain excellent corrosion protection properties on the aluminum alloy substrates.
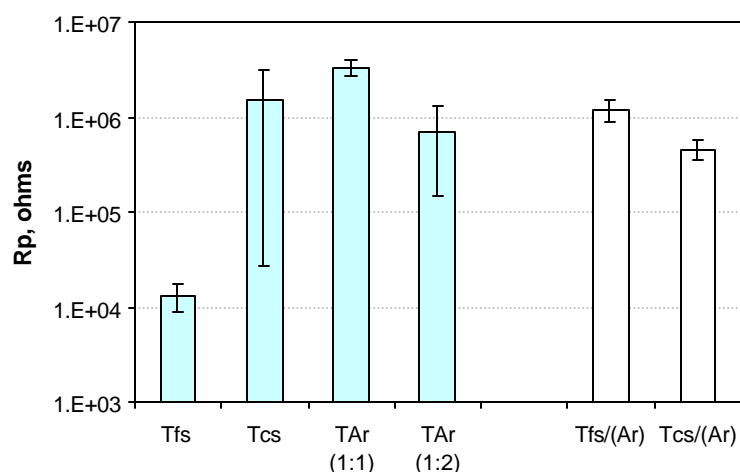
Figure 11. Polarization resistance of TMS plasma coated Alcad 7075-T6 (Ace/O) aluminum substrates under IVD conditions (without anode assembly) with or without second plasma treatment. Plasma conditions are 25 mTorr TMS + Ar (based on TMS/Ar ratios), DC 1000 V, 2 min for closed system TMS; 1 sccm TMS, 50 mTorr, DC 5 W, 1 min for flow system; 2 sccm oxygen or argon, 50 mTorr, 1 min for second plasma treatments.

Corrosion test results for (IVD)/Plasma Polymerization System

Two types of corrosion tests, SO_2 salt spray and Prohesion salt spray (as employed in parts 1 and 2 of this series), were used for evaluation of the corrosion protection characteristics of plasma coating systems produced by DC cathodic polymerization in a closed reactor system on IVD Al-coated Al. After the corrosion tests, the corrosion test results were evaluated and the corrosion widths along the scribe lines were measured and calculated according to the procedures described in part 1 of this series.

Fig. 12 shows the comparison of average corrosion widths from both (a) SO_2 salt spray and (b) Prohesion salt spray tested IVD panels. Both SO_2 and Prohesion test results, as observed in Fig. 12, show that **chromate-free** plasma coating systems provided excellent corrosion protection on IVD Al-coated Al alloys, having comparable or lower corrosion widths after the tests than their **chromated controls** of CC/A and CC/E on IVD Al-coated Al panels.

In comparison with flow system TMS plasma coatings (**T**fs), plasma coating systems based on close system TMS plasma polymers (**T**cs) provide equally good corrosion protection of IVD Al-coated Al alloys. From Fig. 12b, it was also noticed that the coating system of [2I](O)/Tcs/(Ar)/D obtained with closed system TMS plasma films (**T**cs) gave acceptable

performance in the Prohesion test, while [2I](O)/Tfs/(Ar)/D prepared in the flow system corroded very badly, having much larger corrosion widths.
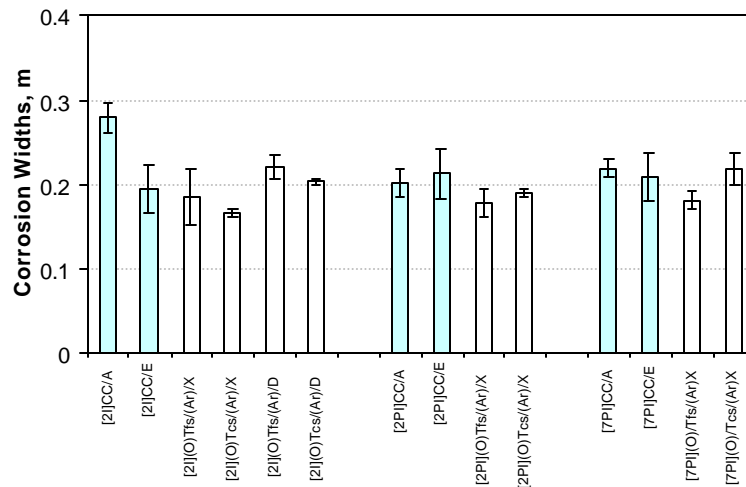
(a) SO$_2$ Test results
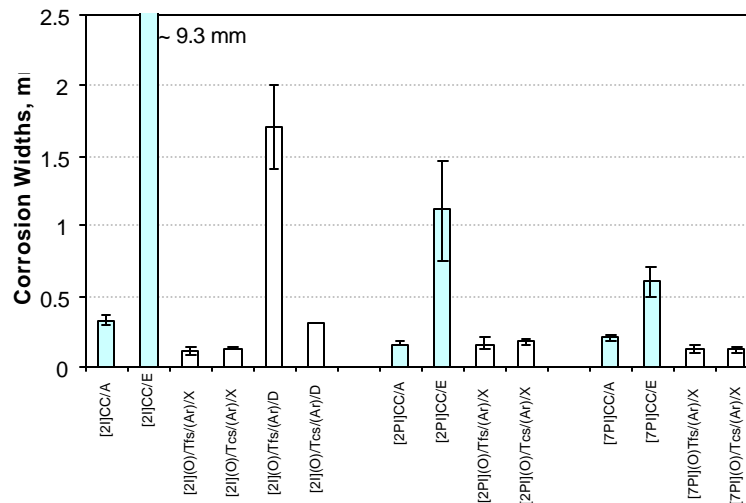
(b) Prohesion test results

Figure 12. Corrosion widths of (a) SO$_2$ salt spray and (b) Prohesion salt spray tested IVD Al-coated Al alloy panels protected with chromate-free plasma coating systems and their chromated controls.

It should be pointed out that the primers in the plasma coating systems applied to the IVD Al-coated Al alloys could not be removed by the commercial Turco paint stripper solution. This tenacious and water insensitive adhesion at the primer/IVD interface achieved by TMS cathodic polymerization in a closed reactor system must be responsible for the excellent corrosion protection performance of these plasma coating systems. In other words, excellent corrosion

protection of IVD Al-coated Al alloys can be accomplished with chromate-free primer coatings with the aid of tenacious and water-insensitive interface adhesion.

Conclusions

DC cathodic polymerization of TMS in a closed reactor system not only possesses the benefit of efficient operation in a large-scale reactor, but also yields high quality plasma coatings as compared with those obtained in a flow plasma reactor. XPS analysis results indicated that the TMS plasma coatings under such operation have unique chemical structures, which have a more organic (carbon rich) top surface and then gradually change through the film bulk to a more inorganic (silicon rich) structure near the aluminum substrate. The organic top surface of the coating provided a compliant adhesion base with subsequent spray paint primers that are usually epoxy type primers. At the other interface of the plasma coating, the inorganic structure was compatible with IVD aluminum, bonding strongly to the aluminum oxide surface. With further argon plasma treatment of TMS coating surfaces, or direct polymerization of TMS mixed with argon, tenacious adhesion was obtained between chromate-free primers and the TMS plasma film coated IVD Al substrates.

DC cathodic polymerization of TMS mixed with argon improved the primer adhesion performance of the closed system TMS plasma polymers. Moreover, the addition of a certain amount of argon into the TMS plasma system further increased the plasma coating quality, reflected in the increase in refractive indices. Based on the higher compatibility with the IVD process, the excellent adhesion performance, and the benefit of one process combining TMS plasma polymerization and the post-deposition plasma treatment, DC cathodic polymerization of TMS mixed with argon in a closed system is being considered as a more realistic approach in practical applications.

With the application of DC cathodic polymerization of TMS in a closed reactor system, the resulting **chromate-free** plasma coating systems have been shown to provide excellent corrosion protection of IVD Al-coated Al alloys. This was verified by both the 4 weeks of SO_2 salt spray and 12 weeks of Prohesion salt spray tests. In conjunction with the industrial IVD process, DC cathodic polymerization in a closed reactor system can use the large-volume IVD vacuum equipment more efficiently with significant savings from lower consumption of monomer gas.

References

[1] Q.S. Yu, J.E. Deffeyes, H.K. Yasuda, " Corrosion Protection of Ion Vapor Deposition (IVD) Al-Coated Al Alloys by Low-temperature Plasma Interface Engineering: part I: DC Cathodic Polymerization with Anode Magnetron Enhancement", Prog. Org. Coat., Submitted.

[2] Q.S. Yu, J.E. Deffeyes, H.K. Yasuda, " Corrosion Protection of Ion Vapor Deposition (IVD) Al-Coated Al Alloys by Low-temperature Plasma Interface Engineering: part II: DC Cathodic Polymerization under Conditions of IVD", Prog. Org. Coat., Submitted.

[3] Q.S. Yu and H.K. Yasuda, "Deposition behavior in low temperature cascade arc torch polymerization process", J. Polym. Sci.: Part A: Polym. Chem., 37 (1999) 967.

[4] B.T. Nevill, 36th Annual Technical Conference Proceedings-Society of Vacuum Coaters, Albuquerque, NM, USA, 1993, p. 379.

[5] K.E. Steube and L.E. McCrary, J. Vac. Sci. Technol., 1(1974) 362.

[6] "SoftCorr^{TM} III Corrosion Measurement Software Instruction Manual", EG&G Instruments Corp., 1997.

[7] ASTM standards D3359-93B, Annual book of ASTM standards, Vol. 06.01.

[8] A. Sharma and H. Yasuda, J. Vac. Sci. Tech., 21(4) (1982) 994.

[9] A. Sharma and H. Yasuda, J. Adhesion, 13 (1982) 201.

[10] ASTM standards G85-94-Annex A4 and A5, Annual book of ASTM standards, Vol. 03.02.

[11] F.J. Himpsel, F.R. McFeely, A. Taleb-Ibrahimi, J.A. Yarmoff, and G. Hollinger, Phys. Rev. B 38 (1988) 6084-6096.

[12] F.R. McFeely, K.Z. Zhang, M.M. Banaszak Holl, S. Lee, and J.E. Bender IV, J.Vac. Sci. Technol. B 14 (1996) 2824-2831.

[13] M.R. Alexander, R.D. Short, F.R. Jones, W. Michaeli, C.J. Blomfield, *Appl. Surf. Sci.* **137** (1999) 179-183.

[14] E.M. Liston, L. Martinu, M.R. Wertheimer, "Plasma surface modification of polymers for improved adhesion: a critical review" in Plasma Surface Modification of Polymers, Utrecht, The Netherlands, VSP 1994: p.3.

[15] C. M. Reddy, Q.S. Yu, C. E. Moffitt, D. M. Wieliczka, R. Johnson, J. E. Deffeyes, and H. K.Yasuda, "Improved Corrosion Protection of Al Alloys by System Approach Interface Engineering: Part I - Alclad 2024-T3", Corrosion, 56 (2000) 819.

[16] Q.S. Yu, C. M. Reddy, C. E. Moffitt, D. M. Wieliczka, R. Johnson, J. E. Deffeyes, and H. K. Yasuda, "Improved Corrosion Protection of Al Alloys by System Approach Interface Engineering: Part II - AA 2024-T3", Corrosion, 56 (2000) 887.

[17] C. E. Moffitt, C. M. Reddy, Q.S. Yu, D. M. Wieliczka, R. Johnson, J. E. Deffeyes, and H. K. Yasuda, "Improved Corrosion Protection of Al Alloys by System Approach Interface Engineering: Part III - AA 7075-T6", Corrosion, 56 (2000) in press.

11. An XPS Study of the Elemental Enrichment on Aluminum Alloy Surfaces from Chemical Cleaning

C.E. Moffitt, D.M. Wieliczka, and H.K. Yasuda

Abstract

The native oxide structure on aluminum alloys is usually modified by chemical treatments prior to the application of corrosion resistant coatings, to increase adhesion and performance. Certain commercial modifications were studied to determine their effects on the alloy surfaces, which might have substantial implications on the interface between the alloys and plasma polymers deposited on them. An x-ray photoelectron spectroscopy (XPS) depth profiling investigation of the effects of these chemical cleaners reveals enrichments of alloying elements on the metal surface beneath the modified oxide. Aspects of the enrichment phenomena show a correlation with data from corrosion-performance testing of interface engineered corrosion protection systems. The authors would like to acknowledge the support of DARPA through U.S. Air Force contract # AF F33615-96-C-5055.

Introduction

Pure aluminum forms a natural oxide on its surface, which acts as a barrier, protecting the aluminum from many types of chemical attack. Al_2O_3 has many desirable qualities, which include being chemically inert over a fairly broad range of pH, having high hardness, and possessing certain barrier properties. The strongest aluminum alloys, used primarily for aerospace applications, are more susceptible to chemical attack and corrosion. This susceptibility is generally associated with the alloying elements, via mechanisms related to combinations of local alloying heterogeneities [1-3].

The current, preferred method of inhibiting corrosion on these alloys is through the use of chromates, either through chromate conversion coating (CCC) or through the use of chromated primers, or both. The conversion coatings also serve to form a surface which is more amiable for coating adhesion [2]. Chromium is a heavy metal, which in its hexavalent state, as it is found in CCC chemistries and chromated primers, is known to be carcinogenic. This factor is driving up costs for these protection systems, due to expenses related to hazardous waste disposal, worker safety issues, and potential long term remediation. This, in turn, has driven research toward more environmentally benign anti-corrosion technology.

One novel approach to developing new coatings for corrosion protection is through the use of thin films formed by plasma polymerization of gaseous monomers[4]. These films have many interesting characteristics, including the ease of modification of the surface energy to enhance the wetting characteristics of various primers. During the course of analyzing plasma deposited films on two aluminum alloys, differing corrosion testing results were observed, which were distinctly dependent on the surface pretreatment used on the alloy. This phenomenon sparked an

investigation into the changes on the alloy surface after the use of wet-chemical surface pre-treatments.

Experimental

The two high strength aluminum alloys investigated in these experiments were AA2024-T3 and AA7075-T6. Panels of 0.040 inch thickness were purchased in batches from a test panel supplier (Q-Panel Lab Products, Cleveland, OH 44145, USA). The panels were treated with combinations of the following cleaning techniques: solvent wipe (acetone or ethanol), alkaline cleaner (Turco Products 4215S), deoxidizer (Parker-Amchem Deoxidizer 7 makeup with HNO_3), a pickle solution (53% HNO_3, 0.8% HF, remainder DI-H_2O) used by the Boeing Corporation in St. Louis, Mo. (formerly McDonnel Douglas Corp. (MDC)), and a 50% HNO_3 and DI-H_2O solution. The treatments followed for the commercial cleaners were those specified in MDC process specification documents.

Alloy panel samples were treated in a particular fashion, and loaded into the XPS chamber load lock. These were under vacuum supplied by a turbomolecular pump within five minutes of completion of each treatment. After a minimum of 30 minutes in the load lock, the samples were transferred into the analysis chamber.

XPS spectra were collected on a Kratos HS x-ray photoelectron spectrometer, using a Mg-Kα x-ray source operating at ~217watts (15mA, 14.5kV). They were collected at a pass energy of 80eV in the fixed analyzer transmission mode, which gives a FWHM of just over 1.4eV for the Ag 3d line. The lower resolution used allowed for more ready observation of the more faint spectral features. Spectra collected included C1s, O1s, Al2p, Cu2p, Mg2p, and Zn2p (7075) core XPS levels, valence band spectra, and Al KLL, Cu LMM (certain data sets) and Zn LMM (certain 7075 sets) x-ray induced Auger spectra. Charge compensation was provided by a low energy electron technique, which is unique to the Kratos magnetic immersion lens system. The charge neutralization parameters were –1.5V bias voltage, 1.85A filament current, and –0.5V filament voltage. The samples were sputter depth profiled by rastering a 4kV Ar^+ beam of roughly 2mmx2mm spot size over a 4mmx4mm area. Spectra were collected from an area of approximately 200μm diameter in the center of the sputtered region, utilizing the hybrid mode of the magnetic lensing capabilities.

After collection, the peak areas of the spectra, above a Shirley background, were calculated. Plots of peak area versus sputter time, depth profiles, give information proportional to the elemental concentrations as a function of sputtered depth. Areas from curve fitting results, using Gaussian-Lorentzian line-shapes with 30% Lorentzian contribution for the 80 eV pass energy, were used to investigate changes in chemical state as a function of depth when more than one state was present. Background calculations and curve fitting were performed using Kratos Vision software.

While the act of depth profiling destroys the use of adventitious carbon for charge referencing, consistent behavior has been observed on this system throughout a sizable number of plasma treated and/or wet chemically treated alloy samples. Preferential sputtering of different elements also has the ability to obfuscate depth-profiling results, but the magnitude of the elemental

enrichments reported here are large with respect to possible preferential sputtering artifacts. This is confirmed by the attainment of fairly consistent bulk concentration values.

Results and Discussion

The experimental results from depth profiles through plasma polymer films on alloys having various pretreatments showed certain irregularities associated with the alloying elements. The data presented here are the results from an ensuing investigation of these effects.

Fig. 1 shows the Cu 2p spectra taken from treated 2024-T3 samples. These were used to generate each trace in the Cu depth profile of Fig. 2. These spectra in figure 1 have a constant background subtracted from each of them for display purposes. The axis into the page and to the right corresponds to a spectrum index. The spectra were collected at various computer controlled sputtering intervals, with longer intervals deeper in the alloy samples, and therefore this axis is not linear with sputtering time. The time differences are properly scaled in the depth profiles of Figs. 2 and 3, which show total elemental contributions independent of possible mixed chemical states. The elemental depth profiles in Figs. 2 and 3 show some striking differences in the concentration levels of particular alloying elements, as well as, a somewhat expected, consistent trend of reduced oxide thickness. The aluminum peak areas have been adjusted to remove any Cu 3p contribution. This was accomplished by subtracting a fraction of the observed Cu 2p peak area at each point from the Al 2p peak area. The scaling fraction was obtained from the area of Cu 2p and 3p peaks in spectra from sputter cleaned, oxygen free, high conductivity (OFHC) copper collected at the same settings used for the alloy samples. The bulk alloy levels of constituent elements provide an internal, self-consistent standard for the concentration differences in the surface region of each sample.

All of the caustic pretreatments reduced the thickness of the total oxygen concentrations. This reduction is associated with the changes of the complex native oxide composed of hydrated MgO, $MgAl_2O_4$, and Al_2O_3 structures, which resides above a non-hydrated barrier film of primarily amorphous Al_2O_3 [1,5].

The elevated Mg levels are associated with the native oxides and are remnants of panel formation and heat treatment, being driven by thermally accelerated diffusion of Mg along grain boundaries and through channels in the mixed structure, to the surface. [3,5-12]. Chemical cleaning treatments are believed to minimize the amount of hydrated, mixed oxide above the more stable Al_2O_3 barrier layer. This allows for the plasma film to bond with the more stable barrier oxide after activation of the surface by the plasma. The effects of the removal of Mg enriched oxides are not often mentioned in standard surface treatment texts, but have been asserted to be the root of the main adhesion and interface stability issues associated with use of Mg containing Al alloys without chemical pretreatment [10,13,14].

The changes in Cu concentrations on the surfaces of both 2024 and 7075 samples, and the changes in Zn concentrations on the surface of 7075 samples, will be the remaining foci of this paper. Cu plays a large role in the corrosion processes involving Al-Cu alloys. This is attributed to galvanic coupling between solid solution portions of the alloy, second phase precipitates, and Cu depleted regions [1,2].
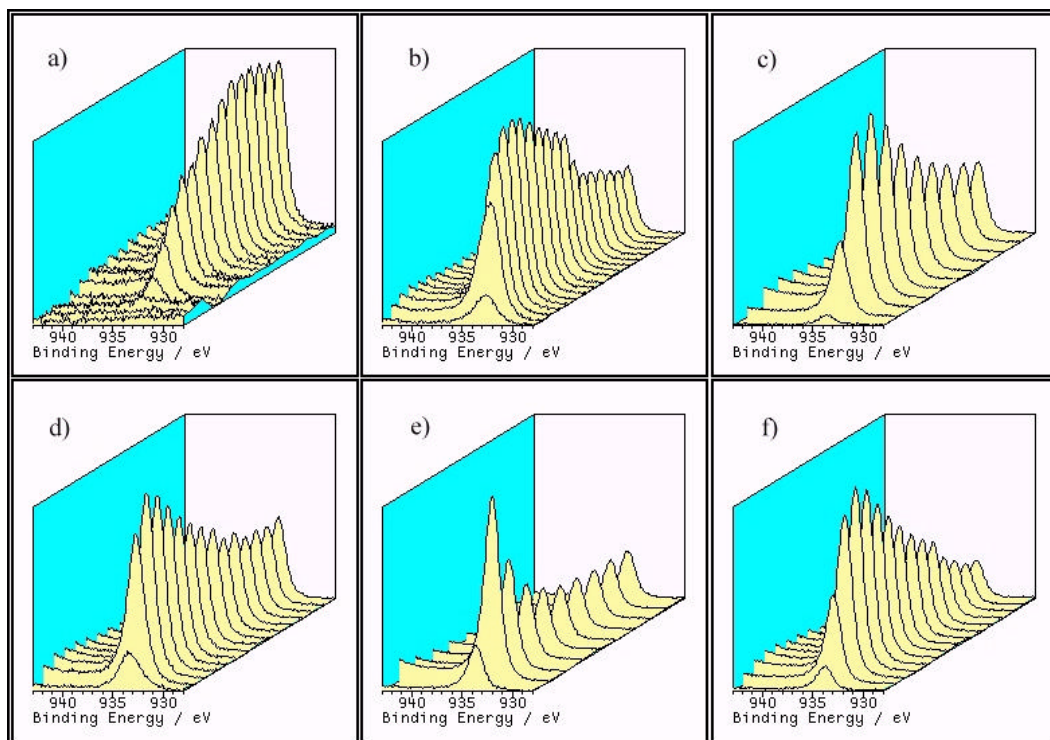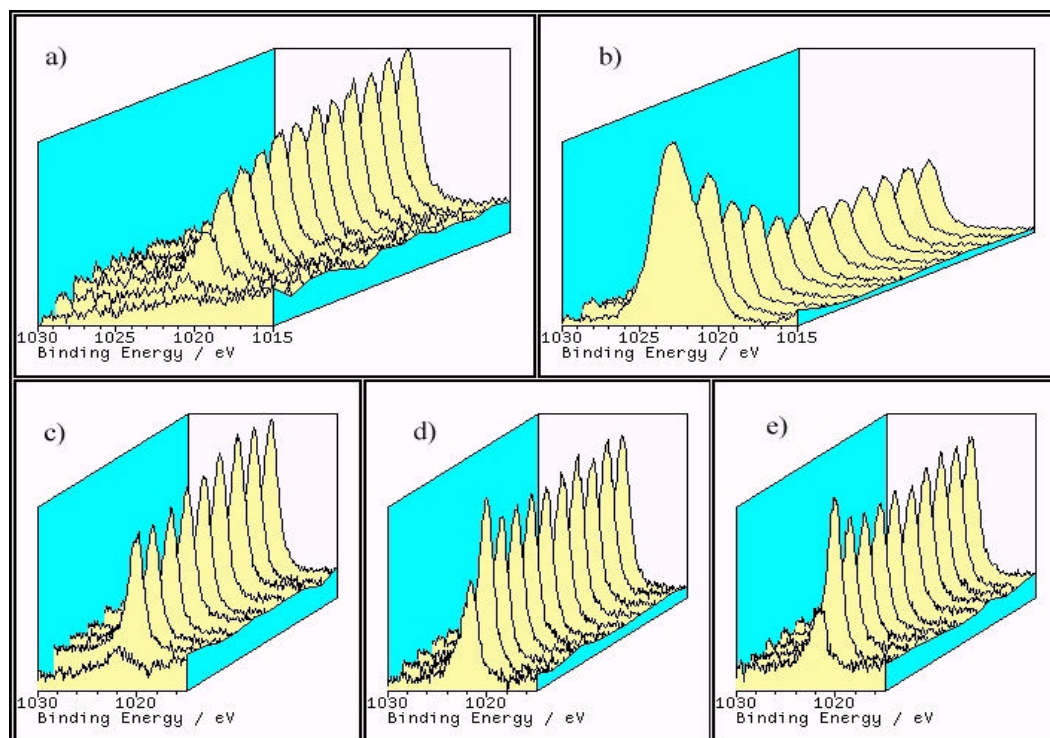
Figure 1. XPS Cu 2p spectra as a function of sputter time for AA2024-T3 after various pretreatments: a) ethanol wiped native surface, b) alkaline cleaned, c) alkaline cleaned and deoxidized, d) pickle treated, e) pickled and deoxidized, and f) alkaline cleaned, deoxidized, and dipped in 50% HNO$_3$-DI water solution for 30 sec.

Figs. 2 and 3 display the large enrichment of Cu on the surfaces of the treated alloy samples. The amount of copper enrichment is on the order of three to seven times the bulk concentrations for both AA2024-T3 and AA7075-T6. Copper enrichment has been observed on these alloys after similar alkaline cleaning and etching using the Forest Products Laboratory (FPL) etch [13]. Copper enrichments have also been reported by others on aluminum alloys [15-24] and relatively pure aluminum [25,26], as well as on copper alloys [27,28], but the implications of this have not been fully explored.

The nature of galvanic attack leads to cathodic deposition of ionic species onto the cathodic site, exposed at weak regions in the oxide. After a large enough potential difference has developed between the cathodic site and a nearby depleted region, the oxide is breached and corrosion of the depleted region begins and accelerates, as has been nicely shown by Kowal, *et. al.* [17]. The Cu enrichment reported here is in itself cause for concern with respect to corrosion performance. This condition would tend to predispose the surface for accelerated attack, once any protective coating is breached.

Although above a Cu enriched surface, plasma film systems, with the plasma films acting as adhesion promoters and barrier films beneath protective coatings, have shown comparable, if not better, corrosion resistance performance on AA2024-T3 panels which had chromate conversion

coatings applied to them beneath coating systems [29]. This was accomplished on alkaline cleaned panels. These same films faired markedly worse on AA7075-T6, until the deoxidation step was included prior to plasma film deposition.

The plot of Zn 2p spectral area as a function of sputter time in Fig. 3 shows striking differences in the effects of the cleaning treatments with respect to the Zn levels at the AA7075-T6 alloy surface. The alkaline cleaned sample has a pronounced enrichment of Zn on the surface, which is approximately the same thickness as the oxide itself. This is readily observed in Fig. 4, which shows the spectra used to generate the depth profiles. Behavior similar to this has also been reported [30,31]. A similar enhancement has been attributed for the detachment of anodic oxide films [31]. This enriched zinc concentration of the alkaline cleaned surface is roughly five times the bulk Zn concentration value.
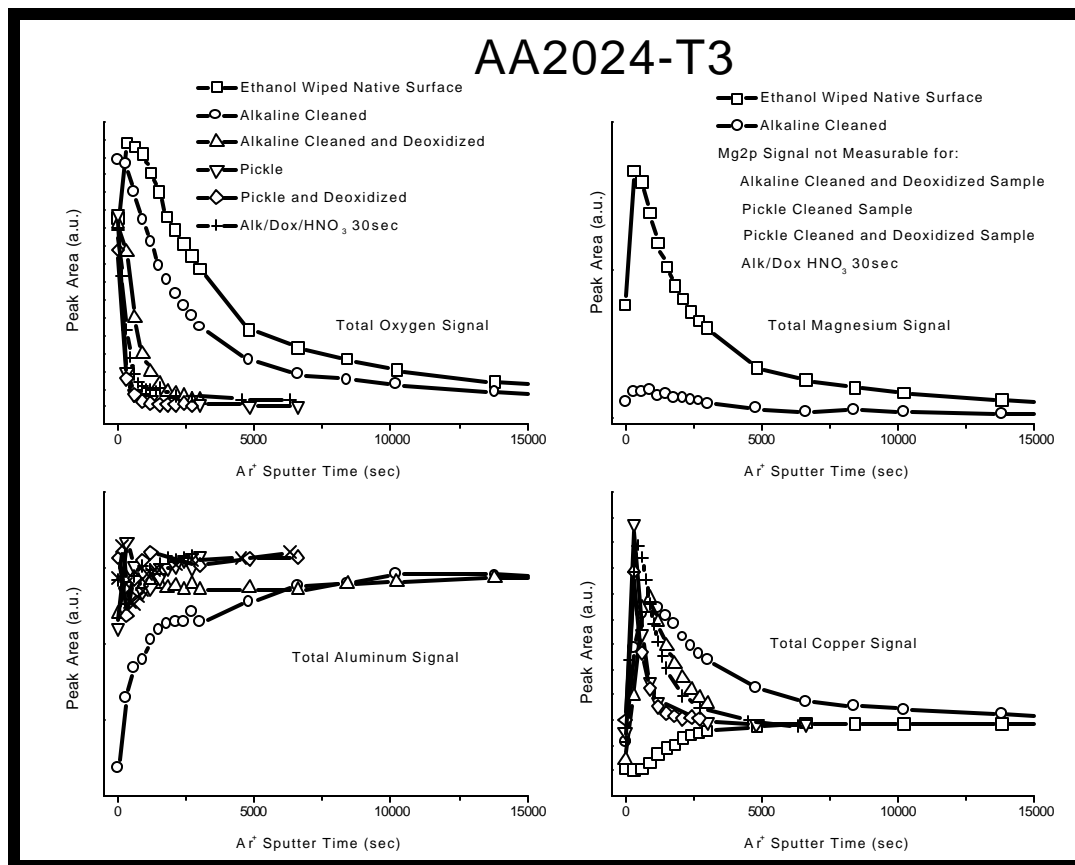
Figure 2. XPS depth profile summary graph for AA2024-T3 showing O1s, Mg2p, Al2p, and Cu2p spectral areas as a function of sputter time.

Another point of interest is the particular condition of the alloy surface after alkaline cleaning, deoxidation, and then dipping the 2024 alloy sample into a 50% mixture of HNO_3 and de-ionized water. The surface, as seen in figure 2, maintains a Cu enriched surface despite the apparently long held claim [18,5], that this eliminates surface Cu enrichments. It should be noted that one of

the original references [32], the apparent origin of this belief, was written before the advances in surface analytical techniques, which measure surface levels at a scale virtually undetectable by the previous methods.
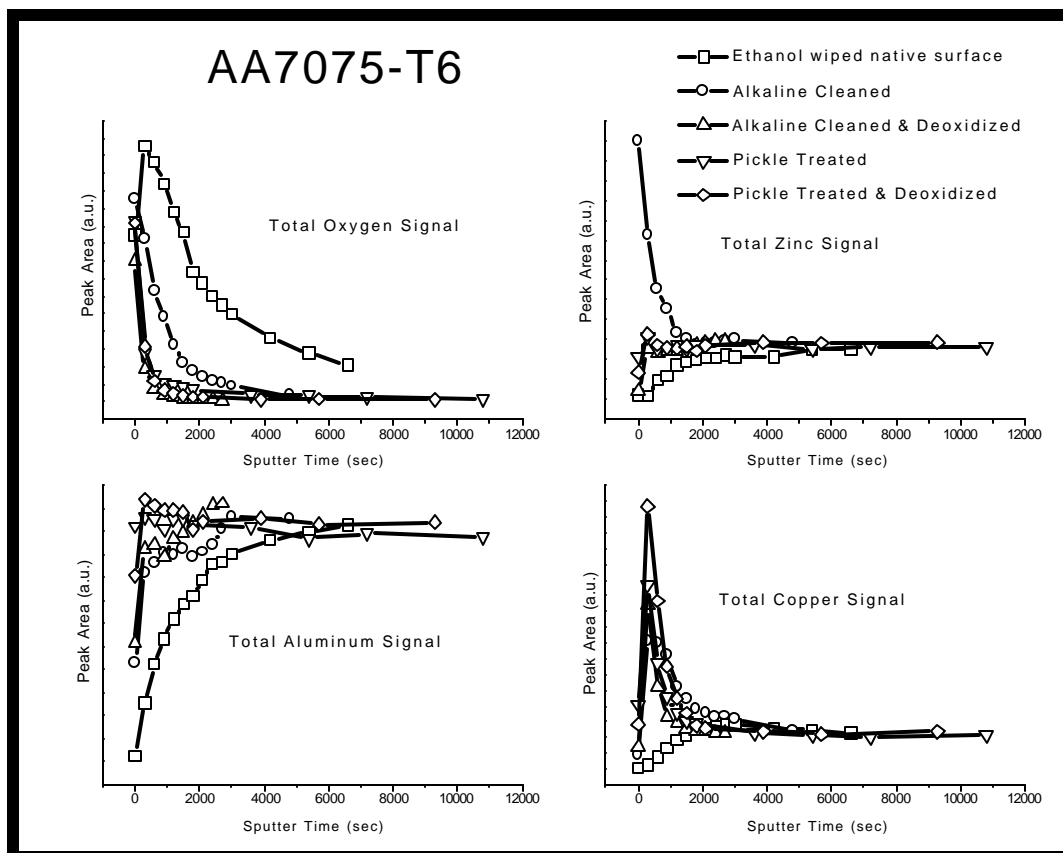
Figure 3. XPS depth profile summary graph for AA7075-T6 showing O1s, Zn2p, Al2p and Cu2p spectral areas as a function of sputter time.

An AA7075-T6 sample, which had been mechanically polished with a final 0.3μm alumina grit and then alkaline cleaned, was investigated using an angular depth profiling technique [33], and the results are shown in Figs. 5 and 6. Variations in take-off angle, with respect to the sample surface, can allow for determination of the origin of certain spectral contributions. The smaller take-off angle corresponds to sampling a thinner region of the surface. This is readily seen in the Al 2p spectra in figure 5, where the metallic contribution to the Al KLL Auger spectrum from the trace corresponding to a 10º take-off angle all but disappears. The C 1s spectra show consistent charging behavior of the adventitious carbon, and the Auger parameters [34, 35] included in Fig. 6 provide a measure that is charge insensitive. As is the case with electron spectroscopies of complex systems, absolute assessments of spectra are generally complicated, but certain relationships bear mentioning. No peak associated with the characteristic CuO shake-up satellite [36,37] was observed in any of the spectra from the alloys, although that region is not displayed in the figure. The shifting of the O1s spectra is seen on all treatments and has been

attributed to hydration effects [14,38-42], but unfortunately hydrogen is undetectable with XPS.

Figure 4. XPS Zn 2p spectra as a function of sputter time for AA7075-T6 after various pretreatments: a) ethanol wiped native surface, b) alkaline cleaned, c) alkaline cleaned and deoxidized, d) pickle treated, and e) pickled and deoxidized.

Zn2p binding energy changes seen in the angular spectra were also noted in the spectra used to compile depth profiles of samples that were alkaline cleaned without polishing. This develops as two particular peaks, as can be seen in Fig. 7. The low binding energy peak is associated with Zn in the alloy, having a binding energy similar to that of metallic zinc[35]. The higher binding energy Zn2p peak does not uniquely match the reported values of anticipated oxide compounds, *i.e.* ZnO or $ZnAl_2O_4$ [35, 43, 44], which can also be said of the angular Zn LMM Auger peaks and the respective Auger parameters.

The effect of the Zn enrichment, as noted earlier, was assumed to diminish the quality of the interface between a plasma polymer film and the alloy. Although the positions of the peak do not absolutely identify the state, the other elements involved limit the possibilities to either an intermetallic or possible hydrated oxide state.   The most stable zinc oxide is soluble in both alkaline and acid environments [45], and metallic Zn itself is anodic to aluminum, let alone Cu intermetallics. It is then asserted that the large Zn enrichment of the alkaline cleaned AA7075-T6 alloy can be related to reduced corrosion protection performance.
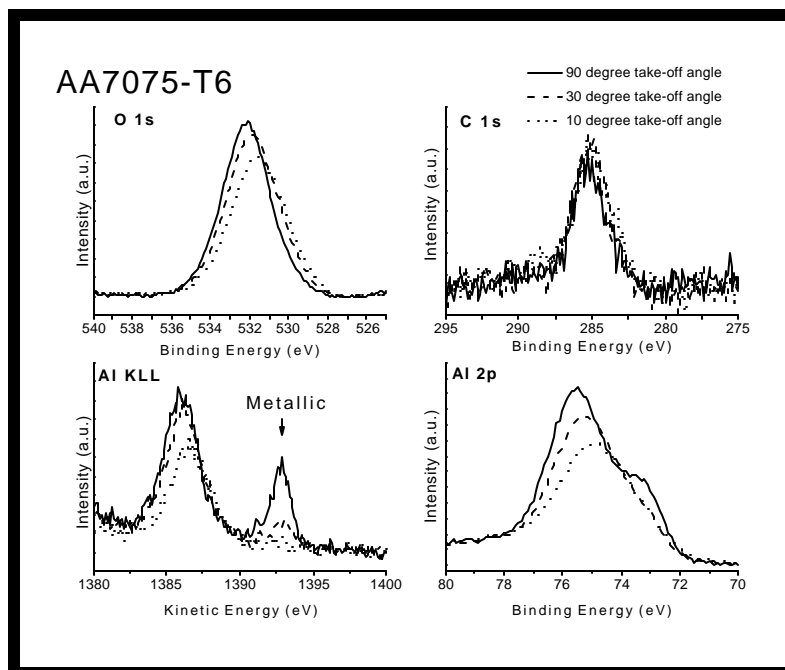
Figure 5. O1s, C1s, Al2p XPS spectra and Al KLL x-ray induced Auger spectra collected at various take-off angles from a polished AA7075-T6 sample, which had been alkaline cleaned after polishing.
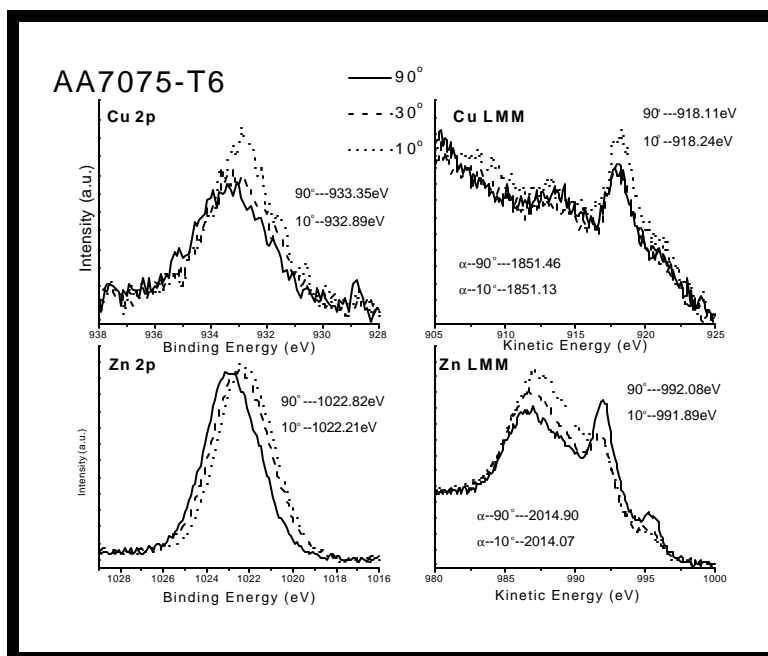
Figure 6. Cu2p and Zn2p XPS spectra and associated Cu LMM and Zn LMM x-ray induced Auger spectra from collected at various take-off angles from the same polished, alkaline cleaned sample as in figure 5. Approximate peak positions and corresponding Auger parameter values are listed.
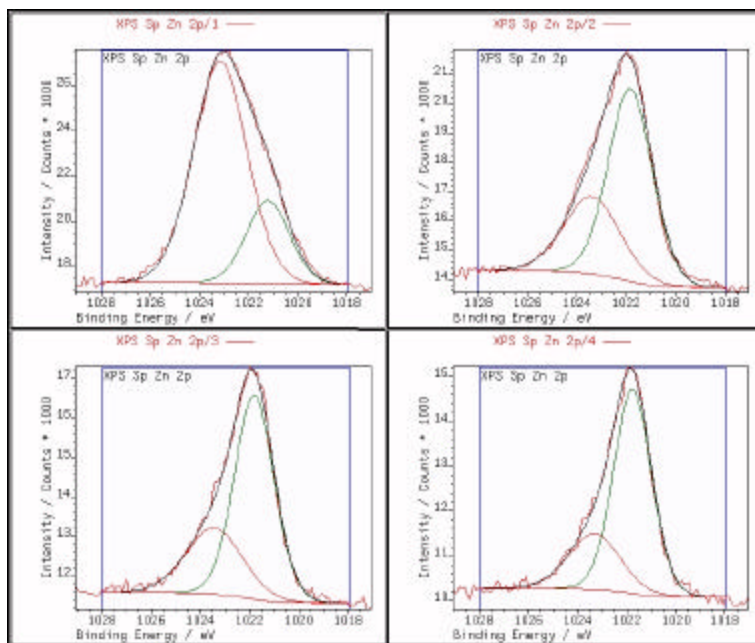
Figure 7. The first four Zn2p spectra from the depth profiling run on the alkaline cleaned AA7075-T6 sample used to generate the alkaline cleaned depth profile in figure 3. The average position of the high binding energy peak is ~ 1023.4eV and the average position of the low binding energy peak is ~ 1021.85eV. The peak positions and Auger parameters are included to show the scale of the energy differences involved in the changes associated with the alloying elements.

Conclusions

The effects of chemical cleaning are seen to do more than simply modify the aluminum oxide structure above complex alloys, *i.e.* thinning it or changing its hydophilicity. The removal of a Mg enriched layer from the as-received panels is accompanied by the enrichment of one or more alloy constituents, using the chemistries employed here. It is conjectured that similar types of preferential enrichments should be present above other aluminum alloys after wet chemical pretreatments, and may play a role in their corrosion behavior. The extent of these enrichments may not be readily apparent from optical or other morphological characterization.

These effects point to a condition where the surface of the alloy immediately beneath, and sometimes penetrating through, the oxide layer is predisposed to accelerated corrosive attack, once the coating and/or the oxide has been penetrated by an electrolytic solution. In addition, larger surface concentrations of more noble metals imply that the cathode to anode area ratio of the system increases. Combinations of different co-enrichments may also have some amplifying effect on surface corrosion beneath protective schemes. This may not be a great concern when chromates are used in a protection scheme, due to their inihibition of the corrosion process, possibly by passivating the cathodic sites [46,47]. However, these factors seem to play a more important role in the prevention of corrosive attack when chromates are not involved in the protection system.

Finally, nitric acid de-smutting may be a practical solution to large deposits of copper compounds, in contact with the bulk alloy surface through the oxide and possibly on top of the oxide. It appears, however, that it does not remove thin enrichments beneath an established oxide.

The information presented here gives rise to certain questions regarding the nature of aluminum alloy surface treatments and indicates that they are an under-explored aspect in the interface engineering of corrosion protection systems. As more sensitive characterization techniques develop they tend to shine new light on systems thought to be well-understood.

References

[1]   <u>ASM Specialty Handbook: Aluminum and Aluminum Alloys</u>, J.R. Davis Editor, (ASM International, Materials Park, OH, USA, May 1994).

[2]   <u>ASM Metals Handbook: Volume 13, Corrosion, Ninth Edition</u>, Edited by ASM Handbook Committee, L.J. Korb and D.L. Olson, Co-Chairman, (ASM International, Materials Park, OH, USA, 1987).

[3]   H. Ebel, M.F. Ebel, J. Wernisch, and J. Pingitzer, *Surface and Interface Analysis*, **12**, No. 1-2, (1988), 228-229.

[4]   <u>Plasma Polymerization</u>, H.K. Yasuda, (Academic Press, New York 1985).

[5]   S. Wernick, R. Pinner, and P.G. Sheasby, <u>Surface Treatment and Finishing of Aluminium and its Alloys</u>, (Finishing Publ. Ltd, Teddington, Middlesex, England, 5th ed. 1987).

[6]   K. Wefers, *Aluminum*, **57**, (1981), 722-726.

[7]   M. Pijolat, V. Chiavazza, and R. Lalauze, *Appl. Surf. Sci.*, **31**, (1988), 179-188.

[8]   Y. Hirome, T. Kobayashi, M. Saito, K. Mizuno, S. Maeda, and K. Honda, *Jap. J. Appl. Physics*, **43**, No. 7, (1993), 372-377.

[9]   J. Bloch, D.J. Bottomley, J.G. Mihaychuk, H.M. van Driel, and R.S. Timsit, *Surface Science*, **322**, (1995), 168-176.

[10]   F.J. Esposto, C.-S. Zhang, P.R. Norton, and R.S. Timsit, *Surface Science*, **302**, (1994), 109-120.

[11]   H. Venugopalan, K. Tankala, and T. Debroy, *Metal. and Mater. Trans. B*, **27B**, (1996), 43-50.

[12]   Y.-N. Xu and W.Y. Ching, *Phys. Rev. B*, **43**, No. 5, (15 Feb. 1991), 4461-4472.

[13]   T.S. Sun, J.M. Chen, J.D. Venables, and R. Hopping, *Appl. Surf. Sci.*, **1**, (1978), 202-214.

[14]   M. Textor and R. Grauer, *Corrosion Science*, **23**, No. 1, (1983), 41-53.

[15]   H.-H. Strehblow and C.J. Doherty, *J. Electrochem Soc.*, **125**, No. 1, (January 1978), 30-33.

[16]   H.-H. Strehblow, C.M. Mellisar-Smith, and W.M. Augustyniak, *J. Electrochem Soc.*, **125**, No. 6, (June 1978), 915-919.

[17]   K. Kowal, J. Deluccia, J.Y. Josefowicz, C. Laird, and G.C. Farrington, *J. Electrochem Soc.*, **143**, No. 8, (August 1996), 2471-2481.

[18]   M.A. Paez, T.M. Foong, , C.T. Ni, G.E. Thompson, K. Shimizu, H. Habazaki, P. Skeldon, and G.C. Wood, *Corrosion Science*, **38**, No. 1, (1996), 59-72.

[19]   H. Habazaki, X. Zhou, K. Shimizu, P. Skeldon, G.E. Thompson, and G.C. Wood, *Electrochimica Acta*, **42**, No. 17, (1997), 2627-2635.

[20]   H. Habazaki, K. Shimizu, P. Skeldon, G.E. Thompson, G.C. Wood, and X. Zhou, *Trans IMF*, **75**, No. 1, (1997), 18-23.

[21]   H. Habazaki, K. Shimizu, P. Skeldon, G.E. Thompson, G.C. Wood, and X. Zhou, *Corrosion Science*, **39**, No. 4, (1997), 731-737.

[22]   X. Zhou, G.E. Thompson, H. Habazaki, K. Shimizu, P. Skeldon, and G.C. Wood, *Thin Solid Films*, **293**, (1997), 327-332.

[23]   K. Shimizu, K. Kobayashi, G.E. Thompson, P. Skeldon, and G.C. Wood, *Corrosion Science*, **39**, No. 2, (1997), 281-284.

[24]   H. Habazaki, M.A. Paez, K. Shimizu, P. Skeldon, G.E. Thompson, G.C. Wood, and X. Zhou, *Corrosion Science*, **38**, No. 7, (1996), 1033-1042.

[25]   X. Wu and K. Hebert, J. Electrochem. Soc., 143, No. 1, (January 1996), 83-91.

[26]   G.M. Brown, K. Shimizu, K. Kobayashi, G.E. Thompson, and G.C. Wood, *Corrosion Science*, **34**, No. 12, (1993), 2099-2104.

[27]   E.A. Ashour and B.G. Ateya, *Electrochimical Acta*, **42**, No. 2, (1997), 243-250.

[28]   T. Surter, E.M. Moser, and H. Böhni, *Corrosion Science*, **34**, No. 7, (1993), 1111-1122.

[29]   H.K. Yasuda and group, group communication and research reports.

[30]   H. Habazaki, X. Zhou, K. Shimizu, P. Skeldon, G.E. Thompson, and G.C. Wood, *Thin Solid Films*, **292**, (1997), 150-155.

[31]   X. Zhou, H. Habazaki, K. Shimizu, P. Skeldon, G.E. Thompson, and G.C. Wood, *Corrosion Science*, **38**, (1996), 1563-1576.

[32]   R.B. Nicholson, G. Thomas, and J. Nutting, *Britt. J. of Appl. Physics*, **9**, (January 1958), 23-27.

[33]   S. Hofmann in Practical Surface Analysis, 2nd Ed., Volume 1: Auger and X-ray Photoelectron Spectroscopy, Edited by D. Briggs and M.P. Seah, (Wiley, NY, 1990), 183.

[34]   C.D. Wagner, H.A. Sic, W.T. Jansen, and J.A. Taylor, *Appl. Surf. Sci.*, **9**, (1981), 203-213.

[35]   C.D. Wagner in Practical Surface Analysis, 2nd Ed., Volume 1: Auger and X-ray Photoelectron Spectroscopy, Edited by D. Briggs and M.P. Seah, (Wiley, NY, 1990), 595.

[36]   S. Hüfner in Photoemission in Solids II: Case Studies, Edited by L. Ley and M. Cardona, (Spriger-Verlag, Berlin, 1979), 173-216.

[37]   B.R. Strohmeier, D.E. Leyden, R.S. Field, and D.M. Hercules, *J. Catalysis*, **94** (1985), 514-530.

[38]   K. Wefers and C. Misra, Oxides and Hydroxides of Aluminum, Alcoa Technical Paper No. 19, Revised, (Alcoa Laboratories, Alcoa Center, Pennsylvania, 1987) pp.64-66.

[39]   E. McCafferty and J. P. Wightman, *Surf. Interface Anal.*, **26,** (1998), 549-564.

[40]   B. R. Strohmeier, *Appl. Surf. Sci.*, **40,** (1989), 249-263.

[41]   B. R. Strohmeier, *Surf. and Interface Anal.* **15,** (1990), 51-56.

[42]   T. Do and N.S. McIntyre, *Surf. and Interface Anal.*, **27,** (1999), 1037-1045.

[43]   C.D. Wagner, W.M. Riggs, L.E. Davis, and J.F. Moulder in Handbook of X-Ray Photoelectron Spectroscopy, Edited by G.E. Muilenberg, (Perkin Elmer Corporation, Eden Prairie, Minn. 1979), 84.

[44]   C.D. Wagner, NIST X-Ray Photoelectron Spectroscopy Database, Version 1.0, (U.S. Commerce Dept., Gaithersburg, MD, 1989).

[45]   CRC Handbook of Chemistry and Physics, 66th Ed., Edited by R. C. Weast, (CRC Press, Boca Raton, Fl, 1985), B-159.

[46]   M.W. Kendig, A.J. Davenport, and H.S. Isaacs, *Corrosion Science*, **34**, No. 1, (1993) 41-49.

[47]   J.R. Waldrop and M.W. Kendig, *J. Electrochem. Soc.*, **145**, No. 1, (1998), L11-L13.

12. A Model Study Investigating the Role of Interfacial Factors in EIS Measurements

M. Chen, Q. S. Yu, C. M. Reddy, and H. K. Yasuda

Abstract

In order to look into the effect of the interfacial factors on Electrochemical Impedance Spectroscopy (EIS), model systems consisting of Parylene C film coated on Alclad 7075-T6 sheets and freestanding Parylene C films were investigated. In order to modify the top surface of Parylene C coating, the coating on aluminum alloy panels were treated with two plasmas: TMS (Trimethylsilane) and a mixture of TMS plus O_2. Plasma polymerization of Trimethysilane (TMS) followed by Hexafluoroethane (HFE) was also applied to the substrate surface prior to the deposition of Parylene C film to improve the adhesion of the film to the surface. The coating performance was evaluated using EIS, and the interfacial factors produced by the plasma treatments were studied by applying suitable equivalent circuit models, which take into account all the interfacial parameters and bulk coating. The simulations performed with the circuit models proposed in this work indicate (1) top surface modification with plasma treatment influences the salt intrusion property of the top layer as well as of the bulk film itself; (2) good adhesion of Parylene C to the panel surface produced by the plasma pretreatment is reflected by the high resistance and low capacitance at the interface; (3) the reduction of the impedance modulus of a Parylene Coated aluminum alloy panel system with increased immersion time in salt solution is largely due to microscopic scale delamination of the film from the panel surface.

Introduction

Electrochemical impedance spectroscopy (EIS) is a valuable method with which to study the barrier property and corrosion protection performance of polymer coated metals; it has been widely used in this field in recent years [1-5]. Many examples, which illustrate the performance deterioration of different coatings, can be found in the literature [3-5]. The time-dependent decline of the impedance has been intuitively attributed to the decline of the barrier characteristics of the bulk phase of the coating. Such an interpretation completely ignores the potential interfacial failures.

Without a parallel study of a freestanding film, the decay characteristics of EIS data cannot be attributed to the decay of the barrier characteristics of the bulk phase of a coating. On the other hand, it is very difficult to obtain a freestanding film of a good corrosion protection coating without altering the bulk characteristics of the coating. Therefore, a parallel study with a freestanding film is not feasible in many cases.

Parylene C coating provides a unique opportunity to investigate the influence of interfacial factors on EIS measurements, because the same polymer with or without adhesion can be deposited on a metal substrate by means of plasma pretreatment of the substrate. Parylene C is an excellent barrier formed by vacuum deposition polymerization [6]. Vacuum deposition eliminates possible complications due to the wetting phenomenon based on the surface

characteristics of the substrate, because monomers in (free) di-radical form in the gas phase polymerize when they strike the substrate surface.

Because the reactive species (paraxylelene) does not react with anything but free radicals, the adhesion of Parylene C to a smooth surface is poor, and a freestanding film can be easily peeled off from the substrate. Adhesion to a smooth surface can be achieved by introducing free radical sites (dangling bonds) on the substrate surface by depositing an ultra-thin layer of a plasma polymer prior to the Parylene deposition [7]. This allows the formation of covalent bonds between the substrate and the coating but does not influence the formation of the bulk phase of the coating.

The overall corrosion protection of a metal depends on the performance of a system as a whole, including its many interfaces and coating layers [8-10]. Any single factor cannot be treated as a dominant one. There is very little work appeared in the literature, which focuses on the role of interfacial factors in the corrosion protection performance of coated systems. Corrosion tests such as salt pray do not yield results that can distinguish the interfacial effects. No EIS study on the interfacial aspects of corrosion protection was found in the literature.
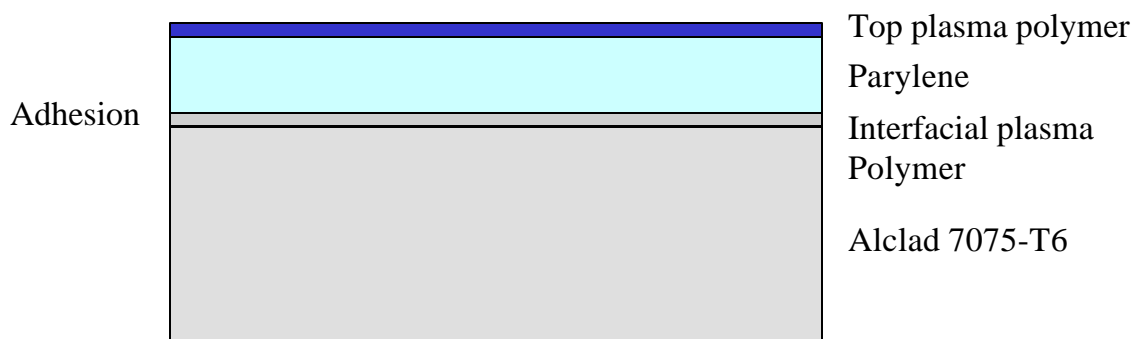
Sample No., & Top Plasma Polymer	Adhesion of Parylene C to Metal	Liquid-contacting Surface	Polymer contacting Metal
(1) None	No	Parylene C	Parylene C
(2) None	Yes	Parylene C	Plasma Polymers of TMS/HFE
(3) Hydrophilic	No	Plasma Polymer of TMS+O_2	Parylene C
(4) Hydrophilic	Yes	Plasma Polymer of TMS +O_2	Plasma Polymers of TMS/HFE
(5) Hydrophobic	No	Plasma Polymer of TMS	Parylene C
(6) Hydrophobic	Yes	Plasma Polymer of TMS	Plasma Polymers of TMS/HFE

Figure 1. Schematic representation of model systems.

Alclad (7075 T-6) was chosen as the substrate in this study, because the nearly pure aluminum (cladded on AA7075-T6) provides a quite reliable surface state by simple organic solvent-wipe cleaning [8]. The two interfaces considered above, i.e., salt solution-Parylene C and Parylene C-Aluminum, can been modified by means of low temperature plasma polymerization. The model systems prepared can be schematically depicted as shown in Fig. 1, in which the interfacial factors to be investigated and the sample prepared accordingly are also summarized.

Using these relatively simple models, the influence of interfacial factors on the outcome of EIS measurements carried out as a function of immersion time is investigated in this study.

Experimental

Materials and plasma treatments

Alcald 7075-T6 panels obtained from Q Panel Lab Products (Cleveland, OH) were used as substrates. The panel surface was cleaned with acetone to remove organic contaminants. The cleaned substrate was placed in a Parylene C vacuum deposition chamber, and approximately 5 μm of Parylene C film was deposited on each panel. Detailed experimental procedures for Parylene C deposition have been described elsewhere [6].
Modification of substrate panels to facilitate the adhesion of Parylene C film (PC) was carried out by depositing a thin layer (~ 50 nm) of plasma polymers of Trimethylsilane (TMS) followed by Hexafluoroethane (HFE) via cathodic plasma polymerization [8, 11].

Modification of the Parylene C surface was performed in an audio-frequency magnetron-plasma reactor [12]. To achieve a hydrophobic surface, plasma polymer of TMS was deposited. To achieve a hydrophilic surface, plasma polymer of a mixture of TMS/O_2 (1:4 molar ratio) was deposited. The thickness of the deposited plasma polymer film was around 20 nm.

Parylene C is a hydrophobic polymer, of which the contact angle of water at 23 ^{0}C was measured as 92 degree. The plasma polymer of TMS, of which the contact angle of water was measured as 120 degree, provides a more hydrophobic surface than as-deposited Parylene C. The plasma polymer of $TMS+O_2$, of which the contact angle of water was measured as 50 degree, provides a hydrophilic surface.

To prepare the freestanding Parylene C films, Pyrex glass plates that had been cleaned with acetone were used as the substrates for deposition. The Parylene C films were easily peeled off of the glass substrates by cutting along the edges of a glass plate. In order to modify the surface property to be either hydrophobic or hydrophilic, both sides of the freestanding Parylene C films were treated with plasma polymers accordingly, as described above.

Equipment for EIS measurements

An electrochemical cell with two compartments separated by the film under study was used for EIS of freestanding Parylene C films, as shown in Fig.2. This is a two-electrode set-up: one Ag/AgCl reference electrode was used as the working electrode and another Ag/AgCl electrode

was used as the counter and reference electrode. The freestanding film has a surface area of 8.56 cm^2 on each side exposed to the electrolyte solution.
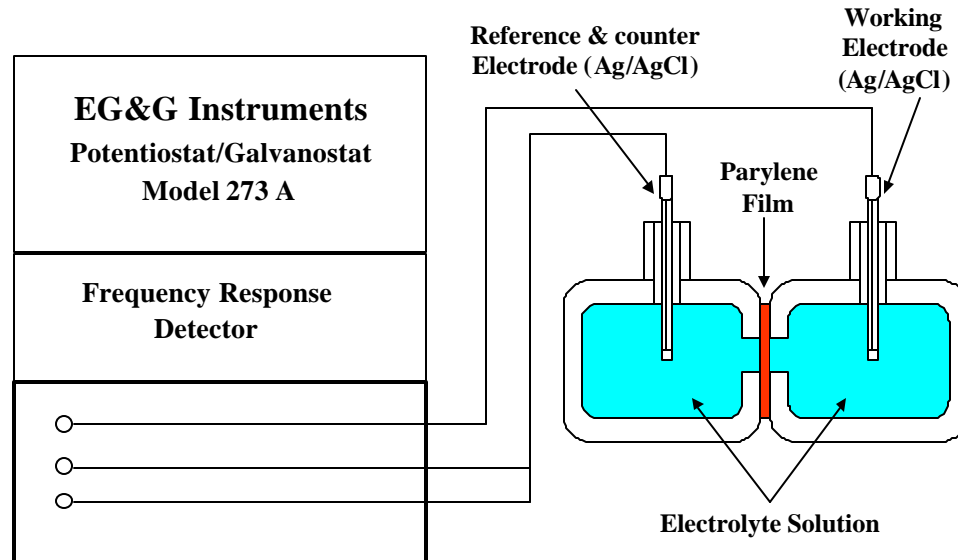
Figure 2. Schematic representation of the electrochemical cell and equipment for EIS of freestanding Parylene C films.
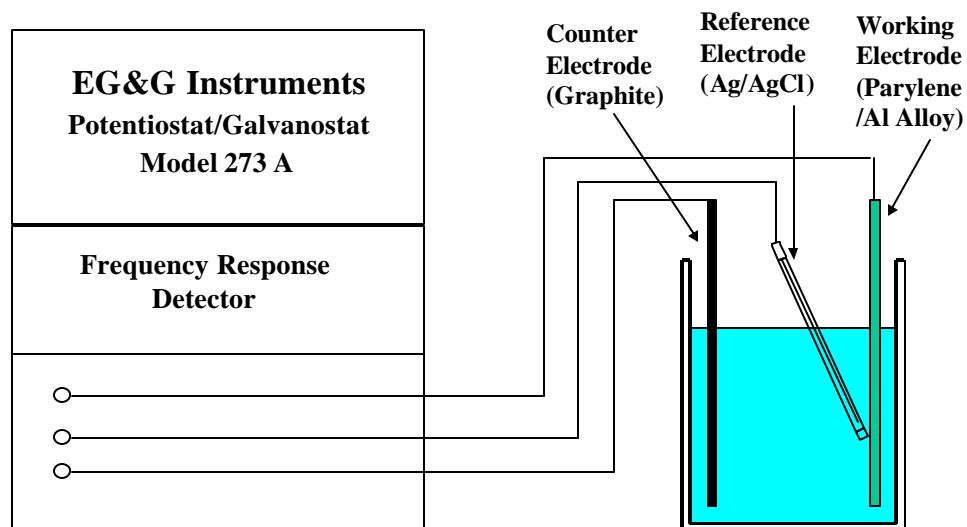
Figure 3. Schematic representation of the electrochemical cell and equipment for EIS of Parylene C polymer coated Alclad 7075-T6 aluminum alloy panels.

Fig. 3 shows the electrochemical cell and EIS set up for Parylene C polymer coated Alclad 7075-T6 aluminum alloy panels. The Parylene C coated Alclad 7075-T6 panel acted as the working electrode with a surface area of 3×3 cm^2 exposed to the electrolyte solution. The Ag/AgCl standard electrode (0.197 V vs. NHE) was used as the reference electrode and was positioned close to the exposed surface of the Parylene C coated Alclad 7075-T6 panel. A graphite rod 0.6 cm in diameter was used as the counter electrode.

Impedance measurements were taken with an EG&G Model 273A Potentiostat/ Galvanostat controlled by Model 398 Electrochemical Impedance Software, Version 1.26. EIS measurements were taken in a 0.9% NaCl aqueous solution for both Parylene C coated Alclad 7075-T6 panels and freestanding Parylene C films. This solution was chosen because it was used in the AC resistivity measurement of low-density polyethylene (LDPE) films [13]. The applied alternating current (AC) signal was 100 mV in the frequency range of 0.1 to 1.0×10^5 Hz.

The film capacitance (C) is determined by the following formula:
$$C = \varepsilon_0 \varepsilon_r S/d \qquad\qquad\qquad\qquad (1)$$
where ε_0 is the vacuum permittivity, and ε_r is the relative permittivity or dielectric constant of the film, d is the film thickness, and S is the working area of the film. For Parylene C film, ε_r is about 3.6, and for water it is 80. Therefore, entry of water into the film will increase the capacitance. The commercially available "Equivalent Circuit" program of Boukamp was used to analyze the impedance spectra [14].

Results and Discussion

Salt intrusion and water permeation

Water permeates through a flawless polymer film via "solution-diffusion" mechanisms. Water molecules are first dissolved into the polymer matrix at the interface; the dissolved water molecules diffuse through the polymer according to the chemical potential gradient across the film. Salt ions are hydrated with numbers of water molecules and are tightly associated with the counter-ions, which are also hydrated. The transport of salt requires larger elementary free volume than does the transport of water molecules. Consequently, salt ions cannot permeate through a hydrophobic polymer, of which the hydration value is low, i.e., less than 0.1 volume percent, by the solution-diffusion principle. Therefore, salt ion permeation through a hydrophobic polymer film such as low-density polyethylene (LDPE) and Parylene C film should not occur.

In reality, however, salt finds or creates paths into a hydrophobic polymer phase and causes the breakdown of an insulating layer or corrosion of the substrate metal. In our previous study of the electric insulation characteristics of LDPE film, it was found that salt ions intrude into the polymer matrix by different mechanisms [13]. The exact mechanisms for salt intrusion are not known, but the phenomenological salt intrusion found in the study can be summarized as follows, in an effort to explain the nature of salt intrusion.

1.   The AC resistivity of LDPE film does not change with water immersion even under electrical stress of 10 kV/mm as shown in Fig.4, where the relative resistivity is plotted as

a function of immersion time.

2.   When an LDPE film is immersed in a salt solution (0.9 % NaCl), the AC resistivity
decreases as a function of the immersion time, as shown in Fig. 5. This figure also shows
the effect of an ultra-thin layer of plasma polymer deposited on the surface of LDPE.
With hydrophobic plasma polymer (HFE + H_2), the decrease of AC resistivity was not
observed.

3.   The insulation breakdown under electrical stress is correlated to the salt intrusion
characteristics of a film.
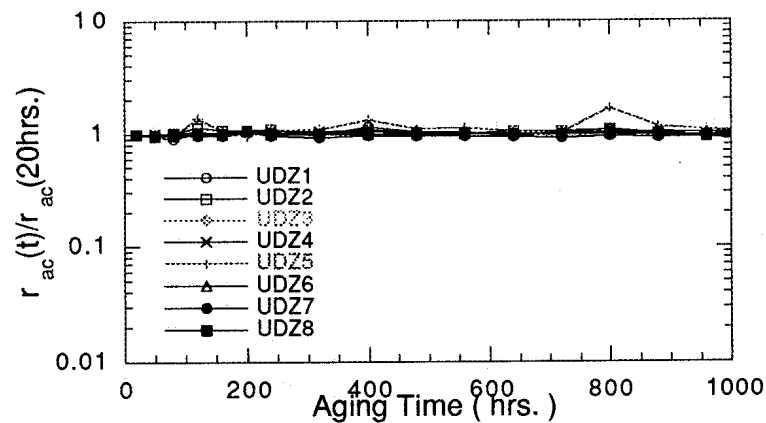
(a) Unstressed LDPE films
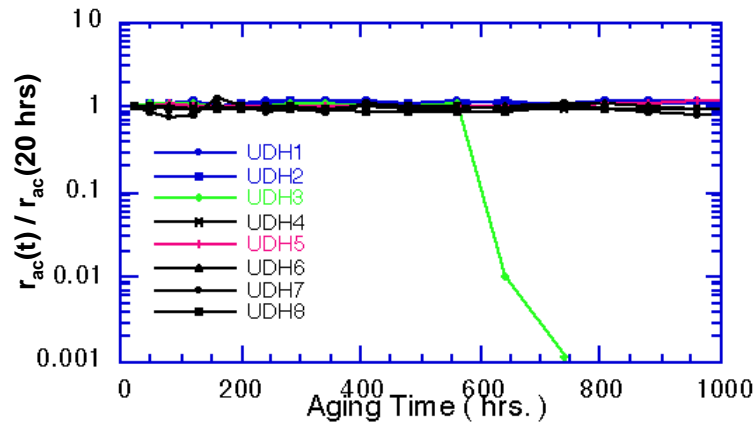
(b) 10 kV/mm stressed LDPE films

Figure 4. AC resistivity ratio versus aging time for untreated LDPE films in a deionized water
environment: (a) unstressed, and (b) 10 kV/mm stressed.
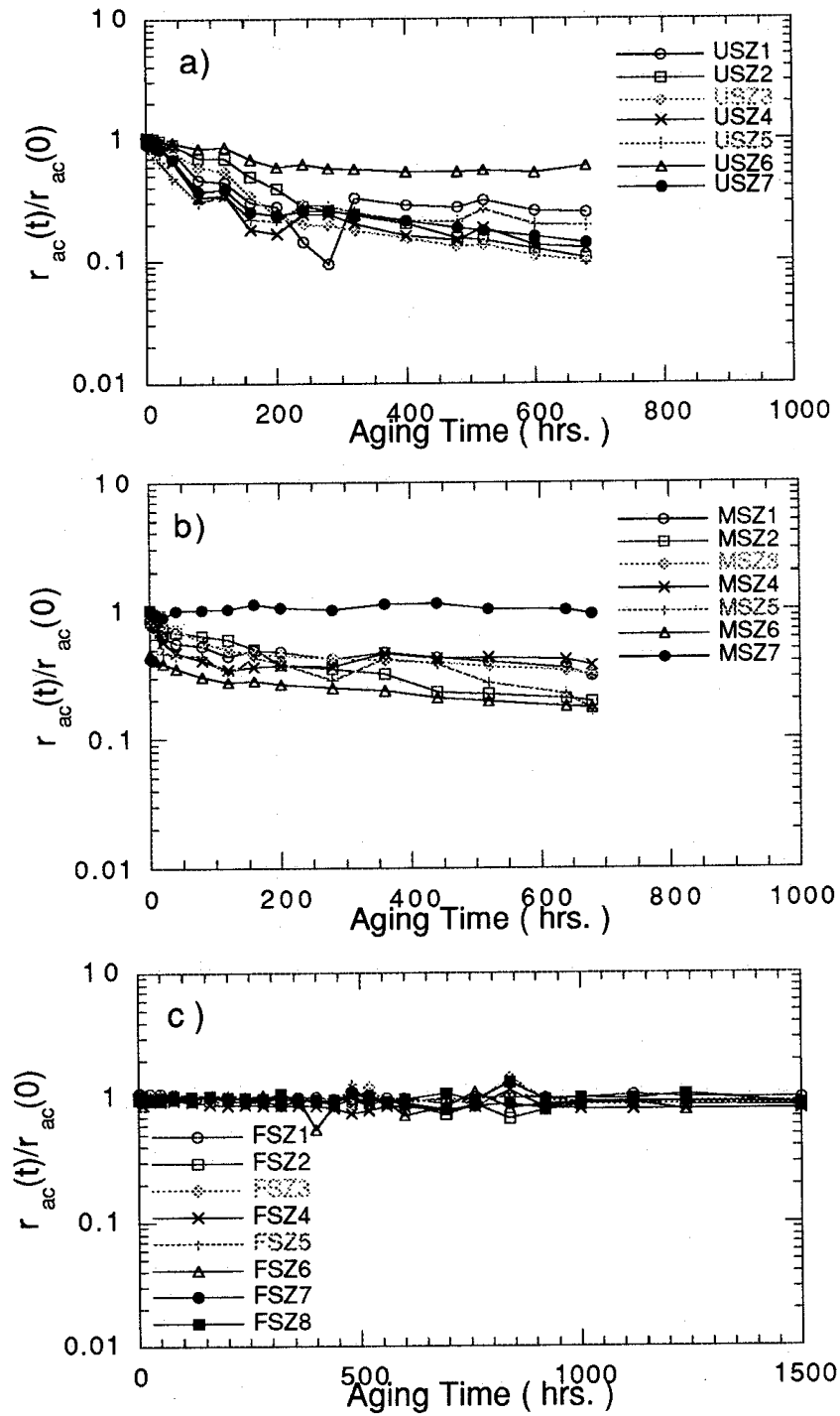
FIGURE 5. AC resistivity ratio versus aging time for unstressed LDPE films in a 0.9% saline environment: (a) untreated, (b) CH_4 plasma treated, and (c) $C_2F_6 + H_2$ (1 : 1) plasma treated.

Water Diffusion Through Coatings
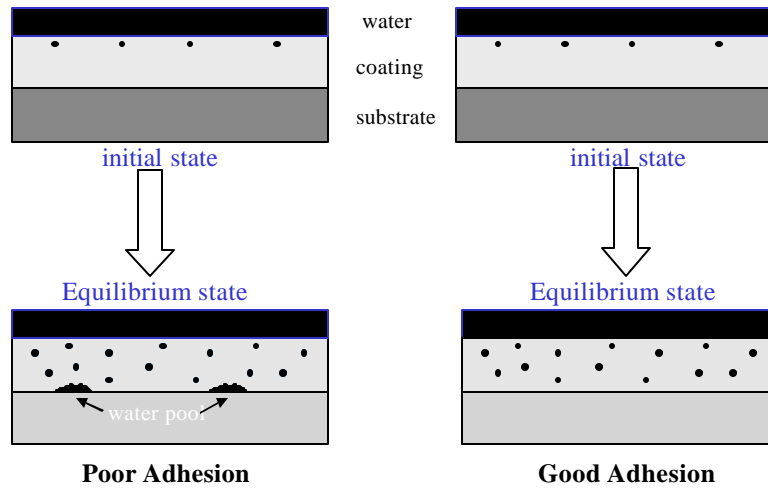
Figure 6. Schematic representation of water diffusion through a coating with and without water-insensitive adhesion of the coating to the substrate.

Salt Intrusion Through Coatings
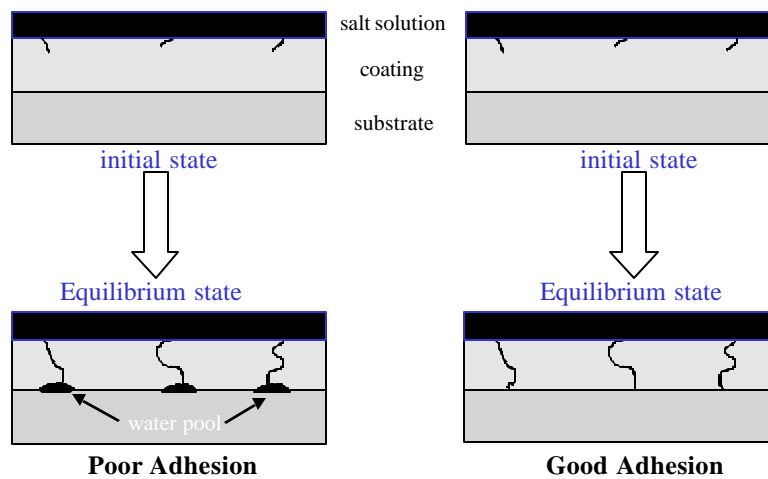
Figure 7. Schematic representation of salt intrusion through a coating with and without water-insensitive adhesion of the coating to the substrate.

Based on these observations, the distinction between water penetration and salt intrusion may be schematically represented as shown in Figs. 6 & 7. In these figures, the effect of lack of water-insensitive adhesion is also depicted. In the absence of water-insensitive adhesion, water

molecules that reach the polymer-metal interface cluster together by breaking weak polymer-metal interaction. If one assumes the diffusion constant of water through a polymer to be 10^{-8} cm^2/s, the time lag of water diffusion through 15 μm thick film is estimated to be 38 s. Any indication of the salt intrusion effect appears over a much longer period of time, i.e., days and months. Therefore, it is appropriate to assume intrusion occurs in a water-saturated polymer matrix.

Change of EIS Bode Plot as a function of Immersion Time

The EIS Bode plots (impedance vs. frequency) at different immersion time for Parylene coated Al panel (Sample 1 in Fig. 1) are shown in Fig. 8, which also includes the Bode plot for a free standing film at immersion time of 0.1 day and 6 days. At the initial run for 0.1 day immersion, the Bode plot for a Parylene C coated sheet, which has no top surface modification nor adhesion modification, shows a typical Bode plot for a good barrier coated sheet; a straight line pointing to a high impedance value at 0.1 Hz. With the increased immersion time, however, the impedance modulus in the low frequency region start to decrease as a function the immersion time.

Changes of the impedance modulus at 0.1 Hz as a function of immersion time are shown in Fig. 9 for Parylene C coated Al sheet without adhesion. The nature of top surface seems to control the rate of the decline. The hydrophilic top surface (Sample 3) accelerates the decline, and the hydrophobic surface (Sample 5) did not show the decline until a threshold time (5 days) is reached. With hydrophilic top surface, the impedance modulus at 0.1 Hz decreased quickly towards that for the freestanding film, and became very close to the freestanding film after 3 days immersion. The influence of the hydrophilic top surface can be seen as the enhancement of the salt intrusion phenomenon [13].

It is also important to point out that, as seen in Fig. 9, little drop of impedance modulus at 0.1 Hz (within 1 order of magnitude) was observed for free-standing Parylene films after 6 days immersion. In contrast, for Parylene coated Al sheets, significant decrease of impedance modulus at 0.1 Hz occurred in the range of 2 to 3 orders of magnitude in the same immersion period. As shown in Fig. 7, the decline of the impedance values in the low frequency region seems to converge to the values observed for a freestanding film of Parylene C. In other words, EIS data of a Parylene C coated sheet seem to converge to that of a free standing film. This trend can be interpreted that the coating is de-laminating so far as EIS can detect, although the film may not be physically detaching from the substrate metal surface in macroscopic sense.

The threshold immersion time observed seems to provide some insight into the nature of the salt intrusion phenomenon in Parylene C film. It is important to recognize that the diffusion time lag of water molecule through 15 μm film is less than a minute and a film would be saturated with water within a day. The threshold immersion time of approximately 6 days indicates that the salt intrusion process is a completely different process from water penetration. It is interesting to note that the threshold immersion time of the same magnitude was also observed with the freestanding film.

The similar plots are shown in Fig. 10 for Parylene C coated sheet with good adhesion. Since the good adhesion can prohibit the water build up at the interface of Parylene C film to the substrate,

the threshold time is extended beyond the time scale of the experiment, and as a consequence the slopes of decay became flatter. Within the immersion time employed, no catastrophic decline was observed. The combination of the hydrophobic top surface and good adhesion to the substrate (Sample 6) showed no decline after immersion for 18 days.
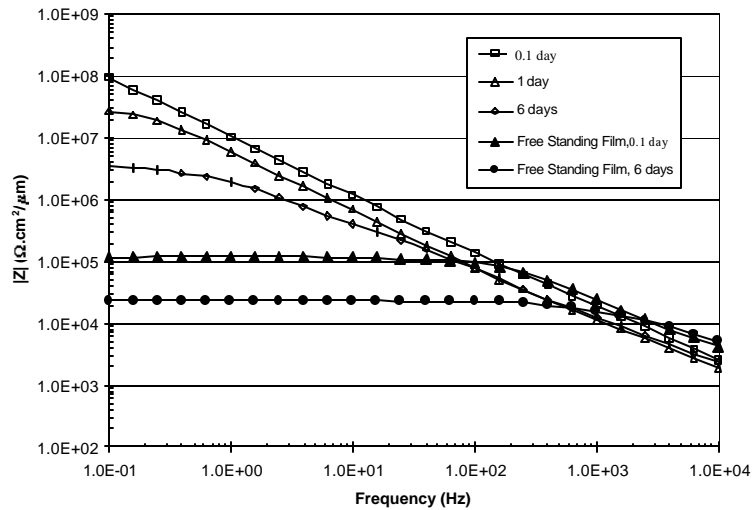

Figure 8. Changes of Bode plots as a function of immersion time for freestanding Parylene C film and Parylene C coated Alclad 7075-T6 aluminum sheets in 0.9% NaCl solution. 0.1 day indicates the initial run after 2 hours immersion of the samples.
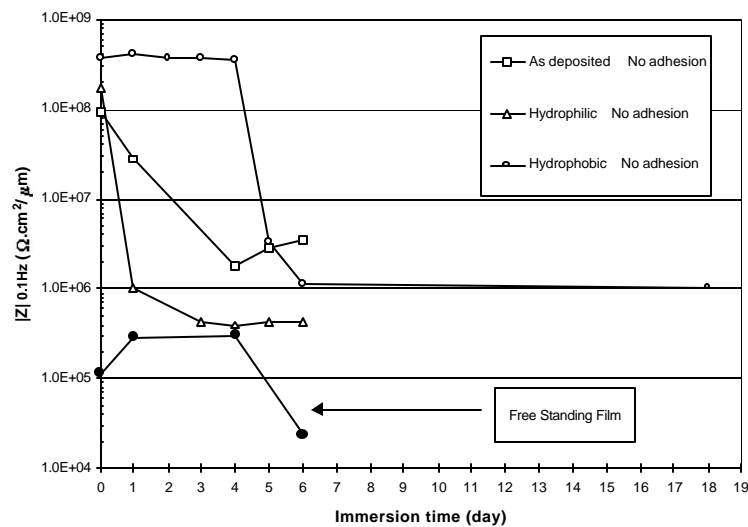
Figure 9. Decline of impedance modulus at 0.1 Hz as a function of immersion time for Parylene C coated Alclad 7075-T6 aluminum sheet. Effect of top surface modification in the case of no adhesion.
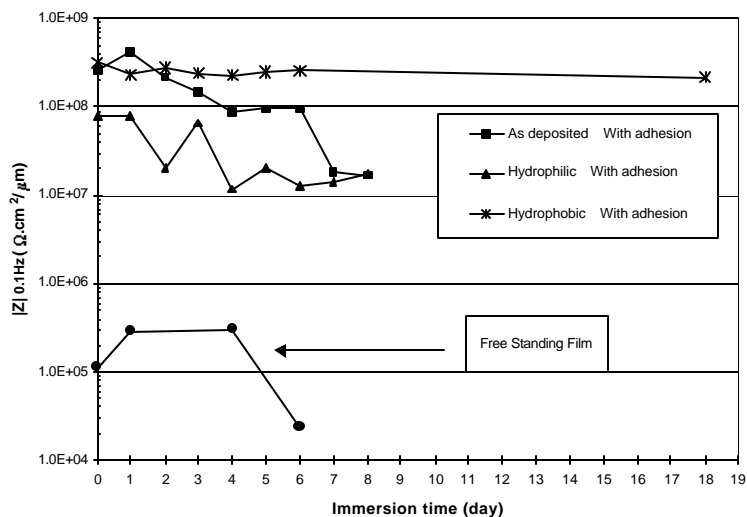
Figure 10. Decline of impedance modulus at 0.1 Hz as a function of immersion time for Parylene C coated Alclad 7075-T6 aluminum sheets. Effect of top surface modification in the case of good adhesion.

Equivalent circuit model analysis

Freestanding film

One time-constant model is typically used to fit EIS data from freestanding films [15]. Such an equivalent mathematical model does not represent the realistic situation with any polymeric film, because the surface region of a film is generally significantly different from the bulk phase of the film, and the entire film cannot be represented by one phase. Such a model merely provides numerical values to express a black box, which does not contribute to the characterization of the film being investigated by EIS.

A new equivalent circuit model, which represents the actual physical state of a polymer film was developed to take into account the interfacial factors of both sides of the freestanding film. The physical model, its equivalent circuit, and the corresponding physical meaning of each circuit element are shown in Fig. 11.

The top surface region can be dealt with as the surface state of a film. The concept of the surface state relevant to the corrosion protection coating has been described in a previous paper [8]. The surface state of both sides of a film should be taken into account in creating an equivalent electrical circuit. The surface state of a plasma polymer coated film represents not just a plasma polymer, but the net result of plasma polymer deposition on the preexisting surface state of a film. In this context, the deposition of a plasma polymer can be considered as the modification of the surface state.

Calculations were carefully performed to find out which factor (interfacial properties of either side of the film or of the bulk film) is the dominant contributor to the decline of the impedance

171

modulus with increased immersion time. The simulation data were plotted, as shown in Fig. 12, to depict the change in parameter values according to immersion time. As anticipated, TMS and TMS+O_2 plasma treated films have higher resistance values than the untreated one. The slight decrease of the salt intrusion resistance of the bulk phase (R_c in Fig. 12(a)) with immersion time was observed for all films. This is exactly what one expects when salt intrusion occurs, since the salt intrusion path short-circuits the resistive layer.

The results indicate the surface states of the two sides of the freestanding film are different (Compare Fig. 12 (b) and (c) for corresponding systems). The difference in the interfacial properties of the two sides of the Parylene C film is due to the preparation procedure in which one side was in contact with the glass substrate, while the other side was subject to growth. One side of a freestanding film is a replica of polymer-substrate interface; the other is a replica of a growing polymer deposition-plasma phase interface. The existence of two different surface states is anticipated with deposited or cast films. It is important to recognize that the EIS model took into account this difference.

It can be clearly seen that, from Fig. 12 (b, c), the TMS plasma treated Parylene surface showed the lowest capacitance due to its hydrophobic nature to resist water adsorption at the surface. In contrast, the TMS+O_2 plasma treated surfaces have higher capacitance, which can be attributed to the hydrophilic surface produced by the plasma treatment and increased water absorption at the surface.
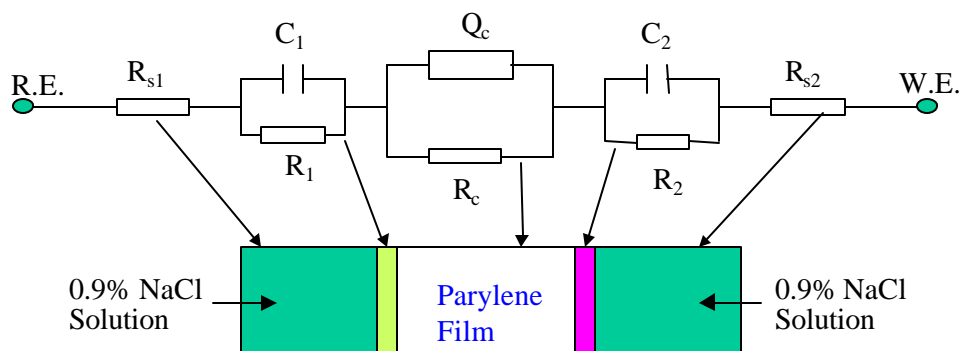
R.E.:   Reference electrode
W.E.:   Working electrode
R_{s1}, R_{s2}: Resistance of salt solution at both sides of the film
R_1, R_2 : Resistance of Parylene surface states at both sides of the film
C_1, C_2 : Capacitance of Parylene surface states at both sides of the film
R_c: Resistance of the Parylene film
Q_c: Constant phase element for Parylene film capacitance

Figure 11. Schematic of the equivalent circuit and physical model for a freestanding Parylene C film.
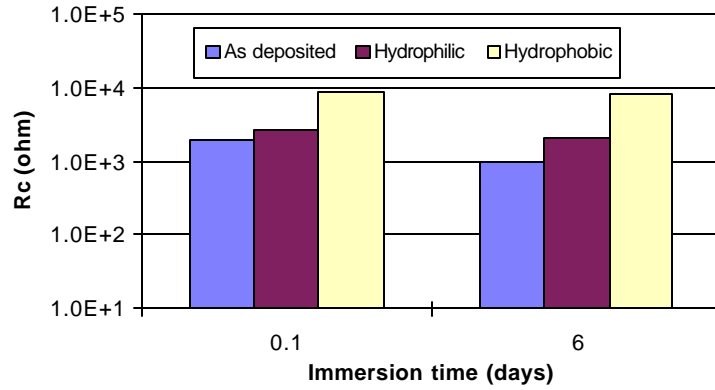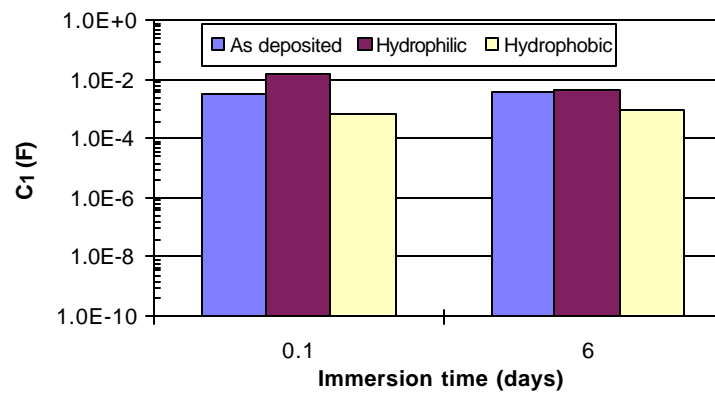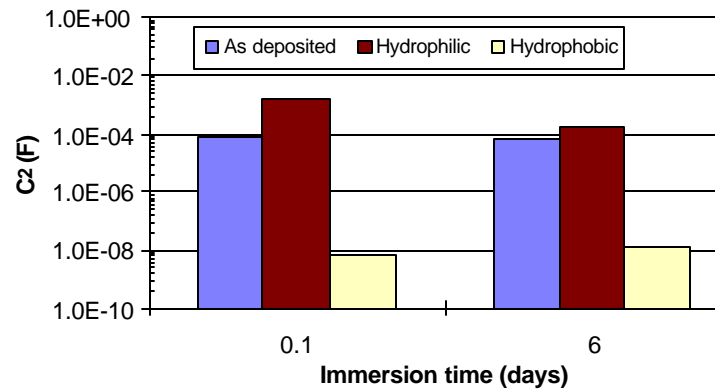
Figure 12. Evaluation of circuit parameters for freestanding Parylene C films: (a) film resistance, (b) interfacial capacitance at one side of the film, (c) interfacial capacitance at the other side. 0.1 day indicates the initial run after 2 hours immersion of the samples.

Equivalent Circuit

Physical Model
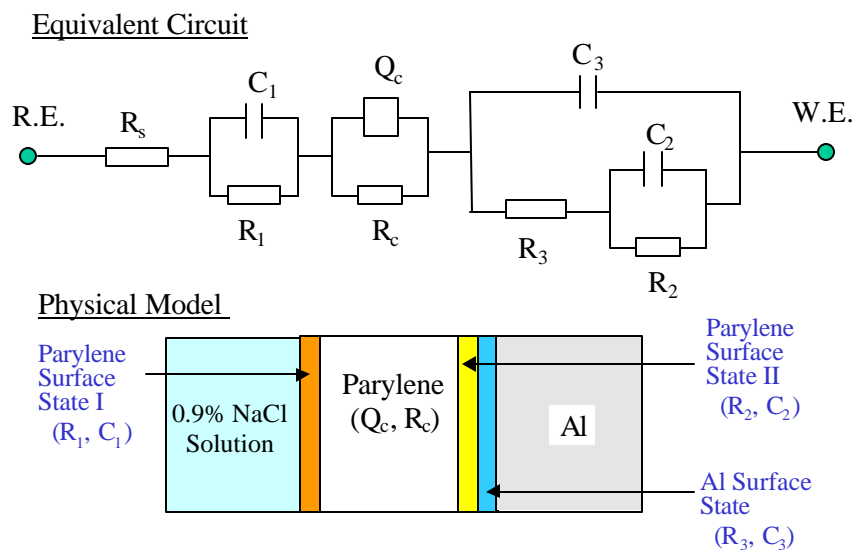
R.E.: Reference electrode, W.E.: Working electrode
R_s: Resistance of electrolyte solution
R_I: Resistance of Parylene surface state I
C_I: Capacitance of Parylene surface state I
R_c: Parylene coating resistance
Q_c: Constant phase element for Parylene coating capacitance
R_2: Resistance of Parylene surface state II
C_2: Capacitance of Parylene surface state II
R_3 : Resistance of Al surface state (Al_2O_3 or Al_2O_3+plasma polymers)
C_3 : Capacitance of Al surface state (Al_2O_3 or Al_2O_3+plasma polymers)

Figure 13. 1Schematic of the equivalent circuit and physical model for a Parylene Coated aluminum panel.

Parylene C coated aluminum sheet

For Parylene C coated Al sheets, the interface between Paryle C coatings and Al panels has to be considered. Therefore, the equivalent circuit suitable for a freestanding film was modified and shown in Fig. 13, which have taken account of the Parylene/Al interfacial properties. Since the surface state of the two contacting materials determines the interface behavior, the equivalent circuit elements that represent the surface state of Al sheet was included in the equivalent circuit model as R_3 and C_3 shown in Fig. 13. The surface state of Al sheet can be considered as the surface oxide layer, and will change to the oxide plus plasma polymers if plasma pretreatment is applied to improve the Parylene adhesion to Al sheet.

As discussed in the previous sections, Parylene C film immersed in salt solution is subject to two penetration processes:
   (1) water uptake into the film, which is reflected by an increase in capacitance, and
   (2) salt-intrusion into the film or at interfaces, which is reflected by a change in resistance.
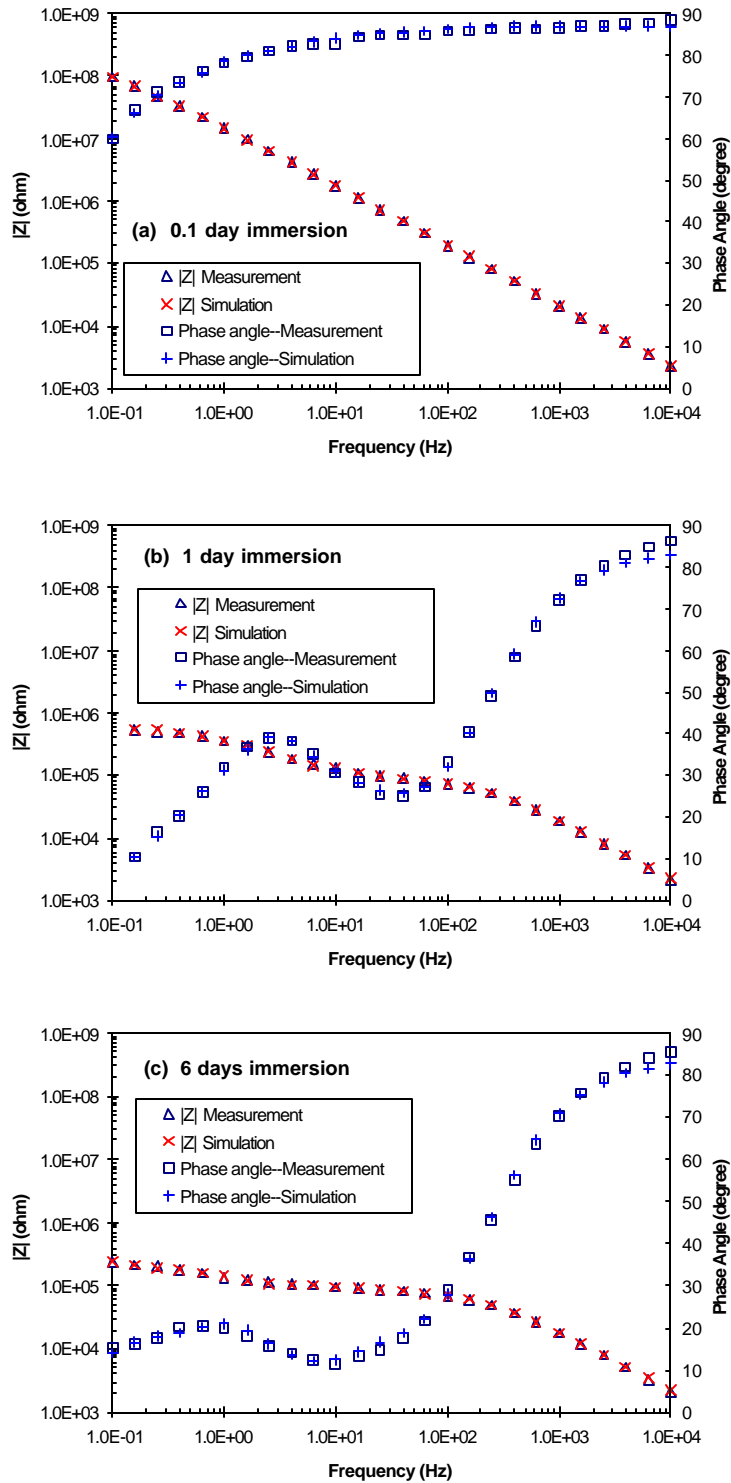
Figure 14. Bode plots of a TMS+O_2 plasma treated Parylene C coated aluminum panel after (a) 0.1 day, (b) 1 day immersion, and (c) 6 days immersion in 0.9 NaCl aqueous solution and fitting curves obtained with the equivalent circuit shown in Figure 13. 0.1 day indicates the initial run after 2 hours immersion of the samples.
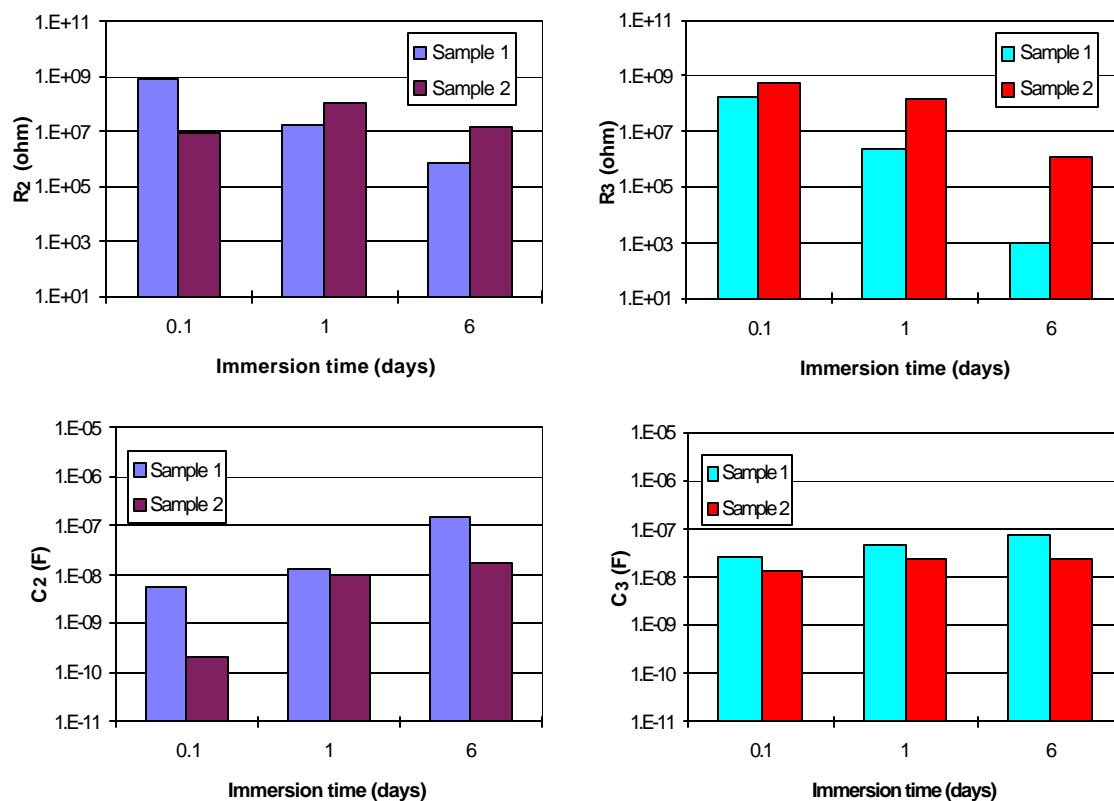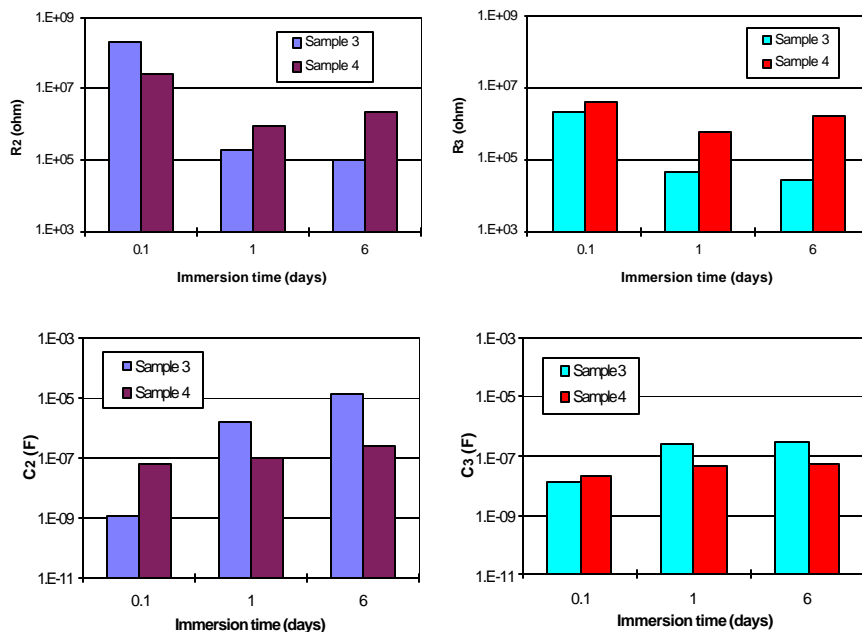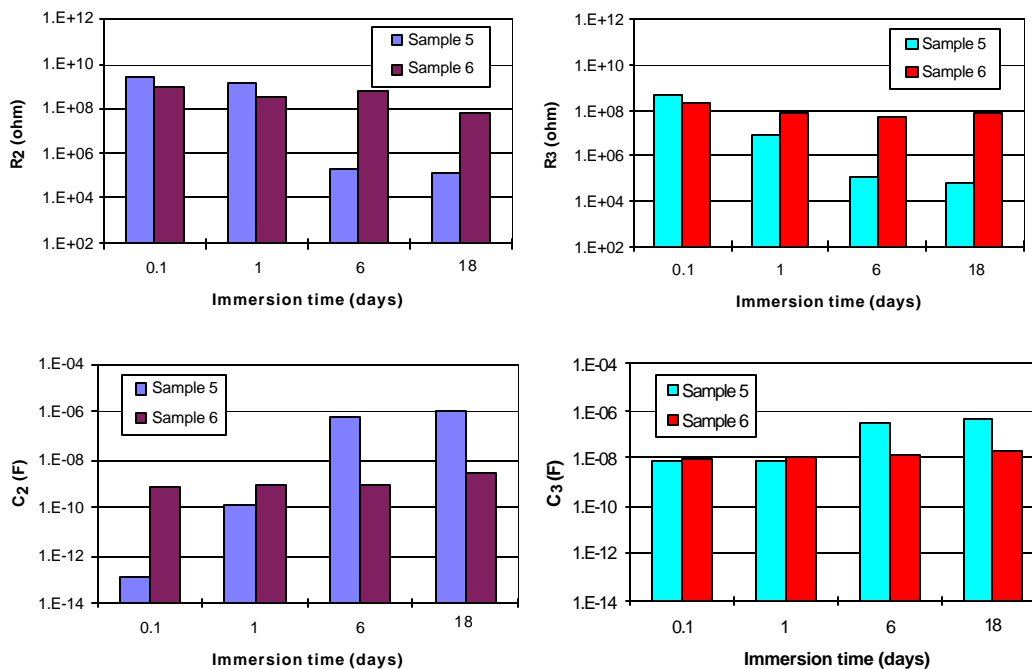
Figure 15. Values of interfacial parameters of samples 1 and 2 versus immersion time of 0.1, 1 and 6 days in 0.9 NaCl aqueous solution. 0.1 day indicates the initial run after 2 hours immersion of the samples.

As illustrated in Fig. 1, the interfacial factors to be investigated and the samples prepared accordingly can be described as follows. Samples 1 and 2 have native Parylene C top surfaces with a water contact angle of 92^0; samples 3 and 4 have more hydrophilic surfaces with a water contact angle of 50^0; samples 5 and 6 have more hydrophobic surfaces with a water contact angle of 120^0. The odd-numbered samples have poor adhesion of Parylene C film to the substrate; while the even-numbered ones have good adhesion achieved by application of plasma polymers.

Fig.14 shows the Bode plot changes with increased salt solution immersion time for sample 3, which has poor adhesion and a hydrophilic surface. It is easy to see that both impedance modulus and phase angle changed with immersion time, indicating the occurrence of water absorption and salt intrusion during immersion. The simulated data with good quality of fit is also presented in the figure.

By performing the simulations, all final values of the parameters were obtained. From the data, it was determined that the decline of impedance modulus at low frequency with increased salt solution immersion time was primarily due to changes in the parameters related to the surface states at the Parylene C/substrate interface, R_2, C_2, R_3 and C_3.

176

Figure 16. Values of interfacial parameters of samples 3 and 4 versus immersion time of 0.1, 1 and 6 days in 0.9 NaCl aqueous solution. 0.1 day indicates the initial run after 2 hours immersion of the samples.

Figure 17. Values of interfacial parameters of samples 5 and 6 versus immersion time of 0.1, 1, 6 and 18 days in 0.9 NaCl aqueous solution. 0.1 day indicates the initial run after 2 hours immersion of the samples.
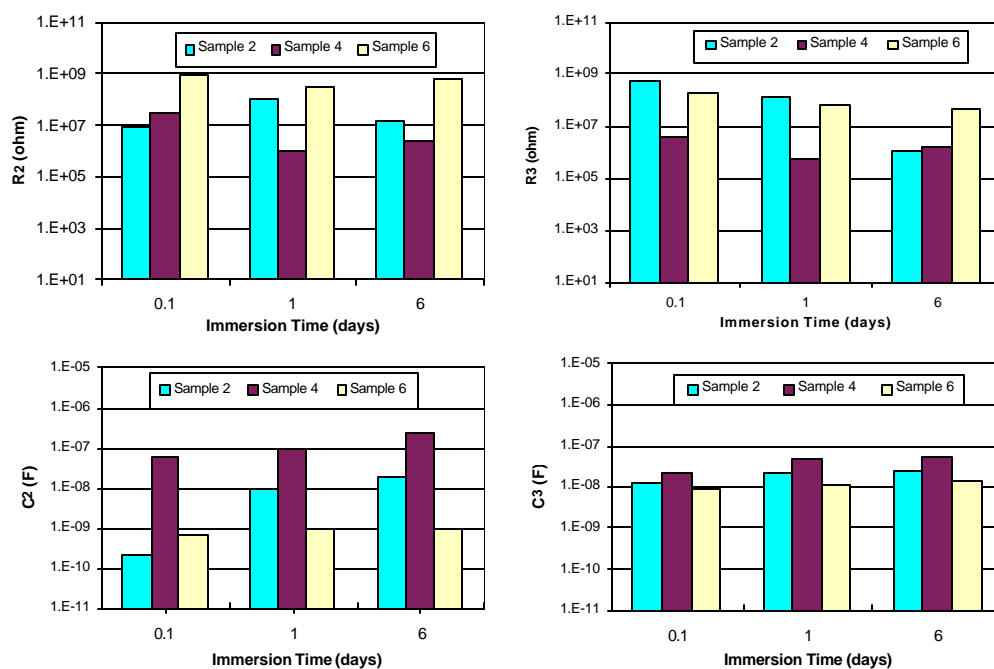
Figure 18. Values of interfacial parameters of good adhesion samples, 2 (native deposited Parylene C surface), 4 (hydrophilic top surface), and 6 (hydrophobic top surface), versus immersion time of 0.1, 1, and 6 days in 0.9 NaCl aqueous solution. 0.1 day indicates the initial run after 2 hours immersion of the samples.

To examine the role of the adhesion factor, three pairs of samples with different top surface properties, as described in Fig. 1, were studied. Figs. 15, 16, and 17 present the values of the related parameters of the equivalent circuit model versus salt solution immersion time for sample pairs 1 and 2 with native Parylene C surfaces, 3 and 4 with hydrophilic surfaces, and 5 and 6 with hydrophobic surfaces, respectively.

From these three figures, a general trend is found for each pair of samples, i.e., higher resistance and lower capacitance were usually observed for the samples with good adhesion (even-numbered samples) than for those with poor adhesion (odd-numbered samples). In organic coated metal systems, increasing interfacial capacitance is usually related to water uptake at the interface. These results clearly showed, as illustrated earlier in Figs. 6 & 7, good adhesion can prevent water uptake or water pool formation at the interface between Parylene C coating and the aluminum substrate.

It is also noted that, for most of the samples, the polarization resistance (R_2 and R_3) decreased with increased immersion time, and the capacitance (C_2 and C_3) increased accordingly. Data after 18 days of exposure were only available for sample pair 5 and 6, since only sample 6 did not show much change in impedance or capacitance. All other samples exhibited a significant decrease in impedance and increase in capacitance after only 6 days of salt solution immersion.

In order to investigate the effect of surface properties on the overall performance of Parylene C coated panels, the values of the four parameters R_2, R_3, C_2 and C_3 for even-numbered samples (good adhesion) are shown in Fig. 18. It can be seen that, for the sample with hydrophilic surface (sample 4), the polarization resistance parameters, R_2 and R_3, have a much lower value with increased immersion time in salt solution than that of the sample with hydrophobic surface (sample 6). Meanwhile, the corresponding interfacial capacitance parameters, C_2 and C_3, showed trends opposite to those of the resistance. These results indicate that the hydrophilic surface could enhance the penetration of salt solution (salt intrusion) through Parylene C coatings to the surface of the aluminum panel. On the other hand, the hydrophobic surface could impede or reduce the possibility of salt intrusion through Parylene C films.

It was especially noted that, as seen in Fig. 17, for sample 6, the values of these four interface parameters showed almost no change with immersion time in salt solution up to 18 days. Because sample 6 has good adhesion and a hydrophobic top surface, these data indicate that the combination of good adhesion and a hydrophobic surface greatly enhance the overall coating barrier property of Parylene C polymers, and thus reduce the chance of electrolyte/metal base contact to initiate corrosion.

It should be noted that the above observations should not be a priori interpreted that a hydrophobic polymer has good salt intrusion resistance. Parylene C and LDPE are very hydrophobic polymers. The salt intrusion occurs into those hydrophobic polymers meaning that hydrophobic polymer surface could have potential gates for the salt intrusion. Hydrophobic plasma polymers close the gates and hydrophilic polymers open them. This stipulation is supported by the data presented here.

VI. CONCLUSIONS

The effect of interfacial factors of Parylene C polymer coatings on the overall protection performance of aluminum alloy was investigated using Electrochemical Impedance Spectroscopy (EIS). From EIS data and the simulation results for freestanding Parylene C film and Parylene C coated Al panels using two equivalent circuit models proposed in this study, the following conclusions were drawn:

(1) Top surface modification affects salt intrusion behavior of the bulk film as well as the interfacial layer. A hydrophilic top surface could enhance the penetration of salt solution (salt intrusion) through Parylene C coatings to the surface of the aluminum panel. On the other hand, a hydrophobic top surface could impede or reduce the possibility of salt intrusion through Parylene C films.

(2) Good interfacial adhesion can prevent water uptake or water pool formation at the interface between Parylene C coating and the aluminum substrate, as reflected by high resistance and low capacitance of the interfacial parameters.

(3) The reduction in the impedance modulus of a Parylene C coated Al panel system with immersion time in salt solution is primarily due to the micro-delamination of film from the panel surface, which results from water uptake or water pool formation at the interface.

(4) The combination of good adhesion and high salt intrusion resistance with a hydrophobic coating surface can greatly enhance the overall protection performance of Parylene C coatings.

Reference

1. E. P. M. van Westing, G. M. Ferrari, and J. H. W. De Wit, "The determination of coating performance with impedance measurements--IV. Protective mechanism of anticorrosion pigments", Corrosion Science, 36, 8 (1994): p.1323.

2. A. Amirudin, and D. Thierry, "Application of electrochemical impedance spectroscopy to study efficiency of anticorrosive pigments in epoxy-polyamide resin", British Corrosion Journal, 30, 2(1995): p. 128.

3. S. M. Cohen, "Electrochemical impedance spectroscopy evaluation of various aluminum pretreatments painted with epoxy primer", J. Coatings Techn., 68, 859 (1996): p. 73.

4. N. Tang, W. J. van Ooij, and G. Górecki, "Comparative EIS study of pretreatment performance in coated metals", Progress in Organic Coatings, 30 (1997): p.255.

5. S. F. Mertens, C. Xhoffer, B. C. De Cooman, and E. Temmerman, "Short-term deterioration of polymer-coated 55% Al-Zn—Part 1: Behavior of thin polymer films", Corrosion, 53, 5 (1997): p. 381.

6. P. Kramer, A. K. Sharma, E. E. Hennecke, and H. Yasuda, "Polymerization of ParaXylylene Derivatives (Parylene Polymerization). I. Deposition Kinetics for Parylene N and Parylene C", J. Polym. Sci.: Polym. Chem. Ed., 22, 475, 1984.

7. H. Yasuda, B. H. Chun, D. L. Cho, T. J. Lin, D. J. Yang, and J. A. Antonelli, "Interface-Engineered Parylene C Coating for Corrosion Protection of Cold-Rolled Steel", Corrosion, **52**, 169, 1996.

8. C. M. Reddy, Q.S. Yu, C. E. Moffitt, D. M. Wieliczka, R. Johnson, J. E. Deffeyes, and H. K. Yasuda, "Improved Corrosion Protection of Al Alloys by System Approach Interface Engineering: Part I - Alclad 2024-T3", Corrosion, accepted.

9. Q.S. Yu, C. M. Reddy, C. E. Moffitt, D. M. Wieliczka, R. Johnson, J. E. Deffeyes, and H. K. Yasuda, "Improved Corrosion Protection of Al Alloys by System Approach Interface Engineering: Part II - AA 2024-T3", Corrosion, accepted.

10. C. E. Moffitt, C. M. Reddy, Q.S. Yu, D. M. Wieliczka, R. Johnson, J. E. Deffeyes, and H. K. Yasuda, "Improved Corrosion Protection of Al Alloys by System Approach Interface Engineering: Part III - AA 7075-T6", Corrosion, accepted.

11. T. F. Wang, H. Yasuda, T. J. Lin, and J. A. Antonelli, "Corrosion protection of cold-rolled steel by low temperature plasma interface engineering; I. Enhancement of E-coat adhesion", Progress in Organic Coatings, **28**, 291, 1996.

12. C.-P. Ho, and H. Yasuda, "Coatings and Surface Modification by Methane Plasma Polymerization", J. Appl. Polym. Sci., **39**, 1541, 1990.

13. Sungyung Lee, "Effects of Plasma Polymer on the Multi-Stress Aging of Organic Insulation and Proposed Degradation Mechanisms", Ph.D. Dissertation, University of Missouri-Columbia, 1995.

14. B. A. Boukamp, Equivalent Circuit, Users Manual, 2nd ed., University of Twente (1989).

15. C. Barreau, D. Massinon, and D. Thierry, "Experimental measurement of the transportation properties of automotive cataphoretic Paints", SAE Transactions, **100**, 1281, 1991.

13. Effect of Scribing Modes on Corrosion Test Results

H.K. Yasuda, C.M. Reddy, Q.S. Yu, J.E. Deffeyes, L. He and G.P. Bierwagen

Abstract

Prohesion salt spray corrosion test was carried out with 32 primer coated AA2024-T3 test panels with four different kinds of scribes (8 test panels each). The scribing width and depth showed little effect on the test results. The extent of damage to the interface between the primer and the substrate alloy produced the greatest influence on the test results. The concurrent Electrochemical Impedance Spectroscopy (EIS) measurement with Prohesion salt spray showed that the sharp drop of the impedance modulus at low frequency ($|Z|_{0.1HZ}$) for the samples scribed with spinning cutter tip started much earlier during the Prohesion exposure than samples scribed without spinning the cutter tip. There was very little difference observed on the impedance modulus values of the samples with different scribe depth and width. The consistent results between the Prohesion test results and EIS data suggested that the concurrent EIS measurement with Prohesion salt spray may provide additional information pertinent to the corrosion protection mechanisms involved in the coating under examination.

Introduction

It is a well-established practice to test corrosion resistance of a coated panel by exposing a scribed coating layer to a corrosive environment such as salt spray for a prolonged period of time [1]. Corrosion resistance of the coating is qualitatively evaluated by examining the corrosion that took place near the scribed line. Such a method certainly provides an estimate of the level of corrosion resistance of the coating; however, this method does not yield information concerning the mechanisms of corrosion protection [2].

The corrosion resistance of a coated metal sheet could be considered to be dependent on at least five factors [3,4,5]. These factors are:

    1) Salt intrusion resistance of the top surface of a coating [6,7],
    2) Barrier characteristics with respect to water and salt and other corrosive chemicals [7,8],
    3) Function of passivating agents [7,8], if any,
    4) Level of adhesion of the coating to the substrate [2,9], and
    5) Surface state of oxides on which the coating is applied [3,10].

All of these factors are important in consideration of corrosion resistance of a coating, which remains intact; i.e., undamaged coating. When the surface of a coating is scribed (damaged coating), the main barrier characteristics of a coating described in 1) and 2) are bypassed. Then the major factors are reduced to 3), 4), and 5). Under such a condition, the exposed interface between metal and coating becomes the major factor. The role of passivating agents or corrosion inhibitors is focused on the exposed metal surface and the new metal surface that will be exposed by the corrosion induced delamination of the coating near the scribed line.

The scribing process is not only exposing the substrate metal but also exposing the interface between coating and metal. Once the coating/metal interface is exposed to a salt solution, the nature and extent of the adhesion of the coating to the substrate metal becomes the utmost important factor that dictates the occurrence of corrosion. The importance of the water-insensitive adhesion in corrosion tests was recently investigated by means of Electrochemical Impedance Spectroscopy (EIS) [11]. EIS could detect the microscopic de-lamination of coating without artificially introduced defects.

EIS study is extended in this study to investigate the nature of scribing, specifically the damage to the coating/metal interface. For this purpose, severe scribing method was included to cause interfacial damage. Questions that arise are: Does a wider scribing width cause more corrosion? Is a deeper scribing depth more damaging? With this background information in mind, 32 sheets of AA2024-T3 were coated with an E-coat under the identical conditions of coating and curing, and were divided into four groups of different scribing modes. Four groups of scribed samples, in which the only difference is the mode of scribing, were exposed to Prohesion salt spray test in two different locations. The coating of not-so-superior adhesion was used intentionally to magnify the interfacial aspect. The results thus obtained are shown in this section.

Experimental

Aluminum alloy panels and surface cleaning

The Al alloy panels (3"×6"×0.032") used for the present study were AA 2024-T3 (2024 specifications are by composition in wt%: Si 0.5, Fe 0.5, Cu 3.8-4.9, Mn 0.3-0.9, Mg 1.2-1.8, Cr 0.1, Zn 0.25, Ti 0.15, total of others 0.15, and Al remainder [12]) procured from Q-Panel Lab Products (Cleveland, OH).

The AA 2024-T3 panels were first cleaned by acetone wiping with Kimwipes® to remove the ink marks and loose organic matters from the surfaces. The chemical cleaning of the aluminum alloy panels was performed by following the method provided by The Boeing Company at St. Louis. Alkaline solution of Turco 4215S (Turco Products, Inc., Wilmington, CA) was prepared and used per McDonnell Douglas Process Specification P.S. 12030 (The Boeing Company, St. Louis). Alkaline cleaning of the panels was conducted by immersion in an alkaline bath at 65 ^{0}C (150 ^{0}F) for about 25 minutes, or until each panel became water break free when rinsed with DI water; they were then thoroughly rinsed with DI water.

Application of primer

Electrodeposition of the E-coat (ED6650, PPG Industries, Cleveland, OH) was carried out in a one gallon electrocoat bath at 90 ^{0}F (32 ^{0}C) using the substrate as the cathode and a stainless steel strip (1.5"×10") as the anode. A Darrah Digital® DC power source with variable voltage facility was used for the electrodeposition. Electrodeposition was carried out at 200V for 2 minutes. The electrocoated panels were then rinsed with DI water to wash the undeposited electrocoat from the surface. Panels were dried in air for 30 minutes and cured in an oven for 20 minutes at 325°F. After baking, the thickness of cured E-coat was about 25 μm as measured using an Elcometer® 355 with a non-ferrous probe.

Scribing procedures

Panels were scribed by using a Computerized Engraver, model Vanguard Unica, (New Hermes Inc., Duluth, GA) with cutter 42-037-000 Diamond Graver (New Hermes Inc., Duluth, GA). It was noted that the cutter used had the tip geometry as shown in schematic diagram in Fig. 1.

Two depths (0.02" and 0.04") of scribes were made using cutter in stationary or spinning mode. Due to the cutting head geometry, a deeper cut yields a wider scribe line. To distinguish the difference of scribe mode, the scribe made in stationary mode, horizontal dragging of the tip across the panel surface, was defined as V shape, and the scribe made with a spinning cutter tip was defined as U shape. The V or U shape definition is used only for identification of different scribes but not the real scribe shapes.

The scribe depth was controlled by adjusting the depth increment of each scribe and the numbers of scribes. Initially the cutter position was zeroed on to the panel surface to be scribed then panels were scribed with increments of 0.25 mm (0.01").
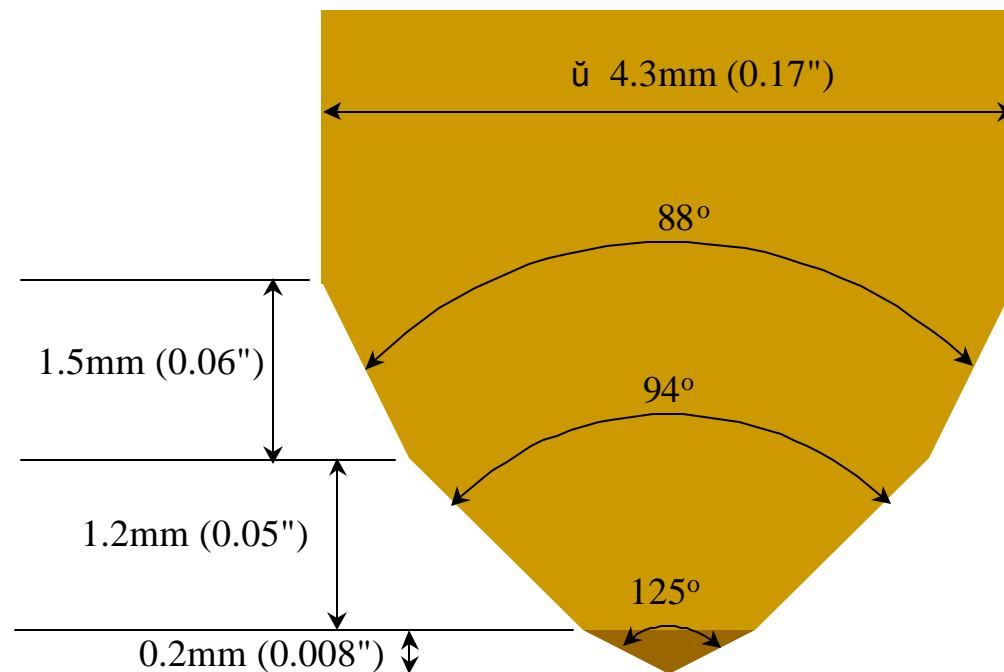
Figure 1. Schematic of the scribing cutter 42-037-000 Diamond Graver (New Hermes Inc., Duluth, GA) tip at 50X magnification.

Prohesion salt spray

The scribed samples were divided into two groups in respective scribing modes, and one group of samples were sent to Boeing, St. Louis (Boeing), and another group to North Dakota State

University (NDSU) for Prohesion salt spray testing. Both labs carried out according to the procedure described in ASTM G85, A5. This test is performed with an electrolyte solution (dilute Harrison's solution) of 0.05% sodium chloride and 0.35% ammonium sulfate by mass. The duration of the test is about 12 weeks (2000 hrs) which is the standard practice followed at Boeing, St. Louis. Wet/dry cycle consists of 1-h fog followed by 1-h dry-off. The fog temperature during the fog period is maintained 25°C. The pH of the collected solution is within the range of 5.0 and 5.4. The dry-off temperature throughout the exposure zone is maintained at $35 \pm 1.5°$C. The dry-off is achieved by purging with fresh air, such that within 3/4-h all visible moisture is dried off of the specimens. The condensate rate is maintained within 1-2 ml/hr. ASTM G85, A5 does not say anything about condensate rate but these recommendations are from the manufacturer of both labs' test chambers, Q-Lab Products, Cleveland OH.

Evaluation of test results

After completing test cycles in Prohesion salt spray, the panels were rinsed with distilled water and visual observations were made. Then the panels are subjected to a commercial paint stripper solution (Turco-5469) to strip off the E-coat on the scribed surface to see the corrosion effect underneath the E-coat film and away from the scribe.

Concurrent EIS measurement with prohesion salt spray

The samples tested at NDSU were also concurrently examined with EIS measurement during the regular Prohesion exposure period. During the 2,000 hours (83.3 days $\approx$ 12 weeks) Prohesion exposure, the tested panels were taken out the Chamber once a week and the EIS measurements were performed on the unscribed parts of the scribed panels. The time to perform the electrochemical measurements was about one hour, and during this time the scribed area was exposed to lab ambient conditions. EIS measurements were performed in dilute Harrison solution (0.05% NaCl and 0.35 $(NH_4)_2SO_4$ aqueous solution) using a Gamry potentiostat controlled by Gamry CMS100 software. Measurements were taken from 0.1 Hz to 5 kHz with 10 mV sign wave potential. Ten points were collected per decade. The reference and counter electrodes were a saturated calomel electrode (SCE) and a platinum electrode respectively. Fig. 2 shows the schematic of the sampling for EIS measurement of scribed panels at NDSU. The circle between the scribe lines is the sampling area for the EIS measurements.

Results and Discussion

Optical Microscopic study

Fig. 3 shows the optical microscopic pictures of the four different scribes at 50X magnification. As seen in Fig. 3, flat scribes were produced by stationary mode (designated as V shape) with horizontal dragging of the cutter tip across the panel surface. In contrast, the spinning tracks were clearly observed in the scribes made in spinning mode (designated as U shape). Spinning left burrs in the scribes and also wider scribes. Since they provided more surface area exposed, the left burrs in the scribe may have more chance to initiate the corrosion.

It should be noted that the V shape scribe with stationary mode is very similar to the knife edge cut of ASTM method D1654 and D3359 [13,14] in preparation of painted specimens for corrosion and adhesion tests. Since the ASTM scribing methods are largely dependent on individual operators, the scribing by an automated engraver machine as employed in this work may provide a more consistent and uniform cut through the coatings on metallic substrates.
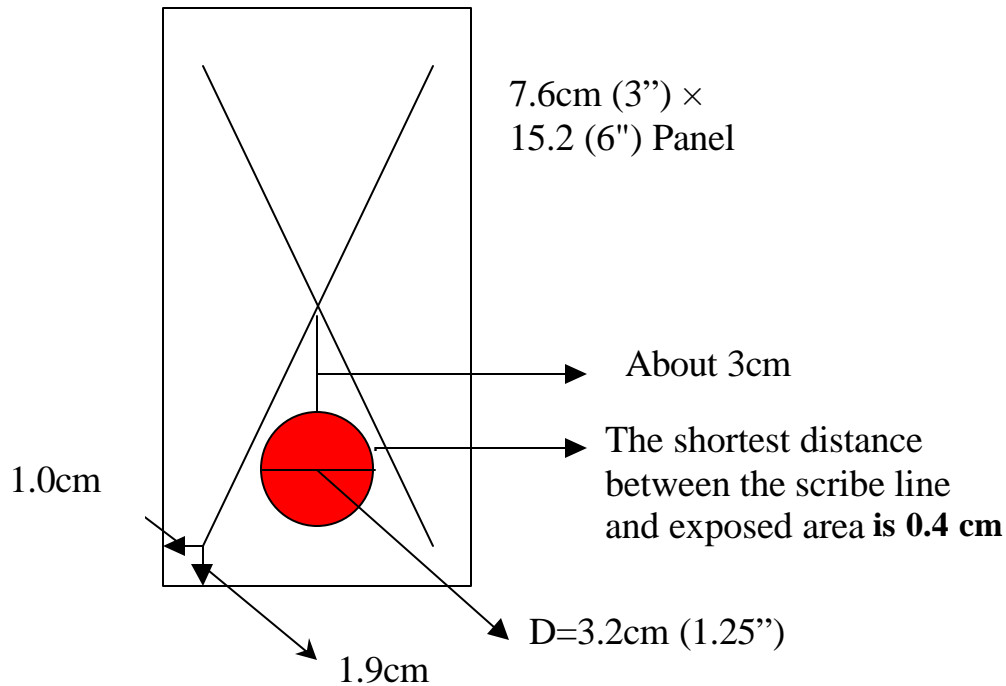

Figure 2. Schematic of the sampling for EIS measurement of scribed panels.

Prohesion test results

Fig. 4 shows the typical pictures of Prohesion tested sheets with different scribes and depths. From the visual examination of the tested panels, a general conclusion can be made that the U type scribe resulted in much more corrosion through the corrosion test, but the scribe depth had very little effect on the corrosion test results. Consistent corrosion test results were also obtained with the samples tested at NDSU.

Due to the cutting head geometry as shown in Fig. 1, the increase of scribe depth also increased the scribed width. Consequently, a general conclusion can be extended to state that the scribing width and scribing depth has little effect on the corrosion test results. The most striking difference in the corrosion results was caused by the different mode of scribing. In a simplified view, V shape scribe gave the least corrosion, and U shape scribe caused severe corrosion.
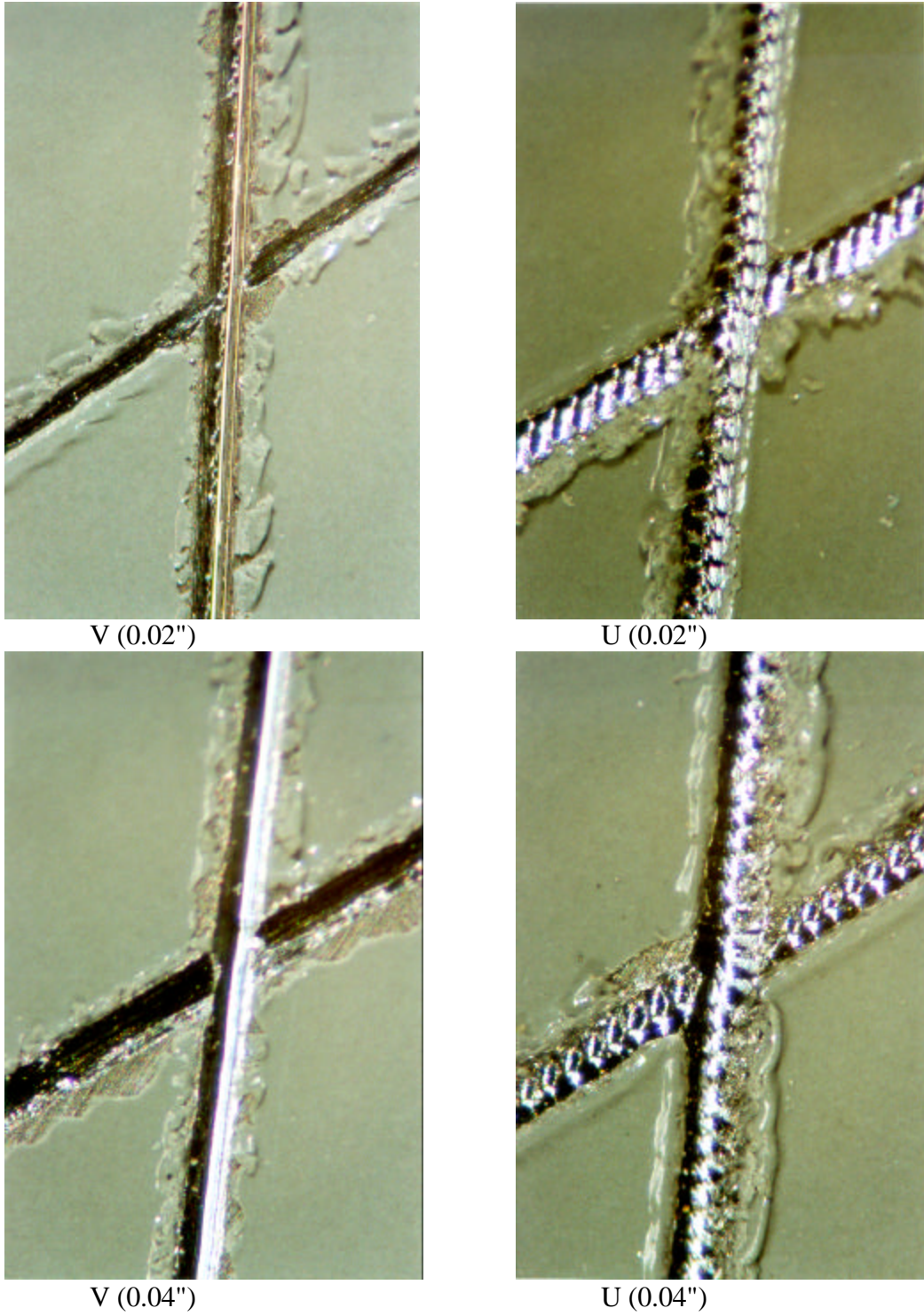
Figure 3. Optical microscopic pictures of the four different scribes at 50X magnification.

V (0.02")   U (0.02")
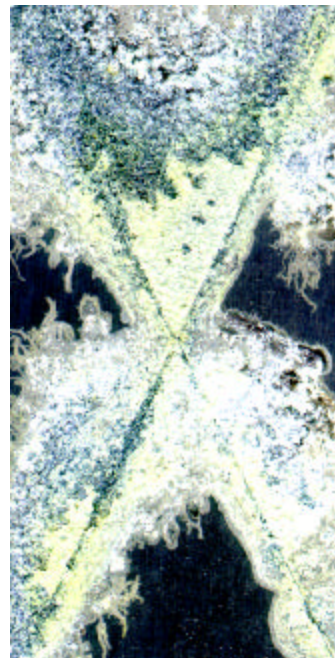
V (0.04")   U (0.04")

Figure 4. Scanned picture of Prohesion tested samples with different scribe types and depths. Tested at Boeing, E-coat removed after test.

It is important to recognize that the major difference in two types of scribing lies on the extent of damage caused on the coating/metal interface as described in more detail in the following section. The scribing with spinning cutter head could cause an extensive damage to the interface between coating and metal, and the striking difference found between V shape scribe and U shape scribe could be translated to the extent of damage to the interface. It is important to note that one out of four samples showed opposite corrosion test results as if the sample was mis-labeled. This means that the damage to the interface is not a sole function of the scribing mode. It simply means that the spinning head has a greater probability of inflicting severe damage.

Concurrent EIS Measurement

EIS technique has been well demonstrated to be an efficient method in evaluating organic coating systems on metallic substrates [15,16]. Recently, Katayama et al. have applied this technique to investigate the degradation of an organic-coated stainless steel with a macroscopic line defect [16]. Their EIS data correlated well with the actual delaminated area of the coating system. In this study, EIS measurement conducted concurrently with Prohesion salt spray test was used to study the scribing effects on the corrosion test results.
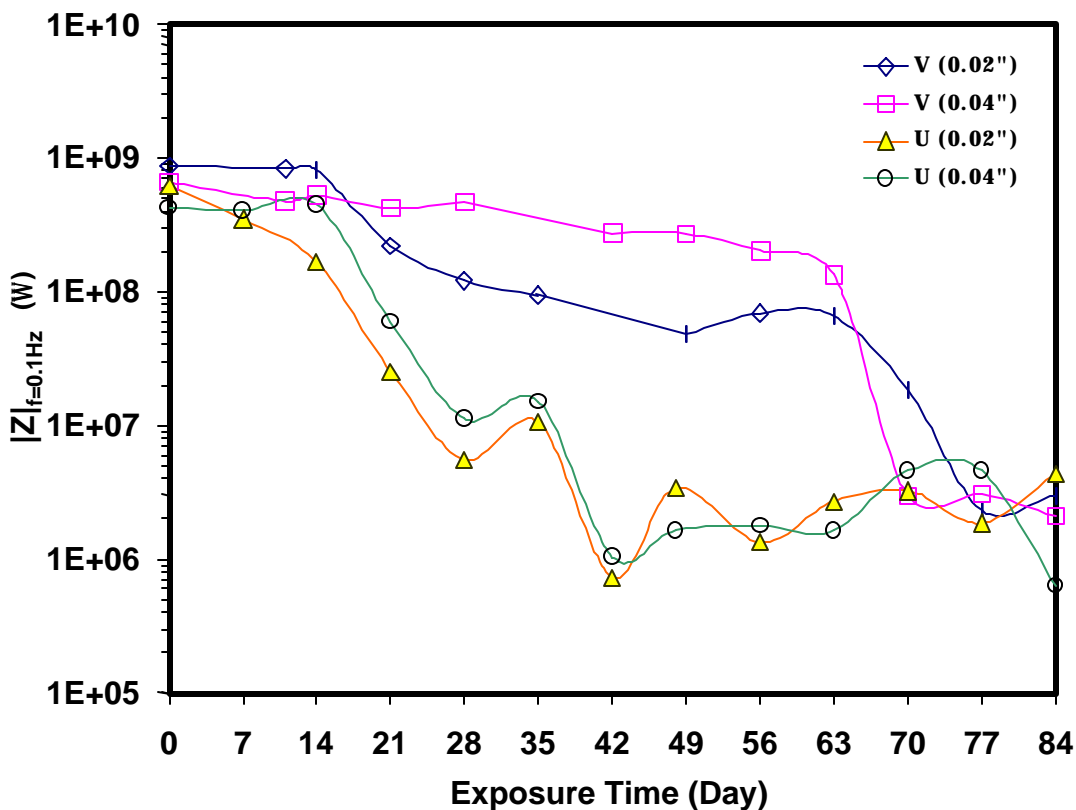
Figure 5. The impedance modulus at low frequency ($|Z|_{0.1HZ}$) dependence on the scribe types and depths and the exposure time in the Prohesion corrosion test chamber.

Fig. 5 shows the dependence of impedance on different modes of scribing. It was noted that the sharp drop of impedance modulus at low frequency ($|Z|_{0.1HZ}$) for U scribed samples of both U (0.02") and U (0.04") started after 14 days of exposure in the Prohesion chamber. The sharp drop of impedance modulus at low frequency ($|Z|_{0.1HZ}$) indicated the coating system failure, which is also evidenced by the onset of a second time constant suggesting partial delamination of the coating [16]. In contrast, there is very little gradual drop of the ($|Z|_{0.1Hz}$) for V scribed samples of both V (0.02") and V (0.04"). The V scribed samples did not start large impedance modulus drop for a long period of exposure time until 70 days in the Prohesion test chamber.

In samples with varying scribe depth, the V (0.04") samples with deeper scribe depth showed slightly better corrosion resistance than V (0.02") samples at the early stage of the exposure. With prolonged exposure, there is little difference on their performance. The U(0.02") and U (0.04") samples showed no significant difference on their corrosion resistance during all the Prohesion test period.

The results of the concurrent EIS measurement are consistent with what were found with Prohesion test results shown above. The earlier failure of the coating system due to partial delamination at the interface resulted in severe corrosion on the U shape scribed panels. The concurrent EIS measurement reveals the importance of the lateral diffusion of salts initiating from the damaged interface. This situation could be explained by Fig. 6, which schematically depicts the pathways of electrolyte to the sampling site of EIS measurement

Since the same primer with controllable coating thickness and characteristics was used, the different scribe modes could not have any effect on the pathways B and C in Fig. 6. If the pathway B or C to be the dominant one, the difference of scribing modes should not influence the EIS impedance values as a function of the immersion time. In the case of V shaped scribes (with minimal interface damage), it is likely that C might be the dominant pathway, and the difference in the scribing depth and width has little effect.
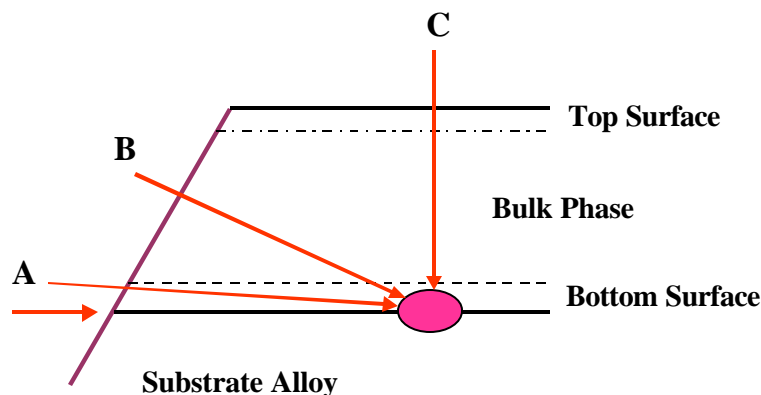
Figure 6. Pathways of corrosive chemicals to the site of EIS measurement.

The most significant factor that can be seen in Fig. 5 is the difference of the critical time at which the impedance modulus value start to drop sharply; i.e., 14 days for U shaped scribe and 70 days for V shaped scribe. This large difference can be explained by the rapid transport by means of pathway A in the case of U shape scribes due to the extensive interface damage, which resulted in the earlier failure of the coating systems with partial delamination of the coating. Even in this case, the scribing depth and width has little effect. This means that the severe damage to the coating/substrate interface caused by the scribing process could cause the largest influence on the outcome of Prohesion salt spray test results. The interfacial damage is considered to be a function of adhesive strength of coating to substrate alloy. Good adhesion might minimize the interfacial damage. Without tenacious, water-insensitive adhesion of a coating layer to the substrate metal, the propagation of the interfacial damage could not be inhibited [11].

The influence of scribing itself on the outcome of corrosion test results is of an important concern in establishing a test method. To obtain test results of narrow distribution is probably the main target of standardizing a test method. On the other hand, from the view point of predicting the best performance of a set of coated samples, it would be better to apply the most severe conditions even though it might results with large scattering. The results shown in this study clearly indicate that the interfacial damage is the most crucial factor in scribed surface corrosion tests.

Summary

1. Prohesion test results conducted both at Boeing, St. Louis and NDSU indicated that the scribe type had a significant effect on the corrosion protection performance of the samples, but the scribe depth and width had very little influence on the corrosion performance of the samples.
2. The concurrent EIS measurement with Prohesion salt spray showed that the sharp drop of impedance modulus at low frequency ($|Z|_{0.1Hz}$) for U scribed samples started much earlier during the Prohesion exposure than V scribed samples. There was very little difference observed on the impedance modulus of the samples with different scribed depths. The consistent results between the Prohesion test results and EIS data suggested that the concurrent EIS measurement with Prohesion salt spray may provide additional information pertinent to the corrosion protection mechanisms involved in the coating under examination.
3. The major factor that caused the largest difference in the corrosion protection performance of samples tested in this study is attributed to the severity of damage inflicted to the interface between the primer and the substrate metal, which was observed by microscope examination and concurrent EIS measurement with Prohesion salt spray test. Scribing by using a spinning cutter tip could inflict severe damage to the interface and thus provides a severer test condition that could distinguish better coated systems. A superior coated system should pass such a severe scribing test.

References

[1] ASTM standards G85-94, Standard Practice for Modified Salt Spray (Fog) Testing, Annex 5.

[2] G.P. Bierwagen, "Reflections on Corrosion Control by Coatings" Prog. Organic Coatings, **28**(1996): p. 43.

[3] C. M. Reddy, Q.S. Yu, C. E. Moffitt, D. M. Wieliczka, R. Johnson, J. E. Deffeyes, and H. K.Yasuda, "Improved Corrosion Protection of Al Alloys by System Approach Interface Engineering: Part I - Alclad 2024-T3", Corrosion, 56 (2000): p.819.

[4] Q.S. Yu, C. M. Reddy, C. E. Moffitt, D. M. Wieliczka, R. Johnson, J. E. Deffeyes, and H. K. Yasuda, "Improved Corrosion Protection of Al Alloys by System Approach Interface Engineering: Part II - AA 2024-T3", Corrosion, 56 (2000): in press.

[5] C. E. Moffitt, C. M. Reddy, Q.S. Yu, D. M. Wieliczka, R. Johnson, J. E. Deffeyes, and H. K. Yasuda, "Improved Corrosion Protection of Al Alloys by System Approach Interface Engineering: Part III - AA 7075-T6", Corrosion, 56 (2000): in press.

[6] Sungyung Lee, "Effects of Plasma Polymer on the Multi-Stress Aging of Organic Insulation and Proposed Degradation Mechanisms", Ph.D. Dissertation, University of Missouri-Columbia, 1995.

[7] G.W. Walter, Corrosion Science, **26** (1986): p.27.

[8] H. Leidheiser, Jr., Corrosion, **38** (1982): p.376.

[9] T.F. Wang, T.J. Lin, D.J. Yang, J.A. Antonelli, H.K. Yasuda, Prog. Org. Coat., **28** (1996): p.291.

[10] H.K. Yasuda, T.F. Wang, D.L. Cho, T.J. Lin, J.A. Antonelli, Prog. Org. Coat., **30** (1997): p.31.

[11] M. Chen, Q.S. Yu, C.M. Reddy, H.K. Yasuda, Corrosion, 56 (2000): p. 709.

[12] ASM Specialty Handbook: Aluminum and Aluminum Alloys, American Society for Metals, 1993.

[13] ASTM D1654, Annual book of ASTM stndards, Vol. 06.01.

[14] ASTM D3359, Annual book of ASTM stndards, Vol. 06.01.

[15] G.P. Bierwagen, C.Jeffcoate, D.J. Mills, J. Li, S. Balbyshev, D.E. Tallman, Prog. Org. Coat. 29 (1996): p. 21.

[16] H. Katayama, K, Yagi, A. Nishikata, T. Tsuru, Electrochimica Acta, 41 (1996): p. 1093.

14. Statistical Evaluation of EIS and ENM Data Collected for Monitoring Corrosion Barrier Properties of Organic Coatings on Al-2024-T3

R.L. De Rosa, G.P. Bierwagen, and D.A. Earl

Abstract

Electrochemical noise (ENM) and impedance (EIS) were used to determine the corrosion protection of epoxy coated aluminum substrates. The noise resistance and impedance values were modeled using multiple linear regression analysis. The discrete variables for the linear regression were time, analysis technique, topcoat, and pretreatment. The model was used to detect contribution from the pretreatment and topcoat separately. The variance generated from ENM confounded any effect from the different components of the coating system. Less variable impedance data was reliable for predicting individual effects from the coatings and pretreatments. Only subjective information was obtained without the aid of statistical modeling.

Introduction

Electrochemical analysis methods are used to monitor and quantify the corrosion protection abilities of organic coatings on metal substrates. Two of the predominant methods are electrochemical impedance spectroscopy (EIS) and electrochemical noise methods (ENM) [1,2,3]. The validity of the quantitative values obtained from EIS and ENM are subject to much discussion. The focus of the work presented was based on the statistical treatment of ENM and EIS data sets from the analysis of coated metal substrates. The statistical treatment, multiple linear regression analysis, was used to elucidate the error associated with each electrochemical method, and to differentiate between discrete variables in the experiment.

Many factors contribute to the extracted values from electrochemical characterization. As with any experimental method, contributions from known and random variables are inherently part of the final data set. It is desirable to separate the contributions of these variables. Known variables are introduced into the experiment in order to determine specific effects on the overall system properties. Typical variables from electrochemical analysis include sample differences, time, and electrolyte composition. Random error is due to variations that are inherent to the analytical technique. Some error can be eliminated if their source can be determined, but most often the unknown variables remain illusive. Examples of random error sources for electrochemical analysis would include effects of electrodes, salt bridges, and noise from the instrumentation.

Linear regression analysis was chosen for this study because it is the most standard statistical method to model multiple variables. It identifies the relationship between known and unknown variables [1]. Presented in this paper is the statistical treatment, using linear regression models, of an experiment designed to quantify the corrosion behavior of electrodeposition (ED) epoxy coated Al 2024-T3. The experiment was designed to differentiate the variables derived from: EIS and ENM analysis methods, time, surface pretreatment, and coating application voltage.

The intent of the work presented is to quantify the contributions from known and random variables (error) related to EIS and ENM analysis of epoxy coated aluminum substrates through a statistical treatment of the data.

Experimental

The coating system used in the experimental design was an epoxy/blocked-isocyanate electrodeposition coating applied to pretreated Al 2024-T3 panels. Variations in the coating system (coating and substrate pretreatment) were made through modification of the coating application and substrate pretreatment. The epoxy coating was modified by varying the application voltage (100V, 150V, and 200V) through voltage or current control during the electrodeposition. The coating was then applied to panels with different surface pretreatments. Overall, three pretreatments were used, acetone cleaned, alkaline cleaned, and plasma deposition poly(trimethylsilane) (PTMS) treatment. Selected combinations of the application voltages and surface pretreatments resulted in six coating systems. The sample identification, pretreatment, and application voltage are given in Table 1.

Table 1. Sample Description

Sample Identification	Pretreatment	E-coat
1 (1V)	alkaline	100 V with voltage control
2 (1.5V)	alkaline	150 V with voltage control
3 (2V)	alkaline	200 V with voltage control
4 (2VI)	Alkaline	200 V with current control
5 (ACE)	Acetone	200 V with current control
6 (N4)	plasma N	200 V with voltage control

Coating systems were prepared in identical sets of two. All panels were prepared for electrochemical analysis by adhering poly(vinyl chloride) pipe with an area of 12.56 cm^2 to the surface of each panel. The area inside the PVC pipe was exposed to a solution of 0.35 weight percent amonium sufate $[(NH_4)_2SO_4]$ and 0.05 weight percent sodium chloride [NaCl]. The collection of the electrochemical data was started one hour after electrolyte exposure. Data was collected five times over a 70-day immersion period on days 1, 7, 14, 60, and 70.

EIS data was collected using a Gamry PC3 potentiostat (Gamry Instruments, Warminster, PA) controlled by Gamry CMS100 software. Measurements were taken between 0.01 Hz to 5-kHz with 10 mV root mean square (RMS) sine-wave potential. Ten points were collected per decade. A saturated calomel reference electrode (SCE) was used with a platinum counter electrode. Sample 5 data for the frequency range sampled is presented as a Bode plot in Fig.1. The impedance modulus, |Z|, at a frequency of 1.02 Hz was used for the data set. The frequency was chosen to reflect the changes in the coating over time. At lower frequencies, error is introduced due to noise within the measurement design, while at higher frequencies, the systems are predominantly capacitive and show very little change. Earlier work done by Tait suggested that

each sample have at least five repeated EIS tests run to achieve *in*significant error in the results[1]. Multiple measurements on a single day were not possible for our analysis due to time constraints. Instead, the |Z| values that were used for the multiple regression analysis were the average between each pair of panels for each coating system.

ENM measurements were done on using a Gamry PC3 potentiostat (zero resistant ammeter) connected to a multiplexer and controlled by Gamry CMS100 software. Electrolytic contact between two nominally identical samples was made through a 0.6 N NaCl agar salt-bridge. A SCE was used as the reference electrode. The data corresponds to the response from both samples. Each R_n value was calculated by collecting one data point (voltage and current) every two seconds to gather 256 data points. These 256 points were averaged, and the standard deviation of the potential was divided by the standard deviation of the current to give R_n. It was possible to perform repeated measurements for ENM over 5 hours, assuming that the effect of such a small time was insignificant with the total time of the test. Therefore, ten measurements (ten repeats) were collected for each of the six pairs of samples on each measurement day.
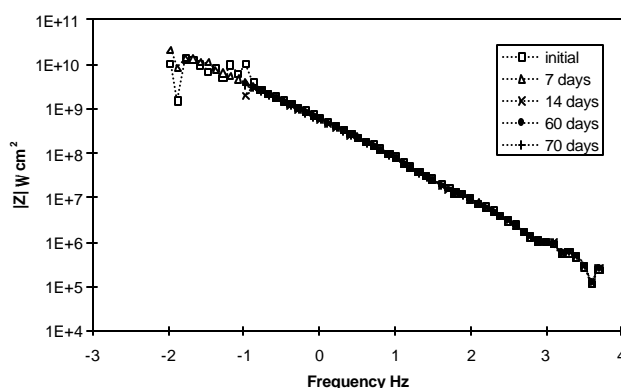
Figure 1. EIS Bode plot for coating system #5 (200 V acetone cleaned) over the 70 day immersion period.

Film thickness measurements were conducted using an Elcometer model 345 film-thickness meter for non-ferrous metals. The closest calibration thickness compared to the range of coating thickness tested was 25 μm.

Results and Discussion

<u>Electrochemical Methods</u>

The data that was used for the statistical treatment was the impedance modulus at 1.0 Hz, $|Z|_{f=1.0Hz}$, and the noise resistance, R_n. It is not uncommon to extract other values, such as noise impedance and pore resistance from ENM and EIS measurements. The use of multiple regression analysis is not limited to the values that are presented in this paper, instead it can be applied to almost all sets of data. The main intent of the information published in this paper is that without a statistical treatment of the data, valuable information can be lost.

The EIS data set is presented in Table 2. Values were divided by 1 x 10^8 for ease in calculations. A plot of the data versus time is given in Fig. 2 with dashed lines showing the general trend with respect to time.

Table 2. EIS Data ($|Z|_{f=1.0Hz} * 1$ x 10^{-8} Ω cm^2)

Sample	Day 1	Day 7	Day 14	Day 60	Day 70
1	5.23	0.82	1.42	1.65	1.58
2	8.14	7.03	6.81	5.83	6.45
3	8.68	7.81	7.42	6.85	6.76
4	9.24	8.21	8.08	7.40	7.35
5	8.62	8.22	7.64	7.21	7.32
6	6.82	6.24	6.00	5.75	6.17
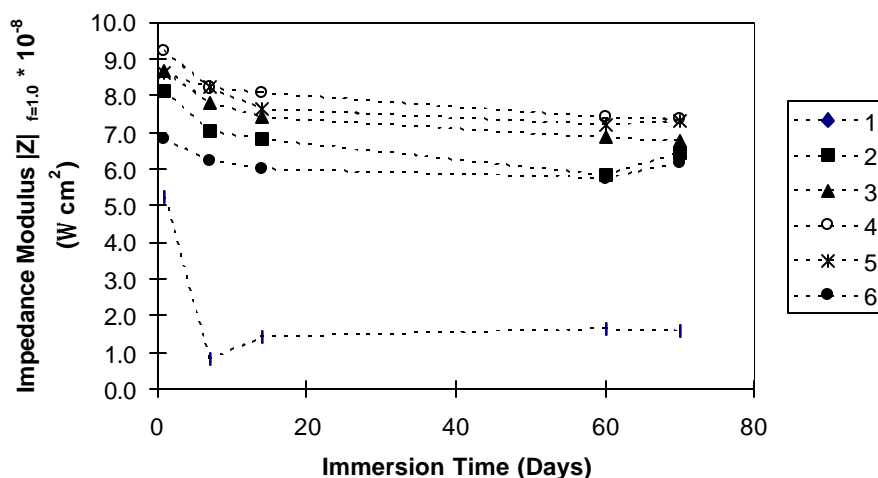
Figure 2. Plot of EIS data with respect to time, $|Z|_{f=1.0\ Hz} * 10^{-8}$.

The averages of the ten repeats for each ENM measurement are presented in Table 3. Values were divided by 1 x 10^8 for ease in calculations. The plot of the ENM data versus time is shown in Fig. 3. Dashed lines indicate the trend in the data over time.

Figs. 2 and 3 convey the behavior of the samples with respect to the measurement technique and time. From the presentation of the data in this manner, it can be seen that the ENM method results in a higher variance in the coating resistance and that it is more sensitive to changes in coating's properties over exposure time. The R_n values are also an order of magnitude higher than the impedance values.

Concerning the differences in coating systems, it can be concluded from both data sets that coating system #1 (100V, alkaline cleaned) resulted in the poorest performance. Beyond this observation, little information can be extracted from the ENM data due to the large variance. The less variable impedance data indicated that coating systems 2-6 have similar barrier protection characteristics with little deviation among their |Z| values and small change over time. No information concerning individual effect of the epoxy and the surface pretreatment can be predicted form the EIS or ENM data sets as they are presented. Multiple linear regression analysis was used to quantify the differences between EIS and ENM data, and the effects of time, application voltage, and surface pretreatment. The following sections present the statistical treatment of the data from the EIS and ENM experiments.

Table 3. ENM Data (R_n * 1 x 10^{-8} Ω cm^2)

Sample	Day 1	Day 7	Day 14	Day 60	Day 70
1	0.37	0.57	0.23	1.01	0.44
2	21.20	4.88	1.77	3.71	1.91
3	3.03	37.80	21.90	2.48	2.71
4	52.60	38.50	15.20	1.00	6.37
5	45.30	34.10	12.50	1.37	2.25
6	25.40	29.40	12.00	0.48	1.50
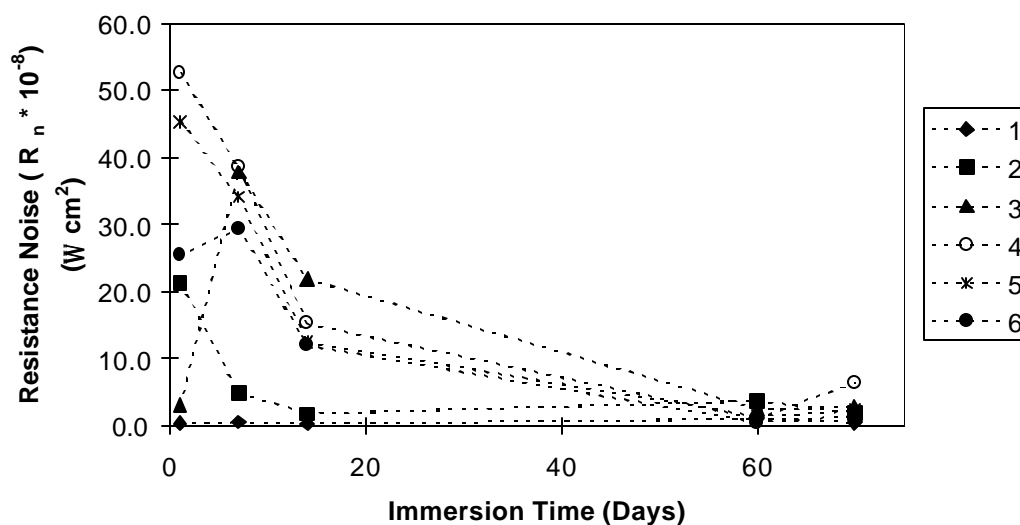
Figure 3. Plot of ENM data with respect to time, R_n * 10^{-8}.

Statistical Evaluation

Raw data from electrochemical analysis continues to be published without any statistical treatment to explain random error or the effects of discrete variables in the experiment[1,2,3].

Multiple regression models were developed from the experimental data presented in Tables 3 & 4 in order to identify any differences between ENM and EIS results and to quantify the effects of immersion time, coating type, and pretreatment [1,2,4]. All of the values presented from the statistical analysis are in units of $10^8 \, \Omega \, cm^2$. A standard 0-1 coding technique [**Error! Bookmark not defined.**] was used to assign x-matrix values to the discrete variables in order to derive unknown β-coefficients for factors. Variables with at least a 95% significance level ($|t_o|>t_{0.025, \, v}$) were included in the models.

Table 4. Dry Film Thickness Measurements

Sample	Dry Film Thickness (μm)	Standard Deviation
1-a	24.17	1.17
-b	23.50	0.55
2-a	29.17	0.40
-b	29.83	0.75
3-a	36.67	1.63
-b	35.67	0.52
4-a	40.67	1.50
-b	37.83	0.75
5-a	27.67	1.03
-b	28.00	0.89
6-a	35.00	1.26
-b	35.83	0.75

The first model was developed with all data from both ENM and EIS methods. The electrochemical measurement method (M), immersion time (T) in days and coating type (C) were all found to have significant effects on the results (R):

$$R = 21.08 - 6.24 \, (M) - 0.17 \, (T) - 11.54 \, (C_1) - 6.10 \, (C_2) - 2.33(C_3)$$

Where $C_1 \ldots C_3$ are the 100V, 150V and 200V coatings with voltage control, and M=0 for EIS or 1 for ENM. When predicting R from the equation, the level of a chosen discrete variable must be assigned a 1 and the others a 0. To predict the effect of the fourth coating (200V with current control), 0 must be input for the values of C_1, C_2, and C_3.

The model identifies that results from ENM (R avg. = 12.7) are significantly higher than EIS (R ave. = 6.4). However, the model accounts for only 40% of the variability in R ($R^2 = 0.40$), which has a large unexplained experimental error (model standard error = 9.29) primarily from the ENM method. This high error level confounded any effects due to the pretreatment ($t_o < 2.0$). The model also indicates that an increase in immersion time and the 100V coating caused R to decrease.

Individual models were also developed for the ENM and EIS methods in order to compare directly their error levels and sensitivity to the experimental variables. Regression models for ENM and EIS results are:

$$R_{ENM} = 28.02 - 0.32 \; (T) - 17.87 \; (C_1) - 11.70 \; (C_2) - 4.81 \; (C_3)$$
and
$$R_{EIS} = 6.62 - 0.01 \; (T) - 6.59 \; (C_1) + 1.20 \; (C_2) + 0.55 \; (C_3) + 1.86 \; (P_1) + 1.61 \; (P_2).$$

Pretreatment P_1 is alkaline and P_2 is acetone. Inputs of 0 for P_1 and P_2 yield predicted results for the PTMS coating pretreatment. From the ENM model, 44% of the variablility in results (R_{ENM}) was still unexplained ($R^2 = 0.56$), and the standard error remained very high at 11.13. In contrast, the EIS model was considerably more accurate, explaining 96% of the variability of R in terms of the experimental variables. The EIS model standard error was 0.50, which was only 4.5% of the level found with ENM. This same trend was found in previously published data comparing ENM to EIS techniques over time, but without the authors using statistical techniques[8]. Unfortunately, without the statistical treatment, the difference between the two techniques cannot be quantified.

The high ENM error confounded any pretreatment effects therefore, differences in data values due to the pretreatment were undetectable using ENM. However, the influences from the pretreatment were detectable using EIS measurements and they were found to influence the final data.

The different behavior from EIS and ENM may possibly be due to the measurement techniques. EIS measurements were done in potentiostatic mode with small amplitude sinusoidal potential fluctuations about the steady state open circuit potential (OCP). The OCP was measured immediately before the potential application. By doing this, drift in the open circuit potential of the system during the experiment was neglected. Alternatively, ENM is based on spontaneous fluctuations in the system without an imposed signal. The method measures the true state of the electrochemical system. The natural fluctuations in the system may contribute significantly to the standard error and variability in the residuals.

By looking at the data from the electrochemical analysis techniques (Tables 2 & 3 or Figs.2 & 3), effects contributed to time, application voltage or pretreatment type could not be determined quantitatively. The significance that the known variables had on the final data was determined through additional statistical modeling. An individual variable's effect was quantified by inputting its range of experimental values into a model, while holding constant the other factor's levels. The resulting deviation from the average response reveals the statistically adjusted, predicted average effect. Initially, the effects that time had on the electrochemical system were modeled. A time derived model that can predict the effect time has on the protection abilities of a coating is invariably useful for lifetime prediction of the coating system [7].

Plots of the residuals versus |Z| and R_n are given in Fig. 4. The residuals are the differences between the actual measured value (|Z| or R_n) and the fitted value from the regression model. It can be seen in Fig. 3 that the ENM residuals were much higher than the EIS residuals, and tended to get larger with higher resistance values. At higher ENM values (≥ 30), an unidentified

factor caused measured values to increase above what was predicted from the experimental variables. EIS variability is shown to be much lower, even though one experiment (1 day immersion time, 100V coating, alkaline pretreatment) was a statistical outlier (standardized residual = 3.2, external studentized residual = 5.2: any residual > 3 is an outlier).
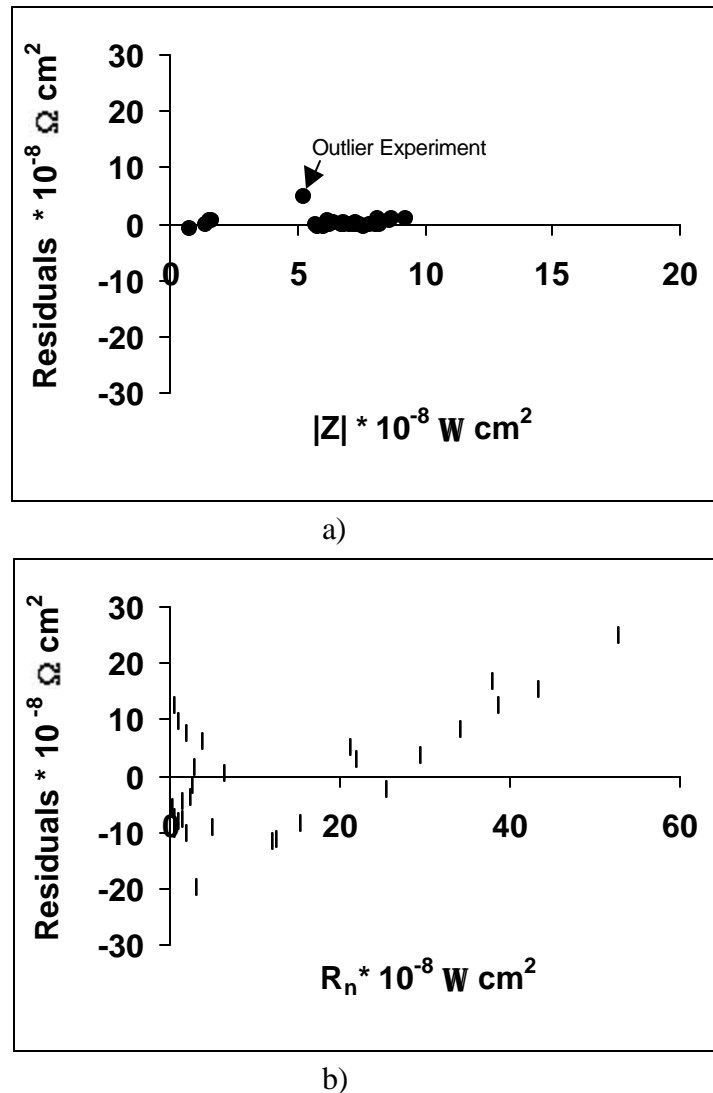

a)

b)

Figure 4. Plot of residuals from linear regression a) EIS data b) ENM data.

A plot of the statistically adjusted resistance and impedance values versus time is given in Fig. 5. The dashed lines indicate the linear rate of decrease in the resistance or impedance with respect to time. For this specific set of data, ENM showed a rate of decay of $3.2*10^7$ Ω cm^2 / day whereas the decay rate from the EIS data was only 1.5×10^6 Ω cm^2 / day. This is a significant difference if one is trying to predict the lifetime of a coating. The decay rate predicted from the ENM data set was 23 times faster than predicted from EIS. Along with the strong decreasing

resistance with respect to time, the plot also shows the large error bars associated with the ENM data. EIS error bars are presented, but are so small that they are barely visible. Therefore, the ENM measurement was more sensitive to changes in the system over time, but one must contend with the high degree of error associated with it when trying to predict time measurement data.
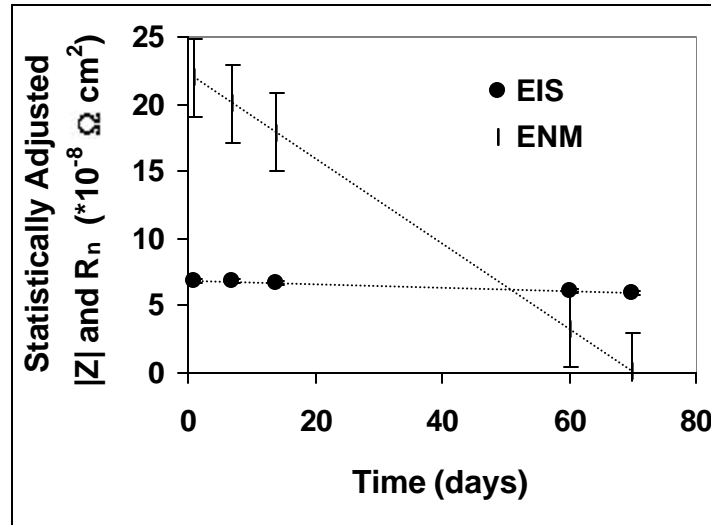
Figure 5. Time effects on ENM (◊) and EIS (•) data based on regression model predictions.

The error associated with the ENM measurements shielded any effects from the coating application voltage or the pretreatment. Therefore, the predictions concerning these two variables made from the regression models were from the EIS data only. First, the application voltage was modeled. The results of the statistically adjusted |Z| values (with error bars) versus ED voltage are presented in Fig. 6. Clearly, the 100V ED coating (#1) showed the lowest impedance response. The trend was also predicted from the raw data (Fig. 2). Also, it was predicted from the raw data set and confirmed by the statistical treatment that no significant difference was found between the 150V, 200V and the 200V-I results.

One could contend that the behavior of the coatings was due to their film thickness. It is known that the impedance or resistance of a coating can be affected to a certain extent by the coating thickness [7,8]. It has been suggested that the resistance of a coating deviates from linearity with thickness as multiple coating layers are introduced. The following equations illustrate the direct relationship between impedance and film thickness. Based on the equivalent circuit model used for the analysis, the impedance modulus was represented by the following equation.

$$|Z| = \frac{R_{po}}{1 + j\omega R_{po} C_c}$$

Where R_{po} is the pore resistance, ω is the frequency and $j = \sqrt{-1}$. The coating capacitance, C_c, is inversely proportional to d.

$$C_c = \frac{\varepsilon \varepsilon_o A}{d}$$

Where d is the coating thickness, ε is the coating's dielectric constant (typically between 3.4 to 3.6), ε_o is the permittivity of free space, and A is the total coating area exposed to electrolyte solution [7]. The film thickness dependence in the denominator cancelled out and the impedance value is directly proportional to d through R_{po}.

$$R_{po} = \frac{d}{kNA_{po}}$$

Where k is the solution conductivity (Ω^{-1} cm^{-1}), N is the number of pores in the coating and A_{po} is the average area of each pore. Therefore, theoretically as d increases, the impedance should also increase.
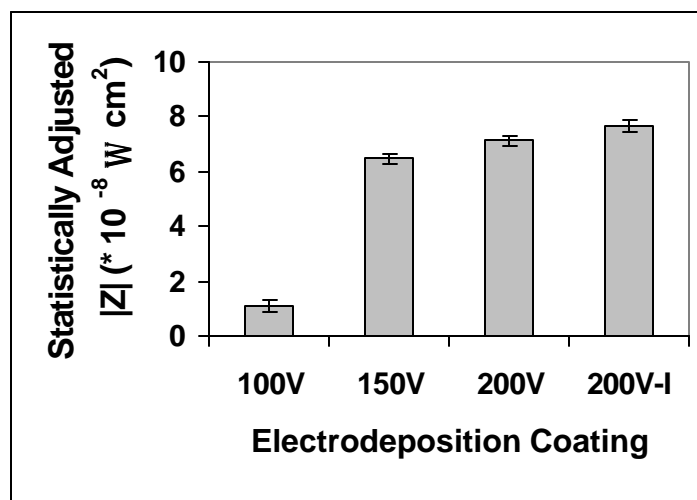
Figure 6. Application voltage effect on EIS results.

Measured film thickness of the six coating systems are given in Table 4. The values between coatings show a difference of up to 15 μm. This variation was due to the application voltage during coating deposition [7,8]. Under potentiostatic control a linear relationship between film thickness and the square root of the voltage exists.

$$d = \sqrt{(2c s_F)(Vt)}$$

Where c is the coulombic efficiency, s_F is the film conductivity, V is voltage and t is time. Under galvanostatic control, the film thickness increases linearly with time after the initial induction time, t. In this equation, i_{app} is the applied current density.

$$d = c i_{app}(t - t)$$

In direct relation to the application voltage, sample #1 (100V) had the lowest film thickness (23.85 μm), and sample #4 (200 V-I) had the highest (39.25 μm). The behavior of coating system 1 correlated with electrochemical theory giving the lowest impedance values. However, coating systems 2 through 6 were indistinguishable through statistical modeling. In fact, sample 5 performed as well as sample 4 despite being an average of 11 μm lower in film thickness. Sample 5 was only an average of 4 μm higher than sample 1 and performed significantly better. A multiple regression analysis using film thickness as an independent variable did not change

any of the statistical predictions. In effect, the thickness of the sample is not an independent variable, since we can see from the above equations it is directly related to both the resulting impedance values and the electrodeposition parameters.

Finally, the pretreatment methods were modeled. The results of the statistically adjusted |Z| values (with error bars) versus pretreatment method are presented in Figure 7. The acetone and alkaline cleaned coating systems produced higher than average results while the plasma treated system resulted in relatively low adjusted impedance values. The difference between alkaline and acetone cleaned systems were statistically insignificant. It must be stressed again that the information concerning the pretreatment effects could not be determined from the raw data without the statistical treatment. By combining the information from the statistical treatment the best performing coating system would be a combination of alkaline cleaning with 200V-I application voltage ED coating, system 4.
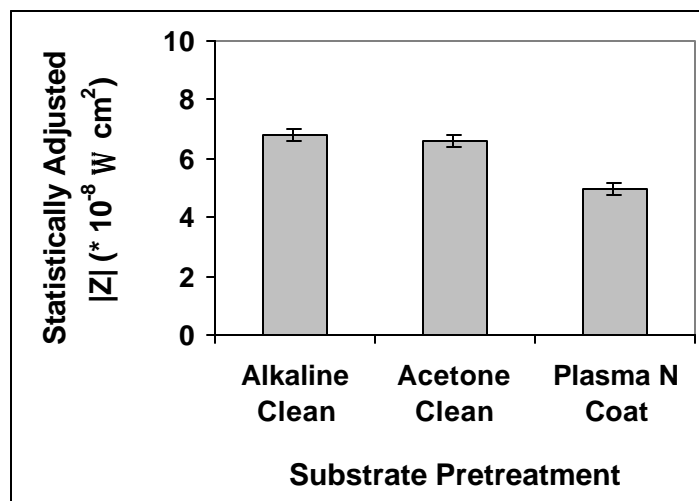
Figure 7. Substrate pretreatment effects on EIS results.

Conclusion

ENM and EIS data were collected for a specific sample set. The raw data indicated certain trends with respect to analysis method and time. We could predict that the ENM data had more variance associated with it and that the resistance values decayed more rapidly with time. The statistical treatment of the data provided a quantitative value attributed to the error associated with ENM data (standard error $= \pm 1.1 * 10^9 \ \Omega \ cm^2$) and EIS data (standard error $= \pm 5.0 * 10^7 \ \Omega \ cm^2$). The EIS error was only 4.9% of the error found with ENM. The effect of time on ENM and EIS was also quantified predicting a decay rate 23 times higher from ENM data than the EIS data. ENM also had a high error associated with multiple measurement over long periods of time with respect to impedance measurements. Finally, the statistical treatment of the EIS data (ENM was too noisy) resulted in the separation of discrete variables introduced into the experiment through the coating system. Effects on the statistically treated data from the application voltage for the ED coating and the pretreatment step were separated. Effects from

film thickness were negligible because it was not a discrete variable in this experimental design. In this specific experiment, it was found that a combination of 200V-I ED coating with alkaline cleaned aluminum would produce a coating system with the highest impedance values.

References

1. G.P. Bierwagen, Organic Coatings for Corrosion Control, ACS Symposium Series 689, Oxford Univ. Press, 1998.
2. A. Amirudin, D. Thierry, Progress in Organic Coatings, 26 (1995) 1-28.
3. B.S. Skerry and D.A. Eden, Progress in Organic Coatings, 15 (1986) 269.
4. D. Montgomery, Design and Analysis of Experiments, 4th Ed., John Wiley & Sons, New York, 1997, pp. 536-565.
5. W.S. Tait, J. Coatings Tech, 66 (834) (1994) 59.

6. Organic Coatings for Corrosion Control, ACS Symposium Series 689, Oxford Univ. Press, G.P. Bierwagen, (Ed.), 1998 p174.
7. 1997 Tri-Service Conference on Corrosion, Office of Naval Research, Wrightsville Beach, NC, Nov. 17-21, 1997.
8. F. Mansfeld, L.T. Han, C. C. Lee, and G. Zhang, Electrochimica Acta, 43(19/20) (1998) 2993.
9. H. Haller and B. Bowles, Multiple Correlation Analysis, Harold S. Haller & Company, Cleveland, OH (1999) pp. 6.1 -6.2, 9.1 - 9.4.
10. H. Haller and B. Bowles, Multiple Correlation Analysis Software, Harold S. Haller & Company, Cleveland, OH, 1999.
11 G. F. Schmitt, SAMPE Journal, 34 (1) (1998) 32.
12. J.R. Scully, J. Electrochemical Soc., 136 (1989) 979.
13. G.P. Bierwagen, J. Li, N. Davis, and D. Tallman, Proc. 5th Nuernberg Congress, Nuernberg, Germany, Vincentz Verlag, Hannover, Germany, Vol. 1, April 12-14, 1999 p.315.
14. A. Amirudin, Pl. Jernberg, D. Thierry, 12th International Corrosion Congress Preceedings: Coatings, Vol. 1, Houston, TX, Sept. 1993, p. 171.
15. Z. Kovac-Kalko, Electrodeposition of Coatings, G.E.F. Brewer (Ed.), American Chemical Society, Washington DC, (1973) 149.
16. M. Wismer, P.E. Peirce, J.F. Bosso, R.M. Christenson, R.D. Jerabek, and R.R. Zwack, J. Coatings Tech., 54(668) (1982) 35.

15. Influence of Surface Pretreatment and Electrocoating Parameters on the Adhesion of Cathodic Electrocoat to the Al Alloy Surfaces

C.M. Reddy, R.S. Gaston, C.M. Weikart, and H.K. Yasuda[*]

Abstract

Adhesion of cathodic electrocoat films to the aluminum alloys 2024-T3 bare and Alclad 2024-T3 with different pretreatments and with different cathodic electrocoat process parameters was investigated. The pretreatments studied were acetone wipe and alkaline cleaning. The cathodic electrocoat process parameters studied include variation of cathodic electrocoating voltage and time. Adhesion performance was evaluated by measuring the delamination time and percent delamination of the electrocoat from the alloy surface by placing the small specimen of the sample in the N-methyl pyrrolidinone (NMP) solution at 60°C until the film lifts off or for 2 hours whichever comes first. NMP times for electrodeposited film delamination from alkaline cleaned surfaces were found to be higher than the acetone wiped and or those of as supplied metal surfaces. There was not much effect of acetone cleaning of these alloy surfaces on the adhesion performance of the cathodic electrocoat. The voltage-current (of cathodic electrocoating process) relationships for alkaline cleaned surfaces were also found to be significantly different from other two types of surfaces. The NMP times of cathodic electrocoat delamination at lower cathodic electrocoating voltage and lower electrocoating times were higher than those at higher cathodic electrocoating voltage and electrocoating times for alkaline cleaned 2024 bare surfaces. Electrocoat thickness developed on the surfaces during the electrodeposition process increased with increasing electrodeposition voltage and time as anticipated.

Introduction

Good adhesion of polymers to the metal surfaces is an important parameter in the protection of the metal from corrosion and mechanical stress. Adhesion improvement of metal polymer bonds has been a topic of research for the past several years(1-4). There have been several pretreatment methods developed in the past to improve the adhesion of the paint to the metal surfaces (2). The adhesion of polymers depends on the characteristics of the metal surfaces which include surface roughness, surface contaminants, nature of chemical bonds on the surface, etc. (3, 4) before the polymer film is applied. Mechanical interlocking of the polymer with porous surfaces was the one of the focused studies in the improvement of the adhesion of metal polymer interfaces(5). In the course of several years, many pretreatments have been investigated to improve the adhesion of polymer to the metal surfaces. The pretreatment processes developed range from the surface cleaning to the surface conversion into different oxides to improve the adhesion of the paints to the metal surfaces(1). The adhesion performances of polymer metal bonds were found to be better for the anodized surfaces of Al alloys because of their porous column structure.

Cathodic electrocoating has been widely used in automotive, industrial and appliance areas in recent years in the corrosion protection system as a primary layer coating or top coat (6). The

chemistry of cathodic electrocoating and electrodeposition parameters have been a subject of several investigations (7-11). Cathodic electrocoating has several advantages including high throw power, superior corrosion protection, high coating utilization (>95%), low level of pollution (aqueous system), easy to automate etc., which makes this system an attractive coating system. Cathodic electrocoating process has been recently used in the painting of the automobile industry, mechanical industry, engineering industry and domestic appliances. Cathodic elctrocoating is a fairly simple process and can be used in different scales. High throw power makes the cathodic electrocoating process attractive in automobile industry as the electrocoat penetrates into cavities and pores of curved shaped parts.

The process parameters of the electrodeposition process have been largely determined by the bonding polymer characteristics (10). The variation of adhesion strengths of the electrocoat to the metal surfaces with electrodeposition parameters as well as the pretreatments of the metal surfaces have not been elucidated in the past. Several investigators have found that the cathodic electrocoated films provide superior corrosion protection of the metal.

Aluminum alloys 2024-T3 bare and Alclad 2024-T3 have been used in aircraft industry because of their higher mechanical strengths. Pure aluminum which has high corrosion resistance properties has limited applications because of its low mechanical strengths(12). By adding small quantities of alloying elements the mechanical strengths of aluminum are increased several folds. Although mechanical strengths have been improved, the addition of alloying elements reduce corrosion resistance of these metals drastically. The chromate conversion coating process, which has excellent corrosion protection property, has been used for the past several years to protect the metal from the corrosion(13). The use of chromates has come under severe restrictions because of their health hazards and necessitated a need for environmentally benign corrosion protection process(14). The electrodeposition is an excellent process for eliminating the environmental hazardous processes because of it's environmental benign nature. The adhesion of the electrodeposited polymer metal bonds is the important factor in the protection of the metal from the corrosion. In the present study we have looked in to the adhesion strengths of electrodposited films on the aluminum alloys AA 2024-T3 bare and AA Alclad 2024-T3 which are used for aircraft building. Cathodic electrocoating technique is being investigated for the application of airplane construction materials as this process has several advantages which can be exploited for our benifit. The objective of this study is to investigate the adhesion strengths of the cathodic electrocoat to different precleaned surfaces of aluminum alloys at different electrodeposition conditions such as elctrocoating voltage and time.

Experimental

Materials

The Al alloys panels, with size 3"X6"X0.034", used for the present study were 2024-T3 bare and Alclad 2024-T3 procured from Q-Panel Lab Products. The cathodic electrocoat used was a mixture of 44 wt% emulsion (BASF U32CD033A), 8 wt% paste (BASF U32AD290), 48 wt% DI water and 4 vol% additive (BASF 20CD0043). Turco 4215S was used as alkaline cleaner for the chemical cleaning of the Al alloys surfaces. The solvents acetone and N-methyl

pirrolidinone were procured from Fisher Scientific Inc.. The thickness of the electrocoat films were measured by elecometer® 355 with non-ferrous probe.

Experimental Procedures

The cathodic electrocoating was carried out on three different kinds of panels: (i) without cleaning, (ii) acetone wiped and (iii) alkaline cleaned at three voltages 170, 200 and 250 and at different electrocoating times from 0.5 to 4.0 minutes. In case of without cleaning, the panels of alloys of both kinds were used as supplied by Q-Panel. When observed visually the panels of 2024-T3 bare had some kind of protecting layer and ink marks of the panel identification tag printing. Alclad 2024-T3 panels had shiny surfaces with panel identification ink marks. In case of acetone wiped, the panels were wiped with acetone using Kimwipes® (Fisher Scientific Inc.) to clean the ink marks and loose organic matter on the surfaces of the panels. In case of alkaline cleaning, the panels were immersed in the alkaline bath (about 4 liter solution) for about 25 minutes, or until panel becomes water break free when rinsed with DI water, and rinsed with DI water and air dried. The composition of the alkaline cleaner solution was maintained such that water breatk free surface is obtained while rinsing with DI water after immersing in the alkaline bath for difinite time. Water contact angles of all the surfaces were measure by Sessile drop method before panels were used for electrodeposition. The electrodeposition was carried out in a one gallon electrocoat bath by using substrate as cathode and stainless steel strip(1.5"X10") as anode. Darrah Digital®'s DC power source with variable voltage facility was used for the electrodeposition.

The electrodeposition was carried out in galvano-potentiostatic mode as follows: the panel was immersed in the electrocoat bath by using paper clip and the DC power source was switched on. The current was controlled under one ampere in the initial stages and voltage was slowly increased to maintain the current at one ampere as the electrodeposition proceeded. Once the current drops sharply (within one minute), the voltage was raised to the predetermined value and maintained throughout the remaining time. Electrocoating times were controlled by automatic function on the DC power supply. The electrocoat deposited panels were then rinsed with deionized (DI) water to wash off the loose electrocoat from the surface. Panels were dried in air for 30 minutes and cured in an oven for 30 minutes at 300°F.

NMP Test

The test specimens of 0.5" diameter were punched out of the cured panels and used for the N-methyl pyrrolidinone (NMP) test as shown in Fig. 1. The NMP test, first developed by van Ooji et.al.(15), is a very good method for distinguishing the adhesion strengths of the electrodeposited polymer films on the metal surfaces. The NMP test has been used to distinguish the adhesion strength of the electrocoat to the substrates. NMP test was performed as follows: first specimens were punched out of the cured electrocoated panels and were placed in the NMP solution which was preheated to 60°C and a stop watch was started. The NMP solution temperature was maintained at 60°C while closely observing the specimen for delamination. When the total electrocoat film lifts off from the specimen, the time was noted as NMP time otherwise the specimen was left in the NMP solution for 120 minutes. Percent adhesion of electrocoat film

was noted by visual observation for the specimen which lasted 120 minutes in the NMP solution without total delamination of the electrocoat film.
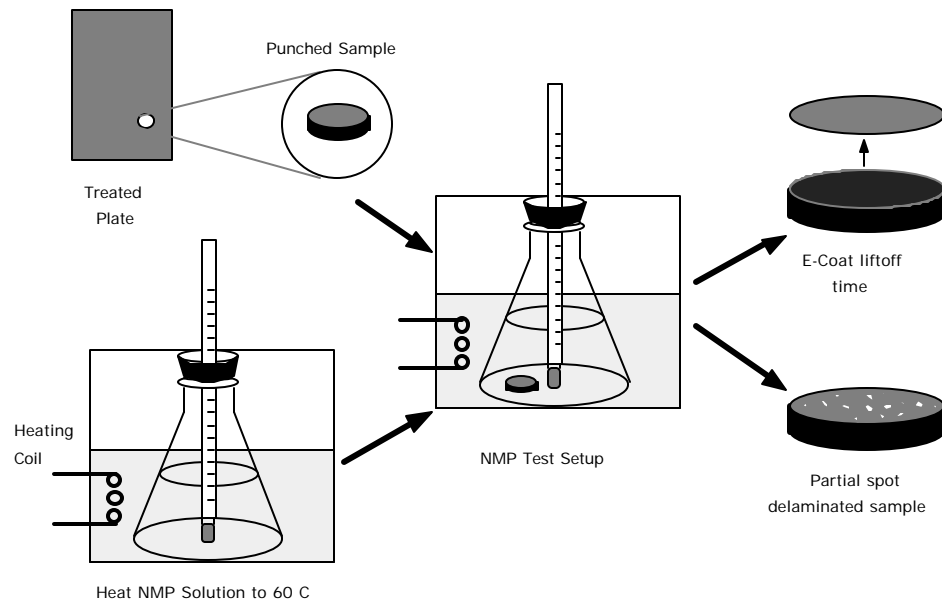
Figure 1. N-methyl pirrolidinone (NMP) Adhesion Test set up.

Results and Discussion

The adhesion of paints and organic coatings to the metallic substrates has been studied for years to understand the nature of the adhesion and many attempts have been made to improve the adhesion. Bond strengths of polymers on Al alloy surface vary depending on the nature of the surface, the surface roughness and chemical bonds before polymer was placed on the substrate(4). Various chemical pretreatments have been found to have varying performance on the corrosion protection of metals (16,17) by the electrocoat deposition.

Electrocoating Process and Electrocoat thickness

Cathodic electrocoating of different surfaces, without cleaning, acetone cleaning and alkaline cleaning, was performed at different voltages and different electrocoating times. As our process was current-voltage control mode operation, the current was maintained at 1 amp while increasing the voltage as currents drops. Typical electrodeposition voltage-time and current-time relationships for electrodeposition on 2024-T3 bare surfaces are shown in Figs. 2 and 3.

The resistance of the electrodeposited film during the deposition process is calculated from the voltage-current relationships for both 2024-T3 bare and Alclad 2024-T3 and are shown in Figs. 4 and 5 respectively. Without cleaning and acetone cleaned surfaces of 2024-T3 bare had the same trend for the current and voltage during the process while alkaline cleaned show lower resistance (Figure 4). Alkaline cleaning removes the organic material, which is difficult to remove by

acetone solvent wipe at room temperature, and loose oxide from the surface which reduces the resistance to the current flow initially.

Once the film attains certain thickness which is about 10 µm for both alloys, then the resistance reaches certain plateau value and increase of resistance is very slow. The resistance of the elctrodeposited films reaches its plateau value within one minute of the deposition process. The behavior of alkaline cleaned surfaces of Alclad 2024-T3 is not so much different from the acetone cleaned surfaces at lower voltage (170V) but slight difference could be observed at higher voltage (250V) as shown in Fig. 5. This may be due to the alkaline cleaning removing the oxide layer on the Alclad 2024-T3 which have little organic layer.
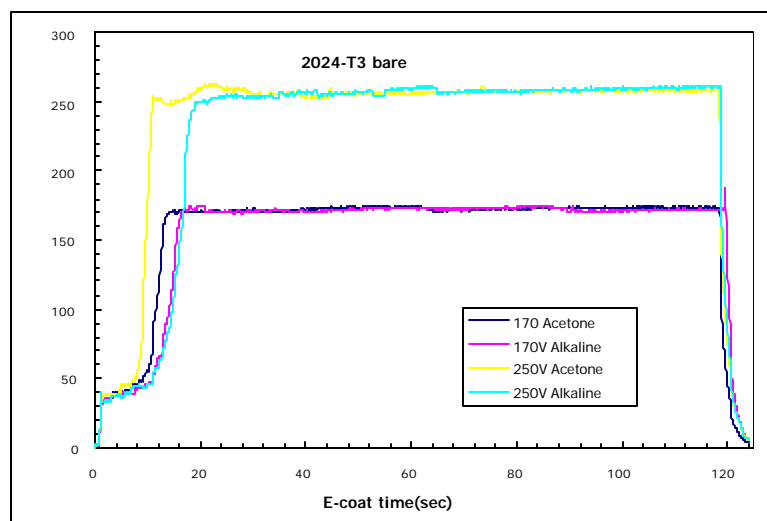
Figure 2. Typical voltage-time relationships of the electrocoating process for 2024-T3 bare. The current was maintained at < 1 amp. at the beginning of the electrocoating and voltage was increased to the set value when current drops down.

Thickness of electrodeposited films of all three types of surfaces of 2024-T3 and Alclad 2024-T3 at different electrodeposition times and voltages are shown in Figs. 6 and 7. The thickness of all types of surfaces increases with electrocoating time and voltage irrespective of pretreatment type. The alkaline cleaned surfaces of both alloys show higher electrocoat film development than other two pretreatment type surfaces. The higher thickness on alkaline cleaned surfaces is easy to understand as the resistances of these surfaces were lower (Figs. 4 and 5).

The electrocoat thickness and time follow more or less linear relationship in the lower electrocoating times (less then 1 min) which can be seen from the Fig. 6 and 7 and the growth of the film is slower after limiting thickness has developed on the surface. Electrocoat thickness developed at lower electrocoating times is higher for Alclad 2024-T3 than that for 2024-T3 bare. This can be explained with same principle of the conductivity of the surface, which is higher for clad alloy. Surface wettability for without cleaned surfaces and acetone cleaned surfaces show that acetone cleaning is not removing all the rolling mill oil from surfaces (see Table I and Table II). It appears that acetone wiping probably removes loose organic matter like ink marks, dust

particles, excessive rolling mill oil etc. from the surfaces, and leaves the more stable organic film on the surface which makes the surface more hydrophobic.
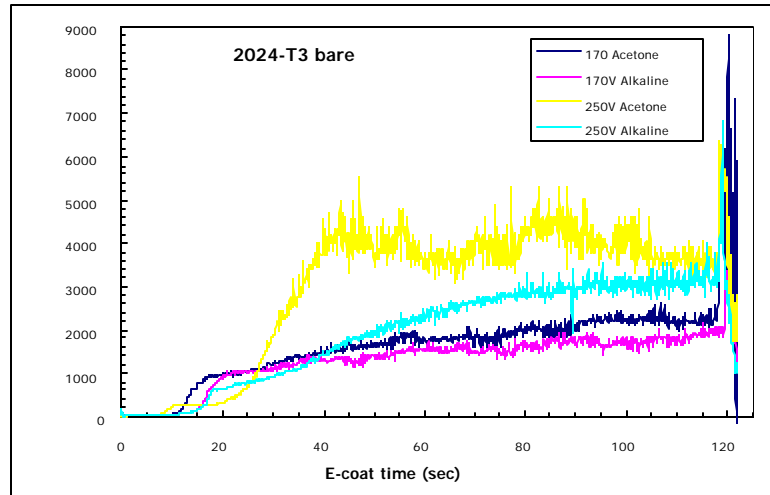
Figure 3. Typical current-time relationships of the electrocoating process for 2024-T3 bare. The current was maintained at < 1 amp. at the beginning of the electrocoating and voltage was increased to the set value when current drops down.
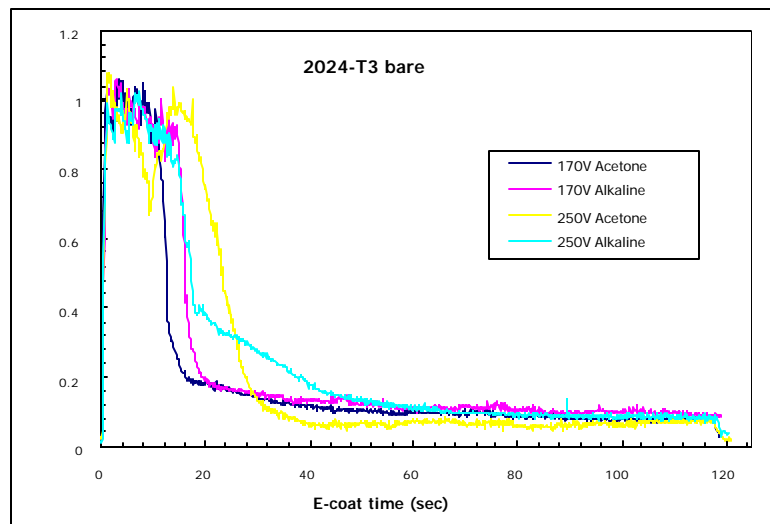
Figure 4. Typical resistance of the electrocoat film during the electrocoating process for 2024-T3 bare. The current was maintained at < 1 amp. at the beginning of the electrocoating and voltage was increased to the set value when current drops down.
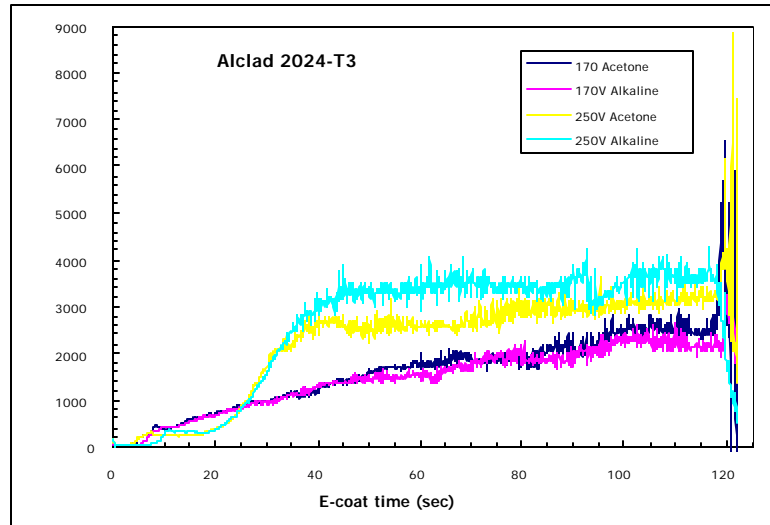
Figure 5. Typical resistance of the electrocoat film during the electrocoating process for Alclad 2024-T3. The current was maintained at < 1 amp. at the beginning of the electrocoating and voltage was increased to the set value when current drops down.
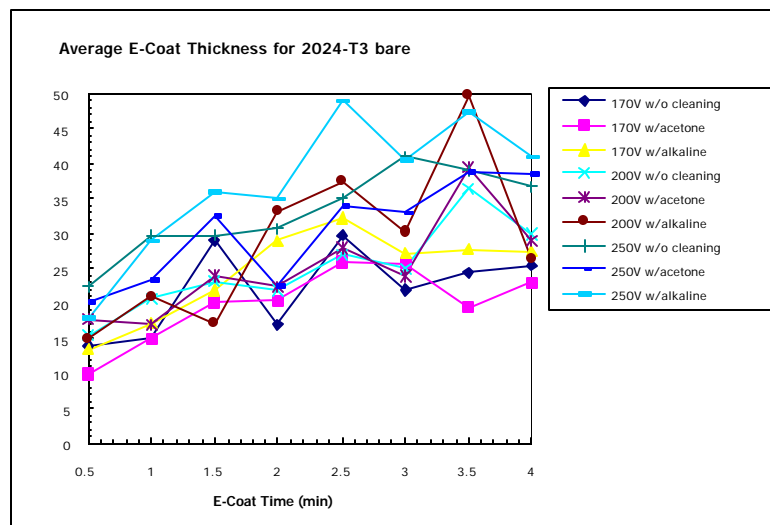
Figure 6. Electrocoat thickness developed for 2024-T3 bare during the electrodeposition process. The current was maintained at < 1 amp. at the beginning of the electrocoating and voltage was increased to the set value when current drops down.

NMP times for acetone wiped and without cleaned samples of 2024-T3 bare are shown in Fig. 8, and for Alclad 2024-T3 in Fig. 9. As can be seen from these figures, adhesion performance was not improved by acetone cleaning of both surfaces. This is not surprising as surface properties of both these alloys are similar as seen from Table 1 and Table 2. This indicates that strong surface contaminants play important role in the adhesion performance of electrocoat on without wiped and acetone wiped surfaces.
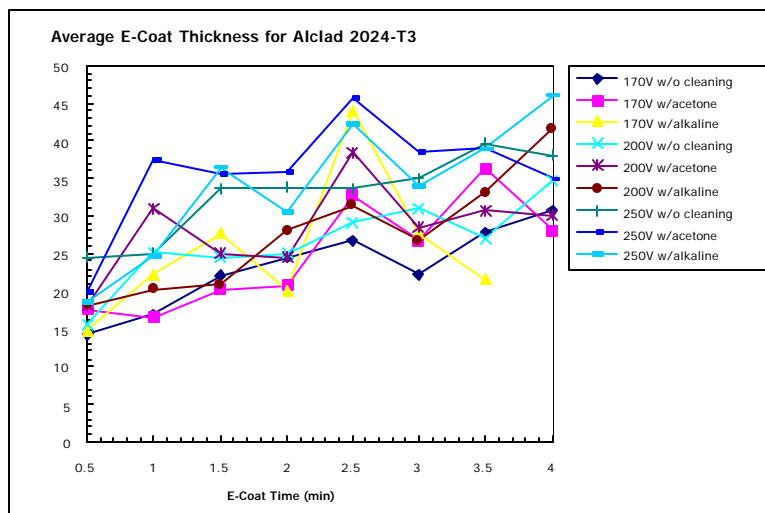
Figure 7. Electrocoat thickness developed for Alclad 2024-T3 during electrodeposition process. The current was maintained at < 1 amp. at the beginning of the electrocoating and voltage was increased to the set value when current drops down.

Table 1. The average contact angles, NMP times and electrocoat thickness for 2024-T3 bare at different treatment conditions.

Treatment Conditions	Average Contact Angle(°)	Average NMP time (min)	Average Thickness (μm)
w/o cleaning	54.5	2.4	26.7
with acetone	58.0	2.7	25.4
with alkaline:	11.2	100.6	30.1
w/o cleaning and with acetone for 170 V	58.2	2.0	21.1
w/o cleaning and with acetone for 200 V	60.0	2.7	25.4
w/o cleaning and with acetone for 250 V	55.5	3.9	31.7
with alkaline for 170 V	10.5	115.6	24.5
with alkaline for 200 V	11.5	108.6	28.8
with alkaline for 250 V	11.5	77.4	37.0

Table 2. The average contact angles, NMP times and electrocoat thickness for Alclad 2024-T3 at different treatment conditions.

| Treatment Conditions	Average Contact angle(°)	Average NMP time (min)	Average Thickness (mm)
w/o cleaning	40.9	6.9	27.5
with acetone	64.6	5.3	29.51
with alkaline:	11.4	43.6	29.1
w/o cleaning or with acetone for 170 V	52	6.2	24.0
w/o cleaning or with acetone for 200 V	53.3	5.8	27.4
w/o cleaning or with acetone for 250 V	47.4	6.5	34.3
with alkaline for 170 V	11.4	51.9	25.36
with alkaline for 200 V	10.9	60.4	27.5
with alkaline for 250 V	12.2	19.4	33.9

Alloys as received versus acetone cleaned
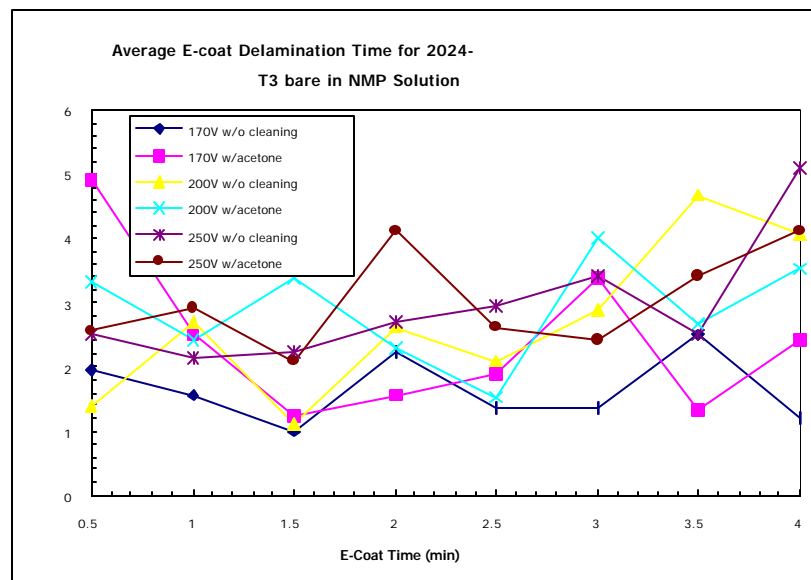
Figure 8. Average delamination time in NMP solution vs electrocoating (e-coat) time for 2024-T3 bare without cleaned and acetone cleaned surfaces at different voltages.
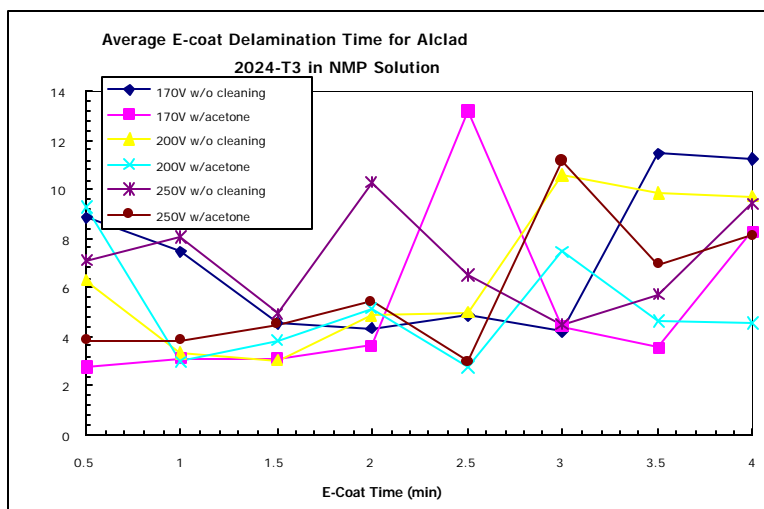
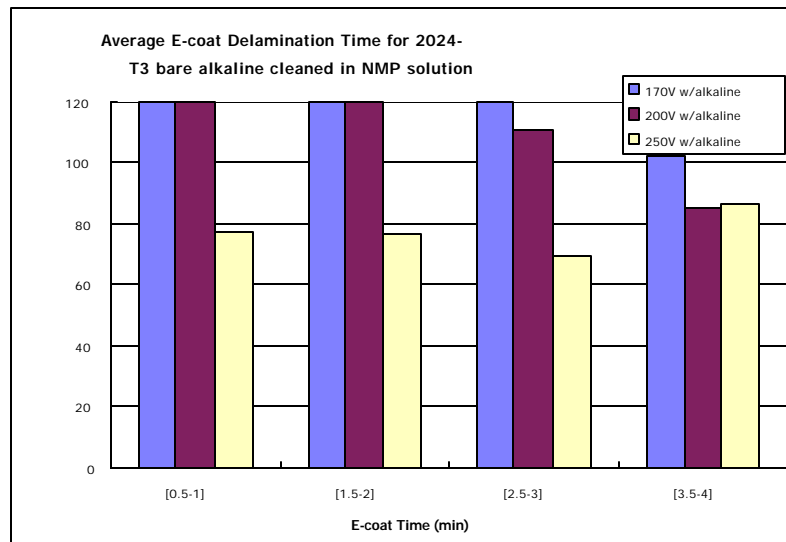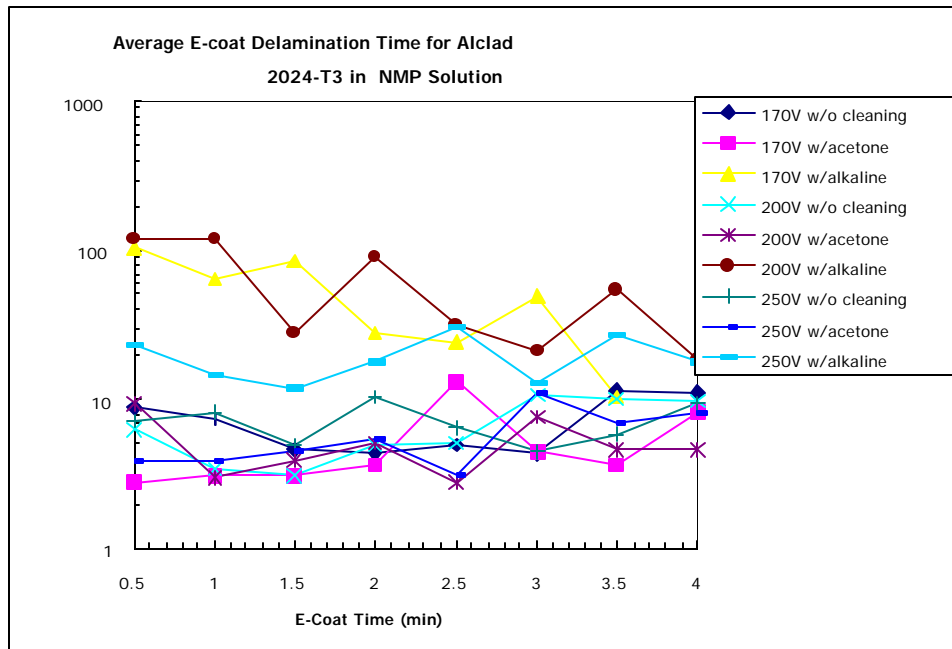Figure 9. Average delamination time in NMP solution vs electrocoating (e-coat) time for Alclad 2024-T3 without cleaned and acetone cleaned surfaces at different voltages.
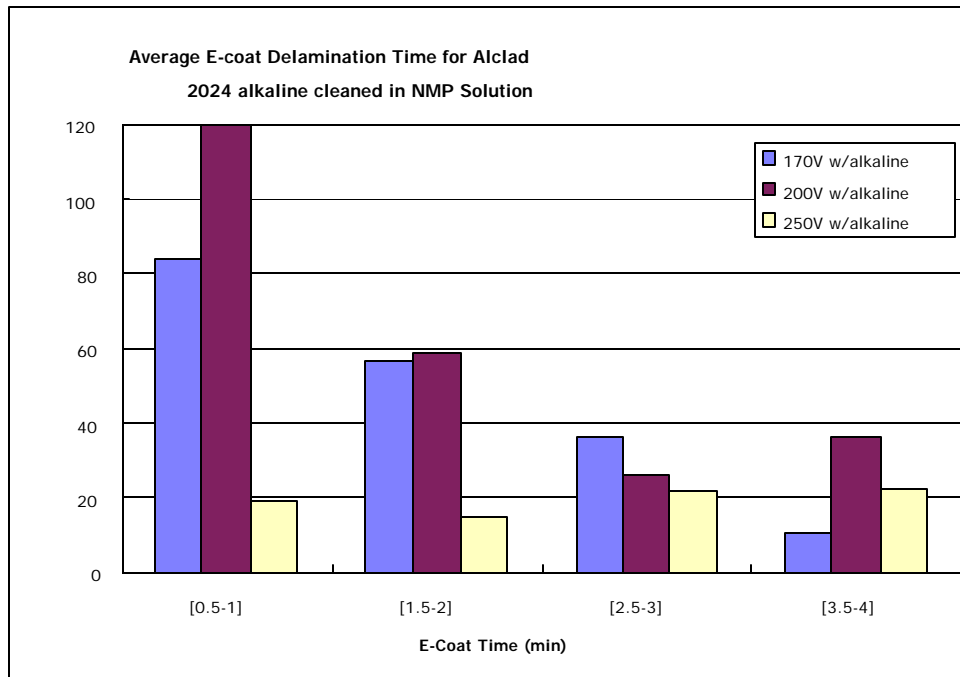
Alkaline cleaning of surfaces

The NMP times for without cleaning, acetone cleaning and alkaline cleaned surfaces at three different electrodeposition voltages 170, 200 and 250 and eight different electrodeposition times, 0.5 to 4 min, of 2024-T3 bare and Alclad 2024-T3 are shown in Figs. 10 and 12 respectively. It is clearly evident from these figures that the alkaline cleaning improves the adhesion of electrocoat by over one order of magnitude in case of 2024-T3 bare and at lower electrocoat times in case of Alclad 2024-T3. The NMP times of more than 2 hours is observed for the alkaline cleaned surfaces of 2024-T3 at all three electrodeposition voltages 170, 200 and 250. To see the average effect on the adhesion performance of alkaline cleaned surfaces, the NMP times of two different electrodeposition times are averaged and shown in Figs. 11 and 13 for both 2024-T3 bare and Alclad 2024-T3 respectively. As seen from these figures, at lower electrodeposition times adhesion performance is better on 2024-T3 bare surfaces for all three voltages studied. For Alclad 2024-T3, all the alkaline cleaned surfaces at different electrodeposition times showed similar behavior as that of 2024-T3 bare but the NMP times were not as high as those of 2024-T3 bare.

Effect of electrocoating voltage on adhesion performance

The adhesion performance of the electrocoat films which exceed 120 minutes of NMP time is evaluated by the observation of the film adhesion on the test specimen after 120 minutes of NMP time. The specimen were rinsed with DI water after 120 minutes in NMP solution and visually observed for the percent adhesion of the electrocoat film to the Al alloy surface and the percent adhesion is recorded from these specimen. Fig. 14 and 15 show the percent adhesion of electrodeposited films on alkaline cleaned surfaces of 2024-T3 bare and Alclad 2024-T3 respectively at different electrocoat voltages and electrocoating times.

From these figures it is clearly seen that at lower electrocoating voltages and times the adhesion performance on 2024-T3 bare is better than higher electrocoating voltages and times. Clearly

170V and lower than 1.5 minutes of electrocoating times favors the adhesion performance on 2024-T3 bare alkaline cleaned surfaces which have almost 100% electrocoat film adhering to the surface. The electrodeposition times of the process depends on the film thickness desired for protection of the material from corrosion as well as mechanical damage. For higher electrocoating voltages(200V), the adhesion performance of these surfaces does not depend on the electrocoating time. This is true in both alloy surfaces of alkaline cleaned. Alclad 2024-T3 has good adhesion performance on the alkaline cleaned surfaces with elctrocoating voltage 170V and electrocoating time of 0.5 min.
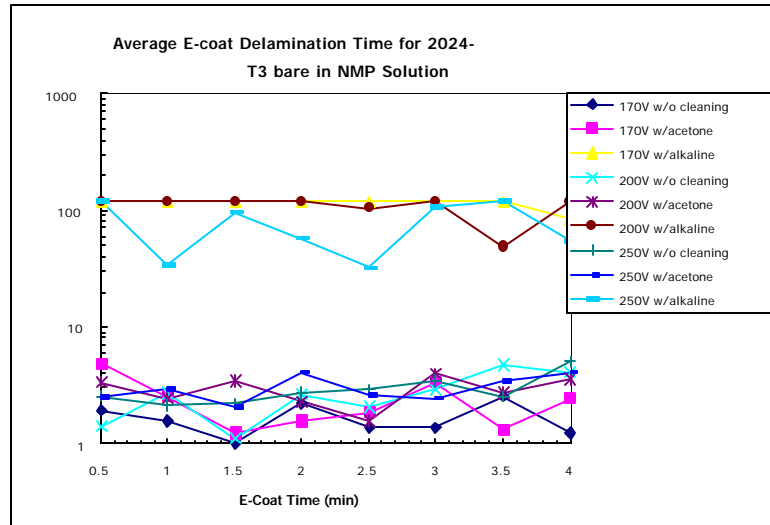
Figure 10. Average delamination time in NMP solution vs electrocoating (e-coat) time for 2024-T3 bare without cleaned, acetone cleaned and alkaline cleaned surfaces at different voltages.

Figure 11. Effect of average delamination time in NMP solution at two different times with electocoating (e-coat) time for 2024-T3 bare alkaline cleaned surfaces at different voltages.

Figure 12. Average delamination time in NMP solution vs electrocoating (e-coat) time for Alclad 2024-T3 without cleaned, acetone cleaned and alkaline cleaned surfaces at different voltages.

Figure 13. Effect of average delamination time in NMP solution at two different times with electrocoat (e-coat) time for Alclad 2024-T3 alkaline cleaned surfaces at different voltages.
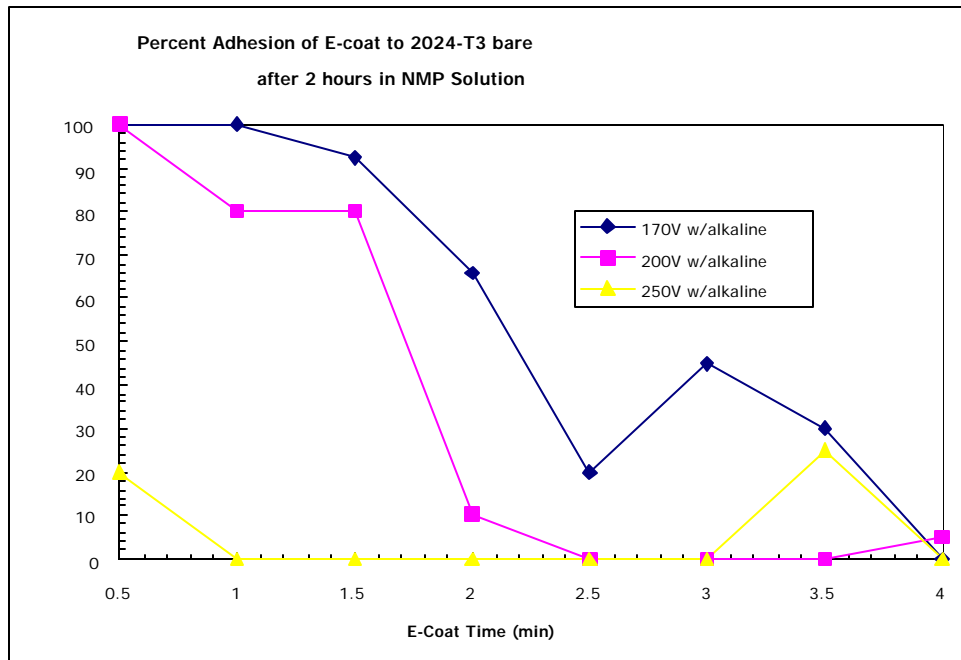
Figure 14. Percent Adhesion of electrocoat (e-coat) after 2 hours in NMP solution vs electrocoating time for 2024-T3 bare alkaline cleaned at different voltages.
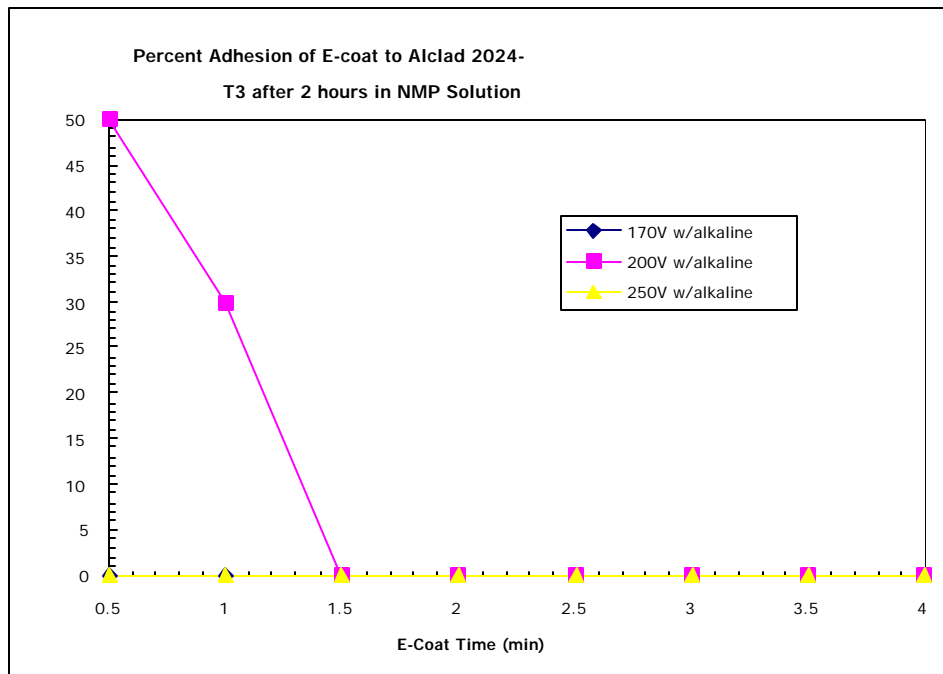
Figure 15. Percent Adhesion of electrocoat (e-coat) after 2 hours in NMP solution vs electrocoating time for Alclad 2024-T3 alkaline cleaned surfaces at diffferent voltages.

Conclusion

<u>2024-T3 bare</u>

1. Acetone cleaned surfaces show higher film resistance during the electrodeposition. This could be due to the surface organic layer which is developed during the manufacturing of the panels when milling oil is used to protect the surface. This organic film is difficult to remove by acetone cleaning.
2. Alkaline cleaning of alloy surfaces improves the adhesion performance by more than one order of magnitude from without cleaning and acetone wiped surfaces. There is not much difference in the adhesion performance of without cleaned and acetone cleaned surfaces.
3. For alkaline cleaned surfaces, lower electrodeposition times and lower electrodeposition voltages (170 and 200V) give better adhesion performance. The percent adhesion declines with increase of electrodepostion time at lower voltage.
4. The adhesion performance does not seems to depend on the electrodeposition time for higher electrodeposition voltage (250V).

<u>Alclad 2024-T3</u>

5. The film resistance of alkaline cleaned and acetone cleaned show similar levels at lower voltages but slight difference at higher voltage (250V). The slight difference in this case looks within experimental error.
6. Alkaline cleaned surfaces show improved adhesion performance but the improvement is not as significant as in the case of 2024-T3 bare.
7. Alkaline cleaned surfaces at lower voltages (170, 200V) and lower electrodeposition times show better adhesion performance.
8. At higher electrodeposition voltage(250V) the adhesion performance does not depend on the electrodeposition time.

References

1. J.D. Venables, Journal of Material Science, 19 (1984) 2431-2453.
2. G.W. Critchlow and D.M. Brewis, Int. J. of Adhesion and Adhesives, 16 (1996) 255-275.
3. J.D. Minford, *Handbook of Aluminum Bonding Technology and Data*, Marcel Dekker, New York, 1993.
4. E.W. Thrall and R.W. Shannon (Eds), *Adhesive Bonding of Aluminum Alloys*, Marcel Dekker, New York, 1985.
5. P.F.A. Bijlmer, J. Adhes. 5 (1973) 319.
6. A.D. Wilson, J.W. Nicholson and H.J. Prosser (eds), *Interface Coatings-2*, Elsevier, London, 1988, Chapter 2, 39-70.
7. C.L. Coon, and J.J. Vincent, Journal of Coatings Technology, Vol. 58, N0. 742, November 1986, 53-60.
8. P.E. Pierce, Journal of Coatings and Technology, 53 (1981), 52-67.

9. P.E. Pierce, Z. Kovac, and C. Higginbotham, Ind. Eng. Chem. Prod. Res. Dev., Vol 17, No. 4, (1978), 317-322.

10. D.R. Hays, and C.S. White, Journal of Paint Technology, Vol. 41 No. 535, August 1969, 461-471.

11. G.L. Burnside, and G.E.F. Brewer, Journal of Paint Technology, 38 (1966), 96-100.

12. L.L. Shreir, R.A. Jarman, and G.T. Burstein (Eds), *Corrosion*; 3rd ed., Vol. 1, Butterworth-Heinemann, Jordan Hill, 1994.

13. T. Biestek, and J. Weber, *Electrolytic and Chemical Conversion Coatings*; Potcullic Press, Redhill, 1976, pp. 1-127.

14. T.S. Sehmbhi, C. Barnes, and J.J.B. Ward, Transactions of the Institue of Metal Finishing 62(1984), 55-58.

15. van Ooji, Sabata, "Effect of Paint Adhesion on the Underfilm Corrosion" in CORROSION/91, Paper No. 417 Houstion, TX: NACE 1991.

16. W.W. Rausch, Metal Finishing, November 1978, 44-48.

17. W.W. Rausch, Metal Finishing, December 1978, 58-61.

16. The Effect of Interfacial Tension on the Adhesion of Cathodic E-coat to Aluminum Alloys

C.M. Reddy, C.M. Weikart, and H.K. Yasuda

Abstract

Adhesion of a cathodically electrodeposited paint (E-coat) to aluminum alloys, Alclad 2024-T3, AA 2024-T3 and AA 7075-T6, was investigated to examine the influence of interfacial tension at the paint/metal interface. The surface energy of an aluminum plate was modified by depositing a plasma polymer of a mixture of trimethyl silane (TMS) and one of three diatomic gases (O_2, N_2, and H_2) by cathodic plasma polymerization. The contact angle (θ) of water of a modified surface changes as a function of the mole fraction of the diatomic gas. The plot of $\cos\theta_{PP}$ of a plasma polymer as a function of the mole fraction of the gas crosses the plot of $\cos\theta_{EC}$ of the E-coat. The difference, $\Delta\cos\theta = \cos\theta_{PP} - \cos\theta_{EC}$, is a parameter which indicates the level of interfacial tension at the paint/metal interface. $\Delta\cos\theta = 0$ represents the minimum interfacial tension. The adhesion of a cured E-coat on a panel was evaluated by the N-methyl pyrrolidinone (NMP) paint delamination time test. The maximum peak of adhesion test values plotted as a function of $\Delta\cos\theta$ occurred around the zero point, $\Delta\cos\theta = 0$, indicating that maximum adhesion is obtained with minimum interfacial tension. Mixtures of TMS and N_2 on all three aluminum alloys studied consistently displayed longer delamination times in the NMP test than mixtures of TMS and O_2 or H_2.

Introduction

Good adhesion of polymer films to metal surfaces is an important parameter in the protection of metal from corrosion and mechanical stress. Improvement in the adhesion of metal-polymer bonds has been a topic of research for the past several years [1-4]. There have been several pretreatment methods developed to improve the adhesion of paint to metal surfaces [2]. The adhesion of polymer films depends on characteristics of the metal surfaces, such as surface roughness, surface contaminants, and the nature of chemical bonds on the surface [3, 4], which exist prior to polymer film application. Mechanical interlocking of a polymer to porous surfaces was one focus of studies on improvement of the adhesion at metal-polymer film interfaces [5]. Over the course of several years, many pretreatments have been investigated in an attempt to improve the adhesion of polymer films to metal surfaces. The pretreatment processes developed range from surface cleaning to surface conversion into different oxides [1]. Because of their porous column structure, anodized surfaces of aluminum alloys were found to result in better adhesion performance of polymer film-metal bonds.

Glow discharge plasma techniques have been used in several areas, such as semiconductors and biological applications, to modify surfaces by non-reacting gas plasma treatment or plasma polymer deposition [6]. Plasma polymers from DC glow discharge have been used for corrosion

protection of metal surfaces because of their superior barrier properties, good adhesion to substrates and chemical inertness [7].

Cathodic electrocoating has been widely used as a primary layer coating or top coat in corrosion protection systems employed in the automotive, industrial and appliance areas for years [8]. The chemistry of cathodic electrocoatings and electrodeposition parameters have been the subject of several investigations [9-13]. Cathodic electrocoating has a number of advantages which make it an attractive coating system; these include high throw power, superior corrosion protection, high coating utilization (>95%), a low level of resulting pollution (aqueous system), and easy automation. Recently the cathodic electrocoating process has been used for painting in the automobile, mechanical, engineering and domestic appliance industries. Cathodic elctrocoating is a fairly simple process and can be used on various scales. High throw power makes the cathodic electrocoating process attractive in the automobile industry, as it ensures the electrocoat penetrates into cavities and pores of curved parts.

Aluminum alloys AA 2024-T3, Alclad 2024-T3 and AA 7075-T6 have been used in the aircraft industry because of their high mechanical strengths. Pure aluminum, which has high corrosion resistance properties, has limited application due to its low mechanical strengths [14]. With the addition of small quantities of alloying elements, the mechanical strengths of aluminum are increased significantly. However, the addition of such alloying elements drastically reduces the corrosion resistance of these metals. For the past several years, this has been overcome with the chromate conversion coating process, which provides excellent corrosion protection for such alloys [15]. Because of their health hazards, the use of chromates has come under severe Environmental Protection Agency restrictions necessitating the development of an environmentally benign corrosion protection process [16].

Electrodeposition is an excellent alternative process due to its environmentally benign nature. In this technique, adhesion of the E-coat polymer-metal bonds is an important factor in the protection of metal from corrosion. In the present study we have looked into the improvement of adhesion strengths of electrodposited films to the aluminum alloys Alclad 2024-T3, AA 2024-T3 and AA 7075-T6 with the application of cathodic plasma polymers. The cathodic electrocoating technique is being investigated for use in the preparation of airplane construction materials, as it has several advantages which can be exploited to our benefit. The objective of this study is to investigate the adhesion strengths of cathodic electrocoat to different plasma polymer surfaces on aluminum alloys to determine a suitable composition of TMS/diatomic gas mixture which maximizes adhesion strengths. Although good adhesion of paint films to a metal surface is an important factor in the corrosion protection of the metal, corrosion performance was not evaluated in this study. The adhesion phenomenon was studied to examine the effect of the composition of the monomer feed gas in plasma polymerization on the adhesion of cathodic E-coat.

Experimental

Materials

Aluminum alloy panels of Alclad 2024-T3 [2A], AA 2024-T3 [2B] and AA 7075-T6 [7B], each $3" \times 6" \times 0.034"$ in size, were procured from Q-Panel Lab Products for use in the present study. The polyurethane-based cathodic electrocoat used was a mixture of 44 wt% resin emulsion (BASF U32CD033A), 8 wt% paste (BASF U32AD290), 48 wt% deionized (DI) water (<10 μmhos conductivity) and 4 vol% additive (BASF 20CD0043). Turco 4215S was utilized as an alkaline cleaner for chemical cleaning of substrate 7B surfaces. Amchem 7 in combination with nitric acid was employed as a deoxidizing agent. The solvents acetone and N-methyl pyrrolidinone were procured from Fisher Scientific, Inc. Trimethylsilane (TMS) with 97% minimum purity was procured from PCR, Inc. and Gelest, Inc. The diatomic gases used were hydrogen (99%), oxygen (99.9%) and nitrogen (99.99%); these were procured from Airgas. All the gases and the monomer were used as received without any further purification.

Experimental Procedures

Reactor system and sample preparation procedure

Low temperature DC plasma technique was used in this study to treat the surface and to deposit plasma polymer films on aluminum alloy surfaces. The bell jar reactor system utilized in this study consisted of six major components: (i) the reactor chamber (about 75 liters), (ii) the anode magnetron electrode setup ($25.4 \text{ cm} \times 25.4 \text{ cm} \times 0.16 \text{ cm}$ stainless steel plates with 8 bar magnets placed equidistantly on the back), (iii) the monomer/gas feeding system, (iv) the pressure and flow rate control systems, (v) the vacuum pump system (Edward Booster with mechanical pump, capacity 240 m^3/h at 0.3 mbar), and (vi) the DC power source. An MDX-1K Magnetron Drive (Advanced Energy Industries, Inc.) was used as the DC power source and was controlled in power mode. The flow and pressure controllers (made by MKS) were used to monitor flow rates of the monomer/gas and reactor chamber pressure.

Three diatomic gases, O_2, H_2 and N_2, were mixed with TMS to create the plasma polymer forming monomer/gas mixtures. Two different initial cleaning processes, acetone wiping and alkaline cleaning followed by deoxidization (in the case of substrate 7B), were used to examine the effect of chemical cleaning on the adhesion of cathodic electrocoat to plasma polymers. The processes examined in this study are shown in Table- 1.

Table 1. Surface treatment processes investigated in this study.

Code	Chemical Pretreatment	Plasma Pretreatment[1]	Plasma polymer deposition[2]
(Ace/O_2)/TMS+O_2	Acetone wipe	O_2	TMS+O_2
(Ace/O_2)/TMS+H_2	Acetone wipe	O_2	TMS+H_2
(Ace/O_2)/TMS+N_2	Acetone wipe	O_2	TMS+N_2
(Alk/Dox/O_2)/TMS+O$_2$	Alkaline clean/ Deoxidization	O_2	TMS+O_2
(Alk/Dox/O_2)/TMS+N$_2$	Alkaline clean/ Deoxidization	O_2	TMS+N_2

1. O_2 plasma pretreatment was carried out at 100 mtorr pressure, 40 watts DC power, 2 sccm O_2
    flow rate for 10 miutes.
2. Plasma polymer deposition was carried at 1 sccm TMS + 1 sccm diatomic gas ($O_2/N_2/H_2$)
    flow rate, 50 mtorr pressure, 5 watts DC power for 1 minute.

Two substrate panels clipped together with alligator clips were placed between two anode
magnetrons used as a cathode. The reactor chamber was evacuated to 1-2 mtorr vacuum after the
panels were installed. Once desired pressure was achieved, the pretreatment gas oxygen (O_2) was
introduced with a 2 cm^3_{STP}/min flow rate, and pressure was set to 100 mtorr. O_2 plasma
pretreatment was carried out for 10 minutes at 100 mtorr and 40 watts DC power. Following the
pretreatment, the reactor was evacuated to 1-2 mtorr pressure before the monomer/gas mixture
was introduced into the reactor chamber. Introduction of the specific monomer/gas mixtures was
then started at a fixed flow rate maintained by the flow controllers. Pressure was set to 50 mtorr
for all the mixture combinations. Plasma polymerization was carried out at 50 mtorr pressure and
5 watts DC power for one minute in the case of each TMS/diatomic gas mixture. Panels were
removed from the reactor after evacuation to 1-2 mtorr pressure. Cathodic E-coat was then
applied on the plasma polymer coated panels within 10 minutes after the samples were taken out
of the plasma chamber. This time was controlled in all cases to eliminate any possible influence
of time-dependent change in adhesion performance. In a previous experiment not reported here,
the adhesion performance of E-coat on plasma polymer films was found to be independent of
time up to 5 days before adhesion performance started to decline.

For the purpose of thickness and refractive index measurement, silicone wafers of the size 1 cm
$\times$ 1 cm were placed on the substrate at different locations before the substrates were installed in
the bell jar reactor. The thickness and refractive indices of plasma polymer films were then
measured on these silicone wafers by an AutoEL-II Automatic Ellipsometer (Rudolph Research
Corporation), which is a null-seeking type with a 632.8 nm helium-neon laser light source.

Within 2 hours after each sample was taken out of the plasma chamber, contact angles of all
plasma polymer surfaces were measured using the sessile drop contact angle measurement
method with the help of a computerized contact angle measurement system, the VCA 2500XE
(AST Products, Billerica, MA). The VCA 2500XE system allows measurement of water contact
angles within a short time, thus avoiding changes in contact angle due to surface dynamics. The
contact angles of plasma polymers and E-coat surfaces were measured by placing a 3 µl DI water
(<10   mhos conductivity) droplet on each surface and capturing the droplet image within few
seconds. Then using each captured image, contact angles were calculated by means of VCA
2500XE software. To eliminate local variation of contact angles, the average of four contact
angles, measured at four different locations on each surface, was figured.

In cases involving acetone wiping, panels were wiped with acetone using tissue paper
(Kimwipes®, Fisher Scientific, Inc.) to clean the ink marks and loose organic matter off of their
surfaces. In the cases involving deoxidization, panels were first alkaline cleaned by immersion in
the alkaline bath (approximately 4 liters of solution) for about 25 minutes until each panel
became water break free when rinsed with DI water. Following this, the panels were immersed in
deoxidizer (approximately 4 liters of solution) for 10 minutes and then rinsed with DI water for 5

minutes. The purpose of alkaline cleaning and deoxidization was to remove the native oxide which is contaminated with milling oil when the alloy is made. The composition of the alkaline cleaning solution was maintained such that a water break free surface would be obtained while rinsing with DI water after immersion in the alkaline bath for a specific amount of time. Water contact angles of all the plasma polymer surfaces were measured by the sessile drop method before electrodeposition. Electrodeposition was carried out in a one gallon electrocoat bath using the substrate as the cathode and a stainless steel strip (1.5" × 10") as the anode. A Darrah Digital® DC power source with variable voltage facility was used for the electrodeposition.

Electrodeposition on each panel was carried out in galvano-potentiostatic mode as described below. The panel was immersed in the electrocoat bath using a paper clip, and the DC power source was switched on. The current was controlled to be under one ampere during the initial stages, and the voltage was slowly increased to maintain the current at one ampere as electrodeposition proceeded. As the current decreased (within one minute), the voltage was increased to 250V and maintained throughout the remaining 2 minutes. Electrocoating duration was controlled by an automatic function of the DC power supply. The electrocoated panels were then rinsed with DI water to remove any loose electrocoat from the surface. Panels were allowed to dry in air for 30 minutes and were then cured in an oven for 30 minutes at 300°F.

Contact angle measurements were carried out on the cured electrodeposited polymer surfaces for comparison with those obtained for the plasma polymer surfaces before E-coating. Adhesion strengths of the electrodeposited polymers to the plasma polymers were evaluated using the NMP test as described below.

The NMP Test

Test specimens 0.5" in diameter were punched out of the cured panels and used for the N-methyl pyrrolidinone (NMP) test. The NMP test, developed by van Ooij, et al. [17], is a good method for distinguishing the adhesion strengths of E-coated polymer films on metal surfaces. The NMP test was used to distinguish the adhesion strength of electrocoats to substrate surfaces coated with plasma polymer. The NMP test was performed as described below. First, three specimens were punched out of each cured electrocoated panel. These were placed in NMP solution, that had been preheated to 60°C, and a stop watch was started. The 60°C temperature of the NMP solution was maintained while the specimens were closely observed for signs of delamination. If the entire electrocoated film lifted off of the specimen, the time was noted as the NMP time, otherwise the specimen was left in the NMP solution for 120 minutes. Percent adhesion of E-coat film was noted by visual observation for the specimens that lasted 120 minutes in the NMP solution without total delamination of the E-coat film. The average NMP time for each set of three specimens was calculated.

Results and Discussion

Plasma Polymer thickness and refractive index

Plasma polymer deposition rate depends on the composition of the monomer-gas mixture. Increases in the concentration of non-polymerizing gas will decrease the deposition rate

considerably when other parameters are kept constant. To examine this relationship, the thickness of plasma polymer developed during a fixed time of deposition was measured at different places on each panel. The average thickness was figured, and this average has been plotted against the mole fraction of diatomic gas. Fig. 1 shows plasma polymer thickness variation plotted against the mole fraction of diatomic gas. Plasma polymer thickness developed during 1 minute of operation at different mole fractions lies in the expected range of 200 to 650 Å. Plasma polymer growth does not seem to depend on the substrate material, but thickness developed in $TMS+H_2$ and $TMS+N_2$ systems is slightly higher than in the $TMS+O_2$ system (Fig. 2). This could be due to SiO_x-type films formed in $TMS+O_2$ systems by the elimination of methyl groups.
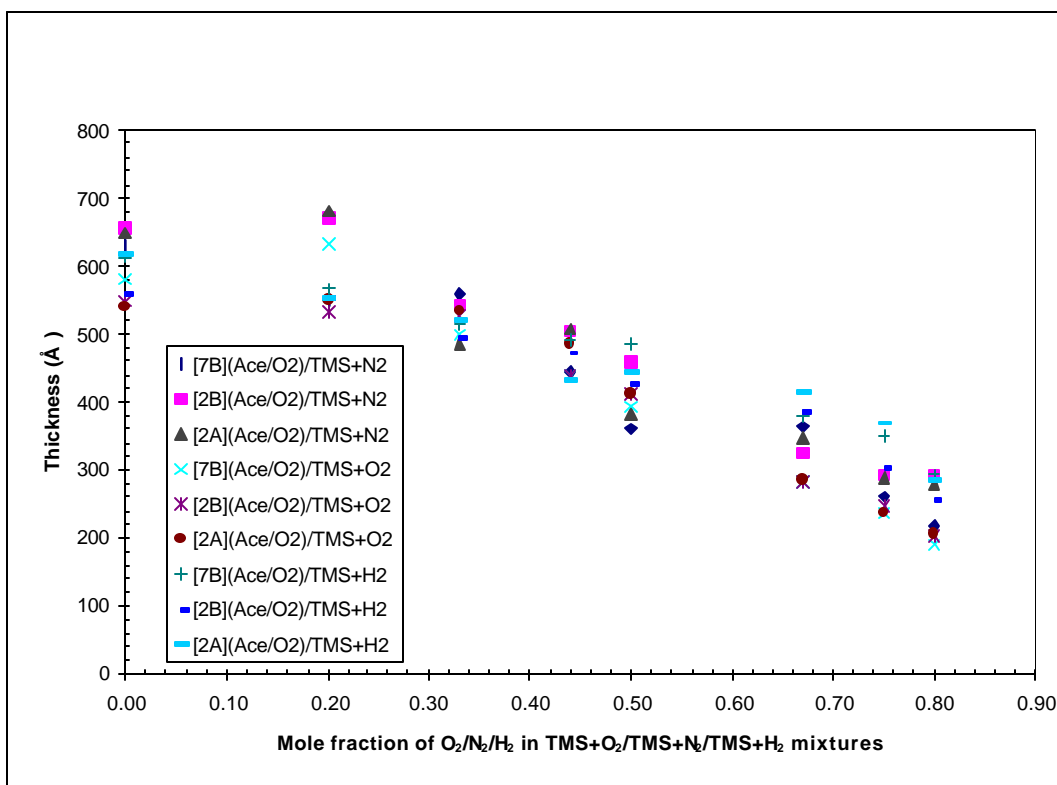
Figure 1. DC plasma polymer thickness variation with mole fraction of O_2, N_2 and H_2 in $TMS+O_2$, $TMS+N_2$ and $TMS+H_2$ mixtures, respectively, on three substrates, 2B (AA 2024-T3), 7B (AA 7075-T6) and 2A (Alclad 2024-T3), with other treatment conditions fixed. Deposition conditions for all concentrations were 5 watts DC power, 50 mtorr pressure and 1 minute deposition time.

Refractive indices of all the plasma polymer films were measured to examine film hardness; these are shown in Fig. 2. Increases in diatomic gas concentration decrease the refractive indices of TMS plasma polymers. Refractive indices of $TMS+H_2$ and $TMS+N_2$ plasma polymers were found to be higher than those of $TMS+O_2$ plasma polymers.

Minimizing interfacial tension

The following working hypothesis has been investigated in this study: ***minimization of the interfacial tension at the E-coat/metal interface can maximize E-coat adhesion***. However, there is no way to measure the interfacial tension between a polymer layer and a metal surface directly. The term <u>surface energy</u> is generally used to describe <u>the interfacial energy between a solid surface and ambient air</u>. Therefore, an attempt to estimate such a surface energy for two contiguous surfaces in an effort to estimate the interfacial energy is not warranted. In other words, air is not a common constituent of the interface under consideration.
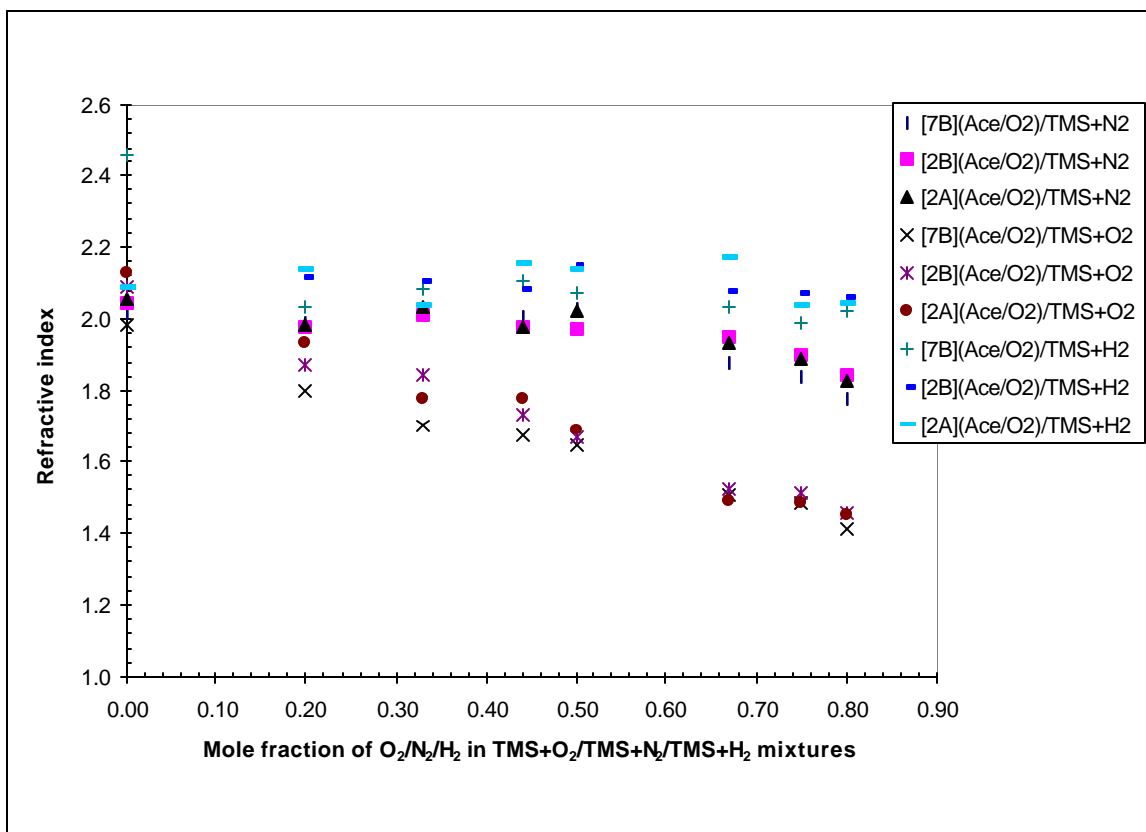
Figure 2. DC plasma polymer refractive index variation with mole fraction of O_2, N_2 and H_2 in TMS+O_2, TMS+N_2 and TMS+H_2 mixtures, respectively, on three substrates, 2B (AA 2024-T3), 7B (AA 7075-T6) and 2A (Alclad 2024-T3), with other treatment conditions fixed. Deposition conditions for all concentrations were 5 watts DC power, 50 mtorr pressure and 1 minute deposition time.

Because water is a common constituent material when an E-coat is applied to a metal surface, a more realistic approach is to compare the contact angles of water on both surfaces to estimate the level of interfacial tension. The value of $\gamma\cos\theta$ is a measurable thermodynamic quantity introduced by Guastalla [18, 19], which is applicable to the situation under consideration. Since the contact angle measurements were made under identical conditions with water, for which γ is

a constant, the change in $\cos\theta$ rather than $\gamma\cos\theta$ was taken to be indicative of the level of interfacial tension for all cases investigated in this study.

This empirical approach works well to show the influence of the interfacial tension on the adhesion of E-coat as is evident in the following sections. The plot of $\cos\theta_{PP}$ of a plasma polymer as a function of the mole fraction of the gas crosses the plot of $\cos\theta_{EC}$ of the E-coat. The difference, $\Delta\cos\theta$, is a parameter which indicates the level of interfacial tension at the paint/metal interface. In the scale of mole fraction of a gas, where $\Delta\cos\theta = 0$, it is assumed that the minimum interfacial tension is attained.
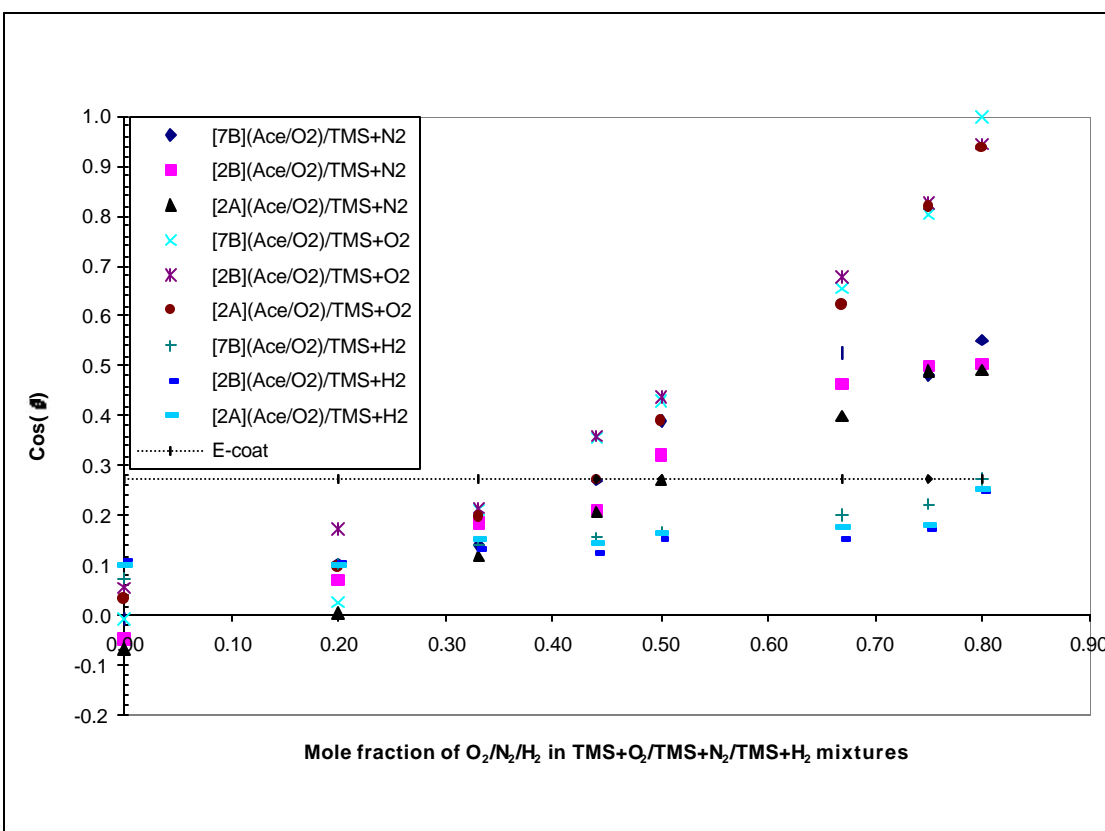
Figure 3. DC plasma polymer contact angle variation with mole fraction of O_2, N_2 and H_2 in TMS+O_2, TMS+N_2 and TMS+H_2 mixtures, respectively, on three substrates, 2B (AA 2024-T3), 7B (AA 7075-T6) and 2A (Alclad 2024-T3), with other treatment conditions fixed. Deposition conditions for all concentrations were 5 watts DC power, 50 mtorr pressure and 1 minute deposition time.

The water contact angles of plasma polymer surfaces are compared with those of a cured E-coat in Fig. 3. The values of $\cos\theta$ of TMS+N_2, TMS+H_2 and TMS+O_2 plasma polymer surfaces are plotted against diatomic gas concentration. As evinced by Fig. 4, $\cos\theta$ variation is significant with the increase of diatomic gas concentration. Water contact angles of a cured E-coat surface

with a corresponding composition of monomer/gas mixture are also shown in Fig. 3; these do not depend on the contact angle of underlying substrate.
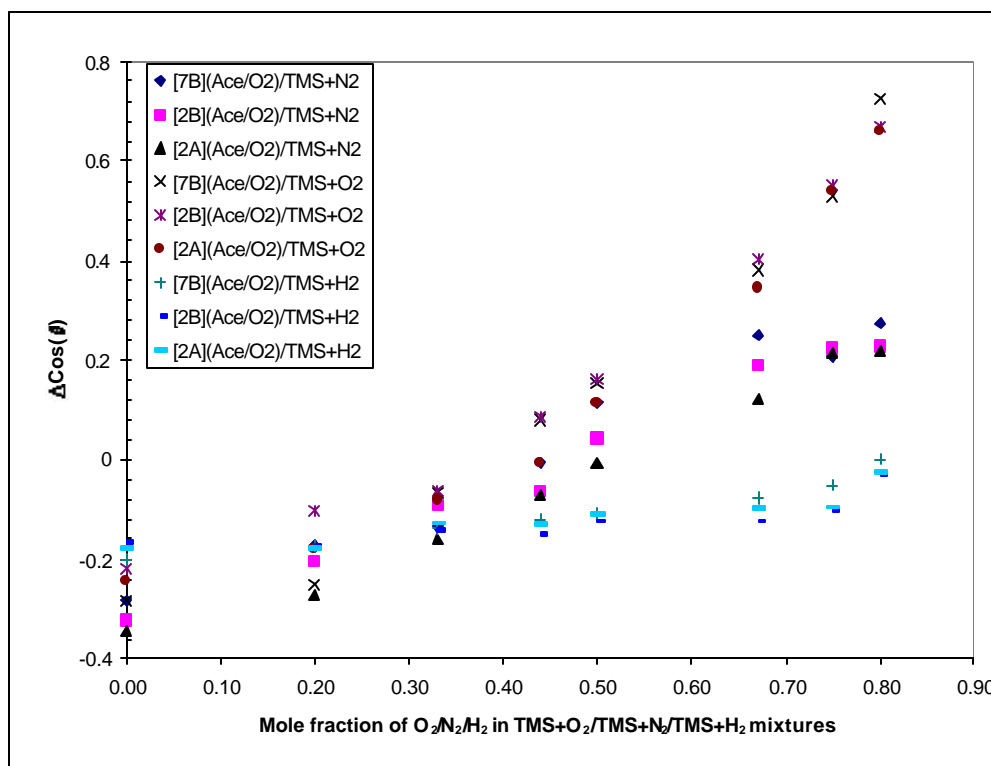
Figure 4. DC plasma polymer $\Delta Cos(\theta)$ variation with mole fraction of O_2, N_2 and H_2 in TMS+O_2, TMS+N_2 and TMS+H_2 mixtures, respectively, on three substrates, 2B (AA 2024-T3), 7B (AA 7075-T6) and 2A (Alclad 2024-T3), with other treatment conditions fixed. Deposition conditions for all concentrations were 5 watts DC power, 50 mtorr pressure and 1 minute deposition time.

The difference between $\cos\theta$ of plasma polymer (PP) surfaces and cured E-coat (EC) surfaces is calculated as follows:

$$\Delta Cos\theta = \cos\theta_{PP} - \cos\theta_{EC}.$$

$\Delta Cos\theta$ variation according to the composition of monomer/diatomic gas mixture is shown in Fig. 4. As anticipated, TMS+O_2 plasma polymers have more hydrophilic surfaces than TMS+N_2 and TMS+H_2 plasma polymers. This figure demonstrates that for TMS+O_2 and TMS+N_2 plasma polymer surfaces, there exists an interfacial tension minimizing point for the composition range studied. The TMS+H_2 system has a wide composition range in which the interfacial tension between the plasma polymer and the E-coat is minimized, while the value of $\cos\theta_{PP}$ remains only below that of $\cos\theta_{EC}$. This minimum interfacial tension exists for all the diatomic gas mixtures which were studied: TMS with H_2, N_2 and O_2. This approach predicts that, if we measure the adhesion strengths of E-coat film to the plasma polymer surfaces, we will be able to see maximum adhesion strengths existing at this minimum interfacial tension.

Adhesion of E-coat to modified AA 2024-T3 alloy surfaces

Adhesion strengths of cathodic E-coat films on metals or modified surfaces of metals are best evaluated by the NMP solution swelling method [17]. The conventional tape test could not be used to distinguish the adhesion strengths of E-coat to the plasma polymer coated metal surfaces in this study, as all the surfaces passed the maximum possible rating available with this method. The NMP solution method is based on the solvent swelling force exerted on the E-coat films in delamination from the surfaces. Film delamination depends on the adhesion strengths of the E-coat-substrate bonds. The NMP solution method was used to differentiate the adhesion performance of the E-coat films on the plasma polymer coated surfaces.
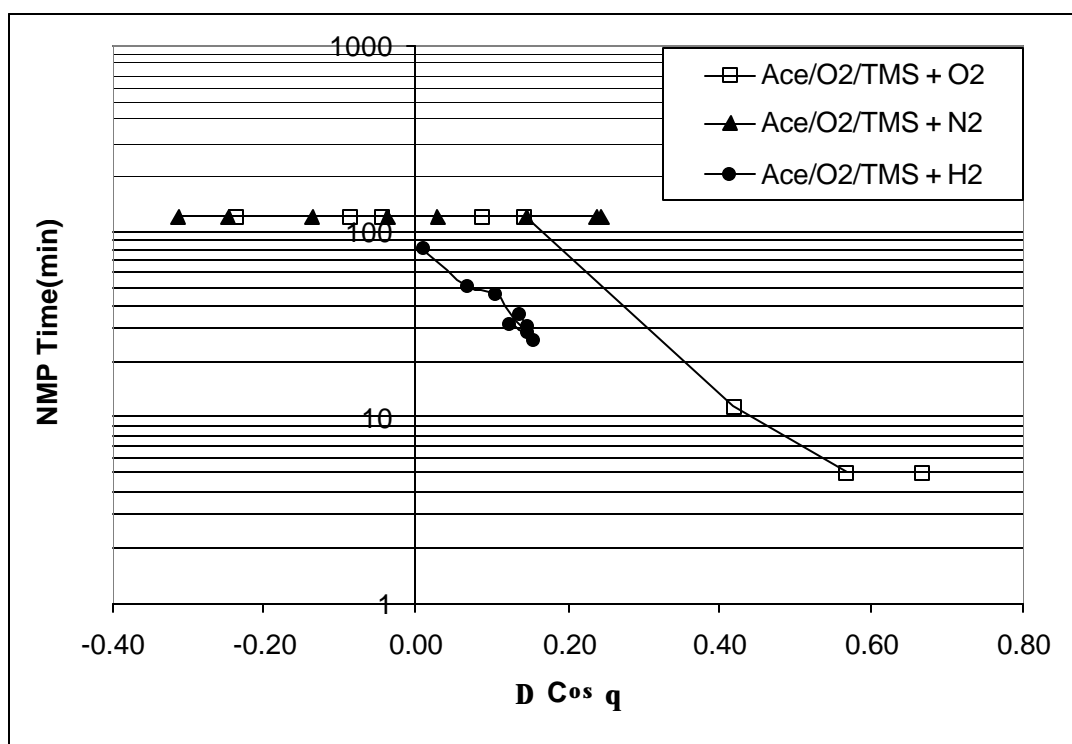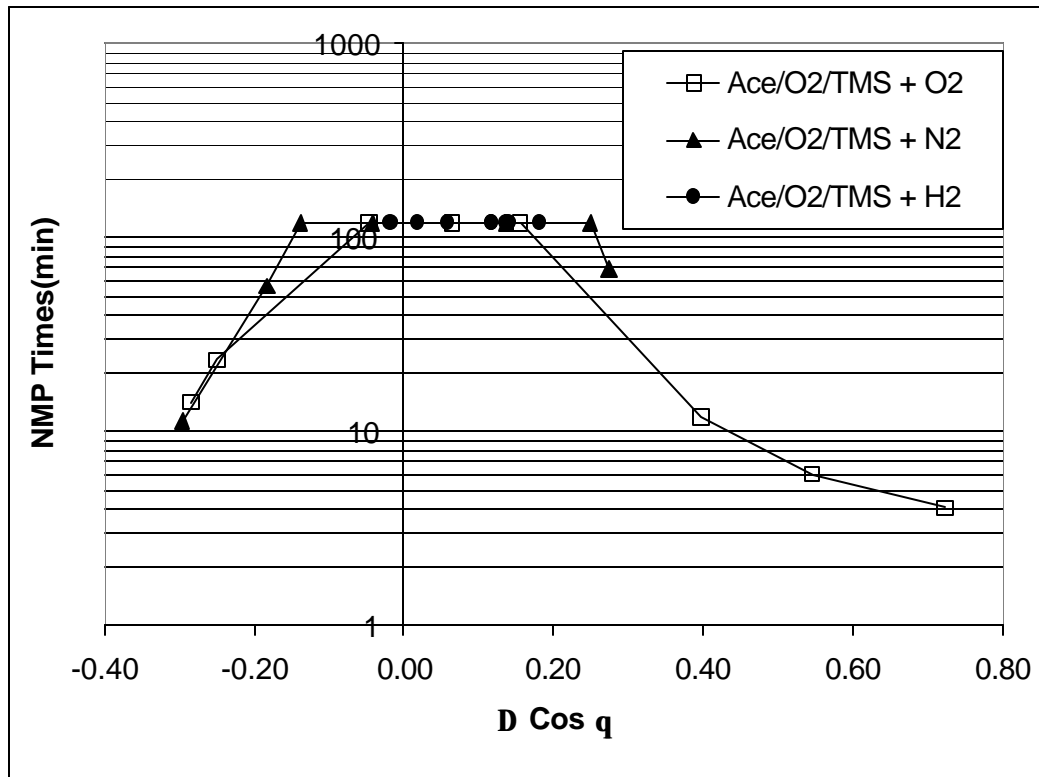

Figure 5. NMP time versus $\Delta Cos(\theta)$ for three plasma polymer systems, TMS+O_2, TMS+H_2 and TMS+N_2, on substrate 2B (AA 2024-T3) with other treatment conditions fixed. Deposition conditions for all concentrations were 5 watts DC power, 50 mtorr pressure and 1 minute deposition time.

The NMP times for substrate 2B coated with the three monomer/diatomic gas mixture systems are shown in Fig. 5. A comparison of the adhesion of E-coat film to the plasma polymers of the different TMS/diatomic gas mixtures deposited on 2B shows that NMP times for all compositions of TMS+N_2 mixtures are the best among all the combinations of the various mixtures. TMS+H_2 mixtures show poor adhesion times in the NMP test as compared to TMS+N_2 mixtures. All three systems show improved adhesion at the interfacial tension minimizing point, which depends on the specific system. The NMP times of E-coat delamination observed on

plasma polymers deposited on substrate 2B are far superior to those observed for E-coat deposited on substrate wiped with acetone (the maximum NMP time for E-coat on acetone-wiped 2B surfaces is 2.0 minutes). Even though plasma polymers of all concentrations show longer NMP times than bare surfaces wiped with acetone, the maximum adhesion achievable with each system is different.

Percent adhesion of the specimen which surpassed 120 minutes of the NMP test without total delamination was recorded by visual observation. Fig. 7 depicts percent adhesion of E-coat to plasma polymer surfaces on substrate 2B plotted against $\Delta Cos(\theta)$. From this figure, it can be seen that adhesion of E-coat to $TMS+N_2$ plasma polymer surfaces is better than to the other two plasma polymer mixtures. Since E-coat films on $TMS+H_2$ plasma polymer surfaces were completely delaminated within 120 minutes of testing time, this system does not appear in Fig. 6. The maximum E-coat adhesion was found at 0.5 mole fraction of N_2 in the $TMS+N_2$ mixture, 0.5 mole fraction of O_2 in the $TMS+O_2$ mixture and 0.67 mole fraction of H_2 in the $TMS+H_2$ mixture.
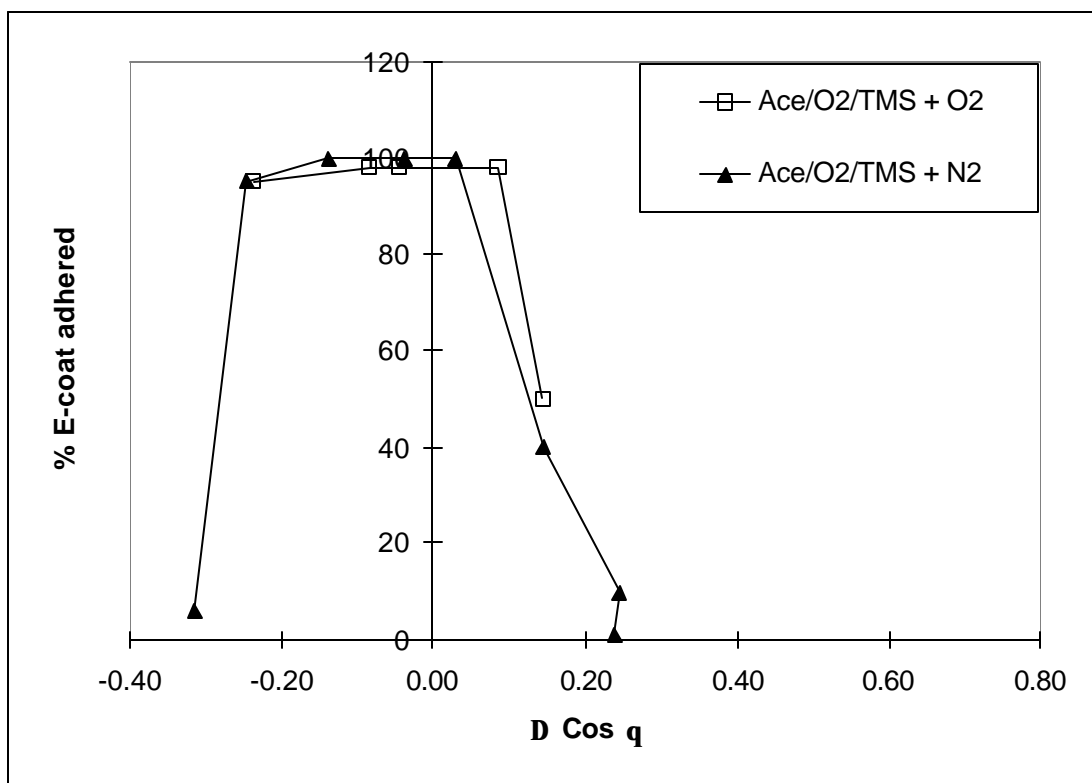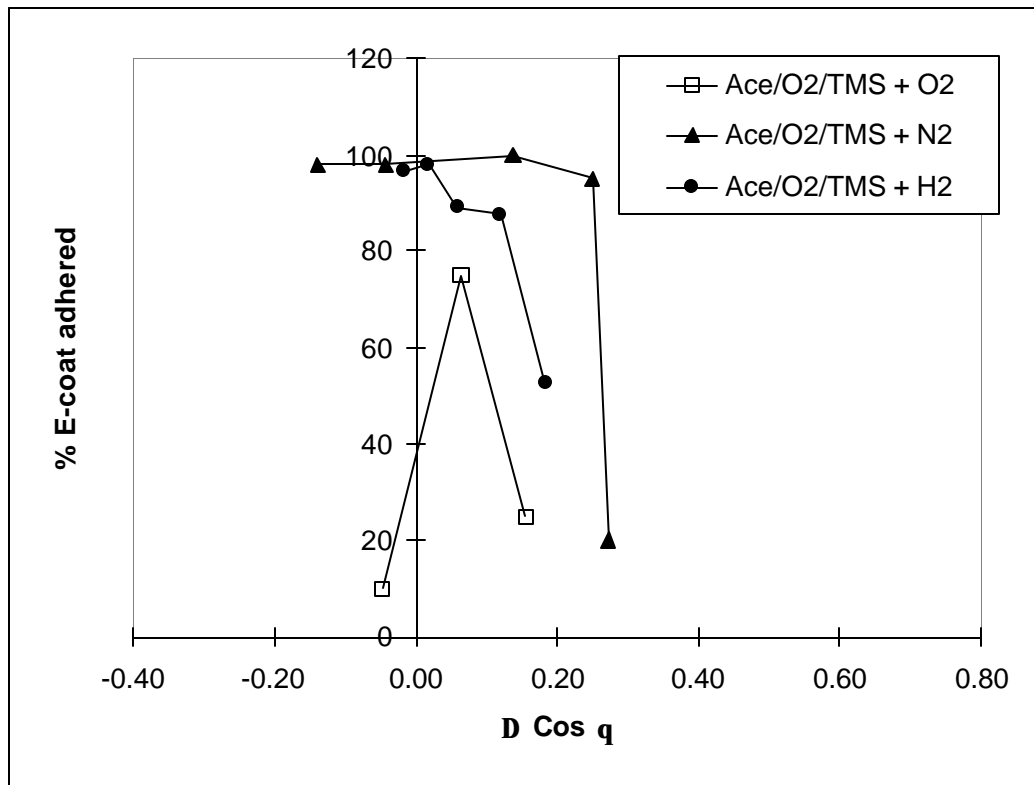

Figure 6. Percent E-coat adhered versus $\Delta Cos(\theta)$ for two plasma polymer systems, $TMS+O_2$ and $TMS+N_2$, on substrate 2B (AA 2024-T3) with other treatment conditions fixed. Deposition conditions for all concentrations were 5 watts DC power, 50 mtorr pressure and 1 minute deposition time.

The maximum adhesion of E-coat to the plasma polymer surfaces does not show dependence on the film thickness or refractive index variation. Plasma polymer film thickness and refractive

indices show gradual change over the diatomic gas mole fraction range (see Figs. 2 and 3) while the NMP delamination times show abrupt change, on either side, near the interfacial tension minimization point, $\Delta \mathrm{Cos}\theta = 0$.

Adhesion of E-coat to modified AA 7075-T6 alloy surfaces

NMP paint delamination times for E-coat on different TMS+O_2, TMS+H_2 and TMS+N_2 plasma polymer surfaces on substrate 7B are plotted in Fig. 7. It can be seen from this figure that NMP delamination times for TMS+H_2 and TMS+N_2 plasma polymer surfaces are longer than those for different TMS+O_2 plasma polymer surfaces. Additionally, it is evident that TMS+H_2 plasma polymer surfaces show longer adhesion times than TMS+N_2 plasma polymer surfaces. However, it should be noted that significantly longer NMP delamination times were found for all three systems near the interfacial tension minimizing point.

Figure 7. NMP time versus $\Delta \mathrm{Cos}(\theta)$ for three plasma polymer s ystems, TMS+O_2, TMS+H_2 and TMS+N_2, on substrate 7B (AA 7075-T6) with other treatment conditions fixed. Deposition conditions for all concentrations were 5 watts DC power, 50 mtorr pressure and 1 minute deposition time.

Average percent adhesion of E-coat to three specimens of TMS+O_2, TMS+H_2 and TMS+N_2 plasma polymer surfaces on substrate 7B is plotted against $\Delta \mathrm{Cos}\theta$ in Fig. 8. The percent adhesion of E-coat on TMS+O_2 and TMS+N_2 plasma polymers on 7B surfaces is slightly lower than on the corresponding 2B surfaces, but TMS+H_2 surfaces show higher percent adhesion on

the 7B surfaces. Among all three systems, TMS+N$_2$ plasma polymer systems have superior percent adhesion of E-coat. Again, as seen on 2B plasma polymer surfaces, there are maximum adhesion points for all three systems of TMS and diatomic gas. Plasma polymer coated AA 7075-T6 surfaces show maximum E-coat adhesion at 0.5 mole fraction of N$_2$ in the TMS+N$_2$ mixture, 0.5 mole fraction of O$_2$ in the TMS+O$_2$ mixture, and 0.67 mole fraction of H$_2$ in the TMS+H$_2$ mixture.

Figure 8. Percent E-coat adhered versus $\Delta Cos(\theta)$ for three plasma polymer systems, TMS+O$_2$, TMS+H$_2$ and TMS+N$_2$, on substrate 7B (7075-T6) with other treatment conditions fixed. Deposition conditions for all concentrations were 5 watts DC power, 50 mtorr pressure and 1 minute deposition time.

The effect of chemical cleaning on the adhesion of E-coat to modified AA 7075-T6 alloy surfaces

Adhesion performance of polymers on bare metal surfaces improves when the surface is cleaned by a chemical process like alkaline cleaning [20, 21]. Chemical alkaline cleaning with Turco 4215S followed by deoxidization with Amchem 7 deoxidizer solution is a common industry practice for cleaning an alloy surface before subjecting it to further processes. To examine the effect of chemical cleaning of the aluminum alloys on the NMP paint delamination times for E-coat on different TMS+O$_2$ and TMS+N$_2$ plasma polymer surfaces on substrate 7B, alkaline cleaning followed by deoxidization was employed. NMP paint delamination times for these systems are plotted in Fig. 9. NMP delamination times for TMS+N$_2$ plasma polymers are longer

than those for TMS+O$_2$ plasma polymer surfaces. Although NMP delamination times have improved slightly from those obtained for acetone-cleaned TMS+N$_2$ plasma polymer surfaces, this improved adhesion performance is not significant, because the acetone-wiped surfaces also show long NMP delamination times. This could be due to the fact that chemical cleaning has little effect on top layer plasma polymer.
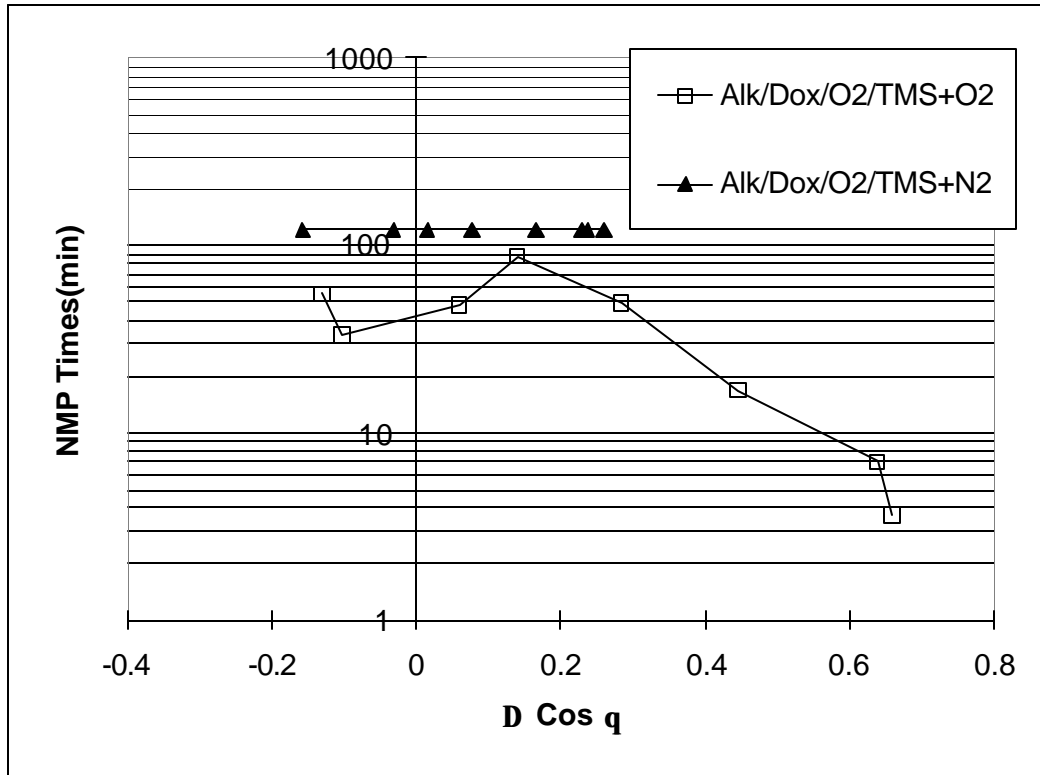
Figure 9. NMP time versus ΔCos(θ) for two plasma polymer systems, TMS+O$_2$ and TMS+N$_2$, on deoxidized substrate 7B (7075-T6) with other treatment conditions fixed. Deposition conditions for all concentrations were 5 watts DC power, 50 mtorr pressure and 1 minute deposition time.

Average percent adhesion of E-coat to TMS+N$_2$ plasma polymer surfaces on (Alk/Dox) substrate 7B is plotted against ΔCosθ in Fig. 10. The adhesion performance of E-coat on all these surfaces is superior to that on acetone-cleaned 7B surfaces. TMS+N$_2$ plasma polymer systems have superior percent adhesion of E-coat to that of TMS+ O$_2$ plasma polymer systems on chemically-cleaned 7B surfaces. Since NMP paint delamination times for TMS+O$_2$ plasma polymer surfaces are below 120 minutes, this system does not appear in Fig. 10.

Adhesion of E-coat to modified Alclad 2024-T3 alloy surfaces
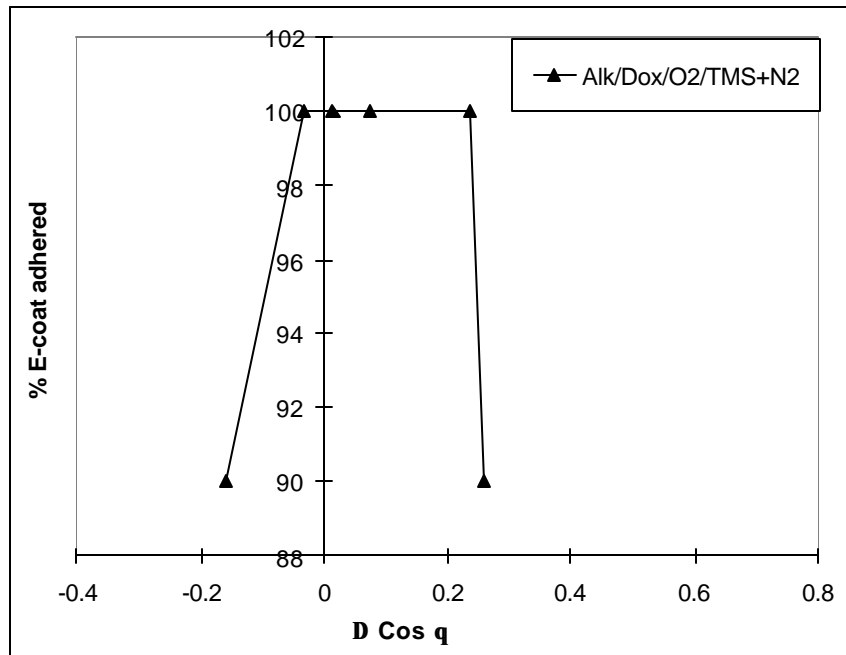
Figure 11. Percent E-coat adhered versus $\Delta Cos(\theta)$ for the TMS+N$_2$ plasma polymer system on deoxidized substrate 7B (7075-T6) with other treatment conditions fixed. Deposition conditions for all concentrations were 5 watts DC power, 50 mTorr pressure and 1 minute deposition time.
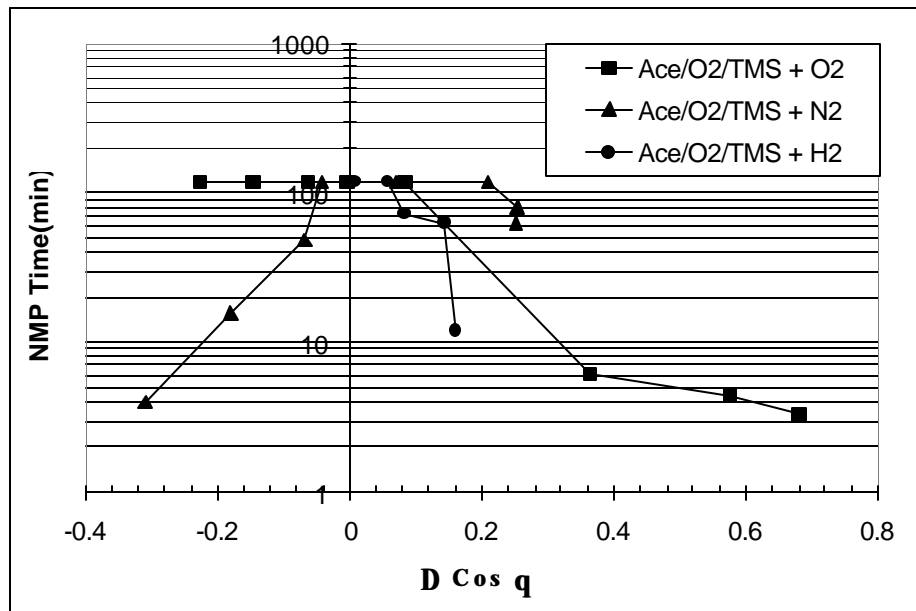
Figure 11. NMP time versus $\Delta Cos(\theta)$ for three plasma polymer systems, TMS+O$_2$, TMS+H$_2$ and TMS+N$_2$, on substrate 2A (Alclad 2024-T3) with other treatment conditions fixed. Deposition conditions for all concentrations were 5 watts DC power, 50 mtorr pressure and 1 minute deposition time.

NMP paint delamination times for E-coat on different TMS+O_2, TMS+H_2 and TMS+N_2 plasma polymer surfaces on substrate 2A are plotted in Fig. 11. From this figure, it can be seen that NMP delamination times for TMS+O_2 and TMS+N_2 plasma polymers are longer than those of plasma polymer surfaces of TMS+H_2. Also, TMS+N_2 plasma polymers show longer delamination times than TMS+O_2 plasma polymers. It is interesting to note that the longer NMP delamination times occur at the minimum interfacial tension point for all three systems on substrate 2A.

Average percent adhesion of three specimens of TMS+O_2, TMS+H_2 and TMS+N_2 plasma polymer surfaces on substrate 2A is plotted against $\Delta Cos\theta$ in Fig. 12. This figure clearly shows that maximum percent adhesion occurs at the minimum interfacial tension point. As compared to results for substrates 2B and 7B, the percent adhesion of E-coat on substrate 2A is lower for all three systems. Of all three systems, the TMS+N_2 plasma polymer system displays superior E-coat adhesion times on substrate 2A.
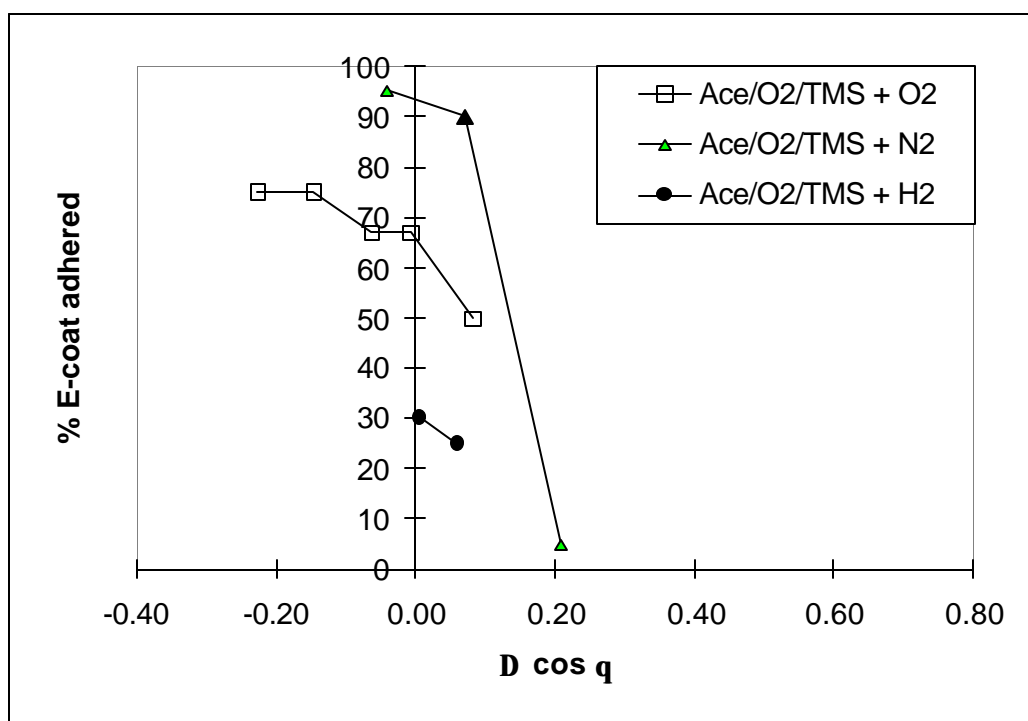
Figure 12. Percent E-coat adhered versus $\Delta Cos(\theta)$ for three plasma polymer systems, TMS+O_2, TMS+H_2 and TMS+N_2, on substrate 2A (Alclad 2024-T3) with other treatment conditions fixed. Deposition conditions for all concentrations were 5 watts DC power, 50 mtorr pressure and 1 minute deposition time.

SEM analysis of substrate surfaces 2B, 7B and 2A

The adhesion improvement of plasma polymer surfaces as compared to untreated substrate surfaces (NMP paint delamination times are about 2-5 minutes maximum) is explained by

interfacial tension minimization. Surface roughness enhances the adhesion of polymers to metal surfaces by means of mechanical interlocking. To examine the effect of plasma polymer deposition on surface morphology, scanning electron microscopy (SEM) studies were conducted for the surfaces of all three alloys without treatment and with typical plasma treatment and plasma polymer deposition. SEM showed that plasma treatment and plasma polymer deposition made the surfaces smoother than the untreated ones. This indicates that surface roughness of the panels was not a significant factor in the adhesion improvement accomplished in this study. The panels, which were cut from larger sheets, were not polished prior to use in the plasma reactor; therefore, they did not contribute to the smoothness observed with SEM. Thus, the dramatic improvements in the adhesion performance of plasma polymer deposited surfaces achieved in this study are due to changes in surface state.

Conclusions

1. The results of this study indicate that minimizing the interfacial tension between the metal/polymer interface maximizes the adhesion of paint.
2. Composition of the plasma polymer gas used in deposition changes cos   of plasma polymer coated metal surfaces.
3. Maximum adhesion for three systems studied, $TMS+O_2$, $TMS+H_2$ and $TMS+N_2$, was obtained when there was minimum interfacial tension between plasma polymer and E-coat film.
4. On all three substrates, AA 2024-T3, Alclad 2024-T3 and AA 7075-T6, the $TMS+N_2$ system showed better adhesion performance than the $TMS+O_2$ and $TMS+H_2$ systems.

References

[1] Venables, J. D., Journal of Material Science, **19**, 2431 (1984).
[2] Critchlow, G. W. and Brewis, D. M., Int. J. of Adhesion and Adhesives, **16**, 255 (1996).
[3] Minford, J. D., *Handbook of Aluminum Bonding Technology and Data* (Marcel Dekker, New York, 1993).
[4] Thrall, E. W. and Shannon, R.W., (Eds), *Adhesive Bonding of Aluminum Alloys* (Marcel Dekker, New York, 1985).
[5] Bijlmer, P. F. A., J. Adhes. **5**, 319 (1973).
[6] Yasuda, H., *Plasma Polymerization* (Academic Press, Orlando, FL, 1985).
[7] Yasuda, H. K., Wang, T.F., Cho, D. L., Lin, T. J., and Antonelli, J.A., Progress in Organic Coatings, **30**, 31 (1997).
[8] Wilson, A. D., Nicholson, J. W. and Prosser, H. J. (eds), *Interface Coatings-2* (Elsevier, London,1988), Chapter 2, pp. 39-70.
[9] Coon, C. L., and Vincent, J. J., Journal of Coatings Technology, **58**, N0. 742, 53 (1986).
[10] Pierce, P. E., Journal of Coatings and Technology, **53,** 52 (1981).
[11] Pierce, P. E., Kovac, Z., and Higginbotham, C., Ind. Eng. Chem. Prod. Res. Dev., **17**, No. 4, 317 (1978).
[12] Hays, D. R., and White, C. S., Journal of Paint Technology, **41**, No. 535, 461 (1969).
[13] Burnside, G. L., and Brewer, G. E. F., Journal of Paint Technology, **38**, 96 (1966).

[14] Shreir, L. L., Jarman, R. A., and Burstein, G. T. (Eds), *Corrosion* (Buttersworth-Heinemann, Jordan Hill, 1994), 3rd ed., Vol. 1.

[15] Biestek, T., and Weber, J., *Electrolytic and Chemical Conversion Coatings* (Potcullic Press, Redhill, 1976), pp. 1-127.

[16] Sehmbhi, T. S., Barnes, C., and Ward, J. J. B., Transactions of the Institute of Metal Finishing, **62**, 55 (1984).

[17] van Ooij, W. J., and Sabata, A., Effect of Paint Adhesion on the Underfilm Corrosion of painted pre-coated steel, CORROSION/91, NACE, Houston, TX, 1991, Paper No. 417.

[18] Guastalla, J., J. Chem. Phys., **49**, 249 (1952).

[19] Guastalla, J., J. Colloid Sci., **11**, 623 (1956).

[20] Rausch, W. W., Metal Finishing, **76,** No. 11, 44 (1978).

[21] Rausch, W. W., Metal Finishing, **76**, No. 12, 58 (1978).

17. The Effect of Magnetic Field Configuration in the Cathodic Polymerization Systems with Two Anode Magnetrons

J. G. Zhao and H. K. Yasuda

Abstract

Direct current (D.C.) glow discharge can be utilized in plasma polymer coating of metal substrates by using the substrate as the cathode (cathodic polymerization). By using an anode equipped with magnetic enhancement, the anode magnetron cathodic polymerization can be effectively operated in low pressure regime, in which a tight barrier type plasma polymer can be formed. When two magnetrons are used against a cathode (substrate), the configurations of magnetic field employed in each magnetron become an important factor of the system. In one case (PM), in which the identical magnetrons are used; magnetic field near the substrate (cathode) emanating from two magnetrons are parallel. In another case (OM), in which magnet arrangement is reversed in one magnetron, magnetic fields near the substrate are opposite. Plasma polymerization with no magnetron (NM) shows the edge effect (higher deposition rate near the edge of cathode). With anode magnetrons (OM or PM), the edge effect is eliminated and higher deposition rates, compared to that obtained without magnetron, were obtained in the majority of electrode area. The uniformity of the deposition rate distribution is better with the OM configuration than with the PM configuration. The distance between electrodes influences the distribution of the deposition rate with the PM configuration (less uniform with small distance), but has little effect with the OM configuration. The advantage of having anode magnetrons diminishes at system pressure higher than 50 mtorr.

Introduction

Direct current (D.C.) plasma polymerization was investigated in the early stage of the development of plasma polymerization (early 1960's). However, it quickly disappeared from literature, and the main stream of plasma polymerization has been carried out by radio frequency (R.F.) glow discharge [1]. The reason why D.C. glow discharge does not appeal to the most practitioners of plasma polymerization is probably that the majority of plasma polymerizations are used for coating of dielectric (substrate) materials, and the use of the substrate as the cathode is out of the consideration. The dominant deposition of a plasma polymer onto the cathode hampers an effective deposition onto the substrate placed in the glow discharge, and a heavy deposition onto the cathode causes the extinction of the discharge. On the other hand, for the treatment of metallic substrates, the cathodic plasma polymerization, in which the substrate is used as the cathode, appears to be an ideal means. The focused dominant deposition onto the substrate is a specific advantage of cathodic (plasma) polymerization in such applications.

A cathodic (plasma) polymer of a monomer is significantly different from the plasma polymer of the same monomer that deposits on a floating substrate [2]. The deposition mechanism is also significantly different from that of most plasma polymerization. The major operational factors in cathodic polymerization are the current density and the local concentration of monomer in the

cathode region, while the flow rate of monomer and the discharge power are two major factors in most plasma polymerizations. It is important to note that the discharge power and the flow rate of monomer are not controlling operational parameters in the cathodic polymerization. The cathode region of a D.C. glow discharge is not in a plasma state in a strict sense because there is the disparity of charged species. Accordingly, the cathodic (plasma) polymerization should be distinguished from the general plasma polymerization. The cathodic polymerization occurs only on the cathode surface. Plasma polymer that deposits on a dielectric substrate placed on the surface of cathode is not a polymer of the cathodic polymerization but is nearly identical to the plasma polymer that deposits on a floating substrate.

When a magnetic field is superimposed on an electrode, such an electrode is generally termed a magnetron. The planar magnetron has been used nearly exclusively as the cathode target (source) of sputter coating [3]. The basic principle of the magnetically enhanced sputtering technique was discovered by Penning [4] and further developed by Kay and others [5 –9].

The cathode magnetron cannot be used for the cathodic polymerization, in which the substrate is used as the cathode in D.C. discharge, because of the sputtering of the cathode material in the vicinity of the characteristic toroidal glow and of very non-uniform deposition distribution. It is also impractical to superimpose magnetic field on various substrates of different shapes and sizes.
A pair of planer magnetrons has been used as electrodes for low frequency to R.F. glow discharges with floating substrates placed between them [1]. By selecting electrode material and choosing plasma polymerization conditions to suppress the sputtering of electrode material, the advantages of confining plasma volume and the low-pressure (e.g., 50 mtorr) operation of plasma polymerization can be achieved.

When a magnetron is used as the anode in the cathodic polymerization, the process can be termed anode magnetron cathodic (AMC) polymerization. The advantages of having magnetic field on the anode are 1) breakdown voltage is lowered, 2) plasma polymerization can be performed in a low- pressure regime, 3) the edge effect of deposition can be minimized, and 4) plasma cleaning of a substrate surface prior to plasma deposition can be effectively performed, because of the absence of the edge effect [10]. Low-pressure operation is generally preferred in obtaining an ultra-thin layer of a tight network system suitable for a barrier by plasma polymerization [11].

AMC polymerization was utilized recently in the corrosion protection of steel [12,13], and of aluminum alloys [14,15,16]. The deposition of an ultra-thin layer (roughly 50 nm) of a plasma polymer or polymers, together with plasma pre-treatment of the surface were used as tools for interface engineering of corrosion protection coated systems. These environmentally benign processes have achieved excellent corrosion protection systems.

A modification of AMC plasma treatment in the form of a torch has been recently explored [17,18]. The anode magnetron torch can achieve sputter cleaning of a metallic substrate, which is considerably larger than the torch itself, by scanning the surface.
When two anode magnetrons are used against a substrate used as the cathode, the configuration of magnetic field employed in each magnetron is an important factor of the discharge system. In

  this paper, the effects of the combination of anode magnetron configuration on AMC polymerization, with respect to the deposition rate and its distribution, are investigated.

Experimental

A bell jar reactor system was used in this study. Fig. 1 depicts the experimental setup schematically. Each anode was a 17.8 cm x 17.8 cm (7" x 7") titanium plate. Eight permanent magnetic bars were placed behind each anode in a circular configuration bridging a center iron plate and an outer iron circular ring plate, with the same poles oriented toward the center (see Fig. 2). The magnetic field strength of each anode was 110 gauss, which was expressed by the maximum Gauss meter reading of the component parallel to the electrode surface. The distance between the two anode electrodes was adjustable. The 7.62 cm x 15.24 cm (3"x6") substrate panel (cathode) was placed midway between the two anode electrodes. The substrate material was aluminum alloy (2024-T3). An MDX-1K Magnetron Drive (Advanced Energy Industries, Inc.) was used as the DC power supply. The power supply was used in wattage mode.

A parallel magnetron (PM) plasma system has a magnetic field configuration in which the south poles of the permanent magnet bars are oriented toward the center of the electrode on both electrodes. In PM configuration, the radial magnetic field fluxes of the two-magnetron electrodes have the same direction (see Fig. 3-a).
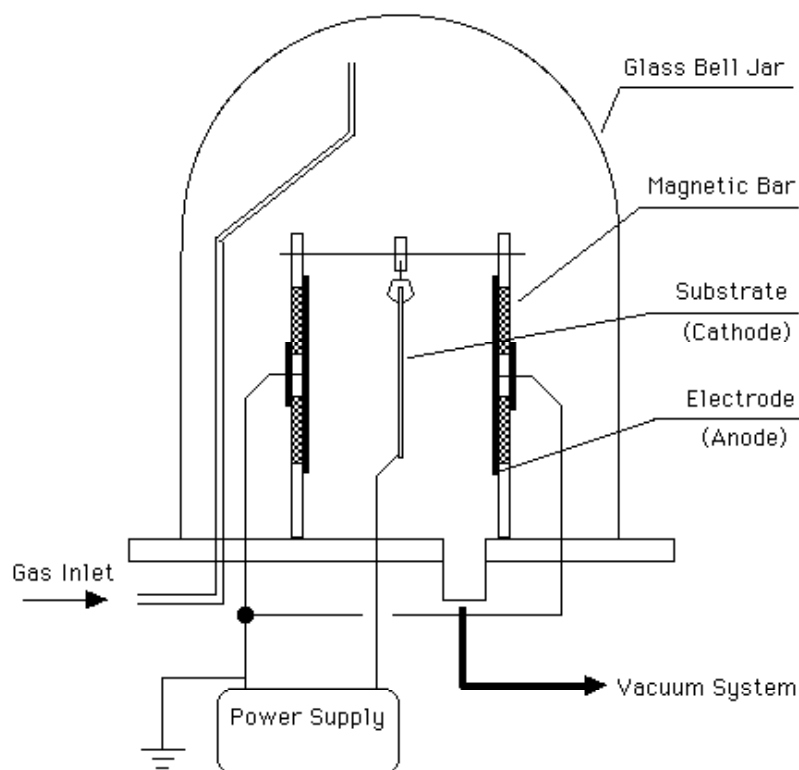
Figure 1. Schematic diagram of the bell jar reactor system.
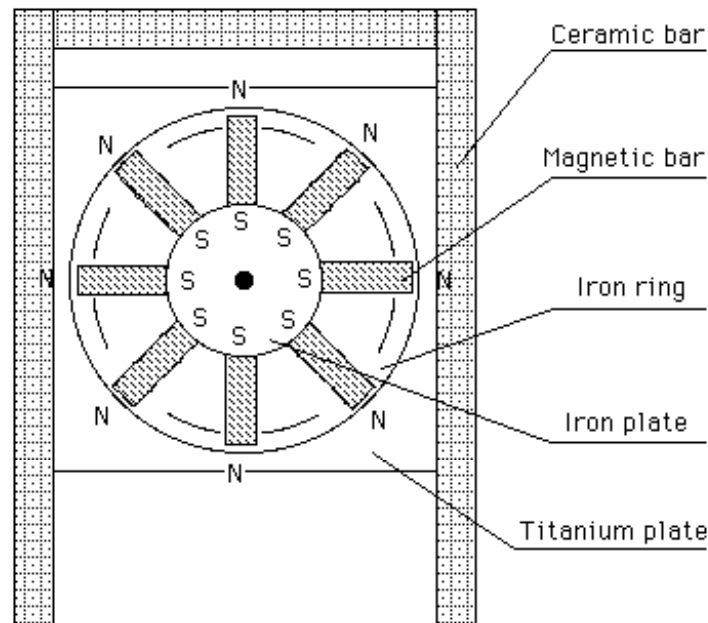
Figure 2. Structure of an anode magnetron electrode.
In an opposite magnetron plasma system (OM), the south poles of the permanent magnet bars are placed on the center in one anode while the north poles of the magnet bars are placed on the center of the other anode. In the OM configuration the radial magnetic field fluxes from the two magnetrons in the midpoint of two anodes are in the opposite direction (see Fig. 3-b). A plasma system with no magnetron (NM) is shown in Fig. 3-c as a reference case.

(a) (b) (c)
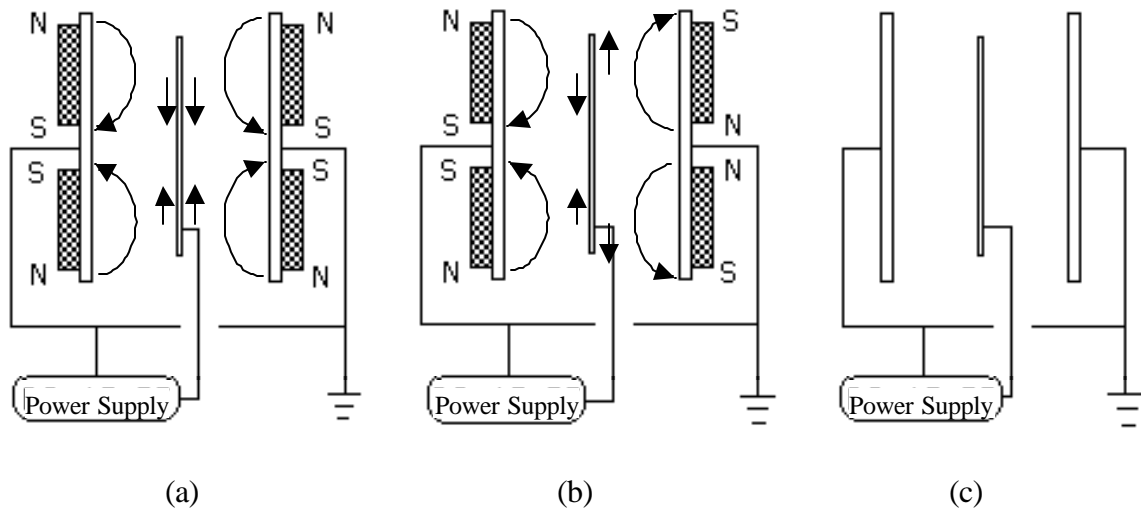
Figure 3. Schematic diagram of different magnetic field configurations on the backside of anode electrodes: (a) parallel magnetic field configuration (PM), (b) opposite magnetic field configuration (OM), and (c) no magnetron (NM).

Small pieces of silicon wafers were placed (maintaining electrical contact) on the substrate surface. An AutoEL-II Automatic Ellipsometer (Rudolph Research Corporation) was used for measurement of the thickness and refractive index of the deposited film (on silicon wafer). The deposition rate was calculated by dividing the deposited thickness by the plasma polymerization time (duration of glow discharge is on). The deposition rates were plotted as a function of distance from the center of the substrate. Trimethylsilane (TMS) of 97% purity, which was supplied by Lancaster Synthesis, Inc., was used as the monomer of plasma polymerization.

Results and discussion

A comparison of PM, OM and NM

The distribution of the deposition rate in an AMC plasma polymerization system with PM, OM, or NM (non-magnetron) anodes is shown in Fig. 4. These results show that the anode magnetron shifts the deposition pattern to the higher deposition rates in the center of the cathode. The edge effect diminishes but a small peak appears in the center. The distribution with OM configuration seems to be more uniform than that with PM configuration.

The edge effect is a serious problem in the case of sputter cleaning a substrate surface by a D.C. argon plasma. Sputtering occurs only near the edge of the cathode and the center part cannot be cleaned. In other words, effective ion bombardment does not occur in the center part of the cathode. With the use of an anode magnetron, the center area can be cleaned.
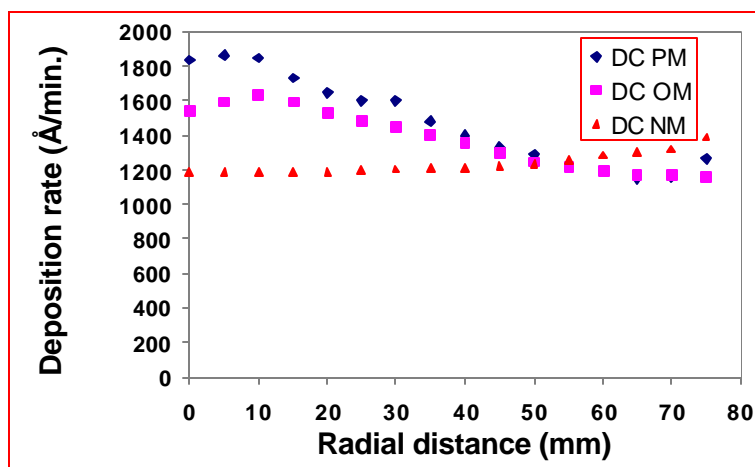
Figure 4. The dependence of the deposition rate distribution on magnetic field configuration (TMS, 50 mtorr, 1 sccm, 5 W, d=100 mm).

The edge effect is less pronounced in plasma polymerization, and the anode magnetrons used in this study seem to be over-compensating the edge effect in plasma polymerization. The refractive indices of plasma polymers prepared by cathodic polymerization are significantly higher than those for plasma polymers of the same monomer deposited on floating substrates [2], indicating that the ion bombardment has significant influence on the properties of plasma

 polymers formed by the cathodic polymerization. However, the less pronounced edge effect in plasma deposition suggests that the ion bombardment is not as important as that in the etching process.

Effect of electrode distance

The experimental results show that electrode distance affects the distribution pattern of deposition rate with the PM configuration (see Figs. 5) but not with the OM configuration. In the PM case, the net magnetic filed strength near the substrate surface is the cumulative magnetic filed emanating from two anodes and consequently is dependent on the inter-electrode distance. In the OM case, on the other hand, the net magnetic filed strength near the substrate surface is nearly nullified by the opposing magnetic fields and consequently is nearly independent of the inter-electrode distance.
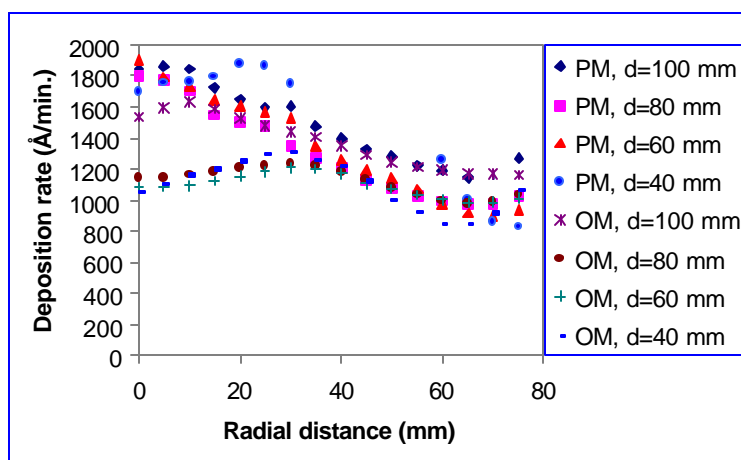
Figure 5. The influence of electrode distance on the deposition rate in AMC plasma polymerization (TMS, 50 mtorr, 1 sccm, 5 W).

The effect of surface area

The influence of the substrate area on the plasma deposition rate is shown in Fig. 6. It is clear that plasma deposition rate decreases with the increase of substrate surface area. This is because plasma deposition rate is proportional to current density in cathodic polymerization [2]. The deposition rate with a 7.62 cm x 15.24 cm (3"x6") substrate is nearly double of that with 15.24 cm x 15.24 cm (6"x6") substrate. The patterns of distribution due to magnetron configuration are similar but the trends are magnified as the deposition rate increases with smaller cathode area.

The effect of system pressure

The influence of system pressure on deposition rate is shown in Fig. 7. The results indicate that the characteristic features of cathodic polymerization (described in introduction) overwhelm the

influence of the magnetic field. The deposition rate of plasma polymer in the cathodic polymerization is proportional to the current density and the concentration of monomer in the cathode region, not the flow rate as mentioned previously.
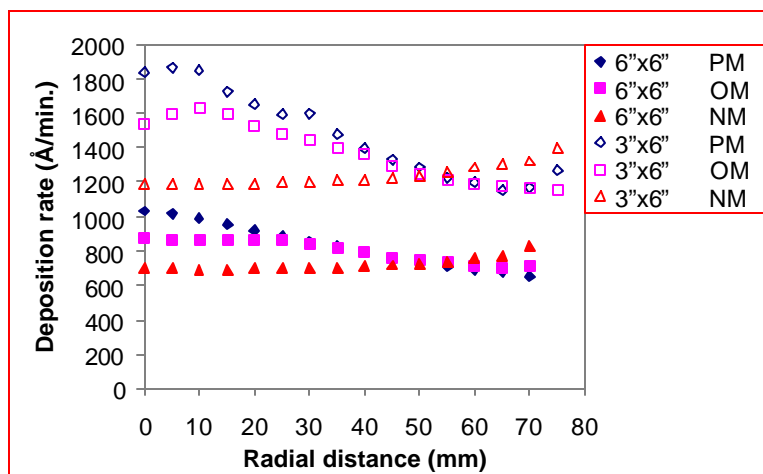
Figure 6. The influence of substrate area on the deposition rate (TMS, 50 mtorr, 1 sccm, 5 W).
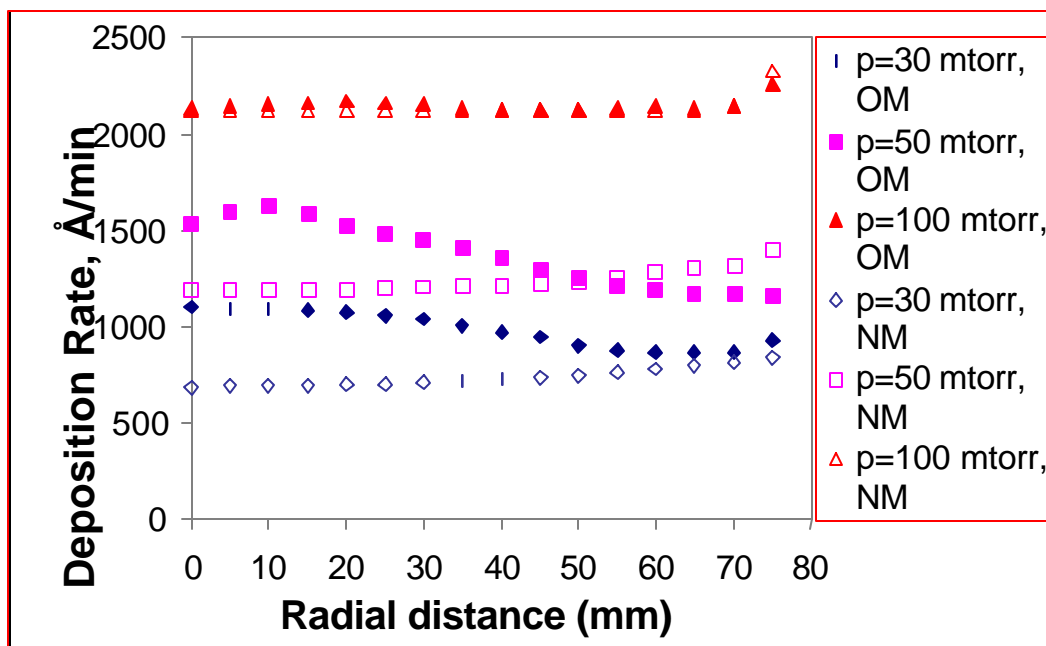
Figure 7. The dependence of deposition rate distribution on system pressure (p) in AMC plasma polymerization (TMS, 1 sccm, 5 W, d=100 mm).

The concentration of monomer in the cathode region increases proportionally to the system pressure. The deposition rates shown in Figs. 7 are nearly proportional to the system pressure while the flow rate is maintained at a fixed value. The typical influences of magnetic field discussed in the previous sections diminish as pressure is increased, and the edge effect of deposition appears at 100 mtorr.

The main purpose of having a magnetically enhanced glow discharge for plasma polymerization is to make it possible to carry out plasma polymerization effectively in a low-pressure regime (e.g., 50 mtorr) [11]. The results shown in Figs. 7 are in accordance with this goal, and confirm that there is no need for a magnetically enhanced or confined discharge for higher-pressure (e.g., 0.5 torr and higher) operation of plasma polymerization. It is important to note, however, that low-pressure operation (e.g., less than 0.1 torr) is highly advantageous and even necessary in some applications of plasma polymers. For instance, in order to obtain tenacious adhesion of a (cathodic) plasma polymer to a metal surface for good corrosion protection [12-16] and surface-dynamically stable plasma coatings (on polymers) [19], low-pressure operation is preferred or mandatory in most cases.

Summary

In AMC polymerization with two anodes against the cathode (substrate), the OM configuration provides slightly more uniform deposition rate distribution than the PM configuration, but at expense of slightly lower deposition rate.

The OM configuration has another advantage that the electrode distance (between two anodes as well as the distance between anode and cathode) has very little effect on deposition rate and its distribution. This feature may be an important factor in coating non-planar substrates.

AMC plasma polymerization can be effectively carried out in the low-pressure regime. The advantages of using magnetron anodes in the cathodic plasma polymerization diminish as system pressure is increased above 50 mtorr ranges.

This study also confirmed that cathodic polymerization is dictated by the conditions in the cathode region of D.C. glow discharge. The operational parameters of general plasma polymerization; i.e., discharge power and flow rate of monomer, do not control the cathodic polymerization.

References
1. H. Yasuda, <u>Plasma Polymerization</u> (Academic Press, Orlando, FL,1985).
2. M. Miyama and H. Yasuda, *J. Appl. Polym. Sci.*, **70**, 237 - 245, (1998)
3. R. K. Waits, Planar Magnetron Sputtering, <u>Thin Film Processes</u>, J. L. Vossen and W. Kern Ed., (Academic Press, New York, 1978).
4. F. M. Penning, *Physica* (Utrecht) **3**, 873, (1936).
5. E. Kay, *J. Appl. Phys*, **34**, 760, (1963).
6. W. D. Gill and E. Kay, *Rev. Sci. Instrum.*, **36**, 277 (1965).

7. E. Kay and A. P. Poenisch, U.S. Patent 2,282,815, (1966).

8. J. R. Mullaly, *Res/Dev*, **22**(2), 40, (1971).

9. K. Wasa and S. Hayakawa, *Rev. Sci. Instrum.*, **40**, 693, (1969).

10. W. H. Tao, M. A. Prelas, and H. K. Yasuda, *J. Vac. Sci. Technol.* **A 14**, 2113 (1996).

11. K. Sato, Y. Iriyama, D. L. Cho, and H. Yasuda, *J. Vac. Sci. Technol.* **A 7** (2), Mar/Apr, 195 (1989).

12. Tinghao F. Wang, H. Yasuda, T. J. Lin , and J. A. Antonelli, *Progree in Organic Coatings*, **28**, 291, (1996).

13. Tinghao F. Wang, D. L. Cho , H. Yasuda, T. J. Lin , and J. A. Antonelli, *Progree in Organic Coatings*, **30**, 31, (1997).

14. C. M. Reddy, Q. S.Yu, C. E. Moffitt, D. M. Wieliczka, R. Johnson, J. E. Deffeyes, and H. K. Yasuda, "Improved Corrosion Protection of Al Alloys by System Approach Interface Engineering: Part I - Alclad 2024-T3", paper submitted to *Corrosion*, 1999.

15. Q. S. Yu, C. M. Reddy, C. E. Moffitt, D. M. Wieliczka, R. Johnson, J. E. Deffeyes, and H. K. Yasuda, "Improved Corrosion Protection of Al Alloys by System Approach Interface Engineering: Part II - AA 2024-T3", paper submitted to *Corrosion*, 1999.

16. C. E. Moffitt, C. M. Reddy, Q. S. Yu, D. M. Wieliczka, R. Johnson, J. E. Deffeyes, and H. K. Yasuda, "Improved Corrosion Protection of Al Alloys by System Approach Interface Engineering: Part III - AA 7075-T6", paper submitted to *Corrosion*, 1999.

17. J. G. Zhao and H. K. Yasuda, Part I., *J. Vac. Sci., & Technol.*, A **18**(1), Jan/Feb, (2000).

18. J. G. Zhao and H. K. Yasuda, Part II., *J. Vac. Sci., & Technol.*, A **17**(6), Nov/Dec (1999).

19. Christopher M. Weikart, Masayo Miyama, Hirotsugu K. Yasuda, *Journal of Colloid and Interface Science*, **211**, 28-38, (1999).

18. Deposition of Trimethylsilane (TMS) in Glow Discharges

H. K. Yasuda and Q. S. Yu

Abstract

The deposition characteristics of trimethylsilane (TMS) on the electrode surface, and on floating substrate are investigated in direct current (DC), 40 kHz, and 13.56 MHz discharges by examining the difference of dependence on operational parameters; flow rate, discharge wattage, and the system pressure. In DC glow discharge, the deposition of materials are caused by the mixture of "dark" *cathodic polymerization*, which is pressure dependent, and "glow" *plasma polymerization* in the negative glow, which is pressure independent. The deposition onto the cathode surface is primarily by the "dark" polymerization, but the deposition onto any non-cathode surface, including the anode surface, is by "glow" *plasma polymerization*. The creation of reactive species occurs by electron-, ion-, and (excited neutrals)- impact dissociations of TMS in the cathode dark region and in the negative glow. With an alternating current discharge, the feature of the "dark" *cathodic polymerization* decreases to the half of the DC because an electrode is the cathode only in one half of the deposition time, but in 13.56 MHz discharge, the influence of the "dark" *cathodic polymerization* totally diminishes as the creation of reactive species changes to that by the oscillating electrons and associating species in the glow.

Introduction

The direct current (DC) glow discharge has been used in the basic studies of glow discharge plasma, and for the sputtering and the etching of the materials. The use of DC glow discharge for plasma polymerization (PCVD) has not been in the mainstream of studies and applications of plasma polymerization coatings, and there is no literature on the subject appeared in recent years. The reasons why DC glow discharge did not attract interests of researchers could be attributed to the fact that most plasma polymerizations have been applied to dielectric materials, which cannot be used as the cathode, and that the deposition of materials occurs mainly on the cathode, which eventually causes extinction of the glow discharge.

When a plasma polymerization coating is applied onto a metallic substrate used as the cathode, on the other hand, the DC cathodic polymerization is a very effective and practical means to apply an ultra-thin layer of barrier coating to the substrate. Cathodic polymerization of trimethylsilane (TMS) has been utilized recently in creating corrosion protecting systems (with a thicker primer coating) for cold rolled steel [1,2], and aluminum alloys [3-5]. Interface engineering by means of cathodic polymerization provided excellent corrosion protection systems, without galvanizing /zinc-phosphating for steel or without chromate conversion coating/chromated primer for aluminum alloys.

In such applications, an approximately 50 nm thick layer of plasma polymer of TMS was deposited on metallic substrates used as the sole cathode, which were pre-cleaned according to the optimal processes characteristics to each substrate material, and an appropriate primer was

applied on the plasma polymer layer. The plasma polymer layer applied is electrically conducting in such an extent that electrochemical deposition of paint (E-coat) can be performed on the surface of plasma polymer coated metal.

The deposition of materials onto the cathode surface is significantly different from that onto a substrate floating in plasma. The relationship between the deposition rate and the operational parameters of glow discharge such as discharge wattage, monomer flow rate, and the system pressure, for the DC cathodic polymerization is distinctively different from that for plasma polymerization that occurs in the diffuse plasma [6]. In this study the difference of the deposition kinetics of TMS in the two different polymerizations are investigated in order to gain more insight into the activation steps of glow discharge polymerizations and of the cathodic polymerization.

Experimental

Materials
        Aluminum alloy panels of 2024-T3 (7.62 cm by 15.24 cm by 0.081 cm) purchased from Q panel Lab Products were used as the metallic substrates. Alkaline solution of Turco 4215S, a commercial alkaline cleaner, was used to clean the aluminum panels for removing the possible surface organic contaminants. Trimethylsilane (TMS) gas of 97% minimum purity was purchased from PCR, Inc. and used without further purification.

Plasma reactor system and operation

The DC cathodic polymerization and audio frequency (AF) and radio frequency (RF) plasma polymerization of TMS were carried out in a bell-jar type reactor. The bell-jar has the dimension of 635 mm in height and 378 mm in diameter. A pair of stainless steel plates (17.8 cm by 17.8 cm by 0.16 cm) was placed inside the bell-jar with spacing of 100 mm and used as two parallel electrodes. The substrate used in the plasma deposition process was an aluminum alloy panel positioned in the midway between the two parallel electrodes.

(a) Substrate as electrode   (b) Substrate floating
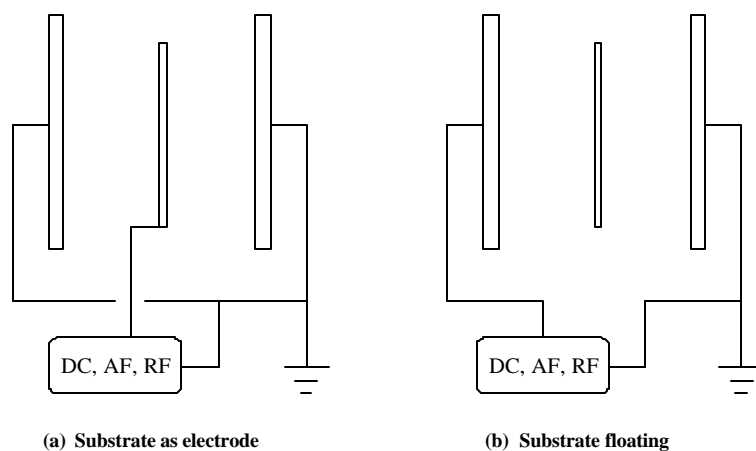
Figure 1. Schematic diagrams of the two configurations of the electrode setup used in the glow discharge polymerization process. (a) Al substrate was used as powered electrode and (b) Al substrate was floating in between the two parallel electrodes.

Two configurations of the electrode-substrate arrangement have been used for TMS deposition in different glow discharges as depicted in Fig. 1. In configuration 1, the Al substrate was used as the powered electrode, which is the cathode in DC process. In such a configuration, the two parallel stainless steel plates were used as grounded electrodes, which are on the same electrical potential. In configuration 2, the Al panel was used as a floating substrate positioned in between the two parallel electrodes. In this configuration, one of the two parallel electrode plates was used as the powered electrode (or cathode in DC process) and another was used as the grounded electrode (or the grounded anode in DC process).

The power supplies used in the present study were MDX-1K magnetron drive for DC plasma process, PE-1000 AC Plasma Source for AF plasma process (40 kHz), and an external RFX-600 generator (13.56 MHz) combined with ATX-600 tuner for RF plasma process. All these power supplies were the products of Advance Energy Industries, Inc.

The reactor system was first pumped down to < 1 mtorr by Edwards EH series vacuum pump system (Model E2M 80 rotary pump and model EH500A booster pump). The TMS monomer gas was then fed into the reactor chamber. An MKS mass flow meter (model 247 C) was used for monitoring the gas flow rate and an MKS pressure controller (model 252) was used to control the gas pressure in the reactor chamber. The system pressure was controlled under a preset flow rate of 1 sccm in this study. After the system pressure stabilized to a preset value, electrical power of DC (or AF or RF) with wattage-control mode was applied to initiate the glow discharge for a preset operation time. In DC discharge, a variable voltage in the range of 600 ~ 1000 V, which was mainly determined by the system pressure, was observed. After the plasma operation, the residual gases were pumped out the reactor chamber and the system pressure was allowed to return to the background pressure before air was allowed to come into the reactor. The samples were then removed from the rector for further measurements.

<u>Measurement of thickness and refractive index</u>

An AutoEL-II automatic ellipsometer (Rudolph Research Corporation), which is a null-seeking type with a 632.8 nm helium-neon laser light source, was used for measurement of the thickness and refractive index of deposited films in different glow discharges. For such a measurement, deposited films were all prepared on silicon wafers, which was sticking to the substrate with double side tape during the deposition. In certain cases, a drop of Silver print was used to stick the silicon wafer to the aluminum substrate in order to achieve a good electrical contact in between. The thickness growth rate or deposition rate of the plasma polymers was calculated from the film thickness divided by deposition time.

Results and Discussion

<u>Creation of Chemically Reactive Species in a DC discharge</u>

The foundation of the chemistry of plasma polymerization and of plasma treatment of material surfaces is based on the chemical reactions of reactive species created by the dissociations of organic molecules caused by the impact of electrons, ions, and exited neutral species in plasma. Although the primary species created by the ionization of organic molecules or fragmented moieties may not play the dominant role, it is quite clear that the whole process does not proceed

without the ionization process. Therefore, it is important to recognize the fundamental step of ionization in a gas discharge system. For this purpose, the simplest case of ionization of argon in a DC glow discharge has been often used in explaining the fundamentals of glow discharge.
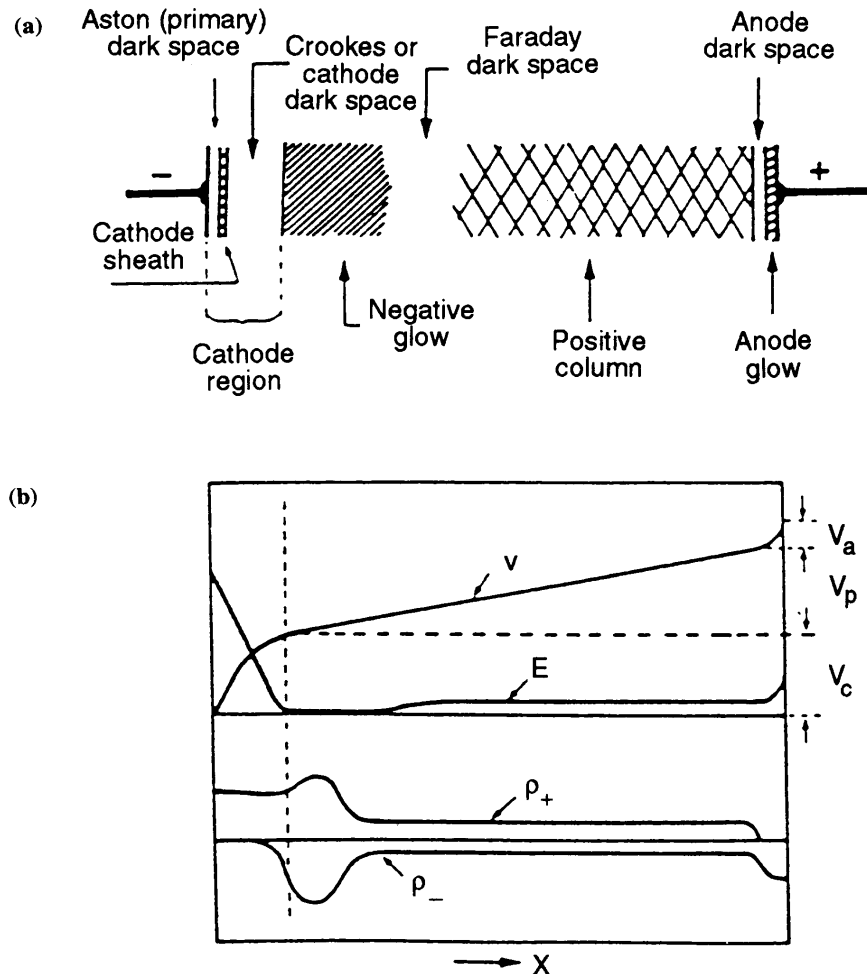

Figure 2. Schematic representation of DC glow discharge: X, distance from cathode: V, Potential: E, electrical field; r+, positive charge density; r-, negative charge density; the shaded areas are luminous.

In a DC discharge, a constant voltage is applied between a cathode and an anode, and the location of luminous glow and profiles of some parameters are shown in Fig. 2. The maximum of the electric field exists near the surface of the cathode, and the acceleration of electrons mainly takes place in this region. The ionization of an argon atom occurs when an electron gains a sufficient energy to ionize the atom. Therefore, the ionization of argon takes place in the vicinity of the cathode glow. The schematic representation of typical DC glow discharge, such as one shown in Fig. 2, has been used in many publications to illustrate low temperature plasmas; however, the figure represents the situation in a long tube under the system pressure of around 1

 torr, which does not represent the situation that is used for DC glow discharge polymerization operated with a shorter distance of electrodes (e.g.,100 mm), and a lower pressure (50 mtorr) in a larger volume reactor (e.g., 30 liters).

In most glow discharge reactors used for plasma polymerization and plasma treatment, the distance between a cathode and an anode is short and the system pressure is relatively lower (compared to the situation in a vacuum tube), so the Faraday dark region and the positive (anode) glow are often not observed. In Fig. 3, DC glow discharge in a plasma polymerization reactor is schematically depicted. The location of negative glow is dependent on the system pressure. At a low system pressure, the negative glow occupies the major part of the inter-electrodes space and reaches near the anode. At a higher system pressure, the cathode dark region and the negative glow moves closer to the cathode and the Faraday dark space appears near the anode, as shown in Figure 3 (b). In the cathode dark region, electrons are being accelerated but the energy of an electron is not high enough to cause sufficient excitation of atoms and ionization to cause luminous glow, and the region thus remains dark. Luminescence in a discharge is due to the process of excited species dissipating energy by emitting photons.

The distribution of electron temperature (energy of electrons) and number of electron in a DC glow discharge reactor used in plasma polymerization is shown in Fig. 4 and Fig. 5 respectively by using data previously presented [7]. The data shown are taken on the plane, which is at the center of the electrode, and perpendicular to the two electrodes (cathode & anode).
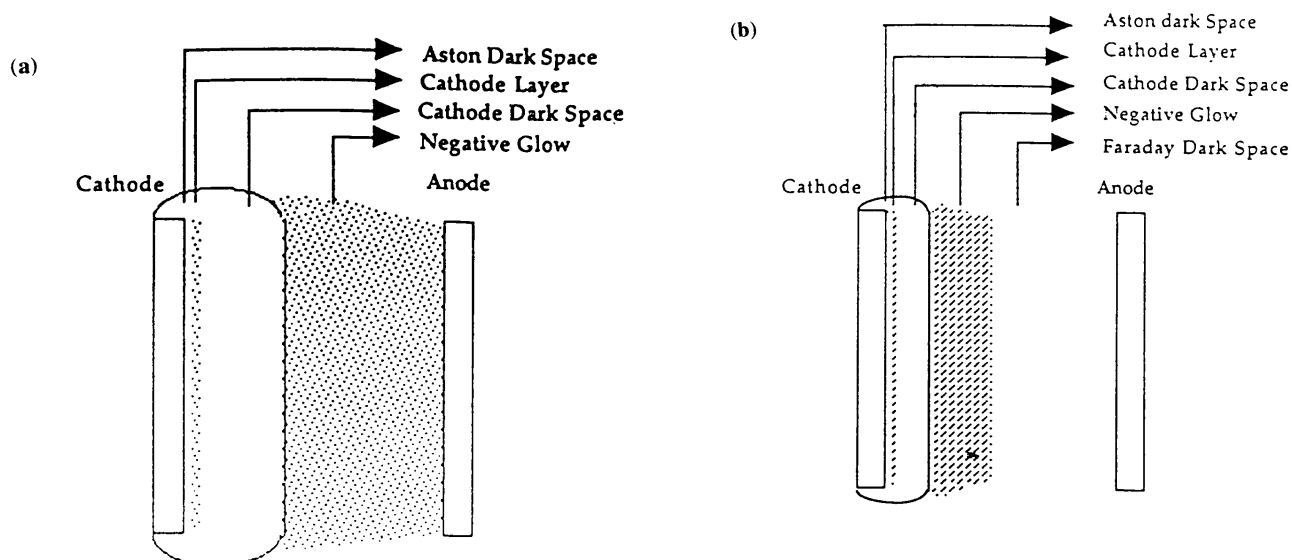
Figure 3. Schematic presentation of DC glow discharge in a plasma polymerization reactor, (a) System pressure < 6.66 Pa (50 mtorr), (b) system pressure > 13.33 Pa (100 mtorr).
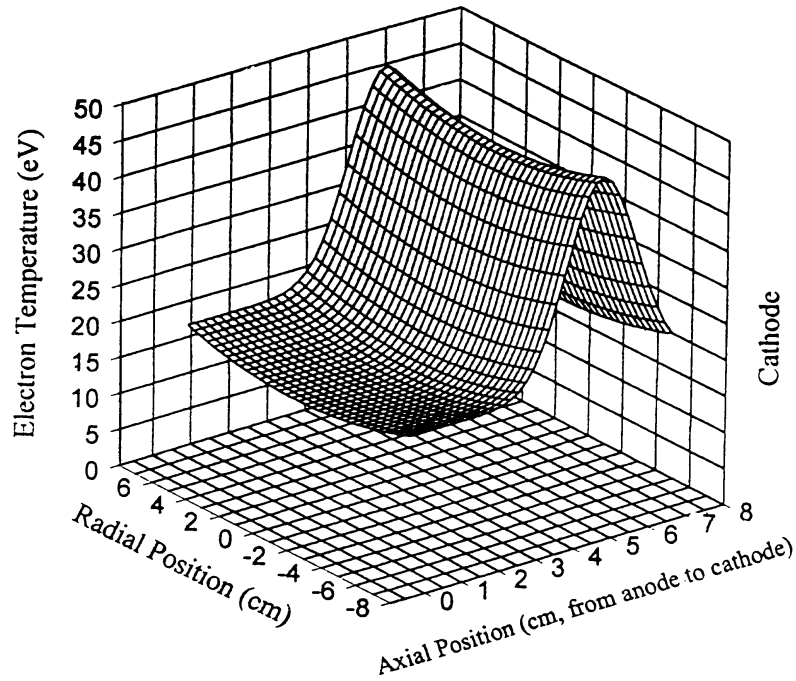
Figure 4. Distribution profile of electron temperature in an argon DC glow discharge in a plasma polymerization reactor
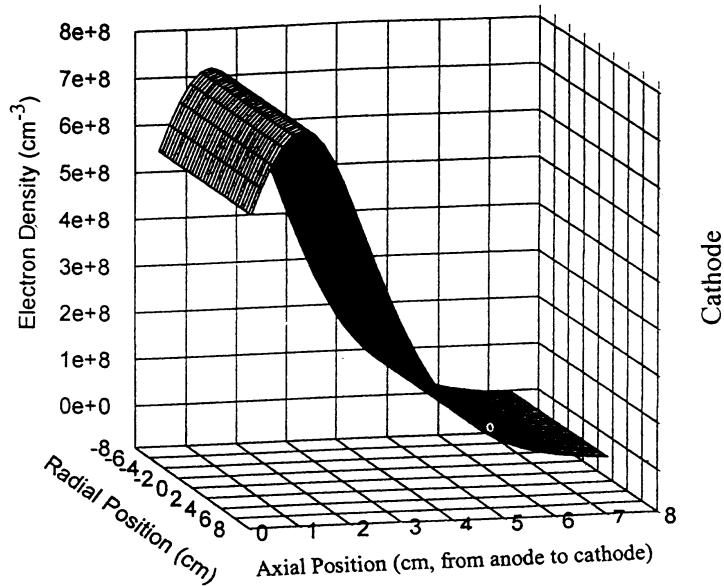
Figure 5. Distribution profile of electron density in an argon DC glow discharge in a plasma polymerization reactor

The electron temperature rises as electrons are accelerated in the electric field. During this process, the number of electrons is relatively small. When the electron temperature reaches the maximum level as a function of the distance, T_e starts to drop significantly, but the number of electrons starts to increase as electrons are pulled towards the anode. The positively charged argon ions will be pulled towards the negatively charged cathode surface and causes the emission of secondary electrons, which will be accelerated while traveling in the cathode fall region. Beyond the cathode fall region, very little electric field exists and no significant acceleration of an electron occurs. The major portion of the negative glow is filled with a large number of electrons, whose energy is not high enough to ionize a significant amount of argon but high enough to create argons in various excited states.

With organic molecules, the consequence of ionization is much more complex than the simple case of the argon glow discharge shown. However, the movement of electrons can be considered to be similar to the case shown for argon glow discharge. In so far as plasma polymerization (PCVD) is concerned, the location where the creation of reactive species occurs and its relative position to the substrate surface, on which plasma polymers deposit, are important factors to be considered.

The well-characterized DC glow discharge is more or less limited to the discharge of inert gases. When an organic gas, instead of an inert gas, is used in the same discharge reactor, a nearly completely different phenomenon occurs, in which the deposition of material occurs and the composition of the gas phase changes continuously as deposition proceeds. This difference could be further illustrated by examples of DC discharge of argon and of acetylene.

In a closed system, e.g., 500 mtorr of argon or acetylene, the discharge is completely different in the following way. DC glow discharge of argon can be maintained indefinitely, and diagnostic measurements such as electron temperature measurement and emission spectroscopy could be carried out in such a steady glow discharge. In contrast to this situation, DC glow discharge of acetylene extinguishes in few seconds to few minutes depending on the size of the tube and the system pressure. This is because acetylene forms polymers and deposits on the wall of the reactor. On this process of plasma polymerization of acetylene, very little hydrogen, or any gaseous species, is created, and the plasma polymerization acts as a vacuum pump. When the system pressure decreases beyond a certain threshold value, the discharge cannot be maintained.

The similar situation can be also seen in a flow system discharge. Again argon discharge can be maintained indefinitely under a steady state flow of argon under a given pressure. This is not the case with acetylene glow discharge. When a relatively low flow rate, e.g., 1 sccm, and the pumping rate is not controlled to adjust the pressure change, e.g., under the full pumping capacity, the acetylene is consumed (by plasma polymerization) faster than it is replenished by the flow of acetylene. Consequently, the system pressure decreases, and the glow discharge extinguish. In the flow system, however, acetylene is fed into the system continuously at a given flow rate, and the system pressure increases as soon as the glow discharge extinguishes. As the system pressure increases to the pressure, where the breakdown of the gas phase could occur under the applied voltage, glow discharge is ignited again, but the re-ignited glow discharge follows the same path of the first discharge. As a consequence of these processes, the glow discharge occurs as a self-pulsating intermittent discharge.

  A significant difference between glow discharge of an inert gas such as argon and that of an organic compound such as acetylene is the fundamental step of creating excited or reactive species. The low energy electron on the slope of increasing energy shown in Fig. 4 is energetic enough to dissociate the organic molecule (electron impact dissociation). Thus, the direct ionization of the entire molecule is rather unlikely event while such a step should be the major and the most important step, if one applies the fundamental knowledge gained by argon discharge without modifications to account for the basic difference. The ionization would occur with fragmented moieties in the case of organic gases.

Species that contribute to the deposition of materials in the cathode region are mainly created by the electron impact dissociation in the cathode dark space. Ions are pulled to the cathode surface by the electrical field. As the energy increases as an ion travels towards the cathode, neutral species, including the monomer, could be dissociated by the ion impact dissociation. The polymer forming (reactive) species thus created in the dark space near the cathode are not photon-emitting species [8]. This aspect is also evidenced by the reduction of the intensity of luminous glow when an organic gas is added to an argon discharge, and also by that the glow discharge of a fast- polymerizing gas such as acetylene is associated with very faint glow.

Polymer-forming species thus created in the cathode region of a DC discharge, presumably free radicals and cation-free radicals, deposit on the cathode surface. In order to maintain glow discharge, however, the secondary electrons must be emitted from the cathode surface. This means that the secondary electrons must come out of the deposited plasma polymer when the cathode surface is sufficiently covered by the plasma polymer. The emission of the secondary electrons from the surface of dielectric materials is well known phenomena. In the case of plasma polymers, it can be understood that the surface state electrons, which are responsible for the contact electrification of polymer surfaces (static charges), could be emitted as the secondary electrons to sustain the glow discharge. In other words, the secondary electron emission is not an ionization process. An ultra-thin layer of plasma polymer (up to ca. 100 nm) is electrically conducting as evidenced by the fact that a plasma coated metal plate can be coated by the electrochemical deposition of paint (E-coating). Thus the plasma polymer layer remains in the same electrical potential of the cathode (within a limited thickness) and the work function for the secondary electron emission does not increase significantly.

Another important factor is the negative glow in DC discharge, which is observed both in argon and acetylene glow discharge. The negative glow constitutes the main body of glow in which plasma polymerization of organic vapors generally occurs in alternating or RF discharges. The negative glow in a DC discharge should also cause plasma polymerization of an organic vapor. The mechanisms of the creation of polymer-forming species in the negative glow must be completely different from that for the cathodic polymerization described above. While the ionization is essential to sustain the glow discharge, the reactive neutral species (free radicals), which can be considered as the byproducts of the ionization, are dominant species that control the deposition an organic compound in plasma[9].

The above explanation of the difference between DC glow discharges of an inert gas and of an organic vapor is a speculative one. However, the deposition data support the concept of the dark space polymerization. The difference in the deposition kinetics in the negative glow and in the cathode dark space, which will be described in detail in the following sections, strongly indicate

 that the cathodic deposition is not the deposition of species that are created in the negative glow and enhanced by the electric field in the cathode fall.

The glow discharge initiated by an alternating current power source can be visualized by an alternating cathode and anode shown in the DC glow discharge, up to a certain frequency; e.g., 50 kHz. Therefore, the polymer deposition in DC discharge as well as in an alternating current discharge is a mixture of DC cathodic polymerization that occurs in the cathode dark region and *plasma polymerization* that occurs in the (negative) glow.

At a higher frequency (e.g., over 100 kHz), an electron can no longer travel in the distance to reach the anode within a cycle, so the oscillation of electrons becomes the major motion of electrons in 13.56 MHz and microwave discharges. In this case the collision of an oscillating electron with an atom or a molecule is the principal mechanism of ionization as well as the creation of polymer-forming species, which occur away from the electrode surface. Thus, the predominant role of the cathode observed in DC and alternating current discharge would diminish in 13.5 MHz discharge.

Deposition Rate as Functions of Operation Parameters

The formation of reactive species and the deposition of materials from them in the cathode region can be termed cathodic polymerization and those occurring in the remainder of the space can be plainly termed *plasma polymerization* for the purpose of discussion. According to this distinction of two processes, the cathodic polymerization takes place in the "dark" space, and the *plasma polymerization* occurs in the "glow". It should be clarified that "dark" and "glow" merely refers to the location where plasma polymerization takes place. Polymerization does not emit photons because the excess energy is dissipated in the chemical reactions to form polymers. Polymerization and photon-emission are both deactivation processes of excited species.

Since the majority of plasma coatings are performed in the latter case (i.e., *plasma polymerization*), it is easy to start the discussion with the deposition rate as a function of operation parameters for *plasma polymerization*.

Deposition in Plasma

In the *plasma polymerization*, the activation (formation of the reactive species) and deactivation (deposition of materials) are coupled, because the power input is directly applied to monomer gases and the polymerization occurs mainly in the glow region of a reactor. In essence, the activation of an organic molecule for the "glow" polymerization starts at the boundary of glow. The supply of the monomer into the glow volume is a crucially important factor because the monomer is consumed in the glow by depositing polymers and the numbers of polymer-forming species in the glow decreases. It has been well established that the *plasma polymerization* is primarily controlled by a composite power parameter, W/FM, where W is discharge power in Watts, and F is volume (or molar) flow rate, and M is molecular weight of the monomer. W/FM represents the energy input per unit mass of the monomer, which is given in J/kg [9].

Based on W/FM, plasma polymerization can be divided into two regimes; an energy deficient regime and a monomer deficient regime. In the energy deficient domain, ample monomer is available but the power input rate is not sufficient. In this domain, the deposition rate increases with the power input. In the monomer deficient (power saturated) domain, sufficient discharge power is available but the monomer feed rate is the determining factor for the deposition. It is important to note that these two domains cannot be identified based simply on the value of operational parameters. The domain can be identified only by the dependence of the deposition rate on operational parameter. In general, however, the following parameters can be used to judge whether the plasma polymerization is in the monomer deficient domain. When the energy input level expressed in J/kg exceeds roughly 20 times of the summation of bond energies in a monomer molecule expressed also in J/kg, the discharge can be considered to be in the monomer deficient regime [9].

Most experiments start from the power deficient domain, where the deposition of a plasma polymer can be expressed by the following expression.

$$k_1 = k'W \tag{1}$$
$$k_1/FM = k_0 = k'W/FM \tag{2}$$
$$k_0 = k' \, (W/FM) \tag{3}$$

where k_1 is the mass deposition rate, and k_0 is the specific (normalized) mass deposition rate.

The specific deposition rate k_0 is the only form of deposition rate that can be used to compare deposition characteristics of different monomers with different chemical structures and molecular weights under different discharge conditions (flow rate, system pressure and discharge power). Similarly W/FM can be considered the normalized discharge energy input. When only one monomer is employed, k_1 can be used to establish the dependency of deposition rate on operational parameters. Even in such a simple case, k_1 cannot be expressed by a simple function of W or F, and its relationship to those parameters varies depending on the domain of plasma polymerization.

As the power input is increased (at a given flow rate), the domain of plasma polymerization approaches the monomer deficient one, which can be recognized by the asymptotical approach of k_0 value to a horizontal line as the power input increases. In the monomer deficient domain, the deposition rate (asymptotic value) will increase as the flow rate is increased and shows a linear dependence on the monomer feed-in rate at a given discharge power and the system pressure, i.e.,

$$k_1 = k'' \, (FM.) \tag{4}$$

The relationship given by Eq. (4) is valid only in the monomer deficient domain. The further increase of the flow rate (FM) will eventually decrease the deposition rate as the domain of plasma polymerization changes to the energy deficient domain. Such a decreasing part can be expressed by Eq. (3). It is important to note that the deposition rate depends on the composite parameter W/FM. Consequently, an increase in flow rate (at a given discharge power) has the same effect as decreasing the discharge power (at a given flow rate), and conversely, an increase of discharge power has the same effect as decreasing the flow rate.

The data to show this relationship (previously presented [6]) are shown in Fig. 6. This figure illustrates how well the thickness growth rate, GR/FM, in 40 kHz and 13.5 MHz *plasma polymerization* of methane and n-butane, can be expressed as a function of the composite input parameter W/FM. It is important to recognize that regardless of the mass of monomer, flow rate, and discharge wattage, a single line fits all data obtained in 40 kHz or 13.5 MHz plasma polymerizations of hydrocarbons employed, in which the deposition occurs on an electrically floating conductor or on a dielectric substrate placed in the glow. This figure shows the asymptotical approach to the monomer deficient domain and also points out that the normalized deposition rate differs depending on the nature of the power source employed when an identical experimental setup, except for the power supply, is used.

<u>Deposition in Cathodic Polymerization</u>

When the same principle for *plasma polymerization* is applied to express the thickness growth rate in DC cathodic polymerization, it becomes quite clear that the cathodic "dark" polymerization is not the "glow" *plasma polymerization*. There is a clear dependence of the deposition rate on W/FM, but no universal curve can be obtained. In other words, the relationship given by Eq. (3) does not apply to the cathodic polymerization. The best universal dependency for DC cathodic polymerization is found between k_1/M and the current density. Fig. 7, reproduced from reference [6], depicts this relationship for all DC cathodic polymerization data, which were obtained in the same study, covering experimental parameters such as flow rate, size of cathode, mass of hydrocarbon monomers but at the same system pressure.
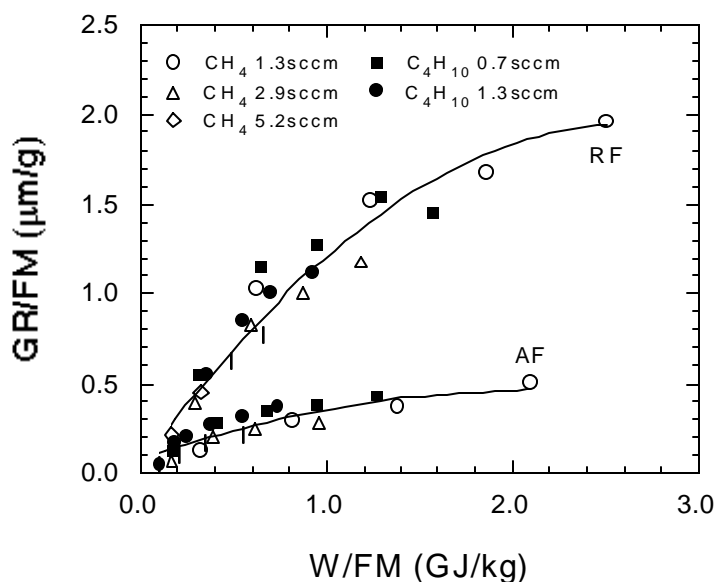
Figure 6. Dependence of GR/FM on W/FM for 40 kHz and 13.56 MHz plasma polymerizations: flow rate; methane 1.3, 2.9, 5.2 sccm, n-butane 0.7, 1.3 sccm.

  The implications of the correlation shown in Fig. 7 are as follows. 1) The energy input parameter (based on the plasma phase) does not control the deposition of material onto the cathode surface. 2) The current density of a DC glow discharge is the primary operational parameter. 3) The flow rate of monomer does not influence the film thickness growth rate. 4) The film thickness growth rate is dependent on the mass concentration of monomer (CM) in the cathode region rather than the mass input rate (FM). (In these experiments, the system pressure was maintained at a constant value of 50 mtorr, and thus C was a constant.)

The cathodic deposition, in general cases, can be expressed by the following equation;

$$k_1/[CM] = k_c [I] \tag{5}$$
$$k_1 = k_c [I][CM] \tag{6},$$

where [I] is the current density, and [CM] is mass concentration of monomer in the cathode regions of a DC discharge.

Since the mass concentration of monomer in the cathode region depends on the system pressure, the deposition rate in the cathode region should depend on the system pressure p;

$$k_1 = k'_c [I] p \tag{7}.$$

The relationship given by Eq. (7) is a conspicuous deviation from that for the "glow" *plasma polymerization*, in which the flow rate rather than the system pressure is the rate determining parameter and hence the deposition rat is independent of the system pressure (under a given flow rate). This difference, the pressure dependency, can be used as a tool to distinguish the "dark" and "glow" polymerizations.
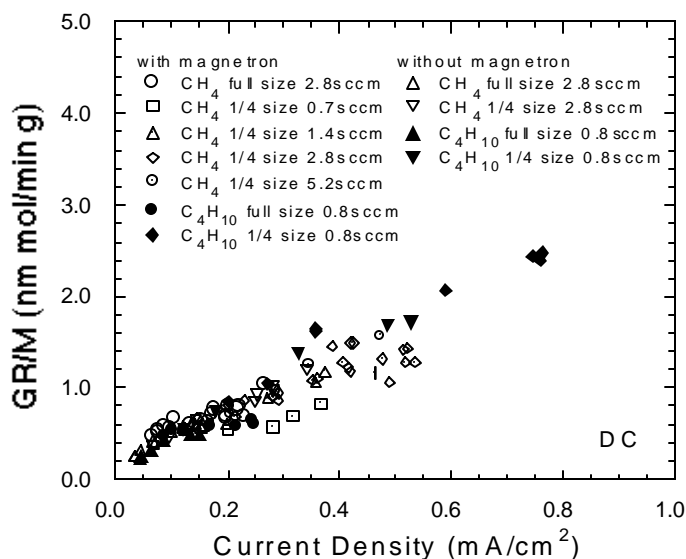
Figure 7. Dependence of GR/M on current density for DC cathodic polymerization with magnetron discharge: cathode size full, flow rate; methane 2.8 sccm, n-butane 0.8 sccm with magnetron discharge; cathode size 1/4; flow rate; methane 0.7, 1.4, 2.8, 5.2 sccm, n-butane 0.8

 sccm without magnetron discharge; cathode size full and 1/4, flow rate; methane 2.8 sccm, n-butane 0.8 sccm.

TMS Deposition on an Electrode in Alternating Current Discharges

An electrode in an alternating current discharge is the cathode in a half of the deposition time and the anode in the other half of the time. Comparing Eq. (3) and Eq. (7), the contribution of the cathodic polymerization can be estimated by examining the system pressure dependence of the deposition rate (at a fixed flow rate). If *plasma polymerization* is the dominant factor, it is anticipated that the deposition rate would be independent of the system pressure. If cathodic polymerization is the dominant factor, the deposition rate onto an electrode is dependent on the system pressure, and the value of deposition rate is expected to be one half of that for DC cathodic polymerization.

TMS deposition rate profiles in DC, 40 kHz and 13.56 MHz discharges are shown for electrode in Fig. 8 and for floating substrate in Fig. 9. It can be seen that, regardless of the frequency of electrical power source used, a uniform deposition of TMS plasma polymers was observed in the three plasma processes, although an appreciable edge effect occurred in the DC and a less pronounced effect occurred in the 40 kHz when the substrate was used as the cathode or powered electrode. The uniform distribution of deposition rates justifies the use of single measurement at the center of electrode.
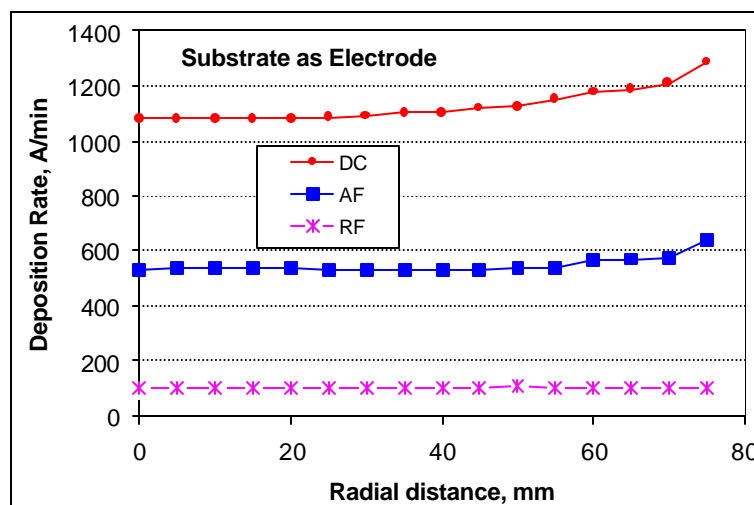
Figure 8. The deposition rate profiles of TMS in DC, 40 kHz, and 13.56 MHz plasma polymerization processes with substrate as electrode. Plasma conditions are 1 sccm TMS, 50 mtorr system pressure, 5 W power input.

Figs. 10 and 11 compare the deposition rates and refractive indices respectively of plasma polymers of TMS formed by DC, 40 kHz, and 13.5 MHz discharges. (Samples were collected at

 the center of the sample plates.) It is interesting to note that the deposition rate by 40 kHz glow discharge is one half of DC cathodic polymerization, when the substrate is used as an electrode. This indicates that an electrode in a 40 kHz discharge acts as the cathode of a DC discharge on the half cycle and that the cathodic polymerization is the main polymerization for the deposition onto the electrode surface, and also that the contribution of *plasma polymerization* to the deposition onto an electrode is minimal.
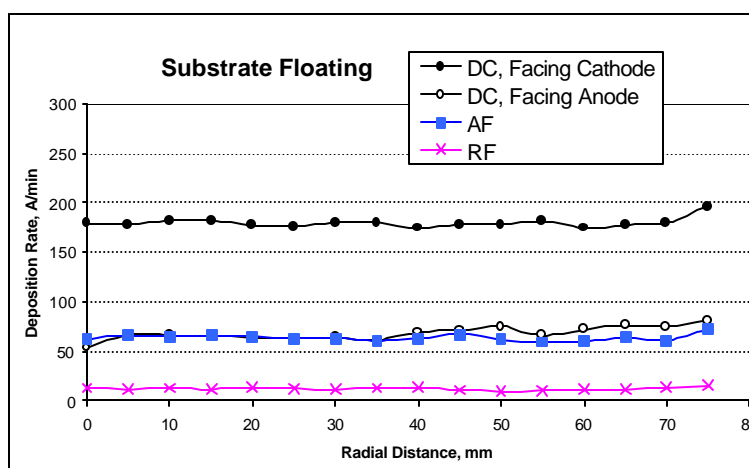
Figure 9. Deposition rate profiles of TMS in DC, 40 kHz, and 13.56 MHz plasma polymerization processes with substrate floating. Plasma conditions are 1 sccm TMS, 50 mtorr system pressure, 5 W power input.
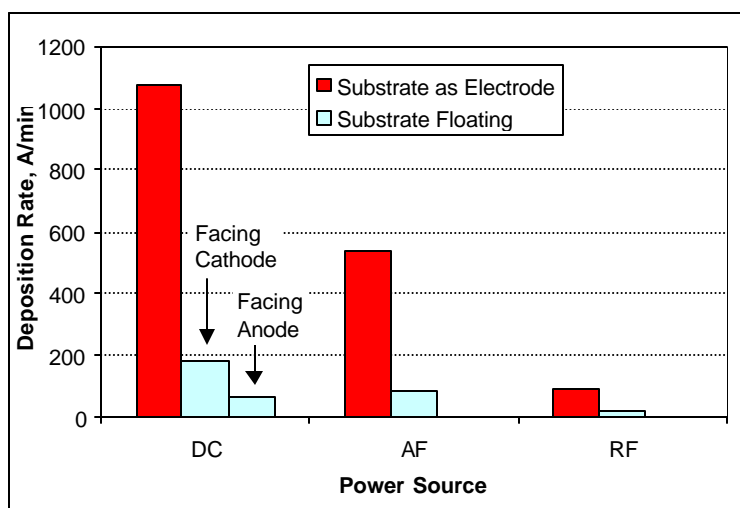
Figure 10. A comparison of deposition rate of TMS plasma polymers in DC, 40 kHz, and 13.56 MHz plasma polymerization processes. Plasma conditions are 1 sccm TMS, 50 mtorr system pressure, 5 W power input.
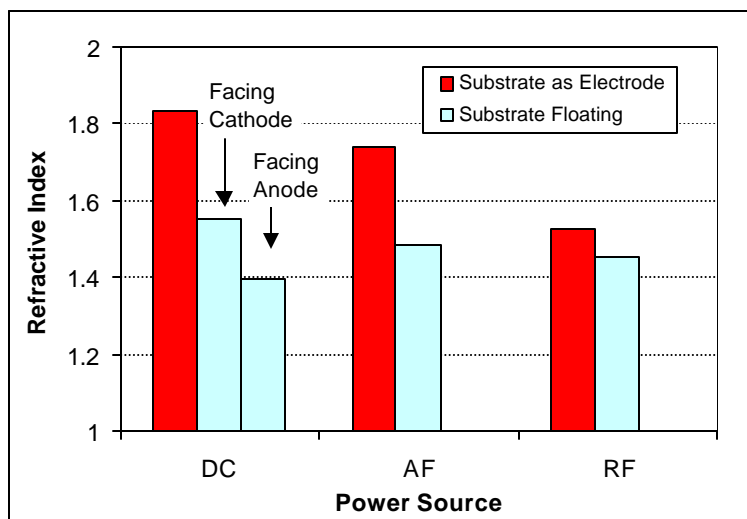
Figure 11. A comparison of refractive index of TMS plasma polymers in DC, 40 kHz, and 13.56 MHz plasma polymerization processes. Plasma conditions are 1 sccm TMS, 50 mtorr system pressure, 5 W power input.
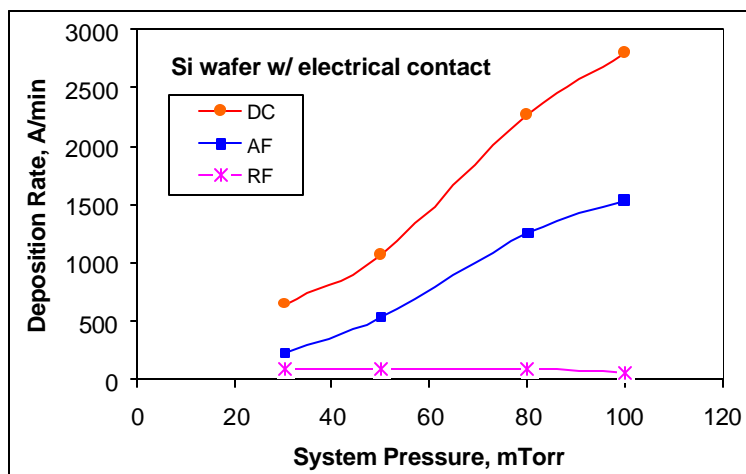
Figure 12. The system pressure dependence of deposition rate of TMS on Si wafer with electrical contact to the substrate used as powered electrode in DC (cathode), 40 kHz, and 13.56 MHz plasma polymerization processes. Plasma conditions are 1 sccm TMS, 5 W power input.

With electrically floating substrates, the deposition rates, as well as the refractive indices, are nearly the same for DC and 40 kHz glow discharges. Under the set of conditions employed, 13.5 MHz discharge yielded the lower deposition rate, but the refractive index was found nearly the same as those samples formed in DC and 40 kHz discharges. This implies that "glow" *plasma polymerization* in the negative glow of DC and those in 40 kHz and 13.56 MHz are essentially the same.
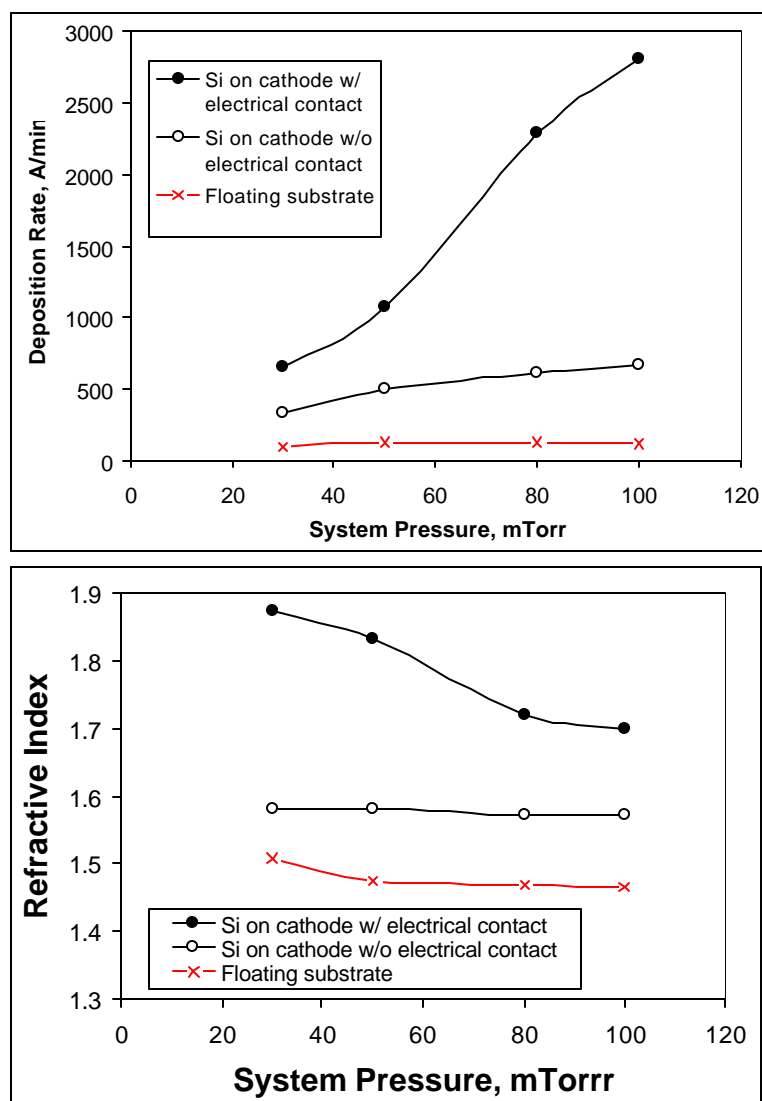
Figure 13. The system pressure dependence of deposition rate and refractive index of TMS in **DC** glow discharge polymerization. Plasma conditions are 1 sccm TMS, 5 W power input.

The system pressure dependence of the deposition rate onto the electrode surface in DC, 40 kHz and 13.56 MHz discharges are shown in Fig. 12. As anticipated from the deposition rate equation, given in Eq. (7), the deposition rate of DC cathodic polymerization is linearly proportional to the system pressure. The deposition rate in 40 kHz discharge was found to be pressure dependent also, but that in 13.56 MHz was found to be independent of system pressure. The deposition rate in the 40 kHz discharge is roughly one half of that in the DC discharge, and the slope of pressure dependence is also roughly one half of that obtained from DC discharge. These findings indicate that cathodic polymerization takes place on the electrode in a 40 kHz discharge.   As the frequency increases to 13.56 MHz, the electrode does not act as the cathode such as in DC or 40 kHz discharges, and the "glow" *plasma polymerization* then governs the

deposition onto the electrode. The species created in the glow deposit on the powered electrode in 13.56 MHz discharge.
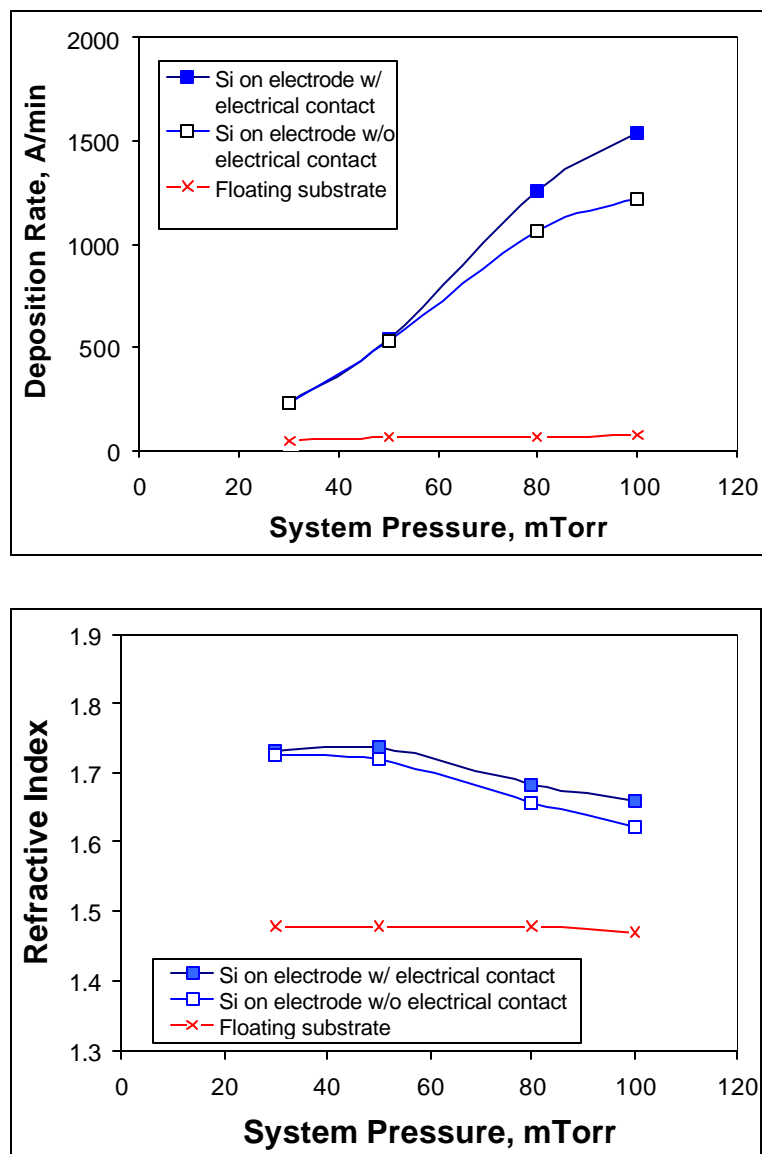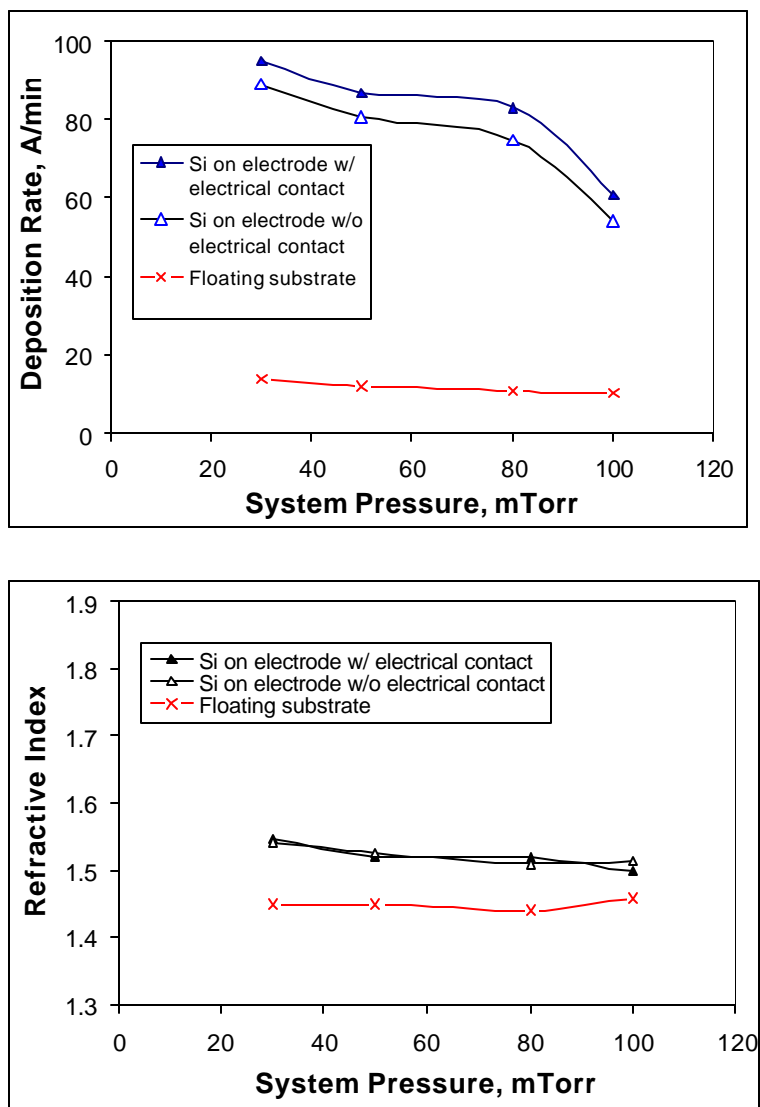

Figure 14. The system pressure dependence of deposition rate and refractive index of TMS on Si wafer with electrical contact and without electrical contact to powered electrode or floating substrate in **40 kHz** plasma polymerization processes. Plasma conditions are 1 sccm TMS, 5 W power input.

The deposition rates so far presented were calculated from the thickness of deposition that took place on a silicon wafer that was electrically connected to the aluminum alloy plate. In order to see the influence of electrical contact, some silicon wafers were electrically insulated from the

substrate plate by placing a thin slide cover glass between the silicon wafer and the substrate. The influence of the electrical contact on deposition rate onto the electrode and onto the floating substrate is shown in Figs. 13 – 15 as a function of system pressure. In the lower part of the figures, the influence of the same factors on the refractive index is shown. The scale of the deposition rate axis is different for each case in order to show the system pressure dependence clearly in each case.

Figure 15. The system pressure dependence of deposition rate and refractive index of TMS on Si wafer with electrical contact and without electrical contact to powered electrode or floating substrate in **13.56 MHz** plasma polymerization processes. Plasma conditions are 1 sccm TMS, 5 W power input.

In a **DC** discharge (Fig. 13), without electrical contact, the deposition rate differs significantly from that for cathodic polymerization (with electrical contact), and the pressure dependence is

marginal. The deposition onto a floating substrate can be characterized as typical "glow" *plasma polymerization*. A major difference in refractive index is seen between the electrode and non-electrode use of the substrates. If one considers that the overall DC plasma polymerization is a mixture of cathodic polymerization and *plasma polymerization*, the deposition on the cathode is primarily "dark" cathodic polymerization. With an insulating layer between the substrate and the cathode surface, there is no cathode dark space, and hence no "dark" cathodic polymerization that deposits polymer on the substrate. The substrate on the cathode surface without electrical contact or any non-cathode surface receives the products of "glow" *plasma polymerization*, which occurs in the negative glow.

In a **40 kHz** discharge (Fig.14), the deposition onto the surface of the electrode, regardless of electrical conductivity or contact, is significantly different from deposition onto a floating substrate. The cathodic aspect of the electrode is less (one half of DC discharge), but because of this the overall cathodic aspects of polymerization extend beyond the surface of the electrode yielding cathodic plasma polymer on an electrically insulated substrate placed on the electrode. Thus, the features of cathodic polymerization dominate in the vicinity of the electrode regardless of electrical contact.

In **13.56 MHz** discharge (Fig.15), the deposition onto the surface of an electrode, regardless of electrical conductivity or contact, is also appreciably different from that onto the floating substrate, although the magnitude of the difference is much smaller than those found in DC or 40 kHz discharges. However, the deposition on to the electrode has no feature of cathodic polymerization. In 13.56 MHz discharge, the deposition of materials is primarily by "glow" *plasma polymerization*, of which deposition rate is given by Eq. (3). The higher deposition rate on the electrode could be explained by the effect of the cathode fall. In RF discharge, however, the site of activation has shifted away from the electrode surface, and the features of cathodic polymerization diminished.

Deposition on Anode in DC discharge

In DC discharge, the relatively smaller amount of deposition occurs onto the anode surface than that occurs onto the cathode. The deposition pattern shows the shape of the cathode; i.e., a rectangular cathode produces a rectangular shape deposition on a larger square anode. The deposition on the anode surface is not pressure dependent as shown in Fig. 16.   When a floating substrate is placed in between the cathode and the anode, the deposition on the anode shows the shadow of the substrate as shown in Fig. 17. The size of shadow, in which no deposition is observed, is proportional to the size of the substrate that is placed in front of the anode (data not shown).

In DC cathodic polymerization, it has been found that the deposition of plasma polymers is controlled by the current density, a parameter of the cathodic region that is not a plasma in a strict sense [3]. To verify the current density dependence of the deposition rate, the deposition rate on the panels (cathodes) were plotted against the current density, which is shown in Fig. 11. It can be seen that, in Fig. 11, a linear dependence of deposition rate on current density was observed.
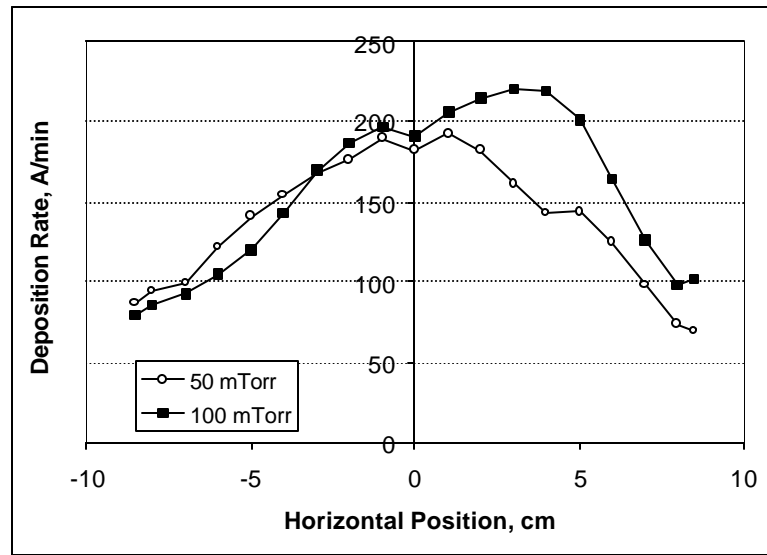
Figure 16. Plasma polymer deposition profile on anode surface in TMS DC polymerization. Conditions are 1sccm TMS, DC 5 W.
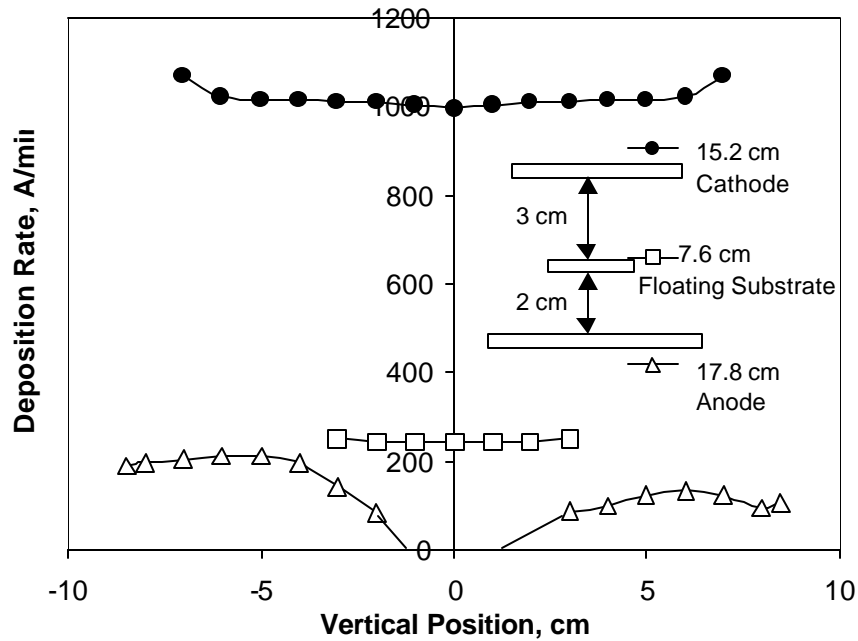

Figure 17. The effect of the floating panels positioned in front of the anode on the deposition rate on Anode surface and Cathode surface in DC glow discharge polymerization. Conditions are: 1 sccm TMS, 50 mtorr, DC 5 W, d = 100 mm.

These results indicate that the anode is a passive surface as far as the plasma polymerization is concerned, and the deposition does not differ from the floating substrate placed in between the cathode and the anode, which receives deposition by the "glow" *plasma polymerization* in the negative glow region. According to these results (within a set of experimental conditions employed), approximately 20 % of deposition is caused by the "glow" *plasma polymerization* in the DC discharge investigated in this study.

Conclusions

In DC glow discharge, the deposition of materials can be considered to be a mixture of "dark" cathodic polymerization, and "glow" *plasma polymerization* in the negative glow. The deposition onto the cathode surface is primarily by the "dark" polymerization, but the deposition onto any non-cathode surface including the anode surface is strictly by "glow" *plasma polymerization*, which occurs in the negative flow.

As the frequency of discharge power source increases, the feature of the "dark" cathodic polymerization decreases to the half of the DC, but in 13.5 MHz discharge, the influence of the "dark" cathodic polymerization totally disappears as the activation mechanisms changes to that by the oscillating electrons in the glow.

The cathodic polymerization yields plasma polymers with high refractive index values when the current density is high, indicating the high density of the materials. The refractive index decreases as the contribution of the "glow" *plasma polymerization* increases. The contribution of the cathodic polymerization decreases as the current density decreases.

References
1. T.F. Wang, T.J. Lin, D.J. Yang, J.A. Antonelli, H.K. Yasuda, *Prog. Org. Coat.*, **28,** 291 (1996).
2. H.K. Yasuda, T.F. Wang, D.L. Cho, T.J. Lin, J.A. Antonelli, *Prog. Org. Coat.*, **30,** 31 (1996).
3. C.M. Reddy, Q.S. Yu, C.E. Moffitt, D.M. Wiliczka, R. Johnson, J.E. Deffeyes, H.K. Yasuda, *Corrosion*, in press.
4. Q.S. Yu, C.M. Reddy, C.E. Moffitt, D.M. Wiliczka, R. Johnson, J.E. Deffeyes, H.K. Yasuda, *Corrosion*, in press.
5. C.E. Moffitt, C.M. Reddy, Q.S. Yu, D.M. Wiliczka, R. Johnson, J.E. Deffeyes, H.K. Yasuda, *Corrosion*, in press.
6. M. Miyama and H.K. Yasuda, *J. Appl. Polym. Sci.*, **70**, 237 (1998).
7. W.H. Tao, M.A. Prelas, H.K. Yasuda, *J. Vac. Sci. Technol.*, **A14**, 2113 (199
8. Q. S. Yu and H. K. Yasuda, *J. Polyme. Sci.: Part A: Polym. Chem.*, **36**, 1583 (1998).
9. H. Yasuda, *Plasma Polymerization*, Academic Press, Inc., Orlando, Florida, 1985.

19. Deposition of Trimethylsilane (TMS) in Glow Discharges, Part II: Direct Current (DC) Cathodic Polymerization on Multiple Cathodes (Substrates) Without Using Anode Assembly

Q.S. Yu and H.K. Yasuda*

Abstract

DC cathodic polymerization of trimethylsilane (TMS) was carried out in plasma reactors with and without using anode assembly. The deposition characteristics of TMS in such a process was examined and compared with conventional audio frequency (AF) and radio frequency (RF) plasma polymerization. In DC cathodic polymerization, the TMS plasma polymers are nearly exclusively deposited on the cathode (substrate) surface. As a result, fast deposition of TMS plasma polymers was easily achieved in DC cathodic polymerization as compared with AF or RF plasma polymerization. DC cathodic polymerization without using anode assembly has its advantageous features that the size and number of substrates (as cathodes) are not restricted by the size and the location of anode assembly. It was found that the maximum deposition rate on the cathode surfaces was obtained without anode assembly. The DC cathodic polymerization of TMS was conducted in a large volume reactor with multiple cathodes (substrates). The deposition mechanisms for DC cathodic polymerization applies also to the multiple cathodes, and uniform deposition on each cathode could be obtained with appropriate spacing and operational parameter based on the current density and the system pressure.

Introduction

Deposition of polymeric materials in a glow discharge, which is often referred to as "plasma polymerization" or "glow discharge polymerization", has been extensively investigated over the passed two decades [1,2]. The major portion of plasma polymerization processes has been done in radio frequency (RF) glow discharges. In RF glow discharge, plasma polymerization results in deposition on every surface exposed to plasmas and also on the surface in the down stream, including the reactor wall. In contrast, when a DC glow discharge is used for plasma polymerization, the deposition of plasma polymers occurs nearly exclusively on the cathode (substrate) surface [3,4]. This is an extremely favorable feature of DC glow discharge applied to conducting materials, because plasma polymers deposit preferably on the substrate (used as the cathode) and cause the least contamination of the reactor. It has been recently demonstrated that the deposition of plasma polymers in a DC glow discharge is a very effective and practical method to apply a thin layer of barrier coating to a metallic substrate that can be used as the cathode [5-12]. Interface engineering by means of plasma polymer deposition in DC glow discharges provided excellent corrosion protection for cold rolled steel [5,6] and aircraft aluminum alloys [7-12].

It is important to recognize that, in DC glow discharge, the deposition of plasma polymers mainly occurs in the cathodic region. The cathode region of a DC glow discharge is not plasma in a strict sense because a disparity exists in the density of positive charges and that of negative

  charges. Therefore, the deposition of plasma polymers in a DC glow discharge is very different from the conventional plasma polymerization, such as plasma polymerization in RF glow discharges. A more appropriate term of "DC cathodic polymerization" has been used to describe the plasma polymer deposition process in the cathodic region of a DC glow discharge [3].

Our recent study [4] indicates that, in DC glow discharge, the deposition of plasma polymers can be considered to be a mixture of "dark" *cathodic polymerization*, which is pressure dependent, and "glow" *plasma polymerization* in the negative glow, which is pressure independent under a fixed flow rate of monomer. The deposition onto the cathode surface is primarily by the "dark*"* *cathodic polymerization*, but the deposition onto any non-cathode surface, including the anode surface, is by "glow" *plasma polymerization*.

In DC glow discharge, the creation of reactive species occurs by electron-, ion-, and (excited neutrals)- impact dissociation of TMS in the cathode dark region and in the negative glow. With an alternating current discharge, the feature of the "dark" *cathodic polymerization* decreases to the half of the DC because an electrode is the cathode only in one half of the deposition time. In a high frequency discharge, such as 13.56 MHz of RF, the influence of the "dark" *cathodic polymerization* totally diminishes as the creation of reactive species changes to that by the oscillating electrons and associating species in the glow, and deposition of plasma polymers is mainly caused by "glow" *plasma polymerization*.

As follow up of our recent study [4] that deals with deposition of TMS in various discharges, this paper focus on the deposition of TMS in DC glow discharges, i.e., DC cathodic polymerization of TMS. Since DC cathodic polymerization mainly occurs in the cathodic region, the cathodic region parameters, such as current density and system pressure (or monomer concentration), have been found to be the controlling factors of the deposition and the characteristics of deposited films in DC discharge [3, 4]. In contrast, the other plasma parameters beyond the cathodic region, e.g., the removal of anode assembly, which is often used to confine the "glow", should have little or negligible effect on the "dark" *cathodic polymerization*. The removal of anode assembly from plasma system is of significant importance in the scaling-up process of DC cathodic polymerization, because the number, size, and shape of the substrates (cathodes) will no longer restricted by the anode assembly. In this study, therefore, the influence of anode on the deposition characteristics in DC cathodic polymerization was studied, and the possibility of DC cathodic polymerization without using anode assembly was investigated.

Experimental

<u>Materials</u>

Aluminum alloy panels of 2024-T3 (7.62 cm by 15.24 cm by 0.081 cm) purchased from Q panel Lab Products were used as the metallic substrates. Alkaline solution of Turco 4215S, a commercial alkaline cleaner, was used to clean the aluminum panels for removing the possible surface organic contaminants. Trimethylsilane (TMS) gas of 97% minimum purity was purchased from PCR, Inc. and used without further purification.

<u>Plasma reactor systems and operation</u>

Bell jar reactor

The DC cathodic polymerization and audio frequency (AF) and radio frequency (RF) plasma polymerization of TMS were carried out in a bell-jar type reactor. Inside the bell-jar, a pair of stainless steel plates (17.8 cm by 17.8 cm by 0.16 cm) was placed inside the bell-jar and used as two parallel electrodes, if not specified, with spacing of 100 mm. The substrate (or cathode) used in the plasma deposition process was an aluminum alloy panel positioned in the midway between the two parallel electrodes. The reactor system and operation procedures are exactly the same as described in our recent report [4].

2. Large volume reactor for DC cathodic polymerization on multiple cathodes
To conduct DC cathodic polymerization on multiple cathodes (substrates), a barrel type plasma reactor, which was fabricated by PlasmaCarb, Inc. Bedford, NH, USA, was employed in this study. The reactor chamber was made of stainless steel with 60 cm ID and 62.5 cm height. There is no anode assembly arranged inside the reactor chamber and the grounded stainless steel barrel functions as the anode during the gas discharge. The Al panels were loaded inside the chamber and used as the substrates (cathodes) for DC cathodic polymerization of TMS. In each batch, over 30 Al panels (7.62 cm by 15.24 cm by 0.081 cm) with spacing of 6 cm between each other can be loaded inside the chamber for plasma deposition.

Vacuum was created by a combined pumping system of Leroy-Somer model LS100L1RP mechanical pump and Cit-Alcatel model RSV600 booster pump. A pressure switch (Tripoint PA30A) is mounted between the mechanical and booster pump. When the vacuum in the reactor chamber reach a certain value, the blower turns on, otherwise turns off. The gas flow rate was controlled with an MKS mass flow meter and the chamber pressure was measured with a MKS 127 Baratron pressure transducer and MKS PRD-D-1 pressure readout. DC glow discharge was initiated by an MDX-1K magnetron drive.

Measurement of film thickness of plasma polymers

An AutoEL-II automatic ellipsometer (Rudolph Research Corporation), which is a null-seeking type with a 632.8 nm helium-neon laser light source, was used for measurement of the thickness and refractive index of deposited films in different glow discharges. For such a measurement, deposited films were all prepared on silicon wafers, which was sticking to the substrate with a drop of Silver print in order to achieve a good electrical contact in between. The thickness growth rate or deposition rate of the plasma polymers was calculated from the film thickness divided by deposition time.

Results and discussion

DC cathodic polymerization versus AF and RF plasma polymerization

In direct current (DC) cathodic polymerization, the activation of reactive species and deposition of polymers mainly occur in the cathodic region. At high frequency, e.g., radio frequency (RF), the oscillating electrons in the glow discharge are mainly responsible for the creation of polymer-

  forming species. As a result, in high frequency discharge, plasma polymerization occurs anywhere in the glow region between or beyond the two electrodes. In a glow discharge initiated by an alternating current power source, e.g., audio frequency (AF), the electrode can be visualized as an alternating cathode in half circle of time and anode in another half circle of time.

The deposition rate profile of TMS on the powered electrode (cathode in DC process) in DC, AF, and RF glow discharges are shown in Fig. 1. It can be seen that a pretty uniform deposition of TMS plasma polymers were observed in the three plasma processes, although a slight edge effect occurred in both DC and AF processes. The uniform distribution of deposition justifies the use of single measurement of deposition rate at the center of electrode.

Form Fig. 1, it was also noticed that, under similar plasma conditions, the deposition rate in DC process is much higher than that in AF or RF plasma polymerization process even when the substrate was used as powered electrode. It is interesting to note that, when the substrate is used as an electrode, the deposition rate in AF glow discharge is half of that in DC cathodic polymerization. This indicates that an electrode in an AF discharge acts as the cathode of a DC discharge on the half circle of time and the cathodic polymerization dominates the polymer deposition on the electrode surface. In RF discharge, however, deposition rate of TMS plasma polymers on the electrode surface is much lower than that in DC or AF discharge, which evidently indicate that the contribution of cathodic polymerization to the deposition onto an electrode diminishes in RF glow discharge.
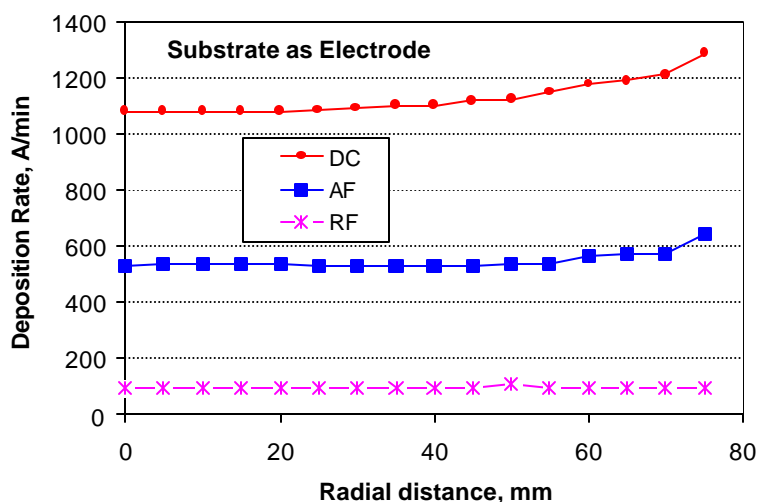
Figure 1. The deposition rate profiles of TMS in DC, 40 kHz, and 13.56 MHz plasma polymerization processes with (a) substrate as powered electrode (cathode in DC discharge). Plasma conditions are 1 sccm TMS, 50 mtorr system pressure, 5 W power input, anode spacing d = 100 mm.

The role of anode in DC cathodic polymerization

  In DC cathodic polymerization conducted in bell jar reactor, the cathode (substrate) is positioned in the middle between the two anodes. In such electrode arrangement, the distance between the cathode and the anode is expected to have some effects on the deposition rate and deposition profile with respect to those without anode assembly. Figs. 2 and 3 show the influence of the two-anode spacing on TMS deposition rate on **Cathode (i.e. substrate)** and **Anode** respectively.

From Fig. 2, it can be seen that, with the increase of anode spacing from 60 mm to 160 mm, the deposition rate on cathode (substrate) showed an increasing trend. The deposition on cathode (substrate) surface seemed to reach a maximum when the anodes were removed from the plasma system, i.e., no anode assembly was present and the grounded reactor wall functioned as anode. In contrast, it is noted that, from Fig. 3, the deposition on anode surface decreased with the increase of anode spacing. These results clearly indicated that the too close anode spacing could not only decline the preferred plasma polymer deposition on substrate (cathode), but also induced more undesired contamination on the anode surface. In other words, DC cathodic polymerization without using anode assembly seems to be a more efficient and realistic way in its practical applications.
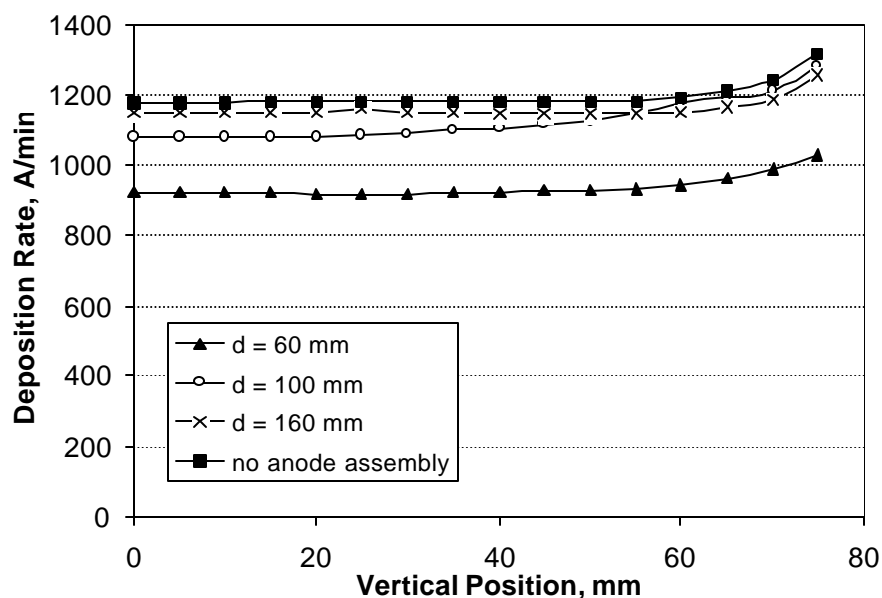
Figure 2. The influence of electrode distance on the deposition rate on **Cathode (i.e. substrate)** in DC cathodic polymerization. Conditions are: 1 sccm TMS, 50 mtorr, DC 5 W, d the distance between two anodes, d/2 is the distance between the cathode and an anode.

The original purpose of using anode magnetron was to eliminate the edge effect of plasma etching and to lower the break down voltage. It was found, however, that the edge effect is not a serious problem in plasma deposition [13]. As seen in Fig. 2, DC cathodic polymerization of TMS without using anode assembly gave rise to higher deposition than that with anode

 assembly. Therefore, the nature of anode and the role it plays in DC cathodic polymerization process need to be further investigated and clarified.
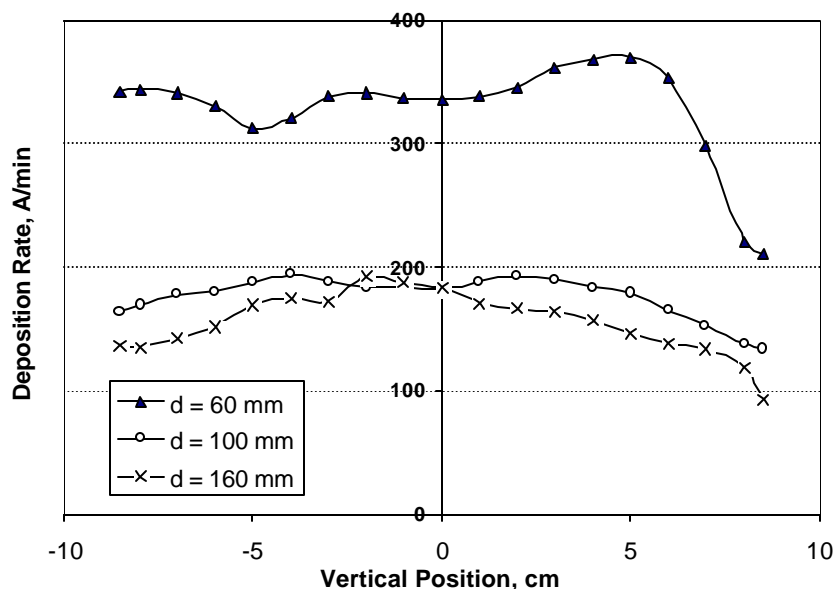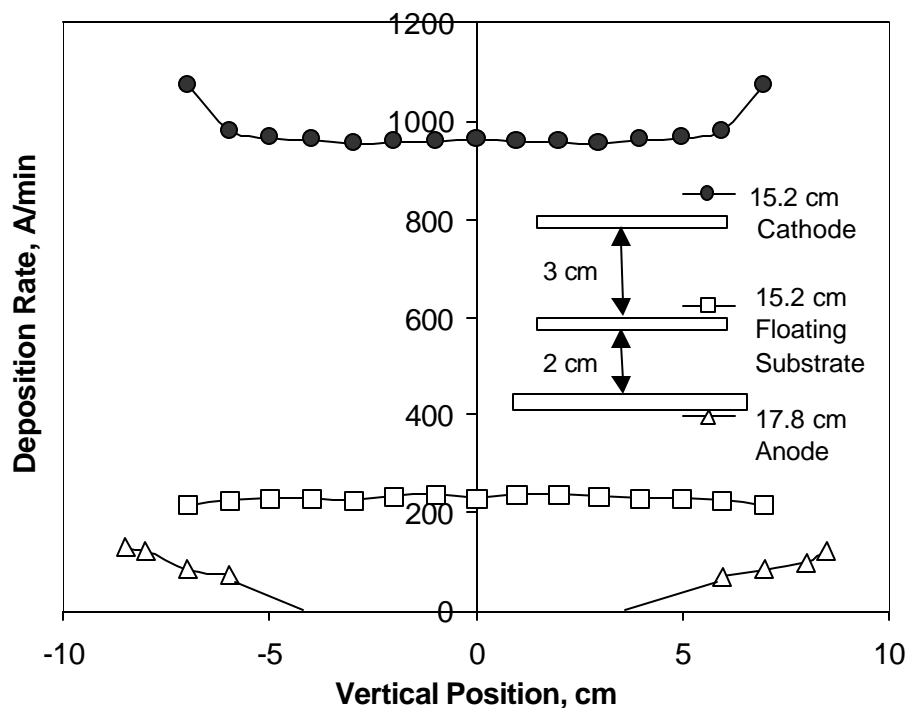

Figure 3. The influence of electrode distance on the deposition rate on **Anode surface** in DC cathodic polymerization. Conditions are: 1 sccm TMS, 50 mtorr, DC 5 W, d the distance between two anodes, d/2 is the distance between the cathode and an anode.

In DC discharge, as noted from Figs. 2 and 3, the relatively smaller amount of deposition occurs onto the anode surface than that occurs onto the cathode. Fig. 4 shows the effect of the floating panels positioned between anode and cathode on the deposition rate on Anode surface and Cathode surface in DC cathodic polymerization. It was noted that, from Fig. 4, the floating panels did not affect the plasma deposition on cathode. In contrast, they acted just as a surface cover of the anode and showed a similar deposition to that on anode. It is interesting to note that a declined deposition near the covered edges and no deposition were detected in the center of the covered anode due to the presence of the floating panels. These results indicate that the anode is a passive surface as far as the plasma polymerization is concerned, and the deposition does not differ from the floating substrate placed in between the cathode and anode. This also means that the anode, as a passive surface, collects polymerizing species created by the glow discharge polymerization and that the glow discharge polymerization deposits on the cathode surface also. When the passive surfaces are eliminated, the majority of the glow discharge polymerization also occurs on to the cathode surface. Thus, as noticed in Fig. 2, the deposition onto cathode increases with removing anodes.
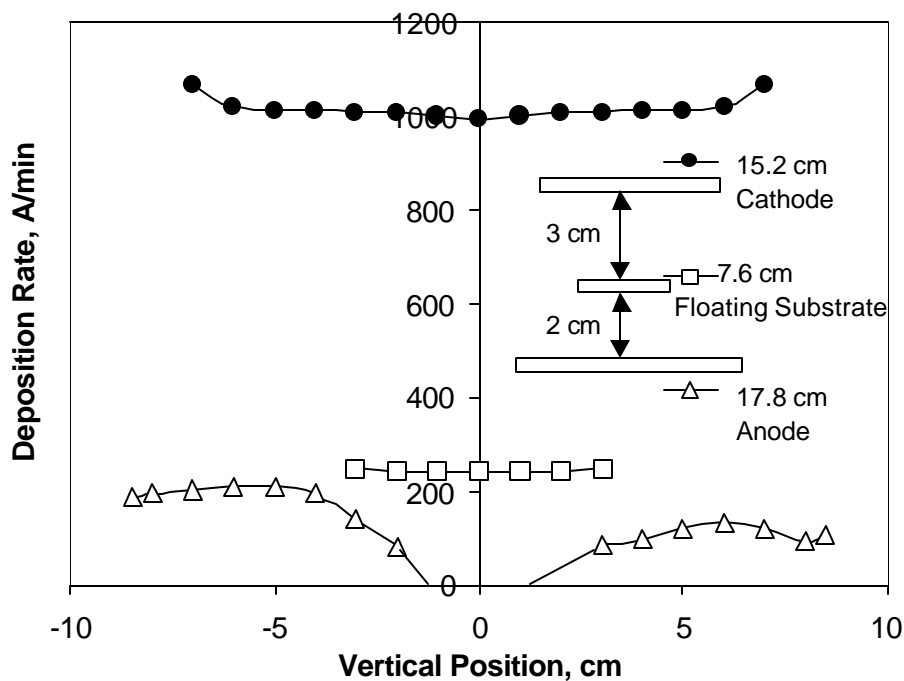
(a) 1/2 piece of Al panel in front of Anode

(b) 1 whole piece of Al panel in front of Anode

Figure 4. The effect of the floating panels positioned in front of the anode on the deposition rate on Anode surface and Cathode surface in DC cathodic polymerization. Conditions are: 1 sccm TMS, 50 mtorr, DC 5 W, anode spacing d = 100 mm, d/2 is the distance between the cathode and an anode.

DC cathodic polymerization of TMS on multiple cathodes without using anode assembly

As an initial step of the scaling-up of plasma polymerization process, DC cathodic plasma polymerization of TMS was carried out and investigated on multiple aluminum panels in a relatively big size (178 liter versus 70 liter bell-jar reactor), barrel type reactor, which was described in detail in experimental section. In such a reactor, no anode assembly was arranged inside the chamber. During the plasma polymerization process, the DC power was directly applied to the aluminum panels, which were loaded inside the reactor and used as the cathodes. The grounded reactor wall functioned as the anode during the DC discharge.

The effect of panel spacing on TMS deposition was studied with 5 Al panels in a row which acted as cathodes. The arrangement of the panels (cathodes) is schematically shown in Fig. 5. The deposition profiles on each panel (cathode) with three different panel spacing of 2, 4 and 6 cm are shown in Fig. 6. It can be seen that, in Fig. 6(a), 2 cm panel spacing is so close as to affect the monomer diffusion between the panels. Thus non-uniform deposition profile was found on all the 5 panels (cathodes).

It can be seen that, form Fig. 6, very uniform TMS deposition profiles were achieved on all the 5 panels in both cases of 4 and 6 cm panel spacing. As noted form Fig. 6 (b & c), one interesting aspect is that, in DC cathodic polymerization with a row of cathodes (panels), the deposition rate on the internal panels is about 200 ~ 300 Å/min higher than that on the outside surface of the external panels.
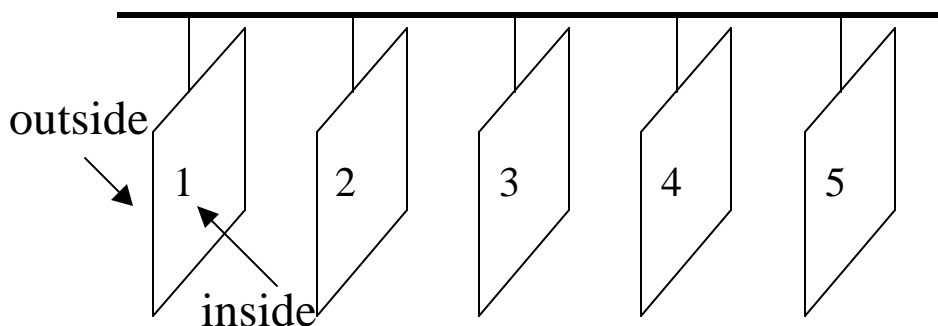
Figure 5. Schematic diagram of the arrangement of 5 panels used as the cathodes in DC cathodic polymerization of TMS without using anode assembly.
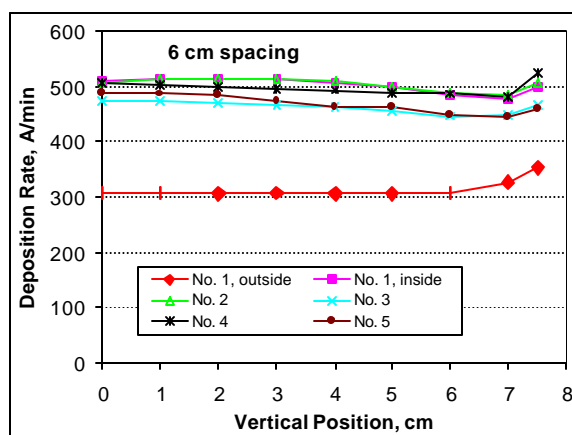
Fig. 7 shows the TMS deposition profile with 5 panels in a row at 100 mtorr under different DC power input. As seen from Fig. 7, the increase of DC power input from 5 watt to 25 watt significantly increased the deposition rate of TMS on the cathodes. Two interesting facts were noted from Fig. 7.
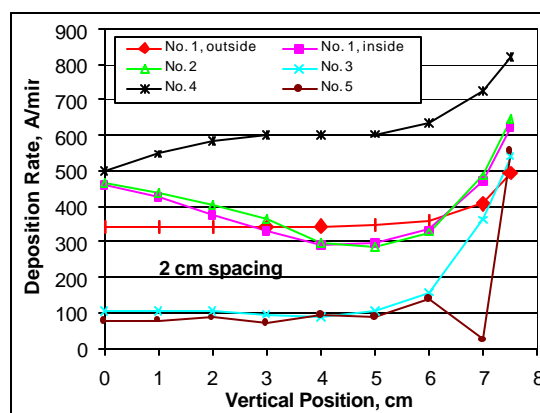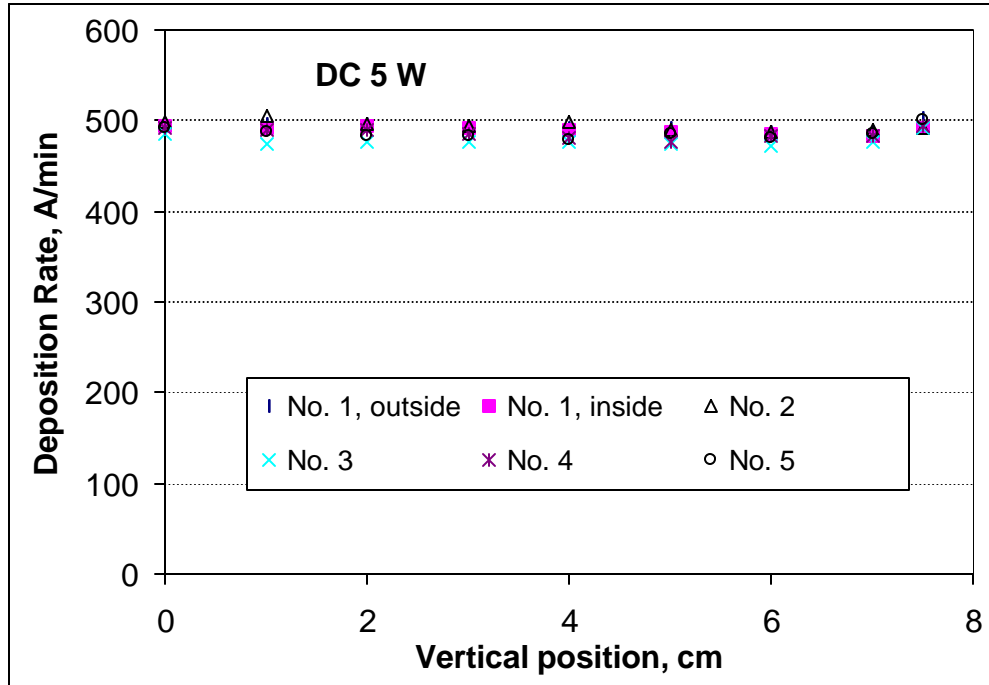
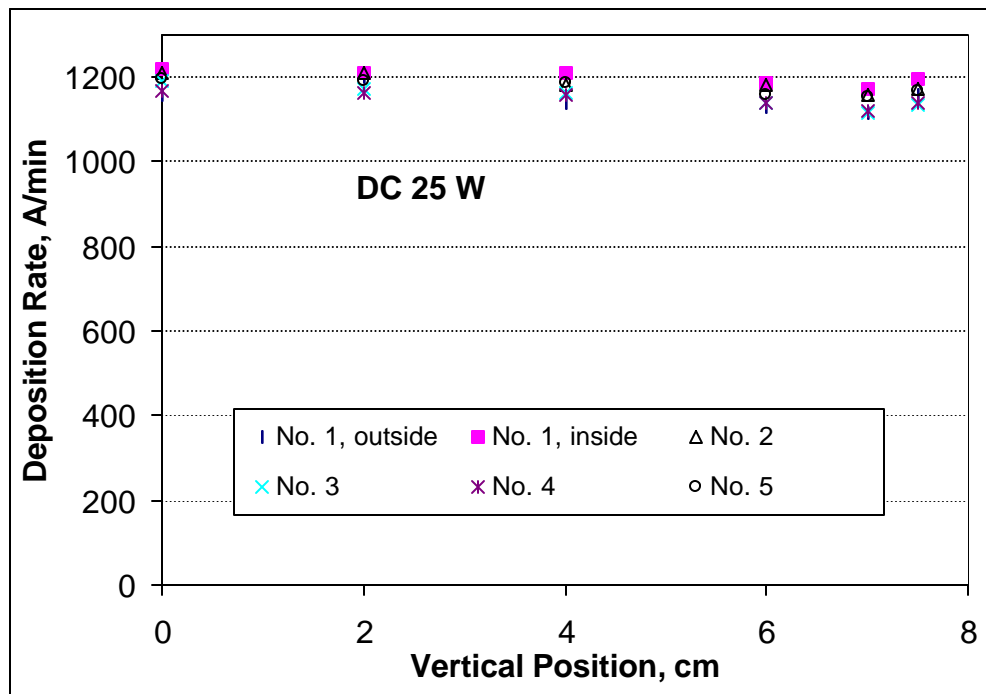(a) 2 cm panel spacing
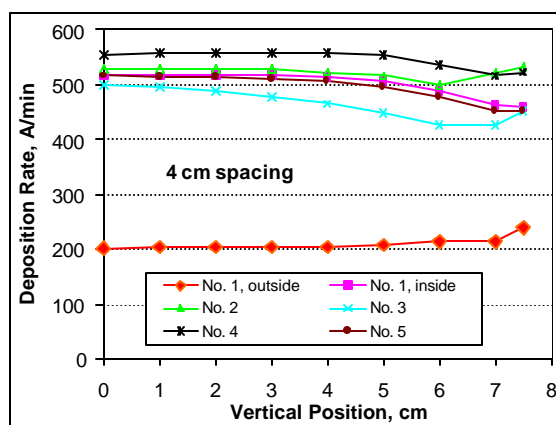
(b) 4 cm panel spacing

(c) 6 cm panel spacing

Figure 6. The effect of panel spacing on the deposition profile with 5 panels in a row as the cathodes of DC cathodic polymerization of TMS. Conditions are: TMS, 1 sccm, 50 mtorr, DC 5 W. Outside deposition was measured only on No. 1 panel.
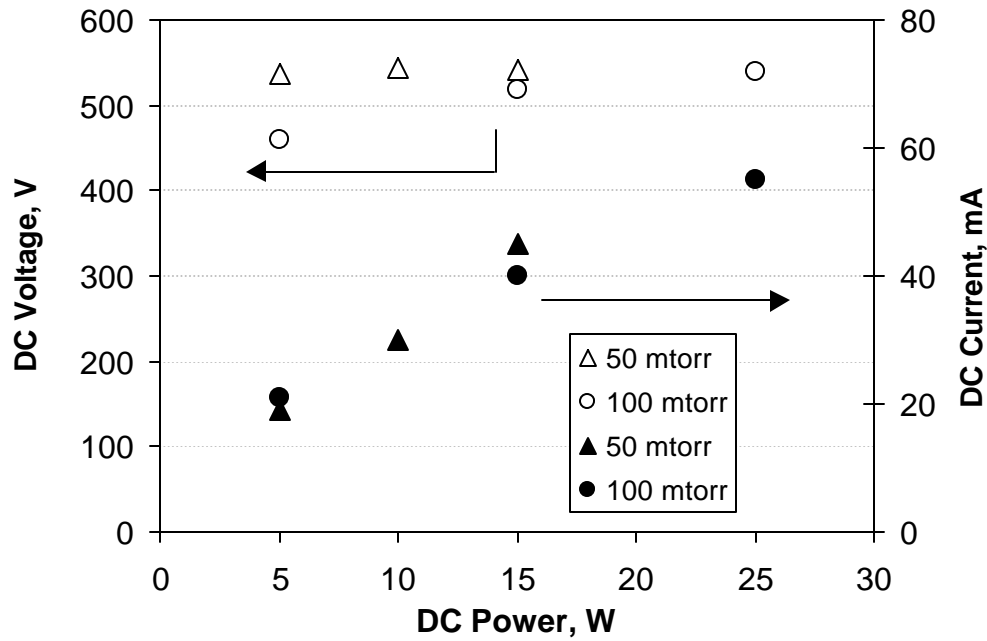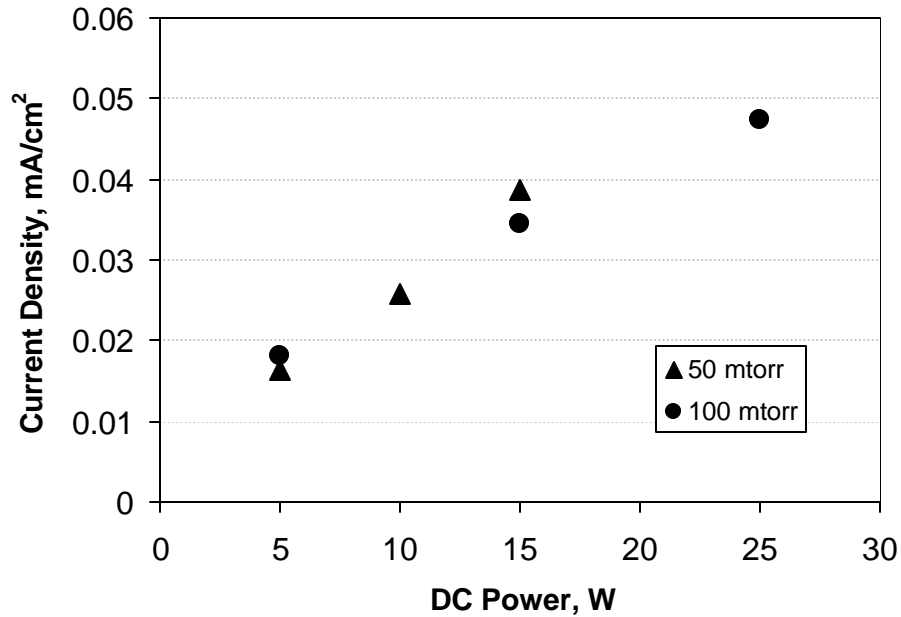
(a) DC 5 watt

(b) DC 25 watt

Figure 7. The effect of DC wattages, (a) 5 watt and (b) 25 watt, on the deposition profiles with 5 panels (cathodes) in a row with panel spacing of 6 cm. Conditions are: TMS, 1 sccm, 100 mtorr, 6 cm panel spacing. Outside deposition was measured only on No. 1 panel.

(a) Change of DC voltage and current

(b) Change of DC current density

Figure 8. The change of (a) voltage and current, and (b) the current density with DC power input in TMS glow discharge. Conditions are: 1 sccm TMS, 5 panels, 6 cm panel spacing.
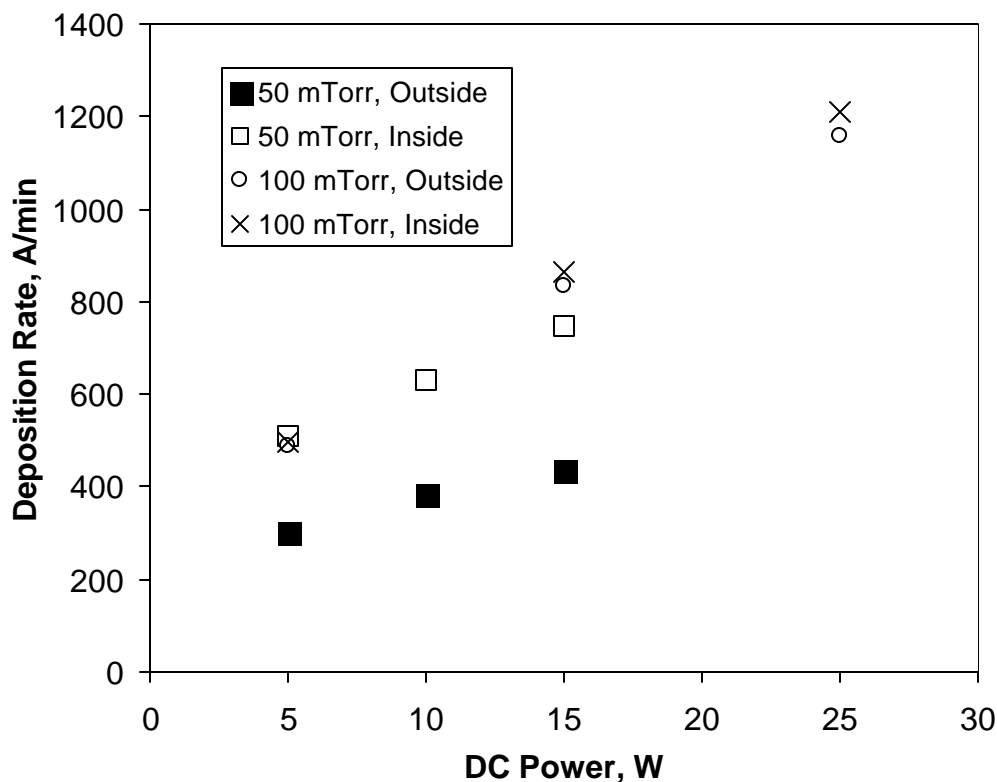
Figure 9. The dependence of TMS deposition rate on DC power input under different system pressures with 5 panels in a row. TMS flow rate was 1 sccm and the deposition rates were obtained on panel #1 as shown in Figure 5 with panel spacing of 6 cm.

The first is that the deposition difference disappeared between the two sides of the outer panels as noticed in Fig. 6. The second; the edge effect was depressed in comparison with that at 50 mtorr as observed in Fig. 6. As a result, an even more uniform plasma deposition was achieved with DC cathodic polymerization that was carried out at higher system pressure.

Fig. 8 shows the change of voltage, current, and the current density with DC power input in TMS discharge. It was noted that, from Fig 8(a), the increase of DC power input had little effect on the voltage but significantly increased the DC current flowing through the discharge. Regardless the system pressure difference, as shown in Fig. 8(b), a linear dependence of DC current density on power input was observed in DC glow discharge of TMS.

Fig. 9 shows the change of TMS deposition rate with DC power input at system pressure of 50 mtorr and 100 mtorr. As anticipated, a linear dependence of the deposition rate on DC power input was observed at both 50 mtorr and 100 mtorr system pressures, because current density had a linear dependence on DC power input. It should be noted that, in spite of multiple cathodes (substrate panels) being used, a pretty high deposition rate (> 1200 Å/min) was also achieved in DC cathodic polymerization of TMS. These results indicated that, in a large-scale plasma

reactor, the deposition rate of TMS on multiple panels can be significantly increased by properly adjusting the DC discharge parameters.
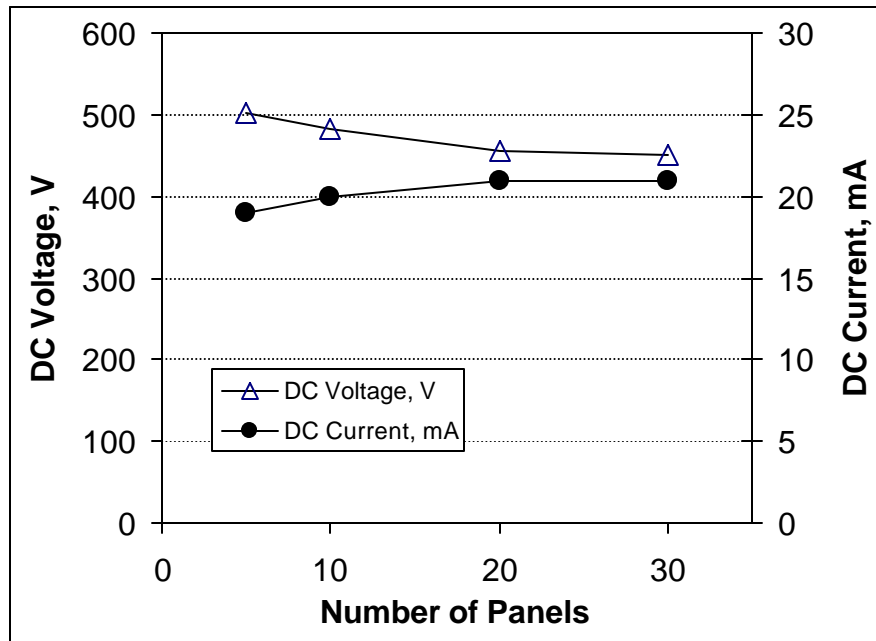
(a) DC voltage and current
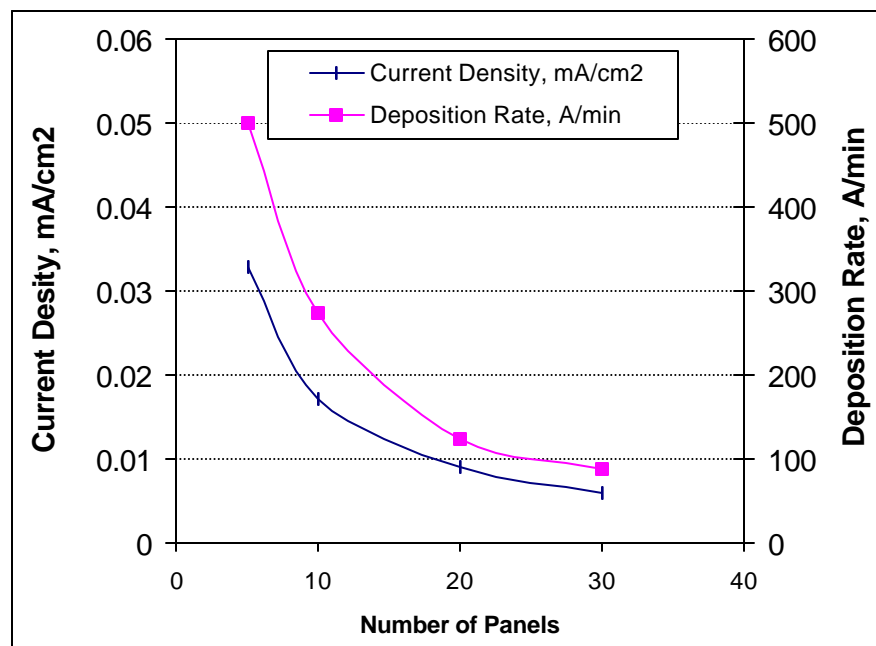
(b) current density and TMS deposition rate

Figure 10. The influence of panel numbers on (a) the plasma voltage and current, as well as (b) the current density and TMS deposition rate on the cathode (the panels). Conditions are: TMS, 1 sccm, 50 mtorr, DC 5 W, 6 cm panel spacing.
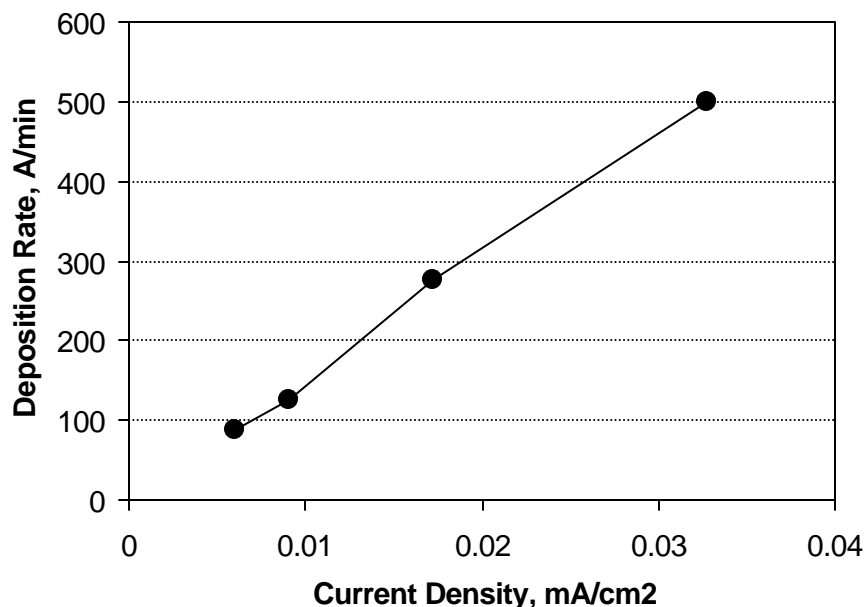
Figure 11. The current density dependence of deposition rate of TMS plasma polymers on the cathode (panels). Conditions are: TMS, 1 sccm, 50 mtorr, DC 5 W, 6 cm panel spacing.

The effects of the number of panels on the plasma parameters are shown in Fig. 10, in which TMS DC cathodic polymerization on multiple panels was conducted with power operation mode under a fixed plasma condition of DC 5 W, 1 sccm TMS and 50 mtorr. As seen from Fig. 10(A), with the same DC power input of 5 W, the increase of the panel numbers showed a little effect on the DC voltage and current during the deposition. As the panel number increased from 5 to 30, the voltage decreased about 50 V on a 500 V base and the current increased about 2 mA on a 20 mA base. Fig. 10(b) shows the panel number dependence of the current density and TMS deposition rate on the panel surfaces. With the increase of the panel numbers, a decreasing trend was observed for the deposition rate due to the decrease of DC current density.

Summary

1. The advantageous features of DC cathodic polymerization were further demonstrated as compared to plasma polymerization in AF and RF glow discharges. DC cathodic polymerization of TMS provided the fastest deposition of plasma polymers.

2. The increase of anode spacing gave an increasing trend of plasma deposition rate on cathode (substrate) surface. Under the similar plasma conditions, the DC cathodic polymerization of TMS performed without anode assembly showed the highest deposition rate on cathode (substrate) surface.

3. The experimental results indicate that, in a DC glow discharge, the anode is a passive surface as far as the plasma polymerization is concerned, and the deposition does not differ from the floating substrate placed in between the cathode and anode. As a result, DC cathodic polymerization can be simply performed without using the anode assembly. In such an

 operation, the size and number of substrates (cathodes) are no longer restricted by the anode assembly.

4. Multiple panels was used as the cathode without anode assembly. With a suitable cathode spacing about 4 cm for 7.6 cm x 15.2 cm panels, very uniform plasma coatings were achieved on all the aluminum panels.

5. The deposition mechanisms found for the cathodic polymerization (single cathode with anode assembly) also applies to the multiple cathodes without anode assembly. Accordingly the deposition rate of TMS on multiple panels (multiple cathodes) can be greatly increased by properly adjusting the DC glow discharge parameters in a large reactor.

References
[1] H. Yasuda, *Plasma Polymerization,* Academic Press, Inc., Orlando, Florida, 1990.
[2] R. d'Agostino, *Plasma Deposition, Treatment, and Etching of Polymers*, Academic Press, Inc., Boston, 1990: p. 163.
[3] M. Miyama and H.K. Yasuda, J. Appl. Polym. Sci., 70 (1998): p. 237.
[4] H.K. Yasuda and Q.S. Yu, "Deposition of Trimethylsilane in Glow Discharges", J. Vac. Sci. Technol., submitted.
[5] T.F. Wang, T.J. Lin, D.J. Yang, J.A. Antonelli, H.K. Yasuda, Prog. Org. Coat. 28 (1996): p. 291.
[6] H.K. Yasuda, T.F. Wang, D.L. Cho, T.J. Lin, J.A. Antonelli, Prog. Org. Coat. 30 (1996): p. 31.
[7] C. M. Reddy, Q.S. Yu, C. E. Moffitt, D. M. Wieliczka, , R. Johnson, J. E. Deffeyes, and H. K. Yasuda, "Improved Corrosion Protection of Al Alloys by Low Temperature Plasma Interface Engineering: Part I-Alclad 2024-T3 ", Corrosion, 56 (2000): p. 819.
[8] Q.S. Yu, C. M. Reddy, C. E. Moffitt, D. M. Wieliczka, R. Johnson, J. E. Deffeyes, and H. K. Yasuda, "Improved Corrosion Protection of Al Alloys by Low Temperature Plasma Interface Engineering: Part II-AA 2024-T3 ", Corrosion, 56 (2000): p. 887.
[9] C. E. Moffitt, C. M. Reddy, Q.S. Yu, D. M. Wieliczka, R. Johnson, J. E. Deffeyes, and H. K. Yasuda, "Improved Corrosion Protection of Al Alloys by Low Temperature Plasma Interface Engineering: Part III-AA 7075-T6", Corrosion, 56 (2000): p. 1032.
[10] Q.S. Yu, C. M. Reddy, C. E. Moffitt, D. M. Wieliczka, R. Johnson, J. E. Deffeyes, and H. K. Yasuda, "Improved Corrosion Protection of Al Alloys by Low Temperature Plasma Interface Engineering: Part IV-Spray Paint Primer Coated Al Alloys ", Corrosion, submitted.
[11] Q.S. Yu, J.E. Deffeyes, H.K. Yasuda, " Corrosion Protection of Ion Vapor Deposition (IVD) Al-Coated Al Alloys by Low-temperature Plasma Interface Engineering: part I: DC Cathodic Polymerization with Anode Magnetron Enhancement", Prog. Org. Coat., accepted.
[12] Q.S. Yu, J.E. Deffeyes, H.K. Yasuda, " Corrosion Protection of Ion Vapor Deposition (IVD) Al-Coated Al Alloys by Low-temperature Plasma Interface Engineering: part II: DC Cathodic Polymerization under Conditions of IVD", Prog. Org. Coat., Submitted.
[13] G. Zhao and H. K. Yasuda, "The Effect of Magnetic Field Configuration in the Cathodic Polymerization Systems with Two Anode Magnetrons", J. Vacuum Sci. & Tech., in press, (2000).

20. Deposition of Trimethylsilane (TMS) in Glow Discharges, Part III; DC Cathodic Polymerization In a Closed Reactor System

Qingsong Yu, C.E. Moffitt, D.M. Wieliczka, Hirotsugu Yasuda

Abstract

DC cathodic polymerization of trimethylsilane (TMS) in a closed reactor system was investigated. The composition of reactive species in the gas phase was monitored during the deposition process by a residual gas analyzer (RGA). It was found that, in such a closed plasma system, the deposition of TMS plasma polymers could be visualized as a three consecutive, time-delayed, fundamental processes. In the early stage of plasma deposition (< 60 sec after initiation of plasma), the deposition of plasma polymers was dominated by the polymerization of silicon-based species because the silicon-based species polymerized much quicker than carbon-based species. In the second stage of plasma deposition (between 60 to 120 sec), the deposition was then dominated by carbon-based species due to consumption of silicon in the early stage. In the final stage (more than 120 sec), because of the total consumption of all the polymerizable species in the system, the deposition stopped and the deposited plasma polymer surface was continuously treated by non-polymer forming gas plasma. As a result, the TMS plasma coatings obtained under such operations have a unique chemical structure that gradually changes from carbon rich (C/Si ratio of ~ 4.7 on the surface) to lower carbon (C/Si ratio of ~ 1.7 at the film/substrate interface), as identified by X-ray photoelectron spectroscopy (XPS) analysis.

Introduction

Deposition of polymeric materials in a glow discharge, which is often referred to as "plasma polymerization" or "glow discharge polymerization", has been extensively investigated over the passed two decades [1,2]. The major portion of plasma polymerization processes has been done in the high frequency regime, such as radio frequency (RF) glow discharges. The use of direct current (DC) glow discharge for plasma polymerization has not been the mainstream of studies and applications of plasma polymerization. Recent studies [3-9] have demonstrated, however, that the deposition of plasma polymers in a DC glow discharge is a very effective and practical method to apply a thin layer of barrier coating to a metallic substrate used as the cathode. Interface engineering by means of plasma polymer deposition in DC glow discharges provided excellent corrosion protection for cold rolled steel [3,4] and aircraft aluminum alloys [5-9].

In high frequency (e.g. RF) glow discharge, plasma polymer deposits on every surface exposed to the plasma and also on upstream and/or downstream surfaces, including reactor walls. In contrast, the deposition of plasma polymers in a DC glow discharge, which has been more appropriately termed as "DC cathodic polymerization" [10-12], has distinguished advantageous features related to coating metallic substrates (as the cathode) as compared with high frequency glow discharges. First, in DC cathodic polymerization, the deposition of plasma polymers occurs nearly exclusively on the surface of cathode (substrate). This is an extremely favorable feature of DC glow discharge applied to conducting materials, because plasma polymers deposit preferably on the substrate (used as the cathode) and cause the least contamination of the reactor.

Second, DC cathodic polymerization can be done without using an anode assembly, in which case the metallic reactor wall and/or the metal base plate function as the anode during the discharge. The removal of the anode assembly from a plasma system is of significant importance in the scaling-up of the DC cathodic polymerization process, because the number, size, and shape of the substrates (cathodes) will no longer restricted by the anode assembly. As a result, DC cathodic polymerization has been conducted on multiple metallic substrates (as cathodes) in a large volume reactor and reported in Part II of this series of studies [12].

In flow system plasma polymerization, a change in reactor size can be adjusted by the following basic principle. It is important to first maintain the same system pressure at which the process was initially developed in a smaller reactor to obtain particular desirable coating characteristics. In a larger volume reactor, a higher flow rate in proportion to the volume ratio should be employed and a higher discharge power should be applied to maintain the same W/F (power to flow) ratio. In cathodic polymerization, however, the controlling factor is not the flow rate, but the concentration of monomer in the vicinity of the cathode, which is proportional to the system pressure [10].   Since the system pressure is one of the main factors that control cathodic polymerization, there is a possibility that large monomer flow could be avoided by employing a closed system. A large volume reactor could provide a sufficient amount of monomer without the expense incurred using a flow regime. The details of cathodic polymerization in a flow system were reported in Part I and Part II of this series of studies.

The merit of closed system polymerization entirely depends on the characteristics of the coating that can be obtained by the method. The deposition process in such a closed system was investigated in this study.

Experimental

Materials

Alclad 7075-T6 Al alloy panels (3"×6"×0.032") used for the present study were procured from Q-Panel Lab Products (Cleveland, OH). Acetone wiping with Kimwipes® was used to clean the aluminum panels for removing the possible surface organic contaminants. Trimethylsilane (TMS) gas of 97% minimum purity was purchased from PCR, Inc. and used without further purification.

Plasma reactor system and operation

DC cathodic polymerization of TMS was carried out in a bell jar type reactor. The bell jar has the dimension of 635 mm in height and 445 mm in diameter (ID). There is no anode assembly arranged inside the bell jar. Two Al panels (forming a 6"×6" square) were placed in the center of the bell jar and used as the cathode of the plasma system. Upon initiating the glow discharge, the bottom stand of the bell jar, which is made of stainless steel, functions as the grounded anode. The DC plasma generator was an MDX-1K Magnetron Drive power supply (Advanced Energy Industries, Inc.).
The reactor chamber was first pumped down to < 1 mtorr. The reactor chamber was then isolated from the pumping system by closing the main valve located in between. TMS gas,

controlled by an MKS mass flow meter (model 247C), was then fed into the reactor. After the system pressure reached the preset point, TMS gas feeding was stopped and DC power was then applied to initiate the glow discharge to start cathodic polymerization. A residual gas analyzer (RGA) is connected to the plasma reactor (Leybold-Inficon Transpector 2 with a range of 200 amu controlled by Transpectorware^{TM}, version 3). The faraday cup sensor employed by this unit is attached to a Leybold-Inficon IPC-2 pressure converter system. The major components are the sampling valve, turbomolecular pump (Leybold-Inficon TMP-150), and rotary van pump. Quantitative RGA data were obtained by recording a mass spectrum for gases present in the isolated IPC-2 to correct background gases, then recording spectra of gases in the plasma reactor.

XPS analysis

X-ray photoelectron spectroscopy (XPS), also referred to as ESCA (electron spectroscopy for chemical analysis), data was acquired with a Kratos AXIS HS instrument, using the Mg-Kα flood source operated at ~217 watts (15 mA, 14.5 kV). Data were acquired in the combined electrostatic and magnetic, hybrid, lensing mode of the instrument. The 2 mm aperture used for these measurements limits collection to a spot size on the order of 200-300 μm in the hybrid mode. XPS depth profiles were done with a rastered Ar$^+$ beam and photoelectrons were collected at 90-degree take-off angle (surface normal) with 80eV pass energy. Peak area above a Shirley background was used in combination with the manufacturer's listed elemental sensitivity factors to generate compositional ratios. While possibly not precise on an absolute scale, this method assures that they are consistent comparisons both within an individual film and also across multiple samples.

The ion beam energy was 4 kV at a filament emission of 10 mA. This gives a current of about 1μA at the sample in a spot size of ~1.1 mm, which was rastered over an area of approximately 3x3 mm^2. Data were collected from near the center of this area. Charge compensation was made with the manufacturer's proprietary system, at settings of: -1.5 V charge balance voltage, 1.85 A filament current, and –0.5 V bias voltage.

 Measurement of thickness and refractive index

An AutoEL-II automatic ellipsometer (Rudolph Research Corporation), which is a null-seeking type with a 632.8 nm helium-neon laser light source, was used for measurement of the thickness and refractive index of deposited films in different glow discharges. For such a measurement, deposited films were all prepared on silicon wafers attached to the panel substrates with double sieeded tape during the deposition. A drop of silver paint was also used in order to achieve a good electrical contact. The thickness growth rate or deposition rate of the plasma polymers was calculated from the film thickness divided by deposition time.

Results and discussion

In flow system plasma polymerization, the system pressure is continuously adjusted by controlling the opening of a throttle valve connected to the pumping system. Because of fragmentation of the original monomer in the plasma state, the composition of the gas phase changes on the inception of the plasma. The increase in the total number of gas molecules is

 compensated by the increased pumping rate in a flow system, and a steady state flow of a consistent composition of gas phase is established at a pre-determined system pressure.

In closed system plasma polymerization, a fixed amount of monomer molecules are contained in the reactor, and glow discharge is initiated. The system pressure in such a system (in a given volume) is proportional to the total number of gas phase molecules. The fragmentation of monomer molecules as well as the ablation of gaseous species from the deposited material will increase the pressure, while deposition will decrease the system pressure. Thus, the change in system pressure with plasma polymerization time will indicate the change in the overall balance between the plasma fragmentation/ablation and the plasma film deposition.

Fig. 1 depicts the system pressure change in a closed system reactor when plasma polymerization of TMS is carried out. The system pressure continuously increases while the glow discharge is on, but remains at a constant value as soon as the glow discharge is turned off. This indicates that the total number of gas phase species increases with time in spite of the deposition of plasma polymer of TMS. A Residual Gas Analyzer (RGA) characterized the gas phase composition of TMS plasma in the closed reactor system. The most significant gas phase species identified in TMS plasma system are summarized in Fig. 2. It can be seen that the main gas phase species from the fragmentation of TMS monomers are hydrogen molecules and carbon-containing or silicon-containing molecular segments.
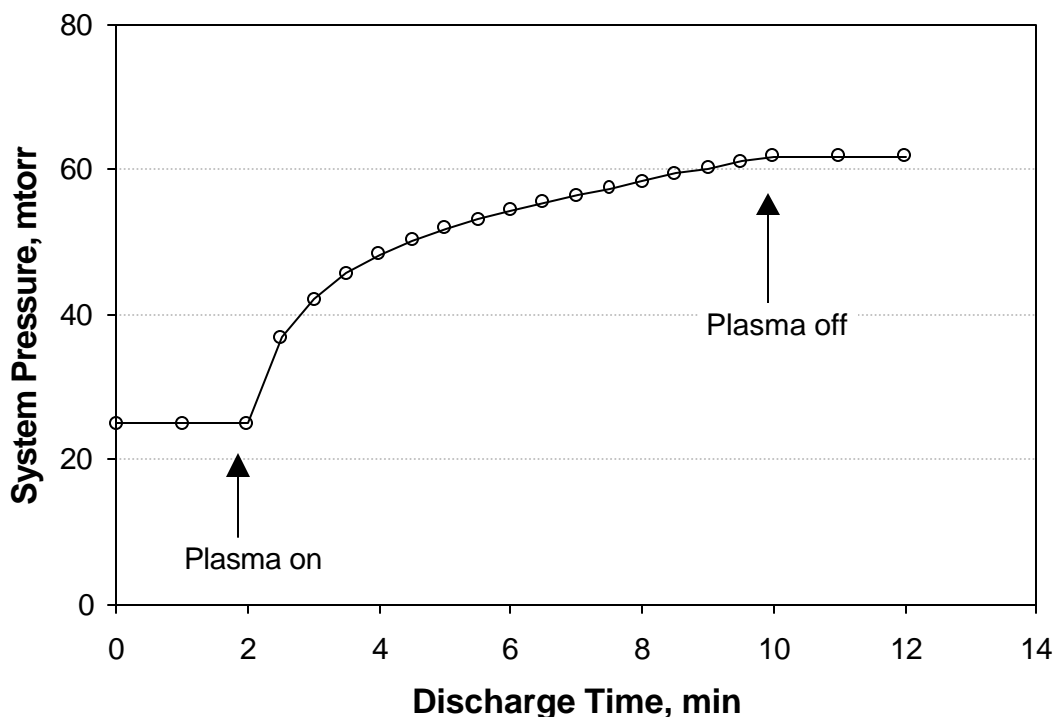

Figure 1. Increase of system pressure during closed system plasma polymerization of TMS. Plasma conditions are: 25 mtorr TMS, 2 panels of Alclad 7075-T6, DC 1000 V.
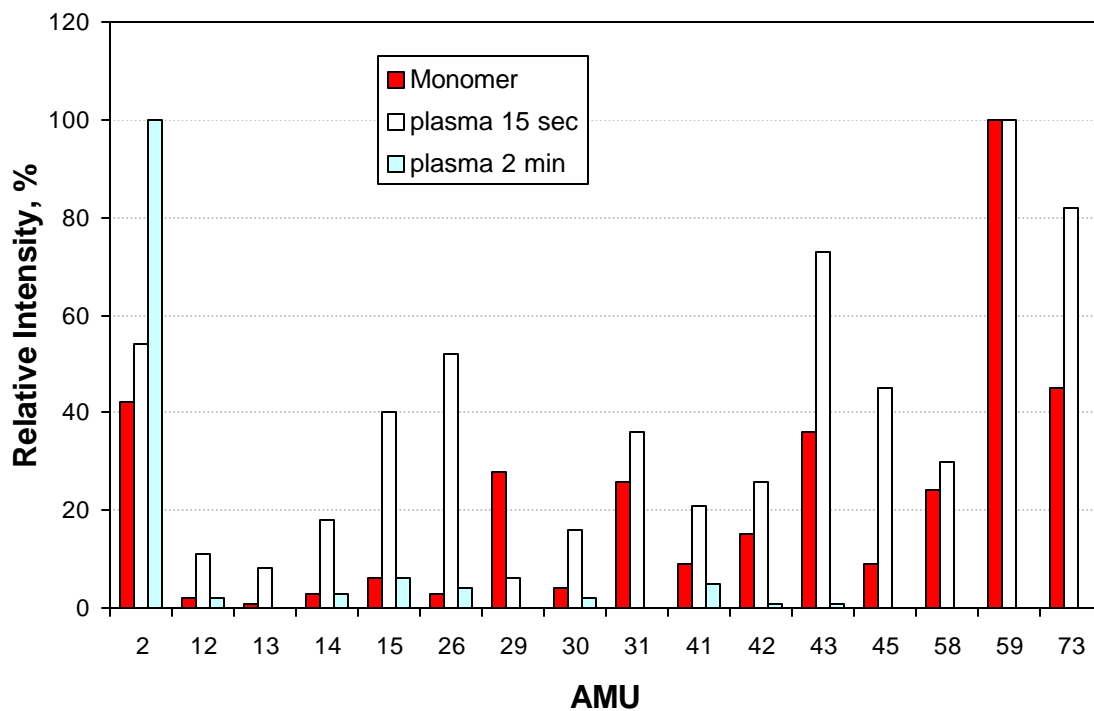
Figure 2. The most significant gas phase components observed in closed system TMS plasmas. Plasma conditions are: TMS 25 mT, 2 panels of Alclad 7075-T6, DC 1000 V.
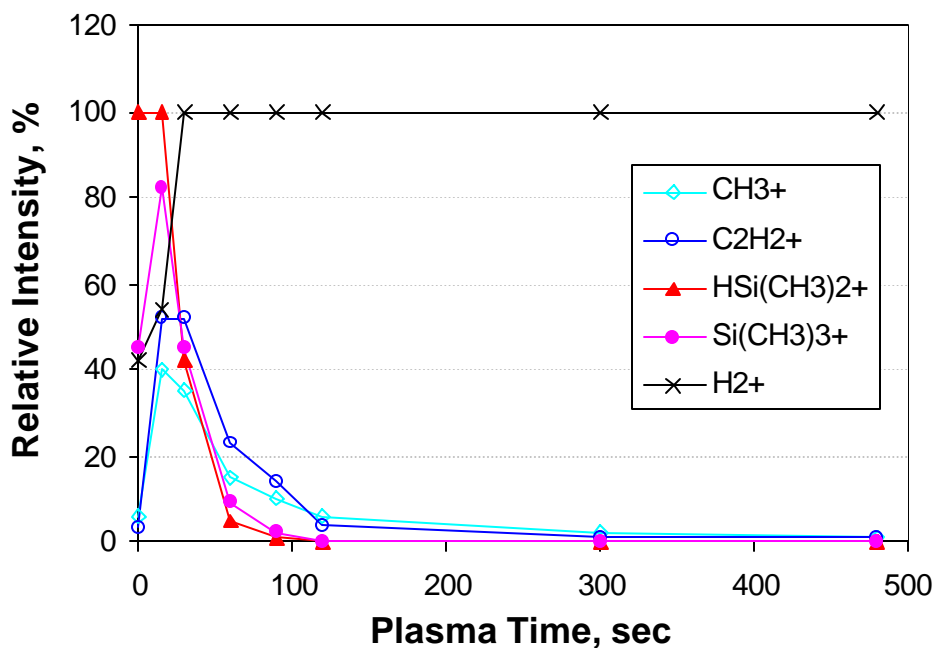

Figure 3. Change of gas phase species in plasma of TMS with plasma time. Plasma conditions are: 25 mtorr TMS, 2 panels of Alclad 7075-T6, DC 1000 V.

Fig. 3 shows the discharge time dependence of several representative gas phase species in the closed TMS plasma system. In the early stage of the discharge, such as in the first 60 seconds, silicon-containing species were the dominant species in the system. Because of the fast deposition characteristics of silicon species [13], the silicon-containing species disappeared very quickly. After 60 seconds of deposition, very few silicon-containing species remained in the gas phase in the plasma system. The similar trends were reported in a closed system polymerization of hexamethyldisiloxane (HMDSO) by R.F. glow discharge [14].

From Fig. 3, it is noted that, in the early stage of discharge, the organic carbon species (no silicon content) had lower intensity than silicon-containing species. After 60 seconds of deposition, the carbon-containing species outnumber the silicon-containing species in the plasma system. At this stage, the deposition is dominated by carbon-containing species due to prior consumption of silicon moieties.

In the final stage, after 120 seconds, both the silicon-containing and carbon-containing species have been consumed by the plasma deposition. In the gas phase, only hydrogen is left in the plasma system and no further deposition occurs. Therefore, it is anticipated that there will be no further thickness growth of the TMS plasma coatings after 120 seconds.
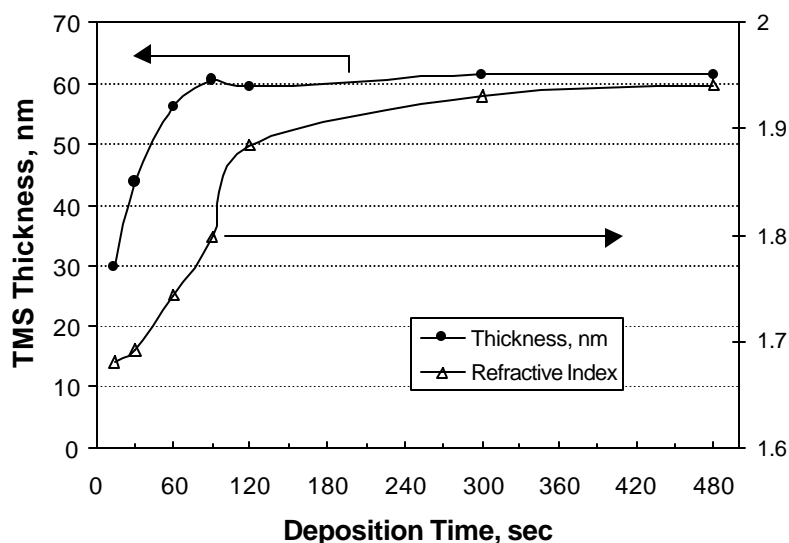

Figure 4. Changes in thickness and refractive index of TMS plasma coatings with discharge time in a closed reactor system. Plasma conditions are: TMS 25 mT, 2 panels of Alclad 7075-T6, DC 1000 V.

Fig. 4 shows the time dependence of the thickness and refractive index of TMS plasma coatings on the plasma polymerization time in a closed reactor system. It can be seen that the coating thickness increases very fast in the first 90 seconds. After 90 seconds, the TMS coating thickness stops growing with additional deposition time. The refractive index of the TMS coating, however, does keep increasing with the deposition time. This increase obviously results from the continuing bombardment by the active plasma species. It should be noted that the times

referred in this discussion are confined to the specific conditions used in the specific reactor. The characteristic times (for TMS) vary depending on the size of reactor, the system pressure, the size of cathode and the current density.

In a separate study, it was found that the characteristic plasma deposition rate of Si-containing organic compounds is nearly six times greater than that of hydrocarbons [13]. In plasma polymerization, a significant extent of fragmentation of the original monomer molecules occurs, and direct deposition of the original molecules is an unlikely event. It is therefore anticipated that Si-containing moieties would deposit faster than C-based moieties leading to a Si-rich depositions from TMS, which contains one Si and three C in the original molecule. This difference in the characteristic deposition rates would be amplified if the plasma polymerization is carried out in a closed system, because the gas phase composition with respect to Si and C changes continuously, and the composition of the deposition changes accordingly. Therefore, it is anticipated that the closed system deposition of TMS would lead to a graded composition film.
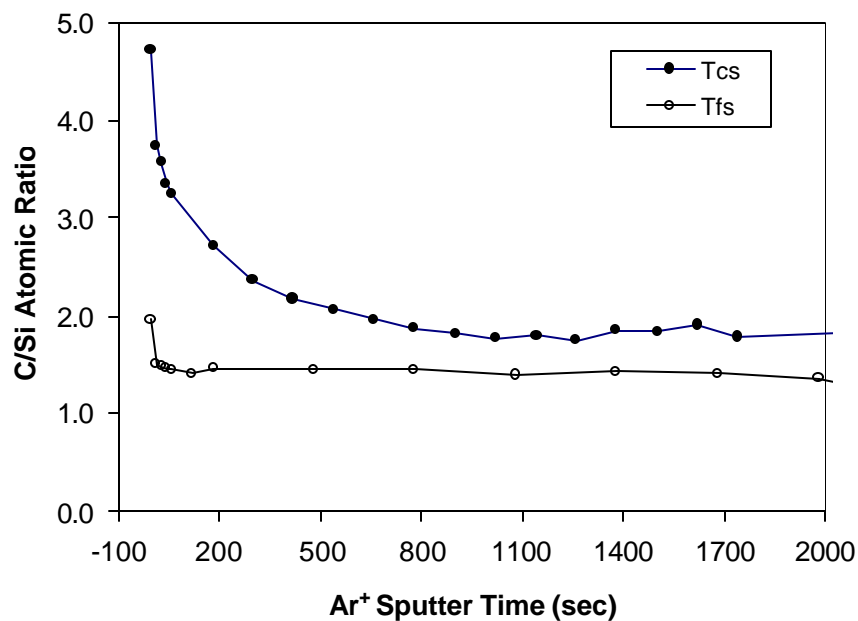

Figure 5. C/Si ratios of plasma polymer films of TMS prepared in a flow system reactor (Tfs) and in a closed system reactor (Tcs), as generated by XPS depth profiling.

According to this scheme of closed system plasma polymerization of TMS, it is anticipated that the atomic composition of the plasma polymer should continuously change with the plasma polymerization time. Fig. 5 depicts the comparison of XPS depth profile generated C/Si ratios for plasma polymers deposited in both a flow system reactor and in a closed system reactor. As noted in Fig. 5, the TMS plasma coating prepared in a closed system shows gradual composition changes from carbon rich (C/Si ratio of ~ 4.7) at the surface to a lower carbon content (C/Si ratio of ~ 1.7) at the interface with the substrate. In contrast, the coating obtained in the flow system

had a uniform composition throughout the film. These results clearly show that closed system plasma polymerization of TMS indeed produces a film with graded composition; i.e., with decreasing carbon content from the surface of the film into the bulk film and to the film/metal interface.

Considering the fact that the system pressure continues to increase after most of the polymerizable species are exhausted in the gas phase, plasma polymerization of TMS in a closed system contains the aspect of plasma treatment of once deposited plasma polymer coating. In the later stage of closed system polymerization, oligomeric moieties loosely attached to three-dimensional network are converted to more stable form, and improved corrosion protection characteristics were found compared to the counterpart in flow system polymerization of TMS, of which details will be presented eslwhere. Thus the merit of closed system cathodic polymerization is well established.

Summary

DC cathodic polymerization of TMS in a closed reactor system can be visualized as a time-delayed, consecutive application of three fundamental processes. The sequence takes the order of 1) deposition of Si-species, 2) deposition of C-species, and 3) plasma treatment and ablation of the deposited plasma polymers by the non-polymer forming plasma. These points clearly explain the gradual structure change, as identified by XPS, of closed system TMS coatings from higher carbon composition at the surface to lower carbon composition in the bulk film and to the film/metal interface. .

References

[1] H. Yasuda, *Plasma Polymerization,* Academic Press, Inc., Orlando, Florida, 1985.

[2] R. d'Agostino, *Plasma Deposition, Treatment, and Etching of Polymers*, Academic Press, Inc., Boston, 1990: p. 163.

[3] T.F. Wang, T.J. Lin, D.J. Yang, J.A. Antonelli, H.K. Yasuda, Prog. Org. Coat. 28 (1996): p. 291.

[4] H.K. Yasuda, T.F. Wang, D.L. Cho, T.J. Lin, J.A. Antonelli, Prog. Org. Coat. 30 (1996): p. 31.

[5] C. M. Reddy, Q.S. Yu, C. E. Moffitt, D. M. Wieliczka, , R. Johnson, J. E. Deffeyes, and H. K. Yasuda, Corrosion, 56 (2000): p. 819.

[6] Q.S. Yu, C. M. Reddy, C. E. Moffitt, D. M. Wieliczka, R. Johnson, J. E. Deffeyes, and H. K. Yasuda, Corrosion, 56 (2000): p. 887.

[7] C. E. Moffitt, C. M. Reddy, Q.S. Yu, D. M. Wieliczka, R. Johnson, J. E. Deffeyes, and H. K. Yasuda, Corrosion, 56 (2000): p. 1032.

[8] Q.S. Yu, C. M. Reddy, C. E. Moffitt, D. M. Wieliczka, R. Johnson, J. E. Deffeyes, and H. K. Yasuda, Corrosion, submitted, 2000.

[9] Q.S. Yu, J.E. Deffeyes, H.K. Yasuda, Prog. Org. Coat., accepted, 2000.

[10] M. Miyama and H.K. Yasuda, J. Appl. Polym. Sci., 70 (1998): p. 237.

[11] H.K. Yasuda and Q.S. Yu, J. Vac. Sci. Technol., submitted, 2000

[12] Q.S. Yu and H.K. Yasuda, submitted, 2000.

[13] Q.S. Yu and H.K. Yasuda, J. Polym. Sci.: Part A: Polym. Chem., 37 (1999) 967.

[14] H.-U. Poll, J. Meichsner, M. Arzt, M. Friedrich, R. Rochotzki and E. Kreyssig, Surface and Coatings Technology, 59 (1993) 365-370.

21. ESR study of the plasma polymerizations of trimethylsilane and methane

F.F. Oldfield, D.L. Cowan, and H.K. Yasuda

Abstract

Electron Spin Resonance (ESR) was used to study, at the molecular level, the plasma polymerization of trimethylsilane (TMS) and methane. Direct ESR analysis of the plasma coated Al substrate required the use of a novel ESR technique. TMS plasma deposit on Al showed a single broad resonance line near g=2.003. The signal was stable in vacuum and decayed on exposure to air, with a significant fraction persisting for days. Results show that this signal arises from silicon dangling bonds. Identical TMS signals were observed from films prepared by the DC cathodic or the AF glow discharge method but their decay rates were different. In contrast, the deposition of methane produced two distinct types of carbon-based signals depending upon the method of deposition. TMS or CH_4 films deposited by the DC cathodic method showed slow signals decay and high refractive indices value. While the use of Al as the substrate showed plasma-coating radicals, only substrate radicals were observed when PE was used as the substrate. The nature of radicals formed depends not only on the deposition method used but also on the substrate type.

Introduction

Electron spin resonance (ESR) was used to study free radicals produced by the plasma treatment and the plasma coating processes[1-9]. Plasma treatment refers to the use of none-polymerizing plasma in the glow discharge while plasma coating or plasma deposition refers to the use of polymerizing plasma. Plasmas contain energetic particles and ultraviolet radiation that can penetrate some substrates and form paramagnetic centers[1]. Ar plasma treatments of the substrate polyethylene (PE) create substrate free radicals, which were comprehensively studied by ESR[2,3].

However, not much information is available about the nature of radicals produced by the plasma coating process. In this system, two types of radicals can form, radicals in the polymer matrix and radicals generated in the substrate[1]. PE was used as the substrate for the deposition of iso-t-pentinol (C_5H_7OH) plasma and carbon tetrafluoride (CF_4)/Ar plasma mixture. ESR was then used to measure the free radical concentrations[4,5]. These reports have been directed mainly towards the analysis of the modified substrate properties.

Glass substrates have been used by a number of investigators for the ESR analysis of plasma deposited films[6-9]. For example, silane (SiH_4) plasma has been deposited by the RF plasma method on a glass substrate for ESR analysis[10]. Other workers used the inner coaxial tube as the substrate for the plasma polymerization of xylene isomers (C_8H_{10}) by corona discharge. The coated films were then collected for ESR analysis[7]. The ESR signal for a glass tube coated with hydrocarbon plasma polymers is a composite signal of the plasma polymer and the glass substrate signals[1,9]. While some studies have confirmed that the ESR spectra observed had not

been contaminated with the glass radicals although details of methods used were not reported[2], other studies appear not to have separated the plasma-polymerization signal from the substrate glass signal.

Quartz substrates were used for ESR analysis of the RF deposition of SiH_4 and for the plasma-enhanced chemical vapor deposition (PECVD) process of SiH_4 /NH_3 mixture[11,12]. Since exposure of quartz to glow discharge plasmas produces paramagnetic centers[13], the ESR signals observed in these systems are likely to include interference of substrate signals.

KBr pellets were also used as the substrates for the deposition of the condensed aromatic ring perylene (C_{20} H_{12}) monomer and its derivatives.   Samples were then milled into fine powder before the ESR analysis[14]. Since the mechanical fracture produces ESR signals[15], signals observed in these systems may therefore include some interfering signals formed by the milling process.

Metal substrates are of particular interest because plasma deposition by the DC cathodic discharge method has been shown to provide corrosion protection to metal substrates[16-18]. There are no published reports of direct analysis of free radicals formed in these systems. Indirect ESR analysis of Al foil substrates coated with silane and H_2 mixture by the PECVD process has been reported. The indirect ESR analysis was then carried out after etching the coated foils with dilute HCl[19]. Metal substrates do not form free radicals when exposed to plasma, they should be suitable substrates for the analysis of plasma polymer coating. But the difficulty in the use of metal in the direct ESR analysis is that metals are conductive materials. A special technique is therefore required to overcome this problem.

The term "free radical" is often used in the context of a reactive intermediate, but the same structure (containing unpaired electron) can and does exist in a kind of immobilized environment. For example, a bulk-polymerized methyl methacrylate (PMMA) contains an appreciable amount of free radicals that can be detected by ESR[20]. "Immobilized" or "trapped" free radicals are often formed in a solid by ionizing radiation. The term "dangling bond" is often used to describe the free radicals[21] created in a solid. Those immobilized free radicals have the same characteristic chemical reactivity as the corresponding mobile free radicals but the net reactivity is severely reduced due to space restriction or the lack of mobility. In some cases, free radicals are well protected and they remain in the solid for a long time. The terms "dangling bond" and "free radical" can be considered synonymous, and are used interchangeably in this paper.

There are three objectives for this study. First, is the direct ESR analysis of metal substrates coated with plasma polymers of trimethylsilane (TMS) and methane (CH_4). Direct analysis of the plasma coated Al required the use of a non-conventional ESR method. Second, is to examine the effect of plasma discharge mode (DC cathodic and AF discharge). Third, is the study of the nature of radicals formed as a function of the type of substrate (Al foils and PE).

Experimental

Materials

The monomer gas trimethylsilane (TMS) with a purity of 97% was purchased from Lancaster Synthesis, Pelham NH. Methane gas (99.5%) was purchased from Scot Specialty Gases Inc. Plumsteadville PA. The Al foil substrates with thickness of 0.01 mm and 0.02 mm were obtained from Goodfellow, Berwyn PA. Kimwipes papers were purchased from Fisher Scientific Inc St. Louis MO. The alkaline chemical cleaner Turco 4215S was purchased from Turco Products, Inc., Wilmington, CA. The laboratory film PARAFILM was purchased from the American National Can, Neenah WI. Ultra-high molecular weight polyethylene (PE) fiber with 0.012 mm diameter was obtained from Goodfellow.

Plasma film deposition

Polymerization by the DC cathodic polymerization method

Al foils were used as the substrate for the DC cathodic polymerization at room temperature. They were first cleaned with an acetone wipe using KIMWIPES papers or by using the alkaline cleaning method. Al foils were immersed in an alkaline bath at 65^oC for 25 minutes, then rinsed with de-ionized water and dried. The cleaned foils, 15.2 cm x 15.2 cm, were then placed inside the plasma reactor and used as the cathode of the glow discharge. Details about the reactor and the DC cathodic discharge polymerization method have been reported earlier[22]. The plasma films were prepared by the DC plasma deposition using TMS and CH_4 monomers. Plasma deposition conditions were with DC power of 5W and pressure of 50 mtorr for periods ranging from one to three minutes.

Polymerization by the AF glow discharge

The AF glow discharge was used after both Al foils and PE fibers were placed in the reactor and plasma coated at the same time. The substrate PE fibers were cleaned by soxhlet extraction with iospropanol for 12 hours[23]. Fibers were cut into 2-3 cm strips before beginning the plasma polymerization process. Substrates were placed in the plasma phase (not on an electrode) of the TMS and CH_4. Plasma polymerization was carried out with an AF power, which ranged from 20 to 115 watts, under a pressure of 100 mtorr. The plasma deposition period varied from 15 to 90 minutes. Rotation of the samples in the plasma reactor during the deposition period required the use of longer deposition periods to obtain larger ESR signals. Details about the AF plasma polymerization method as well as the type of reactor have been reported earlier[22].

Refractive index measurements

Measurements of refractive index and film thickness were carried out using an AutoEL-II automatic ellipsometer (Rudolph Research Corporation), which is a null-seeking type with a 632.8-nm helium laser light source. Details about the measurements have been reported earlier[22].

ESR analysis

PE as the substrate

Care was taken to ensure that the first ESR spectra were measured at approximately 20 minutes after the removal of the coated fibers from the plasma reactor. About 120 mg of the coated PE fibers was placed in a 0.4 cm diameter quartz tube, and then analyzed by ESR at room temperature.

Al foils as the substrate

After plasma polymerization, Al foils were removed from the plasma reactor and samples were immediately prepared for ESR analysis. Foils were cut into 1.5 cm x 0.25 cm strips and ten strips were then sandwiched between eleven strips of 0.024 mm PARAFILM. The purpose of PARAFILM is to insulate the Al foils and improve the geometry of the sample by forming a uniform spacing between the closely packed Al foils. The Al foil sandwich was then placed near the E = 0 mode of the TE 102 X-band microwave cavity of the ESR spectrometer with the metal planes normal to the microwave E field (Fig. 1). The first ESR spectra were measured at approximately 20 minutes after removal of the coated foils from the plasma reactor. Digitized spectra were measured using a conventional X-band electron paramagnetic resonance spectrometer with a 100 KHz field modulation. All the ESR measurements were performed at room temperature.

Results and Discussion

In plasma polymerization of an organic monomer, the fragmentation of the molecule or opening of multiple bonds precedes the ionization. The detachment of H, the opening of π-bond, and the cession of σ-bonds create free radicals. The film deposition occurs as these free radicals react at the surface [1]. Thus, the process of plasma polymerization is not an ordinary polymerization, and the resulting polymer in solid state is not the same material as what one might anticipate from the structure of the monomer.

As a film deposits on a substrate surface, many free radicals cannot find another free radicals to combine at the time of deposition and free radicals can be also created on the deposited film by the interaction with plasma. In other words, the rate of free radical formation is greater than the dissipation rate of free radicals. Consequently, many free radicals are trapped in the three dimensional network of amorphous C-H or amorphous Si-H. These trapped free radicals or "dangling bonds" are free radicals with greatly restricted mobility but with the same chemical reactivity. Unlike free radicals formed on a long chain polymer, the dangling bonds in a plasma polymer show no hyper structure.

When a plasma polymer is exposed to the ambient air, oxygen reacts with the free radicals residing at the surface or free radicals that has access to oxygen. Oxygen is the best scavenger of free radicals, and convert a free radical to a peroxy radical and then further to a carbonyl or carboxyl moieties. Because of this mechanism, nearly all plasma polymers of hydrocarbons, which do not contain oxygen atom, show oxygen atoms at the surface. XPS analysis reveals the presence of approximately 20 atomic percent of oxygen at the surface of nearly all plasma polymers derived from various hydrocarbons.
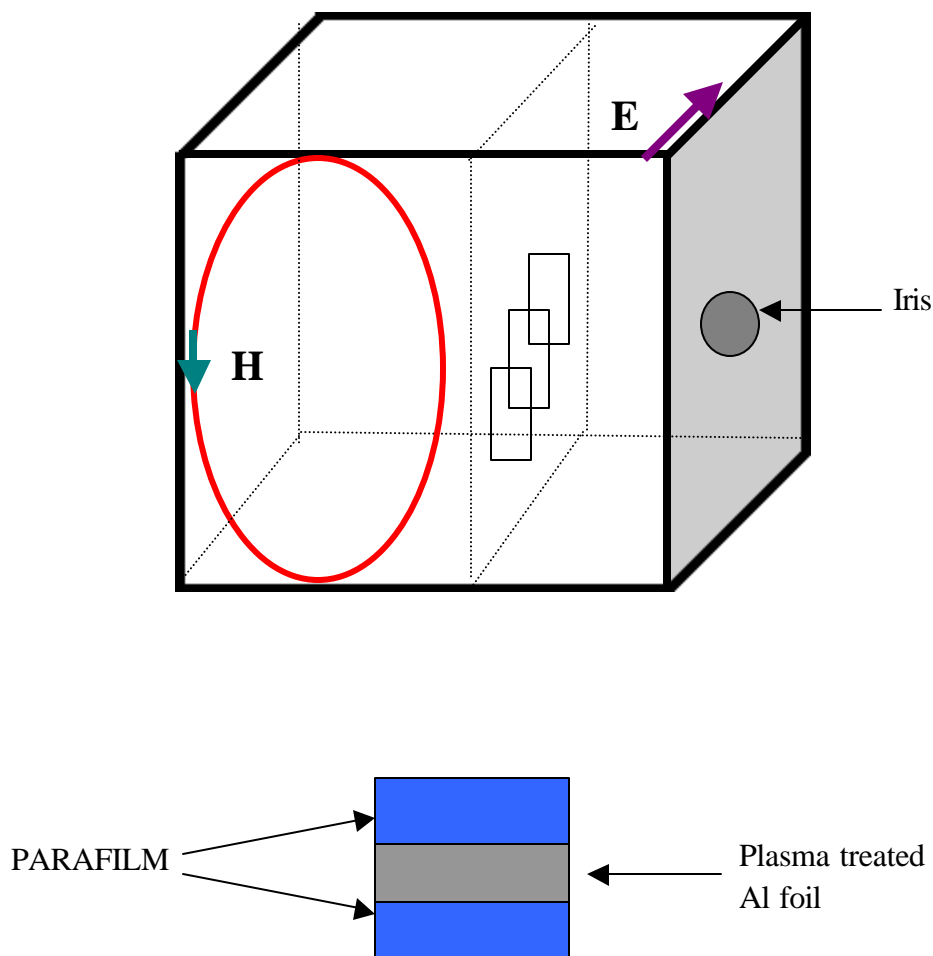
Figure 1. Orientation of the Al foils sample in the TE 102 microwave cavity of the ESR spectrometer and the composition of the sample as a sandwich of the Al foils and the PARAFILM layers.

If a plasma polymer structure is not very tight, eventually all trapped free radicals will be quenched by reacting with oxygen or by recombining them, although it might take few minutes to few days. If the structure is very tight, oxygen molecules cannot reach the dangling bond, and consequently the trapped free radicals remain in the film for very long time. The decay of free radicals in a plasma polymer due to the first exposure to air is generally very fast but does not involve the change of free radical signal; the intensity only decreases. The reaction of oxygen with surface free radicals is mainly responsible for the fast decay as mentioned above. This stage of decay slows-down within a few minutes to an hour, in general, and is followed by the second stage of slow decay.

It is desirable to study the first stage of decay; however, it is very difficult because of the space limitation of the ESR cavity and also of the difficulty to create plasma in a very narrow space. Furthermore, the great perturbation in operational conditions of plasma polymerization necessary to carry out such experiments often offsets the merit of such efforts. Plasma polymerization is system dependent, which means that a plasma polymer formed in a set of condition is different from another one of the same monomer polymerized in different set of conditions.

We are mainly concerned with plasma polymers deposited on an aluminum substrate in this study. It requires the special technique, which should be done in air as described in this paper. Accordingly our efforts are focused on the second stage decay of the trapped free radicals, which is related to the tightness of plasma coatings.

ESR measurement for plasma polymers

The most useful form of plasma polymers is the ultra-thin films deposited on various kinds of substrates in different shapes. It has been known that free radicals play key roles in the formation of materials in plasma, and it has been known also that a large amount of free radicals reside in the plasma formed solids. On the other hand, there are only limited number of papers, which address the nature and quantities of free radicals in plasma. This is due to the technical difficulty of directly measuring free radicals in plasma polymers.
ESR study of an ultra-thin layer of plasma polymer deposited on a substrate solid has an inherent difficulty due to the limitation of mass available for the signal detection. In many cases, the mass of substrate is far greater than the mass of plasma polymer. Because of the low mass ratio of sample/substrate, it is often necessary to insert multiple samples in the tube. If the substrate is glass, quartz, or polymer, the signal from the substrate cannot be ignored. Metal substrates are generally free of substrate signals due to their exposure to plasmas; however, alignment of multiple metal samples causes another problem because of the conductive nature of metals.

In order to examine the plasma polymers formed by cathodic polymerization, an aluminum foil can be used as the cathode. An aluminum foil coated with a plasma polymer layer can be sliced and placed in a quartz tube. An arbitrarily placed Al sample, however, will drastically distort the resonant electromagnetic fields of a microwave cavity, making the cavity useless for ESR purposes. However, there exist configurations where the Al itself can become part of a resonant cavity mode suitable for ESR. One of these configurations is a single Al sheet placed on the midline of a TE 102 cavity, converting it into two weakly coupled TE 101 cavities.

In our system, a single plasma-coated Al sheet gave a very weak signal. Increasing the plasma polymerization duration will increase the ESR signal, but, when Al is used as the cathode in the DC plasma system, there was a maximum of three-minutes before changes occurred in the film characteristics. We achieved an increase in the signal intensity by using an alternative geometry that allowed the use of multiple sheets (Fig. 1). In order to ensure electrical isolation of the Al sheets and to maintain a good parallel geometry, foils were sandwiched between strips of PARAFILM.

Detection of ESR signals from TMS plasma polymerization using Al substrate

The above-described method was successfully used to detect free radicals from Al foils coated with TMS plasma, with good spectrometer sensitivity (Fig. 2a). A ten layer configuration gave considerable enhancement over a single layer regardless of the foil thickness (Fig. 2b). The overall signal enhancement showed some sensitivity to foil thickness, with thin foils working better as expected (Fig. 3a).

In order to confirm that the ESR signal was the result of the TMS plasma polymerization, two control experiments were carried out. First, the untreated Al foils were found to show no ESR signal after being cleaned by the acetone wipe or by the alkaline method. The other control experiment involved treating Al foils with Ar plasma (non-polymer forming plasma) and, as a result, no ESR signal was observed. These results confirmed that the observed ESR signal was due to the TMS plasma polymerization. In addition, if the observed ESR signal were the result of the TMS plasma polymerization, there would be a direct proportionality between the signal intensity and the deposition time. The experimental results did show that the signal intensity increased proportionally with the deposition time (Fig. 3b).

Decay of the TMS signal

The ESR signal decayed over time as it fell by a factor of two in eight hours (Fig. 4a) and with a significant fraction of the signal persisting for several days. Approximately 10% of the signal remained after 90 days. This decay might be due to the recombination of free radicals or it might represent the reaction of trapped free radicals with ambient oxygen.

Two identical TMS plasma coated samples were therefore studied where one sample was stored in air for three days, while the other sample was held in vacuum for the same length of time. A comparison of the ESR signals from the two samples showed that after 72 hours the signal intensity from the vacuum sample was much stronger than the sample exposed to air. In addition, as soon as the protected sample was exposed to air its ESR signal fell very sharply, and, after only a few hours, the two samples showed nearly identical free radical concentrations (Fig. 4b). These results demonstrate that the ESR signal decay represents reaction of the trapped free radicals with ambient oxygen.

Effect of the mode of plasma discharge on the TMS signal

Comparison between the DC cathodic deposition method and the AF glow discharge was carried out in order to have a better understanding of the molecular process. Results showed that the DC cathodic discharge deposition of TMS plasma (5W, 50 mtorr, one minute) gave identical ESR signal with the same intensity as those produced by the AF discharge method (115W, 100 mtorr, 15 minutes). But these two signals showed differences in their decay rate. TMS deposition by the DC cathodic showed the ESR signal fell by 40% in 420 minutes. In comparison, when the polymerization was carried out by the AF glow discharge, the signal fell by 40% in only 150 minutes. In addition, differences were also observed in the refractive index measurements of these films. Results showed that the refractive indices for films prepared by the DC cathodic method were higher than those prepared by the AF glow discharge (Table 1).
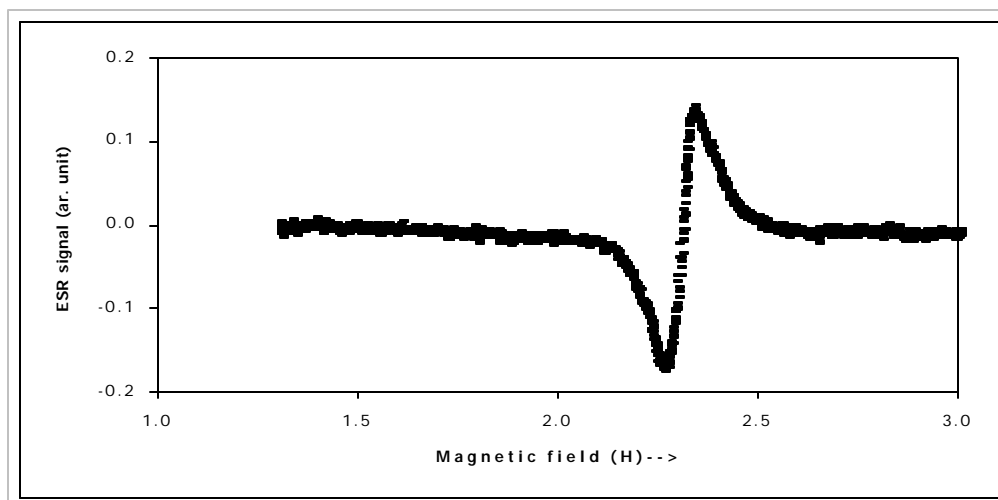
(a)
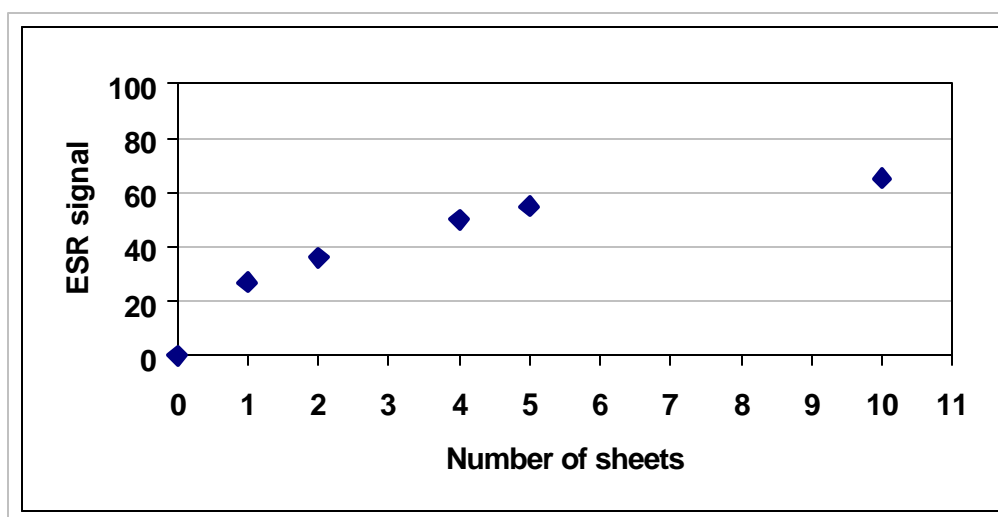
(b)

Figure 2. ESR signal obtained by the TMS plasma polymerization using the DC cathodic method (5W, 50 mtorr, 3min) (a) ESR signal observed using a sandwich of ten Al foils of 0.02 mm thick and eleven PARAFILM layers. Each unit (1.0) on the horizontal axis corresponds to 18.0 mT field sweep centered on g = 2.000. (b) Variation of signal intensity with the number of the coated Al foils.
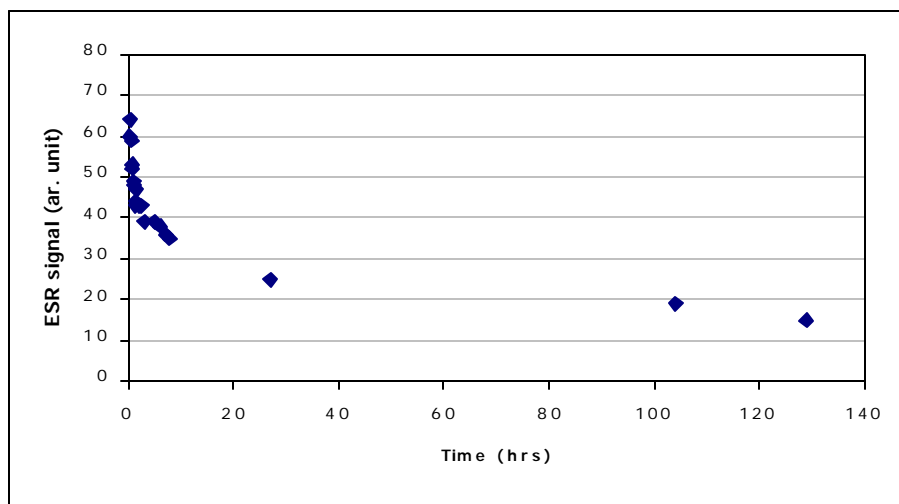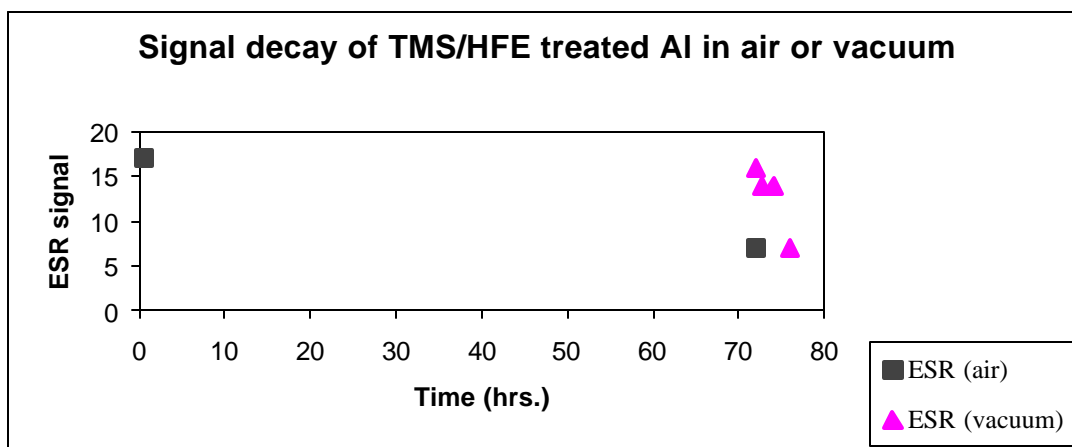
(a)

(b)
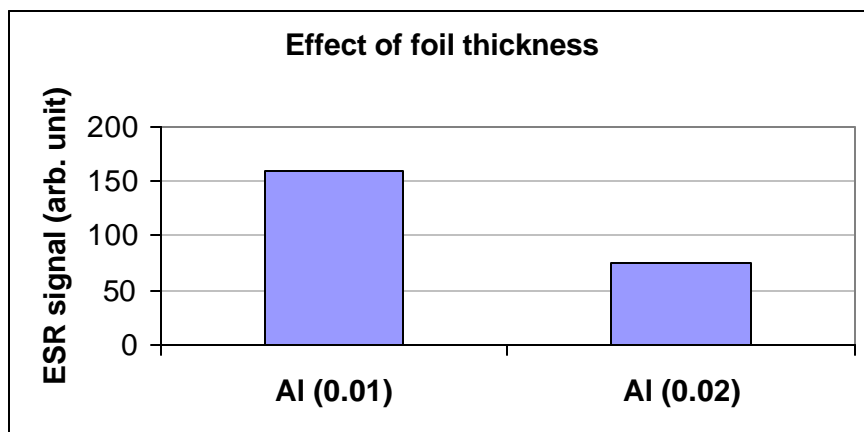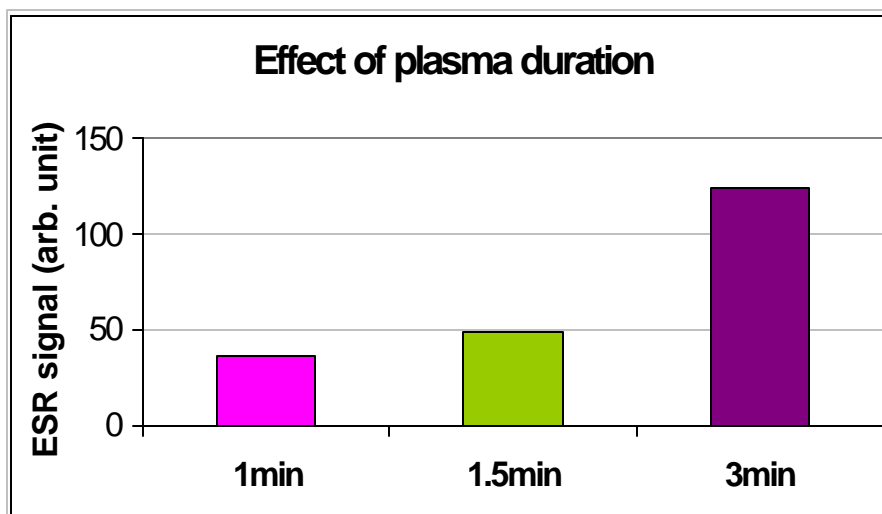
Figure 3. ESR signal as a function of foil thickness and plasma duration using the DC cathodic polymerization (5W, 50 mtorr, 3 min.) of TMS plasma (a) ESR signal intensity as a function of foil thickness of 0.01 mm and 0.02 mm (b) ESR signal intensity as a function of plasma duration.

(a)

(b)

Figure 4. Effect of air exposure on the ESR signal obtained by the DC cathodic plasma deposition (5W, 50 mtorr, 3 min.) of TMS (a) ESR signal decay with storage time in air (b) ESR signal intensity from two identical samples. One sample was held in vacuum for 72 hours showing no decay in vacuum and rapid decay when exposed to air. The other identical sample was exposed to air for 72 hours showing decay with time.

Films deposited by the DC cathodic polymerization have a tighter network compared to the deposition by the AF discharge method[22]. Since signal decay represents reaction of trapped radicals with ambient oxygen (Fig.3), tighter network will restrict the diffusion of oxygen and the signal will show a slower decay. These results demonstrate that the nature and the decay rate of the ESR signals positively correlate to the film characteristics.
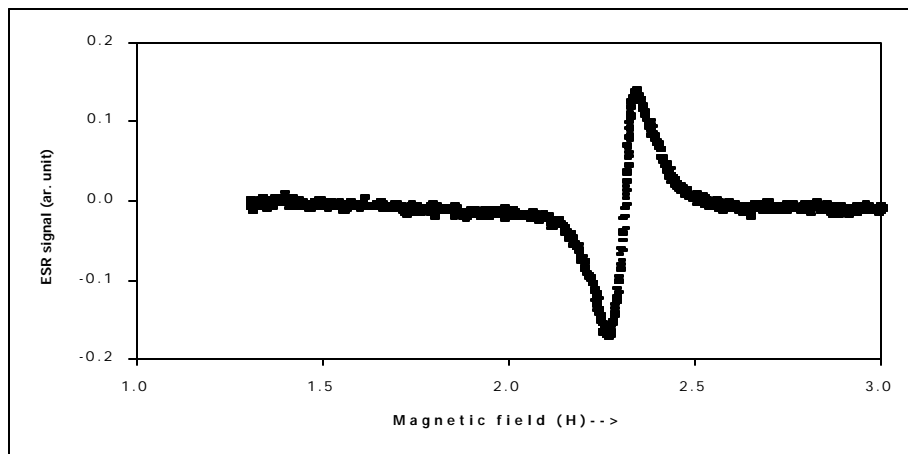
(a)
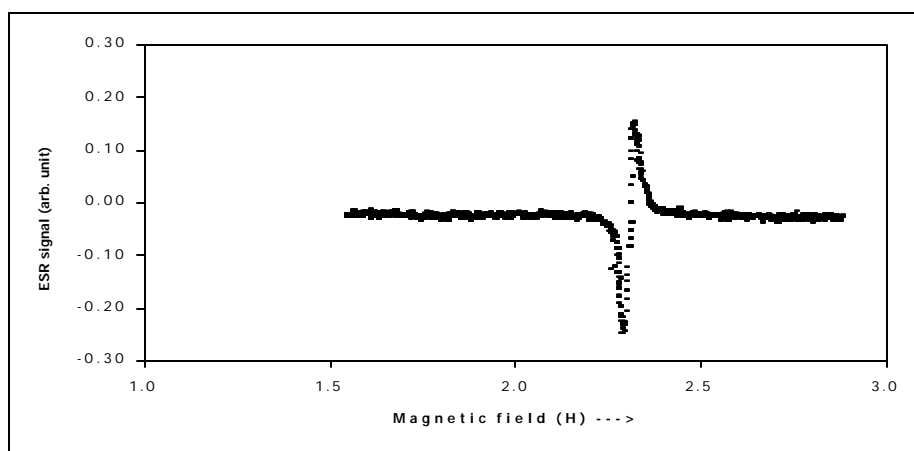
(b)

Figure 5. Comparison between the TMS and the CH$_4$ signals obtained by the DC cathodic plasma polymerization method (5W, 50 mtorr, 3min.) (a) TMS plasma (b) CH$_4$ plasma. Field sweep settings as in (2a).

Table 1. ESR signal decay and refractive index measurements as a function of plasma type and deposition method

Plasma	Method	Type of radical	ESR signal decay	Refractive index	
TMS	DC cathodic[a]	Silicon	40% in 420 min.	2.04	
TMS	AF discharge[b]	Silicon	40% in 150 min.		1.55
CH$_4$	DC cathodic[a]	Graphitic carbon	10% in 4320 min.	2.40[*]	
CH$_4$	AF discharge[b]	Hydrocarbon	80% in 20 min.	1.67[*]	

[a](5W, 50 mtorr, one min.); [b](115W, 0.5sccm, 100 mtorr, 15 min.); [*]From Mayama and Yasuda[20]

Comparison between TMS and CH$_4$ plasma deposition signals

Since the TMS monomer gas contains both carbon and silicon, the TMS signal could originate from either carbon or silicon radicals. A comparison of the TMS signals with carbon-based signals obtained by methane plasma deposition disclosed some interesting features.
First, under the same condition, the DC cathodic plasma polymerization of TMS produced a broad single line (Δ Hpp ~ 15 Gauss) but CH$_4$ deposition gave a narrow line (Δ Hpp ~ 6 Gauss) (Fig. 5). The TMS signal with its unique shape and line-width is clearly very different from the CH$_4$ signal (Fig. 6). Analysis of signal decay showed that TMS signal decayed by 40 % in 420 minutes while methane signal showed only 10% decay in 4,320 minutes. The stability of the methane signal is a key feature of a graphite type radical. The features of CH$_4$ signal are also similar to those radicals in amorphous carbon (a microcrystalline form of graphite) films obtained by the microwave plasma chemical vapor deposition of CH$_4$/H$_2$ mixture[24].

Second, in contrast to the TMS systems where identical signals can be obtained using the DC or the AF discharge, the deposition of CH$_4$ by these two methods produced two different signals (Fig. 7). While the DC cathodic produced a narrow signal (Δ Hpp ~ 6 Gauss) (Fig. 7b) with very little decay (10% decay in 4,320 minutes), the AF discharge produced a broad signal (Δ Hpp ~ 12 Gauss) (Fig. 7a) with very fast decay (~ 80% in 20 minutes). This fast decaying signal has the spectral feature that is similar to those radicals in hydrocarbon films obtained by the RF plasma discharge of unsaturated hydrocarbons[8]. These results demonstrate that the TMS signal is very different from carbon-based signals (Table 1).

Identification of the TMS signal

The TMS polymerization signal represents a large number of free radicals with concentration in the order of c ~ 1.3×10^{14} spins/cm^2 in a typical 50 nm layer. The signal provides only a few diagnostic clues for a microscopic interpretation. We observed a single line, centered near the free electron g value (g   2.003), with no suggestion of underlying fine or hyperfine structure (Fig. 2a). The most unusual feature is the large line width (Δ Hpp ~ 15 Gauss). It may be reasonable to assume that the TMS signal is a composite of more than one signal, but there was no observable change in the line shape as the signal decayed with time.

The spin orbit broadening is given by
$$\Delta \ H/H \sim \Delta \ g/g \sim \lambda_{(so)} /\delta \ E$$
For carbon, the spin orbit constant $\lambda_{(so)}$ is very small and the contribution to line broadening is normally negligible. But the significantly larger $\lambda_{(so)}$ leads to substantial g-shift in silicon. The interactions between the spin system and its environment are also directly related to $\lambda_{(so)}$. Both intrinsic g-shifts and lifetime broadening effects are less than 15 gauss for carbon but 15 gauss is a typical broadening for silicon at the X band. Broadening is; therefore, more apparent in silicon compared to carbon radicals[25].
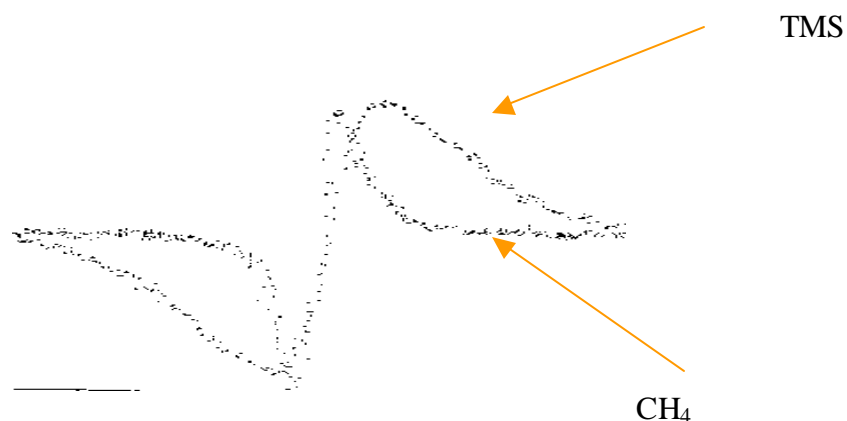
Figure 6. A picture of the overlap of the ESR signals from TMS and CH_4 plasma polymerization. The DC cathodic plasma polymerization method was used (5W, 50 mtorr, 3 min).

However, one cause of significant line broadening for carbon radicals is the anisotropic hyperfine in immobilized molecules, such as radicals produced in frozen hydrocarbon glasses[26] or radicals trapped in polymer matrix[20]. These large hyperfine effects also show resolved structure.

None of these objections apply to the interpretation of our ESR signal as a dangling silicon bond. The absence of hyperfine structure is a strong argument in favor of the model. Also on the experimental side, the comparisons of the TMS signals with methane plasma polymerization signal, which is due to carbon-based radicals with graphitic nature, clearly show that they are very different (Fig. 6).

Furthermore, the broad TMS signal is similar to the reported silicon-dangling bond centers observed from silane plasma deposition[10,19]. In addition, a well-studied class of paramagnetic silicon defects, (the P_b centers)[27,28], has precisely the g anisotropy (δ g 0.006) required to account for the width of the TMS signal. The overall effect of including all these P_b defects together would be to produce a nearly isotropic line about 15 gauss wide. Since the P_b centers are known to be associated with the Si-SiO_2 interface, this is in agreement with our system, of Si on AlO_X. Therefore, the uniqueness of the TMS signal with its shape, line-width and absence of hyperfine structure are consistent with a highly localized silicon-based dangling bond.

A hypothetical chemical structure that is compatible with our ESR results would be an organo-silicon oxide polymer. This polymer interpretation is also supported by the ESCA analysis of similar TMS films where freshly prepared samples showed Si/O/C atomic ratios close to 1/1/2 respectively [Wieliczka and Yasuda unpublished results]. The structure is also in agreement with the reported results of TMS films on cold-rolled steel as characterized by XPS[29].

(a)

(b)
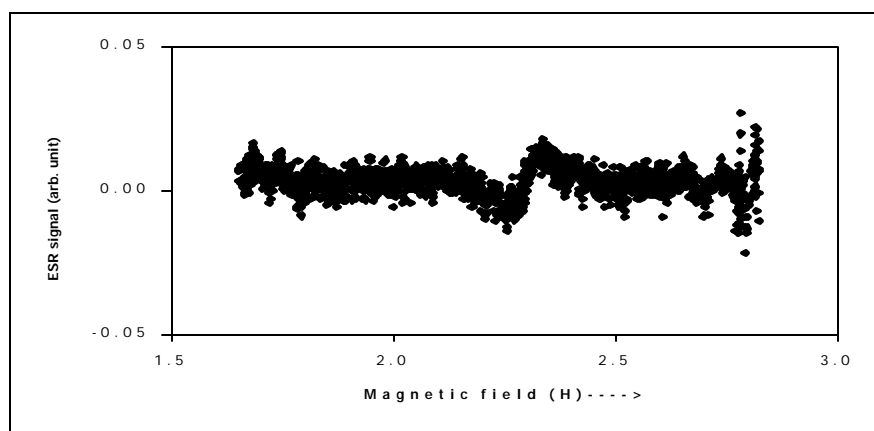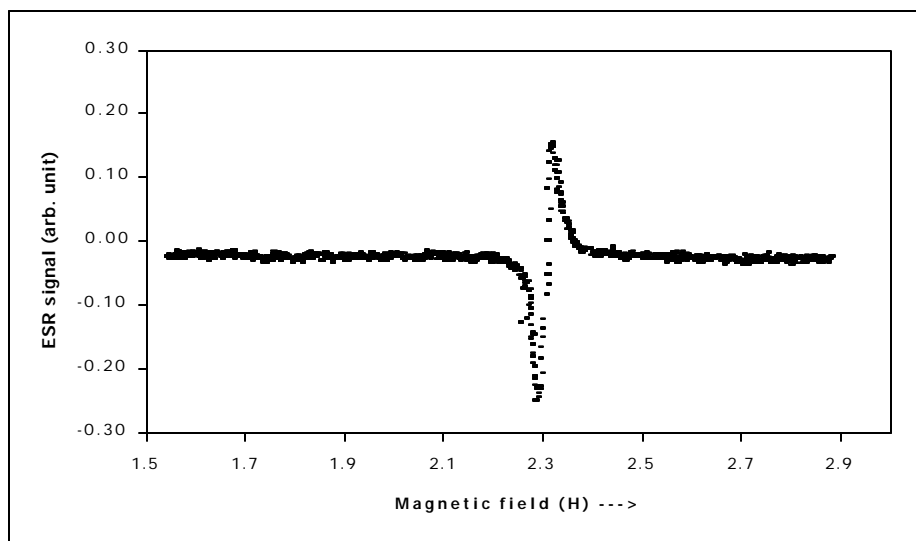
Figure 7. Effect of plasma deposition mode on the ESR signal of CH_4 obtained by (a) the AF discharge method (115W, 100 mtorr, 90 min.) (b) the DC cathodic method (5W, 50 mtorr, 3 min.). Field sweep settings as in (2a).

Effect of substrate on the ESR signals

While PE was used as the substrate for plasma deposition by several workers[4,5], the nature of radicals formed is lacking. Therefore ESR results of plasma deposition on the substrate PE were compared with those using Al substrate.
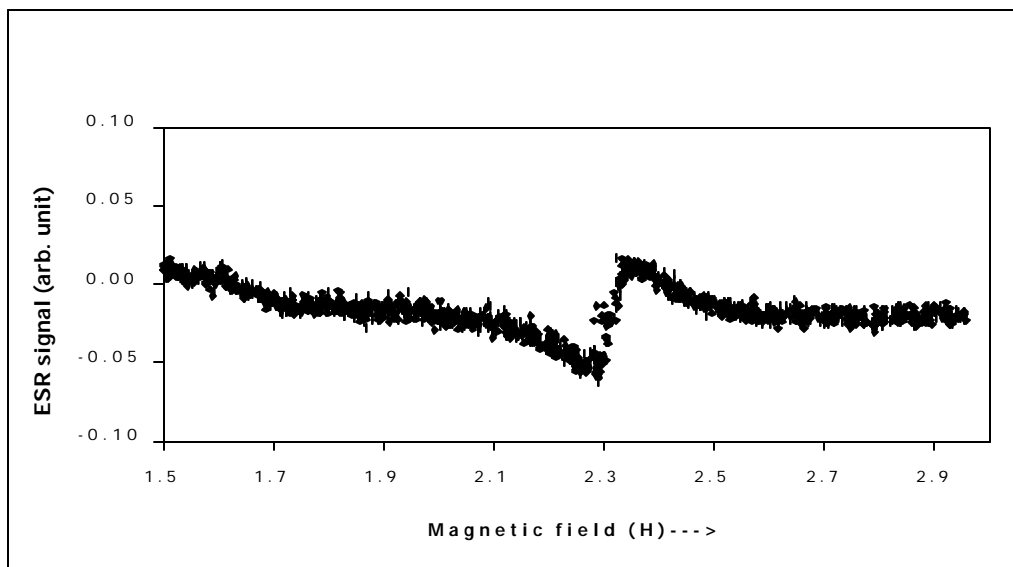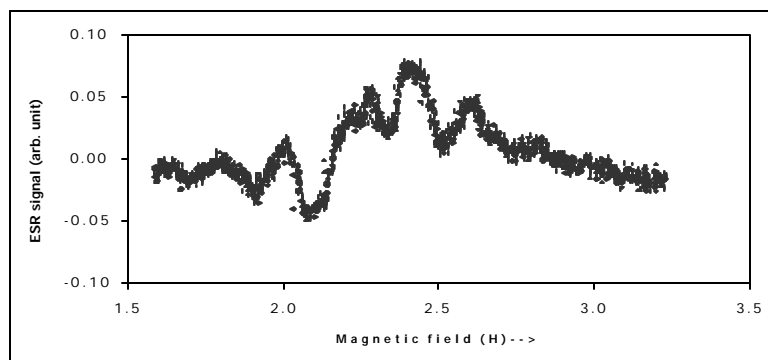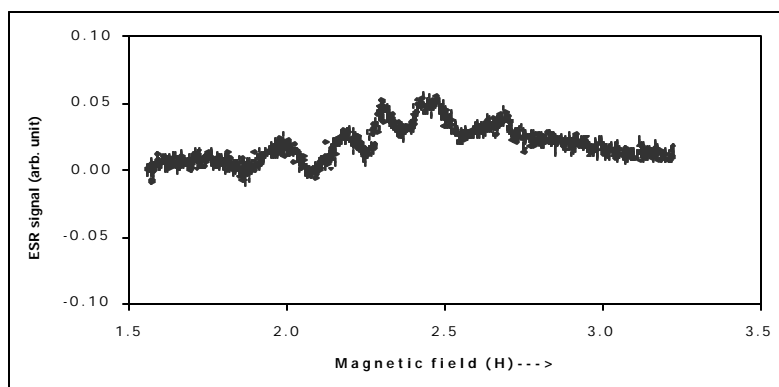
(a)
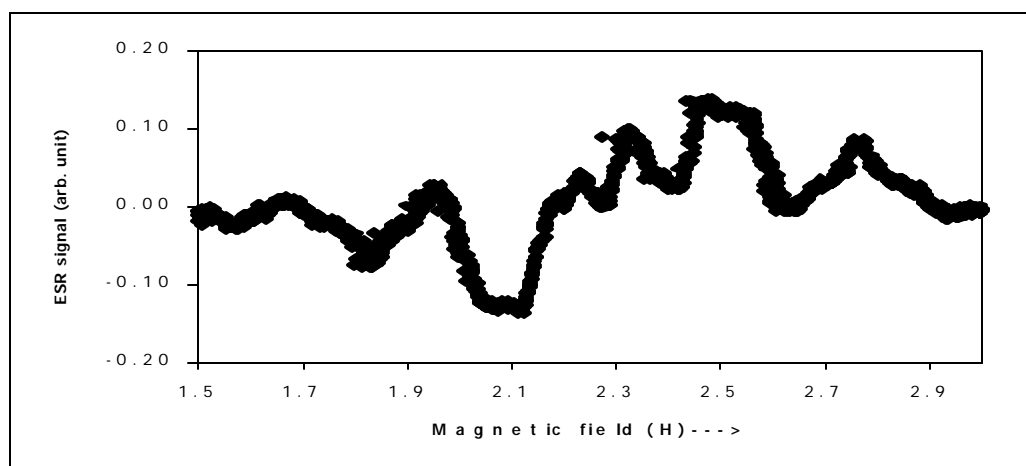
(b)

Figure 8. Variation of the ESR signals as a function of substrates. TMS plasma polymerization obtained by the AF discharge method (115W, 100 mtorr, 15 min) deposited on (a) Al foils (b) PE fibers. Field sweep settings as in (2a).

(a)

(b)

Figure 9. Effect of air exposure on the ESR signals obtained by TMS plasma coated PE fibers using the AF glow discharge method (115W, 100 mtorr, 15 min.) (a) 40 minutes after air exposure (b) one day after air exposure. Field sweep settings as in (2a).
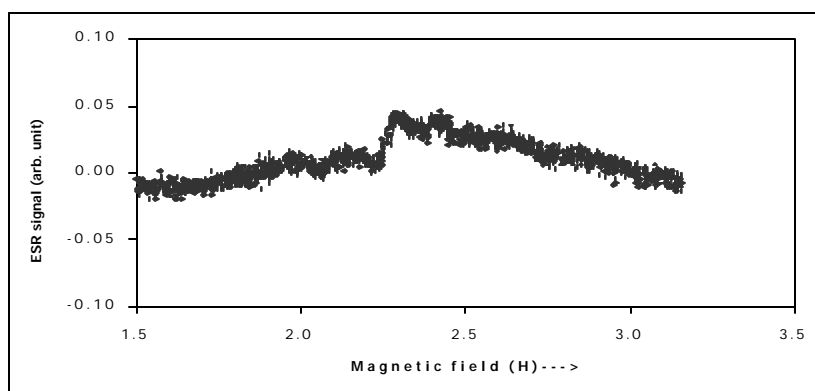

Figure 10. Effect of long-term storage on the ESR signal from PE fibers coated with TMS plasma using the AF glow discharge method (115W, 100 mtorr, 15 min.). Signal observed after seven days of air exposure. Field sweep settings as in (2a).

When the substrate PE is placed on the cathode, unlike Al, it will not act as a part of the cathode, and the film produced is nearly identical to that prepared by the AF discharge where the substrate is floating in the plasma. For comparison, both the substrates Al foils and PE fibers, were placed in the reactor and plasma coated at the same time. Results showed that signals from TMS plasma deposition on PE are very different from that of TMS polymerization on Al (Fig. 8). Unlike the broad ESR line observed when Al was used as the substrate, hyperfine structures were observed by using the substrate PE (Fig. 8).

While the ESR signal decay showed only a decrease in intensity when Al was used as the substrate, the complex spectrum observed when PE was used as the substrate continued to change its pattern. A decrease in the spectral intensity and sharpening of the central ESR line were observed (Fig. 9). In addition, long term of air exposure (7 days) of the coated fibers resulted in a major change, where only the central line was observed (Fig. 10). Similar signals were also observed due to the CH_4 plasma deposition, Ar plasma treatment or by the gamma irradiation (with approximate dose of 2.5 M Rads) of the PE fibers. These complex spectra together with the change of pattern are very similar to the reported carbon-based signals observed from PE powder treated with Ar plasma[2]. Radicals generated by the Ar plasma treatment are hydrocarbon-based signals derived from the substrate PE. Kuzuya and colleagues assigned these PE radicals as the overlap of a sextet spectrum due to mid-chain alkyl radicals (-$CH_2\cdot CHCH_2$-), a septet spectrum due to mid-chain allylic radicals (-$CH_2\cdot CHCH=CHCH_2$-) and a broad line due to immobilized dangling-bond sites[2].

TMS deposition on PE showed only substrate signals and with no detectable TMS signal (Figs 8, 9). The absence of the TMS signal in this system could be due to the fast reaction of TMS radicals with the surface radicals generated from PE. The more likely explanation is that the amount of free radicals in the plasma polymer layer is too small compared to the free radicals created in the bulk of the substrate, PE. What we see in Fig. 9 and 10 is the decay of PE free radicals created by the plasma of TMS. Since subjecting PE to plasma form substrate PE radicals independent of the type of plasma, PE or polymeric substrates in general are not suitable for free radical study of plasma polymers.

Summary

1. ESR was used to directly study the TMS and CH_4 plasma polymers.
2. A novel ESR method was employed to examine the deposited films directly on the conducting Al substrate.
3. TMS signals were found to arise from silicon dangling bonds.
4. Deposition by the DC cathodic or the AF plasma discharge methods showed identical TMS signals but with differences in decay rates and refractive index value.
5. The nature of the CH_4 signal depends on the deposition method used. While the DC cathodic gave carbon-based signals with graphitic nature, the AF discharge method produced hydrocarbon signals.
6. Deposition of TMS or CH_4 on the hydrocarbon substrate PE produced hydrocarbon signals; i.e., the substrate signals predominate.
7. ESR can be used to examine the plasma film deposits directly on the Al substrate without interference of substrate signals.

REFERENCES

1. H. K. Yasuda, *Plasma polymerization*, Academic Press, Orlando, FL, 1985.
2. M. Kuzuya, J. Niwa and H. Ito, *Macromolecules*, **26**, 1990 (1993).
3. M. Kuzuya, S. Kondo and M. Sugito, *Macromolecules*, **31(10)**, 3230, (1998).
4. J. Salansky, *J. Appl. Poly. Sci.*, **71**, 677 (1999).
5. J. Amouroux, F. Arefi, P. Spartacus, S. Mournet, and M. Goldman, *Polymer Materials Sci, Eng.*, **56**, 332, (1987).
6. H. K. Yasuda, and T. Hsu, *J. Polym. Sci: Polym. Chem. Ed.*, **15**, 81 (1977).
7. T.W. Scott, K. C. Chu, and M. Venugopalan, *J. Polym. Sci: Polym. Chem. Ed.* **17**, 267 (1979).
8. M. Kuzuya, M. Ishikawa, A. Noguchi, H. Ito, K. Kamiya, and T. Kawaguchi, *J. Mater. Chem.,* **1(3)**, 387 (1991).
9. N. Morosoff, B. Crist, M. Bumgarner, T. Hsu, and H. K. Yasuda, *J. Macromol. Sci. Chem.,* **A10**, 451 (1976).
10. T. Inokuma, L. He, Y. Kurata and S. Hasegawa, *J. Electrochem. Soc.*, **142 (7)**, 2346, (1995).
11. H. Kirimura, H. Maeda, H. Murakami, T. Nakahigashi, S. Ohtani, T. Tabata, T. Hayashi, M. Kobayashi, Y. Mitsuda, N. Nakamura, H. Kuwahara and A. Doi, *Jpn. J. Appl. Phys.*, **33 (1, 7B)**, 4389, (1994).
12. W. L. Warren and C. H. Seager, *J. Appl. Phys.*, **77(11)**, 5730, (1995).
13. T. Endo, S. Taniguchi, I. Inaba, M. Katoh and K. Sugiyama, *Jpn . J. Appl. Phys. Part 1-Regular Papers,* **27(5)** 710, (1988).
14. K. Tanaka, S. Nishio, Y. Matsuura, and T. Yamabe, *Synthetic Metals*, **64**, 209 (1994).
15. M. Kuzuya, K. Kamiya, and K. Sawanda, Proc. *Jpn. Symp. Chem. Plasma Chem.*, **4**, 317 (1991).
16. C. M. Reddy, Q. S. Yu, C. E. Moffitt, D. M. Wieliczka, R. Johnson, J. E. Deffeyes and H. K. Yasuda,"Improved Corrosion Protection of Al Alloys by System Approach Interface Engineering: Part I-Alclad 2024-T3" *Corrosion, in press,* (2000).
17. Q. S. Yu, C. M. Reddy, C. E. Moffitt, D. M. Wieliczka, , R. Johnson, J. E. Deffeyes, and H. K.Yasuda ,"Improved Corrosion Protection of Al Alloys by System Approach Interface Engineering: Part II-AA 2024-T3" *Corrosion, in press,* (2000).
18. C. E. Moffitt, C. M. Reddy, Q. S. Yu, D. M. Wieliczka, R. Johnson, J. E. Deffeyes and H. K. Yasuda, ,"Improved Corrosion Protection of Al Alloys by System Approach Interface Engineering: Part III-AA 7075-T6" *Corrosion, in press,* (2000).
19. P. Hari, P. C. Taylor, and F. Finger, *Amorphous silicon technology Materials Research Society Symposium Proceedings,* **420**, 491 (1996).
20. F. F. Oldfield and H. K. Yasuda, *J. Biomed. Mater. Res.*, **44**, 436-445, (1999).
21. S. R. Elliot, *Physics of amorphous materials*, John Wiley & Sons, New York, 1990, pp 339-380.
22. M. Miyama and H. K. Yasuda, *J. Appl. Poly. Sci.*, **70**, 237 (1998).
23. C. C. Wang and G. H. Hsiue, *J. Poly. Sci. A: Poly. Chem.*, **31**, 1307, (1993).
24. I. Watanabe and K. Sugata, *Jpn. J. Appl. Phys.*, **27**, 1808, (1988).
25. P.W. Atkins and M. C. R. Symons, *The structure of inorganic radicals: an application of electron spin resonance to the study of molecular structure*, Elsvier, New York, 1967.
26. D. J. E. Ingram, *Free radicals as studied by electron spin resonance*, Academic Press, Butterworth, London. 1958, pp. 171-181.
27. P. J. Caplan and E. H. Poindexter, *J. Appl. Phys.*, **50(9)**, 5847, (1979).
28. E. H. Poindexter, P. J. Caplan, B. E. Deal and R. R. Razouk, *J. Appl. Phys.*, **52**, 879, (1981).
29. A. Sabata, W. J. van Ooij, and H.K. Yasuda, *Surface and Interface Analysis*, **20(10)**, 845 (1993).

22. ESR study of trimethyl silane plasma polymer, Part II; Effect of consecutive treatments and mixed gases

F.F. Oldfield[1], D.L. Cowan[1], and H.K. Yasuda[2,*] E. Moffitt[3], D. M. Wieliczka[3]

Abstract

An ESR study has indicated that a second plasma treatment on plasma deposited films from trimethylsilane (TMS) monomer gas has the ability to modify the characteristics of the primary plasma polymer significantly in a favorable manner for many applications. The effect of the second plasma polymerization on the primary plasma polymer of TMS depends on the nature of the second monomer. A plasma of F-containing monomer; hexafluoroethane (HFE) and tetrafluoromethane (CF_4), decreases the ESR signal of TMS and no detectable signal due to F-containing monomer was found. The decay rate of the signal decreased significantly. In contrast to this situation, CH_4 plasma treatment yields an ESR signal that is a composite of that observed from TMS and CH_4 films individually. The overall signal increased in this instance, but didn't show appreciable decay in 24 hours period. When the sequence was reversed, CH_4/TMS also yields a composite signal, but it is not the same composite signal as observed from the TMS/CH_4 system. A second treatment by non-polymer forming plasmas also decreased the ESR signal of TMS, and decreased the decay rate, indicating that the second gas plasma treatment yields a somewhat similar effect found with the HFE plasma treatment. Plasma polymerization of mixtures of TMS and non-polymer-forming gases increased the ESR signal but decreased the decay rate, except in the case of oxygen. A mixture of (TMS+O_2) behaved as a completely different monomer. No ESR signal was found in this system.

Introduction

Reactions of free radicals such as the coupling of free radicals and the hydrogen abstraction from polymer molecules constitute the major growth mechanisms of plasma polymerization or of material formation in plasma chemical deposition (PCVD). Because of these growth mechanisms, most plasma polymers contain a great number of free radicals that can be detected by Electron Spin Resonance (ESR) spectroscopy [1]. However, there are few ESR studies on plasma polymers published, probably due to the technical difficulties associated with this application to plasma polymers.

Two major difficulties are as follows. 1) Although the concentration of free radicals in a unit volume of a plasma polymer is high, the total number of free radicals that can be placed in the ESR cavity is small due to the fact that plasma polymers are generally prepared in the form of ultra-thin films, of which thickness is in the range of 10 - 100 nm, deposited on a substrate material. 2) Another inherent problem is the difficulty of identifying and separating the ESR signals due to plasma polymer and that due to the substrate. In most ESR studies on plasma polymers, glass fibers, glass rods, polymer fibers, and polymer films are used. All these substrate materials form free radicals when they are exposed to a plasma environment, due to UV photon emission of plasmas [2,3]. UV penetrates through nearly the entire volume of substrates

used in ESR studies, i.e., thin film or small diameter rod or fiber. Consequently, the ratio of ESR signal due to a plasma polymer layer to that of the substrate material is very small. This problem becomes even larger when a substrate is exposed to the plasma for longer periods of time in an effort to increase the thickness, because the substrate signal becomes overwhelmingly large so as to obscure the sample signal.

Unfortunately, many papers published have not addressed this issue appropriately, and hence the validity of results is uncertain. In this respect, it is vitally important to use substrate materials that do not create an ESR signal by plasma exposure and can be placed in a small ESR cavity. In a previous study, a novel technique was developed to use thin foil of aluminum, which does not create ESR signal from interaction with plasmas [4]. By this approach, the problem due to the substrate signal could be totally eliminated, although the first problem mentioned above still exists.

Free from hampering substrate signals, it is now possible to examine the subtle but very important factors, such as the influence of the second gas and the effect of sequential plasma processes, of plasma polymerization. The new technique was extended to examine these effects on the deposition of trimethylsilane (TMS).

Experimental

Materials

The following gases were used in plasma pretreatment and plasma polymerization process. The diatomic gases, hydrogen (99%), oxygen (99.9%) and argon (99.9%), were procured from Airgas. Trimethlysilane (TMS) gas of 97% minimum purity was procured Lancaster Synthesis, Inc. (Windham, NH). Methane (CH_4) of 99.5% purity was purchased from Scot Specialty Gases, Inc. (Plumsteadville, PA), and Hexafluoroethane (HFE) from Specialty Gases (Maumee, OH). Tetrafluoromethane (CF_4) of 99% purity was procured from PCR, Inc. All the gases and monomers were used as received without any further purification.

The Al foil substrates with thickness of 0.02 mm were obtained from Goodfellow, Berwyn PA. Kimwipes papers were purchased from Fisher Scientific Inc St. Louis MO. The laboratory film PARAFILM was purchased from American National Can, Neenah WI.

Plasma film deposition by the DC cathodic polymerization method

Al foils were used as the substrate for the DC cathodic polymerization at room temperature. They were first cleaned with an acetone wipe using Kimwipes tissue papers. The cleaned foils, 15.2 cm x 15.2 cm, were then placed inside the plasma reactor and used as the cathode of the glow discharge. Details about the reactor and the DC cathodic discharge polymerization method have been reported earlier [5]. The plasma films were prepared by the DC cathodic polymerization of TMS. Plasma deposition conditions were with DC power of 5W and pressure of 50 mtorr for periods ranging from one to three minutes.

ESR analysis

After plasma polymerization, Al foils were removed from the plasma reactor and samples were immediately prepared for ESR analysis. Foils were cut into 1.5 cm x 0.25 cm strips and ten strips were then sandwiched between eleven strips of 0.024 mm PARAFILM. The Al foil sandwich was then placed near the E = 0 mode of the TE 102 X-band microwave cavity of the ESR spectrometer with the metal planes normal to the microwave E field. Details about the ESR method have been reported earlier [4]. The first ESR spectra were measured at approximately 20 minutes after removal of the coated foils from the plasma reactor. Digitized spectra were measured using a conventional X-band electron paramagnetic resonance spectrometer with a 100 KHz field modulation. All the ESR measurements were performed at room temperature.

XPS Analysis

X-ray photoelectron spectroscopy (XPS) analysis was performed with a Kratos Axis HS spectrometer, using the Mg-Ká flood source, which has the advantage of exciting the Si KLL Auger transition with Bremsstrahlung. Since the intensity of this transition is lower than the core level emission excited by the primary Mg x-ray (Ká), a mid-range resolution with 80eV pass energy was used for collection. This yields a FWHM of the Ag 3d 5/2 line of just over 1.4eV. Charging compensation was provided by the Kratos electron technique in the magnetic field of the lens system. This generally overcompensates insulating samples, so discussion of adjusted peak positions is included in the results section.

Results and Discussion

In dealing with various combinations of plasma processes, the following notations are used. Two plasma processes are expressed by inserting / between two plasma processes, in the order of sequence. Plasma polymerization of TMS followed by plasma of hydrogen is expressed as TMS/H_2. When two gases are used simultaneously, the two gases are placed in a parenthesis; e.g., (TMS+H_2) represents plasma polymerization of a mixture of TMS and H_2. Thus, TMS/(HFE+H_2) means that the plasma polymerization of TMS is followed by the plasma polymerization of a mixture of HFE and H_2. All sequential processes are carried out in the same reactor without breaking the vacuum.

Sequential Plasma Polymerizations

TMS/HFE

The post-deposition plasma modifications to the plasma polymer of TMS have been seen to greatly improve bonding to various primers and paints [6,7,8]. One particular system has been observed to have tremendous adhesion between plasma coated alloy panels and paint applied to them. This system involves cathodic DC plasma deposition of a roughly 50nm primary plasma polymer film from trimethylsilane (TMS) onto a properly pretreated alloy substrate, followed by the deposition of an extremely thin fluorocarbon film by DC plasma deposition of HFE. It was

the super adhesion aspect of this particular system that triggered the current series of ESR studies.

It is important to note that HFE is not a monomer of general plasma polymerization, because it does not polymerize in absence of hydrogen [9]. When it is applied onto a polymer surface, however, hydrogen is abstracted form the surface and forms a very thin layer of plasma polymer. It is essentially a self-terminating deposition process leading to an extremely thin layer of HFE plasma polymer. ESCA analysis indicated that the thickness of F containing layer in the TMS/(HFE) system is less than few nanometer [10].

It is also important to recognize that HFE plasma is a good etching agent for silicon, and the substrate (plasma polymerized TMS) contains silicon. Consequently, the deposition of HFE plasma polymers on the surface might partially etch the TMS plasma polymer layer. The plasma polymerization may increase the free radical concentration, while the latter may decrease it. ESR signals of TMS and that of TMS/HFE are shown in Fig. 1 as a function of time (decay).
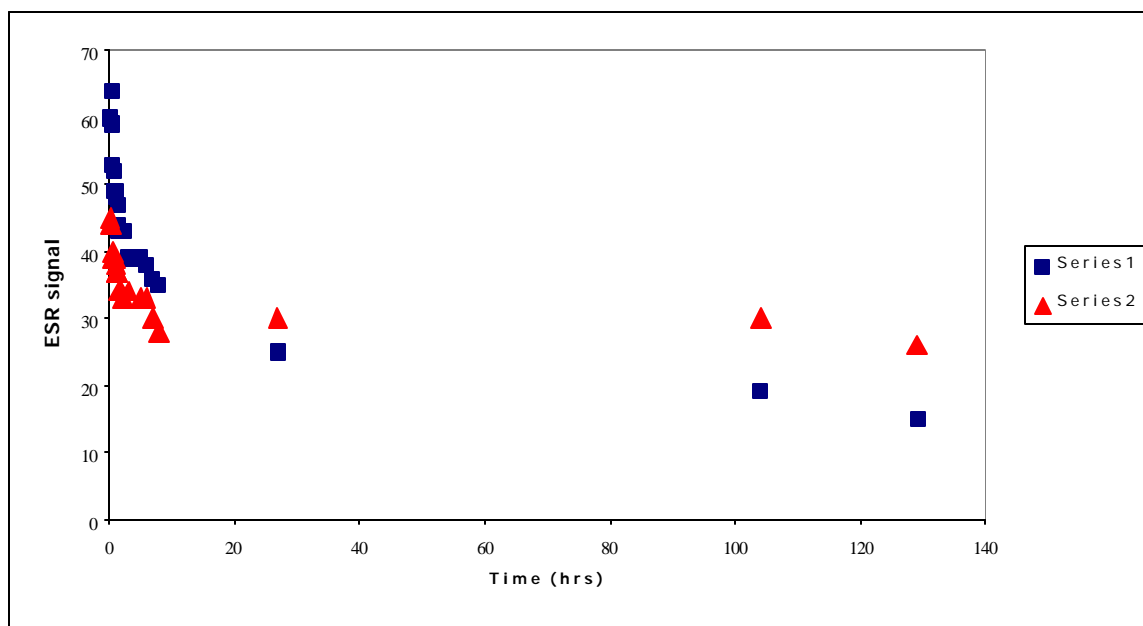

Figure 1. Difference in the ESR signal and its decay rate of TMS (Series 1) and TMS/HFE (Series 2) plasma polymer coatings on Al foil.

The ESR data contain at least one interesting clue as to why the TMS/HFE plasma coating provides strongly bonded films, namely that there is a consistent reduction in the free radical signal from the TMS under-layer when an HFE layer is deposited on top. The magnitude of the reduction is about 20% of the total, or about 2.6×10^{13} spins/cm^2. This number may represent nearly all of the silicon dangling bonds in the upper 20% of the TMS plasma polymer film. If this 10 nm thick transition region (20 % of TMS layer) did contain 2.6×10^{13} crosslinks/cm^2, as these numbers suggest, that would suffice to remove loosely kept oligomeric structures, which

would yield exceptionally strong surface adhesion for the HFE derived film by the principle of converting a week boundary to a strong top surface structure.
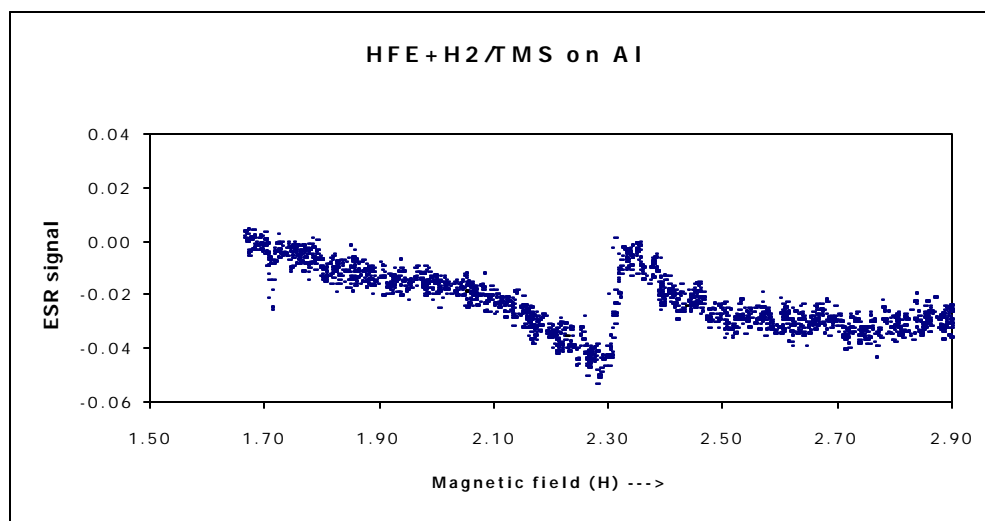

(a)
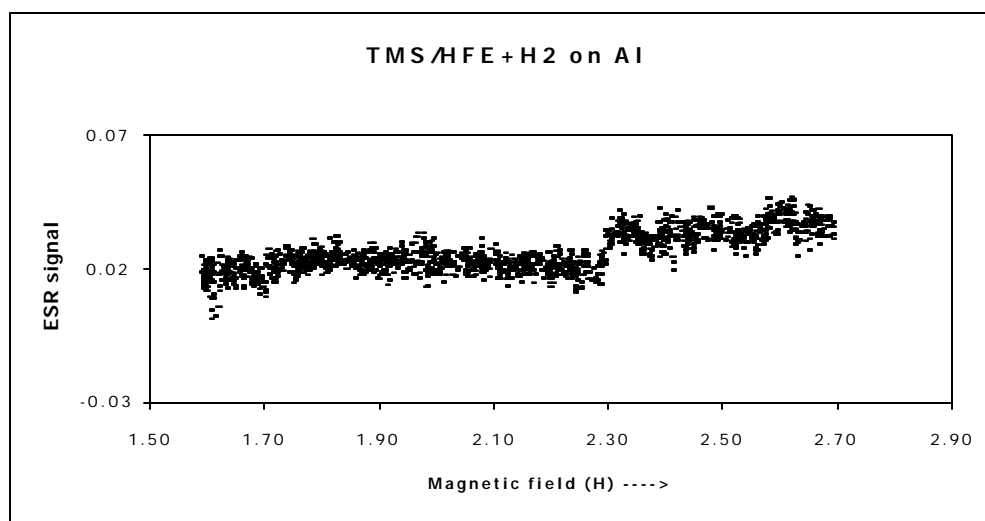
(b)

Figure 2. Comparison of the ESR signals from (a) (HFE+H2)/TMS and (b) TMS/(HFE+H2).

Plasma deposition with HFE is a self-terminating plasma polymerization process. Namely, when a polymer substrate surface is sufficiently covered by the plasma polymer of HFE, the deposition ceases as the supply of hydrogen diminishes. Consequently it is extremely difficult to detect ESR signals from the HFE plasma polymer. Attempts were made to investigate the etching effects described above with plasma of (HFE+H_2), because this system is not a self-terminating

system and this enables to the investigation of the effect by depositing a thicker layer. The ESR signal of TMS/(HFE+H2) is compared with that of (HFE+H2)/TMS in Fig. 2.

(a)

(b)
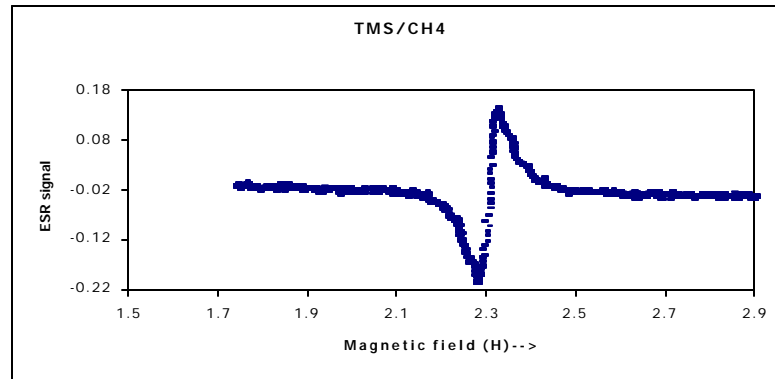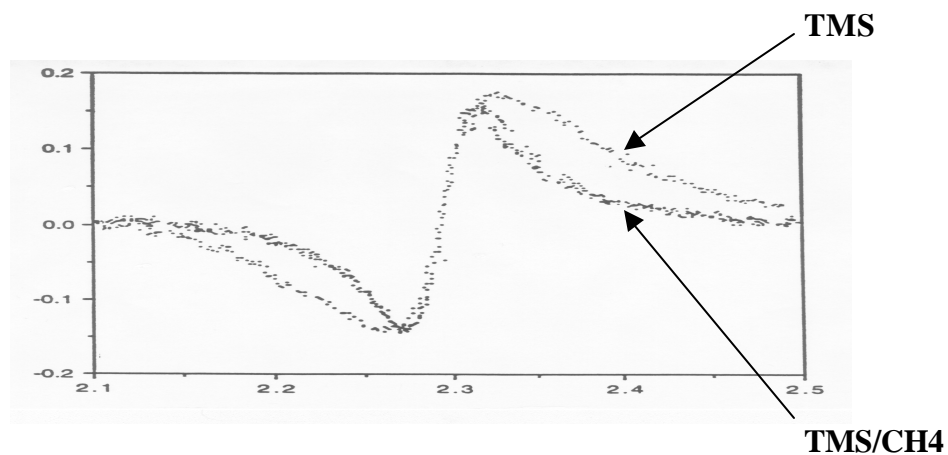
Figure 3. ESR signals from TMS/CH4 (b) picture of the overlap of TMS and TMS/CH4 signals.

TMS/(HFE+H_2)

The etching effect is clearly evident since the ESR signal of the TMS film almost completely disappeared due to the second deposition of plasma polymer of (HFE+H_2). There is still no ESR signal attributable to (HFE+H_2) plasma polymer.

(HFE+H_2)/TMS

The presence of plasma polymer of (HFE+H_2) on the substrate surface didn't influence the free radical characteristics of plasma polymer of TMS, which deposits on the surface of (HFE+H2), whereas the adhesion of TMS in this sequence was found to be extremely poor [10].

TMS/CH_4

The ESR signal of TMS/CH_4 and a comparison with the TMS signal is shown in Fig. 3. Analysis of the TMS/CH_4 showed that it is a composite signal of TMS and CH_4 film signals, which is different from the TMS signal and also from the CH_4 signal. This composite signal showed that the TMS portion of the signal was larger than the signal from TMS alone. The second plasma polymerization, of CH_4, increases the ESR signal intensity dramatically. The ESR signal intensity and its decay characteristics for various combinations of sequential treatments are depicted in Fig. 4. The large increase of ESR signal intensity from that portion due to the TMS component, as well as its small percentage of decay over 24 hours, suggests that the second layer of CH_4 plasma polymer is acting as a barrier to O_2 diffusion.
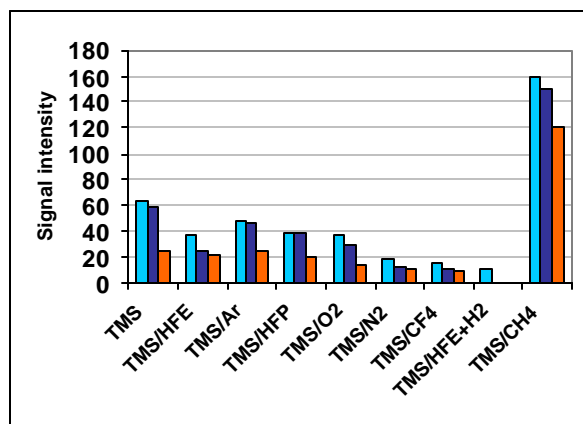
(a)
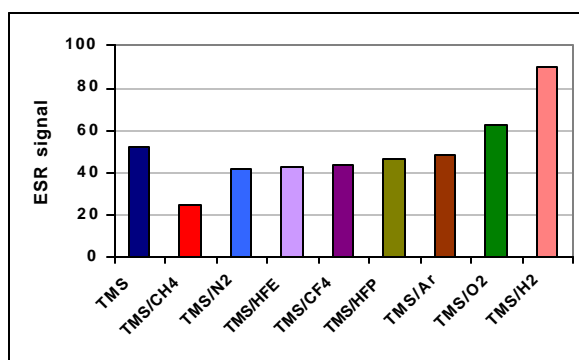
(b)

Figure 4. (a) comparison of the ESR signal decay after 0.3 and 24 hours from the plasma coating of one minute TMS followed by one minute of plasma treatment of O2, H2, Ar, HFE and the plasma coating of CH4; (b) percentage decay of the ESR signal in 24 hours.

The decay of the ESR signal in general consists of two parts. The first part is the very quick first order decay immediately following the exposure of plasma polymer to ambient air. The second part is a relatively slow decay, which follows the first decay. The first decay cannot be measured by the experimental set up employed in this study. The second part of decay, which is dealt in this study, may be due to the diffusion-controlled reaction of free radicals with oxygen, or the recombination of trapped free radicals in the plasma polymer network. In either mechanism, the slow decay indicates that the network in the combined system is tighter than the system that yields a faster decay rate.

CH4/TMS

The ESR signal from CH4/TMS is also a composite signal of TMS and CH_4; however, the composite signal is not the same composite signal of TMS/CH_4.

Plasma Treatment of the Plasma Deposited TMS Film

ESR results for the TMS/HFE system, together with adhesion characteristics of the system, strongly suggests that the etching of oligomers, or the conversion of oligomers in the plasma polymerized TMS to more stable polymeric networks [12], seems to be an important factor that accounts for the strong adhesion with this system. It is likely that a second plasma treatment with non-polymerizing gases might produce a similar effect observed with TMS/HFE system. From this point of view, various plasma post-treatments of plasma polymerized TMS were investigated.

TMS/Ar: TMS/Ar showed a transient (O_2^+ radical) and a decrease in the TMS signal.

TMS/O_2:   TMS/O_2 showed a transient signal (peroxy radical) and a decrease in the TMS signal.

TMS/N_2:   TMS/N_2 showed a transit signal (nitroxide radical) and a decrease in the TMS signal.

TMS/H2:   TMS/H_2 showed a decrease in the TMS signal.

CH4/H_2:   CH$_4$/ H_2 showed an increase in the CH_4 signal. The effect of H_2 plasma treatment on the plasma polymers of TMS and that of CH_4 is completely different. ESR signal intensity and the decay characteristics for these two systems are shown in Fig. 5.
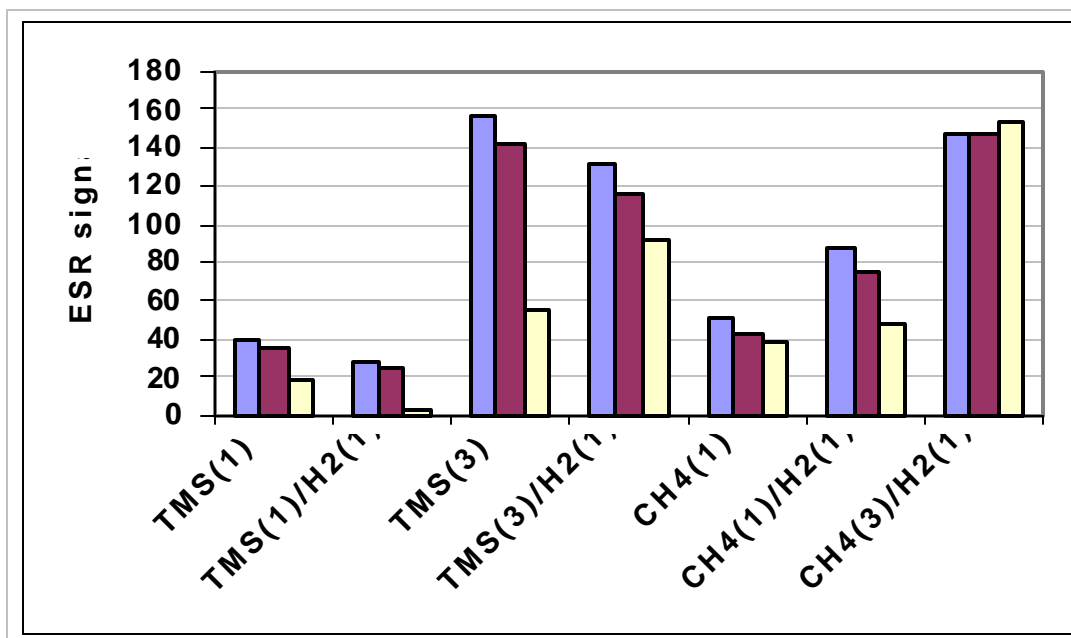
Figure 5. Decay of the ESR signals with time. Data taken at 20 minutes, 30 minutes and 24 hours after the exposure of plasma treated Al surfaces to air.

Plasma Polymerization of Mixed Gas

(TMS+H2)

   A drastic change occurred when hydrogen was mixed in the TMS plasma polymerization. As a result, the initial ESR signal intensity increased but no significant decay was observed over a 24-hour period. The ESR signal intensity and its decay characteristics for (TMS+H2), (TMS+Ar), and (TMS+O2) are compared with those for TMS in Fig. 6.

(TMS+Ar)

   Addition of Ar to the TMS plasma also increases the ESR signal significantly from that for TMS alone. The relative decay rate decreased but not as much as when H_2 was mixed with TMS.
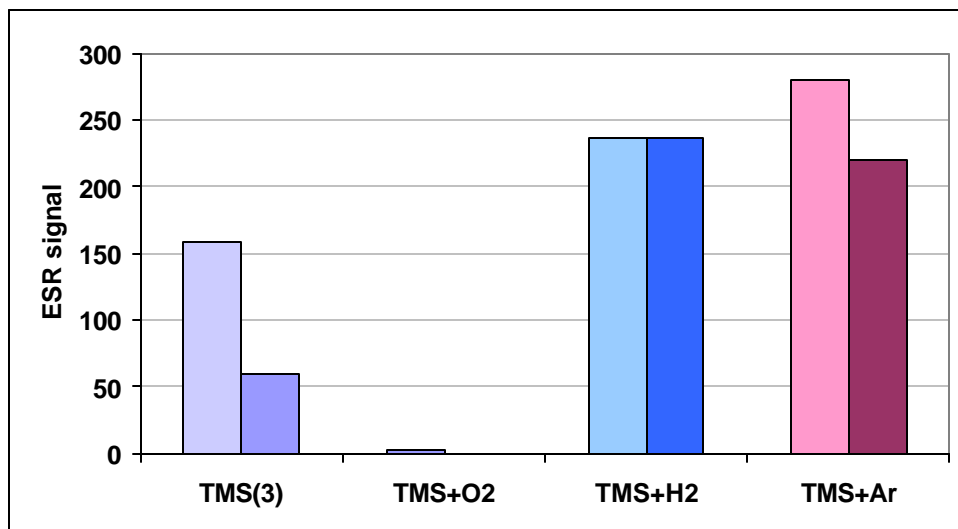
Figure 6. Comparison between the ESR signal intensities of TMS (3min), TMS+O2 (3minute), TMS+H2 (3minute) and TMS+Ar (3minute). Signal intensities were measured after 0.3 hours and 24 hours after air exposure.
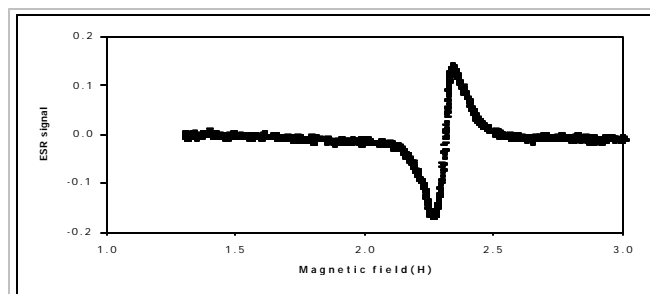

(TMS+O2)

Results show that when a sufficient amount of oxygen was added to the TMS plasma, the ESR signal was virtually extinguished as shown in Fig. 7. This indicates that plasma polymer of (TMS+O2) is a completely different material from plasma polymer of TMS. Oxygen mixed with TMS reacts with TMS during the process of plasma polymerization yielding more inorganic character of the structure, which does not contain Si dangling bonds. This is a completely different process from O_2 plasma treatment of plasma polymer of TMS, in which the O_2 plasma react with Si dangling bonds on the surface.

XPS data also support this assessment of the effects. Fig. 8 shows photoelectron spectra from the surface of several films at normal emission (90° take-off angle). It is immediately observed that the post-deposition treatments and combined gas deposition yield different surface chemistries from the as-deposited, pure TMS film. All of the post-deposition treatments leave the surface of the films in a silica-like state, even treatment with the more inert gas plasmas. This is reasoned to be from the creation of free radicals by the plasmas, which are quickly oxidized upon exposure to atmosphere prior to analysis.

The peak positions in the figure bear some discussion in reference to the charging compensation technique, as mentioned in the experimental section. When optimized for the best resolution, this compensation technique overcompensates the sample surface by ~1V. Without a clear signal from adventitious hydrocarbons on the surface of the actual samples, some uncertainty lies in the actual position, but approximate positions can readily be deduced. An initial argument for the proper correction lies in measuring the position of the adventitious carbon above a thermal oxide on silicon, of approximately the same thickness as the plasma polymer films. This agrees

with the approximation of 1V over-compensation, and has been reliably consistent throughout a number of experiments.

(a)

(b)
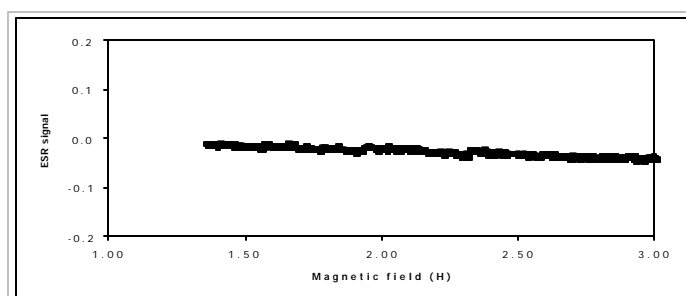
Figure 7. Effect of oxygen as a mixture to the TMS plasma (a) ESR signal from TMS plasma coating of Al foils (b) ESR signal from TMS+O_2 (1scm + 4scm) plasma coating of Al foils.

The second argument lies in the actual positions of the film sample peaks. The relation of the oxidized silicon peak and the separation from the untreated TMS film peak and those of other samples, coupled by the modified Auger parameter [12,13], indicate that the higher binding energy Si peak is likely due to the formation of SiO_2. This is particularly distinct on the O_2 plasma treated film, with the other more inert plasma treatments having some sub-oxide components [14]. A value of 1711.6 for the modified Auger parameter of the oxygen plasma treated film is quite consistent with those reported for various forms of silica type bonding [15].

Then using a shift of ~1.2eV for all of the peaks, it is seen that the high binding energy peak in the C 1s spectra is now at 284.8eV, which is a standard position for the graphitic and hydrocarbon bonding generally used for charge neutralization. There is some contribution at even higher binding energy, appearing around 286-7eV in the uncorrected spectra, which is consistent with some C-O bonding due to the plasma treatment. The charging shift of the lower binding energy C 1s peak from the untreated, plain TMS film then makes it lie in a region consistent with Si-C or Si-CH$_x$ bonding. This, and the associated position of the Auger peak then yield a value of 1713.0 for the modified Auger parameter, just slightly lower than that observed on pure SiC. The point of this lengthy argument is that the treatment with oxygen

plasma modifies both the silicon and carbon bonding, forming Si-O and C-C structures from the Si-CH$_x$ structure of the original film. The incorporation of oxygen with TMS in the deposition process also yields a distinct modification of the local bonding structure, beyond the surface effects observed in the post-deposition treatments.
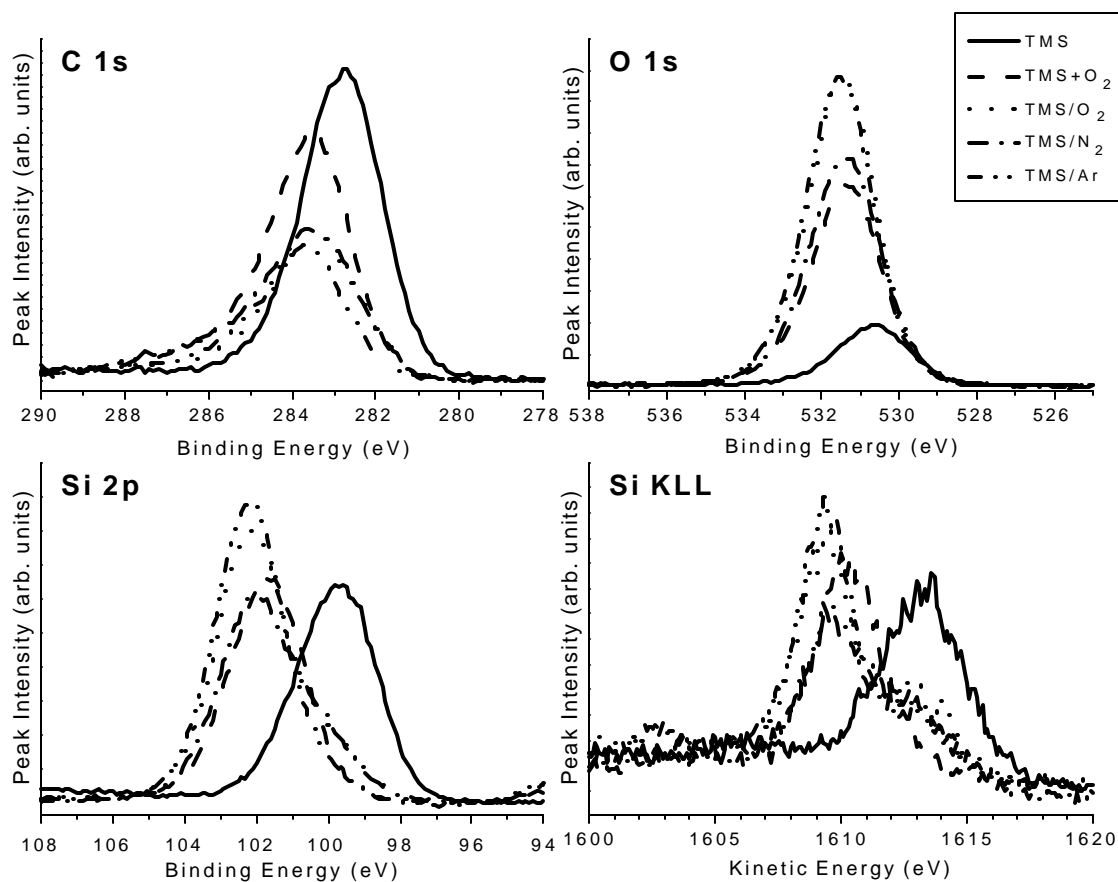

Figure 8. Normal emission photoelectron and x-ray excited Auger spectra from the surface of various films, including a plain TMS film, a mixed TMS+O$_2$ deposited film, and several TMS films with post deposition plasma treatments.

Fig. 9 shows spectra from the same films deep beneath the modified surfaces, after inert ion sputtering, with the addition of a second spectra set from the TMS film at an advanced stage of aging. It now becomes apparent that while the treated films maintain a high degree of Si-C bonding in the bulk, the film formed with the addition of O$_2$ in the plasma does not. It has the carbon bound in C-C structures while the silicon is fairly exclusively bound to oxygen, similar to the surface of the treated films. The level of oxidation is not as complete as on the surface of the O$_2$ treated film, with the peak positioned at slightly lower binding energy and some additional sub-oxide tailing on the low binding energy side, but some level of oxidation is visible

throughout. The level of Si oxidation in some of the plasma treated films appears somewhat misleading, due to the fact that they were not all analyzed immediately after formation, having varying lengths of exposure to atmosphere. The trend toward higher binding energy Si 2p and lower kinetic energy Si KLL peaks, however, is consistent with the longer exposures, as evidenced by the spectra from the same plain TMS film at two different ages.
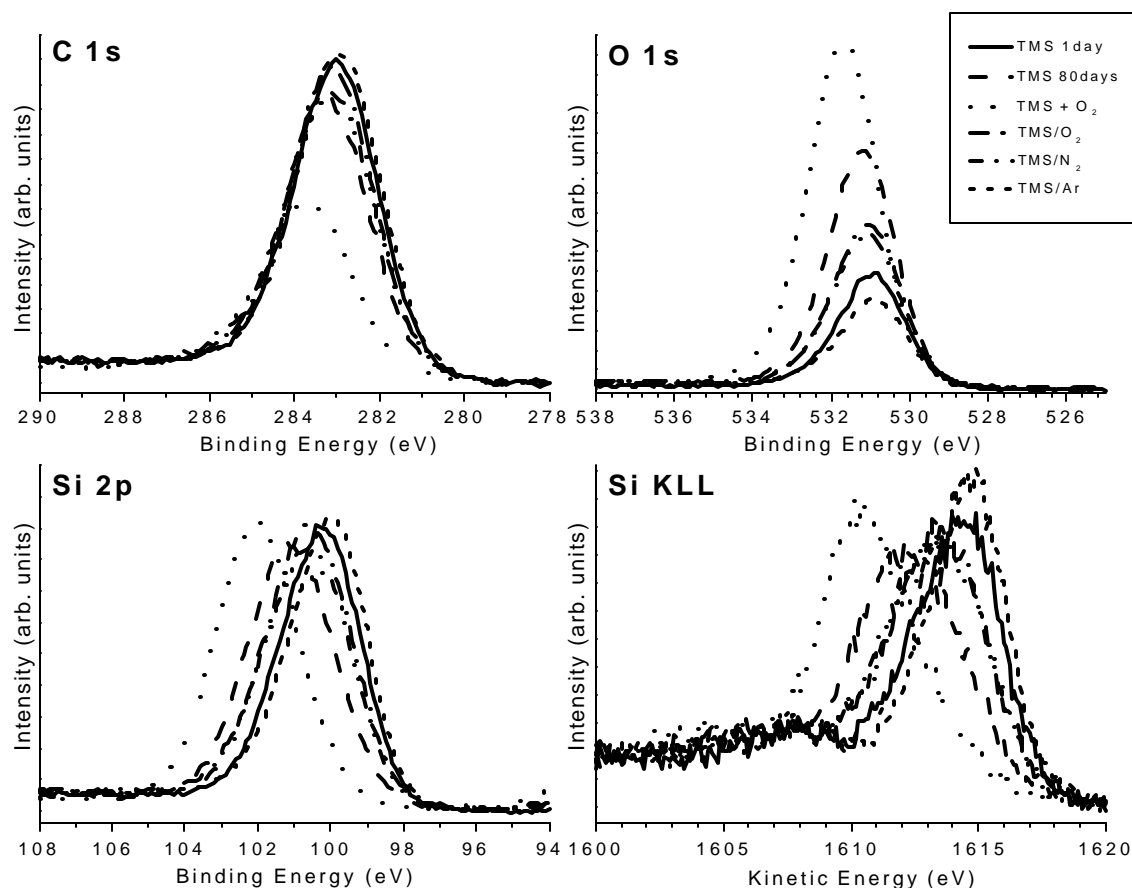

Figure 9. Normal emission photoelectron and x-ray excited Auger spectra taken from the bulk of various films, after the surface regions have been removed with substantial inert ion sputtering.

Fig. 10 complements these arguments. It shows spectra taken as a function of take-off angle, which indicates that the modification is restricted to a thin region on the surface of the film. At smaller take-off angles, a more shallow volume of the material is sampled. It is clear that the underlying structure from the bulk of the TMS film is present in both of the Si spectra, when sampling at the higher take-off angles, which looks deeper into the film. Although not as markedly obvious, the carbon spectra also support the points discussed earlier. The spectra taken at higher take-off angles (deeper) show that the component associated with Si-CH$_x$ bonding resides below the C-C structure, essentially disappearing at the lower take-off angles that sample

the outermost, treated region of the film. As mentioned earlier, some C-O bonding is associated with the small component on the high binding energy side at ~287-8eV in this figure.
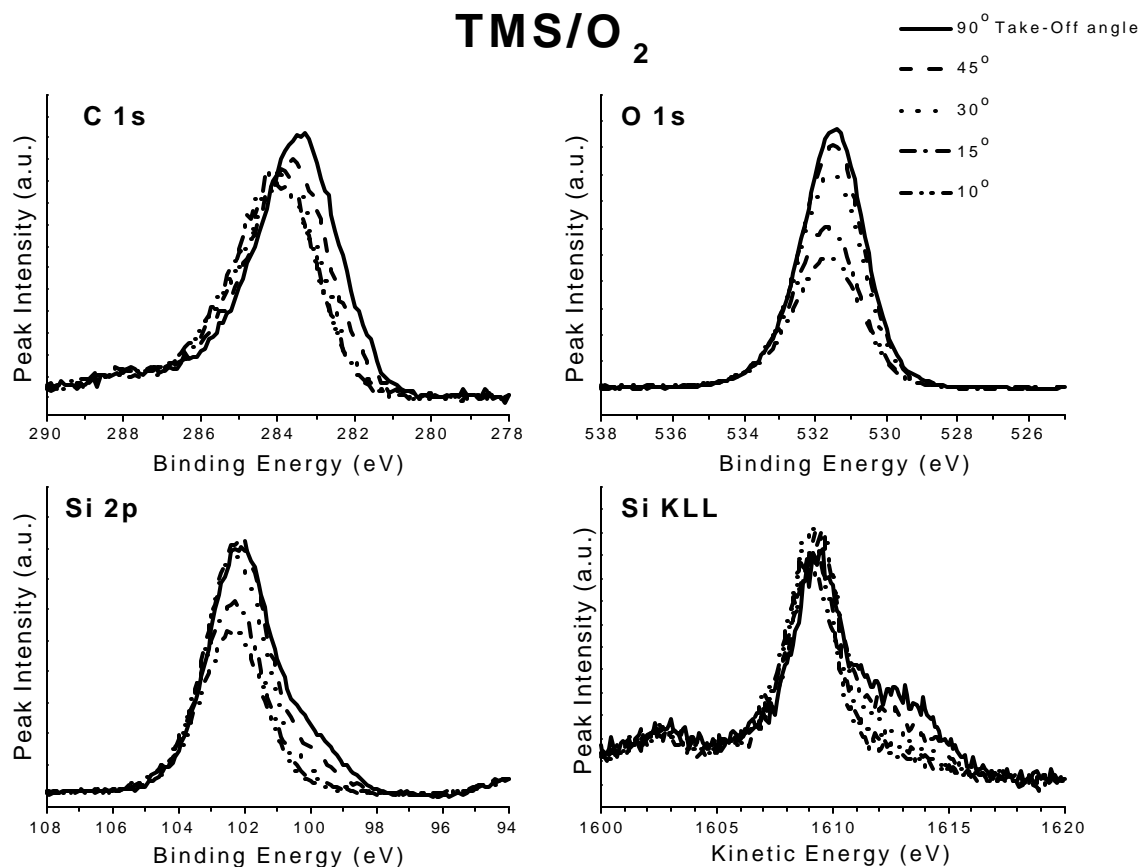

Figure 10. Photoelectron and x-ray excited Auger spectra taken at various take-off angles from the surface of the TMS film treated with an O_2 plasma, showing how the contribution from the underlying bulk TMS film disappears at low take-off angle, revealing the layered structure left after the plasma treatment.

Using a simple model, a rough estimate of the modified layer thickness can be obtained. Since atomic densities are not known for these materials, an approximation based on XPS sensitivity factors gives a plausible value. Using elemental ratios calculated from the 10° take-off angle for the outer region, and values from deep in the bulk after sputtering for the bulk values, an approximate ratio of 1.36 is found for the number of silicon atoms in the inner-versus-outer regions. Likewise, effective attenuation lengths (EAL) of Si 2p electrons ejected by Mg-Ká excitation for these materials are not well known, but again approximate values could be used. Using the average value (2.7nm) from a recent review by Powell and Jablonski [16] for SiO_2 as the outer layer EAL, and a rough guess of 2.5nm for the bulk film, isn't unreasonable. The value for close packed crystalline Si is ~2.3 [16], and above 3.0nm for traditional polymers [17].

Strohmeir's method [18] for calculating the thickness from the normal emission spectrum then yields:

$$d = 2.7 * \ln[(1.36)(\frac{2.5}{2.7})(\frac{I_t}{I_b}) + 1],$$

where I_t and I_b are the intensities of the top and bulk contributions of the normal emission spectrum, respectively. The intensities are calculated from curve fitting the normal emission Si 2p peak with two Gaussian-Lorentzian peaks (30% Lorentzian for the 80eV pass energy), one for the surface oxide and one for the bulk. This gives a thickness d of roughly 6.3nm, with large error from the approximations. So it is seen that the thickness of the treated layer is roughly 10-15% of the thickness of the film, when discussing films on the order of 50nm thick, depending on whether any sputtering/ablation of the original TMS film occurred during the post-deposition plasma treatment. Depth profiling of the treated films also indicates that a substantial decrease in carbon content, as compared to the bulk composition or the untreated TMS film, takes place in this layer.

The XPS analysis supports the ESR data and yields insight into the mechanisms responsible for the changes in free radical concentrations in both the treated films and the mixture, and points to the overall mechanism responsible for the changes in the pure film with exposure to atmosphere. The ESR data showed that the incorporation of oxygen in the plasma polymerization process quenched the free radical signal. This directly correlates to the XPS data showing that in this combined deposition the silicon is now dominantly bonded with oxygen, and the carbon no longer has the binding energy characteristic of Si-C type bonds. The post deposition treatment with O_2 directly oxidizes the surface, again converting the local bonding in a similar manner as the mixture with O_2 in the deposition, but only in the outer region of the film. Likewise, treatment with the other more inert plasmas causes the surface region to oxidize upon exposure to atmosphere, likely due to the breaking of relevant bonds and the creation of free radicals during treatment. This new silcated/oxidized structure on the surface is then void of the free radicals that contribute to the pure TMS ESR signal, and may have some inhibiting effect on the diffusion of oxygen into the bulk.

Conclusion

The effect of the second plasma polymerization on the primary plasma polymer of TMS depends on the nature of the second monomer. Plasma of F-containing monomers decrease ESR signal of TMS and no detectable signal due to F-containing monomer was found. The decay rate of signal decreased significantly (approximately 20%). The etching effect is dominant in these systems.

In contrast to this situation, CH_4 plasma yield ESR signal that is a composite signal of TMS and CH_4. The overall signal increased, but didn't show appreciable decay in 24 hours period. When the sequence was reversed, CH_4/TMS also yield a composite signal that is not the same composite signal from TMS/CH_4 system, and ESR signal intensity increased.

The second treatment by non-polymer forming plasmas also decreased ESR signal of TMS, and decreased the decay rate, indicating that the second gas plasma treatment yields somewhat similar effect found with HFE plasma treatment.

Plasma polymerization of mixtures of TMS and non-polymer-forming gases increased ESR signal but decreased the decay rate, except in the case of oxygen. A mixture of (TMS+O_2) behaved as a completely different monomer. No ESR signal was found in this system.

XPS results help to elucidate some of the relationships observed in the ESR measurements. The incorporation of oxygen in the deposition process is seen to oxidize the silicon sites, while restructuring the carbon bonding, such that it is no longer bound to silicon. This same effect is observed on the surface of the TMS films that were plasma treated with various non-polymerizing gases. This dominant chemical change, associated with the total loss of the ESR signal in the case of the O_2 mixture and the decrease of the ESR signal on the films treated with the post-deposition plasmas, is thus related to the extinction of the free radicals in the film.

Reference

1. H. Yasuda, "Plasma Polymerization", Academic Press, Orlando, FL, 1985.
2. M. Hudis, J. Appl. Polym. Sci. 16, 2397 (1972).
3. N. Morosoff, B. Crist, M. Bumgarner, T. Hsu, and H. Yasuda, J. Macromol. Sci., Chem. A10, 451 (1976).
4. F.F. Oldfield, D.L. Cowan, and H.K. Yasuda, paper submitted to this journal; Part I.
5. Masayo Miyama and Hirotsugu Yasuda, J. Appl. Polym. Sci., **70**, 237 - 245, (1998).
6. C. M. Reddy, Q. S.Yu, C. E. Moffitt, D. M. Wieliczka, R. Johnson, J. E. Deffeyes, and H. K. Yasuda, Corrosion, **56**, No. 8, 819-831, (2000)
7. Q. S. Yu, C. M. Reddy, C. E. Moffitt, D. M. Wieliczka, R. Johnson, J. E. Deffeyes, and H. K. Yasuda, Corrosion, **56**, No. 9, 887-900, (2000).
8. C. E. Moffitt, C. M. Reddy, Q. S. Yu, D. M. Wieliczka, R. Johnson, J. E. Deffeyes, and H. K. Yasuda, Corrosion, 56, No. 10, 1032-1045, (2000).
9. T. Masuoka and H. Yasuda, J. Polym Sci., Polym. Chem. Ed., 20, 2633 (1982)
10. C.E. Moffitt, C.M. Reddy, Q.S. Yu, D.M. Wieliczka, and H.K. Yasuda, Appl. Surf. Sci., 161, n. 3-4 (July 2000), 481-496.
11. H. K. Yasuda, Q. S.Yu, C. M. Reddy, C. E. Moffitt, and D. M. Wieliczka, paper submitted to J. Vac. Sci., & Tech.
12. Hirotsugu Yasuda and Takeshi Yasuda, J. Polymer Sci., Part A: Polymer Chem., 38, 943 (2000)
13. C. D. Wagner, H. A. Six, W. T. Jansen, and J. A. Taylor, *Appl. Surf. Sci.,* **9** (1981) 203.
14. S.D. Waddington, in <u>Practical Surface Analysis, 2nd Ed., Vol. 1-Auger and X-ray Photoelectron Spectroscopy</u>, edited by D. Briggs and M. P. Seah (Wiley, New York, 1990) 587-594.
15. F.J. Himpsel, F.R. McFeely, A. Taleb-Ibrahimi, J.A. Yarmoff and G. Hollinger, *Phys. Rev. B*, **38** (1988) 6084.
16. C. D. Wagner, in <u>Practical Surface Analysis, 2nd Ed., Vol. 1-Auger and X-ray Photoelectron Spectroscopy</u>, edited by D. Briggs and M. P. Seah (Wiley, New York, 1990) 602.
17. C. J. Powell and A. Joblonski, *J. Phys. Chem. Ref. Data*, **28** (1999) 19.
18. D. Briggs, in <u>Practical Surface Analysis, 2nd Ed., Vol. 1-Auger and X-ray Photoelectron Spectroscopy</u>, edited by D. Briggs and M. P. Seah (Wiley, New York, 1990) 443.
19. B. R. Strohmeier, *Surf. and Interface Anal.* 15 (1990) 51.

23. Selective Adsorption of Fluorocarbons and Its Effects on the Adhesion of Plasma Polymer Protective Coatings

C.E. Moffitt[1], C.M. Reddy, Q. S. Yu, D.M. Wieliczka, and H.K. Yasuda

Abstract

Cathodic D.C. plasma deposited films have shown promise as int ermediate adhesion and barrier layers for use in the interface engineering of corrosion protection systems on various materials. The surface treatment of plasma deposited trimethylsilane (TMS) films with various post-deposition plasma treatments can improve the adhesion of various paints to these films, which are usually strongly adhered to underlying substrates. Research into the application of these systems for corrosion protection of aluminum alloys included post-deposition treatments of the TMS films with hexafluoroethane plasmas, which was seen to significantly improve the adhesion of primers. Oxygen plasma cleaning of the alloy surfaces, prior to deposition of the TMS film, is normally employed to remove organic contaminants.   During testing of sample aluminum panels, one batch was processed without the oxygen plasma treatment and exhibited extensive adhesion failures. The investigation of these results shows that low levels of fluorocarbon contaminants readily react with the alloy surface and deposit a fluorine containing carbonaceous layer, which dramatically interferes with the adhesion of the plasma polymer to the alloys, but the adhesion with primer coatings remains tenacious. XPS studies also show that the presence of even low levels of these contaminants in the chamber, during the oxygen cleaning process, is sufficient to induce the conversion of the surface from oxide to a mixture of oxide and fluoride. This conversion is considered detrimental to the corrosion resistance of these systems.

Introduction

Surface modification by plasma treatment and by plasma deposition of thin films has given rise to an exciting realm of interface engineering. These techniques allow for the tailoring of surface chemistry to deliver certain desired properties and to facilitate interface formation between various materials. The application of plasma deposited films, generally referred to as plasma polymers[1] or films formed by plasma chemical vapor deposition or plasma deposition, to specific materials has been seen to promote corrosion resistance, change the wettability of the surface, and promote adhesion of coatings [2-7]. This type of interface engineering requires the selection of particular treatments and film types depending on the desired effect and the specific material to be modified. The advantages of this type of thin film application have spurred commercial endeavors, such as the Vitrinite® finish by Metroline Surfaces, Inc. and the Silcosteel® finish by the Restek Corporation.

Various methods may be used to initiate plasma formation, including microwave coupling in the radio frequency range, audio frequency coupling, DC coupling, as well as other emerging techniques. Each method has its own optimal range of operational parameters, depending on the desired result and the monomers used. One distinct advantage of the DC method is the deposition of a large percentage of the monomer gases. Most of the material introduced to the vacuum chamber is thus deposited on the substrate, which minimizes problems associated with

the venting of unreacted monomer or intermediate gases. Another advantage to the cathodic technique is the increase in adhesion between plasma polymers and metal substrates, as compared to other types of plasma deposition [7].

A better understanding of environmental complications associated with current anti-corrosion technology for protection of aluminum alloys, primarily the use of chromates containing Cr^{6+}, is spurring research into new approaches and coatings for these systems. Amorphous plasma polymers based on silane and siloxane chemistries have shown great promise as viable corrosion protection alternatives that can also increase paint adhesion to parts.[8] While some films have desirable surface properties when they are formed from pure monomers or mixes of process gases, other post-deposition plasma modifications to the primary plasma polymers have been seen to greatly improve bonding to various primers and paints. One particular system has been observed to have tremendous adhesion between plasma film covered alloy panels and paint applied to them. This system involves cathodic DC plasma deposition of a roughly 50nm primary plasma polymer film from trimethylsilane (TMS) onto a properly pretreated alloy substrate, followed by the deposition of an extremely thin fluorocarbon film by DC plasma deposition of hexafluoroethane (HFE).

This film system was seen to outperform others not incorporating the adhesion promoting HFE film. The alloy panels were always treated with an O_2 plasma to remove any organic contaminants from the alloy surface prior to film deposition. After a large number of depositions, one set of panels missed the O_2 plasma treatment but still had the plasma film system deposited on them. These panels were destined for testing with various primers in the Joint Group for Acquisition Pollution Prevention program (JG-APP, which is now JG-PP, the Joint Group for Pollution Prevention). After paint application, they were seen to experience miserable adhesion failures in scribed wet tape testing. The entire paint layer delaminated where it was in contact with tape. Other films deposited with the O_2 plasma treatment, in this same time interval, experienced some diminished corrosion resistance but maintained good primer adhesion. A study of the pretreatment application and the surface prior to deposition indicates that the aluminum alloy panels have a remarkable sensitivity to the build-up of a fluorocarbon background in the plasma reactor. This study also showed that the application of the O_2 plasma treatment modified the alloy surface, changing it from one composed of aluminum oxide to a surface composed of mixed oxide and aluminum fluoride, and in extreme cases, to a mostly mixed fluoride chemistry incorporating some oxygen. These modifications are seen to relate to the diminished corrosion resistance of samples treated in the presence of the fluorocarbon contaminant.

Fluorine contamination in plasma processing environments has been reported and discussed regarding various scenarios [9-16], as has cross contamination from storage in contaminated containers or with contaminated samples [13, 17]. Modification of aluminum deposited on fluoropolymer substrates and other polymers having fluorine based plasma treatments has also been observed [18-20]. Fluorocarbon lubricants have also been observed to modify the oxide structures on aluminum alloys [21, 22]. Likewise Al_2O_3 catalytic supports have been observed to degrade by fluoride conversion during reactions with fluorocarbons [23], and alloy oxide modification has also been well noted in the presence of fluorine compounds not of the fluorocarbon family [24].

Most of these discussions regarding fluorine contamination of aluminum surfaces have focused on the conversion of aluminum oxide to fluoride or oxy-fluoride. Evidence for similar conversions will be presented in this study, and in extreme cases conversion to aluminum bonding quite similar to that in AlF_3 will be seen. The poor adhesion of the samples skipping the O_2 plasma treatment, however, will be seen to be related not to the fluorine contamination as such, but rather to the carbonaceous nature of the initial adsorbate. Oxygen plasma cleaning removes this carbonaceous component, while the surface fluorine concentration is enhanced.

Experimental

All of the plasma polymer films discussed here were deposited using the cathodic DC technique described elsewhere [4]. Likewise, any of the pre-deposition surface treatments were also performed in a DC mode of operation. The trimethylsilane (TMS) monomer was procured from PCR Inc. and Gelest Inc., having 97% minimum purity. The hexafluoroethane (HFE) was purchased from Specialty Gas (Maumee, Ohio). These monomer gases were used with no additional purification. The specific parameters used for the oxygen pre-cleaning were 2sccm O_2, 40watts DC power, 100mTorr, for 2 minutes, and the film deposition parameters were 1sccm, 5watts, 50mTorr for 1 minute each of TMS followed by HFE.

99+% assayed AlF_3 was purchased from Alpha Aesar to use as a reference standard. It was mounted on double-sided tape and used in both its as-received form and after exposure to steam for approximately 2 minutes.

The primary aluminum alloy used in this study was Alclad 7075-T6, although similar results were observed on wet chemically cleaned 2024-T3 and 7075-T6. The alloy panels were 3"x6"x0.032 and all were obtained from Q-Panel Lab Products. Wet chemical pretreatment of the alloys, when performed, was done with Turco Products 4215-S alkaline cleaner and Parker-Amchem Deoxidizer 7.

Films were also deposited on pieces of Si wafer attached to alloy panels, in some instances, allowing for ellipsometry measurements to be made. The Si wafers were obtained from Silicon Quest International, Inc., and were 5", n-type, (111) wafers.

The samples from the JG-APP program whose analyses are included here were selected from a number of panels submitted for the program testing. All the panels used in this testing were Alclad 7075-T6. The primers used on these particular panels are identified as follows:

JG-APP#5—Spraylat EWDG275 A/B, waterborne Type I Non-Chromated Test Primer

JG-APP#6—Dexter/Crown Metro 10PW22-2/ECW-119, Type I Non-Chromated Control Primer

JG-APP#10—MMS 436 Solvent based; Courtaulds 519X303/910X357/020X324 1/, Type I Chromated Control Primer

JG-APP#3—Dexter/Crown Metro PD 218-166/ PD 232-106, waterborne Type I Non-Chromated Test Primer

Although the individual primers are identified here to fit standard norms of reporting experimental details, all of the primers deposited on the panels that missed the oxygen plasma cleaning failed in the same dramatic fashion. The intent is not in any way to attribute the failure to any of the primers. The application of the primers was always within four days after plasma polymer deposition and usually within three days. The spray-applied primers had dry film thickness of 0.8 to 1.2 mils and were air cured at room temperature for a minimum of two weeks prior to any testing.

X-ray photoelectron spectroscopy (XPS) data was acquired with a Kratos AXIS HS instrument, using the Mg-Kα flood source operated at ~217 watts (15mA, 14.5kV). It is better to use the term electron spectroscopy for chemical analysis (ESCA) in this instance since relevant Auger electrons were collected to enhance the chemical information obtained from the samples, but the convention is to include these in the XPS designation. All of the XPS data were acquired in the hybrid mode of the instrument, which combines electrostatic and magnetic lensing. The 2mm aperture, used in the hybrid mode, limits electron collection to a spot size on the order of 200-300µm. Most spectra, and all those shown, were collected with the analyzer set at a pass energy of 80eV, including the individual core spectra. This gives a FWHM of just over 1.4eV for the Ag 3d line. The choice of the lower energy resolution mode of operation was based on the fact that early samples were analyzed in the interest of only obtaining elemental concentrations, where higher elemental sensitivity in a relatively short period of time was the primary concern. This allowed for many samples to be analyzed quickly in hope of identifying gross process irregularities. Once these early analyses were made, it did not seem appropriate to change resolution on the standards or any additional samples whose spectra would be compared to those already analyzed. Charge compensation was made with the manufacturer's proprietary system, at settings of: -1.5V bias voltage, 1.85A filament current, and –0.5V filament voltage (charge balance voltage).

XPS depth profiles were done with a rastered Ar^+ beam. The beam energy was 4kV at a filament emission of 10mA. This gives a current of about 1µA at the sample in a spot size of ~1.1mm, which was rastered over an area of approximately $3x3mm^2$. Data were collected from near the center of this area. Exact depth information was not pursued in this experiment, but for similar TMS films on Si wafer pieces examined in this same frame, where thickness was measured with ellipsometry, a sputter rate of ~2.4nm/min was obtained with this specific arrangement.

Results and Discussion

The initial dramatic failure of a wide range of primers on an entire set of panels gave rise to immediate concern that a potential systematic problem existed. Past results with TMS films having the HFE treatment had shown tenacious adhesion to a wide range of primers, including spray primers, in all forms of testing. Analysis of the failed specimens was quickly undertaken. The adhesion on this particular set of panels after the scribed wet tape test was so bad that the primer could be removed by just lightly pressing a sample stub, with double sided tape on it, against a panel and lifting. This method allowed for the analysis of both sides of the failed

interface. The exposed alloy surface is referred to as the metal side, while the interface side of the lifted primer is referred to as the back of the primer.

Brief surface analysis of the first sample with XPS revealed virtually no silicon on the alloy surface beneath the lifted primer, but did indicate a rather substantial fluorine presence. Analysis of the interface side of the removed primer showed a strong silicon level, indicating that it was possible that the entire plasma film had delaminated at the interface with the alloy, rather than the primer delaminating from the plasma film. Additional samples from the failed set were prepared in a similar manner and were analyzed, with the inclusion of light sputtering and sputter depth profiling, in an effort to confirm the nature of the adhesion failure.

Fig. 1 shows the fluorine 1s spectra taken from the exposed alloy beneath the removed primer from a panel identified as JG-APP#3. Using changes in take-off angle (angle between the sample surface and direction of emission/collection of electrons) and light sputtering, it is seen that the fluorine on the alloy is in two distinct chemical states, one on the outer surface (10° take-off angle) and one just below (90° take-off angle). Angular depth profiling of an additional alloy panel beneath the peeled primer showed similar results to those displayed for JG-APP#3 in Fig. 1. Higher resolution (20 eV pass energy) angular spectra simply repeated the structure with more noise and gave little additional information. Sputtering of these and additional samples further confirmed this two-layer system with respect to fluorine bonding.

The normal emission spectra from the various samples are shown in Fig. 2. The two-state nature is fairly apparent on all of the panels.   JG-APP#6 had a more exclusive contribution from the top-level, lower binding energy state, indicating a thicker layer on this sample. The measurements at the various take-off angles also revealed that Al, O and C were also present in two distinct states in the two layers. While the position of the high binding energy fluorine peak is often related to organic bonding[21], the carbon spectra do not support this assessment on these samples. Higher binding energy fluorine peaks have also been assigned to $Al(OF)_x$ [13,17], which appears to be the case here as well. The lower binding energy peak is generally associated with metal fluoride bonding, but the position of the aluminum 2p peak was not consistent with a direct AlF_x assessment and could be associated with AlC bonding [19]. The peak positions of the other elements in the two layers indicated that a more complicated relationship might exist.

These alloy oxides were thin enough to see a metallic contribution from the underlying alloy in the Al 2p spectra at the sample-normal electron collection angle (90° take-off) after the first sputter. For all of these samples, little silicon was seen on the remaining alloy surfaces.

The surface of the primers opposing the alloy panels, however, had a strong silicon signal. Fig. 3 shows the sputter depth profiles from the back of the removed primer from three of the JG-APP panels. The regions of strong silicon signal in the plots indicate that the tenacious adhesion between the plasma polymer and the primer is still intact and that the mode of failure was purely adhesive at the plasma polymer/aluminum alloy interface. The increase in fluorine signal coupled with the decrease in silicon signal indicates the interface region between the TMS film and the primer, where the HFE plasma polymer resides.
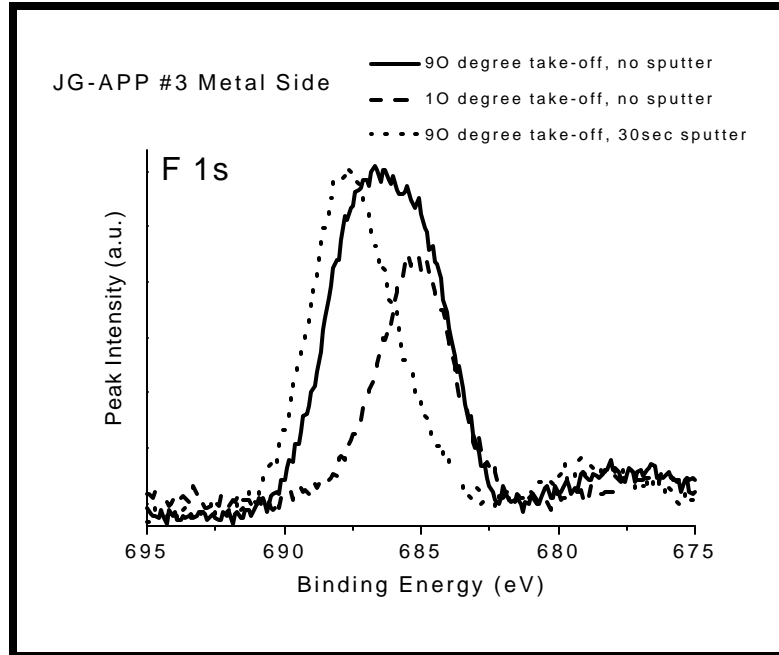
Figure 1. Fluorine 1s photoelectron spectra taken from the exposed alloy surface beneath the removed primer for sample JG-APP#3.
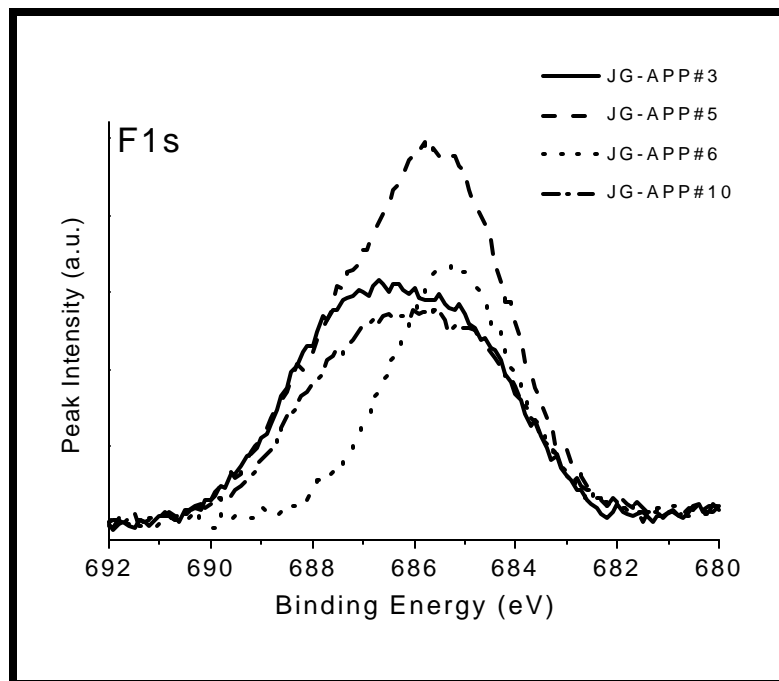

Figure 2. Normal emission (90° take-off angle) F 1s spectra from the exposed alloy, beneath the removed primer, from each of four of the JG-APP samples.

Fig. 4 shows the relative atomic ratios calculated from the depth profiling of the films still attached to the removed primers. This type of plasma polymer has been observed to have fairly consistent ratios as a function of depth in past measurements of similar films. The ratio changes in the region near the interface will be seen to be indicative of the problem with these particular films.
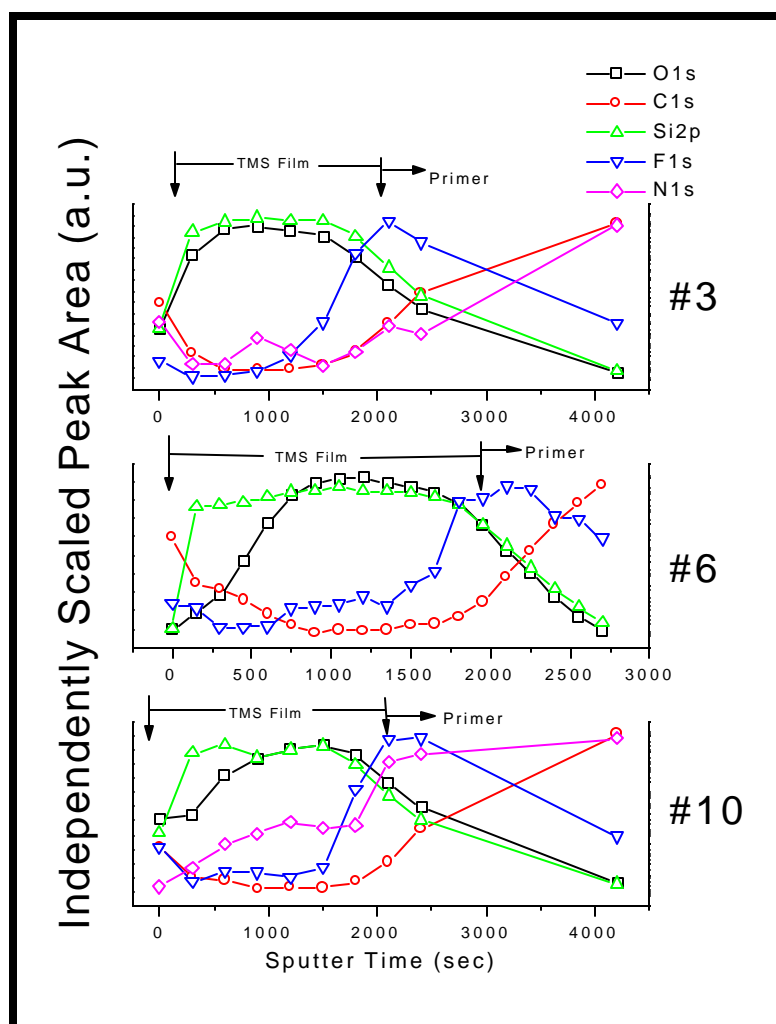

Figure 3. XPS sputter depth profile of the removed paint from three of the JG-APP samples, showing that the TMS film is still intact to the primer.

The high level of fluorine on the exposed aluminum from these failed panels certainly indicated that fluorine played some significant role in the adhesion failure. An extensive investigation ensued to better understand the source of the fluorine at the film/alloy interface and the nature of its role in this systematic failure.

The HFE precursor for the fluorinated plasma polymer treatment was the obvious candidate as the source of the surface fluorine contamination in the plasma reactor. Samples were prepared

for surface analysis to determine the extent of the interaction, assuming that perhaps a leak in a source line was responsible. Prior to any modification of the chamber, a panel was exposed to an oxygen plasma and shipped to the XPS facility for analysis. XPS analysis indeed indicated that it had a substantial level of fluorine on the surface, (fluorine comprised roughly 20 atomic percent of the sampling volume). A panel that was simply introduced to the reactor, the chamber evacuated to the base pressure and then vented was also analyzed. It too showed a certain level of fluorine on its surface, roughly five atomic percent, with a different binding energy. The fluorine on the surface had persisted even after exposure to the atmosphere for a full day while being shipped for XPS analysis. This, and the fact that larger fluorine incorporation on the surface was seen after oxygen plasma cleaning, indicated that a relatively complex interaction was occurring, not just simply a physisorbed contaminant in the reactor. A logical progression of experiments to elucidate the source ensued.
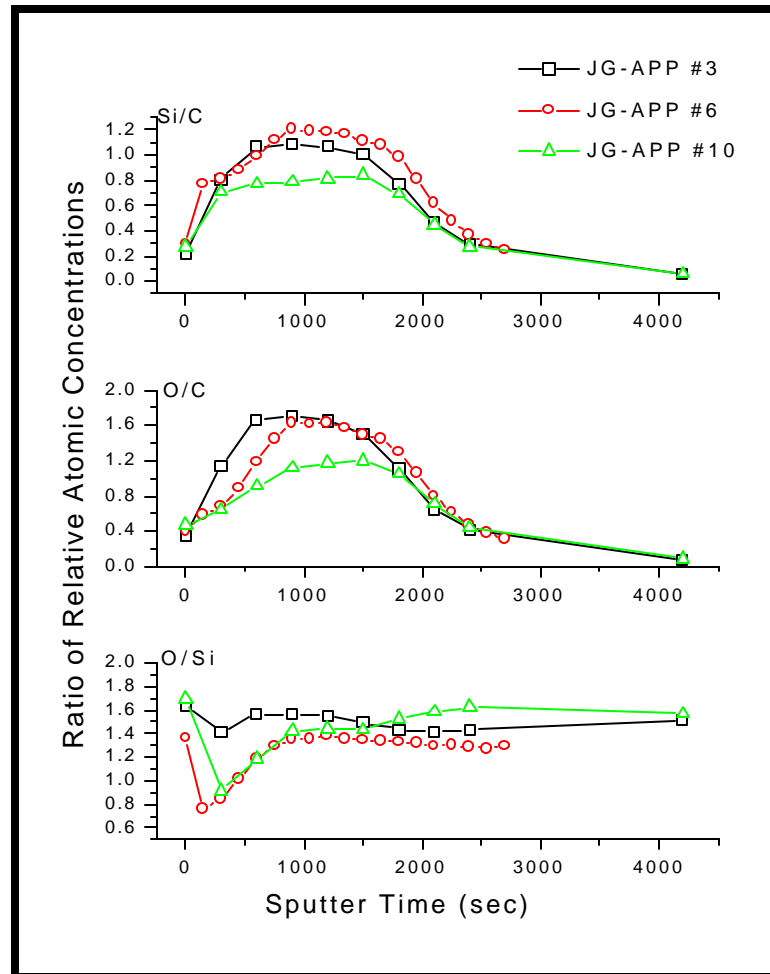

Figure 4. Atomic ratios of the TMS films shown as a function of sputtering time, taken from the back of primers removed from three failed panels.

The most likely source seemed to be a leaking HFE supply line, so it was removed from the reactor and the port was sealed. Samples were prepared similar to those just mentioned, and shipped for analysis. They were examined with XPS the day following their preparation, and showed nearly identical levels to those made with the HFE line attached. Both the carbon 1s and fluorine 1s spectra are shown as Figs.5a and 6a, respectively. Again, the oxygen plasma dramatically increased the fluorine content on the surface of the alloy panel, while decreasing the high level of carbon observed on the panel not having undergone this step. Likewise, the other parts of figure 5 and figure 6 show the respective spectra taken from similarly prepared samples during different stages of reactor cleaning through the course of this investigation.
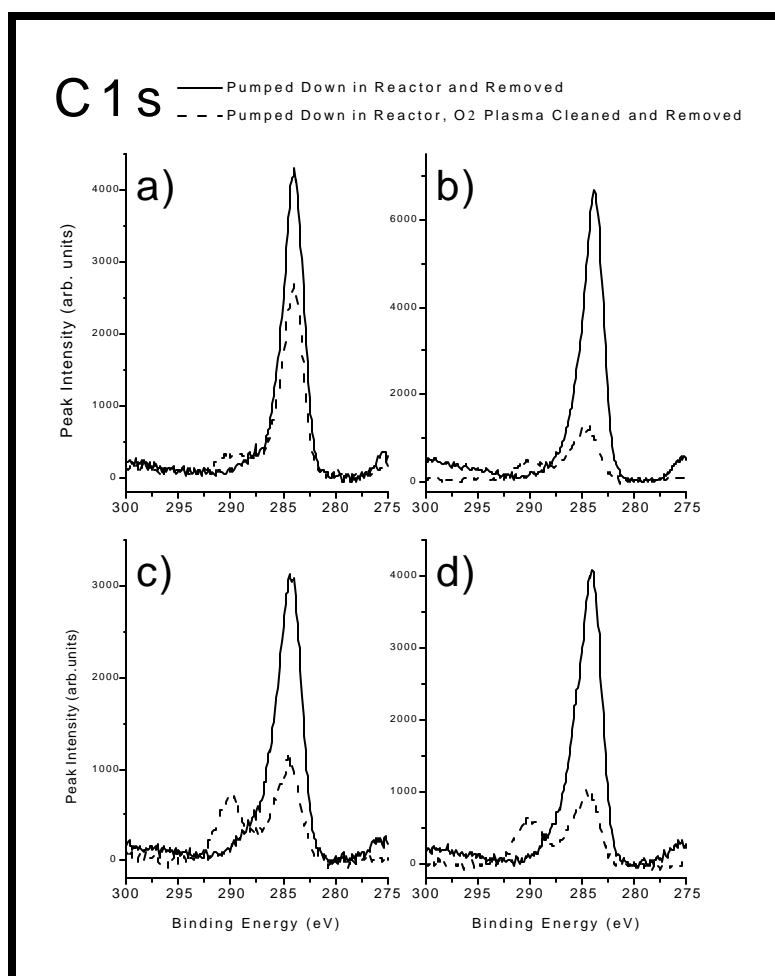

Figure 5. C 1s spectra taken from panels which were pumped down and removed from the reactor or oxygen plasma cleaned and removed from the reactor after four different stages of reactor cleaning. The progression is: a) HFE feed line disconnected; b) just prior to cleaning bell jar; c)after cleaning bell jar; d) after changing pump oil.

All of these samples exhibit the same characteristic features, to some degree. Evacuation of the reactor with an alloy panel present is seen to allow for some fluorine to deposit on the panel,

accompanied by a large carbon concentration with the 1s peak centered near 283.8eV binding energy, just below that of the ubiquitous, adventitious carbon peak. The process of oxygen plasma cleaning greatly increases the fluorine concentration on the alloy oxide, and changes its chemical state, while greatly decreasing the carbon concentration.
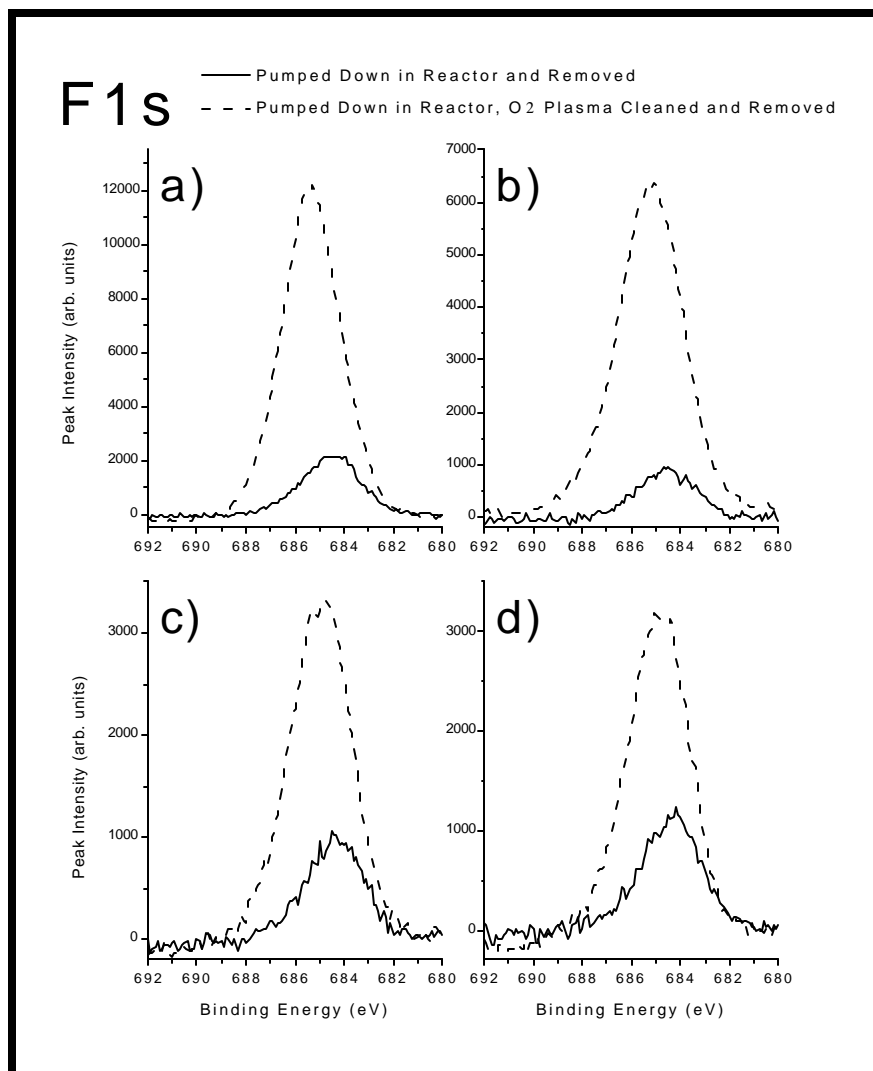

Figure 6. F 1s spectra taken from panels which were pumped down and removed from the reactor or oxygen plasma cleaned and removed from the reactor after four different stages of reactor cleaning. The progression is: a) HFE feed line disconnected; b) just prior to cleaning bell jar; c) after cleaning bell jar; d) after changing pump oil.

It can be seen early in the progression of cleaning steps that even after the oxygen plasma cleaning, the same carbon peak near 284eV develops again (Fig. 5a), while at the later stages (Fig. 5, b-d) it does not persist as dramatically. Over two weeks had passed and a progression of plasma cleaning cycles and TMS depositions had taken place between when the samples in Figs.

5a and 6a were prepared and when the samples shown in Figs. 5b-d and 6b-d were made. No additional fluorocarbon treatments were performed in this chamber during this time. Other samples were made in this interim with an LN_2 trap in place as well, but are not shown here. They showed similar levels of contamination, with a general reduction in the level of contamination and incorporation in the photoelectron sampling volume.

At the reduced levels of contamination, the carbon remaining after the oxygen plasma treatment and the subsequent transport for analysis is in two distinct states; one of which appears to be associated with adventitious carbon (general hydrocarbon contamination from the atmosphere). The position of the low binding energy peak (~284.5eV) is still slightly lower than that of adventitious carbon (~285.0eV) on untreated panels with the same charge neutralization settings used here, which might indicate that some Al-C bonding has taken place or that some remnant of the contaminant remains. On first analysis, the second, higher binding energy peak centered near 290eV seems that it could be associated with CF_2 bonding, but appears more likely to be associated with a carbonate species or carboxylates [25, 26]. There is a distinct lack of any of the other carbon peaks generally associated with fluorocarbon plasma polymerization [1, 27-31], and the F 1s shows no peak at a higher binding energy position consistent with CF_2 bonding. Also, panels that were oxygen plasma cleaned in a different reactor exhibited this same peak at roughly the same strength but had just trace levels of fluorine on the surface. This fluorine level was well below (~30x) that required to fit CF_2 stoichiometry, which seems to confirm the non-fluorocarbon assignment.

As mentioned earlier, oxygen plasma cleaning in the presence of the contaminant caused an increase in the concentration of fluorine on the surface of panels. It is seen in figure 6 that this increase is accompanied by a change in chemical state. The samples that were simply exposed to the evacuation process in the reactor had fluorine 1s binding energies at 684.4eV, prior to any sputtering. This, when coupled to the kinetic energies of the fluorine $KL_{23}L_{23}$ Auger transition from 655.4 to 656.1eV, gives modified Auger parameters from 1339.8 to 1340.5. The associated composite peak positions for the surface prior to sputtering are given in table 1 for the cleaning progression.

After oxygen cleaning, both of the fluorine photoelectron and Auger peaks are shifted in comparison to the position of those from the evacuation samples. As the chamber cleans up the position of the composite fluorine peak on the oxygen plasma cleaned samples changes, as seen in Table 1. Curve fitting these peaks was attempted to ascertain what components or species might contribute to these shifts. The curve fitting was performed above Shirley backgrounds using mixed Gaussian/Lorentzian lineshapes, with 10% Lorentzian composition for the fluorine peaks. The choice of composition was based on fitting the leading edge of the peak envelope and was then assumed similar for deeper peaks. Choice of components was based on peak asymmetries and comparisons of peak behavior between samples at various levels of contamination, after oxygen plasma cleaning, and during sputtering of the samples.

The use of one peak for the fluorine spectra exposed to the evacuation process could not fit an asymmetry on the higher binding energy side, which sometimes presented itself as a shoulder on other spectra that are not shown. An additional peak allowed for a much better fitting solution for all of the spectra, but was of quite small magnitude on several of them. The initial peak

widths were obtained by fitting samples after the contamination decreased in the reactor, leaving a better-defined individual peak on the samples simply exposed to the evacuation process. These same components, frozen in position and width, were unable to fit the fluorine spectra from the oxygen plasma treated samples. A reasonable fit of these was obtained with two components only if the positions and widths were allowed to float. One component then maintained a relatively stable position and width, but the other varied in position, unidirectionally, through almost 0.8eV as the contaminant was cleaned from the reactor. This shifting was considered unrealistic, so it was then that a third component was added, which allowed the positions and peak widths to be fixed and obtain a good fit for all of the similar spectra.

Table 1. Listing of fluorine 1s binding energies and KLL kinetic energies through cleaning progression. Letter indications a-d reference spectra from Figure 6.

	Evacuated and Vented			Oxygen Plasma Cleaned		
	F 1s	F KLL	α	F 1s	F KLL	α
HFE feed line disconnected a)	684.4	655.8	1340.2	685.6	654.5	1340.1
Prior to cleaning bell jar b)	684.4	655.4	1339.8	685.2	655.0	1340.2
After cleaning bell jar c)	684.4	655.9	1340.3	684.9	655.4	1340.3
After changing pump oil d)	684.4	656.1	1340.5	684.8	655.4	1340.2

Once an optimized number of components were obtained, their peak widths were frozen and this composition applied to other samples with varying levels of contamination to determine if the model fit all stages of contamination. This method revealed two F 1s peaks on the samples just exposed to the reactor evacuation. A lower binding energy peak at 684.4-684.5eV and a higher binding energy peak of 686.8-686.9eV. On the oxygen plasma treated samples a third dominant peak was necessary to fit the spectra. This had a binding energy of 685.7eV and its contribution to the composite spectra was seen to monotonically decrease as the chamber cleaning progressed. The energy of this additional peak is the same as that attributed to fluoride formation, but not exactly AlF_3 [19].

Brief depth profiling was undertaken on many of these samples and shows that either the chemistry after sputtering, or the surface charging, is somewhat different than that discussed to this point. Figure 7 shows the associated spectra taken before and after the first 15 second sputter cycle from the panel exposed to the evacuation process and removed, while figure 8 shows similar spectra taken from the oxygen plasma treated panel. The two panels used in Figs. 7 and 8 were those samples prepared just prior to cleaning the bell jar. The change in carbon binding energies on the oxygen plasma cleaned sample confuses the interpretation. The peak positions from these spectra are listed in Table 2 and the modified Auger parameters for aluminum are listed in Table 3. The fluorine peak positions reference the composite peak position while the aluminum peak positions reference the non-metallic components of the spectra. Curve fitting of the fluorine peak was performed with the same components used for the surface prior to sputtering, mentioned earlier. A reasonable fit was obtained by simply adjusting the amplitudes of these components. After the first sputter the primary fluorine peak is the high binding energy peak at 686.9-687eV, and it decreases as the reactor is further cleaned. Curve

fitting was also used to distinguish the non-metallic components of the Al spectra. Additional peaks were used for the aluminum and oxygen spectra when necessitated by large asymmetries or additional features. Although helpful in determining whether additional components might be present, curve-fitting results are not always unique solutions and should thus be treated with caution when discussing component positions.
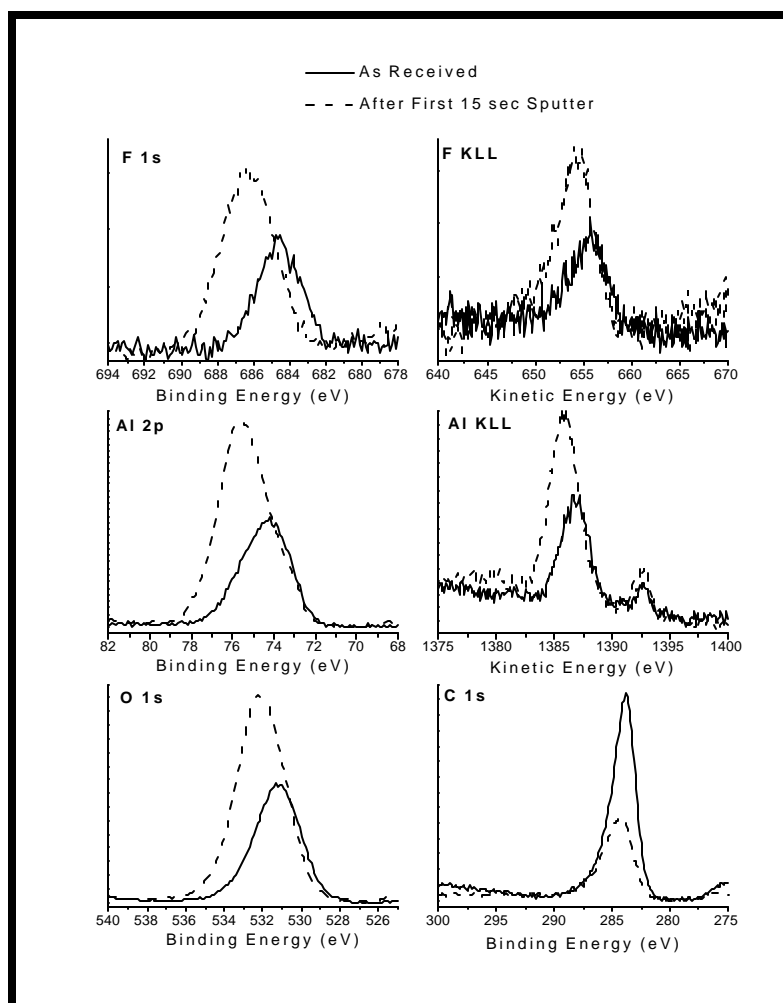

Figure 7. Spectra before and after the first sputter cycle from the panel exposed to the evacuation process and removed just prior to cleaning the bell jar.

The shift in spectral positions after sputtering could be attributed to the removal of a hydroxylated layer, known to reside on the surface of aluminum oxides exposed to atmosphere [24, 32, 33]. The direction of the shift of the oxygen peak, in particular, is wrong for this to be the case, though, according to the references just listed. The aluminum photoelectron and Auger electron lines exhibit a substantial shift (on the order of 1eV) after sputtering, but the Auger parameters shift just slightly. This same behavior was observed on other alloy surfaces, and could be related to the use of charge neutralization. The surface could be overcompensated by

the charge neutralizer prior to the first sputtering, supported by the largest C1s peak at 284.6eV, below the accepted value of 285eV for adventitious carbon [34]. After sputtering, pathways opened to the metal could limit this overcompensation. If it were the case, this same effect should also disallow any shifts to appreciably higher binding energy from positive charging, particularly when the charge neutralizer is also used. The origins of this shifting are unclear, but it was considered prudent to point this effect out, for the proper reporting of results. Because of the elements involved, a sample of AlF_3 was used as a comparison standard.

Table 4 shows the positions of the relevant peaks from this standard, a fair amount of carbon remained after sputtering the steam exposed sample, so its binding energy is also reported in the carbon reference column. Since hydrating/hydroxylating effects are known to pertain to alumina surfaces, the AlF_3 sample was also exposed to steam to help determine how hydration affected its surface. A high binding energy tail was observed on the dry AlF_3 standard, which was not seen on the sample exposed to steam. An additional peak with a binding energy of 689.8eV was required to fit the spectrum. The origin of this additional peak is not apparent, but peaks with these energies have been attributed to fluoropolymers (F-C bonding) and bonding with oxygen containing ligands [19], and a similar peak has been observed on fluorine contaminated aluminum [24]. The appearance here seems to be related to some contamination on the dry sample, which also had second oxygen and carbon peaks, similar to the reports of data taken from AlF_3 standards by others [19]. The position of the additional carbon peak (288.7eV) indicates that this contaminant is likely an organic compound incorporating fluorine, which appears to confirm that this contaminant peak is not associated with $Al(OF)_x$ on this sample. The values of the modified Auger parameter associated with the dominant AlF_3 peaks were close to those obtained by Du and Gardella [19], but the binding energies were not exactly in accord with those observed by Strohmeier [24]. The spectra from the sample exposed to steam appear relatively pristine prior to sputtering, which seems to imply that any AlF_3 taken into solution with the water then deposits out as AlF_3 when exposed to the vacuum, and the AlF_3 does not form a hydrated phase in this manner.

Table 2. Listing of component energies for samples made just prior to cleaning the bell jar.

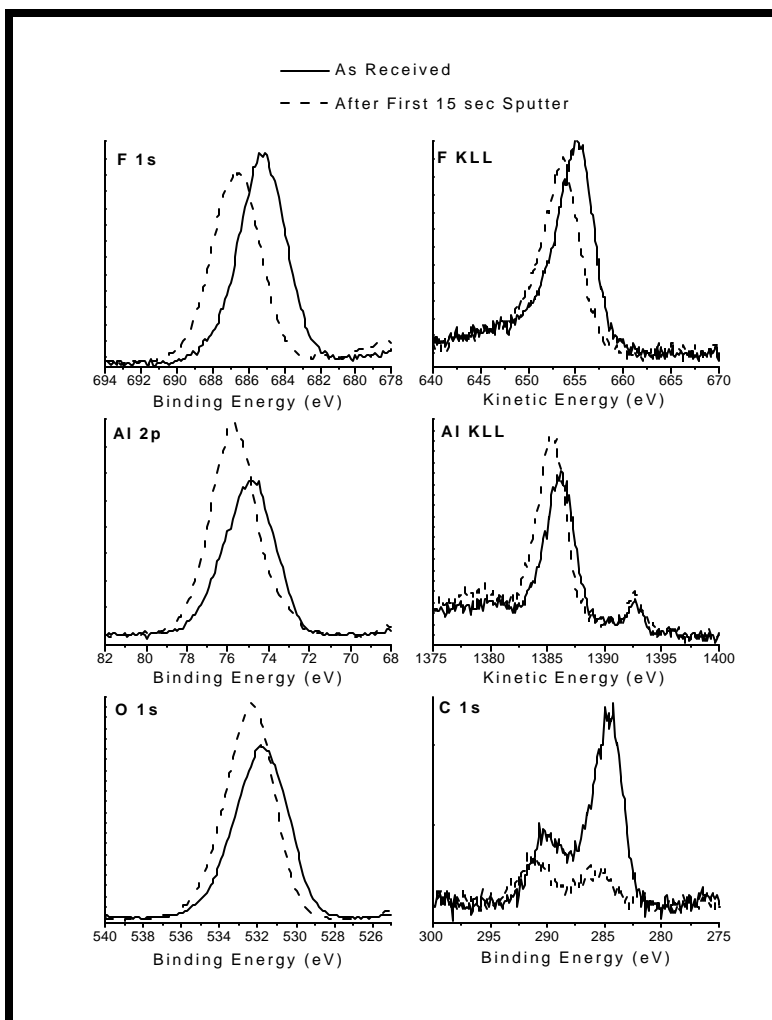|	Before Sputtering		After first 15 second Sputter	
	Evacuated and Vented	Oxygen Plasma Cleaned	Evacuated and Vented	Oxygen Plasma Cleaned
F 1s (binding energy)	684.4	685.2	686.3	686.7
F KLL (kinetic energy)	655.4	655.0	654.3	653.5
Al 2p (binding energy)	74.6	74.9,76.9	75.6	75.8
Al KLL (kinetic energy)	1386.9	1386.2	1385.8	1385.4
O 1s (binding energy)	531.1, 532.9	531.7, 533.7	532.1	532.2, 533.5
C 1s (binding energy)	283.8, 285.6	284.6, 286.9, 290.1	284.3, 286.5	285.8, 291.0

Figure 8. Spectra before and after the first sputter cycle from the panel that was oxygen plasma treated and removed just prior to cleaning the bell jar.

Table 3. Listing of aluminum modified Auger parameters for samples made just prior to cleaning the bell jar.

	Before Sputtering		After first 15 second Sputter	
	Evacuated and Vented	Oxygen Plasma Cleaned	Evacuated and Vented	Oxygen Plasma Cleaned
Aluminum non-metallic α	1461.5	1461.1 (lower BE peak used)	1461.4	1461.2

Table 4. Peak positions from aluminum fluoride standard in each of three conditions

	Fluorine			Aluminum			Carbon Reference
	1s	KLL	α	2p	KLL	α	1s
AlF$_3$ as-received	686.7 689.8	652.3	1339.0	76.7	1382.8	1459.5	285.0 288.7
AlF$_3$ exposed to steam	686.4	652.6	1339.0	76.65	1383.0	1459.65	284.4
AlF$_3$ exposed to steam and sputtered	687.4	651.8	1339.2	77.3	1382.5	1459.8	284.5

A comparison of spectra from the various samples is shown in Fig. 9. The spectra from the alloy panels are those taken after the first sputter cycle. Fig. 9 also contains spectra taken from an aluminum panel exposed to an extreme contamination condition. It was treated with a plasma formed by a 1:1 ratio of O$_2$ and HFE. The aluminum photoelectron and Auger peaks from this sample show distinct overlap with those from the AlF$_3$ sample, although the primary fluorine peaks do not. It appears that in this extreme, aluminum fluoride bonding is a likely occurrence, with fluorine also in an additional structure. This, coupled with the positions of peaks from the various samples and the two layer structure on the JG-PP samples, indicates that many mixed species seem to be present on the surface of these samples, with some likely related to the formation of aluminum fluorides and oxy-fluorides.

Aluminum fluoride is known to be water-soluble [35], so a test of the solubility of the contaminated surface was made. A piece of the panel that was O$_2$ plasma treated after the HFE line was disconnected (same panel used in figures 5a and 6a) was depth profiled with argon sputtering. A second piece from the same sample was washed in de-ionized (DI) water and then depth profiled. A decrease in fluorine concentration was observed throughout the surface layer, but the fluorine was not removed entirely. Prior to washing in the DI water, the maximum concentration of fluorine was ~21.5 atomic percent of the sampling volume. This maximum occurred after the first 15 seconds of the sputter cycle. Fig. 10 shows fluorine 1s spectra from the sample in each condition both before and after 15 seconds of sputtering. The maximum concentration after the DI wash was just over 7 atomic percent, and again occurred after the first sputter cycle. This was not as low as the fluorine level on panels that had simply been exposed to the evacuation process but still substantially lower than the level before the wash. This partial solubility aspect seems to indicate that there are indeed aluminum fluorides present on the oxygen treated samples, as well as insoluble oxy-fluorides that were not readily removed. Strohmeier [24] has noted that hydrated aluminum fluoride is also insoluble in cold water.

During the course of studying various plasma polymers deposited on aluminum alloys, spectroscopic ellipsometry was employed to aid in the interpretation of XPS results and to follow the evolution of the films. The rough surface of alloys is not a viable substrate for this, hence Si (111) wafer pieces were attached to alloy panels and had the plasma polymers deposited on them, as well as the mounting panel. While investigating the source of failure of the particular JG-APP sample set, it was observed that some panels had films that were easily removed with ethanol. This was a very visible phenomenon due to thin film interference effects, but was also

verified with XPS. It was then observed that the films on the Si pieces, deposited in the same deposition as those easily removed from the alloy, could not be removed with ethanol, even after more than one hour in an ultrasonic cleaner. An experiment to understand this difference was undertaken.
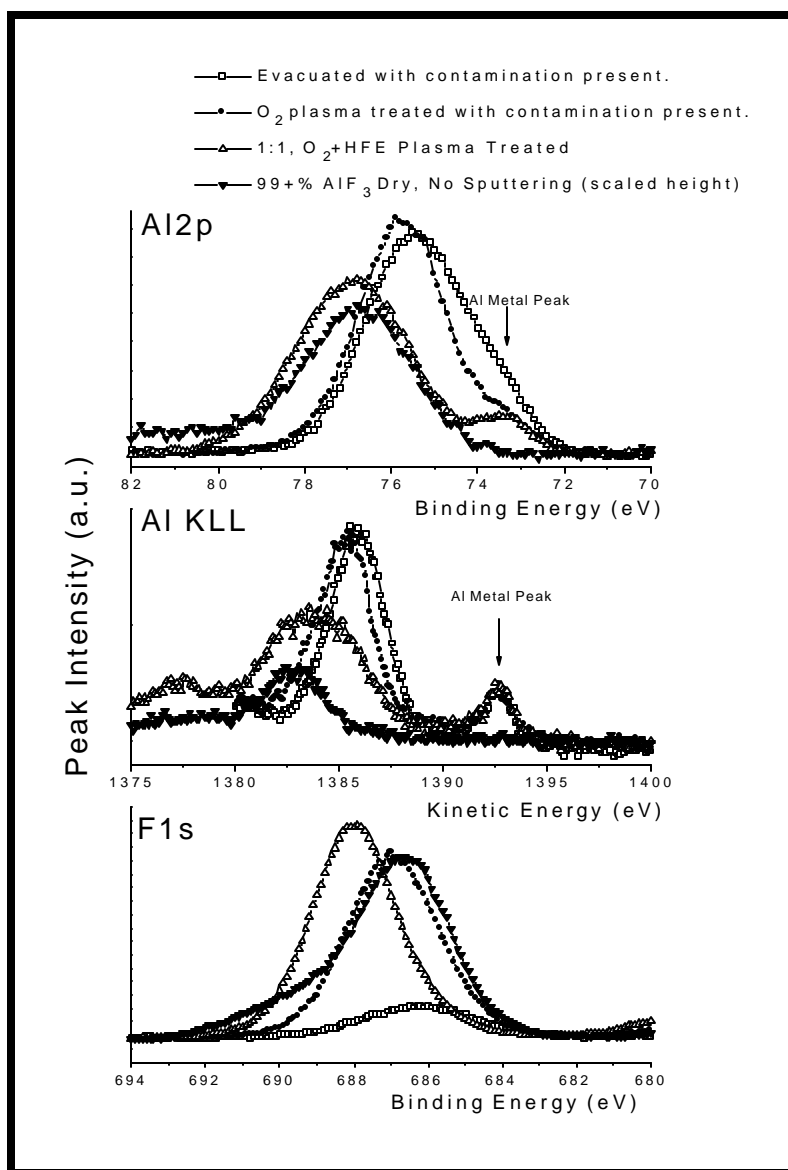

Figure 9. Comparison of spectra between panels exhibiting the fluorine contamination and an AlF$_3$ reference.
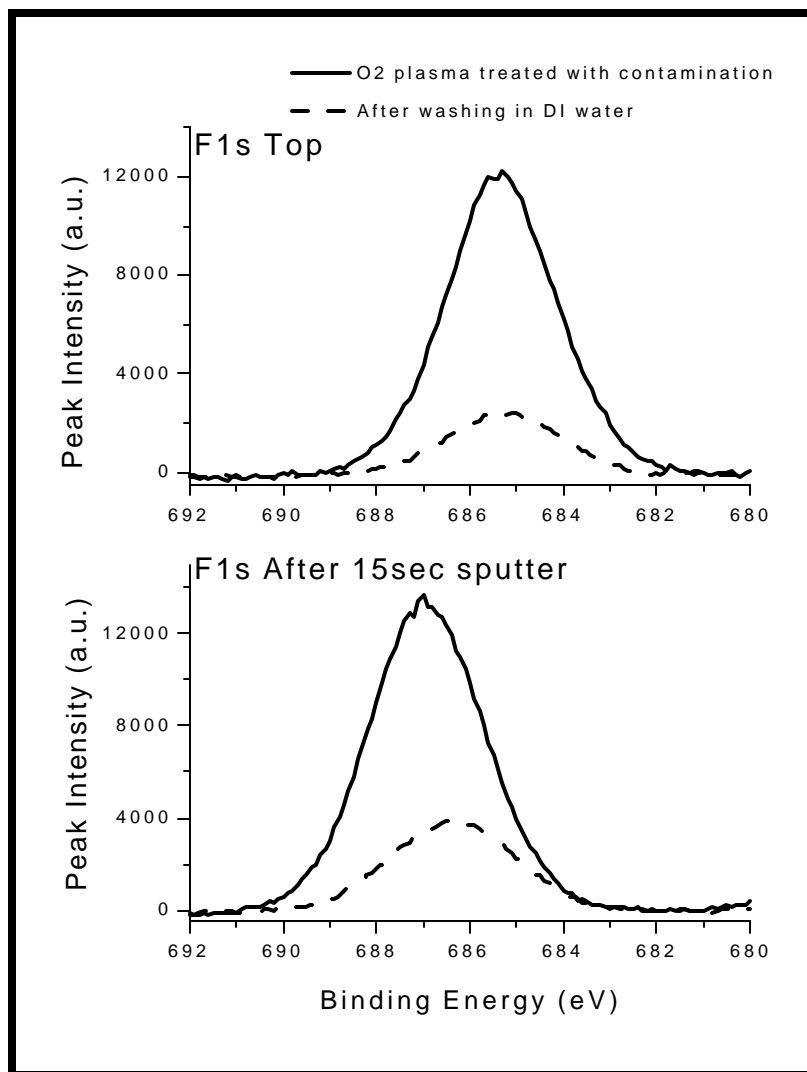
Figure 10. Fluorine 1s spectra from a sample that was O_2 plasma "cleaned" in the presence of the contamination. Spectra shown were taken from a piece without additional modification and a second piece that was washed in DI water. The top set of spectra is from the surfaces as placed in the vacuum chamber. The bottom set was taken after the first sputter cycle in a depth profile.

Panels with Si pieces attached to them were then exposed to the evacuation process and the oxygen plasma treatment, just as the samples discussed in Figs. 5 and 6. The results of XPS analysis of the Si pieces and the alloy panels are shown in Figs. 11 and 12. The top panel of each figure corresponds to the samples being exposed to the evacuation process and the bottom panels corresponds to the samples being oxygen plasma treated. It is very evident in Figs. 11 and 12 that the long-lived contamination only affects the alloy panel and not the Si wafer. After the evacuation process, the alloy panel has both fluorine and the large, low binding energy carbon signal, while the Si wafer piece has no fluorine on it and only carbon associated with adventitious hydrocarbons. There is fluorine on the silicon wafer piece after oxygen plasma cleaning, but aluminum was also observed to be deposited on it from sputtering effects, which

certainly complicates any interpretation of the origin of the fluorine on the silicon. The oxygen plasma treatment again removed the large carbon concentration from the alloy panel. This preferential adsorption of the fluorocarbon contaminant thus fully explained the differences in adhesion of the plasma polymer on the alloy as compared to on the attached silicon.
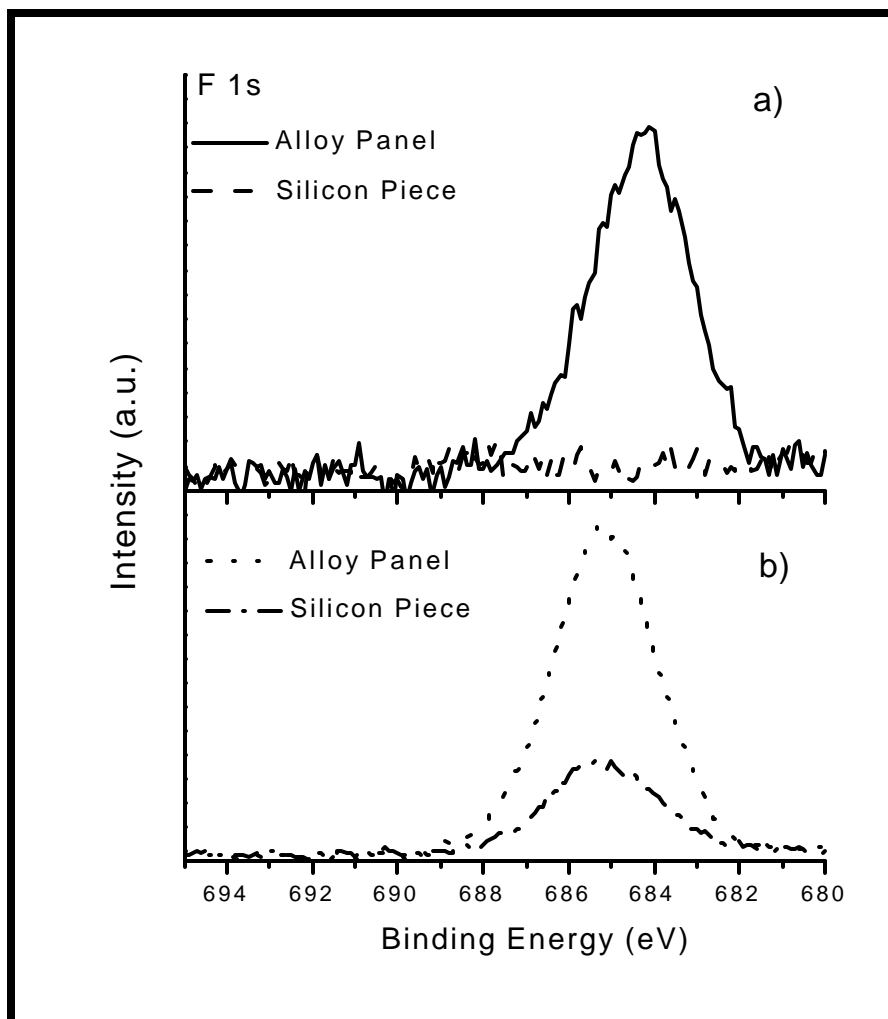

Figure 11. Fluorine 1s spectra from both alloy panels and Si wafer pieces attached to them after: a) exposure to the evacuation process and b) oxygen plasma treatment.

The role of this contaminant on the interface characteristics between the TMS film and the alloy is also quite evident in the sputter depth profiling results shown in Fig. 13 and the focus profiles shown in Fig. 14. These were from two samples; the first of which had the TMS and HFE films deposited on Alclad 7075-T6 after a acetone wiping, while the second sample was O_2 plasma treated prior to film application. Although the carbon depth profile alone shows little variation between the two samples, the Si/C ratio shows the effect of the fluorocarbon adsorption on the interface film properties. The O_2 treated sample maintains a consistent ratio through the interface, while the sample with no plasma cleaning exhibits a definite decrease in this ratio,

indicating increased carbon concentrations at the interface. This Si/C ratio was seen to be a good indicator of film stability, with extremely poor films having a markedly lower ratio. The effect of the oxygen plasma treatment in the presence of the contaminant is again borne out in the fluorine profile, showing the large increase in fluorine concentration at the interface on the oxygen plasma treated sample. The fluorine depth profile from the sample without plasma treatment also shows the more moderate fluorine level at the interface from the adsorption on the alloy oxide, associated with the carbon increase.
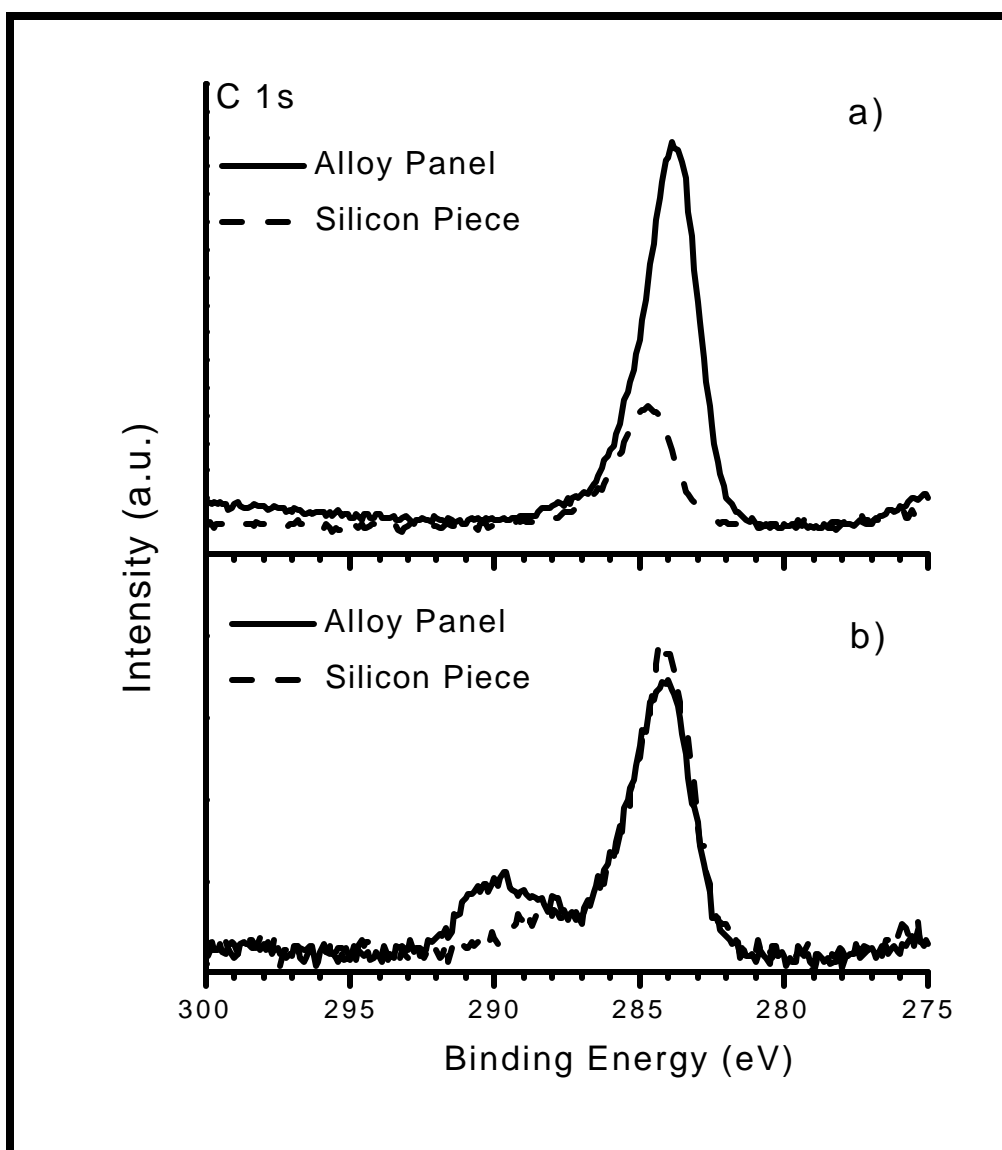

Figure 12. Carbon 1s spectra from both alloy panels and Si wafer pieces attached to them after: a) exposure to the evacuation process and b) oxygen plasma treatment.
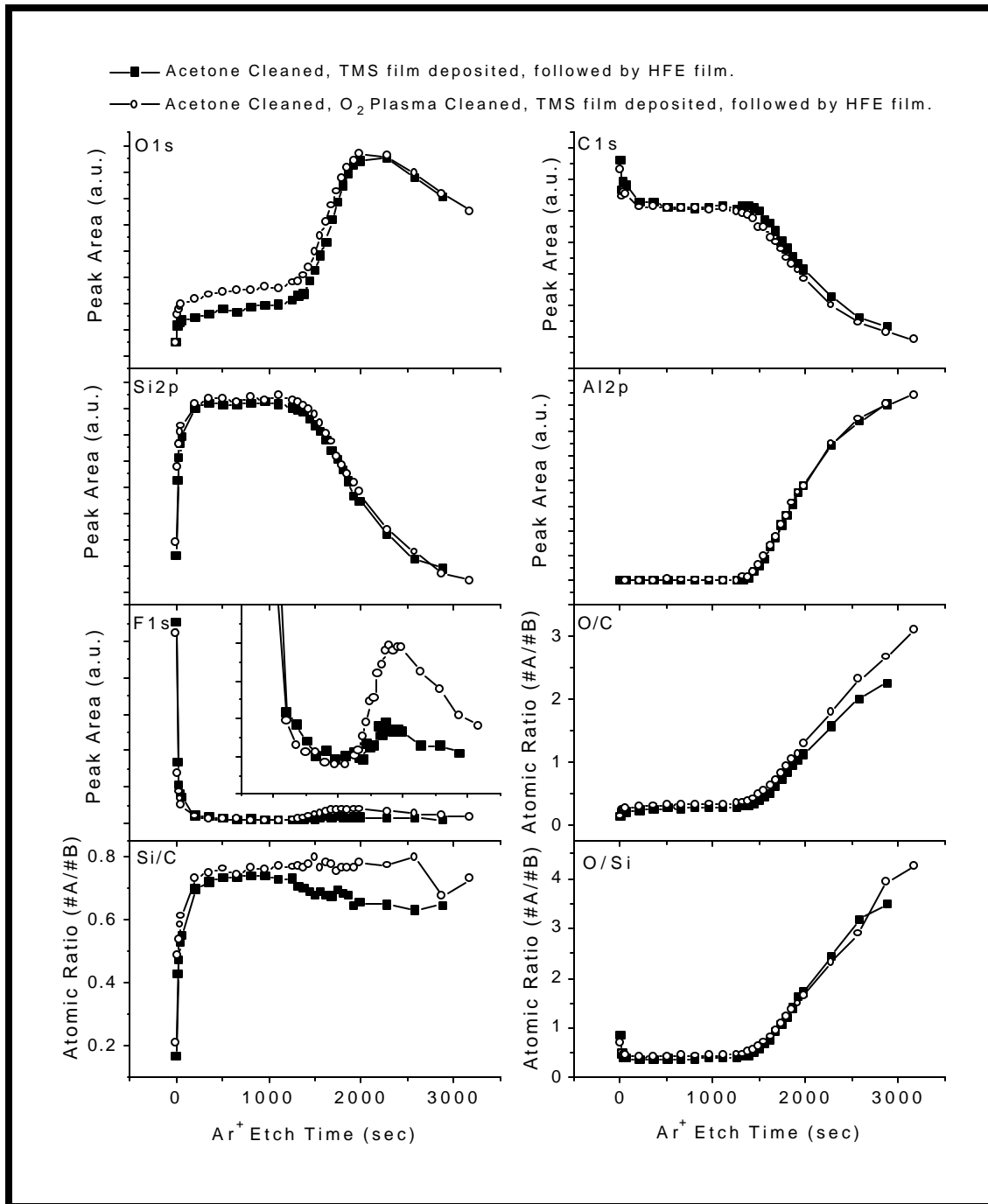
Figure 13. Depth profiles showing peak area and selected atomic ratios from two films on aluminum alloy Alclad 7075-T6. The TMS and following HFE films were deposited on one sample after just acetone cleaning while the second had the O_2 plasma treatment prior to film deposition.
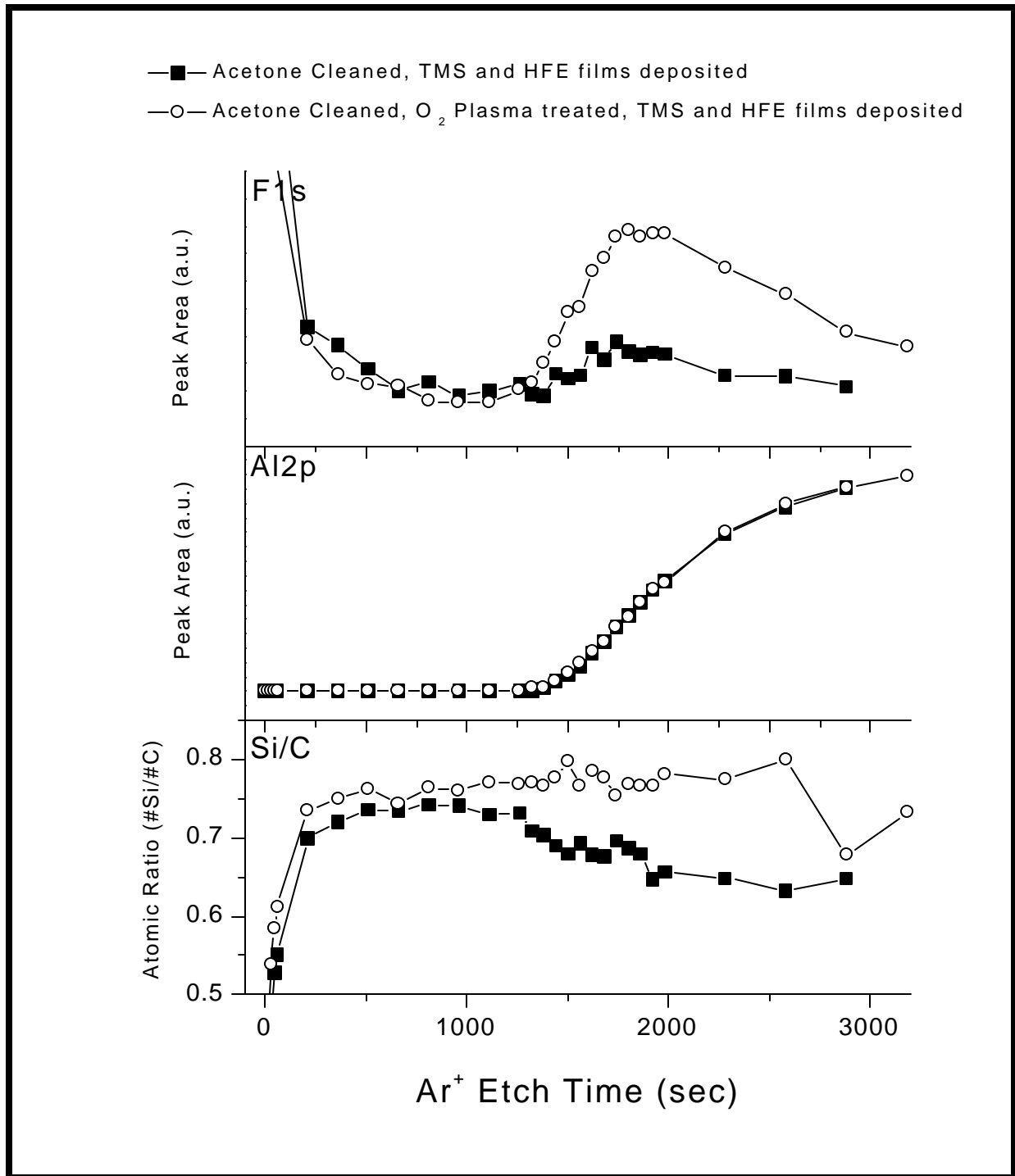
Figure 14. Enlarged depth profiles from figure 15 focussing on the increase in fluorine concentration at the interface on the O_2 plasma treated sample and the decrease in the Si/C ratio at the interface on the panel without the O_2 plasma treatment.

Summary

A dramatic failure of a set of panels sent for adhesion testing has been shown to be related to the adsorption of a fluorocarbon contaminant. The adsorbed contaminant caused the purely adhesive failure between the plasma film and the alloy substrate, which is related to the increased carbon level. Tenacious adhesion of primers to the TMS/HFE plasma polymer combination was shown to remain intact when entire coating systems were easily removed from alloy panels. The adhesion was restored by oxygen plasma treatment prior to film deposition, but in the presence of the contaminant this changed the alumina on the alloy panel into an oxy-fluoride that was seen to be water-soluble. The adsorption was shown to be selective to the alloy surface, not at all affecting the SiO_2 surface of attached silicon wafers.

Conclusions

Interface modification with plasma processes has the capability to tailor adhesion of coatings substantially. Certain reactions within the plasmas are still not well understood, however. The hard deposits left by plasma polymerization of gaseous monomers are the desired result of particular modifications, but volatile species formed in intermediary processes have been seen to play a large role in interface formation. The contaminant species discussed here were formed from a very low molecular weight monomer gas (hexafluoroethane), and persisted after many cleaning cycles. Their origin is speculated to be from oligomer formation during previous plasma treatments with the HFE monomer. These oligomers persist in the reactor, on walls and hardware, but are easily displaced by the evacuation process, allowing their movement to newly inserted surfaces, essentially appearing as fluorocarbon oils. Their stable adsorption to and modification of aluminum oxides preferentially over silicon oxides is perhaps related to the often catalytic and Lewis nature of aluminum oxides. The inability to easily control the contamination level was viewed as highly problematic. The use of fluorocarbon plasma processing for adhesion promotion on TMS films has been temporarily halted on the aluminum alloys by this group, despite early results indicating that tenacious adhesion could be achieved between primers and surfaces treated this way. The corrosion aspects of oxide to fluoride conversion on aluminum and other metals have large ramifications in many fields, and need to be considered when fluorocarbons are employed.

References

[1]   H.K. Yasuda, Plasma Polymerization, (Academic Press, Orlando, Fla., 1985).
[2]   T. J. Lin, J. A. Antonelli, D. J. Yang, H. K. Yasuda, and F. T. Wang, Prog. in Org. Coat. 31 (1997) 351.
[3]   H. K. Yasuda, T. F. Wang, D. L. Cho, T. J. Lin, and J. A. Antonelli, Prog. Org. Coat. 30 (1997) 31.
[4]   T. F. Wang. T. J. Lin, D. J. Yang, J. A. Antonelli, and H. K. Yasuda, Prog. Org. Coat. 28 (1996) 291.
[5]   Y. Lin and H. Yasuda, J. of Appl. Polym. Sci. 60 (1996) 543.
[6]   H, Yasuda, B. H. Chun, D. L. Cho, T. J. Lin, D. J. Yang, and J. A. Antonelli, Corrosion 52 (1996) 169.
[7]   T. F. Wang and H. K. Yasuda, J. of Appl. Polymer Sci. 55 (1995) 903.

[8]   C. M. Reddy, Q. S. Yu, C. E. Moffitt, D. M. Wielizka, R. Johnson, J. E. Deffeyes, and H. K. Yasuda, Corrosion, submitted.

[9]   P. C Karulkar and N. C. Tran, J. Vac. Sci. Tech. B 3 (1985) 889.

[10]   S. Jimbo, K. Shimomura, T. Ohiwa, M. Sekine, H. Mori, K. Horioka, and H. Okano, Jpn. J. Appl. Phys. 32 (1993) 3045.

[11]   Y. Shacham-Diamond and R. Brener, J. Electrochem. Soc. 137 (1990), 3183.

[12]   D. A. Bohling, M. A. George, and J. G. Langan, in IEEE/SEMI Advanced Semiconductor Manufacturing Conference and Workshop: ASMC '92 Proceedings   (IEEE, New York, 1992) p.111.

[13]   K.-H. Ernst, D. Grman, R. Hauert, and E. Holländer, Surface and Interface Anal. 21 (1994) 691.

[14]   J. H. Thomas, III, C. E. Bryson, III, and T. R. Pampalone, Surface and Interface Anal. 14 (1989) 39.

[15]   D. Grman, R. Hauert, E. Holländer, and M. Amstutz, Solid State Tech., 35, n 2 (Feb. 1992) 43.

[16]   J. H. Thomas, III, C. E. Bryson, III, and T. R. Pampalone, J. Vac. Sci. Tech. B 6 (1988) 1081.

[17]   D. Grman, K.-H. Ernst, R. Hauert, and E. Holländer, Microcontamination, 12, n 7 (July 1994) 57.

[18]   C. Seidel, B Gotsmann, H. Kopf, K. Reihs, and H. Fuchs, Surface and Interface Anal., 26 (1998) 306.

[19]   Y. Du and J. A. Gardella, Jr., J. Vac. Sci. Tech. A 13 (1995) 1907.

[20]   P. K. Wu, in: Polymer/Inorganic Interfaces II; MRS Proceedings Vol. 385, Eds. L.T. Drzal, R. L. Opila, N. A. Peppas, and C. Schutte (MRS, Pittsburgh, 1995) 79.

[21]   P. J. John and J. Liang, J. Vac. Sci. Tech. A 12 (1994) 199.

[22]   P. H. Kasai, W. T. Tang, and P. Wheeler, Appl. Surf. Sci. 51 (1991) 201.

[23]   M. M. Farris, A. A. Klinghoffer, J. A. Rossin, and D. E. Tevault, Catalysis Today 11 (1992) 501.

[24]   B. R. Strohmeier, Appl. Surf. Sci. 40 (1989) 249.

[25]   M. Textor and R. Grauer, Corrosion Science 23 (1983) 41.

[26]   S.-G. Hong, Polymer Degradation and Stability 48 (1995) 211.

[27]   D. F. O'Kane and D. W. Rice, J. Macromol. Sci. Chem. A10 (1976) 567.

[28]   D. T. Clark and D. Shuttleworth, J. Polym. Sci. 18 (1980) 27.

[29]   F. Huber, J. Springer, and M. Muhler, J. Appl. Polym. Sci. 63 (1997) 1517.

[30]   T.E.F.M. Standaert, M. Schaepkens, N. R. Rueger, P.G.M. Sebel, G.S. Oehrlin, and J. M. Cook, J. Vac. Sci. Technol. A 16 (1998) 239.

[31]   T.E.F.M. Standaert,, P. J. Marsuo, S. D. Allen, G.S. Oehrlin, and T. J. Dalton, J. Vac. Sci. Technol. A 17 (1999) 741.

[32]   B. Strohmeier, Surface and Interface Anal. 15 (1990) 51.

[33]   E. McCafferty and J. P. Wightman, Surf. Interface Anal. 26 (1998) 549.

[34]   M. P. Seah in Practical Surface Analysis, Vol 1, 2nd Ed, D. Briggs and M. P. Seah, eds., (Wiley, New York, 1990) pp. 541-553.

[35]   R. C. Weast, Ed., Handbook of Chemistry and Physics, 66th ed. (CRC Press, Boca Raton, FL, 1985) p. B-69.

24. Effects of Wall Contamination on Consecutive Plasma Processes

H. K. Yasuda, Q. S.Yu, C. M. Reddy, C. E. Moffitt, and D. M. Wieliczka

Abstract

Plasma processes often go beyond the primary objectives focused on the substrate, or targeted materials. For instance, sputtered materials deposit on surfaces other than the substrate, and plasma deposition extends to the walls of the reactor. In the process of plasma polymerization, or plasma chemical vapor deposition (PCVD), every surface (not just the substrate surface) participates in the overall plasma deposition process. Consequently the chemical and physical natures of all surfaces within a reactor are very important factors that determine the fate of the PCVD process. The materials deposited on the wall surface (wall contaminants) are created in the previous run in a batch operation of PCVD. In a sequential plasma process, where plasma polymerization of trimethylsilane (TMS) was followed by plasma polymerization of hexafluoroethane (HFE), F-containing oligomers (low molecular weight compounds), created during the plasma polymerization of HFE in the previous run, remain on surfaces in the reactor. The wall contaminants were found to migrate to the new substrate (aluminum alloy) surface in the subsequent run upon the evacuation of the reactor. If an O_2 plasma treatment is applied, F-containing organic compounds chemi-sorbed on the new substrate surface are converted to F-containing inorganic compounds, which decreases the plasma-ablatable F on the surface. If no O_2 plasma treatment is applied, the F-containing organic compounds are exposed to the environment of the TMS plasma. From the viewpoint of the sequence of plasma processes, a new HFE/TMS sequence is created without the O_2 plasma treatment. The HFE/TMS system (reversed order to the normal cycle) causes adhesion failure at the interface between the plasma polymers and the aluminum alloys, whereas the TMS/HFE system yields good adhesion of plasma deposited layers to the substrate and provides superior adhesion of a primer applied on the plasma polymer coating. This difference was created by the difference in handling of the wall contaminants.

Introduction

The combination of plasma processes has various advantages when they are executed properly. The factors that influence the sequence of a plasma process are not limited to the substrate and plasma polymers that deposit on the substrate. Wall contamination also influences the sequential aspect of plasma processes. A very dramatic demonstration of this effect has been recently reported [1].

Post-deposition plasma modifications to primary plasma polymers have been seen to greatly improve bonding to various primers and paints [2-4]. One particular system has been observed to have tremendous adhesion between plasma coated alloy panels and paint applied to them. This system involves cathodic DC plasma deposition of a roughly 50nm primary plasma polymer film from trimethylsilane (TMS) onto a properly pretreated alloy substrate, followed by the

deposition of an extremely thin fluorocarbon film by DC plasma deposition of hexafluoroethane (HFE).

It is important to note that HFE is not a monomer of general plasma polymerization, because it does not polymerize in the absence of hydrogen [5]. When it is applied onto a TMS plasma polymer surface, however, hydrogen is abstracted from the surface and forms a very thin layer of plasma polymer. It is essentially a self-terminating deposition process leading to an extremely thin layer of HFE plasma polymer. ESCA analysis indicated that the thickness of F containing layer in the TMS/(HFE) system is less than few nanometers [1].

This film system was seen to outperform others not incorporating the adhesion promoting HFE film. The alloy panels were always treated with O_2 plasma to remove any organic contaminants from the alloy surface prior to film deposition. The entire steps involved in the plasma coating process are:
1. Solvent cleaning of the alloy surface with acetone
2. Oxygen plasma treatment of the cleaned surface,
3. Cathodic polymerization of TMS, and
4. Cathodic polymerization of HFE.

The steps 2 – 4 were carried out in a vacuum reactor consecutively. Thus, the plasma reactor follows the cycle; 1) pump down from ambient environment – 2) O_2 plasma – 3) TMS plasma – 4) HFE plasma – 5) Exposure to ambient air. The sequences of plasma processes are; O_2/TMS, TMS/HFE, and HFE/O_2.

After a large number of sample preparations by this set of plasma coatings, one set of panels inadvertently missed the O_2 plasma treatment but still had the plasma film system deposited on them. These panels were destined for testing with various primers in the effort to evaluate various primers in a pollution prevention program. After paint application, they were seen to experience miserable adhesion failures in scribed wet tape testing. The entire paint layer delaminated where it was in contact with tape. The inadvertent omission of the O_2 plasma treatment changed the coating system from one with super adhesion to one with extremely poor or practically no adhesion. This dramatic change of adhesion is depicted in Fig. 1; (a) showing the properly treated sample surviving a very severe paint stripping test, while Fig. 1 (b) indicating absolute failure caused by the omission of the O_2 plasma treatment on a simple water soaking test.

The paint could be peeled off as a freestanding film from the failure samples. This gave us the unique opportunity to investigate the changes introduced to the interface between the substrate alloy and the plasma polymer of TMS, which turned out to be the influence of wall contamination on the plasma deposition of TMS films. The authors wish to present results of a series of studies carried out to identify the cause of the catastrophic adhesion failure, and the conclusion gained on the effect of wall contamination to the deposition process of TMS.
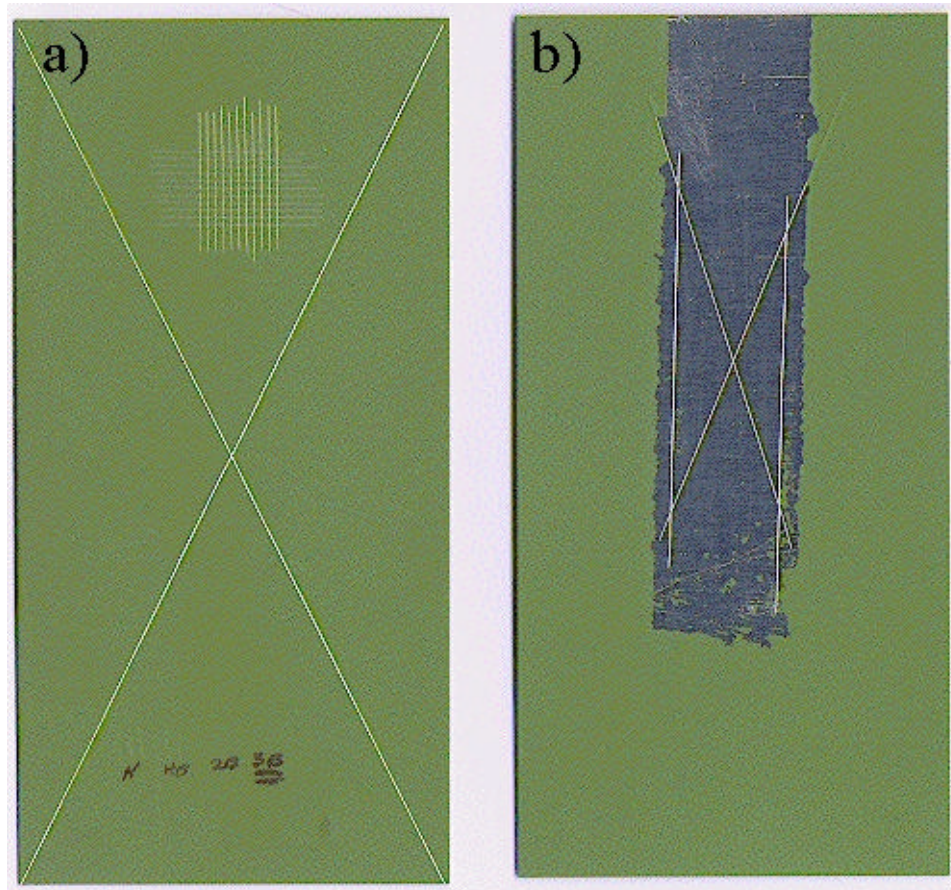
Figure 1. Scanned image of the surface of two alloy panels showing adhesion failure caused by the omission of O_2 plasma treatment of the substrate prior to plasma film deposition and application of the primer (Deft 44-GN-72 MIL-P-85582 Type I Waterbased Chromated Control Primer). a) Panel after Skydrol LD4[®] fluid resistance test, which had the O_2 plasma treatment prior to film deposition and primer application. b) Panel after scribed wet (24-hour immersion in tap water) tape test, which had not been treated with the O_2 plasma treatment prior to film deposition and primer application.

Experimental

Materials

Alclad 7075-T6 Al alloy ([7A]) panels (7.62 cm by 15.2 cm by 0,08 cm) used for the present study were procured from Q-Panel Lab Products (Cleveland, OH).
The following chemicals were used in plasma pretreatment and plasma polymerization process. The diatomic gases, hydrogen (99%) and oxygen (99.9%) were procured from Airgas. Trimethlysilane (TMS) gas of 97% minimum purity was procured from PCR, Inc. (Gainesville,

FL) and Lancaster Synthesis, Inc. (Windham, NH). Hexafluoroethane (HFE) was obtained from Specialty Gases (Maumee, OH). All the gases and monomers were used as received without any further purification.

Surface preparation

As obtained, Alclad 7075-T6 panels had shiny surfaces with panel identification ink marks. Acetone wiping with Kimwipes® was first used to clean the ink marks and loosen organic matter from the surfaces of the panels. Before plasma polymer deposition, plasma pretreatment by oxygen plasmas was applied to aluminum panel surfaces to remove possible contaminants and thus to promote plasma polymer adhesion. The plasma conditions for oxygen plasma treatment were 1sccm O_2, 100 mTorr, DC 40 W, 2 min.

Plasma reactor system and operation

The D.C. plasma reactor system used in this study was a bell jar type reactor as described elsewhere [2]. The D.C. plasma generator was an MDX-1K Magnetron Drive power supply (Advanced Energy Industries, Inc.). Two anodes consisting of stainless steel plates ($25.4 \times 25.4 \times 0.16$ cm) with magnetron enhancement were placed 15.5 cm apart in parallel. An iron ring (17.5 cm outside diameter, 13.8 cm inside diameter, 0.16 cm thick) and an iron center plate (5 cm in diameter, 0.16 cm thick) were attached coaxially on the backside of each anode plate as magnetic field distributor. Eight pieces of permanent magnet bars were equidistantly attached on the iron ring and iron plate with the south pole pointing to the center of the iron plate. The magnetic field strength of each magnet ranged from 700 to 800 Gauss. Two [7A] panels (forming a 6"×6" square) were placed in the middle of the two parallel anodes and used as the cathode of the plasma system.

The cleaned [7A] panels were placed inside the plasma reactor as the cathode. The reactor chamber was first pumped down to less than 1 mTorr with the vacuum system (Edwards Booster with mechanical pump, capacity 240 m^3/h at 0.3 mbar). A monomer was then fed into the reactor chamber. An MKS mass flow meter (Model 247 C) was used for monitoring the monomer/gas flow rates and an MKS pressure controller (Model 252 A) was used to control the gas pressure in the reactor chamber. Plasma conditions for TMS or HFE plasma polymerization were 1 sccm TMS or 1 sccm HFE, 50 mTorr, DC 40 W, 1 min.

After the system pressure stabilized, D.C. power was applied to create the plasma for a preset operation time. After the plasma operation, the residual gases were pumped out and the system pressure allowed to return to the background pressure. The vacuum of the reactor system was then released and the samples were then removed for further sample preparation steps.

XPS analysis

X-ray photoelectron spectroscopy (XPS) data was acquired with a Kratos AXIS-HS instrument, using the Mg-Kα flood source operated at ~217 watts (15 mA, 14.5 kV) or the Al-Kα monochromatic source operated at the same power. All of the XPS data were acquired in the hybrid mode of the instrument, combining electrostatic and magnetic lensing. The collection

spot was limited to a spot size of 200-300 μm, using a 2mm aperture in the hybrid mode. A pass energy of 80eV was used for spectra collected with the flood source, which gives a FWHM of just over 1.4 eV for the Ag 3d line with Mg-Kα excitation. Displayed spectra taken with the monochromatic source were taken at a pass energy of 20eV, which yields a FWHM of just under 0.7eV for the same silver line. All depth profiling was done at 90-degree take-off angle. Charge compensation was made with the manufacturer's proprietary system, at settings of: -1.5 V charge balance voltage, 1.85 A filament current, and –0.5 V bias voltage.

XPS depth profiles were done with a rastered Ar^+ beam. The beam energy was 4 kV at a filament emission of 10 mA. This gives a current of about 1μA at the sample in a spot size of ~1.1 mm, which was rastered over an area of approximately 3x3 mm^2. Data were collected from near the center of this area.

Results and Discussion

<u>Adhesion Failure Caused by Wall Contamination</u>

It is important to note that plasma deposition occurs predominantly onto the cathode surface in the cathodic polymerization scheme adopted in this study, and a new cathode (substrate) was used in every plasma coating operation. In other words, the contamination of the reactor is considered to be minimal. However, there was a small metal clip, which was used to hold the substrate panel in place, left on the cathode system after each deposition. This can be considered a main source of reactor contamination from the prior depositions. There are also small amounts of deposition on the center portion of the anode magnetron, and very small amounts (each time) of deposition on wall surfaces, which are other sources of contamination from the previous runs.

A particular point needs to be made regarding the application cycle of the plasma processes. In the general scheme of the progression of process steps, ignoring venting and substrate replacement, the O_2 plasma treatment followed the HFE plasma treatment and HFE plasma treatment followed TMS plasma application in the regular operation. With the omission of the O_2 plasma treatment, the order of the sequential plasma polymerization processes has changed; i.e., the plasma polymerization of TMS followed the HFE plasma treatment, which was performed in the preceding run. This reversal of the sequence from TMS/HFE to HFE/TMS is one of the major issues dealt in this study. A second major issue is the effect of the O_2 plasma treatment on the fluorine containing contaminants. The extremely poor adhesion of primer coating (30 μm thick) enabled us to investigate the effect on the interface between the alloy and the plasma polymer formed in the TMS treatment.

The XPS analysis of an initial sample revealed virtually no silicon on the alloy surface beneath the lifted primer, but did indicate a rather substantial fluorine presence. The appearance of a strong silicon signal on the interface side of the removed primer indicated that the entire plasma film had likely delaminated at the interface with the alloy. Analysis of additional samples confirmed that the entire film and primer system de-laminated from the alloy panels.

Fig. 2 shows the core spectra taken from the exposed alloy beneath the removed primer from a panel. Using changes in take-off angle (angle between the sample surface and direction of

emission/collection of electrons) and light sputtering, it is seen that the fluorine on the alloy is in two distinct chemical states, one on the outer surface (10° take-off angle) and one just below (90° take-off angle and the remnant after sputtering). This same figure shows that the carbon level on the panel is associated with the outer fluorine state. It is also apparent that the presence of this outer contamination is associated with a modification of the aluminum oxide. This is not unique to just one of the failed panels, with virtually identical states observed on another failed panel beneath the removed coating.
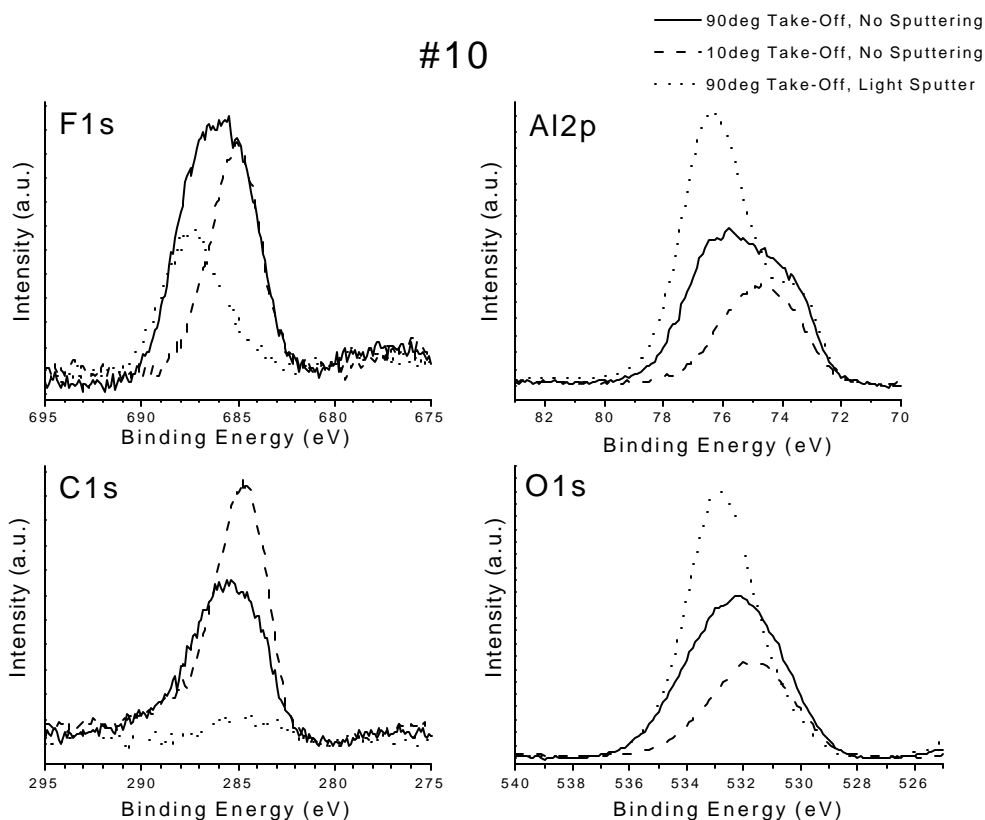
Figure 2. Spectra from the exposed alloy surface beneath the failed coating system on sample #10. The spectra shown were acquired at two different take-off angles prior to sputtering and then also at normal emission after a light sputtering.

The carbon contamination associated with the fluorine on the surface of the alloy panels is not however a fully formed plasma polymer like that formed on the TMS films. Fig. 3 shows C 1s and F 1s spectra from an HFE plasma polymer on a TMS film taken with the monochromatic source at high resolution. The relative composition of fluorocarbon plasma polymers can vary extensively, but the multiple lines in the C 1s spectrum associated with various C-F bonds are quite characteristic of the variations investigated by many researchers. Previous investigations of these types of films with similar carbon binding structure have focussed on areas from general plasma polymer properties and characteristics [6-12], to low dielectric constant materials[13-14],

and to things such as preferential membrane separation techniques[15]. There is some tail at higher binding energy in the C 1s spectra in Figure 2, but nothing like that from the HFE plasma polymer film. Also, the position of the fluorine signal in the failed samples is not consistent with the polymer formation. The higher binding energy component on the contaminated samples is associated with the underlying inorganic modified alumina, and not with the increased carbon level on the surface. The conclusion that must be reached based on the structure of the spectra, is that the contaminating fluorine deposit is not a well-developed plasma polymer film.
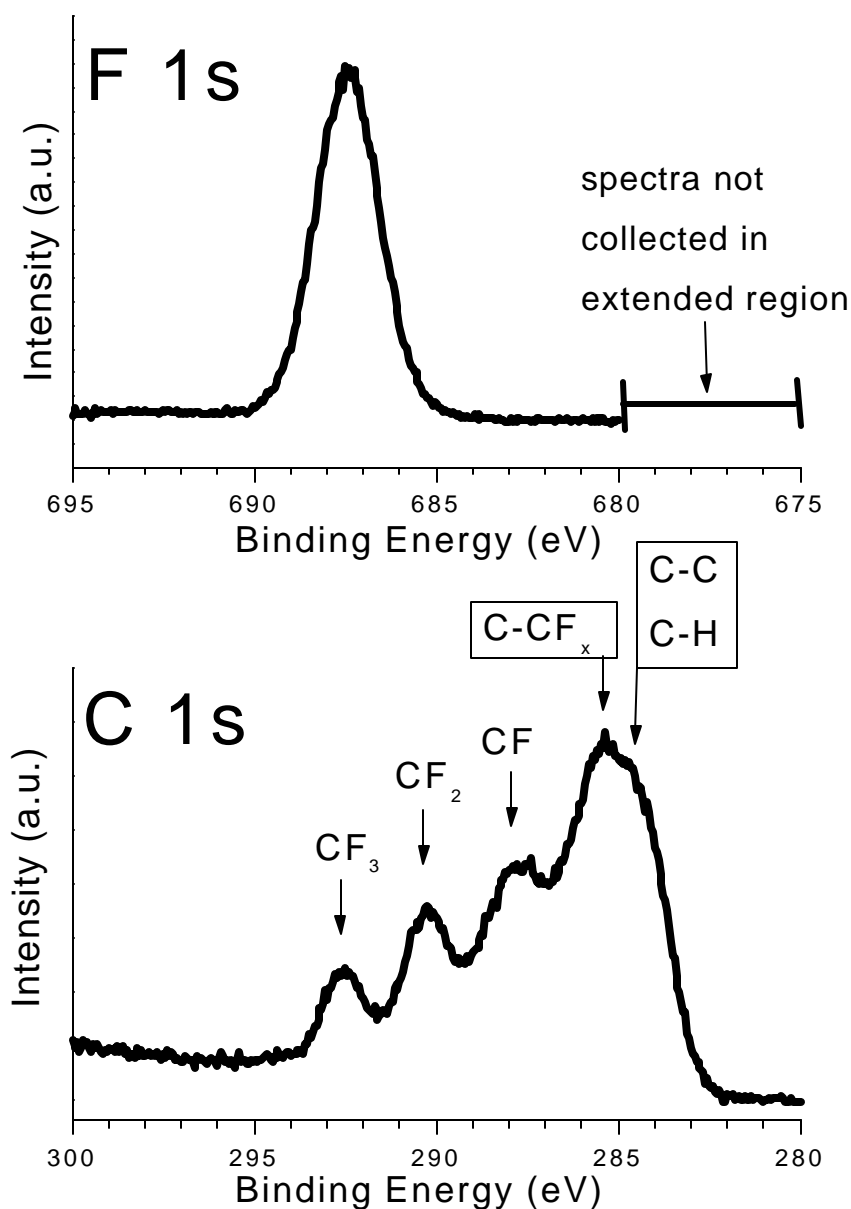
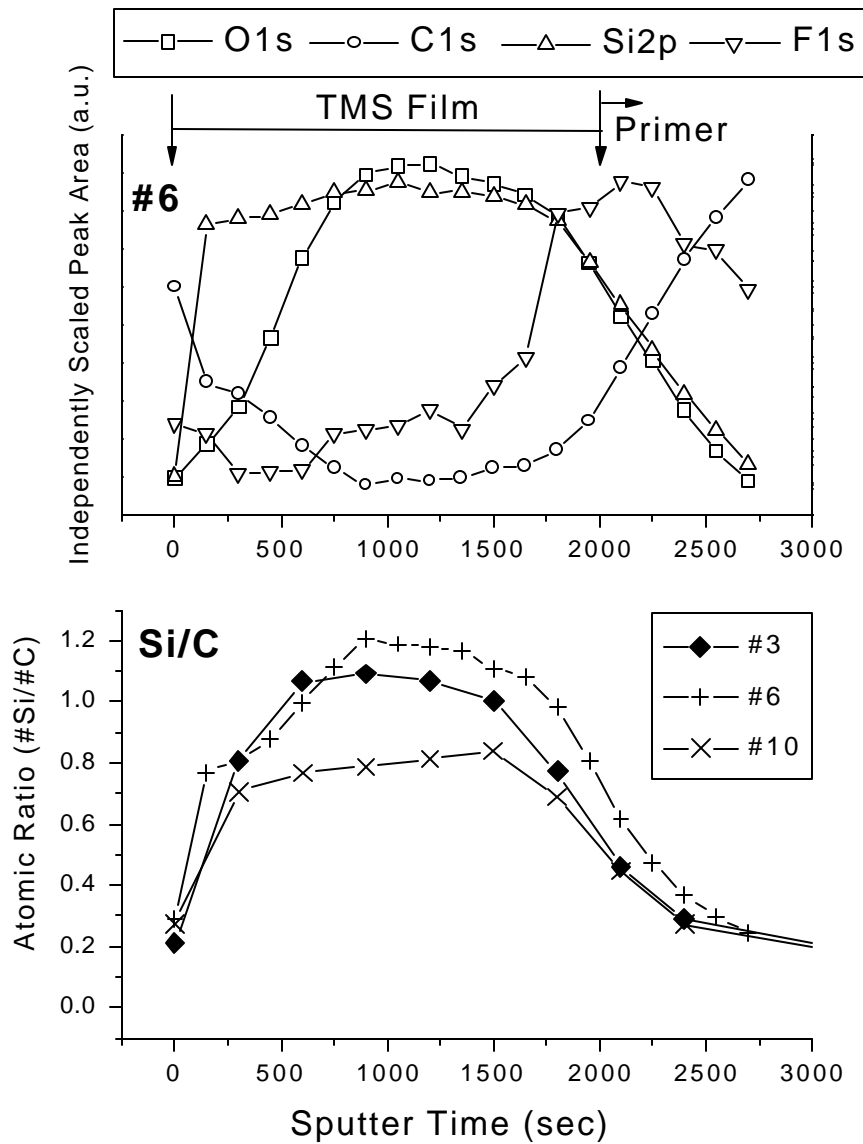Figure 3. Monochromatic generated F 1s and C1s spectra from HFE film on a TMS plasma polymer.

Figure 4. (Top Panel) Elemental area plot from XPS sputter depth profile of interface side of lifted primer on one failed sample. (Bottom Panel) Summary Si/C ratio information from depth profiles of the interface side of the primers lifted from three failed panels.

The surface of the primers opposing the alloy panels was found to have the full TMS film still strongly adhered to the primer, with the HFE film in the TMS/Primer interface. Fig. 4 shows the elemental sputter depth profile from the interface side of the removed primer from one of the failed panels. The region of strong silicon signal in the plot indicates that the tenacious adhesion between the plasma polymer and the primer is still intact and that the mode of failure was purely adhesive at the plasma polymer/aluminum alloy interface. The bottom panel in Figure 5 shows the summary Si/C elemental ratio information from the same interface combined with the information obtained from depth profiles of additional lifted coatings.

The increase in fluorine signal coupled with the decrease in silicon signal in the depth profile indicates the interface region between the TMS film and the primer, where the HFE film formed the strong adhesion. The slightly increased fluorine at the beginning of the depth profile (indicating the surface where the coating was originally in contact with the alloy) shows that fluorine was present when cathodic polymerization of TMS was applied to a new freshly cleaned aluminum alloy panel, and interfered with the normal deposition of TMS. The effect on the TMS film formation is apparent in the bottom panel of Figure 5 where the carbon rich contamination causes the Si/C ratio to be much lower than the bulk level, persisting into the TMS film. The contribution from carbonaceous contamination cannot solely be responsible for the lowered Si/C ratio at the initial portion of the depth profile, since this lowered level persists through more material than the thickness of the deposit on any test panel. This indicates that the contaminant interfered with the normal TMS deposition, causing preferential deposition of carbon rich films at the outset.

An obvious question arises is how did the fluorine come to the surface of the new substrate before the first plasma process (of TMS) was applied, and what is its origin. The answer to this is that fluorine must come from the fluorine-containing contaminants existing within the plasma reactor. This fact was confirmed by a series of experiments to identify the source [1].

Knowing the source of the contamination, the questions are narrowed to,
1) How are fluorine-containing contaminants brought to the surface that would become the interface between alloy and TMS plasma polymer?
2) How does the O_2 plasma treatment eliminate the effect of the fluorine-containing contaminants and restore adhesion at the interface?

A study of the pretreatment application and the surface prior to deposition indicates that the aluminum alloy panels have a marked sensitivity to the build-up of a fluorocarbon background in the plasma reactor. This study also showed that the application of the O_2 plasma treatment modified the alloy surface, changing it from one composed of aluminum oxide to a surface composed of mixed oxide and aluminum fluoride, and in extreme cases, to a mostly mixed fluoride chemistry incorporating some oxygen.

Fluorine contamination has been reported in various environments and applications in the past. It has shown up in plasma processing [16-24], as cross contamination from storage in contaminated containers or with contaminated samples [20, 24], and modification of aluminum deposited on fluoropolymer substrates and other polymers having fluorine based plasma treatments has also been observed [25-27]. Fluorocarbon lubricants have also been noted to modify the oxide structures on aluminum alloys [28, 29] and the degradation of Al_2O_3 catalytic supports has been associated with fluoride conversion during reactions with fluorocarbons [30]. Alloy oxide modification has also been well noted in the presence of fluorine compounds not of the fluorocarbon family [31].

Most of these discussions regarding fluorine contamination of aluminum surfaces have focused on the conversion of aluminum oxide to fluoride or oxy-fluoride. Evidence for similar conversions was included in the study, and in extreme cases conversion to aluminum bonding quite similar to that in AlF_3 was found. The poor adhesion of the samples skipping the O_2

plasma treatment, however, is related not to the fluorine contamination as such, but rather to the carbonaceous nature of the adsorbed materials, which is subjected to the plasma polymerization of TMS. Oxygen plasma cleaning removes this carbonaceous component, while the surface fluorine concentration is enhanced.
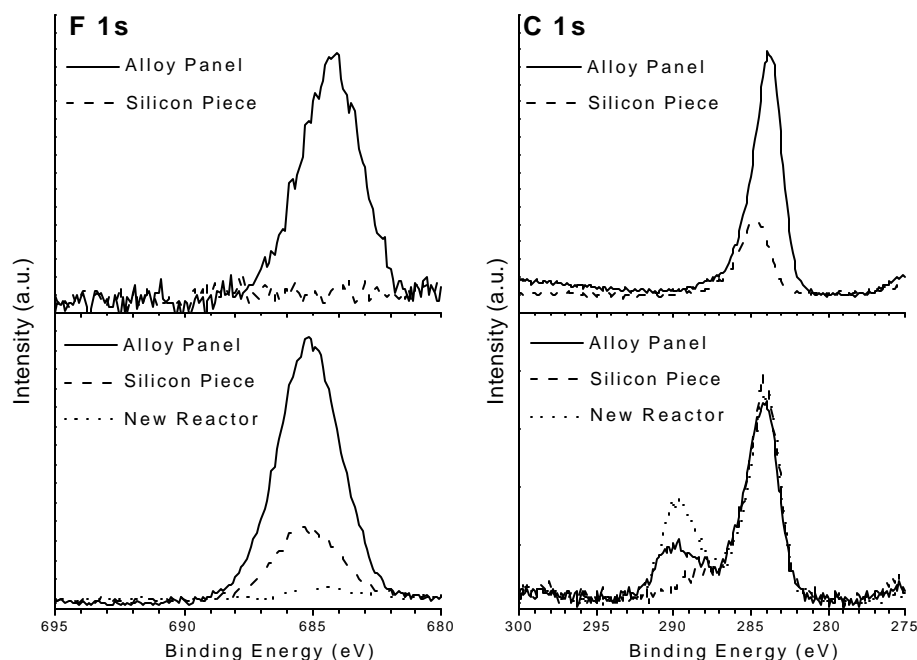

Figure 5. F 1s and C 1s spectra from both alloy panels and Si wafer pieces attached to them. Top figure panels are from samples exposed to the evacuation process and bottom panels are from samples exposed to the O_2 plasma cleaning process. The third trace in each of the bottom panels is from an alloy panel that was O_2 plasma cleaned in a new reactor with minimal fluorine contamination, indicating that the high binding energy C 1s peak is not associated with fluorocarbon bonding.

In order to get insight into the adsorption of F-containing contaminants, Al alloy panels with Si pieces attached to them were subjected to the evacuation process after previous HFE treatments and loading of a fresh sample and then the oxygen plasma treatment. The results of XPS analysis of the Si pieces and the alloy panels are shown in Fig. 5. The top panels in the figure correspond to the samples being exposed to the evacuation process and the bottom panels corresponds to the samples being oxygen plasma treated. In order to show the details of line shapes, the top and the bottom parts of the figures are shown with different vertical scale. The F1s signal in the bottom figure is roughly five times greater than that is the top figures at the same vertical scale. .

After the evacuation process, the alloy panel has both fluorine and the large, low binding energy carbon signal, while the Si wafer piece has no fluorine on it and only carbon associated with

adventitious hydrocarbons. After oxygen plasma treatment (in the contaminated reactor) the fluorine level on the aluminum panel substantially increases. There is fluorine on the silicon wafer piece after oxygen plasma cleaning, but aluminum was also observed on it from sputtering effects, which complicates any interpretation of the origin of the fluorine on the silicon. The oxygen plasma treatment then removed the large carbon concentration from the alloy panel, while converting the surface oxide into the mixed oxy-fluoride structure, incorporating more fluorine than initially present.

Some discussion regarding the high binding energy C 1s peak left on the alloy is required. An additional spectrum is included of an alloy panel that was O_2 plasma treated in a new reactor with minimal fluorine contamination. The C 1s peak from this sample shows an even larger contribution from the high binding energy peak. A peak with this binding energy might be assumed to be associated with C-F bonding (CF_2 specifically), but the panel from the new reactor does not have enough fluorine for this to be the case. It is then more likely that this peak is due to the formation of carbonates or carboxylates, either during the O_2 plasma process or after exposing an activated surface to the hydrocarbons present in the atmosphere. This sample shows a significant contribution from a lower binding energy shoulder on the main peak in the O 1s spectrum, consistent with the addition of an O-C bonding peak. The full interpretation with the incorporation of oxy-fluorides on the surface of the panel treated in the contaminated reactor is unclear, but F-C polymerization is not a likely answer, based on this additional information.

The fluorine containing contaminants were created by the HFE plasma treatment in the previous run. HFE does not form polymeric deposition in the absence of F-capturing agents, such as hydrogen in a plasma environment. HFE forms an extremely thin layer of plasma polymer of HFE on the initial plasma polymers by utilizing the abstraction of H from the plasma polymer of TMS. Thus, anything formed by the HFE plasma treatment and found away from the TMS plasma polymer coated panel is bound to be in oligomer form, not polymeric. Therefore, it is reasonable to assume that those F-containing contaminants are oligomers formed by the HFE plasma treatment.

The results shown above indicate that the following sequence of events occurs. The F-containing oligomers, residing on the reactor walls, are mobile enough to be transferred to the surface of new substrates when the reactor is evacuated, and bind with aluminum oxides so strongly that they are not disturbed by exposure to atmosphere and cannot be pumped out in vacuum, even in high vacuum environment for XPS analysis. Without a specific strong interaction on other surfaces, including the sample silicon wafers attached to the panels, the adsorbed materials, if adsorption occurred, would be pumped out in high vacuum or dissociate upon exposure to atmosphere and cannot be detected by ex-situ XPS analysis.

The role of this contaminant on the interface characteristics between the TMS film and the alloy is also quite evident in the sputter depth profiling results shown in Fig. 6. These results were generated from two samples representative of the two process steps in question from the contaminated reactor; the first of which had the TMS and HFE films deposited on Alclad 7075-T6 after acetone wiping, while the second sample was O_2 plasma treated prior to film application. The Si/C ratio shows the effect of the fluorocarbon adsorption on the interface film properties. The O_2 plasma treated sample maintains a consistent ratio through the interface,

while the sample with no O_2 plasma cleaning exhibits a definite decrease in this ratio, indicating decreased silicon concentrations at the interface. This Si/C ratio was seen to be a good indicator of the integrity of plasma film/alloy interface, with extremely poor films having a markedly lower ratio.
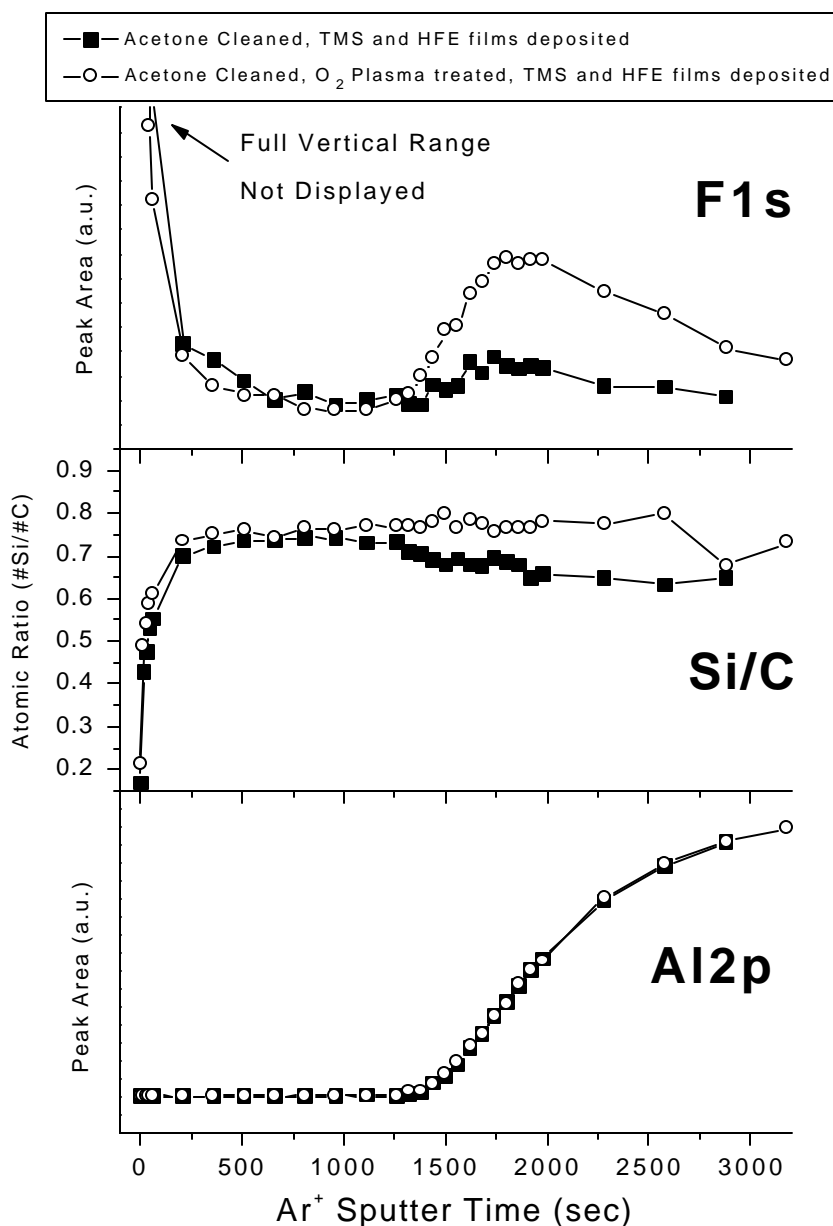

Figure 6. Depth profiles focusing on the increase in fluorine concentration at the interface on the O_2 plasma treated sample and the decrease in the Si/C ratio at the interface on the panel without the O_2 plasma treatment. The aluminum peak area serves as a reference to when the film is removed from each panel and shows that the film thickness and sputtering rates are quite similar. The both samples were prepared by using the contaminated reactor.

The effect of the oxygen plasma treatment in the presence of the contaminant is again seen in the fluorine trace from the depth profile, showing the increase in fluorine concentration at the interface on the oxygen plasma treated sample. The fluorine depth profile from the sample without plasma treatment also shows the more moderate fluorine level at the interface from the adsorption on the alloy oxide, associated with the carbon increase.

Significant factors found by the series of studies on the sudden change from a super adhesion system to no adhesion system can be summarized as follows;
1. Fluorine was found on the interface between the alloy and the first layer of plasma polymer of TMS <u>even for the good adhesion samples, which were prepared without the inadvertent omission of O$_2$ plasma treatment occurred</u>. Fluorine containing oligomers produced in the preceding process migrate to the new substrate placed in the subsequent operation. Those F-containing oligomers interact strongly with aluminum oxides and remain on the new aluminum substrate after the evacuation process.
2. The O$_2$ plasma treatment changed the (low molecular weight) F-containing organic contaminants to F-containing inorganic aluminum compounds (oxy-fluorides).
3. Without the O$_2$ plasma treatment, the chemisorbed F-containing oligomers on to the surface of the alloy interact directly with the TMS plasma on the subsequent plasma process, which leads to substantially decreased Si content at the interface.

The decrease of Si due to F-containing contaminants and the role of the oxygen plasma treatment can be explained by the fundamental principle of plasma polymerization. The key factor to explain the change of elementary composition at the interface is the plasma sensitivity of elements involved on the surface and in the plasma phase. The ablation of materials exposed to plasmas appears to follow the plasma sensitivity series of the elements involved, which is in the order of the electro-negativity of the elements; i.e., elements with higher electro-negativity in the condensed phase are more prone to ablate in plasma that contain elements with lower electro-nagativity [32].

When the thin layer of F-containing oligomers is exposed to the TMS plasma, some of F-atoms are removed from the layer and form Si-F moieties in the plasma. Fluorine atoms (high electro-negativity) in the contaminants are easily detached from the surface by the interaction of plasma of low electro-negative Si (TMS), forming stable species (with Si-F bonds) in the plasma phase, which will be pumped out of the system. The critically important initial stage of TMS plasma polymer deposition is interfered by this process. The scheme of the interference based on the concept of plasma sensitivity of elements is illustrated in Fig. 7. It is important to emphasize that only the interactive (not passive) coating process can create excellent bonding of a coating layer. The interaction between the depositing species and the substrate surface in the initial stage of plasma deposition is extremely important to create good adhesion.

Oxygen plasma treatment of the Al alloy surface with F-containing oligomers is in the similar situation but with different consequence because oxygen plasma does not form polymeric deposition. Oxygen (lower electro-negativity) plasma ablates F-containing oligomers from the substrate surface. In plasma phase, F atoms are detached from the organic moieties, which is a well establish fundamental process of the fragmentation of organic compounds in plasma, and become F-containing plasma, which reacts with elements with lower electro-negativity in the

condensed phase such as O in metal oxides. Thus, plasma sensitive F-containing oligomers are converted to more stable (in plasma environment) F-containing inorganic compounds such as aluminum fluoride-oxide, aluminum fluoride, etc, although the details of species are not well known.
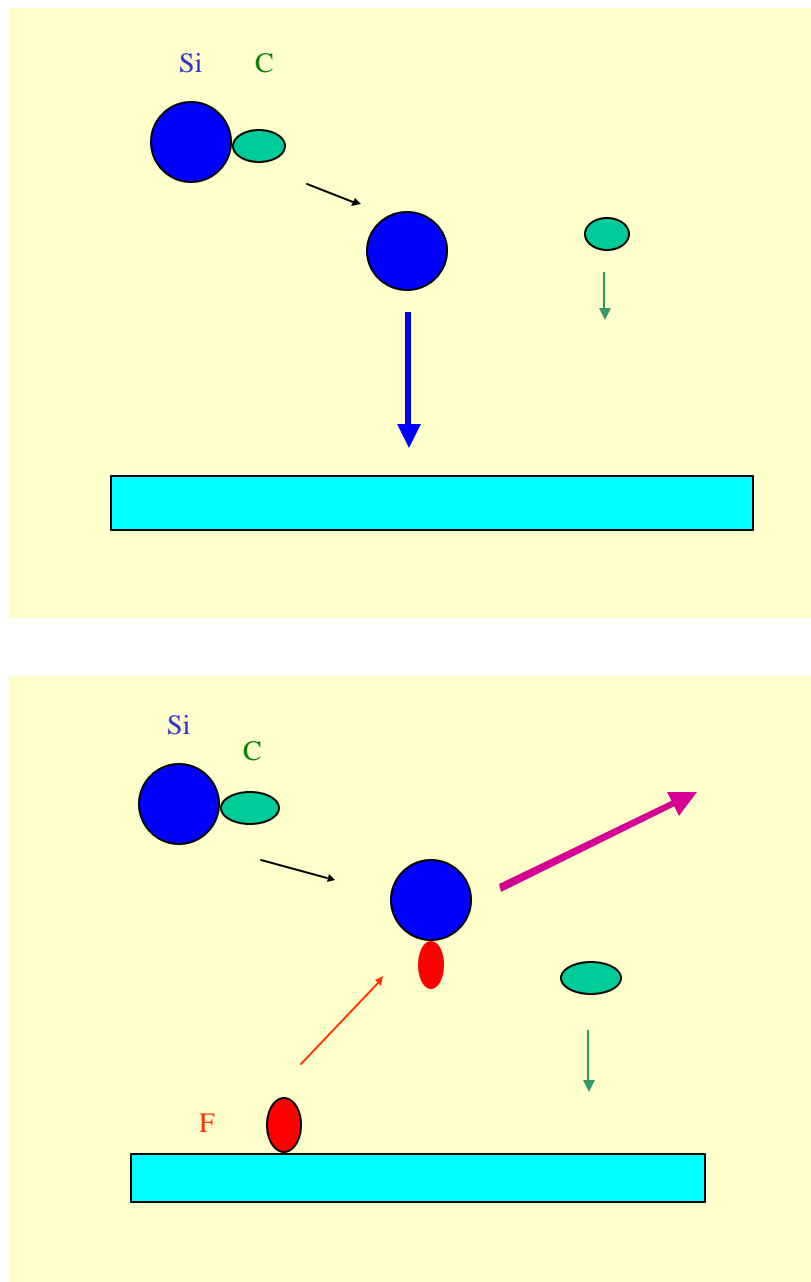

Figure 7. Schematic representation of plasma polymerization of trimethylsilane (TMS): fragmentation of TMS, and different deposition rates for Si moieties and C moieties, and of the change in plasma polymerization of TMS caused by fluorine-containing moiety emanating from the substrate surface.

Although F remains on the surface after the oxygen plasma treatment, the concentration of plasma-ablatable F at the surface is reduced, which virtually eliminates the interference of TMS polymerization by F-containing oligomers. The interference of TMS polymerization by F-containing oligomers creates a weak boundary zone at the interface, which can be characterized by the reduced Si/C XPS ratios.

As a model case to confirm the major principles being discussed above; 1) the interference of TMS plasma polymerization by fluorine ablating from the substrate surface, and 2) the elimination of plasma-ablatable F by O_2 plasma pre-treatment of the substrate surface, the following experiments were performed. First, a very thin layer (less than few nm) of (HFE + H_2) plasma polymer was deposited on an aluminum sheet by 5 seconds of plasma polymerization. One sample was prepared by depositing TMS plasma polymer directly onto this surface. The second sample was prepared by treating the (HFE+H_2) plasma modified surface with oxygen plasma before depositing TMS plasma polymer. Without oxygen plasma treatment, the TMS plasma polymer did not adhere to the substrate surface, whereas with the oxygen plasma treatment, excellent adhesion was obtained. These results confirm the mechanisms by which the wall contamination caused catastrophic damage to the quality of film formed by the plasma CVD process.

Persistence of Wall Contaminants

Once a reactor is contaminated to a certain level, it is very difficult to get rid of the persistent influence of the contaminants. During an arbitrarily chosen one-month period, a contaminated rector was used only for the following two kinds of samples. One sample designated as (Ace) in the legend of Figure 8 was prepared by placing an acetone-cleaned Alclad 7075 coupon in the reactor and pumped down to the base vacuum of approximately 1 mTorr and then removed from the reactor. Another sample designated as (Ace/O_2) was prepared by applying O_2 plasma treatment for 2 minutes. Figure 8 depicts the persistence of the contamination examined by following the XPS fluorine contents on the Al alloy surfaces as a function of time.

The following conclusion could be drawn from the results shown in Fig. 8.
1. O_2 plasma treatment incorporates more fluorine (approximately 5 times) on the Al alloy panel than the sample just loaded to the reactor and pumped down.
2. XPS studies on the panels prepared with the HFE line disconnected, the liquid N_2 trap, and the vacuum pump oil change confirmed that these are not possible sources of fluorine contamination. The F-content gradually decreases with the evacuation time and intermittent O_2 plasma discharges.
3. From the gradual decrease of the level of contamination with evacuation time with intermittent O_2 or Ar processing, it can be speculated that the fluorine level in the regular operation never reached the level shown at the end of 30 days in Figure 8. This is because the HFE/O_2 sequence, which was maintained in the regular operation before the inadvertent omissions occurred, served as a cleaning process for the contaminant in the reactor.

It is important to note that O_2 plasma treatment collects much more F-containing contaminants on the alloy surface than without O_2 plasma treatment, although this treatment virtually eliminated the interference of the contaminants to the subsequent TMS deposition as described in

the previous section. In other words, O_2 plasma treatment does not reduce the amount of fluorine on aluminum alloy surface, but reduces plasma-ablatable fluorine on aluminum alloy surface.
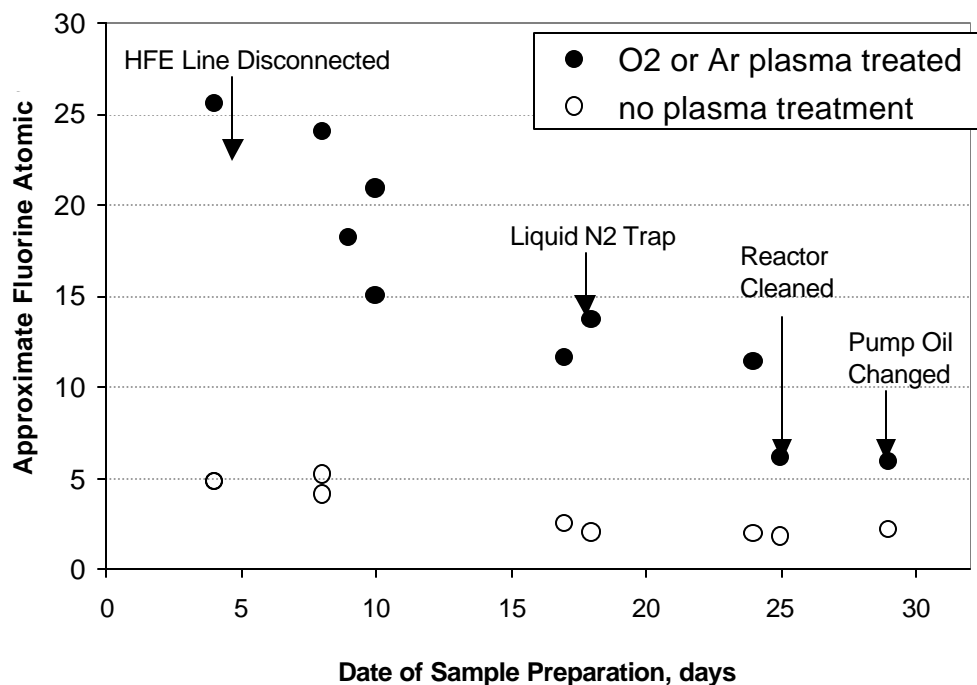

Figure 8. The decay of fluorine contamination with continued reactor use, involving multiple intermittent chamber evacuations and O_2 and Ar plasma-treatments of new substrates. Other than this intermittent use and times when chamber-cleaning procedures were employed, the reactor is continually under vacuum, indicating that this contamination does gradually pump out.

SUMMARY

F-containing oligomers (low molecular weight compounds) created during the plasma polymerization of HFE in previous run cycles remain on surfaces in the reactor (wall contaminants). These oligomers are volatile enough to migrate in vacuum, but not volatile enough to be pumped out completely. The wall contaminants migrate to new substrate (aluminum alloy) surfaces in subsequent runs upon the evacuation of the reactor. When these oligomers deposit on a cleaned aluminum alloy surface, they are strongly chemisorbed and cannot be pumped out even in the high vacuum in XPS instrument.

If an O_2 plasma treatment is applied, oxygen (lower electro-negativity) plasma ablates F-containing oligomers from the substrate surface. In plasma phase, F atoms are detached from the organic moieties (fragmentation of organic compounds in plasma), and become F-containing plasma, which reacts with elements with lower electro-negativity in the condensed phase such as O in metal oxides. Thus, plasma sensitive F-containing oligomers are converted to more stable

363

(in plasma environment) F-containing inorganic compounds such as aluminum fluoride-oxide, aluminum fluoride, etc.

Without O_2 plasma treatment, a new HFE/TMS sequence is created. The HFE/TMS system (reversed order to the normal cycle) yields adhesion failure at the interface of plasma polymers, whereas the TMS/HFE system yields good adhesion to the substrate and provides superior adhesion of a primer applied on the plasma coating.

The repeated use of a reactor for plasma CVD always leave some extent of wall contamination. Because of the wall contamination, the overall plasma processes must include a process that is aimed to minimize or eliminate, if possible, the inadvertent effect of the wall contamination. The O_2 plasma pretreatment of the substrate surface, which was included without a clear aim other than an added insuring cleaning effect to remove residual organics, turned out to be the key process to cope with the problem associated with the wall contamination in the case presented in this study.

The implications of these types of reactions may be far reaching, since similar fluorocarbons are used in Si etching and the cleaning of CVD reactors. The effects on subsequent processing could be significant, particularly with aluminum as a fundamental component of semiconductor technology.

Reference

1. C.E. Moffitt, C.M. Reddy, Q.S. Yu, D.M. Wieliczka, and H.K. Yasuda, Appl. Surf. Sci., **161**, No. 3-4, July, 481 (2000).
2. C. M. Reddy, Q. S.Yu, C. E. Moffitt, D. M. Wieliczka, R. Johnson, J. E. Deffeyes, and H. K. Yasuda, Corrosion, **56**, No. 8, 819 (2000).
3. Q. S. Yu, C. M. Reddy, C. E. Moffitt, D. M. Wieliczka, R. Johnson, J. E. Deffeyes, and H. K. Yasuda, Corrosion, **56**, No. 9, 887 (2000).
4. C. E. Moffitt, C. M. Reddy, Q. S. Yu, D. M. Wieliczka, R. Johnson, J. E. Deffeyes, and H. K. Yasuda, Corrosion, **56**, No. 10, 1032 (2000).
5. Yu Iriyama and H. Yasuda, "Fundamental Aspect and Behavior of Saturated Fluorocarbon in Glow Discharge in Absence of Potential Source of Hydrogen", J. Polym. Sci., Polym. Chem. Ed., **30**, 1731, (1992).
6. H. K. Yasuda, Plasma Polymerization (Academic Press, New York, 1985) pp. 160-166.
7. D. F. O'Kane and D. W. Rice, J. Macromol. Sci. Chem. A **10**, 567 (1976).
8. D. T. Clark and D. Shuttleworth, J. Polym. Sci. **18**, 27 (1980).
9. M. J. O'Keefe and J. M. Rigsbee in Polymer/Organic Interfaces: MRS Proceedings Vol. 304, Eds. R. L. Opila, F. J. Boerio, A. W. Czanderna (MRS, Pittsburgh, 1993) pp. 179-184.
10. T. R. Gegenbach, R. C. Chatelier and H. J. Greisser, Surf. Interface Anal. **24**, 271 (1996).
11. T. R. Gegenbach, and H. J. Greisser, Surf. Interface Anal. **26**, 498 (1998).
12. S. Agraharam, D. W. Hess, P. A. Kohl, and S. A. Bidstrup Allen, J. Vac. Sci. Technol. A **17**, 3265 (1999).
13. J. P. Chang, H. W. Krautter, W. Zhu, R. L. Opila, and C. S. Pai, J. Vac. Sci. Technol. A **17**, 2969 (1999).
14. L. M. Han, R. B. Timmons, and W. W. Lee, J. Vac. Sci. Technol. B **18**, 799 (2000).

15. F. Huber, J. Springer, and M. Muhler, J. Appl. Polym. Sci. **63**, 1517 (1997).

16. P. C Karulkar and N. C. Tran, J. Vac. Sci. Tech. B **3**, 889 (1985).

17. S. Jimbo, K. Shimomura, T. Ohiwa, M. Sekine, H. Mori, K. Horioka, and H. Okano, Jpn. J. Appl. Phys. **32**, 3045 (1993).

18. Y. Shacham-Diamond and R. Brener, J. Electrochem. Soc. **137**, 3183 (1990).

19. D. A. Bohling, M. A. George, and J. G. Langan, in IEEE/SEMI Advanced Semiconductor Manufacturing Conference and Workshop: ASMC '92 Proceedings   (IEEE, New York, 1992) p.111.

20. K.-H. Ernst, D. Grman, R. Hauert, and E. Holländer, Surface and Interface Anal. **21**, 691 (1994).

21. J. H. Thomas, III, C. E. Bryson, III, and T. R. Pampalone, Surface and Interface Anal. **14**, 39 (1989).

22. D. Grman, R. Hauert, E. Holländer, and M. Amstutz, Solid State Tech. **35**, n 2, 43 (Feb. 1992).

23. J. H. Thomas, III, C. E. Bryson, III, and T. R. Pampalone, J. Vac. Sci. Tech. B **6**, 1081 (1988).

24. D. Grman, K.-H. Ernst, R. Hauert, and E. Holländer, Microcontamination, **12**, n 7, 57 (July 1994).

25. C. Seidel, B Gotsmann, H. Kopf, K. Reihs, and H. Fuchs, Surface and Interface Anal. **26**, 306 (1998).

26. Y. Du and J. A. Gardella, Jr., J. Vac. Sci. Tech. A **13**, 1907 (1995).

27. P. K. Wu, in: Polymer/Inorganic Interfaces II; MRS Proceedings Vol. **385**, Eds. L.T. Drzal, R. L. Opila, N. A. Peppas, and C. Schutte (MRS, Pittsburgh, 1995) p. 79.

28. P. J. John and J. Liang, J. Vac. Sci. Tech. A **12**, 199 (1994).

29. P. H. Kasai, W. T. Tang, and P. Wheeler, Appl. Surf. Sci. **51**, 201 (1991).

30. M. M. Farris, A. A. Klinghoffer, J. A. Rossin, and D. E. Tevault, Catalysis Today **11**, 501 (1992).

31. B. R. Strohmeier, Appl. Surf. Sci. **40**, 249 (1989).

32. H. Yasuda and T. Yasuda, J. Polymer Science, Polymer Chemistry Ed., **38**, 943 (2000).

25. Engineering the Surface and Interface of Parylene C Coatings by Low-Temperature Plasmas

Qingsong Yu[a], Joan Deffeyes[b], Hirotsugu Yasuda[a, 1]

Abstract

There is a need for the development of environmentally benign processes by which to protect aluminum alloys from corrosion. Vacuum-deposited Parylene C conformal coating is a very good candidate to provide such protection due to its excellent bulk properties: its moisture barrier, high mechanical strength and thermal stability. However, its poor adhesion to most smooth or non-porous substrates has restricted its application. In this study, low-temperature plasma deposition and treatment has proved to be a powerful approach to engineer the surface and interface of Parylene C coatings. After applying a special plasma polymer coating, which acts as an inter-layer to provide good adhesion to the substrate as well as to the subsequent primer, an excellent adhesion of Parylene C coating to a smooth 7075-T6 aluminum alloy has been achieved. After the surface has been functionalized by plasma treatment, the naturally hydrophobic Parylene polymer became paintable with both solventborne and waterborne spray primers.

Introduction

Parylene C, or monochloro-substituted poly(para-xylylene), is a polymer that has excellent bulk properties, and also maintains barrier properties for various gases, organic solvents and water [1]. Gas phase polymerization makes Parylene C absolutely uniform and conformal on all surfaces. These advantageous features make Parylene C extremely useful in all technologies requiring high quality coatings.

The process of Parylene polymerization is presented schematically in Fig. 1. Parylene dimer is heated until it sublimes. This dimer vapor passes through a high temperature pyrolysis zone where it cracks and becomes monomer vapor. The monomer polymerizes and polymer is deposited in the deposition chamber which is usually at room temperature.

Parylene C deposition, completed in a vacuum, is a process with no solvents, no curing and no liquid phase. Its use introduces essentially no concern with regard to the operator's health and safety, air pollution or waste disposal. As a dry process, non-solvent based coating, Parylene C is not affected by VOC restriction [2].

Parylene C, however, does have one major deficiency, i.e., its adhesion to most substrates with smooth or nonporous surfaces is very poor as noted in Fig. 2. This deficiency has restricted its application. Methods to improve its adhesion have been developed, but improvement is limited due to the lack of specific chemical interactions in the interface [3].

Low-temperature plasma deposition has proven to be a very effective process in improving the adhesion properties of materials while maintaining their desirable bulk properties. Enhanced adhesion of Parylene C and Parylene N to smooth surface materials has been reported with the application of plasma depositions [3, 4]. Most recently, it was reported that an excellent adhesion of Parylene C coating to a cold-rolled steel surface was achieved using plasma polymer coatings, in turn giving rise to corrosion protection of the metal [5].
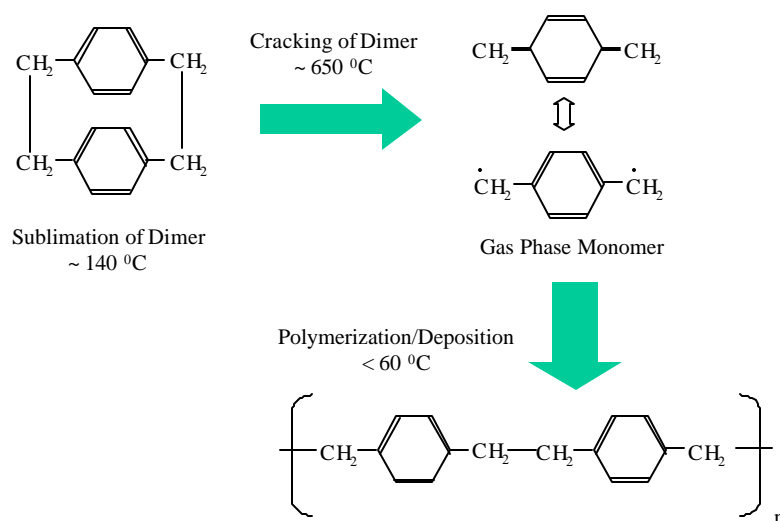
Figure 1. Parylene polymerization steps.

Scheme to utilize chemical inertness of Parylene
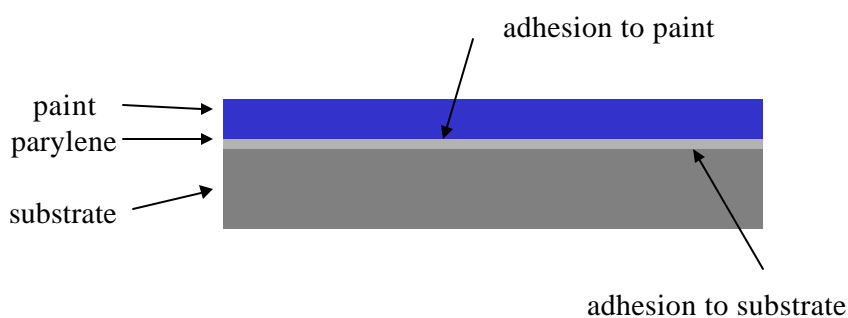
- Poor adhesion to smooth surfaces
    - No chemical bonding ⇒ Plasma interface modification ⇒ Free radicals ⇒ Chemical bonding
- Not paintable
    - Hydrophobic surface ⇒ Plasma surface treatment ⇒ Hydrophilic surface ⇒ Paintable

Figure 2. The plasma treatment effects on the surface and interface of chemically inert Parylene C coating.

Another major deficiency of Parylene C is its poor painting properties, due to its extremely hydrophobic surface. Because of this, surface modification of Parylene films is necessary to enhance their adhesion performance with spray primers.

In this study, low-temperature plasma technique has been utilized to engineer the surface and interface of Parylene C coating. The aim is to make Parylene C strongly adhere to a smooth aluminum alloy, and also to make it paintable with various types of spray primers.

Experimental

Plasma polymer coating

The deposition of plasma polymer was carried out in a bell jar-type glass reactor [5]. The direct current (DC) plasma generator was a Magnetron MDX-1K power supply (Advanced Energy Industries, Inc.). Two anodes consisting of stainless steel plates with magnetic enhancement were placed 6 inches apart. The 7075-T6 aluminum alloy panels (3×6 inches) were cleaned thoroughly with acetone and then placed in-between the two anodes as the cathode and substrate.

The pressure of the reactor chamber was first pumped down to a background pressure (< 2 mtorr [0.26 Pa]). A monomer gas was then fed into the reactor chamber to reach a preset pressure of 50 mtorr that was controlled by MKS 252A exhaust valve controller. DC power was applied to create plasma for a preset time to complete the plasma polymer deposition on the aluminum panels.

Parylene C deposition

The parylene reactor is composed of several units: the sublimation tube, cracking chamber, deposition chamber, and cold trap chamber. Bare 7075-T6 aluminum alloy panels with smooth surface were used to examine the interface adhesion between Parylene C coating and the substrates. Ion vapor deposition (IVD) aluminum coated 7075-T6 panels with porous surface were used as the substrates for Parylene C deposition to investigate the Parylene C surface paintability due to the good adhesion of Parylene coating to porous substrates [3]. The aluminum panels were placed in the deposition chamber and approximately 15 µm of Parylene C film was deposited on each panel. The detailed experimental procedures has been described elsewhere [6].

Plasma treatment of Parylene C coating

Because of its highly efficient nature and large-scale advantage [7, 8], low temperature cascade arc torch plasmas was selected for plasma surface treatment of Parylene C films. The three-torch low-temperature cascade arc reactor was fabricated by PlasmaCarb, Inc. Bedford, NH, USA. The detailed experimental procedures has been described elsewhere [9].

Primer spray

Primers were sprayed onto Parylene C surfaces with an air brush. After painting, the primer coated Parylene C samples were cured under the conditions provided by the primer suppliers. After curing, the thickness of primer coatings was measured with an Elcometer 355 (Elcometer Inc., Rochester Hill, Michigan). The thickness of the primer coatings was controlled to be around 1.0 mil (25.4 µm).

Tape adhesion test

Adhesion performance was evaluated via the Tape Test according to the guideline of the American Society for Testing and Materials (ASTM 3359-93B). This test method provides semi-quantitative results given in grades 0 to 5 (5 indicating that the film cannot be peeled off by the tape). Poor adhesion can be easily detected by this simple Adhesion Tape Test.

The upper limit of adhesive strength measurable by this method is relatively low, because the adhesive strength of the tape is limited. Therefore, if the specimens pass the tape test, the following simple test developed by Sharma and Yasuda [3, 4] was utilized to examine the adhesive characteristics. The cross-shaped cuts with 1 mm apart were first made on the plasma polymer layer by a razor blade according to the procedure of the Adhesive Tape Test. Then the specimens were immersed in boiling water and periodically examined via the Tape Test.

Results and Discussion

Enhancement of Parylene C adhesion to 7075-T6 aluminum by plasma interface modification

Table 1 summarized the advantageous features of plasma polymers in interface modification. It should be emphasized that plasma polymers provide not only the interfacial bonding to enhance the adhesion, but also a chemically inert barrier to further protect the substrate from corrosive environment.

Table 1. Advantageous features of plasma polymer for interface modification.

• Forms a thin protective layer
    – A pinhole-free, chemically inert coating
    – An excellent barrier for gases & solvents
 • Enhances interfacial adhesion
    – Works as an interlayer, strongly adhering to substrate
    – Forms functional groups on the surface
    – Leaves reactive sites for further chemical bonding

Parylene C coating usually does not adhere to materials with a smooth surface, such as bare aluminum alloys. With the aid of plasma interface modification, it is possible to achieve a strong adhesion of Parylene coatings to such smooth surfaces. Therefore, it is possible to protect aluminum alloys with Parylene C coating. In this study, a strong adhesion of Parylene C coating to bare 7075-T6 panels was achieved with the application of plasma polymers.

Fig. 3 shows the scanned picture of Parylene C coating on bare 7075-T6 aluminum alloy after the tape Test. Fig. 3 (a) and (b) are from the same sample, which passed the dry tape test. However, after boiling in water for 6 hours, the Tape Test pulled off the Parylene C coating leaving the blue color of the trimethylsilane (TMS) plasma polymer visible. The samples in Fig. 3 (c) and (d) all passed the dry Tape Test. After boiled in water for 8 hours, the Tape Test could not remove the Parylene C coating from the substrate, which indicates that a strong adhesion of the Parylene C coating to the smooth surface was obtained with proper TMS/CH$_4$ plasma treatments.

(a) Dry Tape Test   (b) Boiled 6 hrs

(c) Boiled 8 hrs   (d) Boiled 8 hrs
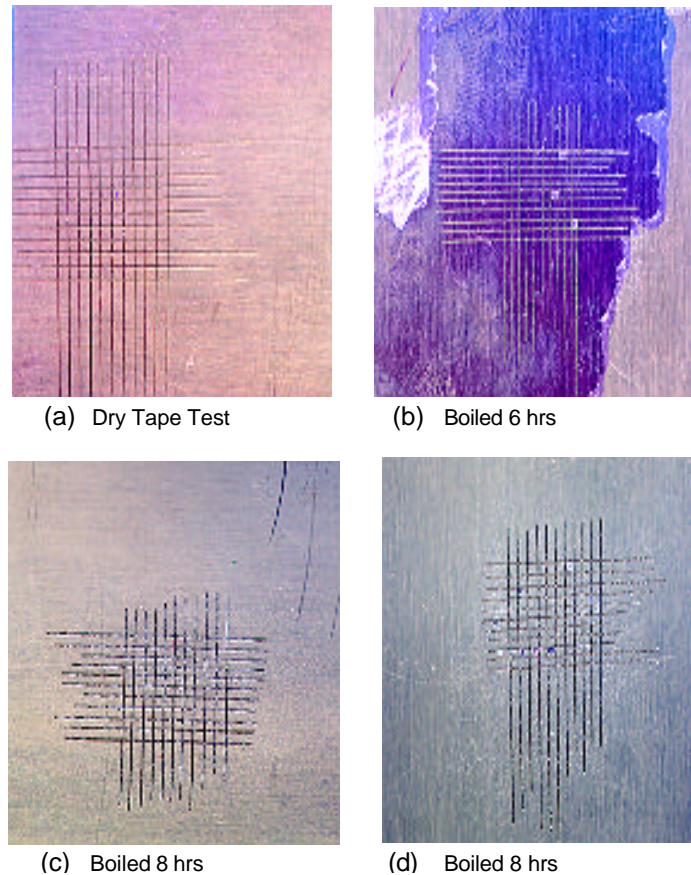
Figure 3. Adhesion improvement of Parylene C to TMS or TMS/CH$_4$ plasma polymer coated 7075-T6 panels with subsequent Ar RF plasma treatment at 100 W and 50 mtorr.   (a) & (b) On TMS plasma polymer, treatment time=1.0 min, (c) On TMS/CH$_4$ plasma polymer, treatment time=2.0 min,   (d) On TMS/CH$_4$ plasma polymer, treatment time=10.0 min.

The adhesion of Parylene C coatings to three different DC plasma polymers coated bare 7075-T6 surfaces was examined; the results are summarized in Table 2. Plasma polymer of TMS/HFE (PP) showed the best results among the three types of plasma polymers. After exposure to air for around one day before deposition of Parylene C, this plasma polymer still showed a very good adhesion to Parylene C coatings. As shown in Table 2, RF argon plasma treatment on the PP

surface in the Parylene reactor was not necessary and such a treatment made the adhesion becomes weaker.

Table 2. Tape Test results of Parylene C coatings on different DC plasma polymer surfaces.

Plasma Polymer Type, Exposure Time in Air		RF Plasma Treatment before Parylene	Tape Test Ratings	
			Dry	Boiled in Water for 1, 2, 4, 6, 8 hrs
PP [a]	0.4 hrs	no	5	5, 5, 5, 5, 5
	1.2 hrs	no	5	5, 5, 5, 5, 5
	23.5 hrs	no	5	5, 5, 5, 5, 5
	63 hrs	no	5	5, 5, 5, 5, 4
	192 hrs	no	4	4, 4, 4, 4, 4
	36 hrs	yes, Ar 20 mT, 100W, 2.0 min	4	4, 4, 4, 4, 4
TMS [b]	0.4 hrs	no	5	5, 5, 4, 4, 3
	22.5 hrs	no	5	5, 5, 4, 4, 4
TMS/CH4 [c]	0.4 hrs	no	4	4, 4, 4, 4, 4
	120 hrs	no	4	4, 4, 4, 4, 3

a: plasma polymer of TMS + plasma polymer of HFE
b: plasma polymer of trimethylsilane
c: plasma polymer of TMS + plasma polymer of CH4

Enhanced primer adhesion of Parylene C by plasma treatment

Paint is necessary to be applied over Parylene in order to:
> 1) apply mission specific markings/survivability coatings.
> 2) add chemical crorrosion inhibitors.
> 3) protect the Parylene from UV exposure.

Surface functionalization of Parylene C

Parylene C polymer films have a very hydrophobic surface, which makes it difficult to improve their painting properties. Surface modification of Parylene C films is necessary to enhance their adhesion performance with respect to paints. Because of its energetically milder characteristics and large-scale advantages [7, 8], low-temperature cascade arc torch (LTCAT) plasma was selected for the surface treatment of Parylene C coating.

The water contact angle of Parylene C coatings is about 90^0 before LTCAT treatment. After argon LTCAT treatment, the surface of Parylene C coatings became more wettable. Changes in the contact angle of the Parylene C surface with LTCAT plasma treatment time are shown in Fig.

4. It should be noted that a more wettable surface was obtained with LTCAT treatment under stronger plasma conditions for a longer time.
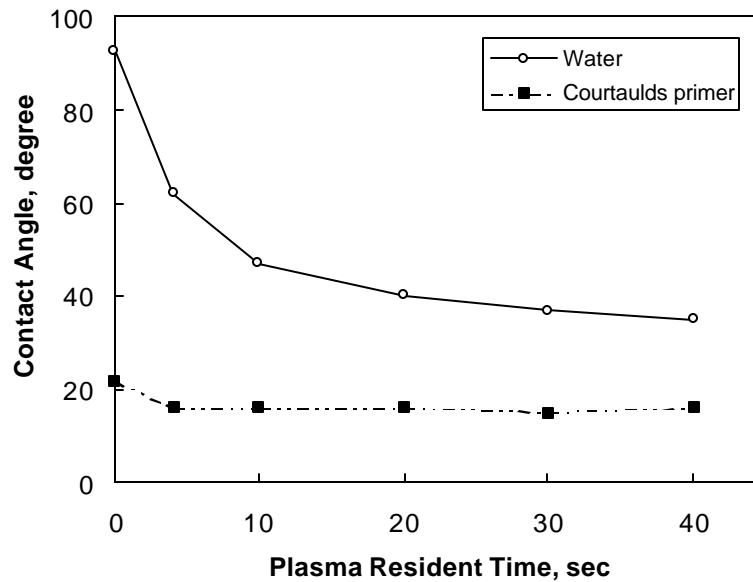

Figure 4. Contact angle changes of water and Courtaulds primer on the Parylene C surfaces with Ar LTCAT treatment time. Treatment conditions: 1000 sccm Ar, 6.0 A arc current.
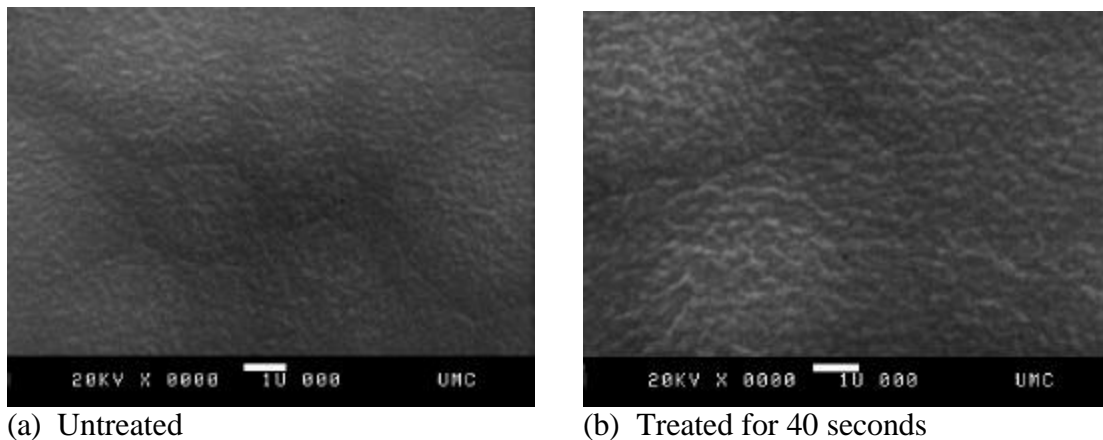

(a) Untreated   (b) Treated for 40 seconds

Figure 5. SEM micrographs of (a) untreated and (b) argon LTCAT treated Parylene C coating surfaces. Treatment conditions: 1000 sccm Ar, 6.0 A arc current.

The surface morphology of Parylene C coatings was examined by SEM. Fig. 5 shows the SEM micrographs of untreated and argon LTCAT treated Parylene C polymer surfaces. Much rougher surfaces were observed on treated samples than untreated ones. It was further noted that the

surface roughening effect became more obvious with longer plasma treatment time, which corresponds to better adhesion test results as shown in Tables 3 - 4. This surface roughening is very important in enhancing adhesion, because it can increase the surface contact area and form mechanical interlock between primer and Parylene C coatings.

The surface roughening effect with argon LTCAT treatment is believed to be induced by the physical sputtering of excited argon neutral species on the Parylene C surface, because excited argon neutrals are the main energetic species in argon CAT plasmas [7, 8].

Improvement of Adhesion of Paint to Parylene C surface

Solventborne primer

After cascade arc torch treatment, Parylene C surfaces were painted with a solventborne primer (519X303, Courtaulds Aerospace). After the primer coatings were cured, the painted samples underwent the adhesion Tape Test under dry conditions and after boiled in water for a certain time period.

Fig. 6 shows the typical scanning pictures of the Tape Test results of primer coatings on untreated and plasma treated Parylene C. It is evident that, without any treatment, the painting properties of Parylene C coatings are very poor (Fig. 6(a)). The dry Tape Test removed all the primers from the Parylene C surface. In contrast, as seen from Fig 6 (b, c, d), plasma treatment by Ar LTCAT significantly improved the primer adhesion of Parylene C.   The samples with longer plasma treatment time passed the cross-cutting tape test even after boiling in water for as long as 8 hours (Fig. 6(c &d)). This indicates that very strong adhesion of the primer coating to the Parylene C polymer has been achieved.

Table 3 summarizes the Tape Test results of Courtaulds primer coating on Parylene C surfaces with and without argon LTCAT plasma treatment. The adhesion performance of Parylene C films with respect to Courtaulds primer was improved in varying degrees depending on treatment conditions and treatment time. This indicates that the adhesion of the Courtaulds primer to Parylene C polymer surfaces can be controlled by adjusting the cascade arc torch treatment conditions. Most of the cases with argon LTCAT plasma treatment passed the Tape Test after 8 hours of boiling in water.

The general trend evident in Table 3 is that the stronger plasma conditions, such as higher arc current, higher argon flow rate, and longer treatment time, give rise to better adhesion of primers to Parylene C films.

Waterborne primer

Plasma treatment of Parylene C films has proved to be very effective in improving the painting properties of Parylene C polymers with respect to a solventborne primer, Courtaulds primer. In this study, the effect of LTCAT plasma treatment on the adhesion of Parylene C polymer to waterborne primer (44-GN-36, Deft Corp.) was also examined.
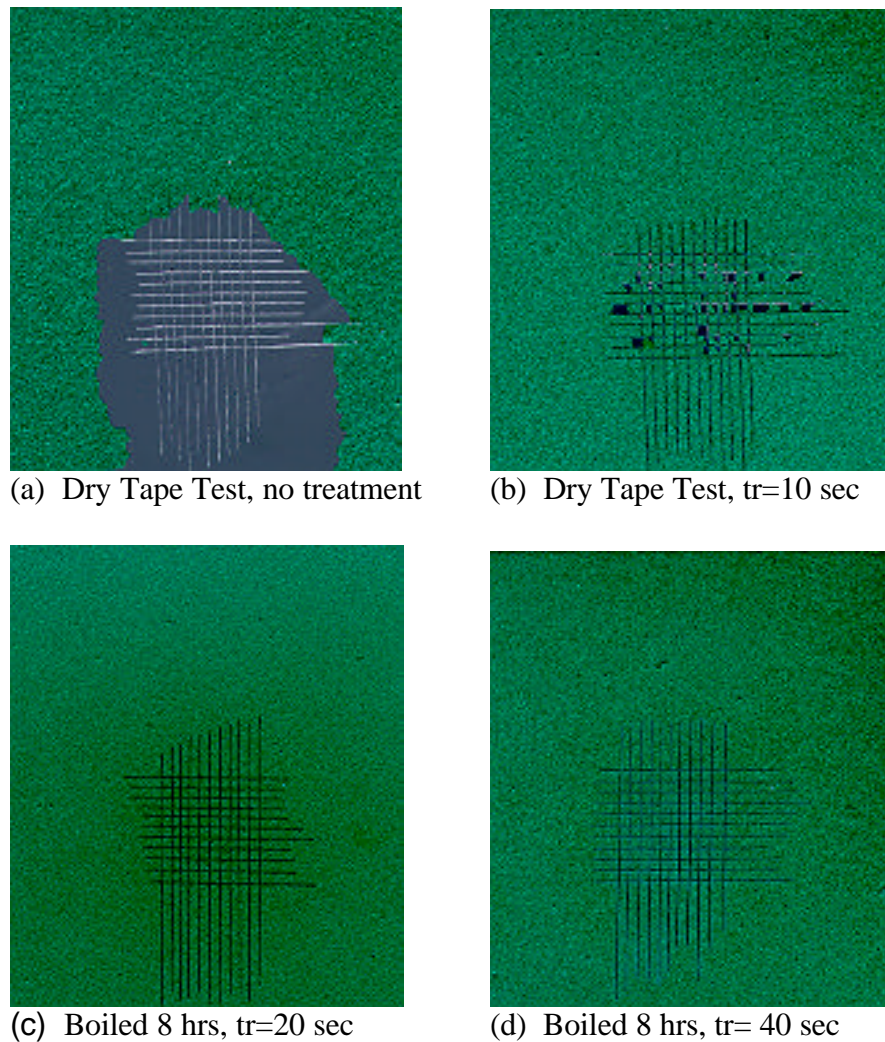
(a) Dry Tape Test, no treatment   (b) Dry Tape Test, tr=10 sec

(c) Boiled 8 hrs, tr=20 sec   (d) Boiled 8 hrs, tr= 40 sec

Figure 6. Adhesion Improvement of solvetborne primer (519X303, Courtaulds Aerospace) to the Parylene C surface after LTCAT plasma treatment at various plasma resident times. Treatment conditions: 1000 sccm Ar, 6.0 A arc current.

Table 4 summarizes the Tape Test results for the Deft primer coatings on Parylene C surfaces treated by LTCAT under different plasma conditions. It is evident that the adhesion performance of Parylene C coatings with respect to the Deft primer was also improved to various degrees, depending on the LTCAT treatment conditions. Some of the samples passed the Dry Tape Test, but failed the Tape Test performed after boiled in water for a certain time period. Samples with stronger LTCAT treatment conditions passed the tape test even after boiled in water for 8 hours, which suggests that a strong adhesion have been achieved. These results indicate that, upon different requirements, the painting properties of Parylene C with respect to the Deft primer can also be controlled simply by adjusting the LTCAT plasma treatment conditions.

Table 3. Tape Test results for solventborne primer (519X303, Courtaulds Aerospace) applied to the argon LTCAT treated Parylene C surfaces.

Plasma Parameters			Tape Test Rating	
Ar Flow Rate	Arc Current	Treatment Time	Dry Test	Boiled in H_2O for 1, 2, 4, 6, 8 hrs
no treatment			0, no adhesion	-
1000 sccm	6.0 A	4 sec	0	-
		10 sec	2	-
		20 sec	5	5, 5, 5, 5, 5
		30 sec	5	5, 5, 5, 5, 5
		40 sec	5	5, 5, 5, 5, 5
1000 sccm	2.0 A	20 sec	0	-
	4.0 A		5	4, 4, 4, 4, 4
	8.0 A		5	5, 5, 5, 5, 5
500 sccm	6.0 A	20 sec	0	-
1500 sccm			5	5, 5, 5, 5, 5
2000 sccm			5	5, 5, 5, 5, 5

Table 4. Tape Test results for waterborne primer (44-GN-36, Deft Corp.) applied to the argon LTCAT treated Parylene C surfaces.

Plasma Parameters			Tape Test Rating	
Ar Flow Rate	Arc Current	Treatment Time	Dry Test	Boiled in H_2O for 1, 2, 4, 6, 8 hrs
no treatment			0, no adhesion	-
1000 sccm	6.0 A	4 sec	0	-
		10 sec	1	-
		20 sec	5	5, 5, 4, 4, 4
		30 sec	5	5, 5, 5, 5, 5
		40 sec	5	5, 5, 5, 5, 5
1000 sccm	2.0 A	20 sec	0	-
	4.0 A		1	-
	8.0 A		5	5, 5, 5, 5, 5
500 sccm	6.0 A	20 sec	0	-
1500 sccm			5	5, 5, 5, 5, 5
2000 sccm			5	5, 5, 5, 5, 5

RF plasma treatment

RF argon plasma treatment of Parylene C surfaces is very attractive because two processes, Parylene deposition and plasma treatment, can be carried out in the same reactor, the Parylene reactor. It was found that an RF plasma source can also be used for the enhancement of Parylene C painting properties. Results of such treatment are shown in Table 5. The difference between RF treatment and LTCAT treatment is that a longer treatment period is necessary for the RF treatment to achieve painting properties similar to those obtained with LTCAT treatment. Therefore, LTCAT treatment seems to be a more efficient method for this purpose than RF plasma treatment.

Table 5. Tape Test results of the adhesion of solventborne primer (519X303, Courtaulds Aerospace) to Parylene C surfaces treated with Ar RF plasma in the Parylene reactor at 50 mtorr.

Power Input	Treatment Time	Tape Test Ratings	
		Dry	Boiled in H_2O for 1, 2, 4, 6, 8 hrs
100 W	20 sec	5	4, 4, 4, 4, 4
	60 sec	5	5, 5, 5, 4, 4
	120 sec	5	5, 5, 5, 5, 5
	240 sec	5	5, 5, 5, 5, 5
50 W	120 sec	5	5, 5, 5, 5, 5
200 W	120 sec	5	5, 5, 5, 5, 5

Conclusions

Low-temperature plasma treatment is a very efficient approach to engineer the surface and interface of Parylene C coatings. The poor adhesion of Parylene C coating to smooth surface can be overcome by plasma interface modification. A strong adhesion of Parylene C coating to a smooth 7075-T6 aluminum surface was achieved with the aid of plasma interface engineering.

The hydrophobic surface of a Parylene C surface can be functionalized by low-temperature plasma treatment. After proper plasma treatment, Parylene C coating became paintable with both solventborne and waterborne spray primers. Low-temperature cascade arc torch treatment had the advantage of shorter treatment time for this purpose over RF plasma treatment.

References

[1] M. Szwarc, Polym. Eng. Sci., 16(7), 473, 1976.

[2] R. Quade, 38th Annual Technical Conference Proceedings, 449, 1995.

[3] A. Sharma and H. Yasuda, J. Vac. Sci. Tech., 21(4), 994, 1982.

[4] A. Sharma and H. Yasuda, J. Adhesion, 13, 201, 1982.

[5] H. Yasuda, B. H. Chun, D. L. Cho, T. J. Lin, D. J. Yang, J. A. Antonelli, Corrosion, 52(3), 169, 1996.

[6] P. Kramer, A. K. Sharma, E. E. Hennecke, and H. Yasuda, J. Polym. Sci.: Polym. Chem. Ed., 22, 475, 1984.

[7] Q. S. Yu and H. K. Yasuda, Plasma Chemistry and Plasma Processing, 18(4), 461, 1998.

[8] S. P. Fusselman and H. K. Yasuda, Plasma Chem. Plasma Process., 14, 251, 1994.

[9] Y.-S. Lin and H. K. Yasuda, J. Appl. Polym. Sci., 67, 855, 1998.

26. Cathodic Plasma Polymerization and Treatment by Anode Magnetron Torch (AMT)
I. The influence of operating parameters on AMT glow discharge

J. G. Zhao and H. K. Yasuda[*]

Abstract

The anode magnetron torch (AMT), which is a physically confined magnetron plasma system, was developed for large-scale applications. It was found that a uniform funnel-shaped negative glow is crucial to achieve uniform plasma treatment in the focused area; this can be attained by adjusting the distance between two electrodes. The relationship between the gap distance (the distance from the edge of the glass tube to the cathode surface) and CDST $e2$ (the cathodic dark space thickness at the edge of the glass tube) is another important factor which affects whether materials removed by sputtering will redeposit on the substrate surface. The CDST shrinks not only with the increase of input power, applied voltage or current, but also with the increase of the magnetic field strength or system pressure. The CDST $e1$ (the CDST at the center of the focused area) will contract and the CDST $e2$ will expand with a decrease in the gap distance. The influence of the electrode distance on the CDST is complicated, because it causes not only a change in magnetic field strength, but also a change in the distribution of the magnetic field strength near the cathode surface.

Introduction

An electrode system superimposed with a magnetic field is generally referred to as a "magnetron" electrode system. The use of a magnetron electrode system provides several obvious advantages in industrial applications. First, it can create a stable glow discharge at low pressure. Second, it can confine the glow discharge to the near inter-electrode space. Third, the magnetron electrode system can apply high energy input without arcing or sparks [1]. In a DC magnetron system, if the magnetic field is superimposed on the cathode, it is called a cathode magnetron system. If it is superimposed on the anode, it is called an anode magnetron system. Cathode magnetron DC glow discharge is widely used in sputter coating [2, 3] and reactive sputter coating [4-8]. This coating usually demonstrates the characteristics of extreme hardness, good wear and corrosion resistance. However, the sputtering rate distribution on the cathode is not uniform, because of the presence of a non-uniform magnetic field at the target surface [9, 10]. This non-uniform sputtering rate distribution limits the application of cathode magnetron DC glow discharge in cathode sputter cleaning or cathodic plasma polymer deposition.

An anode magnetron system, which generates a funnel-shaped negative glow, can yield a relatively uniform sputtering rate on the cathode surface. Therefore, it can be used in a cathodic plasma sputter cleaning and deposition [11]. The use of anode magnetron DC glow discharges in surface treatment and plasma polymer deposition can improve interface adhesion [12] and surface corrosion protection [12-15]. However, for a very large substrate surface treatment, if we use a similarly large electrode system, a high input power is required to keep the desired current density. Such a high level of input energy is limited in actual application. In a large

system, it is also difficult to maintain uniformity in the monomer/gas distribution in the plasma zone. Consequently, the experimental parameters found in a laboratory-scale experiment can not be directly applied to a large-scale reactor. The anode magnetron torch (AMT) plasma system is an asymmetrical electrode system (small anode and large cathode) which has the capability to overcome these problems. If AMT glow discharge could be effectively confined in a local area, the AMT plasma system could be considered as a method to treat a large substrate surface via a scanning process at a low level of input power. Furthermore, the operating parameters used in a laboratory-scale experiment could be directly applied in a large substrate surface treatment or coating.

Because the AMT plasma system is a new technique, many influencing factors, such as magnetic field strength, the distance between electrodes, the gap distance, system pressure and input power, need to be studied. In this chapter, we focus on an investigation of the AMT glow discharge. The spatial distribution of the magnetic field strength and the influence on substrate material are reported. The influence of operating parameters on the AMT glow discharge is discussed.

Experimental

A schematic diagram of the anode magnetron in the AMT plasma system is shown in Fig. 1. The anode is round and made of aluminum. Its diameter (f) is 95 mm. At its center lies the monomer/gas inlet, a hole one-quarter inch in diameter. Six permanent magnets have been plugged symmetrically into the body of the anode. One iron disk and one iron ring, both made of soft iron, have been placed in the electrode and a titanium plate over them. Due to the placement of the magnets, the center iron disk and outer iron ring become the north and the south poles, respectively, of the magnetron system. Two sets of permanent magnets, with average magnetic field strengths of 4600 gauss (N pole) for a strong magnetic field, and 500 gauss (N pole) for a weak magnetic field , were used in this study.

The round anode has been placed snugly inside a glass tube. However, its position within the tube can be easily varied. The glass tube provides physical confinement of the monomer/gas flow, as well as support and insulation of the anode. This anode system is called the anode magnetron torch (AMT) (see Fig. 5b). If an anode system has no anode magnetron, it is simply called an anode torch (AT) (see Fig. 5a).

A schematic diagram of the entire experimental system is shown in Fig. 2. The glass tube is fixed on a stand by an aluminum support frame. A glass rod is used to fix the distance between the electrodes, as they may be attracted to each other under the strong magnetic field, if a cold rolled steel (CRS) panel is used as the cathode. The gas or monomer is fed through a small hole placed in the center of the anode electrode. Two physical parameters, a which is defined as the gap distance between the cathode surface and the edge of the glass tube and b which is defined as the distance between the two electrodes, are adjustable in the experiments. The cathode is made of a 7 in $\times$ 7 in square CRS plate. The ratio of cathode surface area to anode surface area is 4.5 to 1.
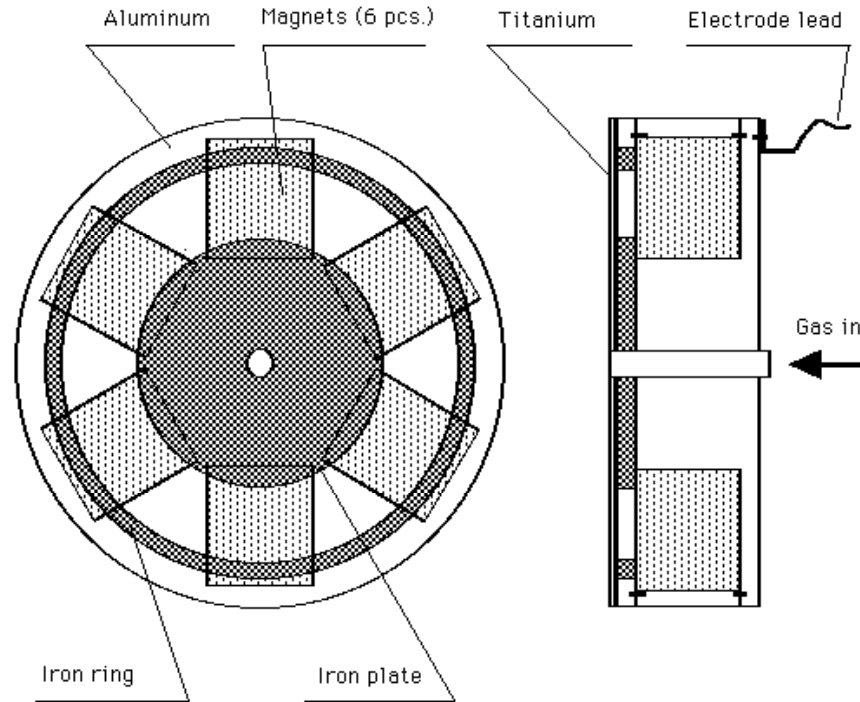
Figure 1. A schematic diagram of the anode magnetron structure.

A vacuum chamber consisting with a bell jar (hieght = 635 mm, diameter = 378 mm) is pumped by Edwards EH series vacuum pump system (Model E2M 80 rotary pump, and Model EH500A booster pump). System pressure is controlled by a throttle valve (MKS 252), which is controlled by an MKS220C pressure sensor, independent of gas flow rate. The typical operation pressure is 50 mtorr and flow rate is 1 sccm at the base system pressure of 2 mtorr.

A Gauss meter (Walker-MG 3D) was used to measure the distribution of the magnetic field strength. The characteristics of an anode magnetron are expressed by the maximum parallel component of the magnetic field at the electrode surface. This was found by scanning the anode surface with the probe.

Cathodic dark space thickness (CDST) was measured from the outside of the bell-jar chamber using vernier calipers. Due to the influence of glass refraction, the CDST measured through the bell-jar chamber is a skewed thickness. The actual CDST can be calculated using the following formula:

$$e_{act} = e_{re} \times R_{act} / R_{re},$$

where, e_{act} is the actual value of the CDST, e_{re} is the value measured through the bell-jar chamber, R_{act} is the actual reference value, and R_{re} is the reference value measured through the bell-jar chamber. For this calculation, it is assumed that the ratio of actual thickness to measured thickness is constant.

Argon gas was used to measure the CDST in this study. CDST *e1* is the CDST at the center of the focused area, and CDST *e2* is the CDST at the edge of the glass tube.
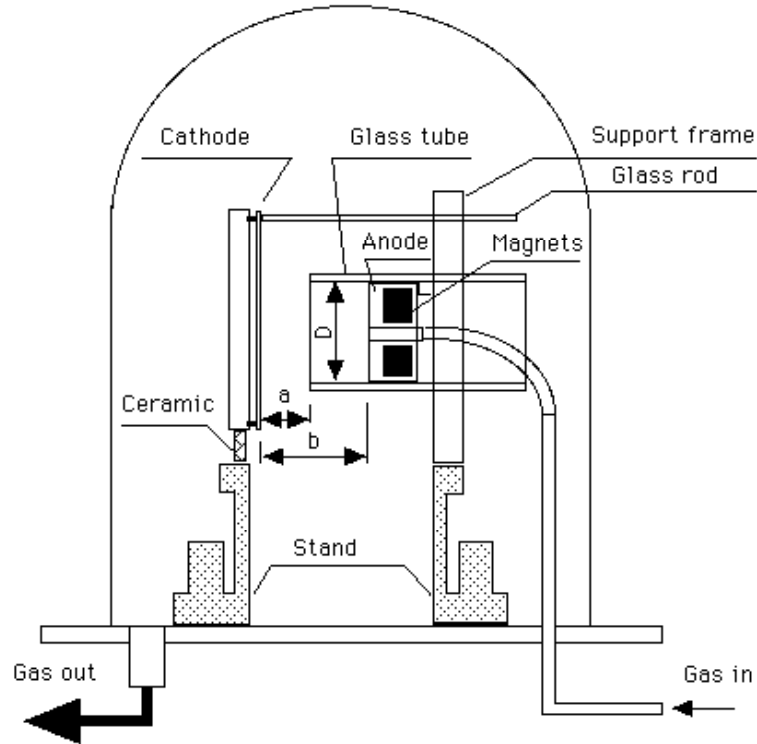
Figure 2. A schematic diagram of the bell-jar reactor system.

It is well known that the color of a thin film corresponds to its thickness. If a CRS panel is coated with trimethylsilane (TMS) using a plasma technique, the significant color changes, light brown, brown, purple, dark blue, light blue, yellow, will appear on the surface respectively as the TMS coating thickness increases. Therefore, various TMS coating thicknesses can be differentiated by the color changes. In order to determine the influence of gap distance and electrode distance on AMT glow discharge, argon plasma was used to sputter CRS which had been coated with TMS and showed a dark blue color. In such an experiment, if the color resulting from the argon plasma treatment is in the brown or purple ranges, it indicates that the sputtering process is predominant. On the other hand, if the resulting color is in the light blue or yellow ranges, the deposition process is predominant.

Results and discussion

The distribution of anode magnetic field strength
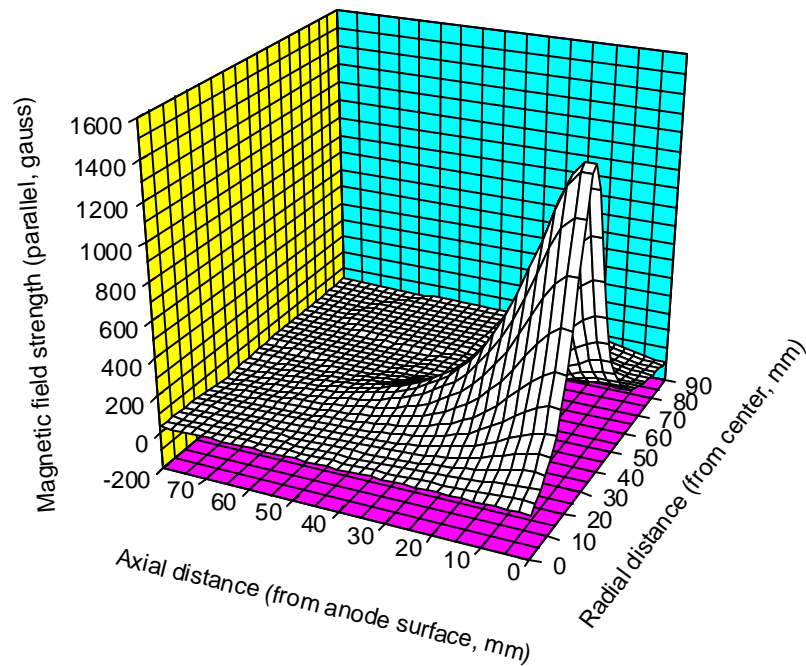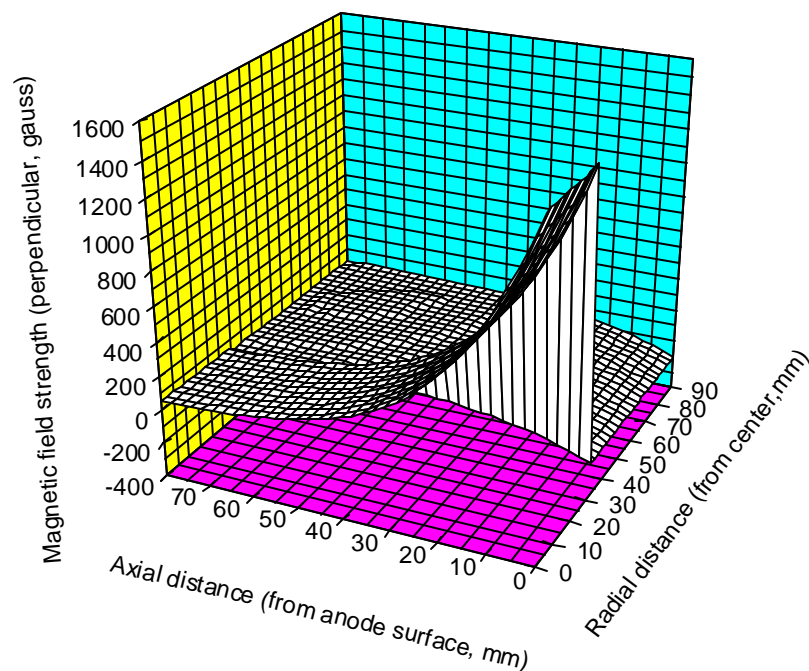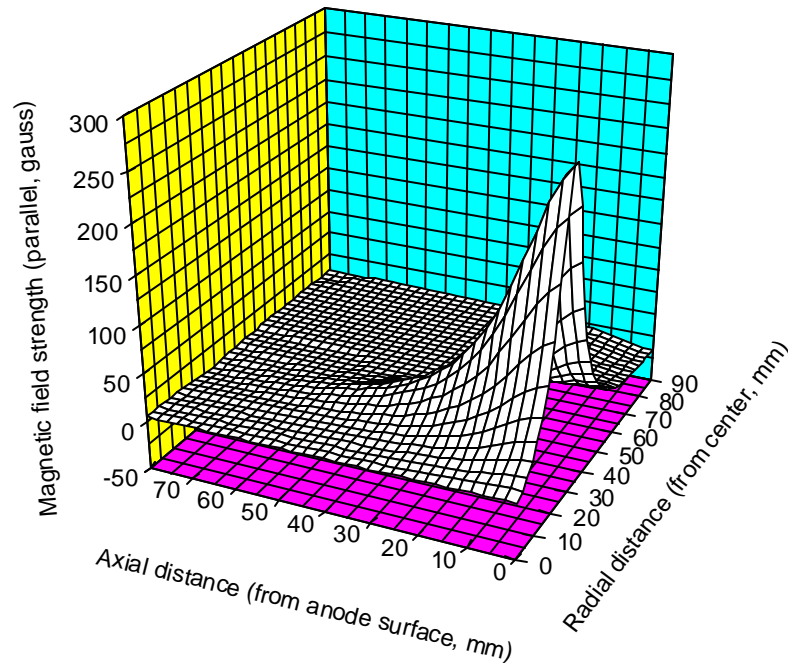
Figure 3a. The spatial distribution of parallel magnetic field strength employing strong magnets ($B_{//stmax}$=1550 gauss) as measured with a Walker-MG 3D gauss meter.

The spatial distributions of anode magnetic field strength are shown in Figs. 3a-d. It was found that, for strong and weak magnetic field strengths, the maximum values are about 1550 (parallel), 1800 (perpendicular) gauss and 280 (parallel), 310 (perpendicular) gauss, respectively. Using the same anode magnetron configuration, the shapes of the distributions of the magnetic field strength are almost identical, but the magnitudes differ. In Figs. 3a-d, r is defined as the radial distance from the center of the anode surface; z is the axial distance from the surface of the anode. For parallel magnetic field strength, the maximum value appears when r is approximately 3 cm and z is approximately 0 cm. For perpendicular magnetic field strength, the maximum value exists when r is about 2 cm and z is about 0 cm. The parallel magnetic field strength decreases as the axial direction distance increases. In the radial direction, following its increase to the maximum, the parallel magnetic field strength decreases as the radial direction increases. Finally, it approaches zero. The distribution of parallel magnetic field strength is almost uniform on the cathode surface when z is larger than 8.0 cm for the strong magnetic field ($B_{//stmax}$=1550 gauss), or larger than 4.0 cm for the weak magnetic field ($B_{//wkmax}$=280 gauss).

It was found that the distribution of magnetic field strength varies little when the cathode is made of materials such as aluminum, or titanium. It varies somewhat more when the cathode is made of CRS; however, the degree to which this influence is observable depends on the distance between the anode and the CRS panel.
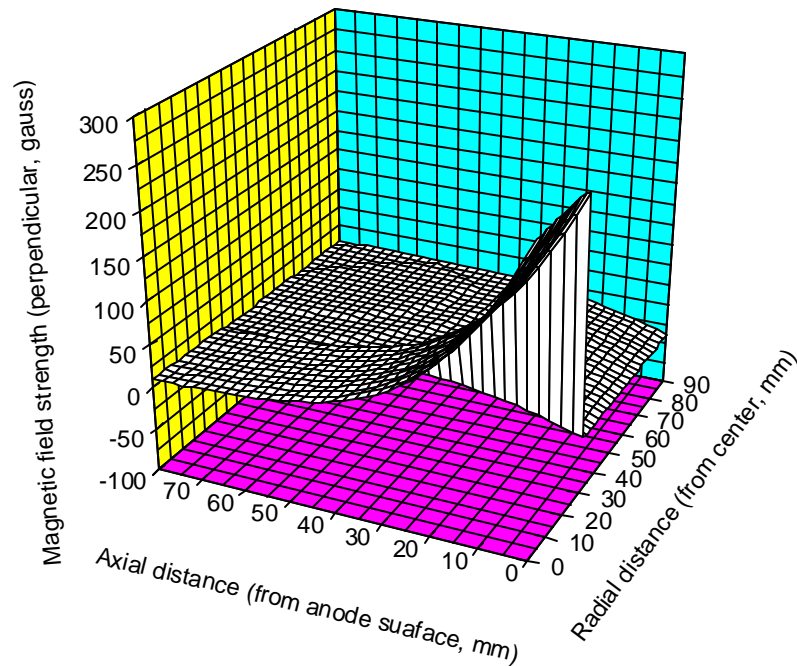

Figure 3b. The spatial distribution of perpendicular magnetic field strength employing strong magnets ($B_{\perp stmax}$=1800 gauss) as measured with a Walker-MG 3D gauss meter.

The influence of the CRS substrate on the distribution of magnetic field strength is shown in Figs. 4a-c. The presence of a CRS plate can create an inductive magnetic field which partially offsets the original magnetic field effect in the vicinity of the CRS plate. The influence of the anode magnetron in the vicinity of the cathode attenuates as the distance between the two electrodes increases. The effect of cathode material can be neglected for large electrode distances (8.0 cm for $B_{//stmax}$=1550 gauss and 4.0 cm for $B_{//wkmax}$=280 gauss).

Figure 3c. The spatial distribution of parallel magnetic field strength employing weak magnets ($B_{//wkmax}$=280 gauss) as measured with a Walker-MG 3D gauss meter.

A comparison of AT and AMT glow discharge

A schematic representation of AT glow discharge is shown in Fig. 5a. The leading edge of the cathode dark space is flat in AT glow discharge. If the system pressure is lower than 30 mtorr, it is difficult to establish a stable glow discharge. There is little change in the shape of the cathode dark space when the gap distance is varied. However, the leading edge of the cathode dark space in the focused area is pushed closer to the surface with the decrease of the gap distance. Outside of the glass tube, the CDST varies little with changes in the gap distance.

A schematic diagram of AMT glow discharge is shown in Fig. 5b. Unlike in the case of AT glow discharge, the cathode dark space in AMT glow discharge is kidney shaped. The CDST in the center region is less than that at the edge region. In other words, the negative glow is pushed closer to the cathode surface at the center of the focused area. The negative glow is funnel-shaped and extends from the center of the anode toward the cathode. The Faraday dark space

forms two hemispherical dark spaces in the cross sectional view. The shape of the glow discharge is similar to that of conventional anode-magnetron glow discharge [16]. The funnel-shaped negative glow still exists even when system pressure is very low (p=10 mtorr).

Figure 3d. The spatial distribution of perpendicular magnetic field strength employing weak magnets ($B_{\perp wkmax}$=310 gauss) as measured with a Walker-MG 3D gauss meter.

The effects of physical parameters in AMT glow discharge

Due to physical confinement, the relationship between the gap distance and the CDST becomes an important factor when large substrate surfaces are to be treated via the AMT technique (Fig. 5b). When Ar plasma was used to treat a TMS plasma polymer coated CRS panel dark blue in color, the resulting multicolored pattern on the CRS panel showed that the materials removed by sputtering may redeposit on the substrate surface near the vicinity or outside of the edge of the glass tube (see Fig. 6). When the value of *a*, defined as the gap distance between the cathode surface and the edge of the glass tube, is greater than the value of the CDST *e2*, the multicolored

pattern on the treated CRS panel does not show any light blue or yellow color. This indicates there has been no redeposition on the substrate surface, if a > e2. However, when the value of *a* is smaller than the value of the CDST e2, (i.e., a < e2) the light blue color will appear near the vicinity or outside of the edge of the glass tube, demonstrating that the redeposition has occurred. Therefore, whether or not materials removed by sputtering redeposit on the substrate surface depends on the relationship between the gap distance and the CDST *e2*. If the gap distance is equal to or greater than the CDST *e2*, materials removed by sputtering will not be redeposited on the substrate surface. Otherwise, the redeposition of such materials occurs near the vicinity or outside of the edge of the glass tube. The value of CDST e2 varies with experimental factors as described bellow but is roughly 15 mm. Therefore, if the gap distance is kept larger than 15 mm, no re-deposition of sputtered materials has been observed.

Radial Distance (from anode center, mm)
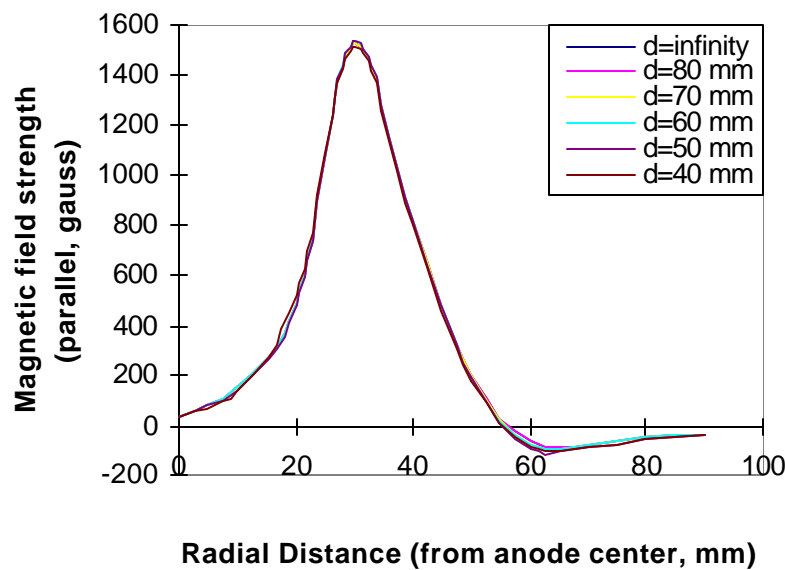
Figure 4a. The dependence of parallel magnetic field strength distribution on electrode distance at *z*=0.0 mm (B$_{//stmax}$=1550 gauss, *d* is the distance between the anode surface and the cathode surface, *z* is the distance from the anode surface to the measurement location, cathode material is a 7 in. $\times$ 7 in. cold-rolled steel plate).

The relationship between gap distance and the CDST *e2* is a crucial condition to control in treatment of large substrate surfaces via the AMT plasma technique. Application of the AMT technique in dealing with large substrate surfaces can be accomplished using a scanning process at a low level of input power. If redeposition on the substrate surface occurs, the cleaned surface can be contaminated again during the AMT scanning process. The actual AMT scanning process must maintain a gap distance equal to or greater than the CDST *e2*. Therefore, the CDST plays an important role in the AMT process. Investigation of the CDST is necessary for successful application of the AMT plasma system. The influence of operating parameters on the CDST is discussed in the next section.
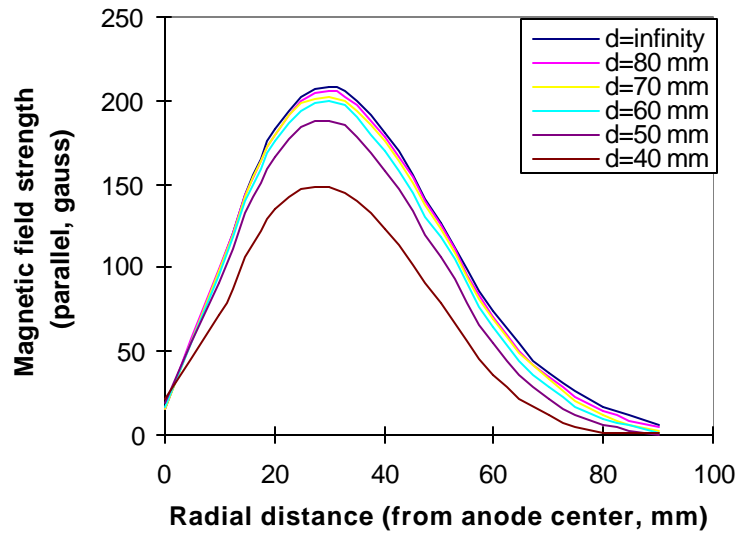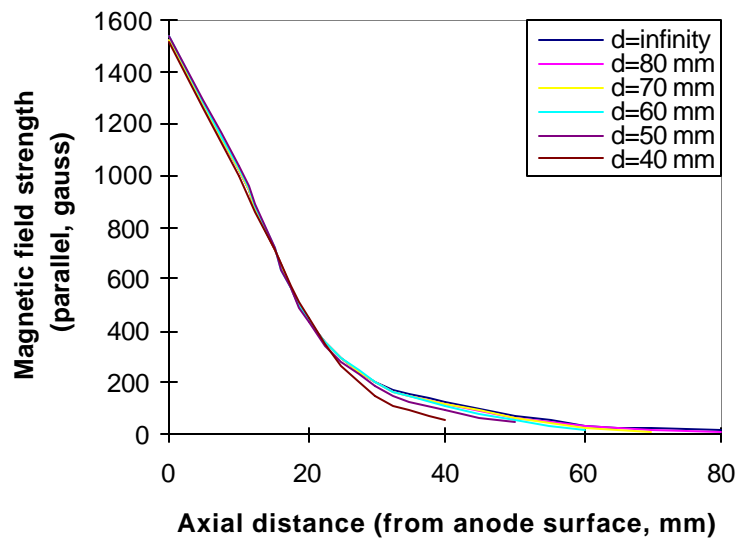
Figure 4b. The dependence of parallel magnetic field strength distribution on electrode distance at z=30 mm ($B_{//stmax}$=1550 gauss, d is the distance between the anode surface and the cathode surface, z is the distance from the anode surface to the measurement location, cathode material is a 7 in. $\times$ 7 in. cold-rolled steel plate).

Figure 4c. The dependence of parallel magnetic field strength distribution on electrode distance at r=30 mm ($B_{//stmax}$=1550 gauss, d is the distance between the anode surface and the cathode surface, r is the radial distance from the center axis of the anode to the measurement location, cathode material is a 7 in. $\times$ 7 in. cold-rolled steel plate).

The distance between electrodes, b, is a vital parameter that can affect the luminosity distribution of the negative glow in AMT glow discharge. In AT glow discharge, the luminosity distribution

of the negative glow does not vary with changes in the distance between electrodes. However, in AMT glow discharge, the luminosity distribution of negative glow does depend on b. A schematic diagram of the luminosity distribution of AMT glow discharge with a small electrode distance is shown in Fig. 7. The tail width of negative glow expands with the decrease of b. The luminosity distribution of the funnel-shaped negative glow is relatively uniform when b is large (>7.0 cm under $B_{//max}$=1550 gauss); it becomes non-uniform when b is small. The luminosity at the center of the funnel-shaped negative glow is less than that at the edge of the glow area. In other words, the luminosity at the center of the funnel-shaped negative glow diminishes as the electrode distance decreases.
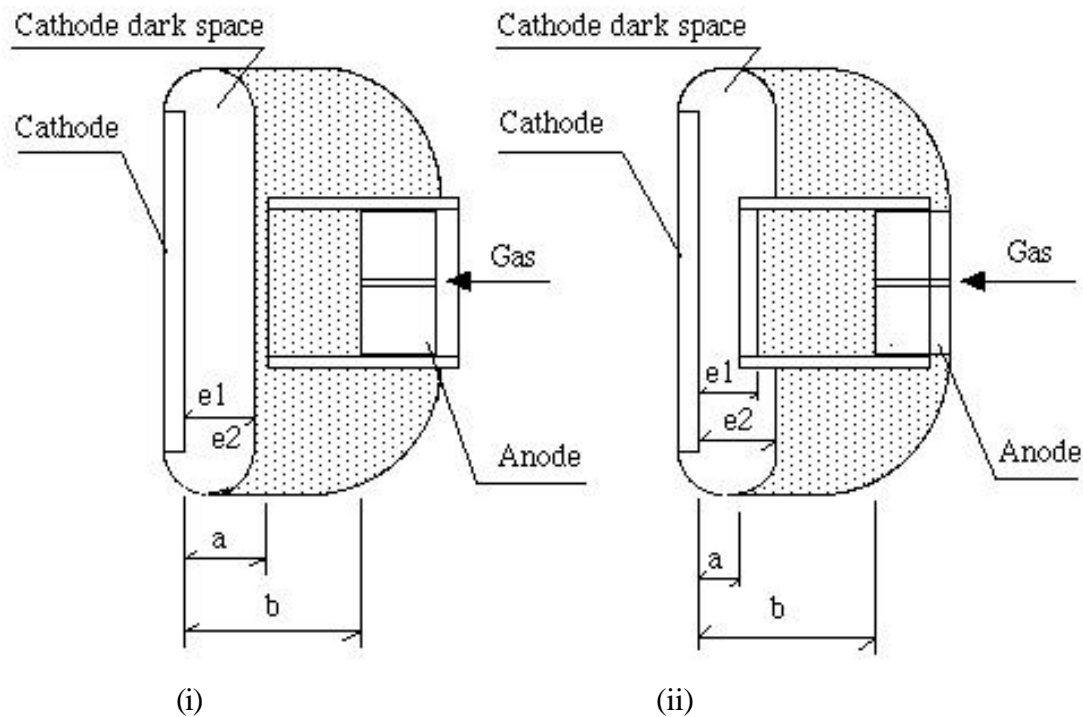
Figure 5a. A schematic diagram of the shape of AT glow discharge. The shaded area is the glow zone. (i) Large gap distance and (ii) Small gap distance.

When argon gas was used to sputter a colored CRS panel at different electrode distances using the AMT plasma technique, the multicolored profile shown in Fig. 8 appeared on the CRS panel. When b is small, the big blue eye appears at the center of focused area, and the luminosity of AMT negative glow becomes non-uniform. The diameter of the blue eye expands as b is decreased, and the luminosity of AMT negative glow becomes more non-uniform. On the contrary, the blue eye disappears as b is increased, and the luminosity of AMT negative glow becomes uniform.

The luminosity of the glow discharge is the result of the excitation and ionization collisions of electrons and gas. These collisions create ions that can bombard the cathode surface. Normally, uniform luminosity of AMT negative glow implies the uniform distribution of excitation and ionization collisions between gas and electrons; this ensures a uniform sputtering rate on the

cathode surface. Therefore, in AMT plasma treatment, creation of a uniform AMT negative glow is essential to achieve a uniform sputtering rate distribution in the focused area.
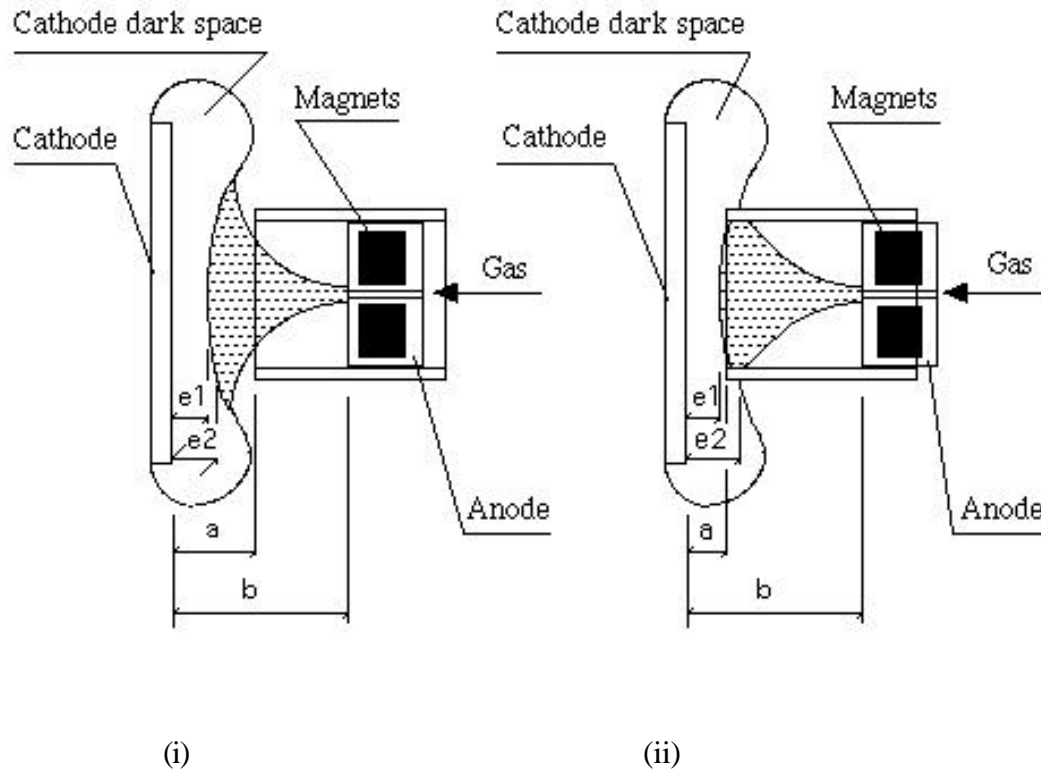

(i)   (ii)

Figure 5b. A schematic diagram of the shape of AMT glow discharge. The shaded area is the glow zone. (i) Large gap distance and (ii) Small gap distance.

The influence of various parameters on the CDST in AMT glow discharge.

The cathode dark space is a region in which electrons travel with high speed because of the high electric field. As a result, the electron density in this region is the lowest in the discharge. Consequently, there are only a few electron-atom collisions, which are not sufficient to cause any detectable glow. The negative glow is due to the excitation and ionization of gas atoms which collide with electrons that have gained high energies after being accelerated through the cathode dark space. The cathodic dark space thickness (CDST), which extends from the cathode to the leading edge of the negative glow, carries most of the voltage [17]. A change in the CDST indicates a difference in the distribution of electron density and electron temperature. A smaller CDST implies the distribution of the high-energy electrons is closer to the cathode surface, if the system pressure has not been altered.

The influence of input power, applied voltage, and applied current on the CDST is shown in Figs. 9-11. The CDST decreases with the increase of input power, applied voltage or applied current. This is because the average energy of electrons increases when the input energy, applied

voltage or applied current increases. More high-energy electrons can easily ionize more gas atoms, resulting in the leading edge of negative glow shifting toward the cathode surface.
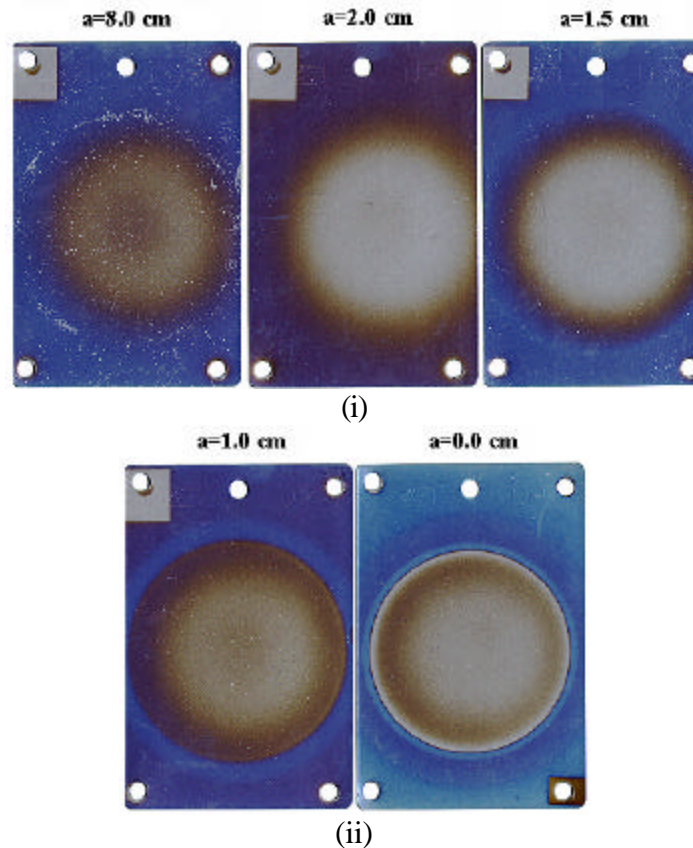

Figure 6. The dependence of Ar sputtering effects on gap distance ($B_{//stmax}$=1550 gauss, b=8.0 cm, w=10 watts, p=50 mtorr, sputtering time: (i) 20 min, (ii) 10 min).

System pressure also influences the CDST in an AMT plasma system. The CDST expands greatly with the decrease of system pressure (see Fig. 12). This is because the mean free path, λ, of gases and of electron is inversely proportional to the system pressure. A higher mean free path, λ, indicates a lower probability of collisions between electrons and gases, thus resulting in the leading edge of negative glow moving far away from the cathode surface. When the system pressure becomes lower (p = 10 mtorr), it is difficult to reach high input power (W = 50 watts), because there are not enough ionized atoms and electrons to keep a high current density. Therefore, no data was visible in Fig. 12 at low system pressure (p = 10 mtorr) and high input power (W = 50 watts).

The magnetic field strength is a vital parameter in the AMT plasma system. The influence of magnetic field strength on the CDST in the AMT system is shown in Fig. 13. The CDST *el* shrinks with the increase of magnetic field strength. Due to the presence of the magnetic field, the movement of electrons is largely restricted and localized. The net pattern of electron activity

is a zigzag spiral motion. Electrons travel along the $E \times B$ drift motion path. Because of the spiral motion of electrons, the possibility of collisions between electrons and gas atoms increases, and higher degrees of ionization occur in magnetron plasma [18]. The peak of electron temperature shifts to the cathode surface, and the electron density rises near the cathode surface with the increase of the anode magnetron [16]. The shifted peak in electron temperature and the increase of electron density result in the distribution of the ionization collisions lying close to the cathode surface
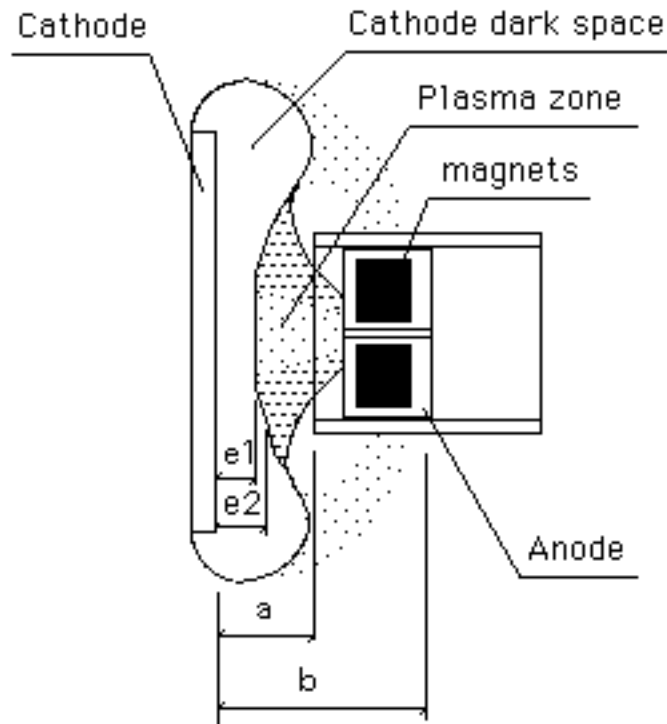
Figure 7. A schematic diagram of the shape of AMT glow discharge with a small electrode distance (< 6.0 cm for $B_{//stmax}=1550$ gauss). The degree of shading in the glow zone indicates the level of brightness, i.e., the center of the glow zone is not as bright as the edges.

As aforementioned, the CDST *e1* become smaller while the CDST *e2* expands with a decrease of the gap distance in AMT glow discharge. The results of this experiment demonstrated this trend (see Fig. 14). Due to high physical confinement (small gap distance), more high-energy electrons are confined in the focused area. This results in an increase of the effective excitation and ionization collisions, shifting the leading edge of negative glow to the cathode surface. The expansion of the CDST *e2* can be attributed to the presence of less high-energy electrons in the unfocused area; this condition obviously arises due to the confinement of more high-energy electrons in the focused area. The presence of less high-energy electrons decreases the possibility of the effective excitation and ionization collisions and pushes the leading edge of the negative glow away from the cathode surface.
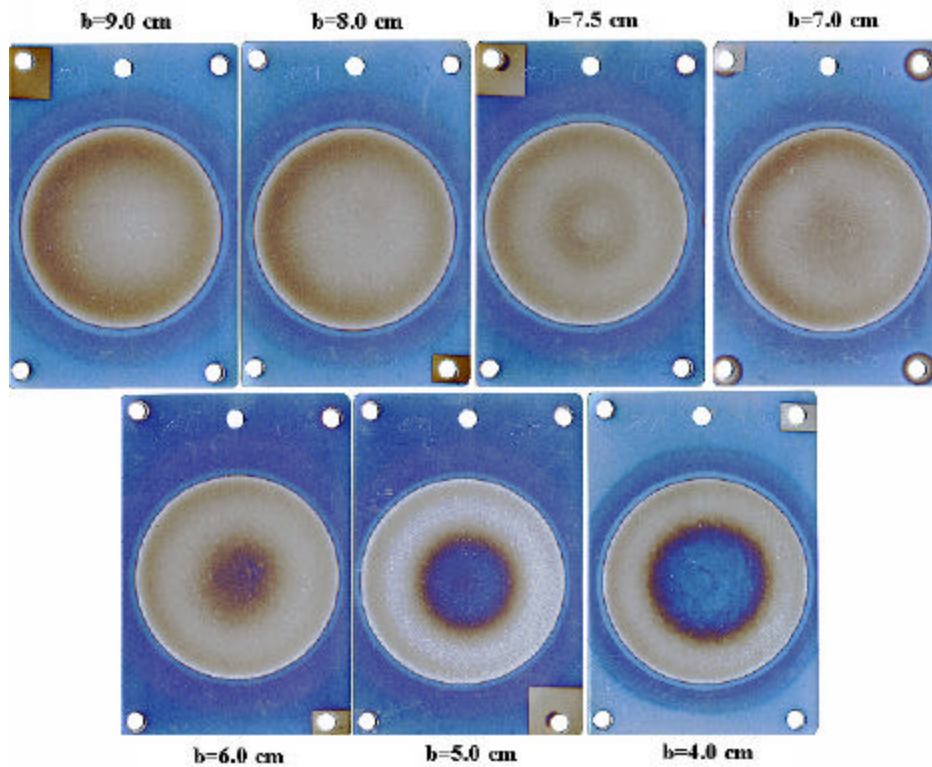
Figure 8. The dependence of sputtering effects on electrode distance ($B_{//stmax}$=1550 gauss, a=0.0 cm, w=10 watts, p=50 mtorr, sputtering time=10 min).
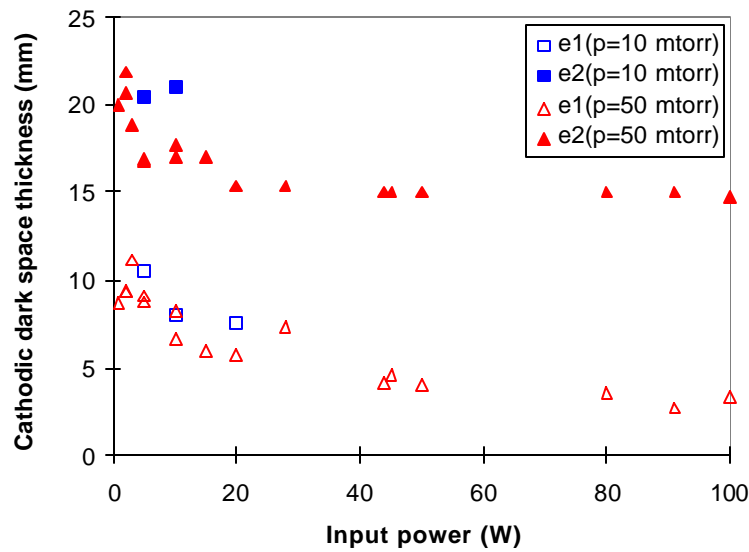

Figure 9. The influence of input power on the cathodic dark space thickness ($B_{//stmax}$=1550 gauss, a=1.5 cm, b=8.0 cm, Ar mass flow rate =1 sccm).
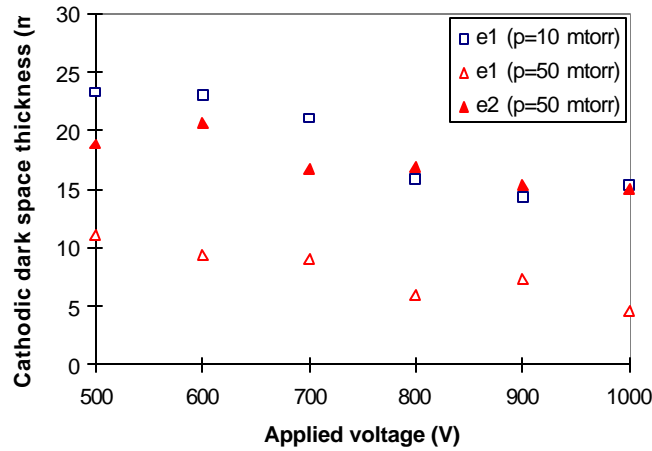
Figure 10. The influence of applied voltage on the cathodic dark space thickness (B$_{//stmax}$=1550 gauss, a=1.5 cm, b=8.0 cm, Ar mass flow rate =1 sccm).
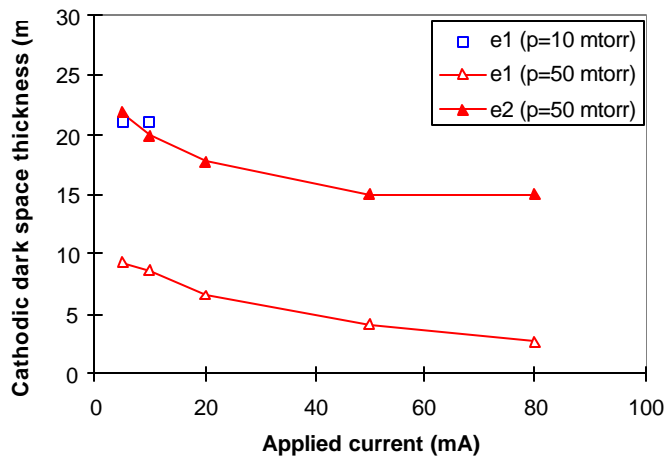

Figure 11. The influence of applied current on the cathodic dark space thickness (B$_{//stmax}$=1550 gauss, a=1.5 cm, b=8.0 cm, Ar mass flow rate =1 sccm).

In AT glow discharge, the electrode distance has almost no influence on the CDST unless it is very close to the CDST. In AMT glow discharge, the influence of the electrode distance, *b,* on the CDST is complicated, because changes in electrode distance cause not only a change in the magnetic field strength near the cathode surface, but also a change in the distribution of the magnetic field strength. Such changes result in variance in the luminosity of AMT negative glow.

A shorter electrode distance may increase the magnetic field strength near the cathode surface and result in shrinkage of the CDST. However, if the electrode distance is too small, due to the influence of the magnetic field strength, more high-energy electrons will be trapped in the high magnetic field strength range where the radial distance is about 3.0 cm from the center of the

anode. The probability of effective electron-atom collisions decreases in the center area. Therefore, the CDST *e1* is expanded. These results are shown in Figs. 15 and 16.
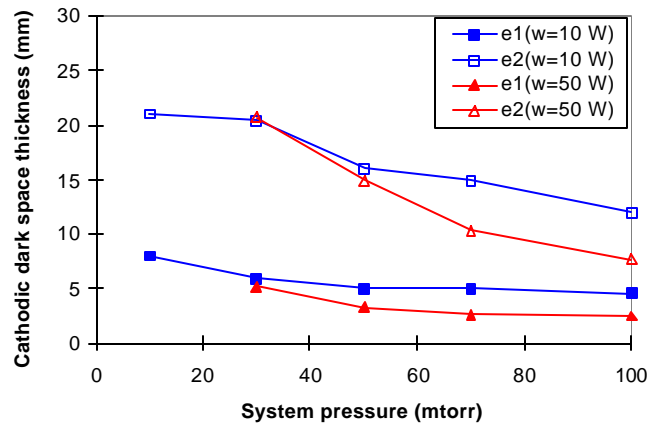

Figure 12. The influence of system pressure on the cathodic dark space thickness ($B_{//stmax}$=1550 gauss, a=1.5 cm, b=8.0 cm, Ar mass flow rate =1 sccm).
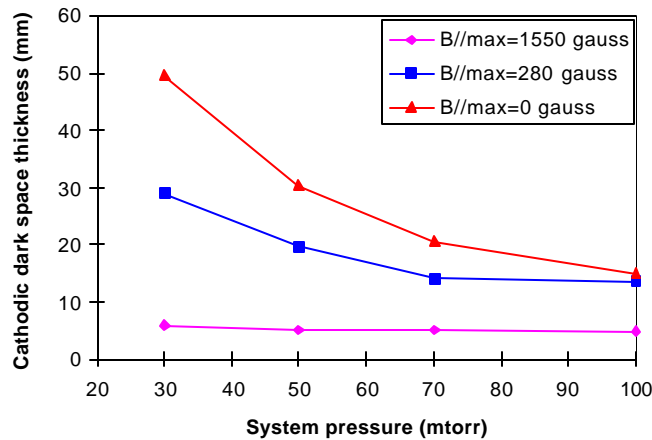

Figure 13. The influence of magnetic field strength on the cathodic dark space thickness (input power=50 W, a=1.5 cm, b=8.0 cm, Ar mass flow rate=1 sccm).

In AMT glow discharge with a weak magnetic field ($B_{//wkmax}$ =280 gauss), the electrode distance does not significantly influence the distribution of the magnetic field strength near the cathode surface; the magnetic field strength distribution is almost uniform unless $b < 3.0$ cm. Therefore, the CDST become smaller with the electrode distance due to the influence of magnetic field strength.
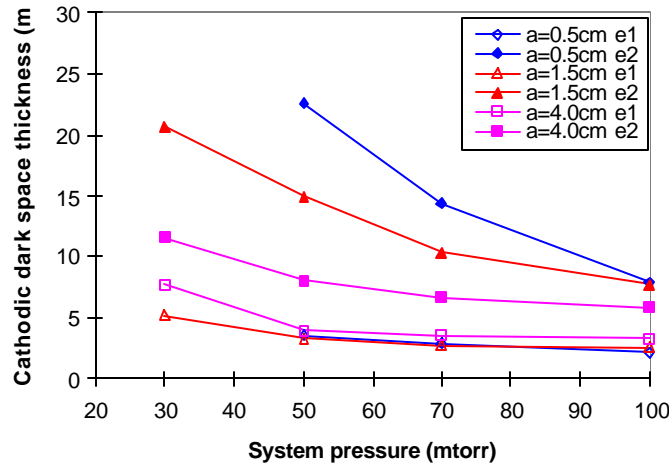
Figure 14. The influence of gap distance on the cathodic dark space thickness ($B_{//stmax}$=1550 gauss, input power=50 W, b=8.0 cm, Ar mass flow rate=1 sccm).
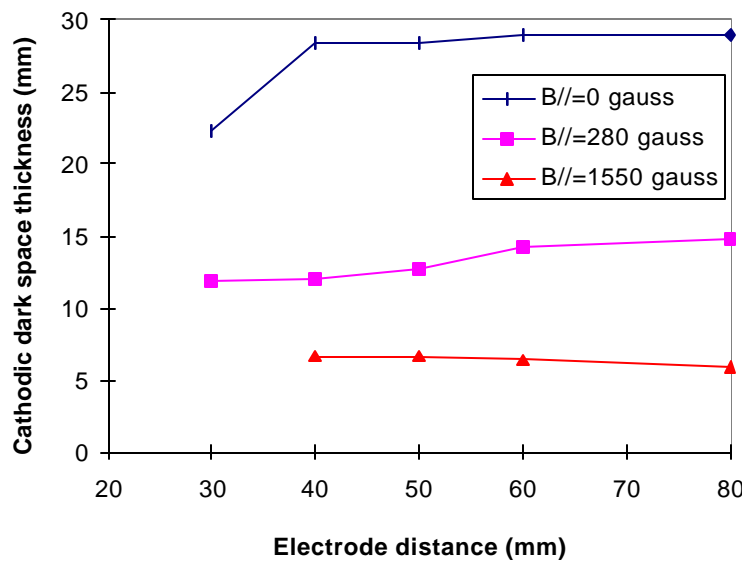

Figure 15. The influence of electrode distance on the cathodic dark space thickness (input power=10 W, a=0.0 cm, Ar mass flow rate=1 sccm).

In AMT with a strong magnetic field ($B_{//stmax}$ =1550 gauss), the CDST $e1$ increases with decreasing electrode distance (from 8.0 to 4.0 cm). This is because, in this case, the electrode distance does significantly influence the distribution of the magnetic field strength near the cathode surface; the magnetic field strength distribution is not uniform when $b < 6.0$ cm. Although the influence of magnetic field strength may shrink CDST $e1$ at small b, the non-uniform magnetic field strength distribution results in less effective collisions between electrons and atoms, which expands the CDST $e1$. This combined influence makes CDST $e1$ expand (see Figs 15 and 16). Nevertheless, the influence of the electrode distance on CDST $e2$ obeys the

same basic principle outside of the focused area: that is, high magnetic field strength will push the cathode dark space closer to the cathode surface (see Fig. 16).
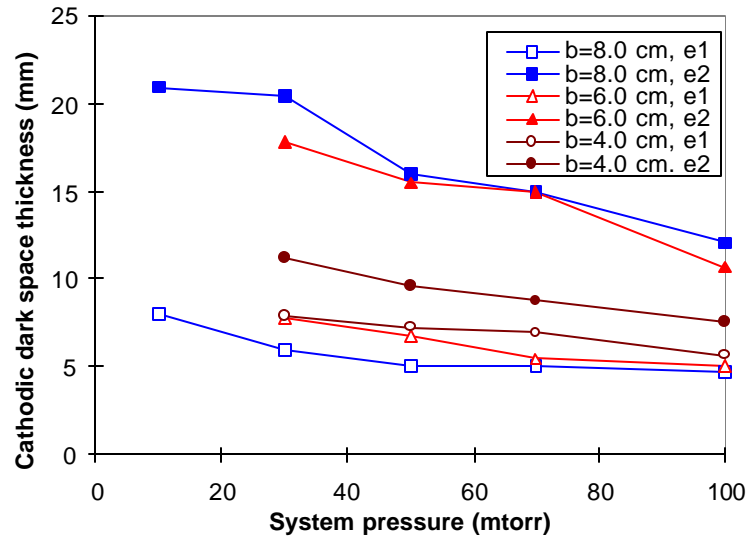

Figure 16. The influence of electrode distance on the cathodic dark space thickness ($B_{//stmax}$=1550 gauss, input power=10 W, a=1.5 cm, Ar mass flow rate=1 sccm).

Conclusion

1. The anode magnetron torch (AMT) system yields stable glow discharge in the low system pressure region (p = 10 mtorr), where stable glow discharge cannot be created without magnetic enhancement.
2. Cold-rolled steel influences the original distribution of the magnetic field strength. The influence attenuates with the increase of the distance between the anode and the CRS.
3. Operating parameters influence AMT glow discharge. A suitable distance between electrodes creates uniform luminosity of the glow discharge in an AMT system. This is an essential condition to achieve a uniform sputtering rate distribution in the focused area.
4. The redeposition of materials removed by sputtering depends on the relationship between gap distance, *a,* and the CDST *e2*. If *a* is equal to or greater than *e2*, no redeposition of materials appears on the substrate. Otherwise, redeposition will occur.
5. The CDST *e1* shrinks not only with the increase of input power, applied voltage, applied current, or system pressure, but also with the decrease of gap distance or anode magnetic field strength.

References

1. D. L. Cho, Y. -S. Yeh, and H. Yasuda, *J. Vac. Sci. Technol*. A **7(5)**, 2960 (1989).
2. R. K. Waits, *J. Vac. Sci. Technol.* **15(2)**, 179 (1978).
3. A. E. Wendt, M. A. Lieberman, and H. Meuth, *J. Vac. Sci. Technol.* A **6(3)**, 1827 (1988).

4. D. Hofmann, A. Rost and H. Schubler, *Mater. Sci. Eng.* A **139**, 290 (1991).

5. S. Kadlec, J. Musil, W. D. Munz, G. Hakanson and J. E. Sundgren, *Surf. Coat. Technol*, **39/40**, 487 (1989).

6. X. Chu, A. Barnett, M.S. Wong and W. D. Sproul, *J. Vac. Sci. Technol.* A **14(6)**, 3124 (1996).

7. G. Este, and W. D. Westwood, *J. Vac. Sci. Technol.* A **2(3)**, 1238 (1984).

8. R. D. Arnell, J. S. Colligon, K. F. Minnebaev, and V. E. Yurasova, *Vacuum*, **47(5)**, 425 (1996).

9. J. Musil, A. Rajsky, A. J. Bell, J. Matous, M. Cepera and J. Zeman, *J. Vac. Sci. Technol.* A **14(4)**, 2187 (1996).

10. A. R. Nyaiesh, *Vacuum*, **36(6)**, 307 (1986).

11. W. H. Tao, Dissertation, University of Missouri-Columbia, Aug. 1994.

12. T. F. Wang, T. J. Lin, D. J. Yand, J. A. Antonelli, and H. K. Yasuda, *Prog. Org.   Coat*. **28(4)**, 291 (1996).

13. H. K. Yasuda, T. F. Wang, D. L. Cho, T. J. Lin, and J. A. Antonelli, *Prog. Org. Coat*. **30(1)**, 31 (1997).

14. H. Yasuda, B. H. Chun, D. L. Cho, T. J. Lin, D. J. Yang, and J. A. Antonelli, *Corrosion J.* **52**, 169 (1996).

15. Y. Lin and H. Yasuda, *J. Appl. Polym. Sci*. **60**, 543 (1996).

16. W. H. Tao, M. A. Prelas, and H. K. Yasuda, *J. Vac. Sci. Technol.* A **14(4)**, 2113 (1996).

17. E. Nasser, Fundamentals of Gaseous Ionization and Plasma Electronics. (Wiley, New York, 1971).

18. J. A. Thornton, *J. Vac. Sci. Technol.* **15(2)**, 171 (1978).

27. Cathodic Plasma Polymerization and Treatment by Anode Magnetron Torch (AMT)
II. The influence of operating parameters on the argon sputtering rate distribution

J. G. Zhao and H. Yasuda[*]

Abstract

In this study, the distribution of argon sputtering rate on the cathode surface was used to investigate the anode magnetron torch (AMT) plasma system, which was developed for large substrate surface treatment. The Ar sputtering rate was estimated using the colorimetric method. The experimental results showed that a uniform sputtering rate could be achieved by adjusting the distance between the two electrodes, because a suitable electrode distance creates a uniform magnetic field near the cathode surface. A small gap distance can increase the Ar sputtering rate in the focused area, but also creates deposition near the vicinity or outside of the edge of the glass tube, which is used to focus the gas flow. The optimum gap distance is equal to the CDST *e2* (cathodic dark space thickness at the edge of the glass tube); this configuration maintains a high sputtering rate in the focused area, but does not allow deposition to occur near the vicinity or outside of the edge of the glass tube. A higher Ar sputtering rate can be achieved under low system pressure. At low system pressure, a high magnetic field strength is important for increasing the Ar sputtering rate, as it improves the magnetic confinement of electrons.

Introduction

In plasma polymerization, DC glow discharge shows its unique advantages in the treatment of metal materials. DC glow discharge not only increases the deposition rate and refractive index, but also improves the adhesion of a plasma polymer on a metal surface as compared to AF or RF glow discharge [2, 3]. Anode magnetron DC glow discharge creates a uniform sputtering or deposition rate on the cathode surface [4]. It has been used in surface treatment for improving adhesion [5] and increasing corrosion protection [5, 6, 7, 8]. Generally, the size of the substrate is more or less the same as that of the magnetron anode in a laboratory-scale experiment. If a large substrate surface is to be treated, there are basically two approaches. One is to use a matching-sized large anode, the other is to use the small anode. The first approach requires a large power supply; it also necessitates a large distance between the cathode and the anode in order to facilitate the supply of monomer into the plasma zone. Consequently, the operating parameters found in a laboratory-scale experiment can not be directly applied to a scaled-up reactor. This approach is analogous to using a five-meter wide brush to paint a five-meter wide wall. The second approach, on the other hand, involves using a small brush to paint the five-meter wide wall. In this approach, if the plasma can be effectively confined to a small portion of the surface area, the operating parameters used on the laboratory scale can be directly applied in plasma treatment and coating on a large scale.

The objectives of this study are twofold: (1) to investigate the influence of operating parameters on the AMT plasma system by examining Ar sputtering rate distribution, and (2) to determine the optimum operating parameters which maintain a high sputtering rate in the focused area but do not allow deposition on the other areas of the substrate. These fundamental aspects of AMT glow discharge are also necessary in developing effective plasma coatings by AMT.

In this study (part II), the colorimetric method was used to estimate the Ar sputtering rate distribution. The influence of operating parameters, including magnetic field strength, electrode distance (*b*), gap distance (*a*), system pressure, input power, gas flow rate and substrate surface area, on sputtering rate distribution, will be presented and discussed.

Experimental

A schematic diagram of the anode magnetron torch (AMT) is shown in Fig. 1. The parameter *a* is the gap distance from the cathode surface to the edge of glass tube, and *b* is the distance between the two electrodes. Both of these parameters are adjustable. Gas is fed from the center of the anode electrode. Details of the experimental setup can be found in the previous paper [1]. In this study, three magnetic field strengths parallel to the anode surface have been used: 1550, 280, and 0 gauss. The CDST *e2* is the cathodic dark space thickness at the edge of the glass tube.
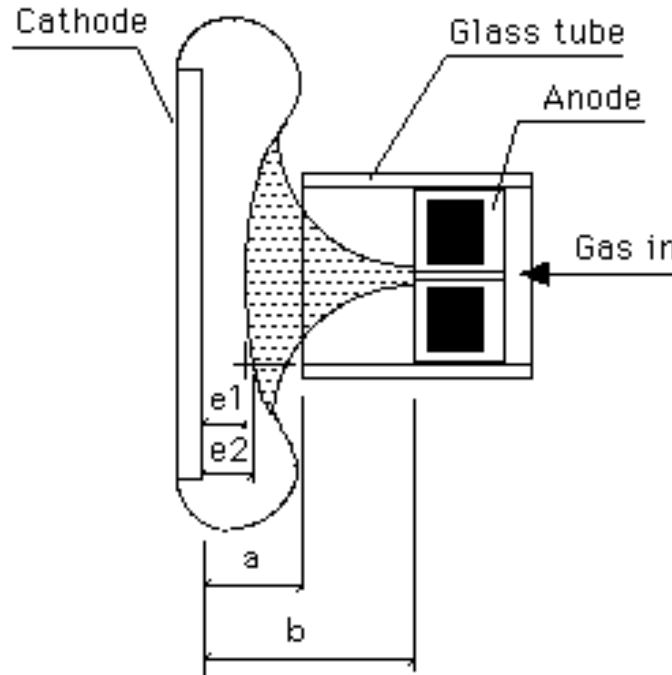

Figure 1. A schematic diagram of the anode magnetron torch (AMT).

Before Plasma Sputtering　　　　　　　**Before Plasma Deposition**

Activated Species

Ar Ions

During Plasma Sputtering　　　　　　　**During Plasma Deposition**

After Plasma Sputtering　　　　　　　**After Plasma Deposition**

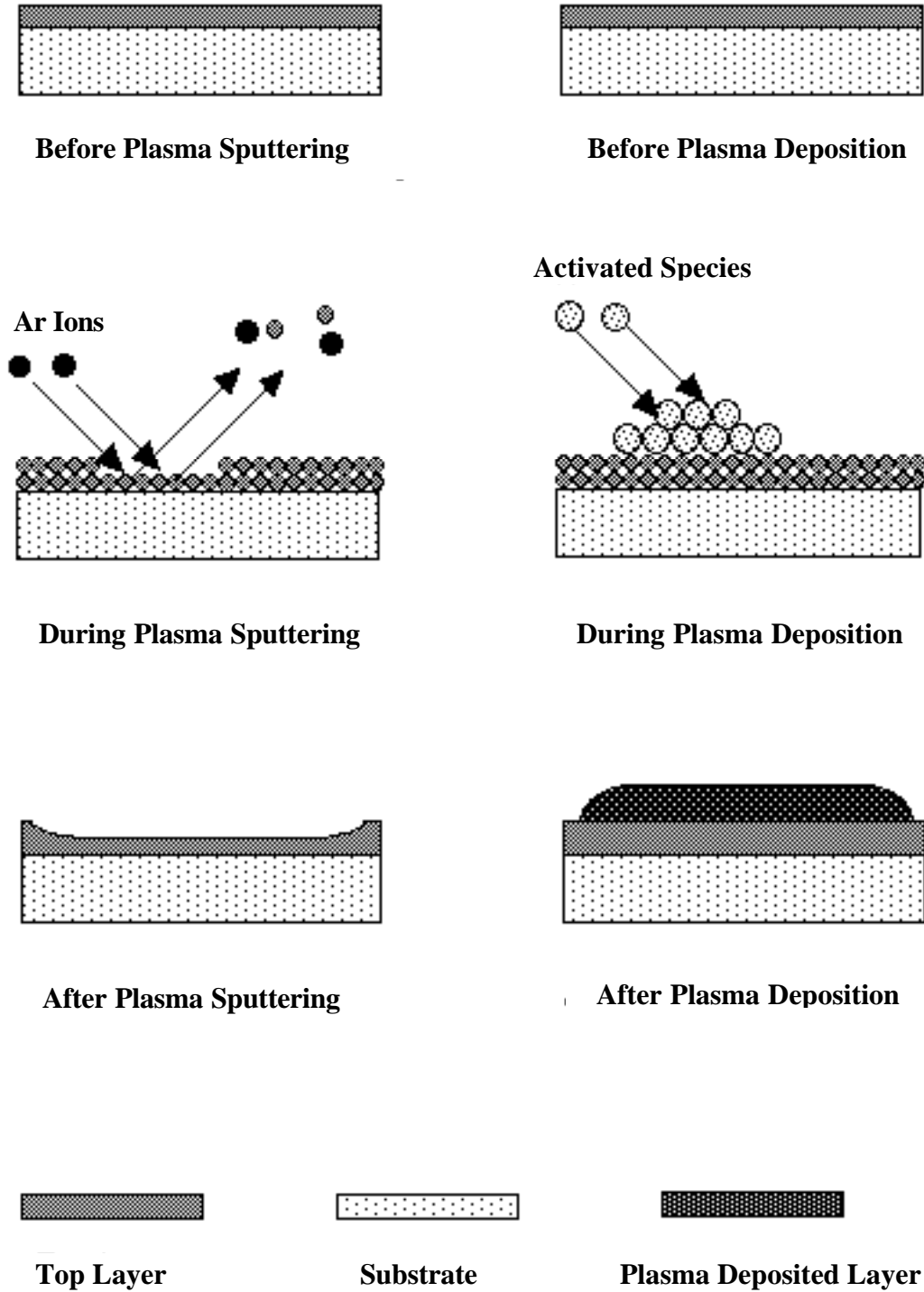**Top Layer**　　　　　**Substrate**　　　　　**Plasma Deposited Layer**

Figure 2. A schematic diagram of plasma sputtering and plasma deposition.

In cathodic plasma polymerization and treatment, the interaction between plasma and substrate surface depends on the bombardment of ionized particles. Whether the ionized

particles (ions) sputter or polymerize on the substrate surface depends on the nature of the gases used [9]. If the gas is a mono-atomic inert gas, the plasma process is sputtering process. If a polymer-forming gas is used, the predominant process on the substrate surface is plasma polymerization (see Fig. 2).

In this study, argon gas has been used as the sputtering gas to study sputtering of plasma polymer of trimethylsilane (TMS) deposited on cold rolled steel. Because of this, the plasma and surface interaction can be limited to the pure sputtering process. The erosion profile (multicolored pattern) on the plasma-treated substrate surface directly shows the results of bombardment with argon ions. A high sputtering rate means increased bombardment of the substrate with argon ions. Therefore, the erosion profile on the substrate surface also holds information about the density distribution of the ions near the cathode surface. If a uniform sputtering rate distribution, indicated by a uniform erosion profile, can be achieved using argon gas, a similar uniform sputtering or deposition rate distribution could be achieved with other gases or monomers by the similar manipulation of operating parameters.

The erosion profile left on the substrate surface following plasma sputtering with argon gas can be evaluated. The evaluation of an erosion profile involves the measurement of the sputtered thickness. Generally, the sputtered film thickness is only between 100 Å and 1000 Å (10 nm to 100 nm). In this range, it is difficult to measure the thickness using normal analytic methods. Most ASTM methods are used to evaluate coating thicknesses from 0.1 μm to 200 μm [10-13], except XPS and ellipsometry. Another difficulty lies in measuring the distribution of sputtered film thickness. XPS can be used to analyze the erosion profile of a thin coating and the sputtered film thickness distribution, but it is a time-consuming process. For very thin film thickness measurements, the most effective method is ellipsometry, which can be used to measure the thickness both quickly and accurately. However, the substrate must be a silicon wafer or some material for which the absorption coefficient is known. For this reason, ellipsometry can not be used directly to measure coated film thickness on other substrates. Fortunately, coated thin films varying in thickness will show different colors on certain substrates. There is a relationship between the thickness of a very thin film and its apparent color. This provides a method with which to evaluate the thickness of very thin films.

Generally, color is a special quality of a mental image perceived by an observer, which can be described by color names [14]. Color is the result of light reflection that has a series of certain wavelengths [15]. Film thickness influences the degree of light absorption and interference; therefore, variance in film thickness will cause changes in color. In other words, the color of thin film is a function of film thickness. If the color of two thin films placed on two panels is identical, the thicknesses of the thin films are same. The apparent color of thin film is influenced by many factors, such as film composition, film thickness, and substrate characteristics. For example, if cold rolled steel (CRS) is coated with pure trimethylsilane (TMS) via a plasma technique, significant color differences will be evident for different coating thicknesses. However, if an

aluminum alloy panel is coated with TMS, color changes are so faint that it is difficult to estimate the thickness of a plasma polymer by colorimetry.

With the increase of TMS film thickness on CRS panels, the apparent color changes in the following sequence: light brown, brown, purple, dark blue, light blue, and yellow. This series of color changes is known to match a corresponding series of TMS film thicknesses. Therefore, CRS panels were used as the substrate in this study.

In order to use the colorimetric method to evaluate plasma sputtering effects, it is necessary to prepare reference color plates. A CRS panel coated by uniform TMS plasma film of known thickness is called a color plate. Reference color plates were prepared in the laboratory using a standard anode magnetron cathodic (AMC) treatment and polymerization system, which has symmetric pairing of electrodes. CRS plates were cleaned with acetone prior to TMS plasma deposition. For each reference plate, TMS plasma was deposited on a CRS plate and a silicon wafer at the same time. The deposited film thickness on the silicon wafer, as measured by ellipsometer, can be considered equal to that on the corresponding CRS plate. Deposited film thickness increases with the increased plasma exposure; each significant increase in thickness corresponds to a relevant color on the CRS plate.

In the AMT Ar sputtering process, a target color plate with a uniform coated film thickness of about 800 Å and an apparent color of dark blue was created. The difference in coated film thickness on a 4 inch × 6 inch CRS panel varied only within 5 %.

After AMT Ar plasma sputtering treatment, because the thickness of TMS film had changed, an erosion profile showing a multicolored pattern was left on the surface of the CRS panel. The residual deposited film thickness was estimated using the colorimetric method. The plasma sputtering rate distribution was calculated by dividing the sputtered film thickness distribution by sputtering time. The sputtered film thickness was the difference between the original coating thickness and the residual coating thickness.

Results and Discussion

Cathodic sputtering treatment using an AMT depends on many operating parameters which influence the motion of electrons and ions; this in turn influences the sputtering rate and its distribution. Fig. 3 shows sample panels, which were treated by AMT Ar plasma under different operating parameters.

From Fig. 3, it is evident that many factors, such as magnetic field strength, input power, system pressure, electrode distance, gap distance, gas flow rate, and cathode area, influence the sputtering rate and its distribution. The specific influence of each parameter is reported and discussed below.
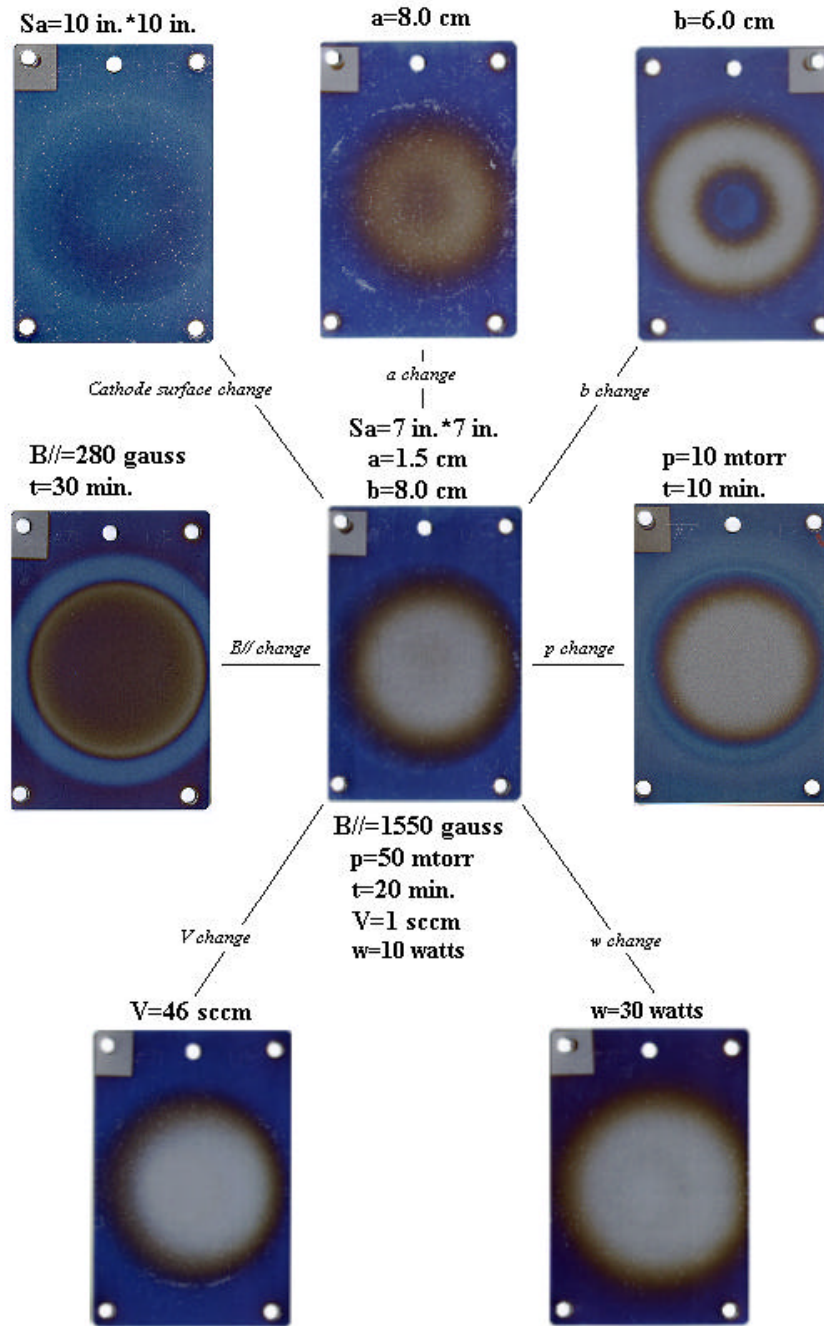
Sa=10 in.*10 in.   a=8.0 cm   b=6.0 cm

Cathode surface change   a change   b change

B//=280 gauss   Sa=7 in.*7 in.   p=10 mtorr
t=30 min.   a=1.5 cm   t=10 min.
                      b=8.0 cm

B// change   p change

B//=1550 gauss
p=50 mtorr
t=20 min.
V=1 sccm
w=10 watts

V change   w change

V=46 sccm   w=30 watts

Figure 3. CRS samples treated by AMT argon plasma under different conditions.

The influence of physical parameters

The gap distance

In the AMT Ar sputtering process, gap distance is an important parameter. It influences the movement pathway of gas or sputtered particles (molecules or atoms). Sputtering rate will change when the gap distance is varied. Fig. 4 shows the relationship between sputtering rate distribution and gap distance. The distribution of sputtering rate according to radius is not uniform. When the gap distance decreases, the total sputtering rate increases in the focused area. So, gap distance plays an important role in achieving a high sputtering rate. At the experimental conditions shown in Fig. 4, the sputtering rate distribution at the center is over 70 Å/min while a is between zero and 2.0 cm. When a is greater than 2.0 cm, the sputtering rate falls quickly. If a is greater than 4.0 cm (from 4.0 cm to 8.0 cm), the sputtering rate hardly changes with variance of the gap distance. When the gap distance is small (<2.0 cm), more electrons emitted from the substrate surface are confined to the focused area, resulting in the ionization of more argon atoms. The high density of argon ions in turn increases the sputtering rate.
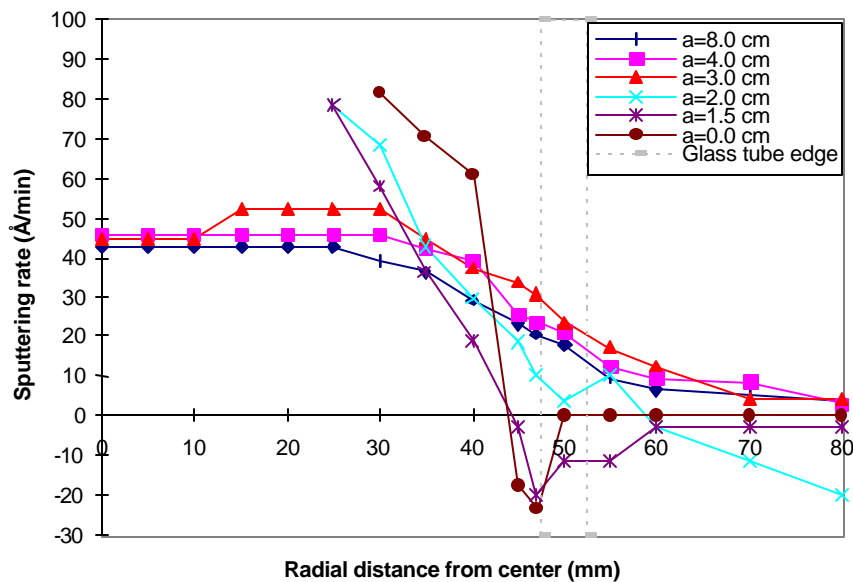
Figure 4. The dependence of the sputtering rate distribution on gap distance ($B_{//max}$ = 1550 gauss, b=8.0 cm, Power=10 w, p=10 mtorr, Ar flow rate=1.0 sccm).

With the decrease of gap distance, redeposition of sputtered particles occurs. The experimental results showed that the CDST $e2$ is a function of operating parameters and tends to increase with the decrease of gap distance [1]. If a is greater than $e2$, the redeposition of sputtered particles does not occur; if it is smaller, redeposition will occur. The reason for this is as follows.

When a particle (charged or non-charged) hits the substrate surface, one of two processes will occur: (1) sputtering or etching of the surface, or (2) deposition or sticking to the surface. An argon ion, because of its high energy and chemical inertness, sputters the surface. However, a sputtered particle, because of its low energy and chemical characteristics, may redeposit on the substrate surface. The former is called an ablation process and the latter a deposition process. If the ablation process is more prevalent than the deposition process, sputtering predominates; in contrast, if deposition exceeds ablation, then polymerization will predominate. This is the principle of competitive ablation and polymerization mechanisms (CAP) [9].

In the AMT plasma system, because of physical and magnetic confinement, more high-energy electrons are confined to the focused area without escape. This results in a higher density of ionized argon atoms in the focused area, so the sputtering rate inside the focused area is much higher than outside. However, because most sputtered particles are electrically neutral, diffusion is their driving force. They cannot get energy from the electric field and, therefore, may stick any place they touch. If a sputtered particle sticks, or redeposits, in the focused area, it will be sputtered again due to the high Ar^+ bombardment. On the contrary, if a sputtered particle redeposits near the vicinity or outside of the edge of the glass tube, the probability that the particle will undergo sputtering a second time decreases dramatically, due to the low Ar^+ bombardment in this area. In this case, the particle typically simply redeposits on the substrate surface.

In the absence of physical confinement ($a = b$), the sputtered particles move and diffuse without any physical barrier to the downstream, because the electrode distance b is much higher than the mean free path λ of the sputtered particles. However, when the gap distance is decreased, the influence of physical confinement (b - a) becomes significant, because the movement path of sputtered particles becomes confined. When a is smaller than $e2$, which is a function of mean free path λ, many sputtered particle s can not easily pass through the gap and deposit near the vicinity or outside of the edge of the glass tube, where less Ar ions bombard the surface (see Fig. 5). Therefore, redeposition occurs when a is smaller than $e2$.
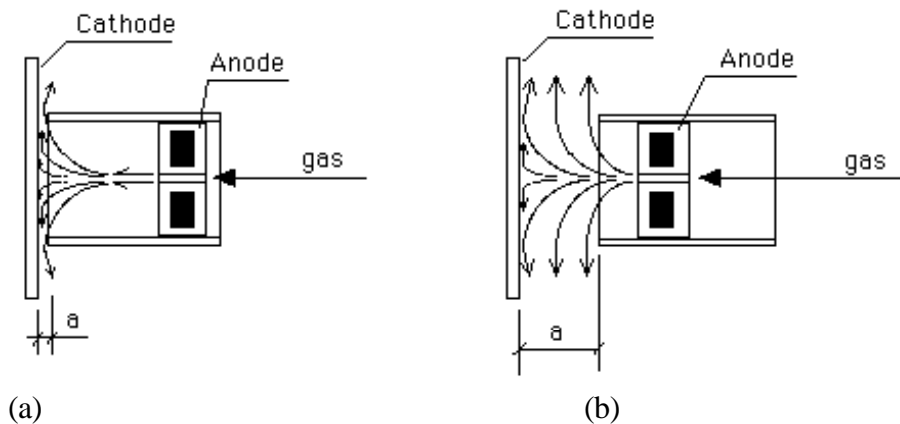

(a)　　　　　　　　　　　　　　　　(b)

Figure 5. A schematic diagram of the influence of the gap distance on the gas stream. (a) Small gap distance, and (b) Large gap distance.

In the AMT plasma system, the relationship between *a* and *e2* becomes a critical condition to control in order to determine whether the redeposition will occur near the vicinity or outside of the edge of the glass tube. This critical condition is very important, because it dictates whether the cleaned surface is recontaminated during the AMT plasma process. In the treatment of a large substrate surface by an AMT scanning process, the gap distance should be equal to or a little higher than the CDST *e2* in order to prevent the recontamination of the cleaned surface.

Fig. 6 shows the influence of gap distance on sputtering rate under higher system pressure (p=50 mtorr). The results display almost the same trend as seen in Fig. 4, aside from the magnitude of the Ar sputtering rate. The sole difference is a sharp peak in sputtering rate near the wall of the glass tube. This sharp peak appears with a small gap distance.
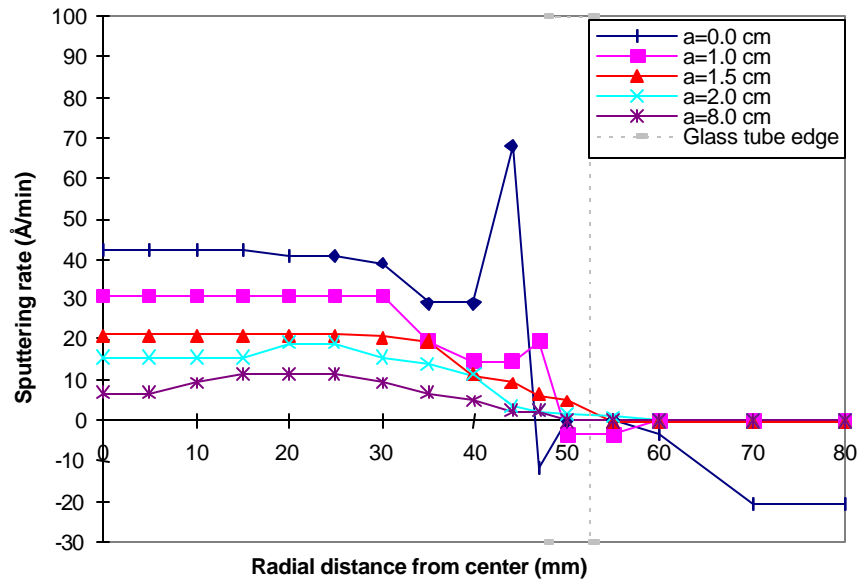
Figure 6. The dependence of the sputtering rate distribution on gap distance ($B_{//max}$= 1550 gauss, b=8.0 cm, Power=10 w, p=50 mtorr, Ar flow rate=1.0 sccm).

The sputtering rate peak near the wall of the glass tube proves the function of physical confinement. Higher physical confinement keeps more argon ions inside of the focused area. Therefore, it increases the sputtering rate in the focused area.

The electrode distance

The distance between the two electrodes influences the magnetic field distribution of the cathode area. Experimental results showed that the electrode distance not only influences the shape of AMT glow discharge, but also the cathodic dark space thickness [1]. Fig. 7a shows the relationship between sputtering rate and the electrode distance under total physical confinement (gap distance *a*=0 cm) and a strong magnetic field ($B_{//max}$=1550 gauss). The distribution of sputtering rate according to radial distance from the center is

not uniform and shifts with changes in electrode distance. When *b* increases, the distribution of the sputtering rate is relatively uniform in the center area; the peak sputtering rate (not the highest peak caused by the wall of the glass tube but the second highest peak) shifts to the center of focused area; and the magnitude of sputtering rate peak decreases relatively.
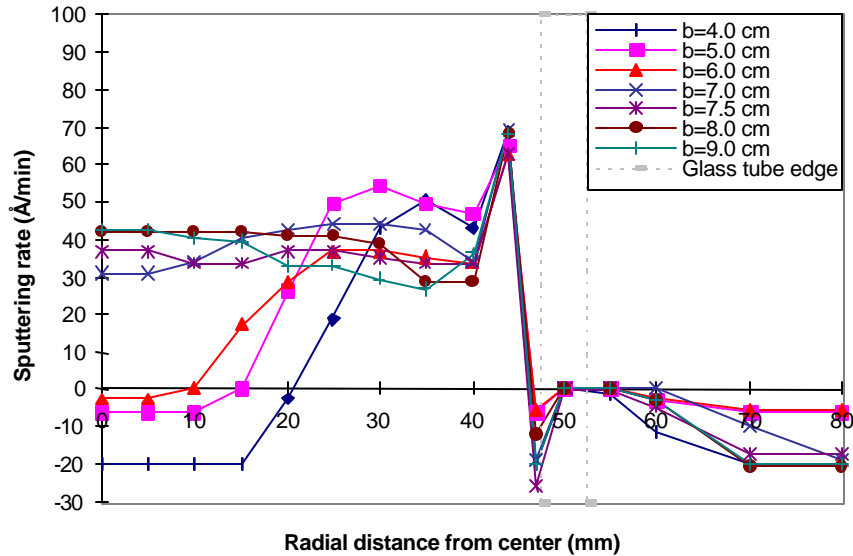

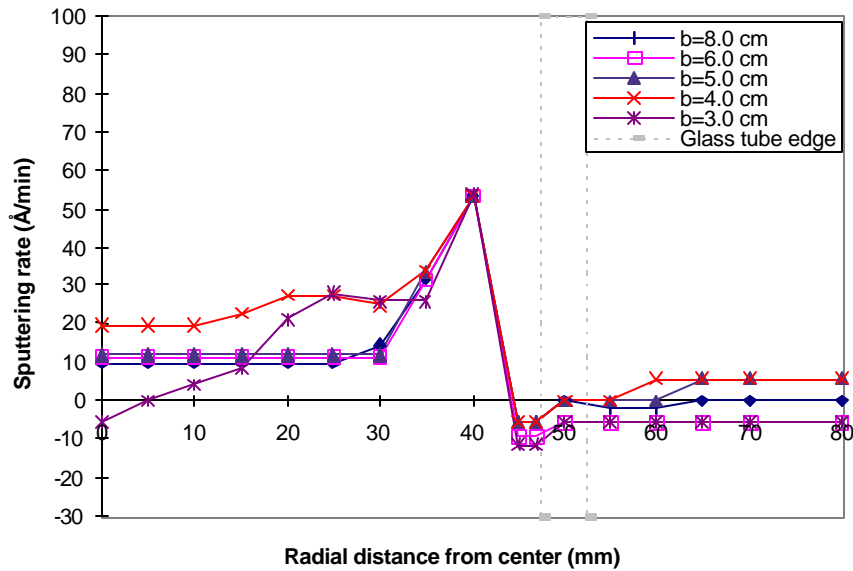Figure 7a. The dependence of the sputtering rate distribution on electrode distance ($B_{//max}$=1550 gauss, a=0.0 cm, Power=10 w, p=50 mtorr, Ar flow rate=1.0 sccm).

While *b* is small, because of the huge difference in Ar sputtering rate, the big blue eye, which will disappear with increasing electrode distance, exists in the center of focused area [1]. This is attributed to non-uniform distribution of the parallel magnetic field strength near the substrate surface. Because of this non-uniformity, secondary electrons emitted by Ar^+ bombardment are easily trapped in the vicinity of the strong magnetic field, resulting in more ionization collisions and a high sputtering rate in this area. The density of Ar^+ at the center of the focused area is much lower due to magnetic field distribution. This causes a lower flux of ion bombardment, so the Ar sputtering rate decreases. On the other hand, the sputtered particles may redeposit on the substrate surface. According to CAP theory, if this deposition rate is higher than the ablation rate, deposition predominates. Otherwise, the sputtering process will predominate. This is why the sputtering rate changes to a negative value at the center of the focused area when *b* is small (see Fig. 7a).

Fig. 7b shows the relationship between electrode distance and sputtering rate distribution under AMT treatment with a weak anode magnetron ($B_{//max}$=280 gauss). The sputtering rate drops as compared to Fig. 7a. The Ar sputtering rate is uniform in the focused area when *b* is greater than 4.0 cm. This uniform sputtering rate is highest at b=4.0 cm and then decreases with the increase of electrode distance. This differs from the sputtering rate distribution under AMT with a strong anode magnetron ($B_{//max}$=1550 gauss). In this

case, the sputtering rate in the focused area rises with the increase of electrode distance, *b,* until b=8.0 cm (see Fig. 7a). This result demonstrates that the electrode distance is not a simple factor in plasma treatment and polymerization with the AMT system. The sputtering rate may drop under large electrode distances, but the distribution of sputtering rate may become non-uniform in the focused area under small electrode distances. The overall effect on sputtering depends on the distribution and strength of the magnetic field near the substrate surface. A suitable electrode distance is one that brings about a uniform magnetic field strength near the cathode surface, ensuring a high and uniform sputtering rate in the focused area.

Figure 7b. The dependence of the sputtering rate distribution on electrode distance ($B_{//max}$=280 gauss, a=0.0 cm, Power=10 w, p=50 mtorr, Ar flow rate=1.0 sccm).

Fig. 7c shows the influence of electrode distance on the sputtering rate without anode magnetron enhancement ($B_{//max}$=0 gauss). In this case, the sputtering rate changes little with variance of the electrode distance. Therefore, electrode distance is not an important parameter in plasma treatment and polymerization if no anode magnetron enhancement is applied.

The influence of magnetic field strength

The magnetic field distribution in the AMT plasma system was reported in an earlier paper [1]. Fig. 8 shows that high magnetic field strength achieves a high and uniform sputtering rate if the electrode distance is large. A large electrode distance can maintain a uniform distribution of magnetic field strength near the substrate surface. However, if the electrode distance is small, such as *b*=4 cm in Figs. 9a and b, the Ar sputtering rate distribution is no longer uniform. This is because the distribution of magnetic field strength created by strong anode magnetron enhancement ($B_{//max}$=1550 gauss) is not uniform near the substrate surface. For weak anode magnetron enhancement ($B_{//max}$=280

gauss), the sputtering rate distribution still remains uniform in comparison to b=8 cm due to a uniform magnetic field distribution near the substrate surface. Without anode magnetron enhancement ($B_{//max}$=0 gauss), the sputtering rate is always very low no matter how other parameters change.
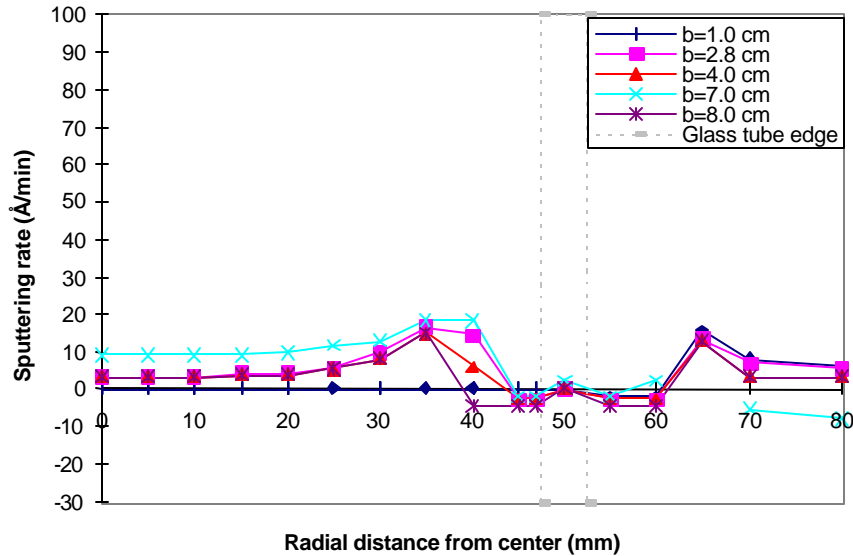

Figure 7c. The dependence of the sputtering rate distribution on electrode distance ($B_{//max}$=0 gauss, a=0.0 cm, Power=10 w, p=50 mtorr, Ar flow rate=1.0 sccm).

It is clear that a strong magnetic field can focus or confine electrons more effectively, increasing the sputtering rate. Nevertheless, a uniform magnetic field strength near the substrate surface plays the same important role in the AMT plasma system. A uniform magnetic field strength can maintain a uniform distribution of electrons. Non-uniform magnetic field strength may attract electrons to a magnetic trap causing a non-uniform distribution of electrons near the substrate surface.

While magnetic fields are used in glow discharges, they are strong enough to influence the energetic plasma electrons, but not the ions due to their higher mass. However, magnetically confined electrons in a glow discharge also provide considerable confinement to the plasma ions, since electrostatic forces prevent the ions from escaping from the electrons [16]. Because of the electrostatic force between electrons and ions, ion distribution becomes non-uniform if electron distribution is not uniform. Thus, the sputtering rate distribution is non-uniform. If uniform magnetic field strength distribution near the cathodic distribution can be created, uniform sputtering rate distribution can be achieved in the focused area.
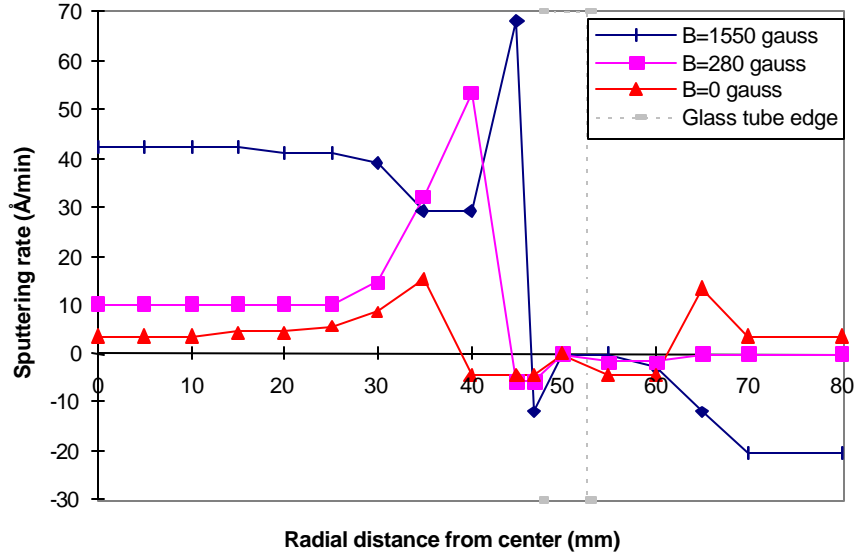
Figure 8. The dependence of the sputtering rate distribution on magnetic field strength (a=0.0 cm, b=8.0 cm, input power=10 w, p=50 mtorr).
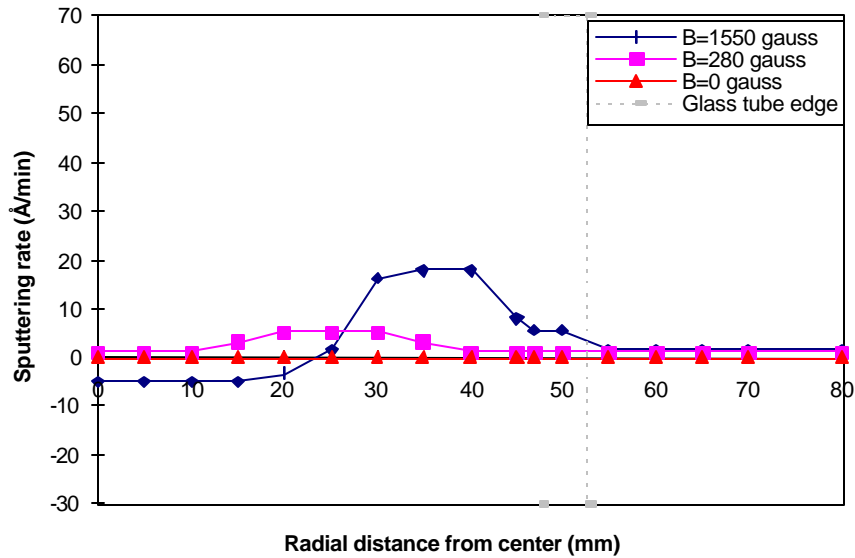

Figure 9a. The dependence of the sputtering rate distribution on magnetic field strength (a=4.0 cm, b=4.0 cm, input power=10 w, p=50 mtorr).
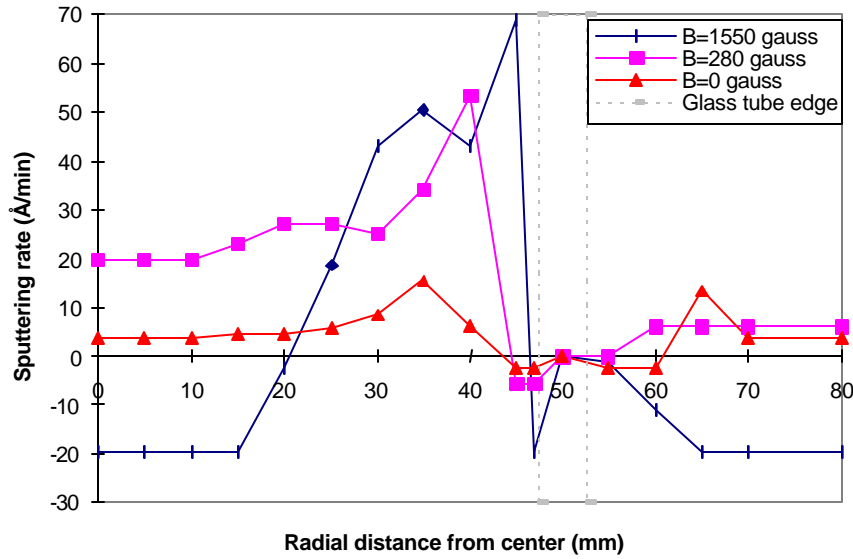
Figure 9b. The dependence of the sputtering rate distribution on magnetic field strength (a=0.0 cm, b=4.0 cm, input power=10 w, p=50 mtorr).

The influence of system pressure

Fig. 10a shows the relationship between Ar sputtering rate and system pressure with a strong anode magnetron. It shows that the Ar sputtering rate distribution is not uniform with respect to radial distance from the center. The Ar sputtering rate increases in the focused area with the decrease of system pressure. In the focused area, the sputtering rate at p=10 mtorr is almost four times greater than that at p=50 mtorr. This is because the mean free path of atoms or other small particles, *l*, is inversely proportional to system pressure. With the decrease of system pressure, the charged particles can get more energy from the electrical field due to the large *l*. High-energy ions that bombard the substrate surface raise the Ar sputtering rate. However, near the vicinity and outside of the edge of the glass tube, when the system pressure is lowered, the Ar sputtering rate can decrease below zero, i.e., deposition occurs. This is because the CDST *e2*, which increases with the decrease of system pressure [1], becomes larger than the gap distance causing the redeposition of sputtered particles as explained earlier.

Fig. 10b shows the influence of system pressure under both a weak anode magnetron ($B_{//max}$=280 gauss) and no anode magnetron ($B_{//max}$=0 gauss). It displays the same results as Fig. 10a. However, the redeposition of sputtered materials occurs at p=50 mtorr, because the gap distance, *a,* is smaller than the CDST *e2*.
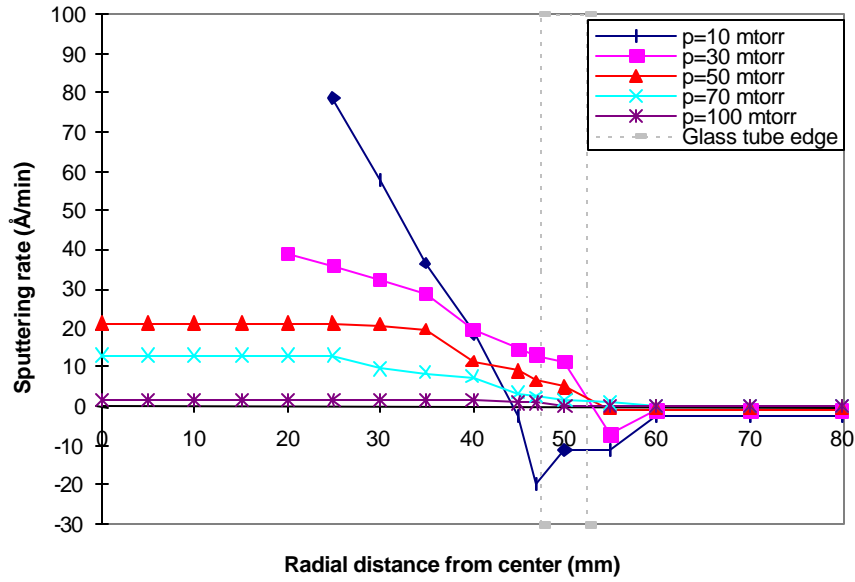
Figure 10a. The dependence of the sputtering rate distribution on system pressure
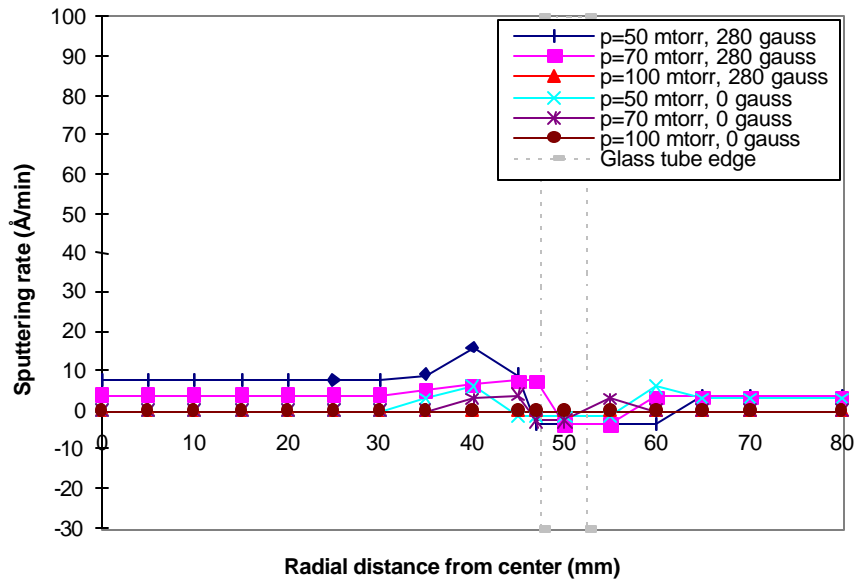($B_{//max}$=1550 gauss, a=1.5 cm, b=8.0 cm, Power=10 w, Ar flow rate=1.0 sccm).

Figure 10b. The dependence of the sputtering rate distribution on system pressure
($B_{//max}$=280 gauss or 0 gauss, a=1.5 cm, b=8.0 cm, Power=10 w, Ar flow rate=1.0 sccm).

The influence of magnetic field strength on the Ar sputtering rate under the different
system pressures can be found by comparing Figs. 10a and b. The results clearly show
the effectiveness of the AMT sputtering system depends on the operating pressure. At

lower system pressures, a stronger magnetic field increases the Ar sputtering rate. However, with the increase of system pressure, the influence of the magnetic field on the Ar sputtering rate is diminished. At high system pressure (p=100 mtorr), the sputtering rate drops to almost zero no matter how high of a magnetic field strength is applied.
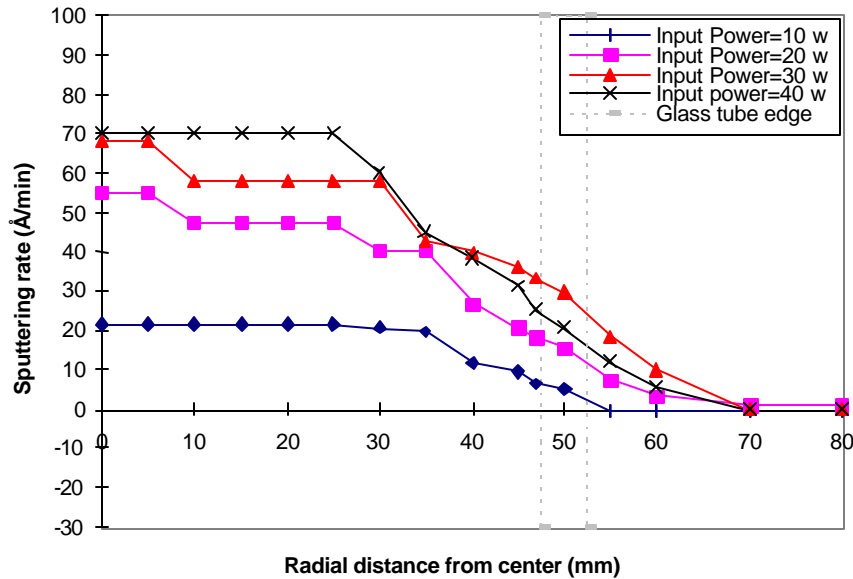
The influence of input power

Figure 11a. The dependence of the sputtering rate distribution on input power ($B_{//max}$=1550 gauss, a=1.5 cm, b=8.0 cm, p=50 mtorr, Ar flow rate=1.0 sccm).

Fig. 11a shows the influence of input power on the Ar sputtering rate distribution. The sputtering rate increases with the increase of input power, but the distribution of the Ar sputtering rate is not uniform with respect to radial distance. Sputtering rate is a function of the energy and the number of ions that bombard the cathodic surface [17]. High input power increases the number of high-energy electrons, raising the probability of ionization collisions between electrons and gas atoms or molecules. Thus, there is a simultaneous increase in both the number of ions and the energy they possess due to increased input power, and, the sputtering rate rises.

Fig. 11b shows the influence of input power on the Ar sputtering rate under both the weak anode magnetron ($B_{//max}$=280 gauss) and no anode magnetron ($B_{//max}$=0 gauss). A trend similar to that evident in Fig. 11a is shown; however, there are two differences. First, the sputtered materials redeposit near the vicinity or outside of the edge of the glass tube, because the CDST $e2$ is larger than the gap distance (a=1.5 cm) under either of these conditions. Second, the input power cannot be increased as high as that under a strong anode magnetron. Thus, one of the merits of the AMT system over plasma

treatment systems without the influence of an anode magnetron is the ability to achieve a higher input power.
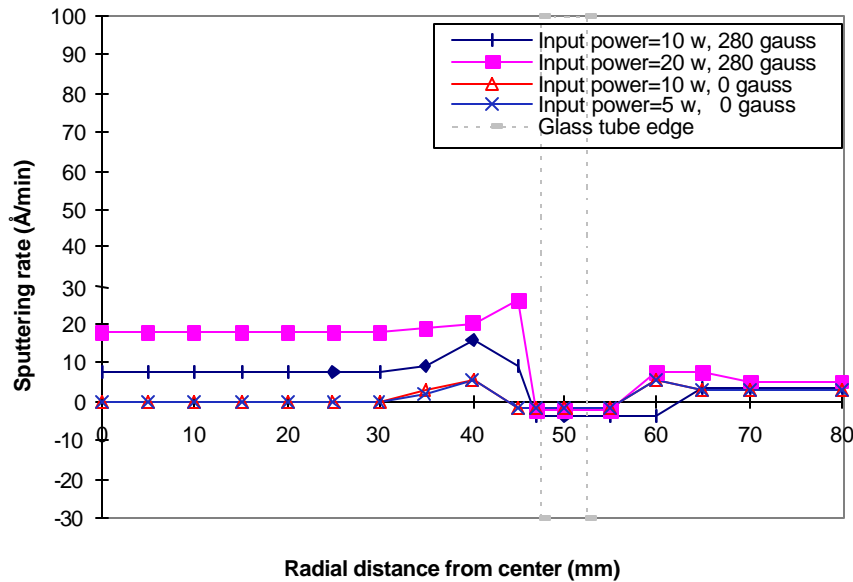

Figure 11b. The dependence of the sputtering rate distribution on input power ($B_{//max}$=280 gauss or 0 gauss, a=1.5 cm, b=8.0 cm, p=50 mtorr, Ar flow rate=1.0 sccm).

The influence of gas flow rate

Fig. 12 shows the influence of Ar gas flow rate (at a fixed pressure) on the Ar sputtering rate distribution in the AMT plasma system. The sputtering rate distribution is almost uniform from the center to r=3.0 cm at a low argon flow rate (V=1 sccm). With the increase of Ar gas flow rate, the sputtering rate increases at the center but hardly changes when r is greater than 2.5 cm. The probable reason is that Ar flow blows out the sputtered particles at the high flow rate, which might have otherwise re-deposited on the center; thus, an increase in the sputtering rate on the center of the focused area occurs. However, this influence is localized. If r is larger than 2.5 cm, which is beyond the area where the Ar gas can blow, the sputtering rate distribution is basically unchanged.

The influence of cathode surface area

The main purpose of developing the AMT system is to treat large substrate surfaces via a scanning process. In order to investigate the effectiveness of AMT plasma treatment of large substrate surfaces, a large CRS panel of 10×10 inches was used as the substrate. The experimental results are shown in Figs. 13a and b.

In Fig. 13a, the sputtering rate does not change much with the increase of cathode surface area at low system pressure (p=10 mtorr). The plasma treatment is localized and effectively confined. However, at a relatively high system pressure (p=50 mtorr), the sputtering rate is almost zero (see Fig. 13b). This case reiterates the importance of

system pressure in AMT Ar sputtering treatment. This can be explained by the influence of the magnetic field, the effect of which is expressed by the ratio of the mean free path of an electron, l_e, to the Larmor radius of an electron, r_e [9].
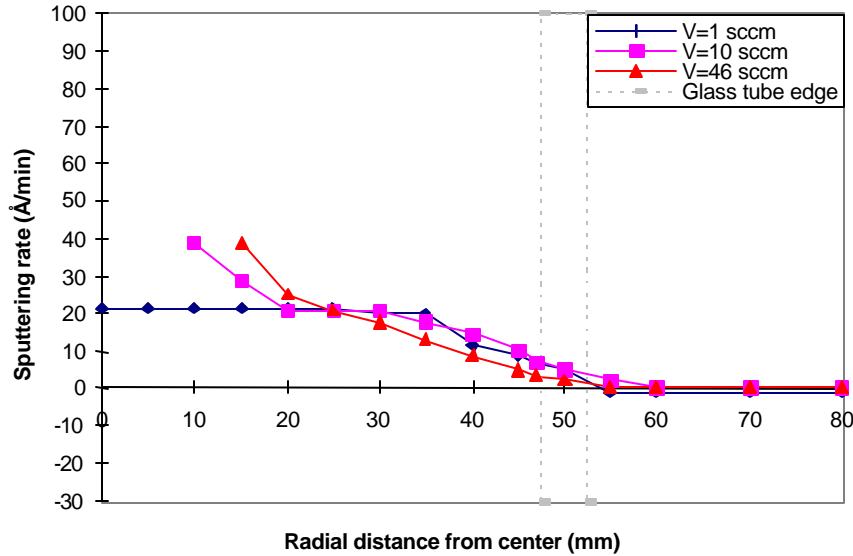

Figure 12. The dependence of the sputtering rate distribution on gas flow rate ($B_{//max}$=1550 gauss, a=1.5 cm, b=8.0 cm, Power=10 w, p=50 mtorr).

When $l_e/r_e \ll 1$, the effect of the magnetic field is negligible. With an increase of the ratio l_e/r_e, the magnetic field starts to influence the motion of electrons and then becomes significant. Lower system pressure means a higher mean free path. Thus, the ratio of l_e to r_e increases with a decrease in system pressure, and the effects of the magnetic field become significant. In other words, the electron path can be confined more effectively and localized under low system pressure. Therefore, the influence of the substrate surface area becomes less significant at low system pressure (p=10 mtorr).

At high system pressure, due to less confinement of electrons, the electrons can scatter over the whole substrate surface, resulting in a decrease in the electron density in the focused area. As a result, the Ar ion bombardment flux decreases, and the sputtering rate drops quickly in the focused area.
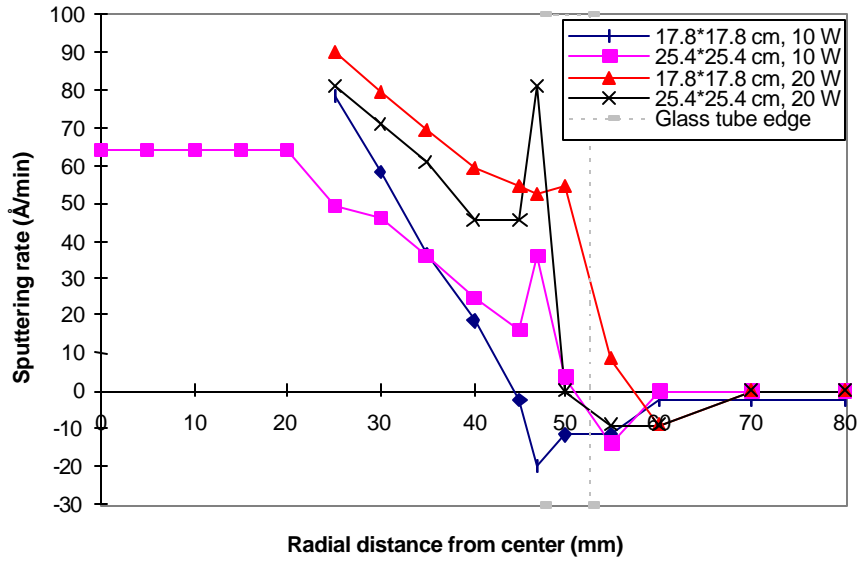
Figure 13a. The dependence of the sputtering rate distribution on cathode surface area ($B_{//stmax}$=1550 gauss, a=1.5 cm, b=8.0 cm, p=10 mtorr).
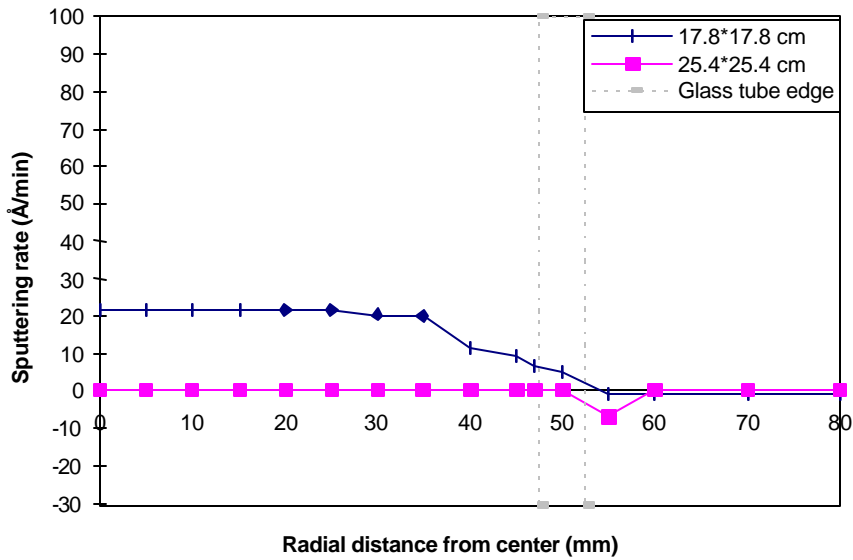

Figure 13b. The dependence of the sputtering rate distribution on cathode surface area ($B_{//stmax}$=1550 gauss, a=1.5 cm, b=8.0 cm, p=50 mtorr).

Conclusions

1.   The argon sputtering effects of the anode magnetron torch (AMT) can be
        effectively confined and localized under low system pressure (p = 10 mtorr).
        Operating parameters influence the effectiveness of AMT Ar sputtering rate.

2.   A small gap distance increases the sputtering rate in the focused area, but creates
        deposition near the vicinity or outside of the edge of the glass tube. A suitable
        gap distance is one, which maintains the highest sputtering rate in the focused
        area without allowing any deposition near the vicinity or outside of the edge of
        the glass tube. This optimal gap distance is equal to the cathodic dark space
        thickness at the edge of the glass tube.

3.   Electrode distance affects the uniformity of the Ar sputtering rate distribution in the
        focused area. The optimum electrode distance is that which brings about uniform
        magnetic field strength distribution near the cathode surface.

4.   High magnetic field strength is important in increasing the Ar sputtering rate,
        because it improves the magnetic confinement of electrons, especially at lower
        system pressures.

5.   High input power and low system pressure can significantly increase the sputtering
        rate.

6.   The increase of Ar gas flow rate improves the sputtering rate only minimally,
        because such improvement is limited by the system pressure and vacuum system
        capacity.

References

 1.   J. G. Zhao and H. Yasuda, (in review).
 2.   T. Wang and H. K.Yasuda, *J. Appl. Polym. Sci*. **55**, 903 (1995).
 3.   A. R. Westwood, *Eur. Polym. J*. **7(4)**, 363 (1971).
 4.   W. H. Tao, Ph. D dissertation, University of Missouri-Columbia, (1994).
 5.   T. F. Wang, T. J. Lin, D. J. Yand, J. A. Antonelli, and H. K. Yasuda, *Prog. Org.
      Coat*. **28(4)**, 291 (1996).
 6.   H. K. Yasuda, T. F. Wang, D. L. Cho, T. J. Lin, and J. A. Antonelli, *Prog. Org. Coat*.
      30(1), 31 (1997).
 7.   H. Yasuda, B. H. Chun, D. L. Cho, T. J. Lin, D. J. Yang, and J. A. Antonelli,
      Corrosion J. **52**, 169 (1996).
 8.   Y. Lin and H. Yasuda, *J. Appl. Polym. Sci*. **60**, 543 (1996).
 9.   H. Yasuda, Plasma Polymerization, (Academic Press, Inc., 1985).
10.   ASTM B748-90, (02.05).
11.   ASTM B588-88, (02.05).
12.   ASTM B499-88, (02.05).

13. ASTM B504-90, (02.05).
14. G. J. Chamberlin and D. G. Chamberlin, <u>Color, Its Measurement, Computation and Application</u>, (Heyden & Son Ltd., 1980).
15. Luigina De Grandis, <u>Theory and Use of Color</u>, (Harry N. Abrams, Inc., New York, 1986).
16. J. A. Thornton, in <u>Deposition Technologies for Films and Coatings, Development and Applications</u>, R. F. Bunshah, J. M. Blocher, Jr., D. M. Mattox, T. D. Bonifield, G. E. McGuire, J. G. Fish, M. Schwartz, P. B. Ghate, J. A. Thornton, B. E. Jacobson, R. C. Tucker, Jr. eds., Noyes Publications, (Park Ridge, New Jersey, 1982), pp 19.
17. B. N. Chapman, <u>Glow Discharge Processes, Sputtering and Plasma Etching</u>, (Wiley, New York, 1980).